Eur. Phys. J. C (2022) 82:869
https://doi.org/10.1140/epjc/s10052-022-10536-1

THE EUROPEAN PHYSICAL JOURNAL C

Review

FLAG Review 2021

Flavour Lattice Averaging Group (FLAG)

Y. Aoki[1], T. Blum[2,3], G. Colangelo[4], S. Collins[5], M. Della Morte[6], P. Dimopoulos[7,8], S. Dürr[9,10], X. Feng[11,12,13,14], H. Fukaya[15], M. Golterman[16], Steven Gottlieb[17], R. Gupta[18], S. Hashimoto[19,20], U. M. Heller[21], G. Herdoiza[22], P. Hernandez[23], R. Horsley[24], A. Jüttner[25,26,27,a], T. Kaneko[19,20], E. Lunghi[17], S. Meinel[28], C. Monahan[29,30], A. Nicholson[31], T. Onogi[15], C. Pena[22], P. Petreczky[32], A. Portelli[24], A. Ramos[23], S. R. Sharpe[33], J. N. Simone[34], S. Simula[35], S. Sint[36], R. Sommer[37,38], N. Tantalo[39], R. Van de Water[34], U. Wenger[4,27], H. Wittig[40]

[1] RIKEN Center for Computational Science, Kobe 650-0047, Japan
[2] Physics Department, University of Connecticut, Storrs, CT 06269-3046, USA
[3] RIKEN BNL Research Center, Brookhaven National Laboratory, Upton, NY 11973, USA
[4] Albert Einstein Center for Fundamental Physics, Institut für Theoretische Physik, Universität Bern, Sidlerstr. 5, 3012 Bern, Switzerland
[5] Institut für Theoretische Physik, Universität Regensburg, 93040 Regensburg, Germany
[6] CP3-Origins and IMADA, University of Southern Denmark, Campusvej 55, 5230 Odense M, Denmark
[7] Dipartimento di Scienze Matematiche, Fisiche e Informatiche, Università di Parma, 43124 Parma, Italy
[8] INFN, Gruppo Collegato di Parma, Parco Area delle Scienze 7/a (Campus), 43124 Parma, Italy
[9] University of Wuppertal, Gaußstraße 20, 42119 Wuppertal, Germany
[10] Jülich Supercomputing Center, Forschungszentrum Jülich, 52425 Jülich, Germany
[11] School of Physics, Peking University, Beijing 100871, China
[12] Collaborative Innovation Center of Quantum Matter, Beijing 100871, China
[13] Center for High Energy Physics, Peking University, Beijing 100871, China
[14] State Key Laboratory of Nuclear Physics and Technology, Peking University, Beijing 100871, China
[15] Department of Physics, Osaka University, Toyonaka, Osaka 560-0043, Japan
[16] Department of Physics and Astronomy, San Francisco State University, San Francisco, CA 94132, USA
[17] Department of Physics, Indiana University, Bloomington, IN 47405, USA
[18] Los Alamos National Laboratory, Theoretical Division T-2, Los Alamos, NM 87545, USA
[19] High Energy Accelerator Research Organization (KEK), Tsukuba 305-0801, Japan
[20] School of High Energy Accelerator Science, The Graduate University for Advanced Studies (Sokendai), Tsukuba 305-0801, Japan
[21] American Physical Society (APS), One Research Road, Ridge, NY 11961, USA
[22] Instituto de Física Teórica UAM/CSIC and Departamento de Física Teórica, Universidad Autónoma de Madrid, Cantoblanco, 28049 Madrid, Spain
[23] IFIC (CSIC-UVEG), Parc Científic de la Universitat de València, 46980 Paterna, Spain
[24] Higgs Centre for Theoretical Physics, School of Physics and Astronomy, University of Edinburgh, Edinburgh EH9 3FD, UK
[25] School of Physics and Astronomy, University of Southampton, Southampton SO17 1BJ, UK
[26] STAG Research Center, University of Southampton, Highfield, Southampton SO17 1BJ, UK
[27] CERN, Theoretical Physics Department, Geneva, Switzerland
[28] Department of Physics, University of Arizona, Tucson, AZ 85721, USA
[29] Department of Physics, The College of William and Mary, Williamsburg, VA 23187, USA
[30] Theory Center, Thomas Jefferson National Accelerator Facility, Newport News, VA 23606, USA
[31] Department of Physics and Astronomy, University of North Carolina, Chapel Hill, NC 27516-3255, USA
[32] Physics Department, Brookhaven National Laboratory, Upton, NY 11973, USA
[33] Physics Department, University of Washington, Seattle, WA 98195-1560, USA
[34] Fermi National Accelerator Laboratory, Batavia, IL 60510, USA
[35] INFN, Sezione di Roma Tre, Via della Vasca Navale 84, 00146 Rome, Italy
[36] School of Mathematics and Hamilton Mathematics Institute, Trinity College Dublin, Dublin 2, Ireland
[37] John von Neumann Institute for Computing (NIC), DESY, Platanenallee 6, 15738 Zeuthen, Germany
[38] Institut für Physik, Humboldt-Universität zu Berlin, Newtonstr. 15, 12489 Berlin, Germany
[39] INFN, Sezione di Tor Vergata, c/o Dipartimento di Fisica, Università di Roma Tor Vergata, Via della Ricerca Scientifica 1, 00133 Rome, Italy
[40] PRISMA Cluster of Excellence, Institut für Kernphysik and Helmholtz Institute Mainz, University of Mainz, 55099 Mainz, Germany

Received: 3 February 2022 / Accepted: 31 May 2022 / Published online: 4 October 2022

[a] e-mail: a.juttner@soton.ac.uk (corresponding author)

Abstract We review lattice results related to pion, kaon, D-meson, B-meson, and nucleon physics with the aim of making them easily accessible to the nuclear and particle physics communities. More specifically, we report on the determination of the light-quark masses, the form factor $f_+(0)$ arising in the semileptonic $K \to \pi$ transition at zero momentum transfer, as well as the decay constant ratio f_K/f_π and its consequences for the CKM matrix elements V_{us} and V_{ud}. Furthermore, we describe the results obtained on the lattice for some of the low-energy constants of $SU(2)_L \times SU(2)_R$ and $SU(3)_L \times SU(3)_R$ Chiral Perturbation Theory. We review the determination of the B_K parameter of neutral kaon mixing as well as the additional four B parameters that arise in theories of physics beyond the Standard Model. For the heavy-quark sector, we provide results for m_c and m_b as well as those for the decay constants, form factors, and mixing parameters of charmed and bottom mesons and baryons. These are the heavy-quark quantities most relevant for the determination of CKM matrix elements and the global CKM unitarity-triangle fit. We review the status of lattice determinations of the strong coupling constant α_s. We consider nucleon matrix elements, and review the determinations of the axial, scalar and tensor bilinears, both isovector and flavor diagonal. Finally, in this review we have added a new section reviewing determinations of scale-setting quantities.

Contents

1 Introduction

Flavour physics provides an important opportunity for exploring the limits of the Standard Model of particle physics and for constraining possible extensions that go beyond it. As the LHC explores a new energy frontier and as experiments continue

to extend the precision frontier, the importance of flavour physics will grow, both in terms of searches for signatures of new physics through precision measurements and in terms of attempts to construct the theoretical framework behind direct discoveries of new particles. Crucial to such searches for new physics is the ability to quantify strong-interaction effects. Large-scale numerical simulations of lattice QCD allow for the computation of these effects from first principles. The scope of the Flavour Lattice Averaging Group (FLAG) is to review the current status of lattice results for a variety of physical quantities that are important for flavour physics. Set up in November 2007, it comprises experts in Lattice Field Theory, Chiral Perturbation Theory and Standard Model phenomenology. Our aim is to provide an answer to the frequently posed question "What is currently the best lattice value for a particular quantity?" in a way that is readily accessible to those who are not expert in lattice methods. This is generally not an easy question to answer; different collaborations use different lattice actions (discretizations of QCD) with a variety of lattice spacings and volumes, and with a range of masses for the u- and d-quarks. Not only are the systematic errors different, but also the methodology used to estimate these uncertainties varies between collaborations. In the present work, we summarize the main features of each of the calculations and provide a framework for judging and combining the different results. Sometimes it is a single result that provides the "best" value; more often it is a combination of results from different collaborations. Indeed, the consistency of values obtained using different formulations adds significantly to our confidence in the results.

The first four editions of the FLAG review were made public in 2010 [1], 2013 [2], 2016 [3], and 2019 [4] (and will be referred to as FLAG 10, FLAG 13, FLAG 16, and FLAG 19, respectively). The fourth edition reviewed results related to both light (u-, d- and s-), and heavy (c- and b-) flavours. The quantities related to pion and kaon physics were light-quark masses, the form factor $f_+(0)$ arising in semileptonic $K \to \pi$ transitions (evaluated at zero momentum transfer), the decay constants f_K and f_π, the B_K parameter from neutral kaon mixing, and the kaon mixing matrix elements of new operators that arise in theories of physics beyond the Standard Model. Their implications for the CKM matrix elements V_{us} and V_{ud} were also discussed. Furthermore, results were reported for some of the low-energy constants of $SU(2)_L \times SU(2)_R$ and $SU(3)_L \times SU(3)_R$ Chiral Perturbation Theory. The quantities related to D- and B-meson physics that were reviewed were the masses of the charm and bottom quarks together with the decay constants, form factors, and mixing parameters of B- and D-mesons. These are the heavy-light quantities most relevant to the determination of CKM matrix elements and the global CKM unitarity-triangle fit. The current status of lattice results on the QCD coupling α_s was reviewed. Last but not least, we reviewed calculations of nucleon matrix elements of flavor nonsinglet and singlet bilinear operators, including the nucleon axial charge g_A and the nucleon sigma term. These results are relevant for constraining V_{ud}, for searches for new physics in neutron decays and other processes, and for dark matter searches.

In the present paper we provide updated results for all the above-mentioned quantities, but also extend the scope of the review by adding a section on scale setting, Sect. 11. The motivation for adding this section is that uncertainties in the value of the lattice spacing a are a major source of error for the calculation of a wide range of quantities. Thus we felt that a systematic compilation of results, comparing the different approaches to setting the scale, and summarizing the present status, would be a useful resource for the lattice community. An additional update is the inclusion, in Sect. 6.2, of a brief description of the status of lattice calculations of $K \to \pi\pi$ decay amplitudes. Although some aspects of these calculations are not yet at the stage to be included in our averages, they are approaching this stage, and we felt that, given their phenomenological relevance, a brief review was appropriate.

For the most precisely determined quantities, isospin breaking – both from the up-down quark mass difference and from QED – must be included. A short review of methods used to include QED in lattice-QCD simulations is given in Sect. 3.1.3. An important issue here is that, in the context of a QED+QCD theory, the separation into QED and QCD contributions to a given physical quantity is ambiguous – there are several ways of defining such a separation. This issue is discussed from different viewpoints in the section on quark masses – see Sect. 3.1.1 – and that on scale setting – see Sect. 11. We stress, however, that the physical observable in QCD + QED is defined unambiguously. Any ambiguity only arises because we are trying to separate a well-defined, physical quantity into two unphysical parts that provide useful information for phenomenology.

Our main results are collected in Tables 1, 2, 3, 4 and 5. As is clear from the tables, for most quantities there are results from ensembles with different values for N_f. In most cases, there is reasonable agreement among results with $N_f = 2, 2+1$, and $2+1+1$. As precision increases, we may some day be able to distinguish among the different values of N_f, in which case, presumably $2+1+1$ would be the most realistic. (If isospin violation is critical, then $1+1+1$ or $1+1+1+1$ might be desired.) At present, for some quantities the errors in the $N_f = 2+1$ results are smaller than those with $N_f = 2+1+1$ (e.g., for m_c), while for others the relative size of the errors is reversed. Our suggestion to those using the averages is to take whichever of the $N_f = 2+1$ or $N_f = 2+1+1$ results has the smaller error. We do not recommend using the $N_f = 2$ results, except for studies of the N_f-dependence of condensates and α_s, as these have an uncontrolled systematic error coming from quenching the strange quark.

Table 1 Summary of the main results of this review concerning quark masses, light-meson decay constants, and hadronic kaon-decay and kaon-mixing parameters. These are grouped in terms of N_f, the number of dynamical quark flavours in lattice simulations. Quark masses are given in the $\overline{\text{MS}}$ scheme at running scale $\mu = 2\,\text{GeV}$ or as indicated. BSM bag parameters $B_{2,3,4,5}$ are given in the $\overline{\text{MS}}$ scheme at scale $\mu = 3\,\text{GeV}$. Further specifications of the quantities are given in the quoted sections. Results for $N_f = 2$ quark masses are unchanged since FLAG 16 [3], and are not included here. For each result we list the references that enter the FLAG average or estimate, and we stress again the importance of quoting these original works when referring to FLAG results. From the entries in this column one can also read off the number of results that enter our averages for each quantity. We emphasize that these numbers only give a very rough indication of how thoroughly the quantity in question has been explored on the lattice and recommend consulting the detailed tables and figures in the relevant section for more significant information and for explanations on the source of the quoted errors

Quantity	Sections	$N_f = 2+1+1$	Refs.	$N_f = 2+1$	Refs.	$N_f = 2$	Refs.
m_{ud} [MeV]	3.1.4	3.410(43)	[6,7]	3.381(40)	[8–12]		
m_s [MeV]	3.1.4	93.40(57)	[6,7,13,14]	92.2(1.0)	[8–11,15]		
m_s/m_{ud}	3.1.5	27.23(10)	[7,16,17]	27.42(12)	[8–10,15,18]		
m_u [MeV]	3.1.6	2.14(8)	[6,19]	2.27(9)	[20]		
m_d [MeV]	3.1.6	4.70(5)	[6,19]	4.67(9)	[20]		
m_u/m_d	3.1.6	0.465(24)	[19,21]	0.485(19)	[20]		
$\overline{m}_c(3\,\text{GeV})$ [GeV]	3.2.2	0.988(11)	[6,7,14,22,23]	0.992(5)	[11,24–26]		
m_c/m_s	3.2.3	11.768(34)	[6,7,14]	11.82(16)	[24,27]		
$\overline{m}_b(\overline{m}_b)$ [GeV]	3.3	4.203(11)	[6,28–31]	4.171(20)	[11]		
$f_+(0)$	4.3	0.9698(17)	[32,33]	0.9677(27)	[34,35]	0.9560(57)(62)	[36]
$f_{K^\pm}/f_{\pi^\pm}$	4.3	1.1932(21)	[16,37–39]	1.1917(37)	[8,40–44]	1.205(18)	[45]
$f_{\pi^\pm}$ [MeV]	4.6			130.2(8)	[8,40,41]		
$f_{K^\pm}$ [MeV]	4.6	155.7(3)	[17,37,38]	155.7(7)	[8,40,41]	157.5(2.4)	[45]
$\text{Re}(A_2)$ [GeV]	6.2			$1.50(4)(14) \times 10^{-8}$	[46]		
$\text{Im}(A_2)$ [GeV]	6.2			$-8.34(1.03) \times 10^{-13}$	[46]		
$\hat{B}_K$	6.3	0.717(18)(16)	[47]	0.7625(97)	[8,48–50]	0.727(22)(12)	[51]
B_2	6.4	0.46(1)(3)	[47]	0.502(14)	[50,52]	0.47(2)(1)	[51]
B_3	6.4	0.79(2)(5)	[47]	0.766(32)	[50,52]	0.78(4)(2)	[51]
B_4	6.4	0.78(2)(4)	[47]	0.926(19)	[50,52]	0.76(2)(2)	[51]
B_5	6.4	0.49(3)(3)	[47]	0.720(38)	[50,52]	0.58(2)(2)	[51]

Our plan is to continue providing FLAG updates, in the form of a peer reviewed paper, roughly on a triennial basis. This effort is supplemented by our more frequently updated website http://flag.unibe.ch [5], where figures as well as pdf-files for the individual sections can be downloaded. The papers reviewed in the present edition have appeared before the closing date **30 April 2021**.[1]

This review is organized as follows. In the remainder of Sect. 1 we summarize the composition and rules of FLAG and discuss general issues that arise in modern lattice calculations. In Sect. 2, we explain our general methodology for evaluating the robustness of lattice results. We also describe the procedures followed for combining results from different collaborations in a single average or estimate (see Sect. 2.2 for our definition of these terms). The rest of the paper consists of sections, each dedicated to a set of closely connected physical quantities, or, for the final section, to the determination of the lattice scale. Each of these sections is accompanied by an Appendix with explicatory notes.[2]

In previous editions, we have provided, in an appendix, a glossary summarizing some standard lattice terminology and describing the most commonly used lattice techniques and methodologies. Since no significant updates in this information have occurred since our previous edition, we have decided, in the interests of reducing the length of this review, to omit this glossary, and refer the reader to FLAG 19 for this information [4]. This appendix also contained, in previous versions, a tabulation of the actions used in the papers that were reviewed. Since this information is available in the discussions in the

[1] Working groups were given the option of including papers submitted to `arxiv.org` before the closing date but published after this date. This flexibility allows this review to be up-to-date at the time of submission. A single paper of this type was included.

[2] In some cases, in order to keep the length of this review within reasonable bounds, we have dropped these notes for older data, since they can be found in previous FLAG reviews [1–4].

Table 2 Summary of the main results of this review concerning heavy-light mesons and the strong coupling constant. These are grouped in terms of N_f, the number of dynamical quark flavours in lattice simulations. The quantities listed are specified in the quoted sections. For each result we list the references that enter the FLAG average or estimate, and we stress again the importance of quoting these original works when referring to FLAG results. From the entries in this column one can also read off the number of results that enter our averages for each quantity. We emphasize that these numbers only give a very rough indication of how thoroughly the quantity in question has been explored on the lattice and recommend consulting the detailed tables and figures in the relevant section for more significant information and for explanations on the source of the quoted errors

Quantity	Section	$N_f = 2+1+1$	Refs.	$N_f = 2+1$	Refs.	$N_f = 2$	Refs.
f_D [MeV]	7.1	212.0(7)	[16,38]	209.0(2.4)	[53–55]	208(7)	[56]
f_{D_s} [MeV]	7.1	249.9(5)	[16,38]	248.0(1.6)	[24,54,55,57]	246(4)	[56,58]
$\frac{f_{D_s}}{f_D}$	7.1	1.1783(16)	[16,38]	1.174(7)	[53–55]	1.20(2)	[56]
$f_+^{D\pi}(0)$	7.2	0.612(35)	[59]	0.666(29)	[60]		
$f_+^{DK}(0)$	7.2	0.7385(44)	[59,61]	0.747(19)	[62]		
f_B [MeV]	8.1	190.0(1.3)	[16,30,63,64]	192.0(4.3)	[54,65–68]	188(7)	[56,69]
f_{B_s} [MeV]	8.1	230.3(1.3)	[16,30,63,64]	228.4(3.7)	[54,65–68]	225.3(6.6)	[56,58,69]
$\frac{f_{B_s}}{f_B}$	8.1	1.209(5)	[16,30,63,64]	1.201(16)	[54,65–68,70]	1.206(23)	[56,69]
$f_{B_d}\sqrt{\hat{B}_{b_d}}$ [MeV]	8.2	210.6(5.5)	[71]	225(9)	[67,72,73]	216(10)	[56]
$f_{B_s}\sqrt{\hat{B}_{B_s}}$ [MeV]	8.2	256.1(5.7)	[71]	274(8)	[67,72,73]	262(10)	[56]
$\hat{B}_{B_d}$	8.2	1.222(61)	[71]	1.30(10)	[67,72,73]	1.30(6)	[56]
$\hat{B}_{B_s}$	8.2	1.232(53)	[71]	1.35(6)	[67,72,73]	1.32(5)	[56]
ξ	8.2	1.216(16)	[71]	1.206(17)	[67,73]	1.225(31)	[56]
B_{B_s}/B_{B_d}	8.2	1.008(25)	[71]	1.032(38)	[67,73]	1.007(21)	[56]

Quantity	Section	$N_f = 2+1$ and $N_f = 2+1+1$	Refs.
$\alpha_{\overline{\rm MS}}^{(5)}(M_Z)$	9.11	0.1184(8)	[11,14,74–79]
$\Lambda_{\overline{\rm MS}}^{(5)}$ [MeV]	9.11	214(10)	[11,14,74–79]
$\Lambda_{\overline{\rm MS}}^{(4)}$ [MeV]	9.11	297(12)	[11,14,74–79]
$\Lambda_{\overline{\rm MS}}^{(3)}$ [MeV]	9.11	339(12)	[11,14,74–79]

separate sections, and is time-consuming to collect from the sections, we have dropped these tables. We have, however, kept a short appendix, Appendix B.1, describing the parameterizations of semileptonic form factors that are used in Sect. 8. Moreover, in Appendix A, we have added a summary and explanations of acronyms introduced in the manuscript. Collaborations referred to by an acronym can be identified through the corresponding bibliographic reference.

1.1 FLAG composition, guidelines and rules

FLAG strives to be representative of the lattice community, both in terms of the geographical location of its members and the lattice collaborations to which they belong. We aspire to provide the nuclear- and particle-physics communities with a single source of reliable information on lattice results.

In order to work reliably and efficiently, we have adopted a formal structure and a set of rules by which all FLAG members abide. The collaboration presently consists of an Advisory Board (AB), an Editorial Board (EB), and nine Working Groups (WG). The rôle of the Advisory Board is to provide oversight of the content, procedures, schedule and membership of FLAG, to help resolve disputes, to serve as a source of advice to the EB and to FLAG as a whole, and to provide a critical assessment of drafts. They also give their approval of the final version of the preprint before it is rendered public. The Editorial Board coordinates the activities of FLAG, sets priorities and intermediate deadlines, organizes votes on FLAG procedures, writes the introductory sections, and takes care of the editorial work needed to amalgamate the sections written by the individual working groups into a uniform and coherent review. The working groups concentrate on writing the review of the physical quantities for which they are responsible, which is subsequently circulated to the whole collaboration for critical evaluation.

Table 3 Summary of the main results of this review concerning LECs, grouped in terms of N_f, the number of dynamical quark flavours in lattice simulations. The quantities listed are specified in the quoted sections. For each result we list the references that enter the FLAG average or estimate, and we stress again the importance of quoting these original works when referring to FLAG results. From the entries in this column one can also read off the number of results that enter our averages for each quantity. We emphasize that these numbers only give a very rough indication of how thoroughly the quantity in question has been explored on the lattice and recommend consulting the detailed tables and figures in the relevant section for more significant information and for explanations on the source of the quoted errors

Quantity	Section	$N_f = 2+1+1$	Refs.	$N_f = 2+1$	Refs.	$N_f = 2$	Refs.
$\Sigma^{1/3}$ [MeV]	5.2.4	286(23)	[80,81]	272(5)	[12,82–86]	266(10)	[80,87–89]
F_π/F	5.2.4	1.077(3)	[90]	1.062(7)	[41,82–84,91]	1.073(15)	[87–89,92]
$\bar{\ell}_3$	5.2.4	3.53(26)	[90]	3.07(64)	[41,82–84,91]	3.41(82)	[87,88,92]
$\bar{\ell}_4$	5.2.4	4.73(10)	[90]	4.02(45)	[41,82–84,91]	4.40(28)	[87,88,92,93]
$\bar{\ell}_6$	5.2.4					15.1(1.2)	[88,92]
$a_0^2 M_\pi$	5.2.4	−0.0441(4)	[94]			−0.04385(47)	[95]
$\Sigma_0^{1/3}$ [MeV]	5.3.5			245(8)	[15]		
Σ/Σ_0	5.3.5			1.48(16)	[15]		
F_0 [MeV]	5.3.5			80.3(6.0)	[41]		
F/F_0	5.3.5			1.104(41)	[15]		
B/B_0	5.3.5			1.21(7)	[15]		
L_4	5.3.5	$+0.09(34)\times10^{-3}$	[37]	$-0.02(56)\times10^{-3}$	[41]		
L_5	5.3.5	$+1.19(25)\times10^{-3}$	[37]	$+0.95(41)\times10^{-3}$	[41]		
L_6	5.3.5	$+0.16(20)\times10^{-3}$	[37]	$+0.01(34)\times10^{-3}$	[41]		
L_8	5.3.5	$+0.55(15)\times10^{-3}$	[37]	$+0.43(28)\times10^{-3}$	[41]		
$a_0^{1/2}\mu_{\pi K}$	5.3.5	0.127(2)	[96]				
$a_0^{3/2}\mu_{\pi K}$	5.3.5	−0.0463(17)	[96]				
$a_0^1 M_K$	5.3.5	−0.388(20)	[97]				

Table 4 Summary of the main results of this review concerning nuclear matrix elements, grouped in terms of N_f, the number of dynamical quark flavours in lattice simulations. The quantities listed are specified in the quoted sections. For each result we list the references that enter the FLAG average or estimate, and we stress again the importance of quoting these original works when referring to FLAG results. From the entries in this column one can also read off the number of results that enter our averages for each quantity. We emphasize that these numbers only give a very rough indication of how thoroughly the quantity in question has been explored on the lattice and recommend consulting the detailed tables and figures in the relevant section for more significant information and for explanations on the source of the quoted errors

Quantity	Section	$N_f = 2+1+1$	Refs.	$N_f = 2+1$	Refs.	$N_f = 2$	Refs.
g_A^{u-d}	10.3.1	1.246(28)	[98–100]	1.248(23)	[101,102]		
g_S^{u-d}	10.3.2	1.02(10)	[98]	1.13(14)	[102]		
g_T^{u-d}	10.3.3	0.989(34)	[98]	0.965(61)	[102]		
g_A^u	10.4.1	0.777(25)(30)	[103]	0.847(18)(32)	[101]		
g_A^d	10.4.1	−0.438(18)(30)	[103]	−0.407(16)(18)	[101]		
g_A^s	10.4.1	−0.053(8)	[103]	−0.035(6)(7)	[101]		
$\sigma_{\pi N}$ [MeV]	10.4.4	64.9(1.5)(13.2)	[22]	39.7(3.6)	[104–106]	37(8)(6)	[107]
σ_s [MeV]	10.4.4	41.0(8.8)	[108]	52.9(7.0)	[104–106,108,109]		
g_T^u	10.4.5	0.784(28)(10)	[110]				
g_T^d	10.4.5	−0.204(11)(10)	[110]				
g_T^s	10.4.5	−0.0027(16)	[110]				

The current list of FLAG members and their Working Group assignments is:

- Advisory Board (AB): G. Colangelo, M. Golterman, P. Hernandez, T. Onogi, and R. Van de Water
- Editorial Board (EB): S. Gottlieb, A. Jüttner, S. Hashimoto, S.R. Sharpe, and U. Wenger

Table 5 Summary of the main results of this review concerning setting of the lattice scale, grouped in terms of N_f, the number of dynamical quark flavours in lattice simulations. The quantities listed are specified in the quoted sections. For each result we list the references that enter the FLAG average or estimate, and we stress again the importance of quoting these original works when referring to FLAG results. From the entries in this column one can also read off the number of results that enter our averages for each quantity. We emphasize that these numbers only give a very rough indication of how thoroughly the quantity in question has been explored on the lattice and recommend consulting the detailed tables and figures in the relevant section for more significant information and for explanations on the source of the quoted errors

Quantity	Section	$N_f = 1+1+1+1$	Refs.	$N_f = 2+1+1$	Refs.	$N_f = 2+1$	Refs.	$N_f > 2+1$	Refs.
$\sqrt{t_0}$ [fm]	11.5.2			0.14186(88)	[37,111,112]	0.14464(87)	[8,113,114]		
w_0 [fm]	11.5.2	0.17236(70)	[115]	0.17128(107)	[37,111,112]	0.17355(92)	[8,114,116]	0.17177(67)	[37,111,112,115]
r_0 [fm]	11.5.2			0.474(14)	[7]	0.4701(36)	[24,116–119]		
r_1 [fm]	11.5.2			0.3112(30)	[37]	0.3127(30)	[41,117–120]		

- Working Groups (coordinator listed first):
  - Quark masses — T. Blum, A. Portelli, and A. Ramos
  - V_{us}, V_{ud} — T. Kaneko, J. N. Simone, S. Simula, and N. Tantalo
  - LEC — S. Dürr, H. Fukaya, and U.M. Heller
  - B_K — P. Dimopoulos, X. Feng, and G. Herdoiza
  - $f_{B_{(s)}}$, $f_{D_{(s)}}$, B_B — Y. Aoki, M. Della Morte, and C. Monahan
  - b and c semileptonic and radiative decays — E. Lunghi, S. Meinel, and C. Pena
  - α_s — S. Sint, R. Horsley, and P. Petreczky
  - NME — R. Gupta, S. Collins, A. Nicholson, and H. Wittig
  - Scale setting — R. Sommer, N. Tantalo, and U. Wenger

The most important FLAG guidelines and rules are the following:

- the composition of the AB reflects the main geographical areas in which lattice collaborations are active, with members from America, Asia/Oceania, and Europe;
- the mandate of regular members is not limited in time, but we expect that a certain turnover will occur naturally;
- whenever a replacement becomes necessary this has to keep, and possibly improve, the balance in FLAG, so that different collaborations, from different geographical areas are represented;
- in all working groups the members must belong to different lattice collaborations;
- a paper is in general not reviewed (nor colour-coded, as described in the next section) by any of its authors;
- lattice collaborations will be consulted on the colour coding of their calculation;
- there are also internal rules regulating our work, such as voting procedures.

As for FLAG 19, for this review we sought the advice of external reviewers once a complete draft of the review was available. For each review section, we have asked one lattice expert (who could be a FLAG alumnus/alumna) and one nonlattice phenomenologist for a critical assessment. The one exception is the scale-setting section, where only a lattice expert has been asked to provide input. This is similar to the procedure followed by the Particle Data Group in the creation of the Review of Particle Physics. The reviewers provide comments and feedback on scientific and stylistic matters. They are not anonymous, and enter into a discussion with the authors of the WG. Our aim with this additional step is to make sure that a wider array of viewpoints enter into the discussions, so as to make this review more useful for its intended audience.

1.2 Citation policy

We draw attention to this particularly important point. As stated above, our aim is to make lattice-QCD results easily accessible to those without lattice expertise, and we are well aware that it is likely that some readers will only consult the present paper and not the original lattice literature. It is very important that this paper not be the only one cited when our results are quoted. We strongly suggest that readers also cite the original sources. In order to facilitate this, in Tables 1, 2, 3, 4, and 5, besides summarizing the main results of the present review, we also cite the original references from which they have been obtained.

In addition, for each figure we make a bibtex file available on our webpage [5] which contains the bibtex entries of all the calculations contributing to the FLAG average or estimate. The bibliography at the end of this paper should also make it easy to cite additional papers. Indeed, we hope that the bibliography will be one of the most widely used elements of the whole paper.

1.3 General issues

Several general issues concerning the present review are thoroughly discussed in Sec. 1.1 of our initial 2010 paper [1], and we encourage the reader to consult the relevant pages. In the remainder of the present subsection, we focus on a few important points. Though the discussion has been duly updated, it is similar to that of Sec. 1.2 in the previous three reviews [2–4].

The present review aims to achieve two distinct goals: first, to provide a **description** of the relevant work done on the lattice; and, second, to draw **conclusions** on the basis of that work, summarizing the results obtained for the various quantities of physical interest.

The core of the information about the work done on the lattice is presented in the form of tables, which not only list the various results, but also describe the quality of the data that underlie them. We consider it important that this part of the review represents a generally accepted description of the work done. For this reason, we explicitly specify the quality requirements used and provide sufficient details in appendices so that the reader can verify the information given in the tables.[3]

On the other hand, the conclusions drawn on the basis of the available lattice results are the responsibility of FLAG alone. Preferring to err on the side of caution, in several cases we draw conclusions that are more conservative than those resulting from a plain weighted average of the available lattice results. This cautious approach is usually adopted when the average is dominated by a single lattice result, or when only one lattice result is available for a given quantity. In such cases, one does not have the same degree of confidence in results and errors as when there is agreement among several different calculations using different approaches. The reader should keep in mind that the degree of confidence cannot be quantified, and it is not reflected in the quoted errors.

Each discretization has its merits, but also its shortcomings. For most topics covered in this review we have an increasingly broad database, and for most quantities lattice calculations based on totally different discretizations are now available. This is illustrated by the dense population of the tables and figures in most parts of this review. Those calculations that do satisfy our quality criteria indeed lead, in almost all cases, to consistent results, confirming universality within the accuracy reached. The consistency between independent lattice results, obtained with different discretizations, methods, and simulation parameters, is an important test of lattice QCD, and observing such consistency also provides further evidence that systematic errors are fully under control.

In the sections dealing with heavy quarks and with α_s, the situation is not the same. Since the b-quark mass can barely be resolved with current lattice spacings, most lattice methods for treating b quarks use effective field theory at some level. This introduces additional complications not present in the light-quark sector. An overview of the issues specific to heavy-quark quantities is given in the introduction of Sect. 8. For B- and D-meson leptonic decay constants, there already exists a good number of different independent calculations that use different heavy-quark methods, but there are only a few independent calculations of semileptonic B, Λ_b, and D form factors and of $B-\bar{B}$ mixing parameters. For α_s, most lattice methods involve a range of scales that need to be resolved and controlling the systematic error over a large range of scales is more demanding. The issues specific to determinations of the strong coupling are summarized in Sect. 9.

Number of sea quarks in lattice simulations

Lattice-QCD simulations currently involve two, three or four flavours of dynamical quarks. Most simulations set the masses of the two lightest quarks to be equal, while the strange and charm quarks, if present, are heavier (and tuned to lie close to their respective physical values). Our notation for these simulations indicates which quarks are nondegenerate, e.g., $N_f = 2+1$ if $m_u = m_d < m_s$ and $N_f = 2+1+1$ if $m_u = m_d < m_s < m_c$. Calculations with $N_f = 2$, i.e., two degenerate dynamical flavours, often include strange valence quarks interacting with gluons, so that bound states with the quantum numbers of the kaons can be studied, albeit neglecting strange sea-quark fluctuations. The quenched approximation ($N_f = 0$), in which all sea-quark contributions are omitted, has uncontrolled systematic errors and is no longer used in modern lattice simulations with relevance to phenomenology. Accordingly, we will review results obtained with $N_f = 2$, $N_f = 2+1$, and $N_f = 2+1+1$, but omit earlier results with $N_f = 0$. The only exception concerns the QCD coupling constant α_s. Since this observable does not require valence light quarks, it is theoretically well defined also in the $N_f = 0$ theory, which is simply pure gluodynamics.

[3] We also use terms like "quality criteria", "rating", "colour coding", etc., when referring to the classification of results, as described in Sect. 2.

The N_f-dependence of α_s, or more precisely of the related quantity $r_0\Lambda_{\overline{\rm MS}}$, is a theoretical issue of considerable interest; here r_0 is a quantity with the dimension of length that sets the physical scale, as discussed in Sect. 11. We stress, however, that only results with $N_f \geq 3$ are used to determine the physical value of α_s at a high scale.

Lattice actions, simulation parameters, and scale setting

The remarkable progress in the precision of lattice calculations is due to improved algorithms, better computing resources, and, last but not least, conceptual developments. Examples of the latter are improved actions that reduce lattice artifacts and actions that preserve chiral symmetry to very good approximation. A concise characterization of the various discretizations that underlie the results reported in the present review is given in Appendix A.1 of FLAG 19.

Physical quantities are computed in lattice simulations in units of the lattice spacing so that they are dimensionless. For example, the pion decay constant that is obtained from a simulation is $f_\pi a$, where a is the spacing between two neighboring lattice sites. (All simulations with results quoted in this review use hypercubic lattices, i.e., with the same spacing in all four Euclidean directions.) To convert these results to physical units requires knowledge of the lattice spacing a at the fixed values of the bare QCD parameters (quark masses and gauge coupling) used in the simulation. This is achieved by requiring agreement between the lattice calculation and experimental measurement of a known quantity, which thus "sets the scale" of a given simulation. Given the central importance of this procedure, we include in this edition of FLAG a dedicated section, Sect. 11, discussing the issues and results.

Renormalization and scheme dependence

Several of the results covered by this review, such as quark masses, the gauge coupling, and B-parameters, are for quantities defined in a given renormalization scheme and at a specific renormalization scale. The schemes employed (e.g., regularization-independent MOM schemes) are often chosen because of their specific merits when combined with the lattice regularization. For a brief discussion of their properties, see Appendix A.3 of FLAG 19. The conversion of the results obtained in these so-called intermediate schemes to more familiar regularization schemes, such as the $\overline{\rm MS}$-scheme, is done with the aid of perturbation theory. It must be stressed that the renormalization scales accessible in simulations are limited, because of the presence of an ultraviolet (UV) cutoff of $\sim \pi/a$. To safely match to $\overline{\rm MS}$, a scheme defined in perturbation theory, Renormalization Group (RG) running to higher scales is performed, either perturbatively or nonperturbatively (the latter using finite-size scaling techniques).

Extrapolations

Because of limited computing resources, lattice simulations are often performed at unphysically heavy pion masses, although results at the physical point have become increasingly common. Further, numerical simulations must be done at nonzero lattice spacing, and in a finite (four-dimensional) volume. In order to obtain physical results, lattice data are obtained at a sequence of pion masses and a sequence of lattice spacings, and then extrapolated to the physical pion mass and to the continuum limit. In principle, an extrapolation to infinite volume is also required. However, for most quantities discussed in this review, finite-volume effects are exponentially small in the linear extent of the lattice in units of the pion mass, and, in practice, one often verifies volume independence by comparing results obtained on a few different physical volumes, holding other parameters fixed. To control the associated systematic uncertainties, these extrapolations are guided by effective theories. For light-quark actions, the lattice-spacing dependence is described by Symanzik's effective theory [121,122]; for heavy quarks, this can be extended and/or supplemented by other effective theories such as Heavy-Quark Effective Theory (HQET). The pion-mass dependence can be parameterized with Chiral Perturbation Theory (χPT), which takes into account the Nambu–Goldstone nature of the lowest excitations that occur in the presence of light quarks. Similarly, one can use Heavy-Light Meson Chiral Perturbation Theory (HMχPT) to extrapolate quantities involving mesons composed of one heavy (b or c) and one light quark. One can combine Symanzik's effective theory with χPT to simultaneously extrapolate to the physical pion mass and the continuum; in this case, the form of the effective theory depends on the discretization. See Appendix A.4 of FLAG 19 for a brief description of the different variants in use and some useful references. Finally, χPT can also be used to estimate the size of finite-volume effects measured in units of the inverse pion mass, thus providing information on the systematic error due to finite-volume effects in addition to that obtained by comparing simulations at different volumes.

Excited-state contamination

In all the hadronic matrix elements discussed in this review, the hadron in question is the lightest state with the chosen quantum numbers. This implies that it dominates the required correlation functions as their extent in Euclidean time is increased. Excited-state contributions are suppressed by $e^{-\Delta E \Delta\tau}$, where ΔE is the gap between the ground and excited states, and $\Delta\tau$ the relevant separation in Euclidean time. The size of ΔE depends on the hadron in question, and in general is a multiple of the pion mass. In practice, as discussed at length in Sect. 10, the contamination of signals due to excited-state

contributions is a much more challenging problem for baryons than for the other particles discussed here. This is in part due to the fact that the signal-to-noise ratio drops exponentially for baryons, which reduces the values of $\Delta\tau$ that can be used.

Critical slowing down
The lattice spacings reached in recent simulations go down to 0.05 fm or even smaller. In this regime, long autocorrelation times slow down the sampling of the configurations [123–132]. Many groups check for autocorrelations in a number of observables, including the topological charge, for which a rapid growth of the autocorrelation time is observed with decreasing lattice spacing. This is often referred to as topological freezing. A solution to the problem consists in using open boundary conditions in time [133], instead of the more common antiperiodic ones. More recently, two other approaches have been proposed, one based on a multiscale thermalization algorithm [134,135] and another based on defining QCD on a nonorientable manifold [136]. The problem is also touched upon in Sect. 9.2.1, where it is stressed that attention must be paid to this issue. While large scale simulations with open boundary conditions are already far advanced [137], few results reviewed here have been obtained with any of the above methods. It is usually *assumed* that the continuum limit can be reached by extrapolation from the existing simulations, and that potential systematic errors due to the long autocorrelation times have been adequately controlled. Partially or completely frozen topology would produce a mixture of different θ vacua, and the difference from the desired $\theta = 0$ result may be estimated in some cases using chiral perturbation theory, which gives predictions for the θ-dependence of the physical quantity of interest [138,139]. These ideas have been systematically and successfully tested in various models in [140,141], and a numerical test on MILC ensembles indicates that the topology dependence for some of the physical quantities reviewed here is small, consistent with theoretical expectations [142].

Simulation algorithms and numerical errors
Most of the modern lattice-QCD simulations use exact algorithms such as those of Refs. [143,144], which do not produce any systematic errors when exact arithmetic is available. In reality, one uses numerical calculations at double (or in some cases even single) precision, and some errors are unavoidable. More importantly, the inversion of the Dirac operator is carried out iteratively and it is truncated once some accuracy is reached, which is another source of potential systematic error. In most cases, these errors have been confirmed to be much less than the statistical errors. In the following we assume that this source of error is negligible. Some of the most recent simulations use an inexact algorithm in order to speed up the computation, though it may produce systematic effects. Currently available tests indicate that errors from the use of inexact algorithms are under control [145].

2 Quality criteria, averaging and error estimation

The essential characteristics of our approach to the problem of rating and averaging lattice quantities have been outlined in our first publication [1]. Our aim is to help the reader assess the reliability of a particular lattice result without necessarily studying the original article in depth. This is a delicate issue, since the ratings may make things appear simpler than they are. Nevertheless, it safeguards against the possibility of using lattice results, and drawing physics conclusions from them, without a critical assessment of the quality of the various calculations. We believe that, despite the risks, it is important to provide some compact information about the quality of a calculation. We stress, however, the importance of the accompanying detailed discussion of the results presented in the various sections of the present review.

2.1 Systematic errors and colour code

The major sources of systematic error are common to most lattice calculations. These include, as discussed in detail below, the chiral, continuum, and infinite-volume extrapolations. To each such source of error for which systematic improvement is possible we assign one of three coloured symbols: green star, unfilled green circle (which replaced in Ref. [2] the amber disk used in the original FLAG review [1]) or red square. These correspond to the following ratings:

- ★ the parameter values and ranges used to generate the data sets allow for a satisfactory control of the systematic uncertainties;
- ○ the parameter values and ranges used to generate the data sets allow for a reasonable attempt at estimating systematic uncertainties, which however could be improved;
- ■ the parameter values and ranges used to generate the data sets are unlikely to allow for a reasonable control of systematic uncertainties.

The appearance of a red tag, even in a single source of systematic error of a given lattice result, disqualifies it from inclusion in the global average.

Note that in the first two editions [1,2], FLAG used the three symbols in order to rate the reliability of the systematic errors attributed to a given result by the paper's authors. Starting with FLAG 16 [3] the meaning of the symbols has changed slightly – they now rate the quality of a particular simulation, based on the values and range of the chosen parameters, and its aptness to obtain well-controlled systematic uncertainties. They do not rate the quality of the analysis performed by the authors of the publication. The latter question is deferred to the relevant sections of the present review, which contain detailed discussions of the results contributing (or not) to each FLAG average or estimate.

For most quantities the colour-coding system refers to the following sources of systematic errors: (i) chiral extrapolation; (ii) continuum extrapolation; (iii) finite volume. As we will see below, renormalization is another source of systematic uncertainties in several quantities. This we also classify using the three coloured symbols listed above, but now with a different rationale: they express how reliably these quantities are renormalized, from a field-theoretic point of view (namely, nonperturbatively, or with 2-loop or 1-loop perturbation theory).

Given the sophisticated status that the field has attained, several aspects, besides those rated by the coloured symbols, need to be evaluated before one can conclude whether a particular analysis leads to results that should be included in an average or estimate. Some of these aspects are not so easily expressible in terms of an adjustable parameter such as the lattice spacing, the pion mass or the volume. As a result of such considerations, it sometimes occurs, albeit rarely, that a given result does not contribute to the FLAG average or estimate, despite not carrying any red tags. This happens, for instance, whenever aspects of the analysis appear to be incomplete (e.g., an incomplete error budget), so that the presence of inadequately controlled systematic effects cannot be excluded. This mostly refers to results with a statistical error only, or results in which the quoted error budget obviously fails to account for an important contribution.

Of course, any colour coding has to be treated with caution; we emphasize that the criteria are subjective and evolving. Sometimes, a single source of systematic error dominates the systematic uncertainty and it is more important to reduce this uncertainty than to aim for green stars for other sources of error. In spite of these caveats, we hope that our attempt to introduce quality measures for lattice simulations will prove to be a useful guide. In addition, we would like to stress that the agreement of lattice results obtained using different actions and procedures provides further validation.

2.1.1 Systematic effects and rating criteria

The precise criteria used in determining the colour coding are unavoidably time-dependent; as lattice calculations become more accurate, the standards against which they are measured become tighter. For this reason FLAG reassesses criteria with each edition and as a result some of the quality criteria (the one on chiral extrapolation for instance) have been tightened up over time [1–4].

In the following, we present the rating criteria used in the current report. While these criteria apply to most quantities without modification there are cases where they need to be amended or additional criteria need to be defined. For instance, when discussing results obtained in the ϵ-regime of chiral perturbation theory in Sect. 5 the finite volume criterion listed below for the p-regime is no longer appropriate.[4] Similarly, the discussion of the strong coupling constant in Sect. 9 requires tailored criteria for renormalization, perturbative behaviour, and continuum extrapolation. Finally, in the section on nuclear matrix elements, Sect. 10, the chiral extrapolation criterion is made slightly stronger, and a new criterion is adopted for excited-state contributions. In such cases, the modified criteria are discussed in the respective sections. Apart from only a few exceptions the following colour code applies in the tables:

- Chiral extrapolation:
  - ★ $M_{\pi,\mathrm{min}} < 200$ MeV, with three or more pion masses used in the extrapolation
    or two values of M_π with one lying within 10 MeV of 135 MeV (the physical neutral pion mass) and the other one below 200 MeV
  - ○ 200 MeV $\leq M_{\pi,\mathrm{min}} \leq 400$ MeV, with three or more pion masses used in the extrapolation
    or two values of M_π with $M_{\pi,\mathrm{min}} < 200$ MeV
    or a single value of M_π, lying within 10 MeV of 135 MeV (the physical neutral pion mass)
  - ■ otherwise

[4] We refer to Sect. 5.1 for an explanation of the various regimes of chiral perturbation theory.

This criterion is unchanged from FLAG 19. In Sect. 10 the upper end of the range for $M_{\pi,\min}$ in the green circle criterion is lowered to 300 MeV, as in FLAG 19.

- Continuum extrapolation:

  ★ at least three lattice spacings and at least two points below 0.1 fm and a range of lattice spacings satisfying $[a_{\max}/a_{\min}]^2 \geq 2$
  ○ at least two lattice spacings and at least one point below 0.1 fm and a range of lattice spacings satisfying $[a_{\max}/a_{\min}]^2 \geq 1.4$
  ■ otherwise

  It is assumed that the lattice action is $\mathcal{O}(a)$-improved (i.e., the discretization errors vanish quadratically with the lattice spacing); otherwise this will be explicitly mentioned. For unimproved actions an additional lattice spacing is required. This condition is unchanged from FLAG 19.

- Finite-volume effects:
  The finite-volume colour code used for a result is chosen to be the worse of the QCD and the QED codes, as described below. If only QCD is used the QED colour code is ignored.
  – *For QCD:*

  ★ $[M_{\pi,\min}/M_{\pi,\text{fid}}]^2 \exp\{4 - M_{\pi,\min}[L(M_{\pi,\min})]_{\max}\} < 1$, or at least three volumes
  ○ $[M_{\pi,\min}/M_{\pi,\text{fid}}]^2 \exp\{3 - M_{\pi,\min}[L(M_{\pi,\min})]_{\max}\} < 1$, or at least two volumes
  ■ otherwise

  where we have introduced $[L(M_{\pi,\min})]_{\max}$, which is the maximum box size used in the simulations performed at the smallest pion mass $M_{\pi,\min}$, as well as a fiducial pion mass $M_{\pi,\text{fid}}$, which we set to 200 MeV (the cutoff value for a green star in the chiral extrapolation). It is assumed here that calculations are in the p-regime of chiral perturbation theory, and that all volumes used exceed 2 fm. The rationale for this condition is as follows. Finite volume effects contain the universal factor $\exp\{-L\ M_\pi\}$, and if this were the only contribution a criterion based on the values of $M_{\pi,\min}L$ would be appropriate. However, as pion masses decrease, one must also account for the weakening of the pion couplings. In particular, 1-loop chiral perturbation theory [146] reveals a behaviour proportional to $M_\pi^2 \exp\{-L\ M_\pi\}$. Our condition includes this weakening of the coupling, and ensures, for example, that simulations with $M_{\pi,\min} = 135$ MeV and $L\ M_{\pi,\min} = 3.2$ are rated equivalently to those with $M_{\pi,\min} = 200$ MeV and $L\ M_{\pi,\min} = 4$.
  – *For QED (where applicable):*

  ★ $1/([M_{\pi,\min}L(M_{\pi,\min})]_{\max})^{n_{\min}} < 0.02$, or at least four volumes
  ○ $1/([M_{\pi,\min}L(M_{\pi,\min})]_{\max})^{n_{\min}} < 0.04$, or at least three volumes
  ■ otherwise

  Because of the infrared-singular structure of QED, electromagnetic finite-volume effects decay only like a power of the inverse spatial extent. In several cases like mass splittings [147,148] or leptonic decays [149], the leading corrections are known to be universal, i.e., independent of the structure of the involved hadrons. In such cases, the leading universal effects can be directly subtracted exactly from the lattice data. We denote $n_{\min}$ the smallest power of $\frac{1}{L}$ at which such a subtraction cannot be done. In the widely used finite-volume formulation QED_L, one always has $n_{\min} \leq 3$ due to the nonlocality of the theory [150]. The QED criteria are used here only in Sect. 3. Both QCD and QED criteria are unchanged from FLAG 19.

- Isospin breaking effects (where applicable):

  ★ all leading isospin breaking effects are included in the lattice calculation
  ○ isospin breaking effects are included using the electro-quenched approximation
  ■ otherwise

  This criterion is used for quantities which are breaking isospin symmetry or which can be determined at the sub-percent accuracy where isospin breaking effects, if not included, are expected to be the dominant source of uncertainty. In the current edition, this criterion is only used for the up- and down-quark masses, and related quantities (ϵ, Q^2 and R^2). The criteria for isospin breaking effects are unchanged from FLAG 19.

- Renormalization (where applicable):

  ★ nonperturbative
  ○ 1-loop perturbation theory or higher with a reasonable estimate of truncation errors
  ■ otherwise

  In Ref. [1], we assigned a red square to all results which were renormalized at 1-loop in perturbation theory. In FLAG 13 [2], we decided that this was too restrictive, since the error arising from renormalization constants, calculated in perturbation theory at 1-loop, is often estimated conservatively and reliably. These criteria have remained unchanged since then.

- Renormalization Group (RG) running (where applicable):
  For scale-dependent quantities, such as quark masses or B_K, it is essential that contact with continuum perturbation theory can be established. Various different methods are used for this purpose (cf. Appendix A.3 in FLAG 19 [4]): Regularization-independent Momentum Subtraction (RI/MOM), the Schrödinger functional, and direct comparison with (resummed) perturbation theory. Irrespective of the particular method used, the uncertainty associated with the choice of intermediate renormalization scales in the construction of physical observables must be brought under control. This is best achieved by performing comparisons between nonperturbative and perturbative running over a reasonably broad range of scales. These comparisons were initially only made in the Schrödinger functional approach, but are now also being performed in RI/MOM schemes. We mark the data for which information about nonperturbative running checks is available and give some details, but do not attempt to translate this into a colour code.

The pion mass plays an important role in the criteria relevant for chiral extrapolation and finite volume. For some of the regularizations used, however, it is not a trivial matter to identify this mass. In the case of twisted-mass fermions, discretization effects give rise to a mass difference between charged and neutral pions even when the up- and down-quark masses are equal: the charged pion is found to be the heavier of the two for twisted-mass Wilson fermions (cf. Ref. [151]). In early works, typically referring to $N_f = 2$ simulations (e.g., Refs. [151] and [87]), chiral extrapolations are based on chiral perturbation theory formulae which do not take these regularization effects into account. After the importance of accounting for isospin breaking when doing chiral fits was shown in Ref. [152], later works, typically referring to $N_f = 2 + 1 + 1$ simulations, have taken these effects into account [7]. We use $M_{\pi^\pm}$ for $M_{\pi,\min}$ in the chiral-extrapolation rating criterion. On the other hand, we identify $M_{\pi,\min}$ with the root mean square (RMS) of M_{π^+}, M_{π^-} and M_{π^0} in the finite-volume rating criterion.

In the case of staggered fermions, discretization effects give rise to several light states with the quantum numbers of the pion.[5] The mass splitting among these "taste" partners represents a discretization effect of $\mathcal{O}(a^2)$, which can be significant at large lattice spacings but shrinks as the spacing is reduced. In the discussion of the results obtained with staggered quarks given in the following sections, we assume that these artifacts are under control. We conservatively identify $M_{\pi,\min}$ with the root mean square (RMS) average of the masses of all the taste partners, both for chiral-extrapolation and finite-volume criteria.

In some of the simulations, the fermion formulations employed for the valence quarks are different from those used for the sea quarks. Even when the fermion formulations are the same, there are cases where the sea and valence quark masses differ. In such cases, we use the smaller of the valence-valence and valence-sea $M_{\pi_{\min}}$ values in the finite-volume criteria, since either of these channels may give the leading contribution depending on the quantity of interest at the one-loop level of chiral perturbation theory. For the chiral-extrapolation criteria, on the other hand, we use the unitary point, where the sea and valence quark masses are the same, to define $M_{\pi_{\min}}$.

The strong coupling α_s is computed in lattice QCD with methods differing substantially from those used in the calculations of the other quantities discussed in this review. Therefore, we have established separate criteria for α_s results, which will be discussed in Sect. 9.2.1.

In the section on nuclear matrix elements, Sect. 10, an additional criterion is used. This concerns the level of control over contamination from excited states, which is a more challenging issue for nucleons than for mesons. In response to an improved understanding of the impact of this contamination, the excited-state contamination criterion has been made more stringent compared to that in FLAG 19.

[5] We refer the interested reader to a number of reviews on the subject [153–157].

2.1.2 Heavy-quark actions

For the b quark, the discretization of the heavy-quark action follows a very different approach from that used for light flavours. There are several different methods for treating heavy quarks on the lattice, each with its own issues and considerations. Most of these methods use Effective Field Theory (EFT) at some point in the computation, either via direct simulation of the EFT, or by using EFT as a tool to estimate the size of cutoff errors, or by using EFT to extrapolate from the simulated lattice quark masses up to the physical b-quark mass. Because of the use of an EFT, truncation errors must be considered together with discretization errors.

The charm quark lies at an intermediate point between the heavy and light quarks. In our earlier reviews, the calculations involving charm quarks often treated it using one of the approaches adopted for the b quark. Since FLAG 16 [3], however, most calculations simulate the charm quark using light-quark actions. This has become possible thanks to the increasing availability of dynamical gauge field ensembles with fine lattice spacings. But clearly, when charm quarks are treated relativistically, discretization errors are more severe than those of the corresponding light-quark quantities.

In order to address these complications, the heavy-quark section adds an additional, bipartite, treatment category to the rating system. The purpose of this criterion is to provide a guideline for the level of action and operator improvement needed in each approach to make reliable calculations possible, in principle.

A description of the different approaches to treating heavy quarks on the lattice can be found in Appendix A.1.3 of FLAG 19 [4]. For truncation errors we use HQET power counting throughout, since this review is focused on heavy-quark quantities involving B and D mesons rather than bottomonium or charmonium quantities. Here we describe the criteria for how each approach must be implemented in order to receive an acceptable rating (✓) for both the heavy-quark actions and the weak operators. Heavy-quark implementations without the level of improvement described below are rated not acceptable (■). The matching is evaluated together with renormalization, using the renormalization criteria described in Sect. 2.1.1. We emphasize that the heavy-quark implementations rated as acceptable and described below have been validated in a variety of ways, such as via phenomenological agreement with experimental measurements, consistency between independent lattice calculations, and numerical studies of truncation errors. These tests are summarized in Sect. 8.

Relativistic heavy-quark actions

✓ at least tree-level $\mathcal{O}(a)$ improved action and weak operators

This is similar to the requirements for light-quark actions. All current implementations of relativistic heavy-quark actions satisfy this criterion.

NRQCD

✓ tree-level matched through $\mathcal{O}(1/m_h)$ and improved through $\mathcal{O}(a^2)$

The current implementations of NRQCD satisfy this criterion, and also include tree-level corrections of $\mathcal{O}(1/m_h^2)$ in the action.

HQET

✓ tree-level matched through $\mathcal{O}(1/m_h)$ with discretization errors starting at $\mathcal{O}(a^2)$

The current implementation of HQET by the ALPHA collaboration satisfies this criterion, since both action and weak operators are matched nonperturbatively through $\mathcal{O}(1/m_h)$. Calculations that exclusively use a static-limit action do not satisfy this criterion, since the static-limit action, by definition, does not include $1/m_h$ terms. We therefore include static computations in our final estimates only if truncation errors (in $1/m_h$) are discussed and included in the systematic uncertainties.

Light-quark actions for heavy quarks

✓ discretization errors starting at $\mathcal{O}(a^2)$ or higher

This applies to calculations that use the twisted-mass Wilson action, a nonperturbatively improved Wilson action, domain wall fermions or the HISQ action for charm-quark quantities. It also applies to calculations that use these light quark actions in the charm region and above together with either the static limit or with an HQET-inspired extrapolation to obtain results at the physical b-quark mass. In these cases, the continuum-extrapolation criteria described earlier must be applied to the entire range of heavy-quark masses used in the calculation.

2.1.3 Conventions for the figures

For a coherent assessment of the present situation, the quality of the data plays a key role, but the colour coding cannot be carried over to the figures. On the other hand, simply showing all data on equal footing might give the misleading impression

that the overall consistency of the information available on the lattice is questionable. Therefore, in the figures we indicate the quality of the data in a rudimentary way, using the following symbols:

- ■ corresponds to results included in the average or estimate (i.e., results that contribute to the black square below);
- □ corresponds to results that are not included in the average but pass all quality criteria;
- □ corresponds to all other results;
- ■ corresponds to FLAG averages or estimates; they are also highlighted by a gray vertical band.

The reason for not including a given result in the average is not always the same: the result may fail one of the quality criteria; the paper may be unpublished; it may be superseded by newer results; or it may not offer a complete error budget.

Symbols other than squares are used to distinguish results with specific properties and are always explained in the caption.[6] Often, nonlattice data are also shown in the figures for comparison. For these we use the following symbols:

- • corresponds to nonlattice results;
- ▲ corresponds to Particle Data Group (PDG) results.

2.2 Averages and estimates

FLAG results of a given quantity are denoted either as *averages* or as *estimates*. Here we clarify this distinction. To start with, both *averages* and *estimates* are based on results without any red tags in their colour coding. For many observables there are enough independent lattice calculations of good quality, with all sources of error (not merely those related to the colour-coded criteria), as analyzed in the original papers, appearing to be under control. In such cases, it makes sense to average these results and propose such an *average* as the best current lattice number. The averaging procedure applied to this data and the way the error is obtained is explained in detail in Sect. 2.3. In those cases where only a sole result passes our rating criteria (colour coding), we refer to it as our FLAG *average*, provided it also displays adequate control of all other sources of systematic uncertainty.

On the other hand, there are some cases in which this procedure leads to a result that, in our opinion, does not cover all uncertainties. Systematic errors are by their nature often subjective and difficult to estimate, and may thus end up being underestimated in one or more results that receive green symbols for all explicitly tabulated criteria. Adopting a conservative policy, in these cases we opt for an *estimate* (or a range), which we consider as a fair assessment of the knowledge acquired on the lattice at present. This *estimate* is not obtained with a prescribed mathematical procedure, but reflects what we consider the best possible analysis of the available information. The hope is that this will encourage more detailed investigations by the lattice community.

There are two other important criteria that also play a role in this respect, but that cannot be colour coded, because a systematic improvement is not possible. These are: (i) the publication status, and (ii) the number of sea-quark flavours N_f. As far as the former criterion is concerned, we adopt the following policy: we average only results that have been published in peer-reviewed journals, i.e., they have been endorsed by referee(s). The only exception to this rule consists in straightforward updates of previously published results, typically presented in conference proceedings. Such updates, which supersede the corresponding results in the published papers, are included in the averages. Note that updates of earlier results rely, at least partially, on the same gauge-field-configuration ensembles. For this reason, we do not average updates with earlier results. Nevertheless, all results are listed in the tables,[7] and their publication status is identified by the following symbols:

- Publication status:
  - A published or plain update of published results
  - P preprint
  - C conference contribution

[6] For example, for quark-mass results we distinguish between perturbative and nonperturbative renormalization, for low-energy constants we distinguish between the p- and ϵ-regimes, and for heavy-flavour results we distinguish between those from leptonic and semi-leptonic decays.

[7] Whenever figures turn out to be overcrowded, older, superseded results are omitted. However, all the most recent results from each collaboration are displayed.

In the present edition, the publication status on the **30th of April 2021** is relevant. If the paper appeared in print after that date, this is accounted for in the bibliography, but does not affect the averages.[8]

As noted above, in this review we present results from simulations with $N_f = 2$, $N_f = 2+1$ and $N_f = 2+1+1$ (except for $r_0\Lambda_{\overline{\rm MS}}$ where we also give the $N_f = 0$ result). We are not aware of an a priori way to quantitatively estimate the difference between results produced in simulations with a different number of dynamical quarks. We therefore average results at fixed N_f separately; averages of calculations with different N_f are not provided.

To date, no significant differences between results with different values of N_f have been observed in the quantities listed in Tables 1, 2, 3, 4, and 5. In particular, differences between results from simulations with $N_f = 2$ and $N_f = 2+1$ would reflect Zweig-rule violations related to strange-quark loops. Although not of direct phenomenological relevance, the size of such violations is an interesting theoretical issue per se, and one that can be quantitatively addressed only with lattice calculations. It remains to be seen whether the status presented here will change in the future, since this will require dedicated $N_f = 2$ and $N_f = 2+1$ calculations, which are not a priority of present lattice work.

The question of differences between results with $N_f = 2+1$ and $N_f = 2+1+1$ is more subtle. The dominant effect of including the charm sea quark is to shift the lattice scale, an effect that is accounted for by fixing this scale nonperturbatively using physical quantities. For most of the quantities discussed in this review, it is expected that residual effects are small in the continuum limit, suppressed by $\alpha_s(m_c)$ and powers of Λ^2/m_c^2. Here Λ is a hadronic scale that can only be roughly estimated and depends on the process under consideration. Note that the Λ^2/m_c^2 effects have been addressed in Refs. [158–162], and found to be small for the quantities considered. Assuming that such effects are generically small, it might be reasonable to average the results from $N_f = 2+1$ and $N_f = 2+1+1$ simulations, although we do not do so here.

2.3 Averaging procedure and error analysis

In the present report, we repeatedly average results obtained by different collaborations, and estimate the error on the resulting averages. Here we provide details on how averages are obtained.

2.3.1 Averaging – generic case

We follow the procedure of the previous two editions [2,3], which we describe here in full detail.

One of the problems arising when forming averages is that not all of the data sets are independent. In particular, the same gauge-field configurations, produced with a given fermion discretization, are often used by different research teams with different valence-quark lattice actions, obtaining results that are not really independent. Our averaging procedure takes such correlations into account.

Consider a given measurable quantity Q, measured by M distinct, not necessarily uncorrelated, numerical experiments (simulations). The result of each of these measurement is expressed as

$$Q_i = x_i \pm \sigma_i^{(1)} \pm \sigma_i^{(2)} \pm \cdots \pm \sigma_i^{(E)}, \tag{1}$$

where x_i is the value obtained by the ith experiment ($i = 1, \ldots, M$) and $\sigma_i^{(\alpha)}$ (for $\alpha = 1, \ldots, E$) are the various errors. Typically $\sigma_i^{(1)}$ stands for the statistical error and $\sigma_i^{(\alpha)}$ ($\alpha \geq 2$) are the different systematic errors from various sources. For each individual result, we estimate the total error σ_i by adding statistical and systematic errors in quadrature:

$$\begin{aligned} Q_i &= x_i \pm \sigma_i, \\ \sigma_i &\equiv \sqrt{\sum_{\alpha=1}^{E} \left[\sigma_i^{(\alpha)}\right]^2}. \end{aligned} \tag{2}$$

With the weight factor of each total error estimated in standard fashion,

$$\omega_i = \frac{\sigma_i^{-2}}{\sum_{i=1}^{M} \sigma_i^{-2}}, \tag{3}$$

[8] As noted above in footnote 1, one exception to this deadline was made, Ref. [61].

the central value of the average over all simulations is given by

$$x_{\rm av} = \sum_{i=1}^{M} x_i\, \omega_i\,. \tag{4}$$

The above central value corresponds to a $\chi^2_{\rm min}$ weighted average, evaluated by adding statistical and systematic errors in quadrature. If the fit is not of good quality ($\chi^2_{\rm min}/{\rm dof} > 1$), the statistical and systematic error bars are stretched by a factor $S = \sqrt{\chi^2/{\rm dof}}$.

Next, we examine error budgets for individual calculations and look for potentially correlated uncertainties. Specific problems encountered in connection with correlations between different data sets are described in the text that accompanies the averaging. If there is reason to believe that a source of error is correlated between two calculations, a 100% correlation is assumed. The correlation matrix C_{ij} for the set of correlated lattice results is estimated by a prescription due to Schmelling [163]. This consists in defining

$$\sigma_{i;j} = \sqrt{\sum_{\alpha}{}' \left[\sigma_i^{(\alpha)}\right]^2}, \tag{5}$$

with $\sum'_\alpha$ running only over those errors of x_i that are correlated with the corresponding errors of the measurement x_j. This expresses the part of the uncertainty in x_i that is correlated with the uncertainty in x_j. If no such correlations are known to exist, then we take $\sigma_{i;j} = 0$. The diagonal and off-diagonal elements of the correlation matrix are then taken to be

$$\begin{aligned} C_{ii} &= \sigma_i^2 \qquad\qquad (i = 1, \ldots, M), \\ C_{ij} &= \sigma_{i;j}\,\sigma_{j;i} \qquad (i \neq j). \end{aligned} \tag{6}$$

Finally, the error of the average is estimated by

$$\sigma^2_{\rm av} = \sum_{i=1}^{M}\sum_{j=1}^{M} \omega_i\,\omega_j\,C_{ij}, \tag{7}$$

and the FLAG average is

$$Q_{\rm av} = x_{\rm av} \pm \sigma_{\rm av}. \tag{8}$$

2.3.2 Nested averaging

We have encountered one case where the correlations between results are more involved, and a nested averaging scheme is required. This concerns the B-meson bag parameters discussed in Sect. 8.2. In the following, we describe the details of the nested averaging scheme. This is an updated version of the section added in the web update of the FLAG 16 report.

The issue arises for a quantity Q that is given by a ratio, $Q = Y/Z$. In most simulations, both Y and Z are calculated, and the error in Q can be obtained in each simulation in the standard way. However, in other simulations only Y is calculated, with Z taken from a global average of some type. The issue to be addressed is that this average value $\overline{Z}$ has errors that are correlated with those in Q.

In the example that arises in Sect. 8.2, $Q = B_B$, $Y = B_B f_B^2$ and $Z = f_B^2$. In one of the simulations that contribute to the average, Z is replaced by $\overline{Z}$, the PDG average for f_B^2 [164] (obtained with an averaging procedure similar to that used by FLAG). This simulation is labeled with $i = 1$, so that

$$Q_1 = \frac{Y_1}{\overline{Z}}. \tag{9}$$

The other simulations have results labeled Q_j, with $j \geq 2$. In this set up, the issue is that $\overline{Z}$ is correlated with the Q_j, $j \geq 2$.[9]

[9] There is also a small correlation between Y_1 and $\overline{Z}$, but we follow the original Ref. [73] and do not take this into account. Thus, the error in Q_1 is obtained by simple error propagation from those in Y_1 and $\overline{Z}$. Ignoring this correlation is conservative, because, as in the calculation of B_K, the correlations between $B_B f_B^2$ and f_B^2 tend to lead to a cancellation of errors. By ignoring this effect we are making a small overestimate of the error in Q_1.

We begin by decomposing the error in Q_1 in the same schematic form as above,

$$Q_1 = x_1 \pm \frac{\sigma_{Y_1}^{(1)}}{\overline{Z}} \pm \frac{\sigma_{Y_1}^{(2)}}{\overline{Z}} \pm \cdots \pm \frac{\sigma_{Y_1}^{(E)}}{\overline{Z}} \pm \frac{Y_1 \sigma_{\overline{Z}}}{\overline{Z}^2}. \tag{10}$$

Here the last term represents the error propagating from that in $\overline{Z}$, while the others arise from errors in Y_1. For the remaining Q_j ($j \geq 2$) the decomposition is as in Eq. (1). The total error of Q_1 then reads

$$\sigma_1^2 = \left(\frac{\sigma_{Y_1}^{(1)}}{\overline{Z}}\right)^2 + \left(\frac{\sigma_{Y_1}^{(2)}}{\overline{Z}}\right)^2 + \cdots + \left(\frac{\sigma_{Y_1}^{(E)}}{\overline{Z}}\right)^2 + \left(\frac{Y_1}{\overline{Z}^2}\right)^2 \sigma_{\overline{Z}}^2, \tag{11}$$

while that for the Q_j ($j \geq 2$) is

$$\sigma_j^2 = \left(\sigma_j^{(1)}\right)^2 + \left(\sigma_j^{(2)}\right)^2 + \cdots + \left(\sigma_j^{(E)}\right)^2. \tag{12}$$

Correlations between Q_j and Q_k ($j, k \geq 2$) are taken care of by Schmelling's prescription, as explained above. What is new here is how the correlations between Q_1 and Q_j ($j \geq 2$) are taken into account.

To proceed, we recall from Eq. (7) that $\sigma_{\overline{Z}}$ is given by

$$\sigma_{\overline{Z}}^2 = \sum_{i',j'=1}^{M'} \omega[Z]_{i'} \omega[Z]_{j'} C[Z]_{i'j'}. \tag{13}$$

Here the indices i' and j' run over the M' simulations that contribute to $\overline{Z}$, which, in general, are different from those contributing to the results for Q. The weights $\omega[Z]$ and correlation matrix $C[Z]$ are given an explicit argument Z to emphasize that they refer to the calculation of this quantity and not to that of Q. $C[Z]$ is calculated using the Schmelling prescription [Eqs. (5)–(7)] in terms of the errors, $\sigma[Z]_{i'}^{(\alpha)}$, taking into account the correlations between the different calculations of Z.

We now generalize Schmelling's prescription for $\sigma_{i;j}$, Eq. (5), to that for $\sigma_{1;k}$ ($k \geq 2$), i.e., the part of the error in Q_1 that is correlated with Q_k. We take

$$\sigma_{1;k} = \sqrt{\frac{1}{\overline{Z}^2} \sum_{(\alpha)\leftrightarrow k}{}' \left[\sigma_{Y_1}^{(\alpha)}\right]^2 + \frac{Y_1^2}{\overline{Z}^4} \sum_{i',j'}^{M'} \omega[Z]_{i'} \omega[Z]_{j'} C[Z]_{i'j'\leftrightarrow k}}. \tag{14}$$

The first term under the square root sums those sources of error in Y_1 that are correlated with Q_k. Here we are using a more explicit notation from that in Eq. (5), with $(\alpha) \leftrightarrow k$ indicating that the sum is restricted to the values of α for which the error $\sigma_{Y_1}^{(\alpha)}$ is correlated with Q_k. The second term accounts for the correlations within $\overline{Z}$ with Q_k, and is the nested part of the present scheme. The new matrix $C[Z]_{i'j'\leftrightarrow k}$ is a restriction of the full correlation matrix $C[Z]$, and is defined as follows. Its diagonal elements are given by

$$C[Z]_{i'i'\leftrightarrow k} = (\sigma[Z]_{i'\leftrightarrow k})^2 \qquad (i' = 1, \ldots, M'), \tag{15}$$

$$(\sigma[Z]_{i'\leftrightarrow k})^2 = \sum_{(\alpha)\leftrightarrow k}{}' (\sigma[Z]_{i'}^{(\alpha)})^2, \tag{16}$$

where the summation $\sum'_{(\alpha)\leftrightarrow k}$ over (α) is restricted to those $\sigma[Z]_{i'}^{(\alpha)}$ that are correlated with Q_k. The off-diagonal elements are

$$C[Z]_{i'j'\leftrightarrow k} = \sigma[Z]_{i';j'\leftrightarrow k}\, \sigma[Z]_{j';i'\leftrightarrow k} \qquad (i' \neq j'), \tag{17}$$

$$\sigma[Z]_{i';j'\leftrightarrow k} = \sqrt{\sum_{(\alpha)\leftrightarrow j'k}{}' (\sigma[Z]_{i'}^{(\alpha)})^2}, \tag{18}$$

where the summation $\sum'_{(\alpha)\leftrightarrow j'k}$ over (α) is restricted to $\sigma[Z]_{i'}^{(\alpha)}$ that are correlated with *both* $Z_{j'}$ and Q_k.

The last quantity that we need to define is $\sigma_{k;1}$.

$$\sigma_{k;1} = \sqrt{\sum_{(\alpha)\leftrightarrow 1}{}' \left[\sigma_k^{(\alpha)}\right]^2}, \tag{19}$$

where the summation $\sum'_{(\alpha)\leftrightarrow 1}$ is restricted to those $\sigma_k^{(\alpha)}$ that are correlated with one of the terms in Eq. (11).

In summary, we construct the correlation matrix C_{ij} using Eq. (6), as in the generic case, except the expressions for $\sigma_{1;k}$ and $\sigma_{k;1}$ are now given by Eqs. (14) and (19), respectively. All other $\sigma_{i;j}$ are given by the original Schmelling prescription, Eq. (5). In this way we extend the philosophy of Schmelling's approach while accounting for the more involved correlations.

3 Quark masses

Authors: T. Blum, A. Portelli, A. Ramos

Quark masses are fundamental parameters of the Standard Model. An accurate determination of these parameters is important for both phenomenological and theoretical applications. The bottom- and charm-quark masses, for instance, are important sources of parametric uncertainties in several Higgs decay modes. The up-, down- and strange-quark masses govern the amount of explicit chiral symmetry breaking in QCD. From a theoretical point of view, the values of quark masses provide information about the flavour structure of physics beyond the Standard Model. The Review of Particle Physics of the Particle Data Group contains a review of quark masses [165], which covers light as well as heavy flavours. Here we also consider light- and heavy-quark masses, but focus on lattice results and discuss them in more detail. We do not discuss the top quark, however, because it decays weakly before it can hadronize, and the nonperturbative QCD dynamics described by present day lattice simulations is not relevant. The lattice determination of light- (up, down, strange), charm- and bottom-quark masses is considered below in Sects. 3.1, 3.2, and 3.3, respectively.

Quark masses cannot be measured directly in experiment because quarks cannot be isolated, as they are confined inside hadrons. From a theoretical point of view, in QCD with N_f flavours, a precise definition of quark masses requires one to choose a particular renormalization scheme. This renormalization procedure introduces a renormalization scale μ, and quark masses depend on this renormalization scale according to the Renormalization Group (RG) equations. In mass-independent renormalization schemes the RG equations read

$$\mu \frac{\mathrm{d}\bar{m}_i(\mu)}{\mathrm{d}\mu} = \bar{m}_i(\mu)\tau(\bar{g}), \tag{20}$$

where the function $\tau(\bar{g})$ is the anomalous dimension, which depends only on the value of the strong coupling $\alpha_s = \bar{g}^2/(4\pi)$. Note that in QCD $\tau(\bar{g})$ is the same for all quark flavours. The anomalous dimension is scheme dependent, but its perturbative expansion

$$\tau(\bar{g}) \overset{\bar{g}\to 0}{\sim} -\bar{g}^2\left(d_0 + d_1\bar{g}^2 + \cdots\right) \tag{21}$$

has a leading coefficient $d_0 = 8/(4\pi)^2$, which is scheme independent.[10] Equation (20), being a first order differential equation, can be solved exactly by using Eq. (21) as the boundary condition. The formal solution of the RG equation reads

$$M_i = \bar{m}_i(\mu)[2b_0\bar{g}^2(\mu)]^{-d_0/(2b_0)} \exp\left\{-\int_0^{\bar{g}(\mu)} \mathrm{d}x \left[\frac{\tau(x)}{\beta(x)} - \frac{d_0}{b_0 x}\right]\right\}, \tag{22}$$

where $b_0 = (11 - 2N_f/3)/(4\pi)^2$ is the universal leading perturbative coefficient in the expansion of the β-function, $\beta(\bar{g}) \equiv d\bar{g}^2/d\log\mu^2$, which governs the running of the strong coupling constant near the scale μ. The renormalization group invariant (RGI) quark masses M_i are formally integration constants of the RG Eq. (20). They are scale independent, and due to the universality of the coefficient d_0, they are also scheme independent. Moreover, they are nonperturbatively defined

[10] We follow the conventions of Gasser and Leutwyler [166].

by Eq. (22). They only depend on the number of flavours N_f, making them a natural candidate to quote quark masses and compare determinations from different lattice collaborations. Nevertheless, it is customary in the phenomenology community to use the $\overline{\text{MS}}$ scheme at a scale $\mu = 2$ GeV to compare different results for light-quark masses, and use a scale equal to its own mass for the charm and bottom quarks. In this review, we will quote the final averages of both quantities.

Results for quark masses are always quoted in the four-flavour theory. $N_f = 2+1$ results have to be converted to the four-flavour theory. Fortunately, the charm quark is heavy $(\Lambda_{\text{QCD}}/m_c)^2 < 1$, and this conversion can be performed in perturbation theory with negligible ($\sim 0.2\%$) perturbative uncertainties. Nonperturbative corrections in this matching are more difficult to estimate. Since these effects are suppressed by a factor of $1/N_c$, and a factor of the strong coupling at the scale of the charm mass, naive power counting arguments would suggest that the effects are $\sim 1\%$. In practice, numerical nonperturbative studies [158,160,167] have found this power counting argument to be an overestimate by one order of magnitude in the determination of simple hadronic quantities or the Λ-parameter. Moreover, lattice determinations do not show any significant deviation between the $N_f = 2+1$ and $N_f = 2+1+1$ simulations. For example, the difference in the final averages for the mass of the strange quark m_s between $N_f = 2+1$ and $N_f = 2+1+1$ determinations is about 1.3%, or about one standard deviation.

We quote all final averages at 2 GeV in the $\overline{\text{MS}}$ scheme and also the RGI values (in the four-flavour theory). We use the exact RG Eq. (22). Note that to use this equation we need the value of the strong coupling in the $\overline{\text{MS}}$ scheme at a scale $\mu = 2$ GeV. All our results are obtained from the RG equation in the $\overline{\text{MS}}$ scheme and the 5-loop beta function together with the value of the Λ-parameter in the four-flavour theory $\Lambda^{(4)}_{\overline{\text{MS}}} = 294(12)$ MeV obtained in this review (see Sect. 9). In the uncertainties of the RGI masses we separate the contributions from the determination of the quark masses and the propagation of the uncertainty of $\Lambda^{(4)}_{\overline{\text{MS}}}$. These are identified with the subscripts m and Λ, respectively.

Conceptually, all lattice determinations of quark masses contain three basic ingredients:

1. Tuning the lattice bare-quark masses to match the experimental values of some quantities. Pseudo-scalar meson masses provide the most common choice, since they have a strong dependence on the values of quark masses. In pure QCD with N_f quark flavours these values are not known, since the electromagnetic interactions affect the experimental values of meson masses. Therefore, pure QCD determinations use model/lattice information to determine the location of the physical point. This is discussed at length in Sect. 3.1.1.
2. Renormalization of the bare-quark masses. Bare-quark masses determined with the above-mentioned criteria have to be renormalized. Many of the latest determinations use some nonperturbatively defined scheme. One can also use perturbation theory to connect directly the values of the bare-quark masses to the values in the $\overline{\text{MS}}$ scheme at 2 GeV. Experience shows that 1-loop calculations are unreliable for the renormalization of quark masses: usually at least two loops are required to have trustworthy results.
3. If quark masses have been nonperturbatively renormalized, for example, to some MOM/SF scheme, the values in this scheme must be converted to the phenomenologically useful values in the $\overline{\text{MS}}$ scheme (or to the scheme/scale independent RGI masses). Either option requires the use of perturbation theory. The larger the energy scale of this matching with perturbation theory, the better, and many recent computations in MOM schemes do a nonperturbative running up to 3–4 GeV. Computations in the SF scheme allow us to perform this running nonperturbatively over large energy scales and match with perturbation theory directly at the electro-weak scale ~ 100 GeV.

Note that many lattice determinations of quark masses make use of perturbation theory at a scale of a few GeV.

We mention that lattice-QCD calculations of the b-quark mass have an additional complication which is not present in the case of the charm and light quarks. At the lattice spacings currently used in numerical simulations the direct treatment of the b quark with the fermionic actions commonly used for light quarks is very challenging. Only two determinations of the b-quark mass use this approach, reaching the physical b-quark mass region at two lattice spacings with $aM \sim 1$. There are a few widely used approaches to treat the b quark on the lattice, which have been already discussed in the FLAG 13 review (see Sec. 8 of Ref. [2]). Those relevant for the determination of the b-quark mass will be briefly described in Sect. 3.3.

3.1 Masses of the light quarks

Light-quark masses are particularly difficult to determine because they are very small (for the up and down quarks) or small (for the strange quark) compared to typical hadronic scales. Thus, their impact on typical hadronic observables is minute, and it is difficult to isolate their contribution accurately.

Fortunately, the spontaneous breaking of $SU(3)_L \times SU(3)_R$ chiral symmetry provides observables which are particularly sensitive to the light-quark masses: the masses of the resulting Nambu–Goldstone bosons (NGB), i.e., pions, kaons, and eta. Indeed, the Gell–Mann–Oakes–Renner relation [168] predicts that the squared mass of a NGB is directly proportional to the sum of the masses of the quark and antiquark which compose it, up to higher-order mass corrections. Moreover, because these NGBs are light, and are composed of only two valence particles, their masses have a particularly clean statistical signal in lattice-QCD calculations. In addition, the experimental uncertainties on these meson masses are negligible. Thus, in lattice calculations, light-quark masses are typically obtained by renormalizing the input quark mass and tuning them to reproduce NGB masses, as described above.

3.1.1 The physical point and isospin symmetry

As mentioned in Sect. 2.1, the present review relies on the hypothesis that, at low energies, the Lagrangian $\mathcal{L}_{\rm QCD}+\mathcal{L}_{\rm QED}$ describes nature to a high degree of precision. However, most of the results presented below are obtained in pure QCD calculations, which do not include QED. Quite generally, when comparing QCD calculations with experiment, radiative corrections need to be applied. In pure QCD simulations, where the parameters are fixed in terms of the masses of some of the hadrons, the electromagnetic contributions to these masses must be discussed. How the matching is done is generally ambiguous because it relies on the unphysical separation of QCD and QED contributions. In this section, and in the following, we discuss this issue in detail. A related discussion, in the context of scale setting, is given in Sect. 11.3. Of course, once QED is included in lattice calculations, the subtraction of electromagnetic contributions is no longer necessary.

Let us start from the unambiguous case of QCD+QED. As explained in the introduction of this section, the physical quark masses are the parameters of the Lagrangian such that a given set of experimentally measured, dimensionful hadronic quantities are reproduced by the theory. Many choices are possible for these quantities, but in practice many lattice groups use pseudoscalar meson masses, as they are easily and precisely obtained both by experiment, and through lattice simulations. For example, in the four-flavour case, one can solve the system

$$M_{\pi^+}(m_u, m_d, m_s, m_c, \alpha) = M_{\pi^+}^{\rm exp.}, \tag{23}$$
$$M_{K^+}(m_u, m_d, m_s, m_c, \alpha) = M_{K^+}^{\rm exp.}, \tag{24}$$
$$M_{K^0}(m_u, m_d, m_s, m_c, \alpha) = M_{K^0}^{\rm exp.}, \tag{25}$$
$$M_{D^0}(m_u, m_d, m_s, m_c, \alpha) = M_{D^0}^{\rm exp.}, \tag{26}$$

where we assumed that

- all the equations are in the continuum and infinite-volume limits;
- the overall scale has been set to its physical value, generally through some lattice-scale setting procedure involving a fifth dimensionful input (see the discussion in Sect. 11.3);
- the quark masses m_q are assumed to be renormalized from the bare, lattice ones in some given continuum renormalization scheme;
- $\alpha = \frac{e^2}{4\pi}$ is the fine-structure constant expressed as function of the positron charge e, generally set to the Thomson limit $\alpha = 0.007297352\ldots$ [165];
- the mass $M_h(m_u, m_d, m_s, m_c, \alpha)$ of the meson h is a function of the quark masses and α. The functional dependence is generally obtained by choosing an appropriate parameterization and performing a global fit to the lattice data;
- the superscript exp. indicates that the mass is an experimental input, lattice groups use in general the values in the Particle Data Group review [165].

However, ambiguities arise with simulations of QCD only. In that case, there is no experimentally measurable quantity that emerges from the strong interaction only. The missing QED contribution is tightly related to isospin-symmetry breaking effects. Isospin symmetry is explicitly broken by the differences between the up- and down-quark masses $\delta m = m_u - m_d$, and electric charges $\delta Q = Q_u - Q_d$. These effects are, respectively, of order $\mathcal{O}(\delta m/\Lambda_{\rm QCD})$ and $\mathcal{O}(\alpha)$, and are expected to be $\mathcal{O}(1\%)$ of a typical isospin-symmetric hadronic quantity. Strong and electromagnetic isospin-breaking effects are of the same order and therefore cannot, in principle, be evaluated separately without introducing strong ambiguities. Because these effects are small, they can be treated as a perturbation,

$$X(m_u, m_d, m_s, m_c, \alpha) = \bar{X}(m_{ud}, m_s, m_c) + \delta m A_X(m_{ud}, m_s, m_c) + \alpha B_X(m_{ud}, m_s, m_c)\,, \tag{27}$$

for a given hadronic quantity X, where $m_{ud} = \frac{1}{2}(m_u + m_d)$ is the average light-quark mass. There are several things to notice here. Firstly, the neglected higher-order $\mathcal{O}(\delta m^2, \alpha\delta m, \alpha^2)$ corrections are expected to be $\mathcal{O}(10^{-4})$ relatively to X, which at the moment is way beyond the relative statistical accuracy that can be delivered by a lattice calculation. Secondly, this is not strictly speaking an expansion around the isospin-symmetric point, the electromagnetic interaction has also symmetric contributions. From this last expression the previous statements about ambiguities become clearer. Indeed, the only unambiguous prediction one can perform is to solve Eqs. (23)–(26) and use the resulting parameters to obtain a prediction for X, which is represented by the left-hand side of Eq. (27). This prediction will be the sum of the QCD isospin-symmetric part $\bar{X}$, the strong isospin-breaking effects $X^{SU(2)} = \delta m A_X$, and the electromagnetic effects $X^{\gamma} = \alpha B_X$. Obtaining any of these terms individually requires extra, unphysical conditions to perform the separation. To be consistent with previous editions of FLAG, we also define $\hat{X} = \bar{X} + X^{SU(2)}$ to be the $\alpha \to 0$ limit of X.

With pure QCD simulations, one typically solves Eqs. (23)–(26) by equating the QCD isospin-symmetric part of a hadron mass $\bar{M}_h$, result of the simulations, with its experimental value $M_h^{\text{exp.}}$. This will result in an $\mathcal{O}(\delta m, \alpha)$ mis-tuning of the theory parameters which will propagate as an error on predicted quantities. Because of this, in general, one cannot predict hadronic quantities with a relative accuracy higher than $\mathcal{O}(1\%)$ from pure QCD simulations, independently on how the target X is sensitive to isospin-breaking effects. If one performs a complete lattice prediction of the physical value of X, it can be of phenomenological interest to define in some way $\bar{X}$, $X^{SU(2)}$, and X^{γ}. If we keep m_{ud}, m_s and m_c at their physical values in physical units, for a given renormalization scheme and scale, then these three quantities can be extracted by setting successively and simultaneously α and δm to 0. This is where the ambiguity lies: in general the $\delta m = 0$ point will depend on the renormalization scheme used for the quark masses. In the next section, we give more details on that particular aspect and discuss the order of scheme ambiguities.

3.1.2 Ambiguities in the separation of isospin-breaking contributions

In this section, we discuss the ambiguities that arise in the individual determination of the QED contribution X^{γ} and the strong-isospin correction $X^{SU(2)}$ defined in the previous section. Throughout this section, we assume that the isospin-symmetric quark masses m_{ud}, m_s and m_c are always kept fixed in physical units to the values they take at the QCD+QED physical point in some given renormalization scheme. Let us assume that both up and down masses have been renormalized in an identical mass-independent scheme which depends on some energy scale μ. We also assume that the renormalization procedure respects chiral symmetry so that quark masses renormalize multiplicatively. The renormalization constants of the quark masses are identical for $\alpha = 0$ and therefore the renormalized mass of a quark has the general form

$$m_q(\mu) = Z_m(\mu)[1 + \alpha Q_{\text{tot.}}^2 \delta_Z^{(0)}(\mu) + \alpha Q_{\text{tot.}} Q_q \delta_Z^{(1)}(\mu) + \alpha Q_q^2 \delta_Z^{(2)}(\mu)] m_{q,0}\,, \tag{28}$$

up to $\mathcal{O}(\alpha^2)$ corrections, where $m_{q,0}$ is the bare-quark mass, $Q_{\text{tot.}}$ and $Q_{\text{tot.}}^2$ are the sum of all quark charges and squared charges, respectively, and Q_q is the quark charge, all in units of in units of the positron charge e. Throughout this section, a subscript ud generally denotes the average between up and down quantities and δ the difference between the up and the down quantities. The source of the ambiguities described in the previous section is the mixing of the isospin-symmetric mass m_{ud} and the difference δm through renormalization. Using Eq. (28) one can make this mixing explicit at leading order in α:

$$\begin{pmatrix} m_{ud}(\mu) \\ \delta m(\mu) \end{pmatrix} = Z_m(\mu)[1 + \alpha Q_{\text{tot.}}^2 \delta_Z^{(0)}(\mu) + \alpha M^{(1)}(\mu) + \alpha M^{(2)}(\mu)] \begin{pmatrix} m_{ud,0} \\ \delta m_0 \end{pmatrix} \tag{29}$$

with the mixing matrices

$$M^{(1)}(\mu) = \delta_Z^{(1)}(\mu) Q_{\text{tot.}} \begin{pmatrix} Q_{ud} & \frac{1}{4}\delta Q \\ \delta Q & Q_{ud} \end{pmatrix} \quad \text{and} \quad M^{(2)}(\mu) = \delta_Z^{(2)}(\mu) \begin{pmatrix} Q_{ud}^2 & \frac{1}{4}\delta Q^2 \\ \delta Q^2 & Q_{ud}^2 \end{pmatrix}, \tag{30}$$

where $Q_{ud} = \frac{1}{2}(Q_u + Q_d)$ and $\delta Q = Q_u - Q_d$ are the average and difference of the up and down charges, and similarly $Q_{ud}^2 = \frac{1}{2}(Q_u^2 + Q_d^2)$ and $\delta Q^2 = Q_u^2 - Q_d^2$ for the squared charges. Now let us assume that for the purpose of determining the

different components in Eq. (27), one starts by tuning the bare masses to obtain equal up and down masses, for some small coupling α_0 at some scale μ_0, i.e., $\delta m(\mu_0) = 0$. At this specific point, one can extract the pure QCD, and the QED corrections to a given quantity X by studying the slope of α in Eq. (27). From these quantities the strong-isospin contribution can then readily be extracted using a nonzero value of $\delta m(\mu_0)$. However, if now the procedure is repeated at another coupling α and scale μ with the same bare masses, it appears from Eq. (29) that $\delta m(\mu) \neq 0$. More explicitly,

$$\delta m(\mu) = m_{ud}(\mu_0)\frac{Z_m(\mu)}{Z_m(\mu_0)}[\alpha\Delta_Z(\mu) - \alpha_0\Delta_Z(\mu_0)]\,, \tag{31}$$

with

$$\Delta_Z(\mu) = Q_{\text{tot.}}\delta Q\delta_Z^{(1)}(\mu) + \delta Q^2\delta_Z^{(2)}(\mu)\,, \tag{32}$$

up to higher-order corrections in α and α_0. In other words, the definitions of $\bar{X}$, $X^{SU(2)}$, and X^{γ} depend on the renormalization scale at which the separation was made. This dependence, of course, has to cancel in the physical sum X. One can notice that at no point did we mention the renormalization of α itself, which, in principle, introduces similar ambiguities. However, the corrections coming from the running of α are $\mathcal{O}(\alpha^2)$ relatively to X, which, as justified above, can be safely neglected. Finally, important information is provided by Eq. (31): the scale ambiguities are $\mathcal{O}(\alpha m_{ud})$. For physical quark masses, one generally has $m_{ud} \simeq \delta m$. So by using this approximation in the first-order expansion Eq. (27), it is actually possible to define unambiguously the components of X up to second-order isospin-breaking corrections. Therefore, in the rest of this review, we will not keep track of the ambiguities in determining pure QCD or QED quantities. However, in the context of lattice simulations, it is crucial to notice that $m_{ud} \simeq \delta m$ is only accurate *at the physical point*. In simulations at larger-than-physical pion masses, scheme ambiguities in the separation of QCD and QED contributions are generally large. Once more, the argument made here assumes that the isospin-symmetric quark masses m_{ud}, m_s, and m_c are kept fixed to their physical value in a given scheme while varying α. Outside of this assumption there is an additional isospin-symmetric $\mathcal{O}(\alpha m_q)$ ambiguity between $\bar{X}$ and X^{γ}.

Such separation in lattice QCD+QED simulation results appeared for the first time in RBC 07 [169] and Blum 10 [170], where the scheme was implicitly defined around the χPT expansion. In that setup, the $\delta m(\mu_0) = 0$ point is defined in pure QCD, i.e., $\alpha_0 = 0$ in the previous discussion. The QCD part of the kaon-mass splitting from the first FLAG review [1] is used as an input in RM123 11 [171], which focuses on QCD isospin corrections only. It therefore inherits from the convention that was chosen there, which is also to set $\delta m(\mu_0) = 0$ at zero QED coupling. The same convention was used in the follow-up works RM123 13 [172] and RM123 17 [19]. The BMW collaboration was the first to introduce a purely hadronic scheme in its electro-quenched study of the baryon octet mass splittings [173]. In this work, the quark mass difference $\delta m(\mu)$ is swapped with the mass splitting ΔM^2 between the connected $\bar{u}u$ and $\bar{d}d$ pseudoscalar masses. Although unphysical, this quantity is proportional [174] to $\delta m(\mu)$ up to $\mathcal{O}(\alpha m_{ud})$ chiral corrections. In this scheme, the quark masses are assumed to be equal at $\Delta M^2 = 0$, and the $\mathcal{O}(\alpha m_{ud})$ corrections to this statement are analogous to the scale ambiguities mentioned previously. The same scheme was used for the determination of light-quark masses in BMW 16 [20] and in the recent BMW prediction of the leading hadronic contribution to the muon magnetic moment [115]. The BMW collaboration used a different hadronic scheme for its determination of the nucleon-mass splitting in BMW 14 [147] using full QCD+QED simulations. In this work, the $\delta m = 0$ point was fixed by imposing the baryon splitting $M_{\Sigma^+} - M_{\Sigma^-}$ to cancel. This scheme is quite different from the other ones presented here, in the sense that its intrinsic ambiguity is not $\mathcal{O}(\alpha m_{ud})$. What motivates this choice here is that $M_{\Sigma^+} - M_{\Sigma^-} = 0$ in the limit where these baryons are point particles, so the scheme ambiguity is suppressed by the compositeness of the Σ baryons. This may sound like a more difficult ambiguity to quantify, but this scheme has the advantage of being defined purely by measurable quantities. Moreover, it has been demonstrated numerically in BMW 14 [147] that, within the uncertainties of this study, the $M_{\Sigma^+} - M_{\Sigma^-} = 0$ scheme is equivalent to the $\Delta M^2 = 0$ one, explicitly $M_{\Sigma^+} - M_{\Sigma^-} = -0.18(12)(6)$ MeV at $\Delta M^2 = 0$. The calculation QCDSF/UKQCD 15 [175] uses a "Dashen scheme," where quark masses are tuned such that flavour-diagonal mesons have equal masses in QCD and QCD+QED. Although not explicitly mentioned by the authors of the paper, this scheme is simply a reformulation of the $\Delta M^2 = 0$ scheme mentioned previously. Finally, MILC 18 [21] also used the $\Delta M^2 = 0$ scheme and noticed its connection to the "Dashen scheme" from QCDSF/UKQCD 15.

Before the previous edition of this review, the contributions $\bar{X}$, $X^{SU(2)}$, and X^{γ} were given for pion and kaon masses based on phenomenological information. Considerable progress has been achieved by the lattice community to include isospin-breaking effects in calculations, and it is now possible to determine these quantities precisely directly from a lattice calculation. However, these quantities generally appear as intermediate products of a lattice analysis, and are rarely directly

communicated in publications. These quantities, although unphysical, have a phenomenological interest, and we encourage the authors of future calculations to quote them explicitly.

3.1.3 Inclusion of electromagnetic effects in lattice-QCD simulations

Electromagnetism on a lattice can be formulated using a naive discretization of the Maxwell action $S[A_\mu] = \frac{1}{4}\int d^4x \sum_{\mu,\nu}[\partial_\mu A_\nu(x) - \partial_\nu A_\mu(x)]^2$. Even in its noncompact form, the action remains gauge invariant. This is not the case for non-Abelian theories for which one uses the traditional compact Wilson gauge action (or an improved version of it). Compact actions for QED feature spurious photon-photon interactions which vanish only in the continuum limit. This is one of the main reason why the noncompact action is the most popular so far. It was used in all the calculations presented in this review. Gauge-fixing is necessary for noncompact actions because of the usual infinite measure of equivalent gauge orbits which contribute to the path integral. It was shown [176,177] that gauge-fixing is not necessary with compact actions, including in the construction of interpolating operators for charged states.

Although discretization is straightforward, simulating QED in a finite volume is more challenging. Indeed, the long range nature of the interaction suggests that important finite-size effects have to be expected. In the case of periodic boundary conditions, the situation is even more critical: a naive implementation of the theory features an isolated zero-mode singularity in the photon propagator. It was first proposed in [178] to fix the global zero-mode of the photon field $A_\mu(x)$ in order to remove it from the dynamics. This modified theory is generally named QED_{TL}. Although this procedure regularizes the theory and has the right classical infinite-volume limit, it is nonlocal because of the zero-mode fixing. As first discussed in [147], the nonlocality in time of QED_{TL} prevents the existence of a transfer matrix, and therefore a quantum-mechanical interpretation of the theory. Another prescription named QED_{L}, proposed in [179], is to remove the zero-mode of $A_\mu(x)$ independently for each time slice. This theory, although still nonlocal in space, is local in time and has a well-defined transfer matrix. Whether these nonlocalities constitute an issue to extract infinite-volume physics from lattice-QCD+QED_{L} simulations is, at the time of this review, still an open question. However, it is known through analytical calculations of electromagnetic finite-size effects at $\mathcal{O}(\alpha)$ in hadron masses [147,148,150,172,179–181], meson leptonic decays [181], and the hadronic vacuum polarization [182] that QED_{L} does not suffer from a problematic (e.g., UV divergent) coupling of short- and long-distance physics due to its nonlocality. Another strategy, first proposed in [183] and used by the QCDSF collaboration, is to bound the zero-mode fluctuations to a finite range. Although more minimal, it is still a nonlocal modification of the theory and so far finite-size effects for this scheme have not been investigated. More recently, two proposals for local formulations of finite-volume QED emerged. The first one described in [184] proposes to use massive photons to regulate zero-mode singularities, at the price of (softly) breaking gauge invariance. The second one presented in [177], based on earlier works [185,186], avoids the zero-mode issue by using anti-periodic boundary conditions for $A_\mu(x)$. In this approach, gauge invariance requires the fermion field to undergo a charge conjugation transformation over a period, breaking electric charge conservation. These local approaches have the potential to constitute cleaner approaches to finite-volume QED. All the calculations presented in this review used QED_{L} or QED_{TL}, with the exception of QCDSF.

Once a finite-volume theory for QED is specified, there are various ways to compute QED effects themselves on a given hadronic quantity. The most direct approach, first used in [178], is to include QED directly in the lattice simulations and assemble correlation functions from charged quark propagators. Another approach proposed in [172], is to exploit the perturbative nature of QED, and compute the leading-order corrections directly in pure QCD as matrix elements of the electromagnetic current. Both approaches have their advantages and disadvantages and as shown in [19], are not mutually exclusive. A critical comparative study can be found in [187].

Finally, most of the calculations presented here made the choice of computing electromagnetic corrections in the electro-quenched approximation. In this limit, one assumes that only valence quarks are charged, which is equivalent to neglecting QED corrections to the fermionic determinant. This approximation reduces dramatically the cost of lattice-QCD+QED calculations since it allows the reuse of previously generated QCD configurations. If QED is introduced perturbatively through current insertions, the electro-quenched approximation avoids computing disconnected contributions coming from the electromagnetic current in the vacuum, which are generally challenging to determine precisely. The electromagnetic contributions from sea quarks to hadron-mass splittings are known to be flavour-$SU(3)$ and large-N_c suppressed, thus electro-quenched simulations are expected to have an $\mathcal{O}(10\%)$ accuracy for the leading electromagnetic effects. This suppression is in principle rather weak and results obtained from electro-quenched simulations might feature uncontrolled systematic errors. For this reason, the use of the electro-quenched approximation constitutes the difference between ★ and ○ in the FLAG criterion for the inclusion of isospin-breaking effects.

3.1.4 Lattice determination of m_s and m_{ud}

We now turn to a review of the lattice calculations of the light-quark masses and begin with m_s, the isospin-averaged up- and down-quark mass m_{ud}, and their ratio. Most groups quote only m_{ud}, not the individual up- and down-quark masses. We then discuss the ratio m_u/m_d and the individual determinations of m_u and m_d.

Quark masses have been calculated on the lattice since the mid-nineties. However, early calculations were performed in the quenched approximation, leading to unquantifiable systematics. Thus, in the following, we only review modern, unquenched calculations, which include the effects of light sea quarks.

Tables 6 and 7 list the results of $N_f = 2+1$ and $N_f = 2+1+1$ lattice calculations of m_s and m_{ud}. These results are given in the $\overline{\text{MS}}$ scheme at 2 GeV, which is standard nowadays, though some groups are starting to quote results at higher scales (e.g., Ref. [188]). The tables also show the colour coding of the calculations leading to these results. As indicated earlier in this review, we treat calculations with different numbers, N_f, of dynamical quarks separately.

$N_f = 2 + 1$ lattice calculations

We turn now to $N_f = 2 + 1$ calculations. These and the corresponding results for m_{ud} and m_s are summarized in Table 6. Given the very high precision of a number of the results, with total errors on the order of 1%, it is important to consider the effects neglected in these calculations. Isospin-breaking and electromagnetic effects are small on m_{ud} and m_s, and have been approximately accounted for in the calculations that will be retained for our averages. We have already commented that the effect of the omission of the charm quark in the sea is expected to be small, below our current precision, and we do not add any additional uncertainty due to these effects in the final averages.

The only new computation since the previous FLAG edition is the determination of light-quark masses by the ALPHA collaboration [18]. This work uses nonperturbatively $\mathcal{O}(a)$ improved Wilson fermions (a subset of the CLS ensembles [137]). The renormalization is performed nonperturbatively in the SF scheme from 200 MeV up to the electroweak scale $\sim$ 100 GeV [203]. This nonperturbative running over such large energy scales avoids any use of perturbation theory at low energy scales, but adds a cost in terms of uncertainty: the running alone propagates to $\approx$ 1% of the error in quark masses. This turns out to be one of the dominant pieces of uncertainty for the case of m_s. On the other hand, for the case of m_{ud}, the uncertainty is dominated by the chiral extrapolations. The ensembles used include four values of the lattice spacing below 0.09 fm, which qualifies for a ★ in the continuum extrapolation, and pion masses down to 200 MeV. This value lies just at the boundary of the ★ rating, but since the chiral extrapolation is a substantial source of systematic uncertainty, we opted to rate the work with a ○. In any case, this work enters in the average and their results show a reasonable agreement with the FLAG average.

We now comment in some detail on previous works that also contribute to the averages.

RBC/UKQCD 14 [8] significantly improves on their RBC/UKQCD 12B [188] work by adding three new domain wall fermion simulations to three used previously. Two of the new simulations are performed at essentially physical pion masses ($M_\pi \simeq 139$ MeV) on lattices of about 5.4 fm in size and with lattice spacings of 0.114 fm and 0.084 fm. It is complemented by a third simulation with $M_\pi \simeq 371$ MeV, $a \simeq 0.063$ fm and a rather small $L \simeq 2.0$ fm. Altogether, this gives them six simulations with six unitary ($m_{\text{sea}} = m_{\text{val}}$) M_π's in the range of 139 to 371 MeV, and effectively three lattice spacings from 0.063 to 0.114 fm. They perform a combined global continuum and chiral fit to all of their results for the π and K masses and decay constants, the Ω baryon mass and two Wilson-flow parameters. Quark masses in these fits are renormalized and run nonperturbatively in the RI-SMOM scheme. This is done by computing the relevant renormalization constant for a reference ensemble, and determining those for other simulations relative to it by adding appropriate parameters in the global fit. This calculation passes all of our selection criteria.

$N_f = 2 + 1$ MILC results for light-quark masses go back to 2004 [197,198]. They use rooted staggered fermions. By 2009 their simulations covered an impressive range of parameter space, with lattice spacings going down to 0.045 fm, and valence-pion masses down to approximately 180 MeV [15]. The most recent MILC $N_f = 2 + 1$ results, i.e., MILC 10A [12] and MILC 09A [15], feature large statistics and 2-loop renormalization. Since these data sets subsume those of their previous calculations, these latest results are the only ones that need to be kept in any world average.

The BMW 10A, 10B [9,10] calculation still satisfies our stricter selection criteria. They reach the physical up- and down-quark mass by *interpolation* instead of by extrapolation. Moreover, their calculation was performed at five lattice spacings ranging from 0.054 to 0.116 fm, with full nonperturbative renormalization and running and in volumes of up to $(6\text{ fm})^3$, guaranteeing that the continuum limit, renormalization, and infinite-volume extrapolation are controlled. It does neglect, however, isospin-breaking effects, which are small on the scale of their error bars.

Finally, we come to another calculation which satisfies our selection criteria, HPQCD 10 [11]. It updates the staggered-fermions calculation of HPQCD 09A [27]. In these papers, the renormalized mass of the strange quark is obtained by

Table 6 $N_f = 2 + 1$ lattice results for the masses m_{ud} and m_s (MeV)

Collaboration	Refs.	Publication status	Chiral extrapolation	Continuum extrapolation	Finite volume	Renormalization	Running	m_{ud}	m_s
ALPHA 19	[18]	A	○	★	★	★	e	3.54(12)(9)	95.7(2.5)(2.4)
Maezawa 16	[189]	A	■	★	★	★	d	–	92.0(1.7)
RBC/UKQCD 14B$^{\ominus}$	[8]	A	★	★	★	★	d	3.31(4)(4)	90.3(0.9)(1.0)
RBC/UKQCD 12$^{\ominus}$	[188]	A	★	○	★	★	d	3.37(9)(7)(1)(2)	92.3(1.9)(0.9)(0.4)(0.8)
PACS-CS 12*	[190]	A	★	■	■	★	b	3.12(24)(8)	83.60(0.58)(2.23)
Laiho 11	[49]	C	○	★	★	○	–	3.31(7)(20)(17)	94.2(1.4)(3.2)(4.7)
BMW 10A, 10B^{+}	[9,10]	A	★	★	★	★	c	3.469(47)(48)	95.5(1.1)(1.5)
PACS-CS 10	[191]	A	★	■	■	★	b	2.78(27)	86.7(2.3)
MILC 10A	[12]	C	○	★	★	○	–	3.19(4)(5)(16)	–
HPQCD 10**	[11]	A	○	★	★	–	–	3.39(6)	92.2(1.3)
RBC/UKQCD 10A	[117]	A	○	○	★	★	a	3.59(13)(14)(8)	96.2(1.6)(0.2)(2.1)
Blum 10†	[170]	A	○	■	○	★	–	3.44(12)(22)	97.6(2.9)(5.5)
PACS-CS 09	[192]	A	★	■	■	★	b	2.97(28)(3)	92.75(58)(95)
HPQCD 09A$^{\oplus}$	[27]	A	○	★	★	–	–	3.40(7)	92.4(1.5)
MILC 09A	[15]	C	○	★	★	○	–	3.25 (1)(7)(16)(0)	89.0(0.2)(1.6)(4.5)(0.1)
MILC 09	[157]	A	○	★	★	○	–	3.2(0)(1)(2)(0)	88(0)(3)(4)(0)
PACS-CS 08	[193]	A	★	■	■	■	–	2.527(47)	72.72(78)
RBC/UKQCD 08	[194]	A	○	■	★	★	–	3.72(16)(33)(18)	107.3(4.4)(9.7)(4.9)
CP-PACS/JLQCD 07	[195]	A	■	★	★	■	–	$3.55(19)(^{+56}_{-20})$	$90.1(4.3)(^{+16.7}_{-4.3})$
HPQCD 05	[196]	A	○	○	○	○	–	3.2(0)(2)(2)(0)‡	87(0)(4)(4)(0)‡
MILC 04, HPQCD/ MILC/UKQCD 04	[197,198]	A	○	○	○	■	–	2.8(0)(1)(3)(0)	76(0)(3)(7)(0)

$^{\ominus}$The results are given in the $\overline{\text{MS}}$ scheme at 3 instead of 2 GeV. We run them down to 2 GeV using numerically integrated 4-loop running [199,200] with $N_f = 3$ and with the values of $\alpha_s(M_Z)$, m_b, and m_c taken from Ref. [201]. The running factor is 1.106. At three loops it is only 0.2% smaller, indicating that perturbative running uncertainties are small. We neglect them here

*The calculation includes electromagnetic and $m_u \neq m_d$ effects through reweighting

$^{+}$The fermion action used is tree-level improved

$^{**}m_s$ is obtained by combining m_c and HPQCD 09A's $m_c/m_s = 11.85(16)$ [27]. Finally, m_{ud} is determined from m_s with the MILC 09 result for m_s/m_{ud}. Since m_c/m_s is renormalization group invariant in QCD, the renormalization and running of the quark masses enter indirectly through that of m_c (see below)

†The calculation includes quenched electromagnetic effects

$^{\oplus}$What is calculated is $m_c/m_s = 11.85(16)$. m_s is then obtained by combining this result with the determination $m_c(m_c) = 1.268(9)$ GeV from Ref. [202]. Finally, m_{ud} is determined from m_s with the MILC 09 result for m_s/m_{ud}

‡The bare numbers are those of MILC 04. The masses are simply rescaled, using the ratio of the 2-loop to 1-loop renormalization factors

a The masses are renormalized nonperturbatively at a scale of 2 GeV in a couple of $N_f = 3$ RI-SMOM schemes. A careful study of perturbative matching uncertainties has been performed by comparing results in the two schemes in the region of 2 GeV to 3 GeV [117]

b The masses are renormalized and run nonperturbatively up to a scale of 40 GeV in the $N_f = 3$ SF scheme. In this scheme, nonperturbative and NLO running for the quark masses are shown to agree well from 40 GeV all the way down to 3 GeV [191]

c The masses are renormalized and run nonperturbatively up to a scale of 4 GeV in the $N_f = 3$ RI-MOM scheme. In this scheme, nonperturbative and N^{3}LO running for the quark masses are shown to agree from 6 GeV down to 3 GeV to better than 1% [10]

d All required running is performed nonperturbatively

e Running is performed nonperturbatively from 200 MeV to the electroweak scale $\sim$ 100 GeV

combining the result of a precise calculation of the renormalized charm-quark mass, m_c, with the result of a calculation of the quark-mass ratio, m_c/m_s. As described in Ref. [202] and in Sect. 3.2, HPQCD determines m_c by fitting Euclidean-time moments of the $\bar{c}c$ pseudoscalar density two-point functions, obtained numerically in lattice QCD, to fourth-order,

Table 7 $N_f = 2+1+1$ lattice results for the masses m_{ud} and m_s (MeV)

Collaboration	Refs.	Publication status	Chiral extrapolation	Continuum extrapolation	Finite volume	Renormalization	Running	m_{ud}	m_s
ETM 21A	[204]	P	★	★	★	★	–	$3.636(66)(^{+60}_{-57})$	$98.7(2.4)(^{+4.0}_{-3.2})$
HPQCD 18†	[13]	A	★	★	★	★	–		94.49(96)
FNAL/MILC/TUMQCD 18	[6]	A	★	★	★	★	–	3.404(14)(21)	92.52(40)(56)
HPQCD 14A ⊕	[14]	A	★	★	★	–	–		93.7(8)
ETM 14⊕	[7]	A	○	★	★	★	–	3.70(13)(11)	99.6(3.6)(2.3)

†Bare-quark masses are renormalized nonperturbatively in the RI-SMOM scheme at scales $\mu \sim 2-5$ GeV for different lattice spacings and translated to the $\overline{\text{MS}}$ scheme. Perturbative running is then used to run all results to a reference scale $\mu = 3$ GeV

⊕As explained in the text, m_s is obtained by combining the results $m_c(5\,\text{GeV}; N_f = 4) = 0.8905(56)$ GeV and $(m_c/m_s)(N_f = 4) = 11.652(65)$, determined on the same data set. A subsequent scale and scheme conversion, performed by the authors, leads to the value 93.6(8). In the table, we have converted this to $m_s(2\,\text{GeV}; N_f = 4)$, which makes a very small change

continuum perturbative expressions. These moments are normalized and chosen so as to require no renormalization with staggered fermions. Since m_c/m_s requires no renormalization either, HPQCD's approach displaces the problem of lattice renormalization in the computation of m_s to one of computing continuum perturbative expressions for the moments. To calculate m_{ud} HPQCD 10 [11] use the MILC 09 determination of the quark-mass ratio m_s/m_{ud} [157].

HPQCD 09A [27] obtains $m_c/m_s = 11.85(16)$ [27] fully nonperturbatively, with a precision slightly larger than 1%. HPQCD 10's determination of the charm-quark mass, $m_c(m_c) = 1.268(6)$,[11] is even more precise, achieving an accuracy better than 0.5%.

This discussion leaves us with five results for our final average for m_s: ALPHA 19 [18], MILC 09A [15], BMW 10A, 10B [9,10], HPQCD 10 [11] and RBC/UKQCD 14 [8]. Assuming that the result from HPQCD 10 is 100% correlated with that of MILC 09A, as it is based on a subset of the MILC 09A configurations, we find $m_s = 92.2(1.1)$ MeV with a $\chi^2/\text{dof} = 1.65$.

For the light-quark mass m_{ud}, the results satisfying our criteria are ALPHA 19, RBC/UKQCD 14B, BMW 10A, 10B, HPQCD 10, and MILC 10A. For the error, we include the same 100% correlation between statistical errors for the latter two as for the strange case, resulting in the following (at scale 2 GeV in the $\overline{\text{MS}}$ scheme, and $\chi^2/\text{dof} = 1.4$),

$$N_f = 2+1: \quad \begin{aligned} m_{ud} &= 3.381(40)\ \text{MeV} && \text{Refs. [8–12,18]},\\ m_s &= 92.2(1.0)\ \text{MeV} && \text{Refs. [8–11,15,18]}, \end{aligned} \tag{33}$$

and the RGI values

$$N_f = 2+1: \quad \begin{aligned} M_{ud}^{\text{RGI}} &= 4.695(56)_m(54)_\Lambda\ \text{MeV} && \text{Refs. [8–12,18]},\\ M_s^{\text{RGI}} &= 128.1(1.4)_m(1.5)_\Lambda\ \text{MeV} && \text{Refs. [8–11,15,18]}. \end{aligned} \tag{34}$$

$N_f = 2+1+1$ lattice calculations

Since the previous review a new computation of m_s, m_{ud} has appeared, ETM 21A [204]. Using twisted-mass fermions with an added clover-term to suppress $\mathcal{O}(a^2)$ effects between the neutral and charged pions, this work represents a significant improvement over ETM 14 [7]. Renormalization is performed nonperturbatively in the RI-MOM scheme. Their ensembles comprise three lattice spacings (0.095, 0.082, and 0.069 fm), two volumes for the finest lattice spacings with pion masses reaching down to the physical point in the two finest lattices allowing a controlled chiral extrapolation. Their volumes are

[11] To obtain this number, we have used the conversion from $\mu = 3$ GeV to m_c given in Ref. [202].

large, with $m_\pi L$ between four and five. These characteristics of their ensembles pass the most stringent FLAG criteria in all categories. This work extracts quark masses from two different quantities, one based on the meson spectrum and the other based on the baryon spectrum. Results obtained with these two methods agree within errors. The latter agrees well with the FLAG average while the former is high in comparison (there is good agreement with their previous results, ETM 14 [7]). Since ETM 21A was not published by the FLAG deadline, it is not included in the averages.

There are three other works that enter in light-quark mass averages: FNAL/MILC/TUMQCD 18 [6] (which contributes both to the average of m_{ud} and m_s), and the m_{ud} determinations in HPQCD 18 [13] and HPQCD 14A [14].

While the results of HPQCD 14A and HPQCD 18 agree well (using different methods), there are several tensions in the determination of m_s. The most significant discrepancy is between ETM 21A and the FLAG average. But also two recent and very precise determinations (HPQCD 18 and FNAL/MILC/TUMQCD 18) show a tension. Overall there is a rough agreement between the different determinations with $\chi^2/\text{dof} = 1.7$ (that we apply to our average according to the standard FLAG averaging procedure). In the case of m_{ud} on the other hand only two works contribute to the average: ETM 14 and FNAL/MILC/TUMQCD 18. They disagree, with the FNAL/MILC/TUMQCD 18 value basically matching the $N_f = 2+1$ result. The large $\chi^2/\text{dof} \approx 1.7$ increases significantly the error of the average. These large values of the χ^2 are difficult to understand in terms of a statistical fluctuation. On the other hand the $N_f = 2+1$ and $N_f = 2+1+1$ averages show a good agreement, which increases our confidence in the averages quoted below.

The $N_f = 2+1+1$ results are summarized in Table 7. Note that the results of Ref. [14] are reported as $m_s(2\,\text{GeV}; N_f = 3)$ and those of Ref. [7] as $m_{ud(s)}(2\,\text{GeV}; N_f = 4)$. We convert the former to $N_f = 4$ and obtain $m_s(2\,\text{GeV}; N_f = 4) = 93.7(8)$MeV. The average of FNAL/MILC/TUMQCD 18, HPQCD 18, ETM 14 and HPQCD 14A is 93.43(70)MeV with $\chi^2/\text{dof} = 1.7$. For the light-quark average we use ETM 14 and FNAL/MILC/TUMQCD 18 with an average 3.410(43)MeV and a $\chi^2/\text{dof} = 1.7$. We note these χ^2 values are large. For the case of the light-quark masses this is mostly due to ETM 14 masses lying significantly above the rest, but in the case of m_s there is also some tension between the recent and very precise results of HPQCD 18 and FNAL/MILC/TUMQCD 18. Also note that the 2+1-flavour values are consistent with the four-flavour ones, so in all cases we have decided to simply quote averages according to FLAG rules, including stretching factors for the errors based on χ^2 values of our fits:

$$N_f = 2+1+1: \quad \begin{aligned} m_{ud} &= 3.410(43)\ \text{MeV} && \text{Refs. [6,7]},\\ m_s &= 93.40(57)\ \text{MeV} && \text{Refs. [6,7,13,14]}, \end{aligned} \tag{35}$$

and the RGI values

$$N_f = 2+1+1: \quad \begin{aligned} M_{ud}^{\text{RGI}} &= 4.736(60)_m(55)_\Lambda\ \text{MeV} && \text{Refs. [6,7]},\\ M_s^{\text{RGI}} &= 129.7(0.8)_m(1.5)_\Lambda\ \text{MeV} && \text{Refs. [6,7,13,14]}. \end{aligned} \tag{36}$$

In Figs. 1 and 2 the lattice results listed in Tables 6 and 7 and the FLAG averages obtained at each value of N_f are presented and compared with various phenomenological results.

3.1.5 Lattice determinations of m_s/m_{ud}

The lattice results for m_s/m_{ud} are summarized in Table 8. In the ratio m_s/m_{ud}, one of the sources of systematic error – the uncertainties in the renormalization factors – drops out. Also other systematic effects (like the effect of the scale setting) are reduced in these ratios. This might explain that despite the discrepancies that are present in the individual quark mass determinations, the ratios show an overall very good agreement.

$N_f = 2+1$ lattice calculations

ALPHA 19 [18], discussed already, is the only new result for this section. The other works contributing to this average are RBC/UKQCD 14B, which replaces RBC/UKQCD 12 (see Sect. 3.1.4), and the results of MILC 09A and BMW 10A, 10B.

The results show very good agreement with a $\chi^2/\text{dof} = 0.14$. The final uncertainty ($\approx 0.5\%$) is smaller than the ones of the quark masses themselves. At this level of precision, the uncertainties in the electromagnetic and strong isospin-breaking corrections might not be completely negligible. Nevertheless, we decided not to add any uncertainty associated with this

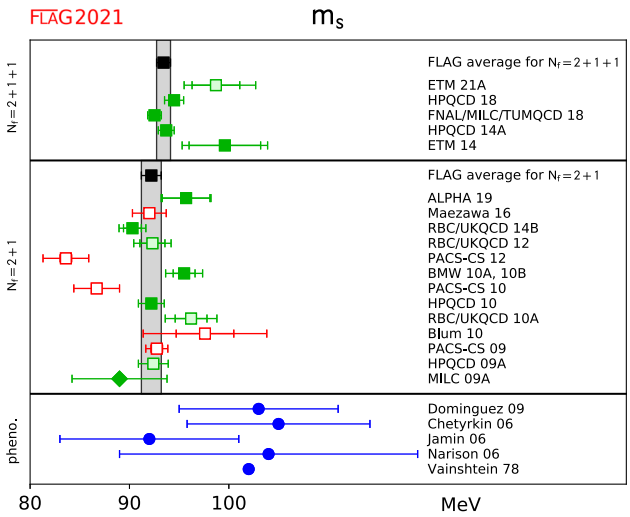

Fig. 1 $\overline{\text{MS}}$ mass of the strange quark (at 2 GeV scale) in MeV. The upper two panels show the lattice results listed in Tables 6 and 7, while the bottom panel collects sum rule results [205–209]. Diamonds and squares represent results based on perturbative and nonperturbative renormalization, respectively. The black squares and the grey bands represent our averages (33) and (35). The significance of the colours is explained in Sect. 2

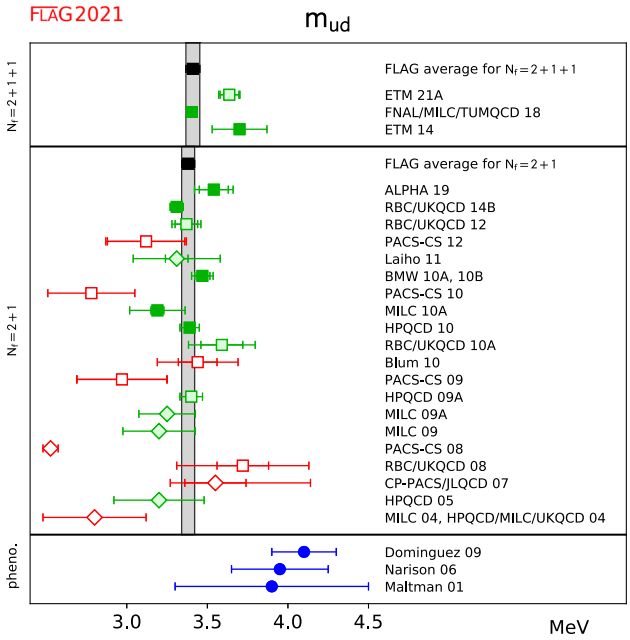

Fig. 2 Mean mass of the two lightest quarks, $m_{ud} = \frac{1}{2}(m_u + m_d)$. The bottom panel shows results based on sum rules [205,208,210] (for more details see Fig. 1)

effect. The main reason is that most recent determinations try to estimate this uncertainty themselves and found an effect smaller than naive power counting estimates (see $N_f = 2 + 1 + 1$ section),

$$N_f = 2 + 1 : \qquad m_s/m_{ud} = 27.42\ (12) \qquad \text{Refs. [8–10,15,18].} \tag{37}$$

$N_f = 2 + 1 + 1$ lattice calculations

For $N_f = 2 + 1 + 1$ there are three results, MILC 17 [16], ETM 14 [7] and FNAL/MILC 14A [17], all of which satisfy our selection criteria.

Table 8 Lattice results for the ratio m_s/m_{ud}

Collaboration	Refs.	N_f	Publication status	Chiral extrapolation	Continuum extrapolation	Finite volume	m_s/m_{ud}
ETM 21A	[204]	2+1+1	P	★	★	★	$27.17(32)^{+56}_{-38}$
MILC 17 ‡	[16]	2+1+1	A	★	★	★	$27.178(47)^{+86}_{-57}$
FNAL/MILC 14A	[17]	2+1+1	A	★	★	★	$27.35(5)^{+10}_{-7}$
ETM 14	[7]	2+1+1	A	○	★	○	26.66(32)(2)
ALPHA 19	[18]	2+1	A	○	★	★	27.0(1.0)(0.4)
RBC/UKQCD 14B	[8]	2+1	A	★	★	★	27.34(21)
RBC/UKQCD 12⊖	[188]	2+1	A	★	○	★	27.36(39)(31)(22)
PACS-CS 12⋆	[190]	2+1	A	★	■	■	26.8(2.0)
Laiho 11	[49]	2+1	C	○	★	★	28.4(0.5)(1.3)
BMW 10A, 10B+	[9,10]	2+1	A	★	★	★	27.53(20)(8)
RBC/UKQCD 10A	[117]	2+1	A	○	○	★	26.8(0.8)(1.1)
Blum 10†	[170]	2+1	A	○	■	○	28.31(0.29)(1.77)
PACS-CS 09	[192]	2+1	A	★	■	■	31.2(2.7)
MILC 09A	[15]	2+1	C	○	★	★	27.41(5)(22)(0)(4)
MILC 09	[157]	2+1	A	○	★	★	27.2(1)(3)(0)(0)
PACS-CS 08	[193]	2+1	A	★	■	■	28.8(4)
RBC/UKQCD 08	[194]	2+1	A	○	■	★	28.8(0.4)(1.6)
MILC 04, HPQCD/MILC/UKQCD 04	[197,198]	2+1	A	○	○	○	27.4(1)(4)(0)(1)

‡The calculation includes electromagnetic effects
⊖The errors are statistical, chiral and finite volume
⋆The calculation includes electromagnetic and $m_u \neq m_d$ effects through reweighting
+The fermion action used is tree-level improved
†The calculation includes quenched electromagnetic effects

All these works have been discussed in the previous FLAG edition [4], except the new result ETM 21A, that we have already examined (and anyway does not appear in the average because it was unpublished at the deadline). The fit has $\chi^2/\text{dof} \approx 2.5$, and the result shows reasonable agreement with the $N_f = 2+1$ result.

$$N_f = 2+1+1: \qquad m_s/m_{ud} = 27.23\ (10) \qquad \text{Refs. [7,16,17]}, \tag{38}$$

which corresponds to an overall uncertainty equal to 0.4%. It is worth noting that [16] estimates the EM effects in this quantity to be $\sim 0.18\%$ (or 0.049 which is less than the quoted error above).

All the lattice results listed in Table 8 as well as the FLAG averages for each value of N_f are reported in Fig. 3 and compared with χPT and sum rules.

3.1.6 Lattice determination of m_u and m_d

In addition to reviewing computations of individual m_u and m_d quark masses, we will also determine FLAG averages for the parameter ϵ related to the violations of Dashen's theorem

$$\epsilon = \frac{(\Delta M_K^2 - \Delta M_\pi^2)^\gamma}{\Delta M_\pi^2}, \tag{39}$$

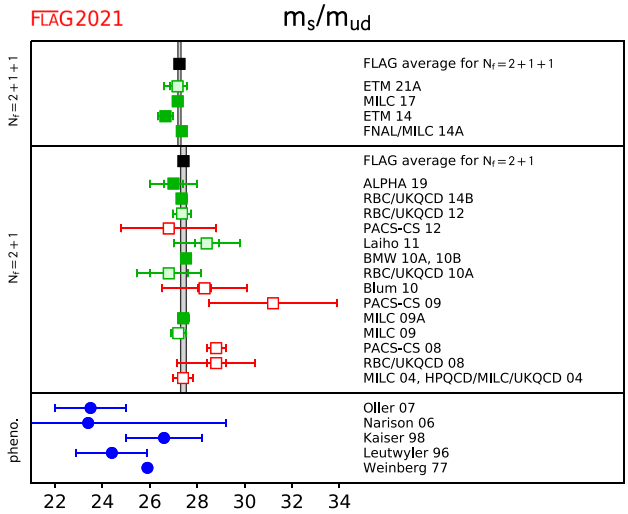

Fig. 3 Results for the ratio m_s/m_{ud}. The upper part indicates the lattice results listed in Table 8 together with the FLAG averages for each value of N_f. The lower part shows results obtained from χPT and sum rules [208,211–215]

where $\Delta M_\pi^2 = M_{\pi^+}^2 - M_{\pi^0}^2$ and $\Delta M_K^2 = M_{K^+}^2 - M_{K^0}^2$ are the pion and kaon squared mass splittings, respectively. The superscript γ, here and in the following, denotes corrections that arise from electromagnetic effects only. This parameter is often a crucial intermediate quantity in the extraction of the individual light-quark masses. Indeed, it can be shown, using the G-parity symmetry of the pion triplet, that ΔM_π^2 does not receive $\mathcal{O}(\delta m)$ isospin-breaking corrections. In other words

$$\Delta M_\pi^2 = (\Delta M_\pi^2)^\gamma \qquad \text{and} \qquad \epsilon = \frac{(\Delta M_K^2)^\gamma}{\Delta M_\pi^2} - 1, \tag{40}$$

at leading-order in the isospin-breaking expansion. The difference $(\Delta M_\pi^2)^{SU(2)}$ was estimated in previous editions of FLAG through the ϵ_m parameter. However, consistent with our leading-order truncation of the isospin-breaking expansion, it is simpler to ignore this term. Once known, ϵ allows one to consistently subtract the electromagnetic part of the kaon-mass splitting to obtain the QCD splitting $(\Delta M_K^2)^{SU(2)}$. In contrast with the pion, the kaon QCD splitting is sensitive to δm, and, in particular, proportional to it at leading order in χPT. Therefore, the knowledge of ϵ allows for the determination of δm from a chiral fit to lattice-QCD data. Originally introduced in another form in [216], ϵ vanishes in the $SU(3)$ chiral limit, a result known as Dashen's theorem. However, in the 1990s numerous phenomenological papers pointed out that ϵ might be an $\mathcal{O}(1)$ number, indicating a significant failure of $SU(3)$ χPT in the description of electromagnetic effects on light-meson masses. However, the phenomenological determinations of ϵ feature some level of controversy, leading to the rather imprecise estimate $\epsilon = 0.7(5)$ given in the first edition of FLAG. Starting with the FLAG 19 edition of the review, we quote more precise averages for ϵ, directly obtained from lattice-QCD+QED simulations. We refer the reader to earlier editions of FLAG and to the review [217] for discussions of the phenomenological determinations of ϵ.

The quality criteria regarding finite-volume effects for calculations including QED are presented in Sect. 2.1.1. Due to the long-distance nature of the electromagnetic interaction, these effects are dominated by a power law in the lattice spatial size. The coefficients of this expansion depend on the chosen finite-volume formulation of QED. For QED_L, these effects on the squared mass M^2 of a charged meson are given by [147,148,150]

$$\Delta_\text{FV} M^2 = \alpha M^2 \left\{ \frac{c_1}{ML} + \frac{2c_1}{(ML)^2} + \mathcal{O}\left[\frac{1}{(ML)^3}\right] \right\}, \tag{41}$$

with $c_1 \simeq -2.83730$. It has been shown in [147] that the two first orders in this expansion are exactly known for hadrons, and are equal to the pointlike case. However, the $\mathcal{O}[1/(ML)^3]$ term and higher orders depend on the structure of the hadron. The universal corrections for QED_TL can also be found in [147]. In all this part, for all computations using such universal formulae, the QED finite-volume quality criterion has been applied with $n_\text{min} = 3$, otherwise $n_\text{min} = 1$ was used.

Since FLAG 19, six new results have been reported for nondegenerate light-quark masses. In the $N_f = 2+1+1$ sector, MILC 18 [21] computed ϵ using $N_f = 2+1$ asqtad electro-quenched QCD+QED_TL simulations and extracted the ratio

m_u/m_d from a new set of $N_f = 2+1+1$ HISQ QCD simulations. Although ϵ comes from $N_f = 2+1$ simulations, $(\Delta M_K^2)^{SU(2)}$, which is about three times larger than $(\Delta M_K^2)^{\gamma}$, has been determined in the $N_f = 2+1+1$ theory. We therefore chose to classify this result as a four-flavour one. This result is explicitly described by the authors as an update of MILC 17 [16]. In MILC 17 [16], m_u/m_d is determined as a side-product of a global analysis of heavy-meson decay constants, using a preliminary version of ϵ from MILC 18 [21]. In FNAL/MILC/TUMQCD 18 [6] the ratio m_u/m_d from MILC 17 [16] is used to determine the individual masses m_u and m_d from a new calculation of m_{ud}. The work RM123 17 [19] is the continuation of the $N_f = 2$ work named RM123 13 [172] in the previous edition of FLAG. This group now uses $N_f = 2+1+1$ ensembles from ETM 10 [218], however, still with a rather large minimum pion mass of 270 MeV, leading to the ○ rating for chiral extrapolations. In the $N_f = 2+1$ sector, BMW 16 [20] reuses the data set produced from their determination of the light-baryon octet-mass splittings [173] using electro-quenched QCD+QED_{TL} smeared clover fermion simulations. Finally, MILC 16 [219], which is a preliminary result for the value of ϵ published in MILC 18 [21], also provides a $N_f = 2+1$ computation of the ratio m_u/m_d.

MILC 09A [15] uses the mass difference between K^0 and K^+, from which they subtract electromagnetic effects using Dashen's theorem with corrections, as discussed in the introduction of this section. The up and down sea quarks remain degenerate in their calculation, fixed to the value of m_{ud} obtained from M_{π^0}. To determine m_u/m_d, BMW 10A, 10B [9,10] follow a slightly different strategy. They obtain this ratio from their result for m_s/m_{ud} combined with a phenomenological determination of the isospin-breaking quark-mass ratio $Q = 22.3(8)$, from $\eta \to 3\pi$ decays [220] (the decay $\eta \to 3\pi$ is very sensitive to QCD isospin breaking, but fairly insensitive to QED isospin breaking). Instead of subtracting electromagnetic effects using phenomenology, RBC 07 [169] and Blum 10 [170] actually include a quenched electromagnetic field in their calculation. This means that their results include corrections to Dashen's theorem, albeit only in the presence of quenched electromagnetism. Since the up and down quarks in the sea are treated as degenerate, very small isospin corrections are neglected, as in MILC's calculation. PACS-CS 12 [190] takes the inclusion of isospin-breaking effects one step further. Using reweighting techniques, it also includes electromagnetic and $m_u - m_d$ effects in the sea. However, they do not correct for the large finite-volume effects coming from electromagnetism in their $M_\pi L \sim 2$ simulations, but provide rough estimates for their size, based on Ref. [179]. QCDSF/UKQCD 15 [221] uses QCD+QED dynamical simulations performed at the $SU(3)$-flavour-symmetric point, but at a single lattice spacing, so they do not enter our average. The smallest partially quenched ($m_{\text{sea}} \neq m_{\text{val}}$) pion mass is greater than 200 MeV, so our chiral-extrapolation criteria require a ○ rating. Concerning finite-volume effects, this work uses three spatial extents L of 1.6 fm, 2.2 fm, and 3.3 fm. QCDSF/UKQCD 15 claims that the volume dependence is not visible on the two largest volumes, leading them to assume that finite-size effects are under control. As a consequence of that, the final result for quark masses does not feature a finite-volume extrapolation or an estimation of the finite-volume uncertainty. However, in their work on the QED corrections to the hadron spectrum [221] based on the same ensembles, a volume study shows some level of compatibility with the QED_{L} finite-volume effects derived in [148]. We see two issues here. Firstly, the analytical result quoted from [148] predicts large, $\mathcal{O}(10\%)$ finite-size effects from QED on the meson masses at the values of $M_\pi L$ considered in QCDSF/UKQCD 15, which is inconsistent with the statement made in the paper. Secondly, it is not known that the zero-mode regularization scheme used here has the same volume scaling as QED_{L}. We therefore chose to assign the ■ rating for finite volume to QCDSF/UKQCD 15. Finally, for $N_f = 2+1+1$, ETM 14 [7] uses simulations in pure QCD, but determines $m_u - m_d$ from the slope $\partial M_K^2/\partial m_{ud}$ and the physical value for the QCD kaon-mass splitting taken from the phenomenological estimate in FLAG 13.

Lattice results for m_u, m_d and m_u/m_d are summarized in Table 9. The colour coding is specified in detail in Sect. 2.1. Considering the important progress in the last years on including isospin-breaking effects in lattice simulations, we are now in a position where averages for m_u and m_d can be made without the need of phenomenological inputs. Therefore, lattice calculations of the individual quark masses using phenomenological inputs for isospin-breaking effects will be coded ■.

We start by recalling the $N_f = 2$ FLAG average for the light-quark masses, entirely coming from RM123 13 [172],

$$N_f = 2: \quad \begin{aligned} m_u &= 2.40(23)\,\text{MeV} && \text{Ref. [172]}, \\ m_d &= 4.80(23)\,\text{MeV} && \text{Ref. [172]}, \\ m_u/m_d &= 0.50(4) && \text{Ref. [172]}, \end{aligned} \tag{42}$$

with errors of roughly 10%, 5% and 8%, respectively. In these results, the errors are obtained by combining the lattice statistical and systematic errors in quadrature. For $N_f = 2+1$, the only result, which qualifies for entering the FLAG average for quark masses, is BMW 16 [20],

Table 9 Lattice results for m_u, m_d (MeV) and for the ratio m_u/m_d. The values refer to the $\overline{\text{MS}}$ scheme at scale 2 GeV. The top part of the table lists the results obtained with $N_f = 2+1+1$, while the lower part presents calculations with $N_f = 2+1$

Collaboration	Refs.	Publication status	Chiral extrapolation	Continuum extrapolation	Finite volume	Isospin breaking	Renormalization	Running	m_u	m_d	m_u/m_d
MILC 18	[21]	A	★	★	★	○	★	–			$0.4529(48)(^{+150}_{-67})$
FNAL/MILC/TUMQCD 18*	[6]	A	★	★	★	○	★	–	2.118(17)(32)(12)(03)	4.690(30)(36)(26)(06)	
MILC 17†	[16]	A	★	★	★	○	★	–			$0.4556(55)(^{+114}_{-67})(13)$
RM123 17	[19]	A	○	★	★	○	★	*b*	2.50(15)(8)(2)	4.88(18)(8)(2)	0.513(18)(24)(6)
ETM 14	[7]	A	★	★	★	■	★	*b*	2.36(24)	5.03(26)	0.470(56)
BMW 16	[20]	A	★	★	★	○	★	–	2.27(6)(5)(4)	4.67(6)(5)(4)	0.485(11)(8)(14)
MILC 16	[219]	C	○	★	★	○	★	–			$0.4582(38)(^{+12}_{-82})(1)(110)$
QCDSF/UKQCD 15	[221]	A	○	■	■	★	–	–			0.52(5)
PACS-CS 12	[190]	A	★	■	■	★	★	*a*	2.57(26)(7)	3.68(29)(10)	0.698(51)
Laiho 11	[49]	C	○	★	★	■	○	–	1.90(8)(21)(10)	4.73(9)(27)(24)	0.401(13)(45)
HPQCD 10‡	[11]	A	○	★	★	■	★	–	2.01(14)	4.77(15)	
BMW 10A, 10B+	[9,10]	A	★	★	★	■	★	*b*	2.15(03)(10)	4.79(07)(12)	0.448(06)(29)
Blum 10	[170]	A	○	■	○	○	★	–	2.24(10)(34)	4.65(15)(32)	0.4818(96)(860)
MILC 09A	[15]	C	○	★	★	■	○	–	1.96(0)(6)(10)(12)	4.53(1)(8)(23)(12)	0.432(1)(9)(0)(39)
MILC 09	[157]	A	○	★	★	■	○	–	1.9(0)(1)(1)(1)	4.6(0)(2)(2)(1)	0.42(0)(1)(0)(4)
MILC 04, HPQCD/ MILC/UKQCD 04	[197,198]	A	○	○	○	■	■	–	1.7(0)(1)(2)(2)	3.9(0)(1)(4)(2)	0.43(0)(1)(0)(8)

*FNAL/MILC/TUMQCD 18 uses ϵ from MILC 18 to produce the individual m_u and m_d masses

†MILC 17 additionally quotes an optional 0.0032 uncertainty on m_u/m_d corresponding to QED and QCD separation scheme ambiguities. Because this variation is not per se an error on the determination of m_u/m_d, and because it is generally not included in other results, we choose to omit it here

‡Values obtained by combining the HPQCD 10 result for m_s with the MILC 09 results for m_s/m_{ud} and m_u/m_d

+The fermion action used is tree-level improved

a The masses are renormalized and run nonperturbatively up to a scale of 100 GeV in the $N_f = 2$ SF scheme. In this scheme, nonperturbative and NLO running for the quark masses are shown to agree well from 100 GeV all the way down to 2 GeV [222]

b The masses are renormalized and run nonperturbatively up to a scale of 4 GeV in the $N_f = 3$ RI-MOM scheme. In this scheme, nonperturbative and N^3LO running for the quark masses are shown to agree from 6 GeV down to 3 GeV to better than 1% [10]

$$N_f = 2+1: \quad \begin{array}{ll} m_u = 2.27(9)\,\text{MeV} & \text{Ref. [20]}, \\ m_d = 4.67(9)\,\text{MeV} & \text{Ref. [20]}, \\ m_u/m_d = 0.485(19) & \text{Ref. [20]}, \end{array} \tag{43}$$

with errors of roughly 4%, 2% and 4%, respectively. This estimate is slightly more precise than in the previous edition of FLAG. More importantly, it now comes entirely from a lattice-QCD+QED calculation, whereas phenomenological input was used in previous editions. These numbers result in the following RGI averages

$$N_f = 2+1: \quad \begin{array}{ll} M_u^{\text{RGI}} = 3.15(12)_m(4)_\Lambda\,\text{MeV} & \text{Ref. [20]}, \\ M_d^{\text{RGI}} = 6.49(12)_m(7)_\Lambda\,\text{MeV} & \text{Ref. [20]}. \end{array} \tag{44}$$

Finally, for $N_f = 2+1+1$, RM123 17 [19] and FNAL/MILC/TUMQCD 18 [6] enter the average for the individual m_u and m_d masses, and RM123 17 [19] and MILC 18 [21] enter the average for the ratio m_u/m_d, giving

$$N_f = 2+1+1: \quad \begin{array}{ll} m_u = 2.14(8)\,\text{MeV} & \text{Refs. [6,19]}, \\ m_d = 4.70(5)\,\text{MeV} & \text{Refs. [6,19]}, \\ m_u/m_d = 0.465(24) & \text{Refs. [19,21]} \end{array} \tag{45}$$

with errors of roughly 4%, 1% and 5%, respectively. One can observe some marginal discrepancies between results coming from the MILC collaboration and RM123 17 [19]. More specifically, adding all sources of uncertainties in quadrature, one obtains a 1.7σ discrepancy between RM123 17 [19] and MILC 18 [21] for m_u/m_d, and a 2.2σ discrepancy between RM123 17 [19] and FNAL/MILC/TUMQCD 18 [6] for m_u. However, the values of m_d and ϵ are in very good agreement between the two groups. These discrepancies are presently too weak to constitute evidence for concern, and will be monitored as more lattice groups provide results for these quantities. The RGI averages for m_u and m_d are

$$N_f = 2+1+1: \quad \begin{array}{ll} M_u^{\text{RGI}} = 2.97(11)_m(3)_\Lambda\,\text{MeV} & \text{Refs. [6,19]}, \\ M_d^{\text{RGI}} = 6.53(7)_m(8)_\Lambda\,\text{MeV} & \text{Refs. [6,19]}. \end{array} \tag{46}$$

Every result for m_u and m_d used here to produce the FLAG averages relies on electro-quenched calculations, so there is some interest to comment on the size of quenching effects. Considering phenomenology and the lattice results presented here, it is reasonable for a rough estimate to use the value $(\Delta M_K^2)^\gamma \sim 2000\ \text{MeV}^2$ for the QED part of the kaon-mass splitting. Using the arguments presented in Sect. 3.1.3, one can assume that the QED sea contribution represents $\mathcal{O}(10\%)$ of $(\Delta M_K^2)^\gamma$. Using $SU(3)$ PQχPT+QED [174,223] gives a $\sim 5\%$ effect. Keeping the more conservative 10% estimate and using the experimental value of the kaon-mass splitting, one finds that the QCD kaon-mass splitting $(\Delta M_K^2)^{SU(2)}$ suffers from a reduced 3% quenching uncertainty. Considering that this splitting is proportional to $m_u - m_d$ at leading order in $SU(3)$ χPT, we can estimate that a similar error will propagate to the quark masses. So the individual up and down masses look mildly affected by QED quenching. However, one notices that $\sim 3\%$ is the level of error in the new FLAG averages, and increasing significantly this accuracy will require using fully unquenched calculations.

In view of the fact that a *massless up quark* would solve the strong CP problem, many authors have considered this an attractive possibility, but the results presented above exclude this possibility: the value of m_u in Eq. (43) differs from zero by 26 standard deviations. We conclude that nature solves the strong CP problem differently.

Finally, we conclude this section by giving the FLAG averages for ϵ defined in Eq. (39). For $N_f = 2+1+1$, we average the results of RM123 17 [19] and MILC 18 [21] with the value of $(\Delta M_K^2)^\gamma$ from BMW 14 [147] combined with Eq. (40), giving

$$N_f = 2+1+1: \quad \epsilon = 0.79(6) \quad \text{Refs. [19,21,147]}. \tag{47}$$

Although BMW 14 [147] focuses on hadron masses and did not extract the light-quark masses, they are the only fully unquenched QCD+QED calculation to date that qualifies to enter a FLAG average. With the exception of renormalization, which is not discussed in the paper, this work has a ★ rating for every FLAG criterion considered for the m_u and m_d quark

masses. For $N_f = 2+1$ we use the results from BMW 16 [20],

$$N_f = 2+1: \qquad \epsilon = 0.73(17) \qquad \text{Ref. [20].} \tag{48}$$

It is important to notice that the ϵ uncertainties from BMW 16 and RM123 17 are dominated by estimates of the QED quenching effects. Indeed, in contrast with the quark masses, ϵ is expected to be rather sensitive to the sea-quark QED contributions. Using the arguments presented in Sect. 3.1.3, if one conservatively assumes that the QED sea contributions represent $\mathcal{O}(10\%)$ of $(\Delta M_K^2)^\gamma$, then Eq. (40) implies that ϵ will have a quenching error of ~ 0.15 for $(\Delta M_K^2)^\gamma \sim 2000\,\text{MeV}^2$, representing a large $\sim 20\%$ relative error. It is interesting to observe that such a discrepancy does not appear between BMW 15 and RM123 17, although the $\sim 10\%$ accuracy of both results might not be sufficient to resolve these effects. On the other hand, in the context of $SU(3)$ chiral perturbation theory, Bijnens and Danielsson [174] show that the QED quenching effects on ϵ do not depend on unknown LECs at NLO and are therefore computable at that order. In that approach, MILC 18 finds the effect at NLO to be only 5%. To conclude, although the controversy around the value of ϵ has been significantly reduced by lattice-QCD+QED determinations, computing this at few-percent accuracy requires simulations with charged sea quarks.

3.1.7 Estimates for R and Q

The quark-mass ratios

$$R \equiv \frac{m_s - m_{ud}}{m_d - m_u} \quad \text{and} \quad Q^2 \equiv \frac{m_s^2 - m_{ud}^2}{m_d^2 - m_u^2} \tag{49}$$

compare $SU(3)$ breaking with isospin breaking. Both numbers only depend on the ratios m_s/m_{ud} and m_u/m_d,

$$R = \frac{1}{2}\left(\frac{m_s}{m_{ud}} - 1\right)\frac{1+\frac{m_u}{m_d}}{1-\frac{m_u}{m_d}} \qquad \text{and} \qquad Q^2 = \frac{1}{2}\left(\frac{m_s}{m_{ud}} + 1\right) R. \tag{50}$$

The quantity Q is of particular interest because of a low-energy theorem [224], which relates it to a ratio of meson masses,

$$Q_M^2 \equiv \frac{\hat{M}_K^2}{\hat{M}_\pi^2}\frac{\hat{M}_K^2 - \hat{M}_\pi^2}{\hat{M}_{K^0}^2 - \hat{M}_{K^+}^2}, \qquad \hat{M}_\pi^2 \equiv \frac{1}{2}(\hat{M}_{\pi^+}^2 + \hat{M}_{\pi^0}^2), \qquad \hat{M}_K^2 \equiv \frac{1}{2}(\hat{M}_{K^+}^2 + \hat{M}_{K^0}^2). \tag{51}$$

(We remind the reader that the $\hat{}$ denotes a quantity evaluated in the $\alpha \to 0$ limit.) Chiral symmetry implies that the expansion of Q_M^2 in powers of the quark masses (i) starts with Q^2 and (ii) does not receive any contributions at NLO:

$$Q_M \overset{\text{NLO}}{=} Q. \tag{52}$$

We recall here the $N_f = 2$ estimates for Q and R from FLAG 16,

$$R = 40.7(3.7)(2.2), \qquad Q = 24.3(1.4)(0.6), \tag{53}$$

where the second error comes from the phenomenological inputs that were used. For $N_f = 2+1$, we use Eqs. (37) and (43) and obtain

$$R = 38.1(1.5), \qquad Q = 23.3(0.5), \tag{54}$$

where now only lattice results have been used. For $N_f = 2+1+1$ we obtain

$$R = 35.9(1.7), \qquad Q = 22.5(0.5), \tag{55}$$

which are quite compatible with two- and three-flavour results. It is interesting to notice that the most recent phenomenological determination of R and Q from $\eta \to 3\pi$ decay [225] gives the values $R = 34.4(2.1)$ and $Q = 22.1(7)$, which are marginally discrepant with some of the averages presented here. The authors of [225,226] point out that this discrepancy is likely due to surprisingly large corrections to the approximation in Eq. (52) used in the phenomenological analysis.

Our final results for the masses m_u, m_d, m_{ud}, m_s and the mass ratios m_u/m_d, m_s/m_{ud}, R, Q are collected in Tables 10 and 11.

Table 10 Our estimates for the strange-quark and the average up-down-quark masses in the $\overline{\text{MS}}$ scheme at running scale $\mu = 2\,\text{GeV}$. Mass values are given in MeV. In the results presented here, the error is the one which we obtain by applying the averaging procedure of Sect. 2.3 to the relevant lattice results.

N_f	m_{ud}	m_s	m_s/m_{ud}
2+1+1	3.410(43)	93.44(68)	27.23(10)
2+1	3.364(41)	92.03(88)	27.42(12)

Table 11 Our estimates for the masses of the two lightest quarks and related, strong isospin-breaking ratios. Again, the masses refer to the $\overline{\text{MS}}$ scheme at running scale $\mu = 2\,\text{GeV}$. Mass values are given in MeV

N_f	m_u	m_d	m_u/m_d	R	Q
2+1+1	2.14(8)	4.70(5)	0.465(24)	35.9(1.7)	22.5(0.5)
2+1	2.27(9)	4.67(9)	0.485(19)	38.1(1.5)	23.3(0.5)

3.2 Charm-quark mass

In the following, we collect and discuss the lattice determinations of the $\overline{\text{MS}}$ charm-quark mass $\overline{m}_c$. Most of the results have been obtained by analyzing the lattice-QCD simulations of two-point heavy-light- or heavy-heavy-meson correlation functions, using as input the experimental values of the D, D_s, and charmonium mesons. Some groups use the moments method. The latter is based on the lattice calculation of the Euclidean time moments of pseudoscalar-pseudoscalar correlators for heavy-quark currents followed by an OPE expansion dominated by perturbative QCD effects, which provides the determination of both the heavy-quark mass and the strong-coupling constant α_s.

The heavy-quark actions adopted by various lattice collaborations have been discussed in previous FLAG reviews [2–4], and their descriptions can be found in Sec. A.1.3 of FLAG 19 [4]. While the charm mass determined with the moments method does not need any lattice evaluation of the mass-renormalization constant Z_m, the extraction of $\overline{m}_c$ from two-point heavy-meson correlators does require the nonperturbative calculation of Z_m. The lattice scale at which Z_m is obtained is usually at least of the order 2–3 GeV, and therefore it is natural in this review to provide the values of $\overline{m}_c(\mu)$ at the renormalization scale $\mu = 3$ GeV. Since the choice of a renormalization scale equal to $\overline{m}_c$ is still commonly adopted (as by the PDG [165]), we have collected in Table 12 the lattice results for both $\overline{m}_c(\overline{m}_c)$ and $\overline{m}_c(3\,\text{GeV})$, obtained for $N_f = 2+1$ and $2+1+1$. For $N_f = 2$, interested readers are referred to previous reviews [2,3].

When not directly available in the published work, we apply a conversion factor using perturbative QCD evolution at five loops to run down from $\mu = 3$ GeV to the scales $\mu = \overline{m}_c$ and 2 GeV of 0.7739(60) and 0.9026(23), respectively, where the error comes from the uncertainty in Λ_{QCD}. We use $\Lambda_{\text{QCD}} = 297(12)$ MeV for $N_f = 4$ (see Sect. 9). Perturbation theory uncertainties, estimated as the difference between results that use 4- and 5-loop running, are significantly smaller than the parametric uncertainty coming from Λ_{QCD}. For $\mu = \overline{m}_c$, the former is about about 2.5 times smaller. Given the high precision of many of these results, future works should take the uncertainties in Λ_{QCD} and perturbation theory seriously.

In the next subsections we review separately the results for $\overline{m}_c$ with three or four flavours of quarks in the sea.

3.2.1 $N_f = 2+1$ results

Since the last review [4], there are two new results, Petreczky 19 [26] and ALPHA 21 [227], the latter of which was not published at the FLAG deadline. Petreczky 19 employs the HISQ action on ten ensembles with ten lattice spacings down to 0.025 fm, physical strange-quark mass, and two light-quark masses, the lightest corresponding to 161 MeV pions. Their study incorporates lattices with 11 different sizes, ranging from 1.6 to 5.4 fm. The masses are computed from moments of pseudoscalar quarkonium correlation functions, and $\overline{\text{MS}}$ masses are extracted with 4-loop continuum perturbation theory. Thus this work easily rates green stars in all categories. ALPHA 21 uses the $\mathcal{O}(a)$-improved Wilson-clover action with five lattice spacings from 0.087 to 0.039 fm, produced by the CLS collaboration. For each lattice spacing, several light sea-quark masses are used in a global chiral-continuum extrapolation (the lightest pion mass for one ensemble is 198 MeV). The authors also use nonperturbative renormalization and running through application of step-scaling and the Schrödinger functional scheme. Finite-volume effects are investigated at one lattice spacing and only for $\sim$ 400 MeV pions on the smallest two

Table 12 Lattice results for the $\overline{\text{MS}}$ charm-quark mass $\overline{m}_c(\overline{m}_c)$ and $\overline{m}_c(3\text{ GeV})$ in GeV, together with the colour coding of the calculations used to obtain them

Collaboration	Refs.	N_f	Publication status	Chiral extrapolation	Continuum extrapolation	Finite volume	Renormalization	$\overline{m}_c(\overline{m}_c)$	$\overline{m}_c(3\text{ GeV})$
ETM 21A	[204]	2+1+1	P	★	★	★	★	$1.339(22)(^{+19}_{-10})(10)^{\dagger}$	$1.036(17)(^{+15}_{-8})$
HPQCD 20A	[23]	2+1+1	A	★	★	★	★	1.2719(78)	0.9841(51)
HPQCD 18	[13]	2+1+1	A	★	★	★	★	1.2757(84)	0.9896(61)
FNAL/MILC/ TUMQCD 18	[6]	2+1+1	A	★	★	★	–	1.273(4)(1)(10)	0.9837(43)(14)(33)(5)
HPQCD 14A	[14]	2+1+1	A	★	★	★	–	1.2715(95)	0.9851(63)
ETM 14A	[22]	2+1+1	A	○	★	○	★	1.3478(27)(195)	1.0557(22)(153)*
ETM 14	[7]	2+1+1	A	○	★	○	★	1.348(46)	1.058(35)*
ALPHA 21	[227]	2+1	A^{+}	★	★	★	★	1.296(19)	1.007(16)
Petreczky 19	[26]	2+1	A	★	★	★	★	1.265(10)	1.001(16)
Maezawa 16	[189]	2+1	A	■	★	★	★	1.267(12)	
JLQCD 16	[25]	2+1	A	○	★	★	–	1.2871(123)	1.0033(96)
χQCD 14	[24]	2+1	A	○	○	○	★	1.304(5)(20)	1.006(5)(22)
HPQCD 10	[11]	2+1	A	○	★	○	–	1.273(6)	0.986(6)
HPQCD 08B	[202]	2+1	A	○	★	○	–	1.268(9)	0.986(10)
PDG	[165]							1.27(2)	

†We applied the running factor 0.7739(60) for $\mu = 3$ GeV to $\overline{m}_c$. The errors are statistical, systematic, and the uncertainty in the running factor
*A running factor equal to 0.900 between the scales $\mu = 2$ GeV and $\mu = 3$ GeV was applied by us
$^{+}$Published after the FLAG deadline

volumes where results are compatible within statistical errors. ALPHA 21 satisfies the FLAG criteria for green-star ratings in all of the categories listed in Table 12, but because it is a new result that was unpublished at the deadline, does not enter the average in this review.

Descriptions of the other works in this section can be found in the last review [4].

According to our rules on the publication status, the FLAG average for the charm-quark mass at $N_f = 2 + 1$ is obtained by combining the results HPQCD 10, χQCD 14, JLQCD 16, and Petreczky 19,

$$N_f = 2 + 1: \quad \overline{m}_c(\overline{m}_c) = 1.275(5)\text{ GeV} \quad \text{Refs. [11,24–26]}, \tag{56}$$

$$\overline{m}_c(3\text{ GeV}) = 0.992(5)\text{ GeV} \quad \text{Refs. [11,24–26]}, \tag{57}$$

where the error on $\overline{m}_c(\overline{m}_c)$ includes a stretching factor $\sqrt{\chi^2/\text{dof}} \simeq 1.16$ as discussed in Sect. 2.2. This result corresponds to the following RGI average

$$M_c^{\text{RGI}} = 1.526(9)_m(14)_\Lambda\text{ GeV} \quad \text{Refs. [11,24–26]}. \tag{58}$$

3.2.2 $N_f = 2 + 1 + 1$ results

For a discussion of older results, see the previous FLAG reviews. Since FLAG 19 two groups have produced updated values with charm quarks in the sea.

HPQCD 20A [23] is an update of HPQCD 18, including a new finer ensemble ($a \approx 0.045$ fm) and EM corrections computed in the quenched approximation of QED for the first time. Besides these new items, the analysis is largely unchanged from

HPQCD 18 except for an added α_s^3 correction to the SMOM-to-$\overline{\text{MS}}$ conversion factor and tuning the bare charm mass via the J/ψ mass rather than the η_c. Their new value in pure QCD is $\overline{m}_c(3\text{ GeV}) = 0.9858(51)$ GeV which is quite consistent with HPQCD 18 and the FLAG 19 average. The effects of quenched QED in both the bare charm-quark mass and the renormalization constant are small. Both effects are precisely determined, and the overall effect shifts the mass down slightly to $\overline{m}_c(3\text{ GeV}) = 0.9841(51)$ where the uncertainty due to QED is invisible in the final error. The shift from their pure QCD value due to quenched QED is about -0.2%.

ETM 21A [204] is a new work that follows a similar methodology as ETM 14, but with significant improvements. Notably, a clover-term is added to the twisted mass fermion action which suppresses $\mathcal{O}(a^2)$ effects between the neutral and charged pions. Additional improvements include new ensembles lying very close to the physical mass point, better control of nonperturbative renormalization systematics, and use of both meson and baryon correlation functions to determine the quark mass. They use the RI-MOM scheme for nonperturbative renormalization. The analysis comprises ten ensembles in total with three lattice spacings (0.095, 0.082, and 0.069 fm), two volumes for the finest lattice spacings and four for the other two, and pion masses down to 134 MeV for the finest ensemble. The values of $m_\pi L$ range mostly from almost four to greater than five. According to the FLAG criteria, green stars are earned in all categories. The authors find $m_c(3\text{ GeV}) = 1.036(17)(^{+15}_{-8})$ GeV. In Table 12 we have applied a factor of 0.7739(60) to run from 3 GeV to $\overline{m}_c$. As in FLAG 19, the new value is consistent with ETM 14 and ETM 14A, but is still high compared to the FLAG average. The authors plan future improvements, including a finer lattice spacing for better control of the continuum limit and a new renormalization scheme, like RI-SMOM. This result has not been published by the deadline, so it does not yet appear in the average.

Five results enter the FLAG average for $N_f = 2+1+1$ quark flavours: ETM 14, ETM 14A, HPQCD 14A, FNAL/MILC/TUMQCD 18, and HPQCD 20A. We note that while the determinations of $\overline{m}_c$ by ETM 14 and 14A agree well with each other, they are incompatible with HPQCD 14A, FNAL/MILC/TUMQCD 18, and HPQCD 20A by several standard deviations. While the latter use the same configurations, the analyses are quite different and independent. As mentioned earlier, m_{ud} and m_s values by ETM are also systematically high compared to their respective averages. Combining all four results yields

$$N_f = 2+1+1: \quad \overline{m}_c(\overline{m}_c) = 1.278(13)\text{ GeV} \quad \text{Refs. [6,7,14,22,23]}, \tag{59}$$

$$\overline{m}_c(3\text{ GeV}) = 0.988(11)\text{ GeV} \quad \text{Refs. [6,7,14,22,23]}, \tag{60}$$

where the errors include large stretching factors $\sqrt{\chi^2/\text{dof}} \approx 2.0$ and 2.5, respectively. We have assumed 100% correlation for statistical errors between ETM results and the same for HPQCD 14A, HPQCD 20A, and FNAL/MILC/TUMQCD 18.

These are obviously poor χ^2 values, and the stretching factors are quite large. While it may be prudent in such a case to quote a range of values covering the central values of all results that pass the quality criteria, we believe in this case that would obscure rather than clarify the situation. From Fig. 5 we note that not only do ETM 21A, ETM 14A, and ETM 14 lie well above the other 2+1+1 results, but also above all of the 2+1 flavour results. A similar trend is apparent for the light-quark masses (see Figs. 1 and 2) while for mass ratios there is better agreement (Figs. 3, 4 and 6). The latter suggests there may be underestimated systematic uncertainties associated with scale setting and/or renormalization which have not been detected. Finally we note the ETM results are significantly higher than the PDG average. For these reasons, which admittedly are not entirely satisfactory, we continue to quote an average with a stretching factor as in previous reviews.

The RGI average reads as follows,

$$M_c^{\text{RGI}} = 1.520(17)_m(14)_\Lambda\text{ GeV} \quad \text{Refs. [6,7,14,22,23].} \tag{61}$$

Figure 5 presents the values of $\overline{m}_c(\overline{m}_c)$ given in Table 12 along with the FLAG averages obtained for $2+1$ and $2+1+1$ flavours.

3.2.3 Lattice determinations of the ratio m_c/m_s

Because some of the results for quark masses given in this review are obtained via the quark-mass ratio m_c/m_s, we review these lattice calculations, which are listed in Table 13, as well.

The $N_f = 2+1$ results from χQCD 14 and HPQCD 09A [27] are from the same calculations that were described for the charm-quark mass in the previous review. Maezawa 16 does not pass our chiral-limit test (see the previous review), though we note that it is quite consistent with the other values. Combining χQCD 14 and HPQCD 09A, we obtain the same result

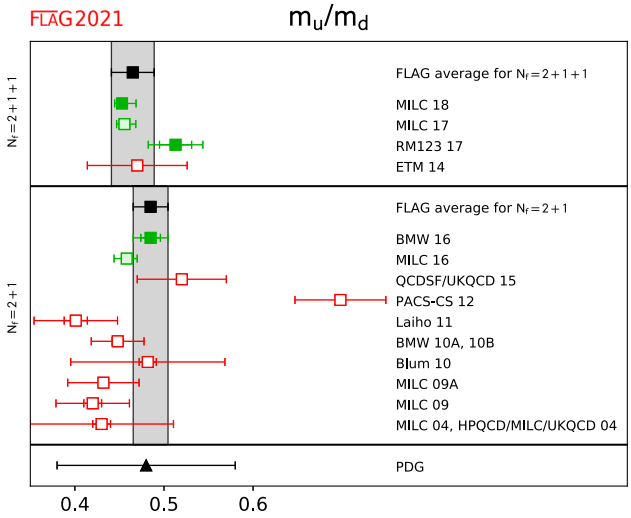

Fig. 4 Lattice results and FLAG averages at $N_f = 2 + 1$ and $2 + 1 + 1$ for the up-down-quark masses ratio m_u/m_d, together with the current PDG estimate

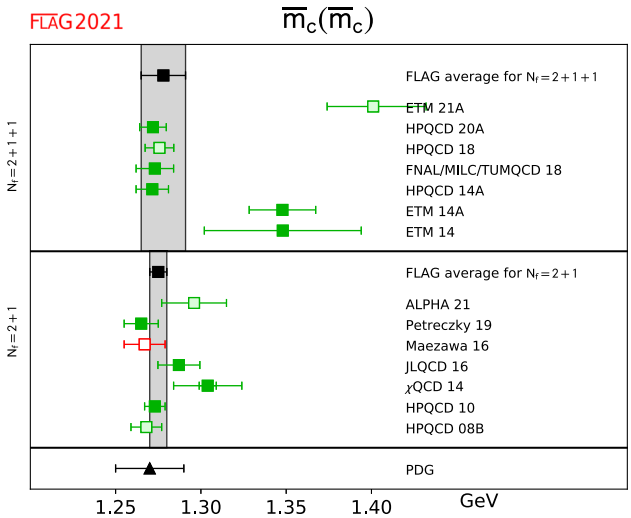

Fig. 5 The charm-quark mass for $2 + 1$ and $2 + 1 + 1$ flavours. For the latter a large stretching factor is used for the FLAG average due to poor χ^2 from our fit

reported in FLAG 19,

$$N_f = 2 + 1 : \qquad m_c/m_s = 11.82(16) \qquad \text{Refs. [24,27]}, \tag{62}$$

with a $\chi^2/\text{dof} \simeq 0.85$.

Turning to $N_f = 2 + 1 + 1$, there is a new result from ETM 21A. The errors have actually increased compared to ETM 14, due to larger uncertainties in the baryon sector which enter their average with the meson sector. Again, ETM 21A does not yet enter the average since it was not published by the deadline for the review. See the earlier reviews for a discussion of previous results.

We note that some tension exists between the HPQCD 14A and FNAL/MILC/TUMQCD results. Combining these with ETM 14 yields

$$N_f = 2 + 1 + 1 : \qquad m_c/m_s = 11.768(34) \qquad \text{Refs. [6,7,14]}, \tag{63}$$

where the error includes the stretching factor $\sqrt{\chi^2/\text{dof}} \simeq 1.5$. We have assumed a 100% correlation of statistical errors for FNAL/MILC/TUMQCD 18 and HPQCD 14A.

Results for m_c/m_s are shown in Fig. 6 together with the FLAG averages for $N_f = 2 + 1$ and $2 + 1 + 1$ flavours.

Table 13 Lattice results for the quark-mass ratio m_c/m_s, together with the colour coding of the calculations used to obtain them

Collaboration	Refs.	N_f	Publication status	Chiral extrapolation	Continuum extrapolation	Finite volume	m_c/m_s
ETM 21A	[204]	2+1+1	P	★	★	★	$11.48(12)(^{+25}_{-19})$
FNAL/MILC/TUMQCD 18	[6]	2+1+1	A	★	★	★	11.784(11)(17)(00)(08)
HPQCD 14A	[14]	2+1+1	A	★	★	★	11.652(35)(55)
FNAL/MILC 14A	[17]	2+1+1	A	★	★	★	$11.747(19)(^{+59}_{-43})$
ETM 14	[7]	2+1+1	A	○	★	○	11.62(16)
Maezawa 16	[189]	2+1	A	■	★	★	11.877(91)
χQCD 14	[24]	2+1	A	○	○	○	11.1(8)
HPQCD 09A	[27]	2+1	A	○	★	★	11.85(16)

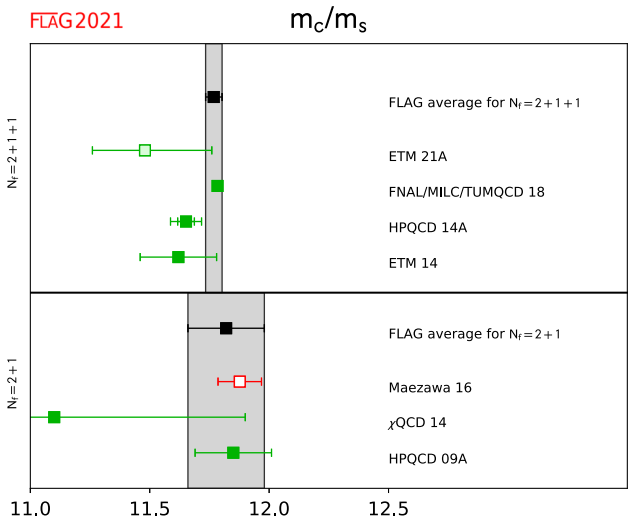

Fig. 6 Lattice results for the ratio m_c/m_s listed in Table 13 and the FLAG averages corresponding to $2+1$ and $2+1+1$ quark flavours. The latter average includes a large stretching factor on the error due a poor χ^2 from our fit

3.3 Bottom-quark mass

Now we review the lattice results for the $\overline{\text{MS}}$ bottom-quark mass $\overline{m}_b$. Related heavy-quark actions and observables have been discussed in previous FLAG reviews [2–4], and descriptions can be found in Sec. A.1.3 of FLAG 19 [4]. In Table 14 we collect results for $\overline{m}_b(\overline{m}_b)$ obtained with $N_f = 2+1$ and $2+1+1$ sea-quark flavours. Available results for the quark-mass ratio m_b/m_c are also reported. After discussing the new results we evaluate the corresponding FLAG averages.

3.3.1 $N_f = 2+1$

There is one new three-flavour result since the last review, Petreczky 19, which was described already in the charm-quark section. The new result rates green stars, so our new average with HPQCD 10 is (both works quote values in the $N_f = 5$ theory, so we simply use those values),

$$N_f = 2+1: \qquad \overline{m}_b(\overline{m}_b) = 4.171(20)\ \text{GeV} \qquad \text{Refs. [11,26].} \tag{64}$$

Table 14 Lattice results for the $\overline{\text{MS}}$ bottom-quark mass $\overline{m}_b(\overline{m}_b)$ in GeV, together with the systematic error ratings for each. Available results for the quark-mass ratio m_b/m_c are also reported

Collaboration	Refs.	N_f	Publication status	Chiral extrapolation	Continuum extrapolation	Finite volume	Renormalization	Heavy-quark treatment	$\overline{m}_b(\overline{m}_b)$	m_b/m_c
HPQCD 21	[28]	2+1+1	A	★	★	★	–	✓	4.209(21)$^{++}$	4.586(12)**
FNAL/MILC/TUM 18	[6]	2+1+1	A	★	○	★	–	✓	4.201(12)(1)(8)(1)	4.578(5)(6)(0)(1)
Gambino 17	[31]	2+1+1	A	○	★	○	★	✓	4.26(18)	
ETM 16B	[30]	2+1+1	A	○	★	○	★	✓	4.26(3)(10)$^{+}$	4.42(3)(8)
HPQCD 14B	[29]	2+1+1	A	★	★	★	★	✓	4.196(0)(23)†	
ETM 14B	[228]	2+1+1	C	○	★	○	★	✓	4.26(7)(14)	4.40(6)(5)
HPQCD 14A	[14]	2+1+1	A	★	★	★	–	✓	4.162(48)	4.528(14)(52)
Petreczky19	[26]	2+1	A	★	★	★	★	✓	4.188(37)	4.586(43)
Maezawa 16	[189]	2+1	A	■	★	★	★	✓	4.184(89)	4.528(57)
HPQCD 13B	[229]	2+1	A	■	○	–	–	✓	4.166(43)	
HPQCD 10	[11]	2+1	A	★	★	★	–	✓	4.164(23)*	4.51(4)
ETM 13B	[56]	2	A	○	★	○	★	✓	4.31(9)(8)	
ALPHA 13C	[230]	2	A	★	★	★	★	✓	4.21(11)	
ETM 11A	[231]	2	A	○	★	○	★	✓	4.29(14)	
PDG	[165]								$4.18^{+0.02}_{-0.03}$	

$^{++}$We quote the four-flavour result. For $N_f = 5$, value is 4.202(21)
**The ratio is quoted in the $\overline{\text{MS}}$ scheme for $\mu = 3$ GeV because of the different charges of the bottom and charm quarks
$^{+}$The lattice spacing used in ETM 14B has been updated here
†Only two pion points are used for chiral extrapolation
*The number that is given is $m_b(10\text{ GeV}, N_f = 5) = 3.617(25)$ GeV

The corresponding four-flavour RGI average is

$$N_f = 2+1: \qquad M_b^{\text{RGI}} = 6.881(33)_m(54)_\Lambda \text{ GeV} \qquad \text{Refs. [11,26].} \tag{65}$$

3.3.2 $N_f = 2+1+1$

HPQCD 21 [28] is an update of HPQCD 14A (and replaces it in our average), including EM corrections for the first time for the b-quark mass. Four flavours of HISQ quarks are used on MILC ensembles with lattice spacings from about 0.09–0.03 fm. Ensembles with physical and unphysical mass sea-quarks are used. Quenched QED is used to obtain the dominant $\mathcal{O}(\alpha)$ effect. The ratio of bottom- to charm-quark masses is computed in a completely nonperturbative formulation, and the b-quark mass is extracted using the value of $\overline{m}_c(3\text{ GeV})$ from HPQCD 20A. Since EM effects are included, the QED renormalization scale enters the ratio which is quoted for 3 GeV and $N_f = 4$. The total error on the new result is more than two times smaller than for HPQCD 14A, but is only slightly smaller compared to the NRQCD result reported in HPQCD 14B. The inclusion of QED shifts the ratio m_b/m_c up slightly from the pure QCD value by about one standard deviation, and the value of $\overline{m}_b(m_b)$ is consistent, within errors, to the other pure QCD results entering our average. Therefore we quote a single average.

HPQCD 14B employs the NRQCD action [29] to treat the b quark. The b-quark mass is computed with the moments method, that is, from Euclidean-time moments of two-point, heavy-heavy-meson correlation functions (see also Sect. 9.8 for a description of the method).

In HPQCD 14B the b-quark mass is computed from ratios of the moments R_n of heavy current-current correlation functions, namely,

$$\left[\frac{R_n r_{n-2}}{R_{n-2} r_n}\right]^{1/2} \frac{\bar{M}_{\rm kin}}{2m_b} = \frac{\bar{M}_{\Upsilon,\eta_b}}{2\bar{m}_b(\mu)} \,, \tag{66}$$

where r_n are the perturbative moments calculated at N^{3}LO, $\bar{M}_{\rm kin}$ is the spin-averaged kinetic mass of the heavy-heavy vector and pseudoscalar mesons and $\bar{M}_{\Upsilon,\eta_b}$ is the experimental spin average of the Υ and η_b masses. The average kinetic mass $\bar{M}_{\rm kin}$ is chosen since in the lattice calculation the splitting of the Υ and η_b states is inverted. In Eq. (66), the bare mass m_b appearing on the left-hand side is tuned so that the spin-averaged mass agrees with experiment, while the mass $\overline{m}_b$ at the fixed scale $\mu = 4.18$ GeV is extrapolated to the continuum limit using three HISQ (MILC) ensembles with $a \approx 0.15, 0.12$ and 0.09 fm and two pion masses, one of which is the physical one. Their final result is $\overline{m}_b(\mu = 4.18\,\text{GeV}) = 4.207(26)$ GeV, where the error is from adding systematic uncertainties in quadrature only (statistical errors are smaller than 0.1% and ignored). The errors arise from renormalization, perturbation theory, lattice spacing, and NRQCD systematics. The finite-volume uncertainty is not estimated, but at the lowest pion mass they have $m_\pi L \simeq 4$, which leads to the tag ★.

The next four-flavour result [30] is from the ETM collaboration and updates their preliminary result appearing in a conference proceedings [228]. The calculation is performed on a set of configurations generated with twisted-Wilson fermions with three lattice spacings in the range 0.06 – 0.09 fm and with pion masses in the range 210–440 MeV. The b-quark mass is determined from a ratio of heavy-light pseudoscalar meson masses designed to yield the quark pole mass in the static limit. The pole mass is related to the $\overline{\rm MS}$ mass through perturbation theory at N^{3}LO. The key idea is that by taking ratios of ratios, the b-quark mass is accessible through fits to heavy-light(strange)-meson correlation functions computed on the lattice in the range $\sim$ 1–2 $\times$ m_c and the static limit, the latter being exactly 1. By simulating below $\overline{m}_b$, taking the continuum limit is easier. They find $\overline{m}_b(\overline{m}_b) = 4.26(3)(10)$ GeV, where the first error is statistical and the second systematic. The dominant errors come from setting the lattice scale and fit systematics.

Gambino et al. [31] use twisted-mass-fermion ensembles from the ETM collaboration and the ETM ratio method as in ETM 16. Three values of the lattice spacing are used, ranging from 0.062 to 0.089 fm. Several volumes are also used. The light-quark masses produce pions with masses from 210 to 450 MeV. The main difference with ETM 16 is that the authors use the kinetic mass defined in the heavy-quark expansion (HQE) to extract the b-quark mass instead of the pole mass.

The final b-quark mass result is FNAL/MILC/TUM 18 [6]. The mass is extracted from the same fit and analysis done for the charm quark mass. Note that relativistic HISQ valence masses reach the physical b mass on the two finest lattice spacings ($a = 0.042$ fm, 0.03 fm) at physical and 0.2 m_s light-quark mass, respectively. In lattice units the heavy valence masses correspond to $aM^{\rm RGI} > 0.90$, making the continuum extrapolation challenging, but the authors investigated the effect of leaving out the heaviest points from the fit, and the result did not noticeably change. Their results are also consistent with an analysis dropping the finest lattice from the fit. Since the b-quark mass region is only reached with two lattice spacings, we rate this work with a green circle for the continuum extrapolation. Note however that for other values of the quark masses they use up to five values of the lattice spacing (cf. their charm-quark mass determination).

All of the above results enter our average. We note that here the ETM 16 result is consistent with the average and a stretching factor on the error is not used. The average and error is dominated by the very precise FNAL/MILC/TUM 18 value,

$$N_f = 2+1+1: \qquad \overline{m}_b(\overline{m}_b) = 4.203(11)\ \text{GeV} \qquad \text{Refs. [6,14,28–31].} \tag{67}$$

We have included a 100% correlation on the statistical errors of ETM 16 and Gambino 17, since the same ensembles are used in both. While FNAL/MILC/TUM 18 and HPQCD 21 also use the same MILC HISQ ensembles, the statistical error in the HPQCD 21 analysis is negligible, so we do not include a correlation between them. The average has $\chi^2/\text{dof} = 0.02$.

The above translates to the RGI average

$$N_f = 2+1+1: \qquad M_b^{\rm RGI} = 6.934(18)_m(55)_\Lambda\ \text{GeV} \qquad \text{Refs. [6,14,28–31].} \tag{68}$$

All the results for $\overline{m}_b(\overline{m}_b)$ discussed above are shown in Fig. 7 together with the FLAG averages corresponding to $N_f = 2+1$ and $2+1+1$ quark flavours.

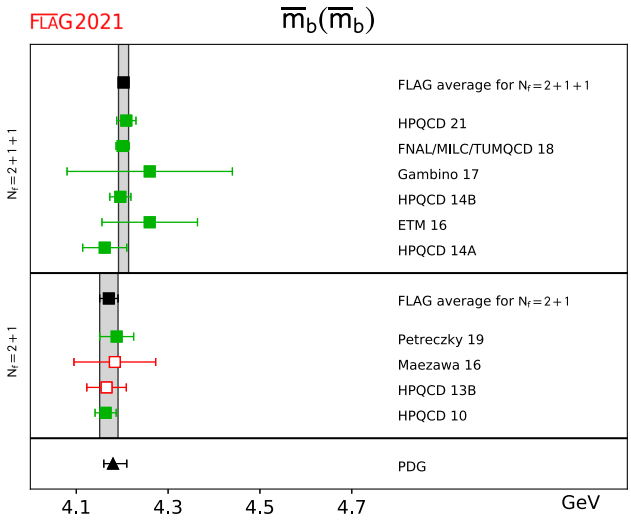

Fig. 7 The b-quark mass for $N_f = 2+1$ and $2+1+1$ flavours. The updated PDG value from Ref. [165] is reported for comparison

4 Leptonic and semileptonic kaon and pion decay and $|V_{ud}|$ and $|V_{us}|$

Authors: T. Kaneko, J. N. Simone, S. Simula, N. Tantalo

This section summarizes state-of-the-art lattice calculations of the leptonic kaon and pion decay constants and the kaon semileptonic-decay form factor and provides an analysis in view of the Standard Model. With respect to the previous edition of the FLAG review [4] the data in this section has been updated. As in Ref. [4], when combining lattice data with experimental results, we take into account the strong $SU(2)$ isospin correction, either obtained in lattice calculations or estimated by using chiral perturbation theory (χPT), both for the kaon leptonic decay constant $f_{K^\pm}$ and for the ratio $f_{K^\pm}/f_{\pi^\pm}$.

4.1 Experimental information concerning $|V_{ud}|$, $|V_{us}|$, $f_+(0)$ and $f_{K^\pm}/f_{\pi^\pm}$

The following review relies on the fact that precision experimental data on kaon decays very accurately determine the product $|V_{us}|f_+(0)$ [232] and the ratio $|V_{us}/V_{ud}|f_{K^\pm}/f_{\pi^\pm}$ [165,232]:

$$|V_{us}|f_+(0) = 0.2165(4)\,, \qquad \left|\frac{V_{us}}{V_{ud}}\right| \frac{f_{K^\pm}}{f_{\pi^\pm}} = 0.2760(4)\,. \tag{69}$$

Here and in the following, $f_{K^\pm}$ and $f_{\pi^\pm}$ are the isospin-broken decay constants, respectively, in QCD. We will refer to the decay constants in the $SU(2)$ isospin-symmetric limit as f_K and f_π (the latter at leading order in the mass difference $(m_u - m_d)$ coincides with $f_{\pi^\pm}$). The parameters $|V_{ud}|$ and $|V_{us}|$ are elements of the Cabibbo–Kobayashi–Maskawa matrix and $f_+(q^2)$ represents one of the form factors relevant for the semileptonic decay $K^0 \to \pi^-\ell\,\nu$, which depends on the momentum transfer q between the two mesons. What matters here is the value at $q^2 = 0$: $f_+(0) \equiv f_+^{K^0\pi^-}(0) = f_0^{K^0\pi^-}(0) = q^\mu \langle \pi^-(p')|\bar{s}\gamma_\mu u|K^0(p)\rangle/(M_K^2 - M_\pi^2)\big|_{q^2\to 0}$. The pion and kaon decay constants are defined by[12]

$$\langle 0|\,\bar{d}\gamma_\mu\gamma_5\,u|\pi^+(p)\rangle = i\,p_\mu f_{\pi^+}\,, \qquad \langle 0|\,\bar{s}\gamma_\mu\gamma_5\,u|K^+(p)\rangle = i\,p_\mu f_{K^+}\,.$$

In this normalization, $f_{\pi^\pm} \simeq 130$ MeV, $f_{K^\pm} \simeq 155$ MeV.

[12] The pion decay constant represents a QCD matrix element – in the full Standard Model, the one-pion state is not a meaningful notion: the correlation function of the charged axial current does not have a pole at $p^2 = M_{\pi^+}^2$, but a branch cut extending from $M_{\pi^+}^2$ to ∞. The analytic properties of the correlation function and the problems encountered in the determination of f_π are thoroughly discussed in Ref. [233]. The "experimental" value of f_π depends on the convention used when splitting the sum $\mathcal{L}_{\rm QCD} + \mathcal{L}_{\rm QED}$ into two parts. The lattice determinations of f_π do not yet reach the accuracy where this is of significance, but at the precision claimed by the Particle Data Group [201,234], the numerical value does depend on the convention used [233,235–237].

In Eq. (69), the electromagnetic effects have already been subtracted in the experimental analysis using χPT. Recently, a new method [238] has been proposed for calculating the leptonic decay rates of hadrons including both QCD and QED on the lattice, and successfully applied to the case of the ratio of the leptonic decay rates of kaons and pions [239,240]. The correction to the tree-level $K_{\mu 2}/\pi_{\mu 2}$ decay rate, including both electromagnetic and strong isospin-breaking effects, is found to be equal to $-1.26(14)\%$[13] to be compared to the estimate $-1.12(21)\%$ based on χPT [164,241]. Using the experimental values of the $K_{\mu 2}$ and $\pi_{\mu 2}$ decay rates the result of Ref. [240] implies

$$\left|\frac{V_{us}}{V_{ud}}\right| \frac{f_K}{f_\pi} = 0.27683\,(29)_{\rm exp}\,(20)_{\rm th}\,[35]\,, \tag{70}$$

where the last error in brackets is the sum in quadrature of the experimental and theoretical uncertainties, and the ratio of the decay constants is the one corresponding to isosymmetric QCD. A large part of the theoretical uncertainty comes from the statistics and continuum and chiral extrapolation of lattice data, which can be systematically reduced by a more realistic simulation with high statistics. We also note that an independent study of the electromagnetic effects is in progress [242]. Therefore, it is feasible to more precisely determine $|V_{us}/V_{ud}|$ using only lattice-QCD+QED for $f_{K^\pm}/f_{\pi^\pm}$ and the ratio of the experimental values of the $K_{\mu 2}$ and $\pi_{\mu 2}$ decay rates.

At present, the superallowed nuclear β transitions provide the most precise determination of $|V_{ud}|$. Its accuracy has been limited by hadronic uncertainties in the universal electroweak radiative correction Δ_R^V. A recent analysis in terms of a dispersion relation [243,244] found Δ_R^V larger than the previous estimate [245]. A more straightforward update of Ref. [245] also reported larger Δ_R^V [246]. In the PDG review, the fourteen precisely measured transitions [247] with the dispersive estimate of Δ_R^V yield [165]

$$|V_{ud}| = 0.97370(14), \tag{71}$$

which differs by $\approx 3\sigma$ from the previous estimate [247]. However, it is not a trivial matter to properly take account of the nuclear corrections at this precision [243,247–255]. For example, the dispersive approach has been applied in a recent update of the so-called inner radiative correction due to quenching of the axial-vector and isoscalar spin-magnetic-moment couplings in nuclei [243], and in a recent estimate of a novel correction due to the distortion of the emitted electron energy spectrum by nuclear polarizabilities [255]. A recent reanalysis of twenty-three β decays [256] obtained

$$|V_{ud}| = 0.97373(31), \tag{72}$$

where the two nuclear corrections tend to cancel with each other and, hence, leave the central value basically unchanged. Their uncertainties, however, doubles that of $|V_{ud}|$. In Sects. 4.4 and 4.5, we mainly use the PDG value (71) but also test Eq. (72) as an alternative input.

The matrix element $|V_{us}|$ can be determined from semi-inclusive τ decays [257–260]. By separating the inclusive decay $\tau \to$ hadrons $+\,\nu$ into nonstrange and strange final states, e.g., HFLAV 18 [261] obtains

$$|V_{us}| = 0.2195(19), \tag{73}$$

and both Maltman et al. [259,262,263] and Gamiz et al. [264,265] arrived at very similar values. Inclusive hadronic τ decay offers an interesting way to measure $|V_{us}|$, but the above value of $|V_{us}|$ differs from the result one obtains from the kaon decays by about three standard deviations (see Sect. 4.5). This apparent tension has been recently solved in Ref. [266] thanks to the use of a different experimental input and to a new treatment of higher orders in the operator product expansion and of violations of quark-hadron duality. A larger value of $|V_{us}|$ is obtained, namely, $|V_{us}| = 0.2231(27)$, which is in much better agreement with the results from the kaon decays. This result is also stable against the choice of the upper limit and weight function of the experimental spectral integrals.[14]

Recently, Ref. [268] proposed a new method to determine $|V_{us}|$ from inclusive strange τ decays. Through generalized dispersion relations, this method evaluates the spectral integral from lattice-QCD data of the hadronic vacuum polarization

[13] This has been updated in Ref. [240] after the previous edition of this review. See also the extended discussion concerning the isospin correction in Sect. 11 on the scale setting.

[14] A recent update can be found in Ref. [267].

function at Euclidean momentum squared in the few-to-several 0.1 GeV^2 region. This method, therefore, does not rely on the operator product expansion, and obtained $|V_{us}|$ consistent with that from the kaon decays. A later analysis yields [267]

$$|V_{us}| = 0.2240(18), \tag{74}$$

by taking account of updates on experimental strange τ branching fractions in 2018. We quote Eqs. (73) and (74) as $|V_{us}|$ from the inclusive hadronic τ decays in Sect. 4.5.

The experimental results in Eq. (69) are for the semileptonic decay of a neutral kaon into a negatively charged pion and the charged pion and kaon leptonic decays, respectively, in QCD. In the case of the semileptonic decays the corrections for strong and electromagnetic isospin breaking in χPT at NLO have allowed for averaging the different experimentally measured isospin channels [269]. This is quite a convenient procedure as long as lattice-QCD simulations do not include strong or QED isospin-breaking effects. Several lattice results for f_K/f_π are quoted for QCD with (squared) pion and kaon masses of $M_\pi^2 = M_{\pi^0}^2$ and $M_K^2 = \frac{1}{2}\left(M_{K^\pm}^2 + M_{K^0}^2 - M_{\pi^\pm}^2 + M_{\pi^0}^2\right)$ for which the leading strong and electromagnetic isospin violations cancel. For these results, contact with experimental results is made by correcting leading $SU(2)$ isospin breaking guided either by χPT or by lattice calculations. We note, however, that the modern trend for the leptonic decays is to include strong and electromagnetic isospin breaking in the lattice simulations (e.g., Refs. [171,172,193,217,238,239,270–272]). After the previous edition, this trend has been extended to the semileptonic decays. Reference [273] discusses an extension of the method in Refs. [239,240], which led to Eq. (70), for the semileptonic decays. References [274–276] pursue an effective field theory setup supplemented by nonperturbative lattice-QCD inputs to estimate the radiative corrections.

4.2 Lattice results for $f_+(0)$ and $f_{K^\pm}/f_{\pi^\pm}$

The traditional way of determining $|V_{us}|$ relies on using estimates for the value of $f_+(0)$, invoking the Ademollo–Gatto theorem [277]. Since this theorem only holds to leading order of the expansion in powers of m_u, m_d, and m_s, theoretical models are used to estimate the corrections. Lattice methods have now reached the stage where quantities like $f_+(0)$ or f_K/f_π can be determined to good accuracy. As a consequence, the uncertainties inherent in the theoretical estimates for the higher order effects in the value of $f_+(0)$ do not represent a limiting factor any more and we shall therefore not invoke those estimates. Also, we will use the experimental results based on nuclear β decay and inclusive hadronic τ decay exclusively for comparison – the main aim of the present review is to assess the information gathered with lattice methods and to use it for testing the consistency of the SM and its potential to provide constraints for its extensions.

The database underlying the present review of the semileptonic form factor and the ratio of decay constants is listed in Tables 15 and 16. The properties of the lattice data play a crucial role for the conclusions to be drawn from these results: range of M_π, size of LM_π, continuum extrapolation, extrapolation in the quark masses, finite-size effects, etc. The key features of the various data sets are characterized by means of the colour code specified in Sect. 2.1. More detailed information on individual computations are compiled in Appendix C.2, which in this edition is limited to new results and to those entering the FLAG averages. For other calculations the reader should refer to the Appendix B.2 of Ref. [3].

The quantity $f_+(0)$ represents a matrix element of a strangeness-changing null-plane charge, $f_+(0) = \langle K|Q^{\bar{u}s}|\pi\rangle$ (see Ref. [278]). The vector charges obey the commutation relations of the Lie algebra of $SU(3)$, in particular $[Q^{\bar{u}s}, Q^{\bar{s}u}] = Q^{\bar{u}u-\bar{s}s}$. This relation implies the sum rule $\sum_n |\langle K|Q^{\bar{u}s}|n\rangle|^2 - \sum_n |\langle K|Q^{\bar{s}u}|n\rangle|^2 = 1$. Since the contribution from the one-pion intermediate state to the first sum is given by $f_+(0)^2$, the relation amounts to an exact representation for this quantity [279]:

$$f_+(0)^2 = 1 - \sum_{n\neq\pi} |\langle K|Q^{\bar{u}s}|n\rangle|^2 + \sum_n |\langle K|Q^{\bar{s}u}|n\rangle|^2 . \tag{75}$$

While the first sum on the right extends over nonstrange intermediate states, the second runs over exotic states with strangeness ± 2 and is expected to be small compared to the first.

The expansion of $f_+(0)$ in $SU(3)$ χPT in powers of m_u, m_d, and m_s starts with $f_+(0) = 1 + f_2 + f_4 + \cdots$ [280]. Since all of the low-energy constants occurring in f_2 can be expressed in terms of M_π, M_K, M_η and f_π [278], the NLO correction is known. In the language of the sum rule (75), f_2 stems from nonstrange intermediate states with three mesons. Like all other nonexotic intermediate states, it lowers the value of $f_+(0)$: $f_2 = -0.023$ when using the experimental value of f_π as input. The corresponding expressions have also been derived in quenched or partially quenched (staggered) χPT [34,281]. At the same order in the $SU(2)$ expansion [282], $f_+(0)$ is parameterized in terms of M_π and two a priori unknown parameters. The latter can be determined from the dependence of the lattice results on the masses of the quarks. Note that any calculation that

Table 15 Colour code for the data on $f_+(0)$. In this and previous editions [4], old results with two red tags have been dropped

Collaboration	Refs.	N_f	Publication status	Chiral extrapolation	Continuum extrapolation	Finite-volume errors	$f_+(0)$
FNAL/MILC 18	[33]	2+1+1	A	★	★	★	0.9696(15)(12)
ETM 16	[32]	2+1+1	A	○	★	○	0.9709(45)(9)
FNAL/MILC 13E	[293]	2+1+1	A	★	★	★	0.9704(24)(22)
PACS 19	[294]	2+1	A	○	■	★	$0.9603(16)(^{+50}_{-48})$
JLQCD 17	[289]	2+1	A	○	■	○	$0.9636(36)(^{+57}_{-35})$
RBC/UKQCD 15A	[35]	2+1	A	★	○	○	0.9685(34)(14)
RBC/UKQCD 13	[295]	2+1	A	★	○	○	$0.9670(20)(^{+18}_{-46})$
FNAL/MILC 12I	[34]	2+1	A	○	○	★	0.9667(23)(33)
JLQCD 12	[296]	2+1	C	○	■	★	0.959(6)(5)
JLQCD 11	[297]	2+1	C	○	■	★	0.964(6)
RBC/UKQCD 10	[298]	2+1	A	○	■	★	$0.9599(34)(^{+31}_{-47})(14)$
RBC/UKQCD 07	[299]	2+1	A	○	■	★	0.9644(33)(34)(14)
ETM 10D	[300]	2	C	○	★	○	$0.9544(68)_{stat}$
ETM 09A	[36]	2	A	○	○	○	0.9560(57)(62)

relies on the χPT formula for f_2 is subject to the uncertainties inherent in NLO results: instead of using the physical value of the pion decay constant f_π, one may, for instance, work with the constant f_0 that occurs in the effective Lagrangian and represents the value of f_π in the chiral limit. Although trading f_π for f_0 in the expression for the NLO term affects the result only at NNLO, it may make a significant numerical difference in calculations where the latter are not explicitly accounted for. (Lattice results concerning the value of the ratio f_π/f_0 are reviewed in Sect. 5.3.)

The lattice results shown in Fig. 8 indicate that the higher order contributions $\Delta f \equiv f_+(0) - 1 - f_2$ are negative and thus amplify the effect generated by f_2. This confirms the expectation that the exotic contributions are small. The entries in the lower part of the left panel represent various model estimates for f_4. In Ref. [283], the symmetry-breaking effects are estimated in the framework of the quark model. The more recent calculations are more sophisticated, as they make use of the known explicit expression for the $K_{\ell 3}$ form factors to NNLO in χPT [284,285]. The corresponding formula for f_4 accounts for the chiral logarithms occurring at NNLO and is not subject to the ambiguity mentioned above.[15] The numerical result, however, depends on the model used to estimate the low-energy constants occurring in f_4 [285–288]. The figure indicates that the most recent numbers obtained in this way correspond to a positive or an almost vanishing rather than a negative value for Δf. We note that FNAL/MILC 12I [34], JLQCD 17 [289], FNAL/MILC 18 [33], and Ref. [290] have made an attempt at determining a combination of some of the low-energy constants appearing in f_4 from lattice data.

4.3 Direct determination of $f_+(0)$ and $f_{K^\pm}/f_{\pi^\pm}$

Many lattice results for the form factor $f_+(0)$ and for the ratio of decay constants, which we summarize here in Tables 15 and 16, respectively, have been computed in isospin-symmetric QCD. The reason for this unphysical parameter choice is that there are only a few simulations of isospin-breaking effects in lattice QCD, which is ultimately the cleanest way for predicting these effects [170–172,178,217,238,239,272,291,292]. In the meantime, one relies either on χPT [197,280] to estimate the correction to the isospin limit or one calculates the breaking at leading order in $(m_u - m_d)$ in the valence quark sector by extrapolating the lattice data for the charged kaons to the physical value of the $up(down)$-quark mass (the result for the

[15] Fortran programs for the numerical evaluation of the form factor representation in Ref. [285] are available on request from Johan Bijnens.

Table 16 Colour code for the data on the ratio of decay constants: f_K/f_π is the pure QCD $SU(2)$-symmetric ratio, while $f_{K^\pm}/f_{\pi^\pm}$ is in pure QCD including the $SU(2)$ isospin-breaking correction. In this and previous editions [4], old results with two red tags have been dropped

Collaboration	Refs.	N_f	Publication status	Chiral extrapolation	Continuum extrapolation	Finite-volume errors	f_K/f_π	$f_{K^\pm}/f_{\pi^\pm}$
ETM 21	[305]	2+1+1	P	★	★	★	1.1995(44)(7)	1.1957(44)(7)
CalLat 20	[39]	2+1+1	A	★	★	★	1.1964(32)(30)	1.1942(32)(31)
FNAL/MILC 17	[16]	2+1+1	A	★	★	★	1.1980(12)$(^{+5}_{-15})$	1.1950(15)$(^{+6}_{-18})$
ETM 14E	[38]	2+1+1	A	○	★	○	1.188(11)(11)	1.184(12)(11)
FNAL/MILC 14A	[17]	2+1+1	A	★	★	★		1.1956(10)$(^{+26}_{-18})$
ETM 13F	[306]	2+1+1	C	○	★	○	1.193(13)(10)	1.183(14)(10)
HPQCD 13A	[37]	2+1+1	A	★	○	★	1.1948(15)(18)	1.1916(15)(16)
MILC 13A	[307]	2+1+1	A	★	★	★		1.1947(26)(37)
MILC 11	[308]	2+1+1	C	○	○	○		1.1872(42)$^{\dagger}_{\text{stat.}}$
ETM 10E	[309]	2+1+1	C	○	○	○	1.224(13)$_{\text{stat}}$	
QCDSF/UKQCD 16	[44]	2+1	A	○	★	○	1.192(10)(13)	1.190(10)(13)
BMW 16	[43,310]	2+1	A	★	★	★	1.182(10)(26)	1.178(10)(26)
RBC/UKQCD 14B	[8]	2+1	A	★	★	★	1.1945(45)	
RBC/UKQCD 12	[188]	2+1	A	★	○	★	1.199(12)(14)	
Laiho 11	[49]	2+1	C	○	★	○		1.202(11)(9)(2)(5)††
MILC 10	[41]	2+1	C	○	★	★		1.197(2)$(^{+3}_{-7})$
JLQCD/TWQCD 10	[311]	2+1	C	○	■	★	1.230(19)	
RBC/UKQCD 10A	[117]	2+1	A	○	○	★	1.204(7)(25)	
BMW 10	[42]	2+1	A	★	★	★	1.192(7)(6)	
MILC 09A	[15]	2+1	C	○	★	★		1.198(2)$(^{+6}_{-8})$
MILC 09	[157]	2+1	A	○	★	★		1.197(3)$(^{+6}_{-13})$
Aubin 08	[312]	2+1	C	○	○	○		1.191(16)(17)
RBC/UKQCD 08	[194]	2+1	A	○	■	★	1.205(18)(62)	
HPQCD/UKQCD 07	[40]	2+1	A	○	○	○	1.189(2)(7)	
MILC 04	[197]	2+1	A	○	○	○		1.210(4)(13)
ETM 14D	[313]	2	C	★	■	○	1.203(5)$_{\text{stat}}$	
ALPHA 13A	[314]	2	C	★	★	★	1.1874(57)(30)	
ETM 10D	[300]	2	C	○	★	○	1.190(8)$_{\text{stat}}$	
ETM 09	[45]	2	A	○	★	○	1.210(6)(15)(9)	
QCDSF/UKQCD 07	[315]	2	C	○	○	★	1.21(3)	

†Result with statistical error only from polynomial interpolation to the physical point
††This work is the continuation of Aubin 08

pion decay constant is always extrapolated to the value of the average light-quark mass $\hat{m}$). This defines the prediction for $f_{K^\pm}/f_{\pi^\pm}$.

Since the majority of results that qualify for inclusion into the FLAG average include the strong $SU(2)$ isospin-breaking correction, we confirm the choice made in the previous edition of the FLAG review [4] and we provide in Fig. 9 the overview of the world data of $f_{K^\pm}/f_{\pi^\pm}$. For all the results of Table 16 provided only in the isospin-symmetric limit we apply individually an isospin correction that will be described later on (see Eqs. (79)–(80)).

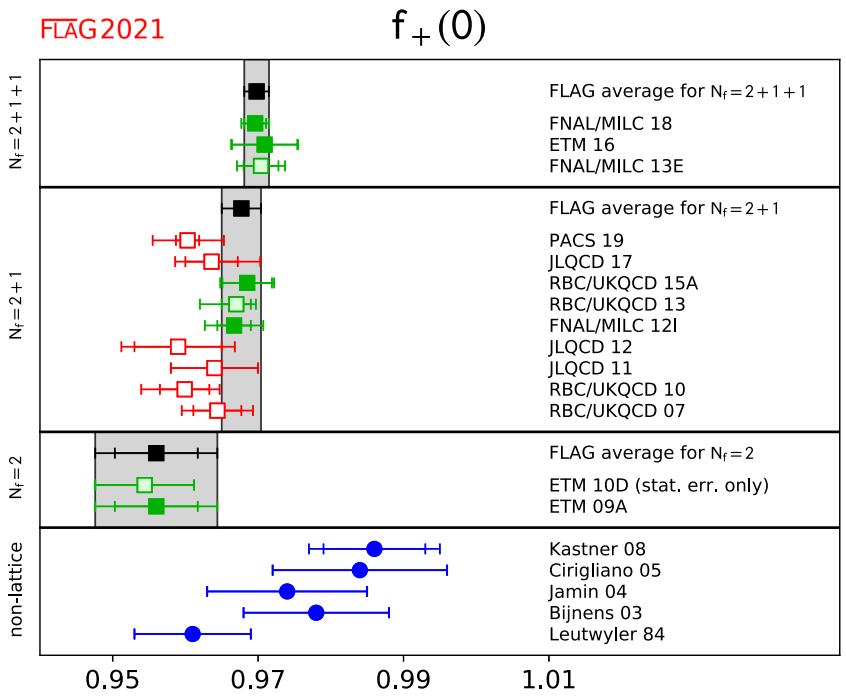

Fig. 8 Comparison of lattice results (squares) for $f_+(0)$ with various model estimates based on χPT [283,285–288] (blue circles). The black squares and grey bands indicate our averages (76)–(78). The significance of the colours is explained in Sect. 2

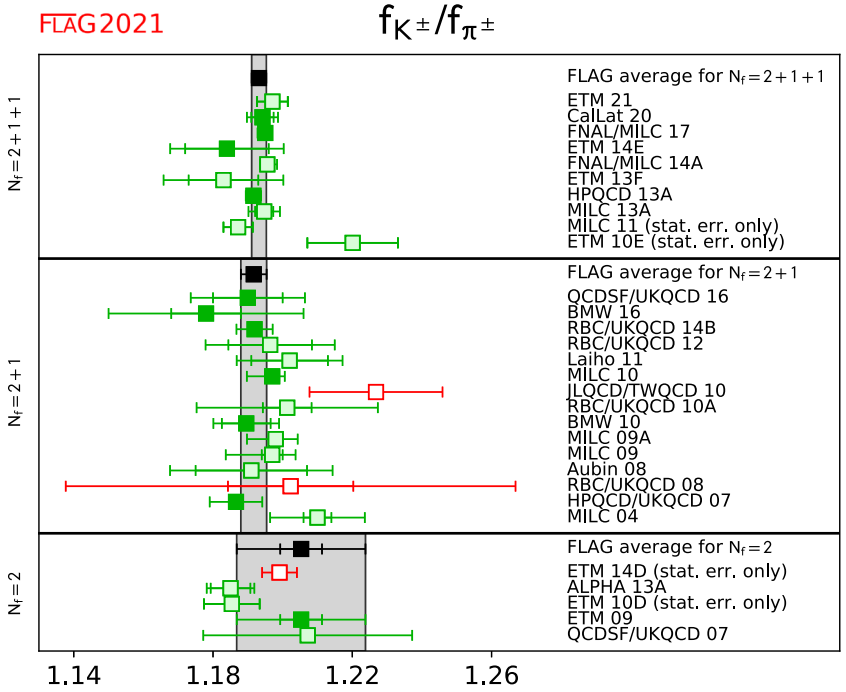

Fig. 9 Comparison of lattice results for $f_{K^\pm}/f_{\pi^\pm}$. This ratio is obtained in pure QCD including the $SU(2)$ isospin-breaking correction (see Sect. 4.3). The black squares and grey bands indicate our averages in Eqs. (81)–(83)

The plots in Figs. 8 and 9 illustrate our compilation of data for $f_+(0)$ and $f_{K^\pm}/f_{\pi^\pm}$. The lattice data for the latter quantity is largely consistent even when comparing simulations with different N_f, while in the case of $f_+(0)$ a slight tendency to get higher values when increasing N_f seems to be visible, even if it does not exceed one standard deviation. We now proceed to form the corresponding averages, separately for the data with $N_f = 2+1+1$, $N_f = 2+1$, and $N_f = 2$ dynamical flavours, and in the following we will refer to these averages as the "direct" determinations.

4.3.1 Results for $f_+(0)$

For $f_+(0)$ there are currently two computational strategies: FNAL/MILC uses the Ward identity to relate the $K \to \pi$ form factor at zero momentum transfer to the matrix element $\langle\pi|S|K\rangle$ of the flavour-changing scalar current $S = \bar{s}u$.

Peculiarities of the staggered fermion discretization used by FNAL/MILC (see Ref. [34]) makes this the favoured choice. The other collaborations are instead computing the vector current matrix element $\langle \pi | \bar{s} \gamma_\mu u | K \rangle$. Apart from FNAL/MILC 13E, RBC/UKQCD 15A, and FNAL/MILC 18, all simulations in Table 15 involve unphysically heavy quarks and, therefore, the lattice data needs to be extrapolated to the physical pion and kaon masses corresponding to the $K^0 \to \pi^-$ channel. We note also that the recent computations of $f_+(0)$ obtained by the FNAL/MILC and RBC/UKQCD collaborations make use of the partially-twisted boundary conditions to determine the form-factor results directly at the relevant kinematical point $q^2 = 0$ [301,302], avoiding in this way any uncertainty due to the momentum dependence of the vector and/or scalar form factors. The ETM collaboration uses partially-twisted boundary conditions to compare the momentum dependence of the scalar and vector form factors with the one of the experimental data [32,300], while keeping at the same time the advantage of the high-precision determination of the scalar form factor at the kinematical end-point $q^2_{max} = (M_K - M_\pi)^2$ [36,303] for the interpolation at $q^2 = 0$.

According to the colour codes reported in Table 15 and to the FLAG rules of Sect. 2.2, only the result ETM 09A with $N_f = 2$, the results FNAL/MILC 12I and RBC/UKQCD 15A with $N_f = 2+1$, and the results ETM 16 and FNAL/MILC 18 with $N_f = 2+1+1$ dynamical flavours of fermions, respectively, can enter the FLAG averages. We note that the new entry in this edition is FNAL/MILC 18 for $N_f = 2+1+1$, which did not enter the previous FLAG average due to its publication status [4].

At $N_f = 2+1+1$ the result from the FNAL/MILC collaboration, $f_+(0) = 0.9704(24)(22)$ (FNAL/MILC 13E), is based on the use of the Highly Improved Staggered Quark (HISQ) action (for both valence and sea quarks), which has been tailored to reduce staggered taste-breaking effects, and includes simulations with three lattice spacings and physical light-quark masses. These features allow to keep the uncertainties due to the chiral extrapolation and to the discretization artifacts well below the statistical error. The remaining largest systematic uncertainty comes from finite-size effects, which have been investigated in Ref. [304] using one-loop χPT (with and without taste-violating effects). In Ref. [33], the FNAL/MILC collaboration presented a more precise determination of $f_+(0)$, $f_+(0) = 0.9696(15)(11)$ (FNAL/MILC 18). In this update, their analysis is extended to two smaller lattice spacings $a = 0.06$ and 0.042 fm. The physical light-quark mass is simulated at four lattice spacings. They also added a simulation at a small volume to study the finite-size effects. The improvement of the precision with respect to FNAL/MILC 13E is obtained mainly by an estimate of finite-size effects, which is claimed to be controlled at the level of $\sim 0.05\,\%$ by comparing two analyses with and without the one-loop correction. The total uncertainty is largely reduced to $\sim 0.2\,\%$. An independent calculation of such high precision would be highly welcome to solidify the lattice prediction of $f_+(0)$, which currently suggests a tension with CKM unitarity with the updated value of $|V_{ud}|$ (see Sect. 4.4).

The result from the ETM collaboration, $f_+(0) = 0.9709(45)(9)$ (ETM 16), makes use of the twisted-mass discretization adopting three values of the lattice spacing in the range 0.06–0.09 fm and pion masses simulated in the range 210–450 MeV. The chiral and continuum extrapolations are performed in a combined fit together with the momentum dependence, using both a $SU(2)$-χPT inspired ansatz (following Ref. [300]) and a modified z-expansion fit. The uncertainties coming from the chiral extrapolation, the continuum extrapolation and the finite-volume effects turn out to be well below the dominant statistical error, which includes also the error due to the fitting procedure. A set of synthetic data points, representing both the vector and the scalar semileptonic form factors at the physical point for several selected values of q^2, is provided together with the corresponding correlation matrix.

The PACS collaboration obtained a new result for $N_f = 2+1$, $f_+(0) = 0.9603(16)\left(^{+50}_{-48}\right)$, by creating an ensemble with the physical light-quark mass on a large lattice volume of $(10.9\,\text{fm})^4$ [294]. Such a large lattice enables them to interpolate $f_+(q^2)$ to zero momentum transfer and study the momentum-transfer dependence of the form factors without using partially-twisted boundary conditions. Their result, however, does not enter the FLAG average, because they only use a single lattice spacing, which is the source of the largest uncertainty in their calculation.

For $N_f = 2+1$, the two results eligible to enter the FLAG average are the one from RBC/UKQCD 15A, $f_+(0) = 0.9685(34)(14)$ [35], and the one from FNAL/MILC 12I, $f_+(0) = 0.9667(23)(33)$ [34]. These results, based on different fermion discretizations (staggered fermions in the case of FNAL/MILC and domain wall fermions in the case of RBC/UKQCD) are in nice agreement. Moreover, in the case of FNAL/MILC the form factor has been determined from the scalar current matrix element, while in the case of RBC/UKQCD it has been determined including also the matrix element of the vector current. To a certain extent both simulations are expected to be affected by different systematic effects.

RBC/UKQCD 15A has analyzed results on ensembles with pion masses down to 140 MeV, mapping out the complete range from the $SU(3)$-symmetric limit to the physical point. No significant cut-off effects (results for two lattice spacings) were observed in the simulation results. Ensembles with unphysical light-quark masses are weighted to work as a guide for small corrections toward the physical point, reducing in this way the model dependence in the fitting ansatz. The systematic

uncertainty turns out to be dominated by finite-volume effects, for which an estimate based on effective theory arguments is provided.

The result FNAL/MILC 12I is from simulations reaching down to a lightest RMS pion mass of about 380 MeV (the lightest valence pion mass for one of their ensembles is about 260 MeV). Their combined chiral and continuum extrapolation (results for two lattice spacings) is based on NLO staggered χPT supplemented by the continuum NNLO expression [285] and a phenomenological parameterization of the breaking of the Ademollo–Gatto theorem at finite lattice spacing inherent in their approach. The p^4 low-energy constants entering the NNLO expression have been fixed in terms of external input [226].

The ETM collaboration uses the twisted-mass discretization and provides at $N_f = 2$ a comprehensive study of the systematics [36,300], by presenting results for four lattice spacings and by simulating at light pion masses (down to $M_\pi = 260$ MeV). This makes it possible to constrain the chiral extrapolation, using both $SU(3)$ [278] and $SU(2)$ [282] χPT. Moreover, a rough estimate for the size of the effects due to quenching the strange quark is given, based on the comparison of the result for $N_f = 2$ dynamical quark flavours [45] with the one in the quenched approximation, obtained earlier by the SPQcdR collaboration [303].

We now compute the $N_f = 2+1+1$ FLAG average for $f_+(0)$ using the FNAL/MILC 18 and ETM 16 (uncorrelated) results, the $N_f = 2+1$ FLAG average based on FNAL/MILC 12I and RBC/UKQCD 15A, which we consider uncorrelated, while for $N_f = 2$ we consider directly the ETM 09A result, respectively:

$$\text{direct, } N_f = 2+1+1: \quad f_+(0) = 0.9698(17) \quad \text{Refs. [32,33],} \tag{76}$$

$$\text{direct, } N_f = 2+1: \quad f_+(0) = 0.9677(27) \quad \text{Refs. [34,35],} \tag{77}$$

$$\text{direct, } N_f = 2: \quad f_+(0) = 0.9560(57)(62) \quad \text{Ref. [36],} \tag{78}$$

where the parentheses in the third line indicate the statistical and systematic errors, respectively. We stress that the results (76) and (77), corresponding to $N_f = 2+1+1$ and $N_f = 2+1$, respectively, include already simulations with physical light-quark masses.

4.3.2 Results for $f_{K^\pm}/f_{\pi^\pm}$

In the case of the ratio of decay constants the data sets that meet the criteria formulated in the introduction are HPQCD 13A [37], ETM 14E [38], FNAL/MILC 17 [16] (which updates FNAL/MILC 14A [17]) and CalLat 20 [39] with $N_f = 2+1+1$, HPQCD/UKQCD 07 [40], MILC 10 [41], BMW 10 [42], RBC/UKQCD 14B [8], BMW 16 [43,310], and QCDSF/UKQCD 16 [44] with $N_f = 2+1$ and ETM 09 [45] with $N_f = 2$ dynamical flavours. Note that only CalLat 20 for $N_f = 2+1+1$ is the new entry for the FLAG average in this edition.

CalLat 20 employs a mixed action setup with the Möbius domain-wall valence quarks on gradient-flowed HISQ ensembles at four lattice spacings $a = 0.06$–0.15 fm. The valence pion mass reaches the physical point at three lattice spacings, and the smallest valence-sea and sea pion masses are below 200 MeV. Finite-volume corrections are studied on three lattice volumes at $a = 0.12$ fm and $M_\pi \sim 220$ MeV. Their extrapolation to the continuum limit and the physical point is based on NNLO χPT [316]. A comprehensive study of systematic uncertainties is performed by exploring several options including the use of the mixed-action effective theory expression, and the inclusion of N^{3}LO counter terms. They obtain $f_{K^\pm}/f_{\pi^\pm} = 1.1942(32)_{\text{stat}}(12)_\chi(20)_{a^2}(1)_{FV}(12)_M(7)_{IB}$, where the errors are statistical, due to the extrapolation in pion and kaon masses, extrapolation in a^2, finite-size effects, choice of the fitting form and isospin breaking corrections.

ETM 14E uses the twisted-mass discretization and provides a comprehensive study of the systematics by presenting results for three lattice spacings in the range 0.06–0.09 fm and for pion masses in the range 210–450 MeV. This makes it possible to constrain the chiral extrapolation, using both $SU(2)$ [282] χPT and polynomial fits. The ETM collaboration includes the spread in the central values obtained from different ansätze into the systematic errors. The final result of their analysis is $f_{K^\pm}/f_{\pi^\pm} = 1.184(12)_{\text{stat+fit}}(3)_{\text{Chiral}}(9)_{a^2}(1)_{Z_P}(3)_{FV}(3)_{IB}$ where the errors are (statistical + the error due to the fitting procedure), due to the chiral extrapolation, the continuum extrapolation, the mass-renormalization constant, the finite-volume and (strong) isospin-breaking effects.

In ETM 21 [305], the ETM collaboration presented an independent estimate of f_K/f_π in isosymmetric QCD with 2+1+1 dynamical flavours of the twisted-mass quarks. Their new set of gauge ensembles reaches the physical pion mass. The quark action includes the Sheikoleslami–Wohlert term for a better control of discretization effects. The finite-volume effects are examined by simulating three spatial volumes, and are corrected by $SU(2)$ χPT formulae [146]. Their new estimate $f_K/f_\pi = 1.1995(44)_{\text{stat+fit}}(7)_{\text{sys}}$ is consistent with ETM 14E with the total uncertainty reduced by a factor of ~ 3.5. While

ETM 21 satisfies all criteria on simulation parameters, it does not enter the FLAG average in this edition due to the publication status.

FNAL/MILC 17 has determined the ratio of the decay constants from a comprehensive set of HISQ ensembles with $N_f = 2+1+1$ dynamical flavours. They have generated 24 ensembles for six values of the lattice spacing (0.03–0.15 fm, scale set with f_{π^+}) and with both physical and unphysical values of the light sea-quark masses, controlling in this way the systematic uncertainties due to chiral and continuum extrapolations. With respect to FNAL/MILC 14A they have increased the statistics and added three ensembles at very fine lattice spacings, $a \simeq 0.03$ and 0.042 fm, including for the latter case also a simulation at the physical value of the light-quark mass. The final result of their analysis is $f_{K^\pm}/f_{\pi^\pm} = 1.1950(14)_{\text{stat}}(^{+0}_{-17})_{\text{a}^2}(2)_{FV}(3)_{f_\pi,PDG}(3)_{EM}(2)_{Q^2}$, where the errors are statistical, due to the continuum extrapolation, finite-volume, pion decay constant from PDG, electromagnetic effects and sampling of the topological charge distribution.[16]

HPQCD 13A has analyzed ensembles generated by MILC and therefore its study of $f_{K^\pm}/f_{\pi^\pm}$ is based on the same set of ensembles bar the ones at the finest lattice spacings (namely, only $a = 0.09-0.15$ fm, scale set with f_{π^+} and relative scale set with the Wilson flow [114,317]) supplemented by some simulation points with heavier quark masses. HPQCD employs a global fit based on continuum NLO $SU(3)$ χPT for the decay constants supplemented by a model for higher-order terms including discretization and finite-volume effects (61 parameters for 39 data points supplemented by Bayesian priors). Their final result is $f_{K^\pm}/f_{\pi^\pm} = 1.1916(15)_{\text{stat}}(12)_{\text{a}^2}(1)_{FV}(10)$, where the errors are statistical, due to the continuum extrapolation, due to finite-volume effects and the last error contains the combined uncertainties from the chiral extrapolation, the scale-setting uncertainty, the experimental input in terms of f_{π^+} and from the uncertainty in m_u/m_d.

Because CalLat 20, FNAL/MILC 17 and HPQCD 13A partly share their gauge ensembles, we assume a 100 % correlation among their statistical errors. A 100 % correlation on the total systematic uncertainty is also assumed between FNAL/MILC 17 and HPQCD 13A with the HISQ valence quarks.

For $N_f = 2+1$ the results BMW 16 and QCDSF/UKQCD 16 are eligible to enter the FLAG average. BMW 16 has analyzed the decay constants evaluated for 47 gauge ensembles generated using tree-level clover-improved fermions with two HEX-smearings and the tree-level Symanzik-improved gauge action. The ensembles correspond to five values of the lattice spacing (0.05–0.12 fm, scale set by Ω mass), to pion masses in the range 130–680 MeV and to values of the lattice size from 1.7 to 5.6 fm, obtaining a good control over the interpolation to the physical mass point and the extrapolation to the continuum and infinite volume limits.

QCDSF/UKQCD 16 has used the nonperturbatively $\mathcal{O}(a)$-improved clover action for the fermions (mildly stout-smeared) and the tree-level Symanzik action for the gluons. Four values of the lattice spacing (0.06–0.08 fm) have been simulated with pion masses down to ~ 220 MeV and values of the lattice size in the range 2.0–2.8 fm. The decay constants are evaluated using an expansion around the symmetric $SU(3)$ point $m_u = m_d = m_s = (m_u + m_d + m_s)^{phys}/3$.

Note that for $N_f = 2+1$ MILC 10 and HPQCD/UKQCD 07 are based on staggered fermions, BMW 10, BMW 16 and QCDSF/UKQCD 16 have used improved Wilson fermions and RBC/UKQCD 14B's result is based on the domain-wall formulation. In contrast to RBC/UKQCD 14B and BMW 16, the other simulations are for unphysical values of the light-quark masses (corresponding to smallest pion masses in the range $220-260$ MeV in the case of MILC 10, HPQCD/UKQCD 07, and QCDSF/UKQCD 16) and therefore slightly more sophisticated extrapolations needed to be controlled. Various ansätze for the mass and cutoff dependence comprising $SU(2)$ and $SU(3)$ χPT or simply polynomials were used and compared in order to estimate the model dependence. While BMW 10, RBC/UKQCD 14B, and QCDSF/UKQCD 16 are entirely independent computations, subsets of the MILC gauge ensembles used by MILC 10 and HPQCD/UKQCD 07 are the same. MILC 10 is certainly based on a larger and more advanced set of gauge configurations than HPQCD/UKQCD 07. This allows them for a more reliable estimation of systematic effects. In this situation we consider both statistical and systematic uncertainties to be correlated.

For $N_f = 2$ no new result enters the corresponding FLAG average with respect to the previous edition of the FLAG review [4], which therefore remains the ETM 09 result, which has simulated twisted-mass fermions down to (charged) pion masses equal to 260 MeV.

We note that the overall uncertainties quoted by ETM 14E at $N_f = 2+1+1$ and by BMW 16 and QCDSF/UKQCD 16 at $N_f = 2+1$ are much larger than the overall uncertainties obtained with staggered (HPQCD 13A, FNAL/MILC 17 at $N_f = 2+1+1$, and MILC 10, HPQCD/UKQCD 07 at $N_f = 2+1$) and domain-wall fermions (RBC/UKQCD 14B at $N_f = 2+1$).

[16] To form the average in Eq. (81), we have symmetrized the asymmetric systematic error and shifted the central value by half the difference as will be done throughout this section.

Table 17 Values of the $SU(2)$ isospin-breaking correction $\delta_{SU(2)}$ applied to the lattice data for f_K/f_π, entering the FLAG average at $N_f = 2+1$, for obtaining the corrected charged ratio $f_{K^\pm}/f_{\pi^\pm}$. The last error in the last column is due to a 100 % uncertainty assumed for $\delta_{SU(2)}$ from $SU(3)$ χPT

	f_K/f_π	$\delta_{SU(2)}$	$f_{K^\pm}/f_{\pi^\pm}$
HPQCD/UKQCD 07	1.189(2)(7)	−0.0040(7)	1.187(2)(7)(2)
BMW 10	1.192(7)(6)	−0.0041(7)	1.190(7)(6)(2)
RBC/UKQCD 14B	1.1945(45)	−0.0043(9)	1.1919(45)(26)

Before determining the average for $f_{K^\pm}/f_{\pi^\pm}$, which should be used for applications to Standard Model phenomenology, we apply the strong-isospin correction individually to all those results that have been published only in the isospin-symmetric limit, i.e., BMW 10, HPQCD/UKQCD 07 and RBC/UKQCD 14B at $N_f = 2+1$ and ETM 09 at $N_f = 2$. To this end, as in the previous editions of the FLAG reviews [2–4], we make use of NLO $SU(3)$ χPT [241,280], which predicts

$$\frac{f_{K^\pm}}{f_{\pi^\pm}} = \frac{f_K}{f_\pi}\sqrt{1+\delta_{SU(2)}}\,, \tag{79}$$

where [241]

$$\delta_{SU(2)} \approx \sqrt{3}\,\epsilon_{SU(2)}\left[-\tfrac{4}{3}\,(f_K/f_\pi - 1) + \tfrac{2}{3(4\pi)^2 f_0^2}\left(M_K^2 - M_\pi^2 - M_\pi^2 \ln\tfrac{M_K^2}{M_\pi^2}\right)\right]. \tag{80}$$

We use as input $\epsilon_{SU(2)} = \sqrt{3}/(4R)$ with the FLAG result for R of Eq. (54), $F_0 = f_0/\sqrt{2} = 80\,(20)$ MeV, $M_\pi = 135$ MeV and $M_K = 495$ MeV (we decided to choose a conservative uncertainty on f_0 in order to reflect the magnitude of potential higher-order corrections). The results are reported in Table 17, where in the last column the last error is due to the isospin correction (the remaining errors are quoted in the same order as in the original data).

For $N_f = 2$ and $N_f = 2+1+1$ dedicated studies of the strong-isospin correction in lattice QCD do exist. The updated $N_f = 2$ result of the RM123 collaboration [172] amounts to $\delta_{SU(2)} = -0.0080(4)$ and we use this result for the isospin correction of the ETM 09 result. Note that the above RM123 value for the strong-isospin correction is incompatible with the results based on $SU(3)$ χPT, $\delta_{SU(2)} = -0.004(1)$ (see Table 17). Moreover, for $N_f = 2+1+1$ HPQCD [37], FNAL/MILC [16] and ETM [318] estimate a value for $\delta_{SU(2)}$ equal to $-0.0054(14)$, $-0.0052(9)$ and $-0.0073(6)$, respectively. Note that the RM123 and ETM results are obtained using the insertion of the isovector scalar current according to the expansion method of Ref. [171], while the HPQCD and FNAL/MILC results correspond to the difference between the values of the decay constant ratio extrapolated to the physical u-quark mass m_u and to the average $(m_u + m_d)/2$ light-quark mass.

One would not expect the strange and heavier sea-quark contributions to be responsible for such a large effect. Whether higher-order effects in χPT or other sources are responsible still needs to be understood. More lattice-QCD simulations of $SU(2)$ isospin-breaking effects are therefore required. To remain on the conservative side we add a 100% error to the correction based on $SU(3)$ χPT. For further analyses we add (in quadrature) such an uncertainty to the systematic error.

Using the results of Table 17 for $N_f = 2+1$ we obtain

$$\text{direct, } N_f = 2+1+1: \quad f_{K^\pm}/f_{\pi^\pm} = 1.1932(21) \quad \text{Refs. [16,37–39],} \tag{81}$$

$$\text{direct, } N_f = 2+1: \quad f_{K^\pm}/f_{\pi^\pm} = 1.1917(37) \quad \text{Refs. [8,40–44],} \tag{82}$$

$$\text{direct, } N_f = 2: \quad f_{K^\pm}/f_{\pi^\pm} = 1.205(18) \quad \text{Ref. [45],} \tag{83}$$

for QCD with broken isospin.

The averages obtained for $f_+(0)$ and $f_{K^\pm}/f_{\pi^\pm}$ at $N_f = 2+1$ and $N_f = 2+1+1$ [see Eqs. (76–77) and (81–82)] exhibit a precision better than $\sim 0.3\%$. At such a level of precision QED effects cannot be ignored and a consistent lattice treatment of both QED and QCD effects in leptonic and semileptonic decays becomes mandatory.

4.3.3 Extraction of $|V_{ud}|$ and $|V_{us}|$

It is instructive to convert the averages for $f_+(0)$ and $f_{K^\pm}/f_{\pi^\pm}$ into a corresponding range for the CKM matrix elements $|V_{ud}|$ and $|V_{us}|$, using the relations (69). Consider first the results for $N_f = 2+1+1$. The average for $f_+(0)$ in Eq. (76) is mapped into the interval $|V_{us}| = 0.2232(6)$, depicted as a horizontal red band in Fig. 10. The one for $f_{K^\pm}/f_{\pi^\pm}$ in Eq. (81)

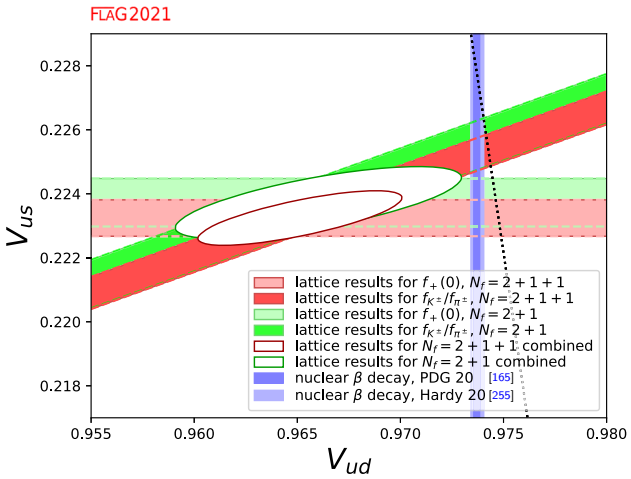

Fig. 10 The plot compares the information for $|V_{ud}|$, $|V_{us}|$ obtained on the lattice for $N_f = 2+1$ and $N_f = 2+1+1$ with $|V_{ud}|$ extracted from nuclear β transitions Eqs. (71) and (72). The dotted line indicates the correlation between $|V_{ud}|$ and $|V_{us}|$ that follows if the CKM-matrix is unitary. For the $N_f = 2$ results see the 2016 edition [3]

and $|V_{us}/V_{ud}|(f_{K^\pm}/f_{\pi^\pm})$ in Eq. (69) is converted into $|V_{us}|/|V_{ud}| = 0.2313(5)$, shown as a tilted red band. The red ellipse is the intersection of these two bands and represents the 68% likelihood contour,[17] obtained by treating the above two results as independent measurements. Repeating the exercise for $N_f = 2+1$ leads to the green ellipse. The vertical light and dark blue bands show $|V_{ud}|$ from nuclear β decay, Eqs. (71) and (72), respectively. The PDG value (71) indicates a tension with both the $N_f = 2+1+1$ and $N_f = 2+1$ results from lattice QCD.

As we mentioned, QED radiative corrections are becoming relevant for the extraction of the CKM elements at the current precision of lattice QCD inputs. We obtain a slightly larger value of $|V_{us}|/|V_{ud}| = 0.2320(5)$ by inputting $|V_{us}/V_{ud}|(f_{K^\pm}/f_{\pi^\pm})$ in Eq. (70) with the QED corrections on the lattice. Figure 11 suggests that the kaon (semi)leptonic decays favour a slightly smaller value of $|V_{ud}|$ than the nuclear transitions.

4.4 Tests of the Standard Model

In the Standard Model, the CKM matrix is unitary. In particular, the elements of the first row obey

$$|V_u|^2 \equiv |V_{ud}|^2 + |V_{us}|^2 + |V_{ub}|^2 = 1\,. \tag{84}$$

The tiny contribution from $|V_{ub}|$ is known much better than needed in the present context: $|V_{ub}| = 3.82(24)\cdot 10^{-3}$ [165]. In the following, we test the first row unitarity Eq. (84) by calculating $|V_u|^2$ and by analyzing the lattice data within the Standard Model.

In Fig. 10, the correlation between $|V_{ud}|$ and $|V_{us}|$ imposed by the unitarity of the CKM matrix is indicated by a dotted line (more precisely, in view of the uncertainty in $|V_{ub}|$, the correlation corresponds to a band of finite width, but the effect is too small to be seen here). The plot shows that there is a tension with unitarity in the data for $N_f = 2+1+1$: Numerically, the outcome for the sum of the squares of the first row of the CKM matrix reads $|V_u|^2 = 0.9813(66)$, which deviates from unity at the level of $\simeq 2.8$ standard deviations. Still, it is fair to say that at this level the Standard Model passes a nontrivial test that exclusively involves lattice data and well-established kaon decay branching ratios.

The test sharpens considerably by combining the lattice results for $f_+(0)$ with the β decay value of $|V_{ud}|$: $f_+(0)$ in Eq. (76) and the PDG estimate of $|V_{ud}|$ in Eq. (71) lead to $|V_u|^2 = 0.99794(37)$, which highlights a $\simeq 5.6\,\sigma$ deviation with unitarity. A lower tension at the three-σ level is suggested either from $f_{K^\pm}/f_{\pi^\pm}$ in Eq. (81) ($|V_u|^2 = 0.99883(37)$) or $|V_{ud}|$ in Eq. (72) with the updated nuclear corrections ($|V_u|^2 = 0.99800(65)$). Unitarity is fulfilled with $f_{K^\pm}/f_{\pi^\pm}$ and $|V_{ud}|$ (72) ($|V_u|^2 = 0.99890(68)$). Note that, when the PDG value of $|V_{ud}|$ (71) is employed, the uncertainties on $|V_u|^2$ coming from the errors of $|V_{ud}|$ and $|V_{us}|$ are of similar magnitude with each other.

[17] Note that the ellipses shown in Fig. 5 of both Ref. [1] and Ref. [2] correspond instead to the 39% likelihood contours. Note also that in Ref. [2] the likelihood was erroneously stated to be 68% rather than 39%.

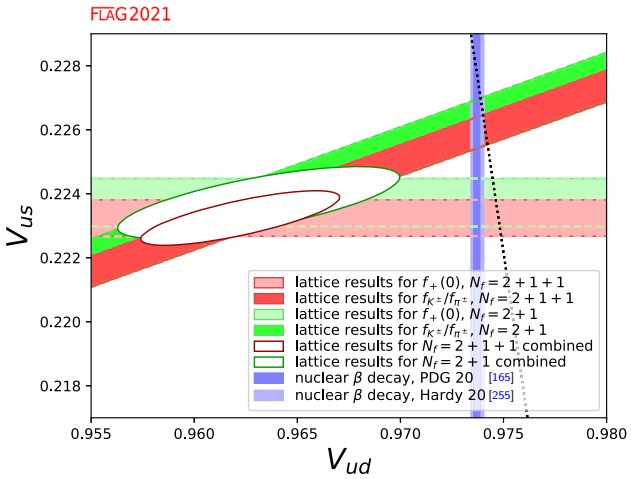

Fig. 11 Same as Fig. 10 but with $|V_{us}|/|V_{ud}|$ through Eq. (70)

The situation is similar for $N_f = 2+1$: with the lattice data alone one has $|V_u|^2 = 0.9832(89)$, which deviates from unity at the level of $\simeq 1.9$ standard deviations. The lattice results for $f_+(0)$ in Eq. (77) with the PDG value of $|V_{ud}|$ (71) lead to $|V_u|^2 = 0.99816(43)$, implying a $\simeq 4.3\,\sigma$ deviation from unitarity, whereas the deviation is reduced to 2.3–2.6 σ with $f_{K^\pm}/f_{\pi^\pm}$ in Eq. (82) ($|V_u|^2 = 0.99896(45)$) and $|V_{ud}|$ in Eq. (72) ($|V_u|^2 = 0.99822(69)$).

For the analysis corresponding to $N_f = 2$ the reader should refer to the 2016 edition [3].

4.5 Analysis within the Standard Model

The Standard Model implies that the CKM matrix is unitary. The precise experimental constraints quoted in Eq. (69) and the unitarity condition Eq. (84) then reduce the four quantities $|V_{ud}|$, $|V_{us}|$, $f_+(0)$, $f_{K^\pm}/f_{\pi^\pm}$ to a single unknown: any one of these determines the other three within narrow uncertainties.

As Fig. 12 shows, the results obtained for $|V_{us}|$ and $|V_{ud}|$ from the data on $f_{K^\pm}/f_{\pi^\pm}$ (squares) are consistent with the determinations via $f_+(0)$ (triangles), while there is a tendency that $|V_{us}|$ ($|V_{ud}|$) from $f_+(0)$ is systematically smaller (larger) than that from $f_{K^\pm}/f_{\pi^\pm}$. In order to calculate the corresponding average values, we restrict ourselves to those determinations that enter the FLAG average in Sect. 4.3. The corresponding results for $|V_{us}|$ are listed in Table 18 (the error in the experimental numbers used to convert the values of $f_+(0)$ and $f_{K^\pm}/f_{\pi^\pm}$ into values for $|V_{us}|$ is included in the statistical error).

For $N_f = 2+1+1$ we consider the data both for $f_+(0)$ and $f_{K^\pm}/f_{\pi^\pm}$, treating ETM 16 and ETM 14E on the one hand and FNAL/MILC 18, CalLat 20, FNAL/MILC 17, and HPQCD 13A on the other hand, as statistically correlated according to the prescription of Sect. 2.3. As shown in Table 19, we obtain $|V_{us}| = 0.2248(7)$, where the error is stretched by a factor $\sqrt{\chi^2/\text{dof}} \sim \sqrt{2.6}$. This result is indicated on the left hand side of Fig. 12 by the narrow vertical band. In the case $N_f = 2+1$ we consider MILC 10, FNAL/MILC 12I and HPQCD/UKQCD 07 on the one hand and RBC/UKQCD 14B and RBC/UKQCD 15A on the other hand, as mutually statistically correlated, since the analysis in the two cases starts from partly the same set of gauge ensembles. In this way we arrive at $|V_{us}| = 0.2249(5)$ with $\chi^2/\text{dof} \simeq 0.8$. For $N_f = 2$ we consider ETM 09A and ETM 09 as statistically correlated, obtaining $|V_{us}| = 0.2256(19)$ with $\chi^2/\text{dof} \simeq 0.7$. The figure shows that the results obtained for the data with $N_f = 2$, $N_f = 2+1$, and $N_f = 2+1+1$ are consistent with each other. However, the larger error for $N_f = 2+1+1$ due to the stretch factor $\sqrt{\chi^2/\text{dof}}$ suggests a slight tension between the estimates from the semileptonic and leptonic decays.

Alternatively, we can solve the relations for $|V_{ud}|$ instead of $|V_{us}|$. Again, the result $|V_{ud}| = 0.97440(17)$, which follows from the lattice data with $N_f = 2+1+1$, is perfectly consistent with the values $|V_{ud}| = 0.97438(12)$ and $|V_{ud}| = 0.97423(44)$ obtained from the data with $N_f = 2+1$ and $N_f = 2$, respectively. We observe the difference of about 3 σ from Eq. (71) from the superallowed nuclear transitions. It is, however, reduced to $\lesssim 2\,\sigma$ with Eq. (72) based on the updated nuclear corrections.

As mentioned in Sect. 4.1, the HFLAV value of $|V_{us}|$ from the inclusive hadronic τ decays differs from those obtained from the kaon decays by about three standard deviations. Assuming the first row unitarity (84) leads to a larger value of $|V_{ud}|$ than those from the kaon and nuclear decays. Such a tension does not appear with $|V_{us}|$ in Eq. (74) from strange hadronic τ decay data and lattice QCD data of the hadronic vacuum polarization function (Table 19).

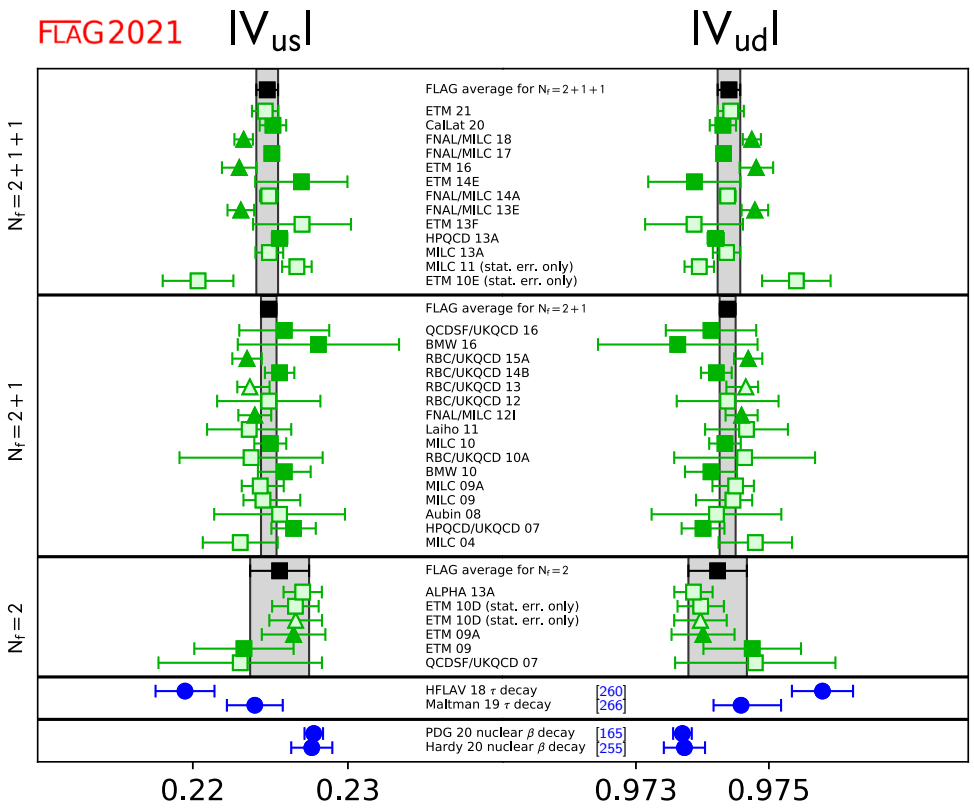

Fig. 12 Results for $|V_{us}|$ and $|V_{ud}|$ that follow from the lattice data for $f_+(0)$ (triangles) and $f_{K^\pm}/f_{\pi^\pm}$ (squares), on the basis of the assumption that the CKM matrix is unitary. The black squares and the grey bands represent our averages, obtained by combining these two different ways of measuring $|V_{us}|$ and $|V_{ud}|$ on a lattice. For comparison, the figure also indicates the results obtained if the data on nuclear β decay and inclusive hadronic τ decay is analyzed within the Standard Model

Table 18 Values of $|V_{us}|$ and $|V_{ud}|$ obtained from the lattice determinations of either $f_+(0)$ or $f_{K^\pm}/f_{\pi^\pm}$ assuming CKM unitarity. The first number in brackets represents the statistical error including the experimental uncertainty, whereas the second is the systematic one

Collaboration	Refs.	N_f	From	$\|V_{us}\|$	$\|V_{ud}\|$
FNAL/MILC 18	[33]	$2+1+1$	$f_+(0)$	0.2233(5)(3)	0.97474(12)(6)
ETM 16	[32]	$2+1+1$	$f_+(0)$	0.2230(11)(2)	0.97481(25)(5)
CalLat 20	[39]	$2+1+1$	$f_{K^\pm}/f_{\pi^\pm}$	0.2252(7)(6)	0.97431(15)(13)
FNAL/MILC 17	[16]	$2+1+1$	$f_{K^\pm}/f_{\pi^\pm}$	0.2251(4)(2)	0.97432(9)(5)
ETM 14E	[38]	$2+1+1$	$f_{K^\pm}/f_{\pi^\pm}$	0.2270(22)(20)	0.97388(51)(47)
HPQCD 13A	[37]	$2+1+1$	$f_{K^\pm}/f_{\pi^\pm}$	0.2256(4)(3)	0.97420(10)(7)
RBC/UKQCD 15A	[35]	$2+1$	$f_+(0)$	0.2235(9)(3)	0.97469(20)(7)
FNAL/MILC 12I	[34]	$2+1$	$f_+(0)$	0.2240(7)(8)	0.97459(16)(18)
QCDSF/UKQCD 16	[44]	$2+1$	$f_{K^\pm}/f_{\pi^\pm}$	0.2259(18)(23)	0.97413(42)(54)
BMW 16	[43,310]	$2+1$	$f_{K^\pm}/f_{\pi^\pm}$	0.2281(19)(48)	0.97363(44)(112)
RBC/UKQCD 14B	[8]	$2+1$	$f_{K^\pm}/f_{\pi^\pm}$	0.2256(3)(9)	0.97421(7)(22)
MILC 10	[41]	$2+1$	$f_{K^\pm}/f_{\pi^\pm}$	0.2250(5)(9)	0.97434(11)(21)
BMW 10	[42]	$2+1$	$f_{K^\pm}/f_{\pi^\pm}$	0.2259(13)(11)	0.97413(30)(25)
HPQCD/UKQCD 07	[40]	$2+1$	$f_{K^\pm}/f_{\pi^\pm}$	0.2265(6)(13)	0.97401(14)(29)
ETM 09A	[36]	2	$f_+(0)$	0.2265(14)(15)	0.97401(33)(34)
ETM 09	[45]	2	$f_{K^\pm}/f_{\pi^\pm}$	0.2233(11)(30)	0.97475(25)(69)

4.6 Direct determination of $f_{K^\pm}$ and $f_{\pi^\pm}$

It is useful for flavour-physics studies to provide not only the lattice average of $f_{K^\pm}/f_{\pi^\pm}$, but also the average of the decay constant $f_{K^\pm}$. The case of the decay constant $f_{\pi^\pm}$ is different, since the the PDG value [234] of this quantity, based on the use of the value of $|V_{ud}|$ obtained from superallowed nuclear β decays [247], is often used for setting the scale in lattice QCD (see Sect. 11 on the scale setting). However, the physical scale can be set in different ways, namely, by using as input the mass of the Ω baryon(m_Ω) or the Υ-meson spectrum (ΔM_Υ), which are less sensitive to the uncertainties of the chiral extrapolation

Table 19 The upper half of the table shows our final results for $|V_{us}|$, $|V_{ud}|$, $f_+(0)$ and $f_{K^\pm}/f_{\pi^\pm}$ that are obtained by analysing the lattice data within the Standard Model (see text). For comparison, the lower half lists the values that follow if the lattice results are replaced by the experimental results on nuclear β decay and inclusive hadronic τ decay, respectively

	Refs.	$\lvert V_{us}\rvert$	$\lvert V_{ud}\rvert$
$N_f = 2+1+1$		0.2248(7)	0.97440(17)
$N_f = 2+1$		0.2249(5)	0.97438(12)
$N_f = 2$		0.2256(19)	0.97423(44)
Nuclear β decay	[165]	0.2278(6)	0.97370(14)
Nuclear β decay	[256]	0.2277(13)	0.97373(31)
Inclusive τ decay	[261]	0.2195(19)	0.97561(43)
Inclusive τ decay	[267]	0.2240(18)	0.97458(40)

in the light-quark mass with respect to $f_{\pi^\pm}$. In such cases the value of the decay constant $f_{\pi^\pm}$ becomes a direct prediction of the lattice-QCD simulations. It is therefore interesting to provide also the average of the decay constant $f_{\pi^\pm}$, obtained when the physical scale is set through another hadron observable, in order to check the consistency of different scale-setting procedures.

Our compilation of the values of $f_{\pi^\pm}$ and $f_{K^\pm}$ with the corresponding colour code is presented in Table 20 and it is unchanged from the corresponding one in the previous FLAG review [4].

In comparison to the case of $f_{K^\pm}/f_{\pi^\pm}$ we have added two columns indicating which quantity is used to set the physical scale and the possible use of a renormalization constant for the axial current. For several lattice formulations the use of the nonsinglet axial-vector Ward identity allows to avoid the use of any renormalization constant.

One can see that the determinations of $f_{\pi^\pm}$ and $f_{K^\pm}$ suffer from larger uncertainties with respect to the ones of the ratio $f_{K^\pm}/f_{\pi^\pm}$, which is less sensitive to various systematic effects (including the uncertainty of a possible renormalization constant) and, moreover, is not exposed to the uncertainties of the procedure used to set the physical scale.

According to the FLAG rules, for $N_f = 2+1+1$ three data sets can form the average of $f_{K^\pm}$ only: ETM 14E [38], FNAL/MILC 14A [17], and HPQCD 13A [37]. Following the same procedure already adopted in Sect. 4.3 for the ratio of the decay constants, we assume 100 % statistical and systematic correlation between FNAL/MILC 14A and HPQCD 13A. For $N_f = 2+1$ three data sets can form the average of $f_{\pi^\pm}$ and $f_{K^\pm}$: RBC/UKQCD 14B [8] (update of RBC/UKQCD 12), HPQCD/UKQCD 07 [40], and MILC 10 [41], which is the latest update of the MILC program. We consider HPQCD/UKQCD 07 and MILC 10 as statistically correlated and use the prescription of Sect. 2.3 to form an average. For $N_f = 2$ the average cannot be formed for $f_{\pi^\pm}$, and only one data set (ETM 09) satisfies the FLAG rules for $f_{K^\pm}$.

Thus, our averages read

$$N_f = 2+1: \quad f_{\pi^\pm} = 130.2\ (0.8)\ \text{MeV} \quad \text{Refs. [8,40,41]}, \tag{85}$$

$$\begin{aligned} N_f &= 2+1+1: & f_{K^\pm} &= 155.7\ (0.3)\ \text{MeV} & &\text{Refs. [17,37,38]},\\ N_f &= 2+1: & f_{K^\pm} &= 155.7\ (0.7)\ \text{MeV} & &\text{Refs. [8,40,41]},\\ N_f &= 2: & f_{K^\pm} &= 157.5\ (2.4)\ \text{MeV} & &\text{Ref. [45]}. \end{aligned} \tag{86}$$

The lattice results of Table 20 and our averages (85–86) are reported in Fig. 13. Note that the FLAG averages of $f_{K^\pm}$ for $N_f = 2$ and $N_f = 2+1+1$ are based on calculations in which $f_{\pi^\pm}$ is used to set the lattice scale, while the $N_f = 2+1$ average does not rely on that.

Table 20 Colour code for the lattice data on $f_{\pi^\pm}$ and $f_{K^\pm}$ together with information on the way the lattice spacing was converted to physical units and on whether or not an isospin-breaking correction has been applied to the quoted result (see Sect. 4.3). The numerical values are listed in MeV units. In this and previous editions [4], old results with two red tags have been dropped

Collaboration	Refs.	N_f	Publication status	Chiral extrapolation	Continuum extrapolation	Finite-volume errors	Renormalization	Physical scale	SU(2)breaking	$f_{\pi^\pm}$	$f_{K^\pm}$
ETM 14E	[38]	2+1+1	A	○	★	○	na	f_π		–	154.4(1.5)(1.3)
FNAL/MILC 14A	[17]	2+1+1	A	★	★	★	na	f_π		–	$155.92(13)(^{+34}_{-23})$
HPQCD 13A	[37]	2+1+1	A	★	○	★	na	f_π		–	155.37(20)(27)
MILC 13A	[307]	2+1+1	A	★	○	★	na	f_π		–	155.80(34)(54)
ETM 10E	[309]	2+1+1	C	○	○	○	na	f_π	✓	–	159.6(2.0)
JLQCD 15C	[319]	2+1	C	○	★	★	NPR	t_0		$125.7(7.4)_{\text{stat}}$	
RBC/UKQCD 14B	[8]	2+1	A	★	★	★	NPR	m_Ω	✓	130.19(89)	155.18(89)
RBC/UKQCD 12	[188]	2+1	A	★	○	★	NPR	m_Ω	✓	127.1(2.7)(2.7)	152.1(3.0)(1.7)
Laiho 11	[49]	2+1	C	○	★	○	na	†		130.53(87)(2.10)	156.8(1.0)(1.7)
MILC 10	[41]	2+1	C	○	★	★	na	†		129.2(4)(1.4)	–
MILC 10	[41]	2+1	C	○	★	★	na	f_π		–	$156.1(4)(^{+6}_{-9})$
JLQCD/TWQCD 10	[311]	2+1	C	○	■	★	na	m_Ω	✓	$118.5(3.6)_{\text{stat}}$	$145.7(2.7)_{\text{stat}}$
RBC/UKQCD 10A	[117]	2+1	A	○	○	★	NPR	m_Ω	✓	124(2)(5)	148.8(2.0)(3.0)
MILC 09A	[15]	2+1	C	○	★	★	na	ΔM_Υ		128.0(0.3)(2.9)	153.8(0.3)(3.9)
MILC 09A	[15]	2+1	C	○	★	★	na	f_π		–	156.2(0.3)(1.1)
MILC 09	[157]	2+1	A	○	★	★	na	ΔM_Υ		$128.3(0.5)(^{+2.4}_{-3.5})$	$154.3(0.4)(^{+2.1}_{-3.4})$
MILC 09	[157]	2+1	A	○	★	★	na	f_π			$156.5(0.4)(^{+1.0}_{-2.7})$
Aubin 08	[312]	2+1	C	○	○	○	na	ΔM_Υ		129.1(1.9)(4.0)	153.9(1.7)(4.4)
RBC/UKQCD 08	[194]	2+1	A	○	■	★	NPR	m_Ω	✓	124.1(3.6)(6.9)	149.4(3.6)(6.3)
HPQCD/UKQCD 07	[40]	2+1	A	○	○	○	na	ΔM_Υ	✓	132(2)	156.7(0.7)(1.9)
MILC 04	[197]	2+1	A	○	○	○	na	ΔM_Υ		129.5(0.9)(3.5)	156.6(1.0)(3.6)
ETM 14D	[313]	2	C	★	■	○	na	f_π	✓	–	$153.3(7.5)_{\text{stat}}$
ETM 09	[45]	2	A	○	★	○	na	f_π	✓	–	$157.5(0.8)(2.0)(1.1)^{\dagger\dagger}$

The label 'na' indicates the lattice calculations that do not require the use of any renormalization constant for the axial current, while the label 'NPR' ('1lp') signals the use of a renormalization constant calculated nonperturbatively (at 1-loop order in perturbation theory)

†The ratios of lattice spacings within the ensembles were determined using the quantity r_1. The conversion to physical units was made on the basis of Ref. [120] and we note that such a determination depends on the PDG value [234] of the pion decay constant

††Errors are (stat+chiral)($a \neq 0$)(finite size)

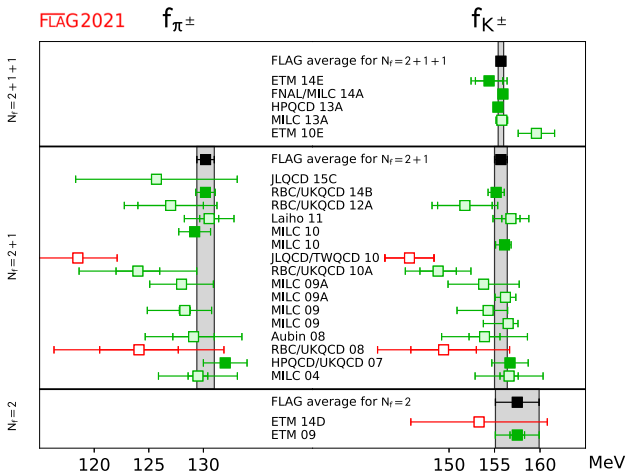

Fig. 13 Values of f_π and f_K. The black squares and grey bands indicate our averages (85) and (86)

5 Low-energy constants

Authors: S. Dürr, H. Fukaya, U. M. Heller

5.1 Chiral perturbation theory and lattice QCD

In the study of the quark-mass dependence of QCD observables calculated on the lattice, it is beneficial to use chiral perturbation theory (χPT). This framework predicts the nonanalytic quark-mass dependence of hadron masses and matrix elements, and it provides symmetry relations among such observables. These predictions invoke a set of linearly independent and universal (i.e., process-independent) low-energy constants (LECs), defined as coefficients of the polynomial terms (in m_q or M_π^2) of different observables.

χPT is an effective field theory approach to the low-energy properties of QCD based on the spontaneous breaking of chiral symmetry, $SU(N_f)_L \times SU(N_f)_R \to SU(N_f)_V$, and its soft explicit breaking by quark-mass terms. In its original implementation (i.e., in infinite volume) it is an expansion in powers of m_q and p^2 with the counting rule $M_\pi^2 \sim m_q \sim p^2$.

If one expands around the $SU(2)$ chiral limit, two LECs appear at order p^2 in the chiral effective Lagrangian,

$$F \equiv F_\pi\Big|_{m_u,m_d\to 0} \quad \text{and} \quad B \equiv \frac{\Sigma}{F^2}\,, \quad \text{where} \quad \Sigma \equiv -\langle\bar{u}u\rangle\Big|_{m_u,m_d\to 0}\,, \tag{87}$$

and seven more at order p^4, called $\bar{\ell}_i$ with $i = 1,\ldots,7$. In the analysis of the $SU(3)$ chiral limit there are again[18] two LECs at order p^2,

$$F_0 \equiv F_\pi\Big|_{m_u,m_d,m_s\to 0} \quad \text{and} \quad B_0 \equiv \frac{\Sigma_0}{F_0^2}\,, \quad \text{where} \quad \Sigma_0 \equiv -\langle\bar{u}u\rangle\Big|_{m_u,m_d,m_s\to 0}\,, \tag{88}$$

but ten more at order p^4, indicated by the symbols $L_i(\mu)$ with $i = 1,\ldots,10$. These "constants" are independent of the quark masses,[19] but they become scale dependent after renormalization (sometimes a superscript r is used). The $SU(2)$ constants $\bar{\ell}_i$ are μ-independent, since they are defined at scale $\mu = M_\pi^{\text{phys}}$ (as indicated by the bar). The $SU(3)$ constants $L_i(\mu)$ are usually quoted at the renormalization scale $\mu = 770\,\text{MeV}$. For the precise definition of these constants and their scale dependence we refer the reader to Refs. [280,320].

In the previous four versions of the FLAG review, we summarized the χPT formulae for the quark-mass dependence of the pion and kaon mass and decay constant, as well as the scalar and vector pion charge radius. We briefly discussed the different regimes of χPT, touched on partially quenched and mixed action formulations, collected and colour-coded the available lattice results for the LECs considered, and formed FLAG estimates or averages, where possible.

Since the fourth edition in 2019 [4] (referred to as FLAG 19 below) only a handful of papers appeared with results on the set of LECs covered in our report, but none that qualifies to be included in an average. We therefore decided to shorten the section on LECs considerably, referring the reader to the 2019 FLAG review for the χPT formulae, description of the results covered there, and the details and explanation of the FLAG estimates and averages. In this edition, we will concentrate on the description of the new results and, for the convenience of our readers, list the FLAG estimates and averages, asking the reader to consult FLAG 19 [4] for the details.

In the 2019 edition, we introduced a section on $\pi\pi$ scattering in the context of $SU(2)$ χPT and collected results, from finite-volume lattice calculations, of the isospin $I = 0$ and $I = 2$ scattering lengths. In this edition, we will keep this section and describe the new results that appeared since the 2019 FLAG review. We will, further, add a section on πK and KK scattering in the context of $SU(3)$ χPT and collect the available results for the scattering lengths from finite-volume lattice calculations.

[18] Here and in the following, we stick to the notation used in the papers where the χPT formulae were established, i.e., we work with $F_\pi \equiv f_\pi/\sqrt{2} = 92.2(1)\,\text{MeV}$ and $F_K \equiv f_K/\sqrt{2}$. The occurrence of different normalization conventions is not convenient, but avoiding it by reformulating the formulae in terms of f_π, f_K is not a good way out. Since we are using different symbols, confusion cannot arise.

[19] More precisely, they are independent of the 2 or 3 light-quark masses that are explicitly considered in the respective framework. However, all low-energy constants depend on the masses of the remaining quarks s, c, b, t or c, b, t in the $SU(2)$ and $SU(3)$ framework, respectively, although the dependence on the masses of the c, b, t quarks is expected to be small [280,320].

5.1.1 $\pi\pi$ scattering

The scattering of pseudoscalar octet mesons off each other (mostly $\pi\pi$ and πK scattering) is a useful approach to determine χPT low-energy constants [321–325]. This statement holds true both in experiment and on the lattice. We would like to point out the main difference between these two approaches is not so much the discretization of space-time, but rather the Minkowskian versus Euclidean setup.

In infinite-volume Minkowski space-time, 4-point Green's functions can be evaluated (e.g., in experiment) for a continuous range of (on-shell) momenta, as captured, for instance, by the Mandelstam variable s. For a given isospin channel $I = 0$ or $I = 2$ the $\pi\pi$ scattering phase shift $\delta^I(s)$ can be determined for a variety of s values, and by matching to χPT some low-energy constants can be determined (see below). In infinite-volume Euclidean space-time, such 4-point Green's functions can only be evaluated at kinematic thresholds; this is the content of the so-called Maiani–Testa theorem [326]. However, in the Euclidean case, the finite volume comes to our rescue, as first pointed out by Lüscher [327–330]. By comparing the energy of the (interacting) two-pion system in a box with finite spatial extent L to twice the energy of a pion (with identical bare parameters) in infinite volume information on the scattering length can be obtained. In particular, in the (somewhat idealized) situation where one can "scan" through a narrowly spaced set of box-sizes L such information can be reconstructed in an efficient way.

We begin with a brief summary of the relevant formulae in $SU(2)$ χPT terminology. In the x-expansion the formulae for a_ℓ^I with $\ell = 0$ and $I = 0, 2$ are found in Ref. [320]

$$a_0^0 M_\pi = +\frac{7M^2}{32\pi F^2}\left\{1 + \frac{5M^2}{84\pi^2 F^2}\left[\bar{\ell}_1 + 2\bar{\ell}_2 - \frac{9}{10}\bar{\ell}_3 + \frac{21}{8}\right] + \mathcal{O}(x^2)\right\}, \tag{89}$$

$$a_0^2 M_\pi = -\frac{M^2}{16\pi F^2}\left\{1 - \frac{M^2}{12\pi^2 F^2}\left[\bar{\ell}_1 + 2\bar{\ell}_2 + \frac{3}{8}\right] + \mathcal{O}(x^2)\right\}, \tag{90}$$

where $x \equiv M^2/(4\pi F)^2$ with $M^2 = (m_u + m_d)\Sigma/F^2$ is one possible expansion parameter of χPT. Throughout this report we deviate from the χPT habit of absorbing a factor $-M_\pi$ into the scattering length (relative to the convention used in quantum mechanics); we include just a minus sign but not the factor M_π. Hence, our a_ℓ^I have the dimension of a length so that all quark- or pion-mass dependence is explicit (as is most convenient for the lattice community). But the sign convention is the one of the chiral community (where $a_\ell^I M_\pi > 0$ means attraction and $a_\ell^I M_\pi < 0$ indicates repulsion).

An important difference between the two S-wave scattering lengths is evident already at tree-level. The isospin-0 scattering length (89) is large and positive at this order, while the isospin-2 counterpart (90) is by a factor ~ 3.5 smaller (in absolute magnitude) and negative. Hence, in the channel with $I = 0$ the interaction is *attractive*, while in the channel with $I = 2$ the interaction is *repulsive* and significantly weaker. In this convention, experimental results, evaluated with the unitarity constraint germane to any local quantum field theory, read $a_0^0 M_\pi = 0.2198(46)_{\text{stat}}(16)_{\text{syst}}(64)_{\text{theo}}$ and $a_0^2 M_\pi = -0.0445(11)_{\text{stat}}(4)_{\text{syst}}(8)_{\text{theo}}$ [324,331–333]. The ratio between the two (absolute) central values is about 4.9, i.e., a bit larger than 3.5. This, in turn, suggests that NLO contributions to a_0^0 and a_0^2 are sizeable, but the expansion seems well behaved.

Equations (89, 90) may be recast in the ξ-expansion, with $\xi \equiv M_\pi^2/(4\pi F_\pi)^2$, as

$$a_0^0 M_\pi = +\frac{7M_\pi^2}{32\pi F_\pi^2}\left\{1 + \xi\frac{1}{2}\bar{\ell}_3 + \xi 2\bar{\ell}_4 + \xi\left[\frac{20}{21}\bar{\ell}_1 + \frac{40}{21}\bar{\ell}_2 - \frac{18}{21}\bar{\ell}_3 + \frac{5}{2}\right] + \mathcal{O}(\xi^2)\right\}, \tag{91}$$

$$a_0^2 M_\pi = -\frac{M_\pi^2}{16\pi F_\pi^2}\left\{1 + \xi\frac{1}{2}\bar{\ell}_3 + \xi 2\bar{\ell}_4 - \xi\left[\frac{4}{3}\bar{\ell}_1 + \frac{8}{3}\bar{\ell}_2 + \frac{1}{2}\right] + \mathcal{O}(\xi^2)\right\}, \tag{92}$$

where $M^2/(4\pi F)^2 = M_\pi^2/(4\pi F_\pi)^2\{1 + \frac{1}{2}\xi\bar{\ell}_3 + 2\xi\bar{\ell}_4 + \mathcal{O}(\xi^2)\}$ has been used. Finally, this expression can be summarized as

$$a_0^0 M_\pi = +\frac{7M_\pi^2}{32\pi F_\pi^2}\left\{1 + \frac{9M_\pi^2}{32\pi^2 F_\pi^2}\ln\frac{(\lambda_0^0)^2}{M_\pi^2} + \mathcal{O}(\xi^2)\right\}, \tag{93}$$

$$a_0^2 M_\pi = -\frac{M_\pi^2}{16\pi F_\pi^2}\left\{1 - \frac{3M_\pi^2}{32\pi^2 F_\pi^2}\ln\frac{(\lambda_0^2)^2}{M_\pi^2} + \mathcal{O}(\xi^2)\right\}, \tag{94}$$

with the abbreviations

$$\frac{9}{2}\ln\frac{(\lambda_0^0)^2}{M_{\pi,\mathrm{phys}}^2} = \frac{20}{21}\bar{\ell}_1 + \frac{40}{21}\bar{\ell}_2 - \frac{5}{14}\bar{\ell}_3 + 2\bar{\ell}_4 + \frac{5}{2}, \tag{95}$$

$$\frac{3}{2}\ln\frac{(\lambda_0^2)^2}{M_{\pi,\mathrm{phys}}^2} = \frac{4}{3}\bar{\ell}_1 + \frac{8}{3}\bar{\ell}_2 - \frac{1}{2}\bar{\ell}_3 - 2\bar{\ell}_4 + \frac{1}{2}, \tag{96}$$

where λ_ℓ^I with $\ell = 0$ and $I = 0, 2$ are scales like the Λ_i in $\bar{\ell}_i = \ln(\Lambda_i^2/M_{\pi,\mathrm{phys}}^2)$ for $i \in \{1, 2, 3, 4\}$ (albeit they are not independent from the latter). Here, we made use of the fact that $M_\pi^2/M_{\pi,\mathrm{phys}}^2 = 1+\mathcal{O}(\xi)$ and thus $\xi\ln(M_\pi^2/M_{\pi,\mathrm{phys}}^2) = \mathcal{O}(\xi^2)$. In the absence of any knowledge on the $\bar{\ell}_i$, one would assume $\lambda_0^0 \simeq \lambda_0^2$, and with this input Eqs. (93, 94) suggest that the NLO contribution to $|a_0^0|$ is by a factor ~ 10.5 larger than the NLO contribution to $|a_0^2|$. The experimental numbers quoted before clearly support this view.

Given that all of this sounds like a complete success story for the determination of the scattering lengths a_0^0 and a_0^2, one may wonder whether lattice QCD is helpful at all. It is, because the "experimental" evaluation of these scattering lengths builds on a constraint between these two quantities that, in turn, is based on a (rather nontrivial) dispersive evaluation of scattering phase shifts [324,331–333]. Hence, to overcome this possible loophole, an independent lattice determination of a_0^0 and/or a_0^2 is highly welcome.

On the lattice a_0^2 is much easier to determine than a_0^0, since the former quantity does not involve quark-line disconnected contributions. The main upshot (to be reviewed below) is that the lattice determination of $a_0^2 M_\pi$ at the physical mass point is in perfect agreement with the experimental numbers quoted before, thus supporting the view that the scalar condensate is – at least in the $SU(2)$ case – the dominant order parameter, and the original estimate $\bar{\ell}_3 = 2.9 \pm 2.4$ is correct (see below). Still, from a lattice perspective it is natural to see a determination of $a_0^0 M_\pi$ and/or $a_0^2 M_\pi$ as a means to access the specific linear combinations of $\bar{\ell}_i$ with $i \in \{1, 2, 3, 4\}$ defined in Eqs. (95, 96).

In passing, we note that an alternative version of Eqs. (93, 94) is used in the literature, too. For instance, Refs. [94,95,334–336] give their results in the form

$$a_0^0 M_\pi = +\frac{7M_\pi^2}{32\pi F_\pi^2}\left\{1 + \frac{M_\pi^2}{32\pi^2 F_\pi^2}\left[\ell_{\pi\pi}^{I=0} + 5 - 9\ln\frac{M_\pi^2}{2F_\pi^2}\right] + \mathcal{O}(\xi^2)\right\}, \tag{97}$$

$$a_0^2 M_\pi = -\frac{M_\pi^2}{16\pi F_\pi^2}\left\{1 - \frac{M_\pi^2}{32\pi^2 F_\pi^2}\left[\ell_{\pi\pi}^{I=2} + 1 - 3\ln\frac{M_\pi^2}{2F_\pi^2}\right] + \mathcal{O}(\xi^2)\right\}, \tag{98}$$

where the quantities (used to quote the results of the lattice calculation)

$$\ell_{\pi\pi}^{I=0} = \frac{40}{21}\bar{\ell}_1 + \frac{80}{21}\bar{\ell}_2 - \frac{5}{7}\bar{\ell}_3 + 4\bar{\ell}_4 + 9\ln\frac{M_{\pi,\mathrm{phys}}^2}{2F_{\pi,\mathrm{phys}}^2}, \tag{99}$$

$$\ell_{\pi\pi}^{I=2} = \frac{8}{3}\bar{\ell}_1 + \frac{16}{3}\bar{\ell}_2 - \bar{\ell}_3 - 4\bar{\ell}_4 + 3\ln\frac{M_{\pi,\mathrm{phys}}^2}{2F_{\pi,\mathrm{phys}}^2}, \tag{100}$$

amount to linear combinations of the $\ell_i^{\mathrm{ren}}(\mu^{\mathrm{ren}})$ that, due to the explicit logarithms in Eqs. (99, 100), are effectively renormalized at the scale $\mu_{\mathrm{ren}} = f_\pi^{\mathrm{phys}} = \sqrt{2}F_\pi^{\mathrm{phys}} = 130.41(20)$ MeV [201]. Note that in these equations the dependence on the *physical* pion mass in the logarithms cancels the one that comes from the $\bar{\ell}_i$, so that the right-hand-sides bear no knowledge of M_π^{phys}. This alternative form is slightly different from Eqs. (93, 94). Exact equality would be reached upon substituting $F_\pi^2 \to F_{\pi,\mathrm{phys}}^2$ in the logarithms of Eqs. (97, 98). Upon expanding $F_\pi^2/F_{\pi,\mathrm{phys}}^2$ and subsequently the logarithm, one realizes that this difference amounts to a term $\mathcal{O}(\xi)$ within the square bracket. It thus makes up for a difference at the NNLO, which is beyond the scope of these formulae.

We close by mentioning a few works that elaborate on specific issues in $\pi\pi$ scattering relevant to the lattice. Reference [337] does mixed action χPT for 2 and 2+1 flavours of staggered sea quarks and Ginsparg–Wilson valence quarks, Refs. [338,339] work out scattering formulae in Wilson fermion χPT, and Ref. [340] lists connected and disconnected contractions in $\pi\pi$ scattering.

5.1.2 πK and KK scattering

The discussion of $\pi\pi$ scattering in the previous subsection carries over, without material changes, to the case of πK and KK scattering. The one (tiny) difference is that results, if contact with χPT is desired, must be matched against the $SU(3)$ version of this framework. In other words, for $\pi\pi$ scattering there is a choice between $SU(2)$ and $SU(3)$, while for πK and KK scattering matching to the $SU(3)$ version of χPT is mandatory.[20]

For completeness we also include, below, the $SU(3)$ χPT result for $I = 2$ $\pi\pi$ scattering. Since, as in the FLAG 19 review, we tabulate the S-wave scattering length with combined isospin I in the dimensionless variable $a_0^I M_\pi$, where the physical pion mass is meant, the result can be converted into specific linear combinations of NLO χPT coefficients in either the $SU(2)$ or $SU(3)$ χPT framework. In this conversion, an extra piece to the systematic error is to be included, to account for higher-order terms in the chiral expansion.

Below, we continue this tradition by summarizing results in the dimensionless variable $a_0^I \mu_{\pi K}$ for πK scattering and $a_0^I M_K$ for KK scattering. Throughout this report, $\mu_{\pi K} \equiv M_\pi M_K/(M_\pi + M_K)$ is the reduced mass of the kaon-pion system at the physical mass point. Again, these results can be converted into linear combinations of the L_i, with proper adjustment of the systematic uncertainty, due to the chiral expansion. In doing so, one should keep in mind that the $SU(3)$ framework does not converge as swiftly as the $SU(2)$ framework, since $m_{ud} \ll m_s$.

We basically follow Ref. [344], but we adopt, for masses and decay constants, the conventions of the LEC section in the FLAG 19 report. We consider the χPT formulae at $\mathcal{O}(p^4)$ in the chiral expansion, as given in Refs. [280,345–349]. The scattering lengths of the $\pi\pi(I = 2)$, $KK(I = 1)$, $\pi K(I = \frac{3}{2})$ and $\pi K(I = \frac{1}{2})$ systems can be written as

$$a^2_{0,\pi\pi} M_\pi = \frac{M_\pi^2}{16\pi F_\pi^2}\left\{-1 + \frac{16}{F_\pi^2}\left[M_\pi^2 L_{\rm scat}(\mu) - \frac{M_\pi^2}{2} L_5(\mu) + \chi^2_{\pi\pi}(\mu)\right]\right\}, \tag{101}$$

$$a^1_{0,KK} M_K = \frac{M_K^2}{16\pi F_K^2}\left\{-1 + \frac{16}{F_K^2}\left[M_K^2 L_{\rm scat}(\mu) - \frac{M_K^2}{2} L_5(\mu) + \chi^1_{KK}(\mu)\right]\right\}, \tag{102}$$

$$a^{3/2}_{0,\pi K} \mu_{\pi K} = \frac{\mu_{\pi K}^2}{8\pi F_\pi F_K}\left\{-1 + \frac{16}{F_\pi F_K}\left[M_\pi M_K L_{\rm scat}(\mu) - \frac{M_\pi^2 + M_K^2}{4} L_5(\mu) + \chi^{3/2}_{\pi K}(\mu)\right]\right\}, \tag{103}$$

$$a^{1/2}_{0,\pi K} \mu_{\pi K} = \frac{\mu_{\pi K}^2}{8\pi F_\pi F_K}\left\{2 + \frac{16}{F_\pi F_K}\left[M_\pi M_K L_{\rm scat}(\mu) + 2\frac{M_\pi^2 + M_K^2}{4} L_5(\mu) + \chi^{1/2}_{\pi K}(\mu)\right]\right\}. \tag{104}$$

These formulae are written in terms of $\mathcal{O}(p^4)$ values of the masses and decay constants (M_π, M_K, F_π and F_K) of the Nambu–Goldstone bosons (which, in turn, depend on the quark masses). We recall that the "Bernese" normalization for the pion decay constant at the physical point is adopted (cf. footnote 18). The constants $L_5(\mu)$ and

$$L_{\rm scat}(\mu) = 2L_1(\mu) + 2L_2(\mu) + L_3(\mu) - 2L_4(\mu) - \frac{1}{2}L_5(\mu) + 2L_6(\mu) + L_8(\mu) \tag{105}$$

are the $SU(3)$ low-energy constants (LECs) at the renormalization scale μ. The objects $\chi^{(I)}_{PQ}(\mu)$ are known functions with chiral logarithmic terms and dependence on the scale μ. In terms of these objects the functions $\chi^I_{PQ}(\mu)$ in Eqs. (101)–(104) read[21]

[20] Note that this could be circumvented if one used a heavy-meson extended version of χPT, in particular $SU(2)$ χPT with an extra (heavy) strange quark [341–343]. However, we have the original Gasser–Leutwyler versions of $SU(2)$ and $SU(3)$ χPT in mind.

[21] There is a typo in the original version of Ref. [344] which made us mistakenly give the last term in the square bracket of Eq. (107) as $\frac{10M_K^2}{9}$ in the arXiv:2111.09849v1 version of this report. The correct expression with the last term $\frac{7M_K^2}{9}$ agrees with Eq. (32) in [348] which, to the best of our knowledge, is the earliest reference for this quantity. Moreover, in the $SU(3)$ limit $(16\pi)^2\chi^2_{\pi\pi}(\mu) \to -\frac{14}{9}M_\pi^2 \log(\frac{M_\pi^2}{\mu^2}) + \frac{4}{9}M_\pi^2$, while the Gell–Mann–Oakes–Renner relation and the substitution $M_K^2 = M_\pi^2 + \epsilon$ yield $(16\pi)^2\chi^1_{KK}(\mu) \to \frac{M_\pi^2(M_\pi^2+\epsilon)}{4\epsilon}\log(\frac{M_\pi^2}{\mu^2}) - (M_\pi^2+\epsilon)\log(\frac{M_\pi^2+\epsilon}{\mu^2}) + \frac{(M_\pi^2+\epsilon)(-20M_\pi^2-20\epsilon+11M_\pi^2)}{36\epsilon}\log(\frac{M_\pi^2+4\epsilon/3}{\mu^2}) + \frac{7}{9}(M_\pi^2+\epsilon)$. In this expression the terms $O(\epsilon^{-1})$ cancel, and with $\log(\frac{M_\pi^2+4\epsilon/3}{\mu^2}) = \log(\frac{M_\pi^2}{\mu^2}) + \frac{4\epsilon}{3M_\pi^2}$ one obtains $(16\pi)^2\chi^1_{KK}(\mu) \to -\frac{14}{9}M_\pi^2\log(\frac{M_\pi^2}{\mu^2}) + \frac{4}{9}M_\pi^2$ in the limit $\epsilon \to 0$. Hence $\chi^2_{\pi\pi}(\mu) = \chi^1_{KK}(\mu)$ in the $SU(3)$ limit. We are indebted to André Walker-Loud and Kiyoshi Sasaki for pointing this out to us and for clarifying details, respectively.

$$\chi^2_{\pi\pi}(\mu) = \frac{1}{(16\pi)^2}\left[-\frac{3M_\pi^2}{2}\log\left(\frac{M_\pi^2}{\mu^2}\right) - \frac{M_\pi^2}{18}\log\left(\frac{M_\eta^2}{\mu^2}\right) + \frac{4M_\pi^2}{9}\right], \tag{106}$$

$$\begin{aligned}\chi^1_{KK}(\mu) = \frac{1}{(16\pi)^2}\Bigg[&\frac{M_\pi^2 M_K^2}{4(M_K^2 - M_\pi^2)}\log\left(\frac{M_\pi^2}{\mu^2}\right) - M_K^2\log\left(\frac{M_K^2}{\mu^2}\right)\\ &+ \frac{-20M_K^4 + 11M_\pi^2 M_K^2}{36(M_K^2 - M_\pi^2)}\log\left(\frac{M_\eta^2}{\mu^2}\right) + \frac{7M_K^2}{9}\Bigg],\end{aligned} \tag{107}$$

$$\begin{aligned}\chi^{3/2}_{\pi K}(\mu) = \frac{1}{(16\pi)^2}\Bigg[&\frac{22M_\pi^3 M_K + 11M_\pi^2 M_K^2 - 5M_\pi^4}{8\left(M_K^2 - M_\pi^2\right)}\log\left(\frac{M_\pi^2}{\mu^2}\right)\\ &+ \frac{9M_K^4 - 134M_\pi M_K^3 + 16M_\pi^3 M_K - 55M_\pi^2 M_K^2}{36(M_K^2 - M_\pi^2)}\log\left(\frac{M_K^2}{\mu^2}\right)\\ &+ \frac{36M_K^4 + 48M_\pi M_K^3 - 10M_\pi^3 M_K + 11M_\pi^2 M_K^2 - 9M_\pi^4}{72(M_K^2 - M_\pi^2)}\log\left(\frac{M_\eta^2}{\mu^2}\right)\\ &+ \frac{43M_\pi M_K}{9} - \frac{8M_\pi M_K}{9}t_1(M_\pi, M_K)\Bigg],\end{aligned} \tag{108}$$

$$\begin{aligned}\chi^{1/2}_{\pi K}(\mu) = \frac{1}{(16\pi)^2}\Bigg[&\frac{11M_\pi^3 M_K - 11M_\pi^2 M_K^2 + 5M_\pi^4}{4(M_K^2 - M_\pi^2)}\log\left(\frac{M_\pi^2}{\mu^2}\right)\\ &+ \frac{-9M_K^4 - 67M_\pi M_K^3 + 8M_\pi^3 M_K + 55M_\pi^2 M_K^2}{18(M_K^2 - M_\pi^2)}\log\left(\frac{M_K^2}{\mu^2}\right)\\ &+ \frac{-36M_K^4 + 24M_K^3 M_\pi - 5M_K M_\pi^3 - 11M_K^2 M_\pi^2 + 9M_\pi^4}{36(M_K^2 - M_\pi^2)}\log\left(\frac{M_\eta^2}{\mu^2}\right)\\ &+ \frac{43M_\pi M_K}{9} + \frac{4M_\pi M_K}{9}t_1(M_\pi, M_K) - \frac{12M_\pi M_K}{9}t_2(M_\pi, M_K)\Bigg],\end{aligned} \tag{109}$$

where $t_1(M_\pi, M_K)$, $t_2(M_\pi, M_K)$ can be written as

$$t_1(M_\pi, M_K) = \frac{\sqrt{(M_K + M_\pi)(2M_K - M_\pi)}}{M_K - M_\pi}\arctan\left(\frac{2(M_K - M_\pi)}{M_K + 2M_\pi}\sqrt{\frac{M_K + M_\pi}{2M_K - M_\pi}}\right), \tag{110}$$

$$t_2(M_\pi, M_K) = \frac{\sqrt{(M_K - M_\pi)(2M_K + M_\pi)}}{M_K + M_\pi}\arctan\left(\frac{2(M_K + M_\pi)}{M_K - 2M_\pi}\sqrt{\frac{M_K - M_\pi}{2M_K + M_\pi}}\right). \tag{111}$$

In short, these formulae show that – in the $SU(3)$ framework – the four scattering lengths $a_0^1 M_\pi$, $a_0^2 M_K$, $a_0^{3/2}\mu_{\pi K}$, $a_0^{1/2}\mu_{\pi K}$ determine three linear combinations of $L_5(\mu)$ and $L_{\rm scat}(\mu)$. Recall that Eq. (105) shows that the latter object is itself a linear combination of the $L_i(\mu)$. Interestingly, $\pi\pi$ and KK scattering determine the same linear combination $L_{\rm scat}(\mu) - \frac{1}{2}L_5(\mu)$, while $a_0^{3/2}\mu_{\pi K}$ and $a_0^{1/2}\mu_{\pi K}$ determine two more (m_s/m_{ud}-dependent) linear combinations. In the last few lines, we established the habit of omitting the particle subscript in $a^I_{0,\pi K}$ and $a^I_{0,KK}$, since the value of I together with the factor M_π, $\mu_{\pi K}$ or M_K already tells the particles involved in the scattering process. The remaining zero subscript is meant to indicate the S-wave component.

5.2 Extraction of SU(2) low-energy constants

5.2.1 New results for individual LO SU(2) LECs

We are aware of four new papers with results on individual $SU(2)$ LECs plus an additional one which we overlooked in FLAG 19 [4]. They all give results on the LO LECs, B and/or F, where B is frequently traded for the condensate $\Sigma \equiv BF^2$ (both B and Σ are renormalized at the scale $\mu = 2\,\text{GeV}$). We start by briefly mentioning their details.

The paper ETM 20A [350] presents an $N_f = 2$ calculation with twisted mass fermions, using three pion masses down to the physical value at a single lattice spacing $a = 0.0914(15)$ fm. They report a value of F as given in Table 22 and a value of $\bar{\ell}_4$ discussed in Sect. 5.2.2 below. The publication status changed from "preprint" to "accepted" after our closing date (as did the quoted uncertainty). In practical terms this change is insignificant, since the quoted number (due to a red tag) would not contribute to the $N_f = 2$ average.

The paper χQCD 21 [351] employs $N_f = 2 + 1$ QCD with domain wall fermions and RI/MOM renormalization. They have two ensembles with physical pion mass (139 MeV) at lattice spacings $a = 0.114$fm and $a = 0.084$fm, one ensemble with $M_\pi = 234\,\text{MeV}$ at $a = 0.071$fm, and one with $M_\pi = 371\,\text{MeV}$ at $a = 0.063$fm that is only used to test the lattice spacing dependence of the scalar renormalization factor. They report the value of $\Sigma^{1/3}$ as listed in Table 21.

The paper ETM 21 [305] uses $N_f = 2 + 1 + 1$ flavours of twisted mass fermions, ten ensembles, three lattice spacings ($a = 0.092, 0.080, 0.068$fm), up to four pion masses $M_\pi \in [135\,\text{MeV}, 346\,\text{MeV}]$, up to two volumes, and $L(M_{\pi,\text{min}}) = 5.55\,\text{fm}$. The scale is set by $f_\pi^{\text{phys}} = \sqrt{2}F_\pi^{\text{phys}} = 130.4(2)\,\text{MeV}$ [201]. They analyze the quark mass dependence of both F_π and the (chiral and finite-volume) log-free quantity $X_\pi = (F_\pi M_\pi^4)^{1/5}$ [352], to determine F and $\bar{\ell}_4$ in two different ways. The two fitting procedures yield nearly identical results for F. The two central values agree exactly, as do the two systematic uncertainties; only the combined statistical plus fitting uncertainty differs a bit among the two approaches. Since the paper does not give preference to one of the fitting procedures, we take the liberty to condense them, assuming 100% correlation, into the single result $F = 87.7(6)(5)\,\text{MeV}$ as listed in Table 22. They also report a value of $\bar{\ell}_4$ to be mentioned in Sect. 5.2.2 below.

The paper ETM 21A [204] is again based on $N_f = 2 + 1 + 1$ flavours of twisted mass fermions, ten ensembles, three lattice spacings, $a = 0.095, 0.082, 0.069$fm, up to four pion masses $M_\pi \in [134\,\text{MeV}, 346\,\text{MeV}]$, up to two volumes, and $L(M_{\pi,\text{min}}) = 5.52\,\text{fm}$. The scale is set by $f_\pi^{\text{phys}} = \sqrt{2}F_\pi^{\text{phys}} = 130.4(2)\,\text{MeV}$ [201], and cross-checked with the nucleon mass. From the analysis of the pion sector they determine values of F and $\Sigma^{1/3}$ as listed in Tables 22 and 21, respectively.

Finally, we should mention Ref. [353] which, regrettably, escaped our attention when preparing the last FLAG report [4]. The authors extract the quark condensate from an OPE analysis of the Landau-gauge quark propagator. They use overlap valence quarks on three ensembles with (2+1)-flavor domain-wall fermions with $a^{-1} = 1.75\,\text{GeV}$ and sea pion masses of 331, 419 and 557 MeV from the RBC/UKQCD collaboration. Their eight valence pion masses range from 220 to 600 MeV. Their result for $\Sigma^{1/3}$ is listed in Table 21. With only a single lattice spacing, their result does not contribute to the FLAG average.

Perhaps it is worth comparing the results for $f \equiv \sqrt{2}F$ in Refs. [204,305]. Carrying all errors along, one finds $\Delta f\,[\text{MeV}] = 124.0(0.9)(0.7) - 122.82(32)(65) = 1.18(1.35)$, which is less than one standard deviation. Given that the two studies were carried out on largely the same ensemble basis, it is perhaps reasonable to assume the statistical error is $\sim 100\%$ correlated. In this case, the difference would be $\Delta f\,[\text{MeV}] = 124.0(0.7) - 122.82(65) = 1.18(0.96)$, which is 1.24σ and thus perfectly acceptable. The chiral analysis in the two papers is treated somewhat differently, which would lead to differences in the neglected NNLO terms, and thus reflects a systematic effect.

The new results for $\Sigma^{1/3}$ and F_π/F, together with the previous ones, are shown in Figs. 14 and 15, respectively.

5.2.2 New results for individual NLO SU(2) LECs

Two of the aforementioned papers contain new results on $\bar{\ell}_4$, i.e., a specific LEC at NLO of the $SU(2)$ framework. ETM 20A [350] quotes $\bar{\ell}_4 = 4.31(4)(2)(11)(5)$ for $N_f = 2$, while ETM 21 [305] finds $\bar{\ell}_4 = 3.44(28)(36)$ for $N_f = 2 + 1 + 1$. These results are listed in Table 23.

If one were to ignore N_f, the two new results would appear inconsistent. While an implicit dependence on the strange- (and highly suppressed) charm-quark mass in the sea is a logical possibility, it seems to us these results should be considered in conjunction with the FLAG 19 averages for the quantity $\bar{\ell}_4$. The FLAG 19 average for $N_f = 2$, based on four papers, was 4.40(28), the average for $N_f = 2 + 1$, based on five papers, was 4.02(45), and the estimate for $N_f = 2 + 1 + 1$,

Table 21 Cubic root of the $SU(2)$ quark condensate $\Sigma \equiv -\lim_{m_u,m_d\to 0}\langle \bar{u}u\rangle$ in MeV units, in the $\overline{\text{MS}}$-scheme, at the renormalization scale $\mu = 2\,\text{GeV}$. All ETM values that were available only in r_0 units were converted on the basis of $r_0 = 0.48(2)$ fm [116,367,368], with this error being added in quadrature to any existing systematic error

Collaboration	Refs.	N_f	Publication status	Chiral extrapolation	Cont. extrapolation	Finite volume	Renormalization	$\sum^{1/3}$
ETM 21A	[204]	2+1+1	P	★	○	★	★	267.6(1.8)(1.1)
ETM 17E	[81]	2+1+1	A	○	★	○	★	318(21)(21)
ETM 13	[80]	2+1+1	A	○	★	★	★	280(8)(15)
χQCD 21	[351]	2+1	P	★	★	★	★	260.3(0.7)(1.7)
JLQCD 17A	[86]	2+1	A	○	★	★	★	274(13)(29)
Wang 16	[353]	2+1	A	○	■	■	★	305(15)(21)
JLQCD 16B	[85]	2+1	A	○	★	★	★	270.0(1.3)(4.8)
RBC/UKQCD 15E	[84]	2+1	A	★	★	★	★	274.2(2.8)(4.0)
RBC/UKQCD 14B	[8]	2+1	A	★	★	★	★	275.9(1.9)(1.0)
BMW 13	[83]	2+1	A	★	★	★	★	271(4)(1)
Borsanyi 12	[82]	2+1	A	○	○	★	★	272.3(1.2)(1.4)
JLQCD/TWQCD 10A	[354]	2+1	A	★	■	■	★	234(4)(17)
MILC 10A	[12]	2+1	C	○	★	★	○	$281.5(3.4)\binom{+2.0}{-5.9}(4.0)$
RBC/UKQCD 10A	[117]	2+1	A	○	○	■	★	256(5)(2)(2)
JLQCD 09	[355]	2+1	A	★	■	■	★	$242(4)\binom{+19}{-18}$
MILC 09A, $SU(3)$-fit	[15]	2+1	C	○	★	★	○	279(1)(2)(4)
MILC 09A, $SU(2)$-fit	[15]	2+1	C	○	★	★	○	$280(2)\binom{+4}{-8}(4)$
MILC 09	[157]	2+1	A	○	★	★	○	$278(1)\binom{+2}{-3}(5)$
TWQCD 08	[356]	2+1	A	■	■	■	★	259(6)(9)
PACS-CS 08, $SU(3)$-fit	[193]	2+1	A	★	■	■	■	312(10)
PACS-CS 08, $SU(2)$-fit	[193]	2+1	A	★	■	■	■	309(7)
RBC/UKQCD 08	[194]	2+1	A	○	■	○	★	255(8)(8)(13)
Engel 14	[89]	2	A	★	★	★	★	263(3)(4)
Brandt 13	[88]	2	A	○	★	○	★	261(13)(1)
ETM 13	[80]	2	A	○	★	○	★	283(7)(17)
ETM 12	[357]	2	A	○	★	○	★	299(26)(29)
Bernardoni 11	[358]	2	C	○	■	■	★	306(11)
TWQCD 11	[359]	2	A	○	■	■	★	230(4)(6)
TWQCD 11A	[360]	2	A	○	■	■	★	259(6)(7)
JLQCD/TWQCD 10A	[354]	2	A	★	■	■	★	242(5)(20)
Bernardoni 10	[361]	2	A	○	■	■	★	$262\binom{+33}{-34}\binom{+4}{-5}$
ETM 09C	[87]	2	A	○	★	○	★	$270(5)\binom{+3}{-4}$
ETM 08	[92]	2	A	○	○	○	★	264(3)(5)
CERN 08	[362]	2	A	○	■	○	★	276(3)(4)(5)
Hasenfratz 08	[363]	2	A	○	■	○	★	248(6)
JLQCD/TWQCD 08A	[364]	2	A	○	■	■	★	$235.7(5.0)(2.0)\binom{+12.7}{-0.0}$
JLQCD/TWQCD 07	[365]	2	A	○	■	■	★	239.8(4.0)
JLQCD/TWQCD 07A	[366]	2	A	★	■	■	★	252(5)(10)

Table 22 Results for the $SU(2)$ low-energy constant F (in MeV) and for the ratio F_π/F. All ETM values that were available only in r_0 units were converted on the basis of $r_0 = 0.48(2)$ fm [116,367,368], with this error being added in quadrature to any existing systematic error. Numbers in slanted fonts have been calculated by us, based on $\sqrt{2}F_\pi^{\text{phys}} = 130.41(20)$ MeV [201], with this error being added in quadrature to any existing systematic error (otherwise to the statistical error). The systematic error in ETM 11 has been carried over from ETM 10

Collaboration	Refs.	N_f	Publication status	Chiral extrapolation	Cont. extrapolation	Finite volume	F	F_π/F
ETM 21A	[204]	2+1+1	P	★	○	★	86.85(23)(46)	*1.062(3)(6)*
ETM 21	[305]	2+1+1	P	★	○	★	87.7(6)(5)	*1.051(7)(6)*
ETM 11	[90]	2+1+1	C	○	★	○	85.60(4)*(13)*	*1.077(2)(2)*
ETM 10	[218]	2+1+1	A	○	■	★	85.66(6)(13)	1.076(2)(2)
RBC/UKQCD 15E	[84]	2+1	A	★	★	★	85.8(1.1)(1.5)	1.0641(21)(49)
RBC/UKQCD 14B	[8]	2+1	A	★	★	★	86.63(12)(13)	1.0645(15)(0)
BMW 13	[83]	2+1	A	★	★	★	88.0(1.3)(0.3)	1.055(7)(2)
Borsanyi 12	[82]	2+1	A	○	○	★	86.78(05)(25)	1.0627(06)(27)
NPLQCD 11	[91]	2+1	A	○	○	○	*86.8(2.1)*$\binom{+3.3}{-3.4}$	1.062(26)$\binom{+42}{-40}$
MILC 10	[41]	2+1	C	○	★	★	87.0(4)(5)	*1.060(5)(6)*
MILC 10A	[12]	2+1	C	○	★	★	87.5(1.0)$\binom{+0.7}{-2.6}$	*1.054(12)*$\binom{+31}{-09}$
MILC 09A, $SU(3)$-fit	[15]	2+1	C	○	★	★	86.8(2)(4)	1.062(1)(3)
MILC 09A, $SU(2)$-fit	[15]	2+1	C	○	★	★	87.4(0.6)$\binom{+0.9}{-1.0}$	*1.054(7)*$\binom{+12}{-11}$
MILC 09	[157]	2+1	A	○	★	★	*87.66(17)*$\binom{+28}{-52}$	1.052(2)$\binom{+6}{-3}$
PACS-CS 08, $SU(3)$-fit	[193]	2+1	A	★	■	■	90.3(3.6)	1.062(8)
PACS-CS 08, $SU(2)$-fit	[193]	2+1	A	★	■	■	89.4(3.3)	1.060(7)
RBC/UKQCD 08	[194]	2+1	A	○	■	○	81.2(2.9)(5.7)	1.080(8)
ETM 20A	[350]	2	A	★	■	○	86.46(0.06)(2.40)	*1.067(1)(30)*
ETM 15A	[368]	2	A	★	■	○	86.3(2.8)	*1.069(35)*
Engel 14	[89]	2	A	★	★	★	85.8(0.7)(2.0)	*1.075(09)(25)*
Brandt 13	[88]	2	A	○	★	○	84(8)(2)	1.080(16)(6)
QCDSF 13	[369]	2	A	★	○	○	86(1)	*1.07(1)*
TWQCD 11	[359]	2	A	○	■	■	83.39(35)(38)	*1.106(5)(5)*
ETM 09C	[87]	2	A	○	★	○	85.91(07)$\binom{+78}{-07}$	1.0755(6)$\binom{+08}{-94}$
ETM 08	[92]	2	A	○	○	○	86.6(7)(7)	1.067(9)(9)
Hasenfratz 08	[363]	2	A	○	■	○	90(4)	*1.02(5)*
JLQCD/TWQCD 08A	[364]	2	A	○	■	■	79.0(2.5)(0.7)$\binom{+4.2}{-0.0}$	*1.167(37)(10)*$\binom{+02}{-62}$
JLQCD/TWQCD 07	[365]	2	A	○	■	■	87.3(5.6)	*1.06(7)*
Colangelo 03	[370]						86.2(5)	1.0719(52)

based on a single paper, was 4.73(10). In terms of standard deviations the difference "old average minus new result" is $4.40(28) - 4.31(13) = 0.09(31)$ or 0.3σ for $N_f = 2$, while it is $4.73(10) - 3.44(46) = 1.29(47)$ or 2.7σ for $N_f = 2+1+1$. Hence, the new $N_f = 2$ result of ETM 20A [350] is in perfect agreement with the corresponding FLAG 19 average. On the other hand, the new $N_f = 2+1+1$ result of ETM 21 [305] is largely *inconsistent* with the corresponding FLAG 19 estimate, which was taken from Ref. [90]. Perhaps one should take a step back at this point, and consider the option that the implicit N_f-dependence (through a dynamical strange and charm quark) is smaller than some unaccounted-for systematic effects in at least one of the works considered. On the practical side neither one of the new results qualifies for a FLAG average (ETM 20A [350] has a red tag, ETM 21 [305] is still unpublished). In summary, the time is not ripe to give an update on the $\bar{\ell}_4$ average given in FLAG 19.

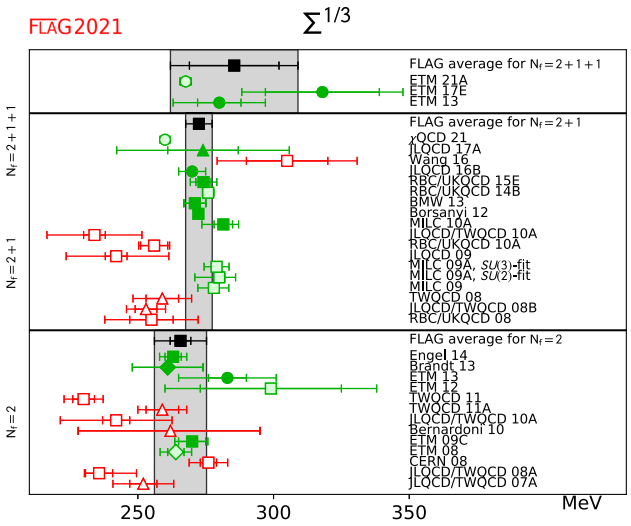

Fig. 14 Cubic root of the $SU(2)$ quark condensate $\Sigma \equiv -\lim_{m_u,m_d\to 0}\langle\bar{u}u\rangle$ in the $\overline{\text{MS}}$-scheme, at the renormalization scale $\mu = 2\,\text{GeV}$. Square symbols indicate determinations from correlators in the p-regime, up triangles refer to extractions from the topological susceptibility, diamonds to determinations from the pion form factor, and bullet points refer to the spectral density method

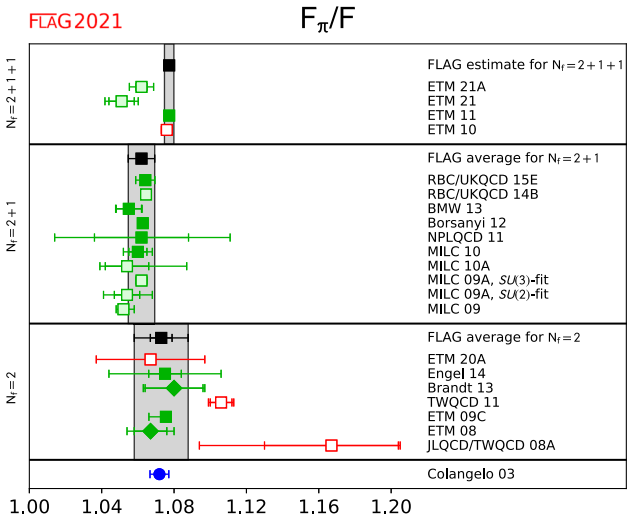

Fig. 15 Comparison of the results for the ratio of the physical pion decay constant F_π and the leading-order $SU(2)$ low-energy constant F. Square symbols indicate determinations from correlators in the p-regime, and diamonds from the pion form factor

The two new results on $\bar{\ell}_4$ in Table 23 are displayed in Fig. 16, along with all previous determinations with systematic error bars. Since there is no new entry in the first column of the table, there is no analogous figure for $\bar{\ell}_3$.

There is also new information on $\bar{\ell}_6$. It appears in three new papers on the slope of the vector form factor at $q^2 = 0$ ("charge radius") of the pion. We follow our tradition of quoting and comparing results in terms of $\langle r^2\rangle_V^\pi$ rather than $\bar{\ell}_6$. As mentioned before, we start with a brief discussion of the particulars of these papers.

The paper Feng 19 [377] is based on $N_f = 2+1$ flavours of domain-wall valence quarks on domain-wall sea. This collaboration uses four ensembles essentially at the physical mass point[22] and another one at $M_\pi = 341\,\text{MeV}$. At the physical mass point they have three lattice spacings in the range $a^{-1} = 1.015{-}1.73\,\text{GeV}$, i.e., none of them satisfies $a < 0.1\text{fm}$. The respective box sizes are $L = [6.22, 4.58, 5.48]\text{fm}$, hence $L(M_{\pi,\text{min}}) = 6.22\text{fm}$.

[22] This earns them a green box on "chiral extrapolation", but the criterion was crafted with the idea of a global fit which takes all available information into account. In the setup of Feng 19 [377] it is barely possible to disentangle a small M_π dependence in the vicinity of M_π^{phys} from cut-off effects.

Table 23 Results for the $SU(2)$ NLO low-energy constants $\bar{\ell}_3$ and $\bar{\ell}_4$. For comparison, the last two lines show results from phenomenological analyses. The systematic error in ETM 11 has been carried over from ETM 10

Collaboration	Refs.	N_f	Publication status	Chiral extrapolation	Cont. extrapolation	Finite volume	$\bar{\ell}_3$	$\bar{\ell}_4$
ETM 21	[305]	2+1+1	P	★	○	★		3.44(28)(36)
ETM 11	[90]	2+1+1	C	○	★	○	3.53(5)*(26)*	4.73(2)*(10)*
ETM 10	[218]	2+1+1	A	○	■	★	3.70(7)(26)	4.67(3)(10)
RBC/UKQCD 15E	[84]	2+1	A	★	★	★	2.81(19)(45)	4.02(8)(24)
RBC/UKQCD 14B	[8]	2+1	A	★	★	★	2.73(13)(0)	4.113(59)(0)
BMW 13	[83]	2+1	A	★	★	★	2.5(5)(4)	3.8(4)(2)
RBC/UKQCD 12	[188]	2+1	A	★	○	★	2.91(23)(07)	3.99(16)(09)
Borsanyi 12	[82]	2+1	A	○	○	★	3.16(10)(29)	4.03(03)(16)
NPLQCD 11	[91]	2+1	A	○	○	○	$4.04(40)\binom{+73}{-55}$	$4.30(51)\binom{+84}{-60}$
MILC 10	[41]	2+1	C	○	★	★	3.18(50)(89)	4.29(21)(82)
MILC 10A	[12]	2+1	C	○	★	★	$2.85(81)\binom{+37}{-92}$	$3.98(32)\binom{+51}{-28}$
RBC/UKQCD 10A	[117]	2+1	A	○	○	■	2.57(18)	3.83(9)
MILC 09A, $SU(3)$-fit	[15]	2+1	C	○	★	★	3.32(64)(45)	4.03(16)(17)
MILC 09A, $SU(2)$-fit	[15]	2+1	C	○	★	★	$3.0(6)\binom{+9}{-6}$	3.9(2)(3)
PACS-CS 08, $SU(3)$-fit	[193]	2+1	A	★	■	■	3.47(11)	4.21(11)
PACS-CS 08, $SU(2)$-fit	[193]	2+1	A	★	■	■	3.14(23)	4.04(19)
RBC/UKQCD 08	[194]	2+1	A	○	■	○	3.13(33)(24)	4.43(14)(77)
ETM 20A	[350]	2	A	★	■	○		4.31(4)(2)(11)(5)
ETM 15A	[368]	2	A	★	■	○		3.3(4)
Gülpers 15	[93]	2	A	★	★	★		4.54(30)(0)
Gülpers 13	[371]	2	A	○	■	○		4.76(13)
Brandt 13	[88]	2	A	○	★	○	3.0(7)(5)	4.7(4)(1)
QCDSF 13	[369]	2	A	★	○	○		4.2(1)
Bernardoni 11	[358]	2	C	○	■	■	4.46(30)(14)	4.56(10)(4)
TWQCD 11	[359]	2	A	○	■	■	4.149(35)(14)	4.582(17)(20)
ETM 09C	[87]	2	A	○	★	○	$3.50(9)\binom{+09}{-30}$	$4.66(4)\binom{+04}{-33}$
JLQCD/TWQCD 09	[372]	2	A	○	■	■		4.09(50)(52)
ETM 08	[92]	2	A	○	○	○	3.2(8)(2)	4.4(2)(1)
JLQCD/TWQCD 08A	[364]	2	A	○	■	■	$3.38(40)(24)\binom{+31}{-00}$	$4.12(35)(30)\binom{+31}{-00}$
CERN-TOV 06	[373]	2	A	○	■	■	3.0(5)(1)	
Colangelo 01	[324]							4.4(2)
Gasser 84	[320]						2.9(2.4)	4.3(9)

The paper χQCD 20 [376] employs overlap valence quarks on $N_f = 2{+}1$ ensembles with domain-wall sea quarks. They use a total of seven ensembles, with three of them being at the physical point. They cover five lattice spacings $a = 0.083{-}0.195$fm, of which only one is below 0.1fm. The relevant box size is 6.24fm at the physical point, where they have $M_\pi L = 4.45$. Renormalization is done nonperturbatively.

The paper Gao 21 [375] is based on $N_f = 2 + 1$ HISQ (staggered) ensembles on which they invert clover valence quarks. They have $M_{\pi,\text{sea}} = M_{\pi,\text{val}} = 140\,\text{MeV}$ at $a = 0.076$fm in a $64^3 \times 64$ volume. In addition, they have $M_{\pi,\text{sea}} = 160\,\text{MeV}$, $M_{\pi,\text{val}} = 300\,\text{MeV}$ at $a = 0.06$fm (in a $48^3 \times 64$ box), and essentially the same sea-valence mass combination at $a = 0.04$fm (in a $64^3 \times 64$ box). The vector form factor is renormalized nonperturbatively. Unfortunately, no continuum

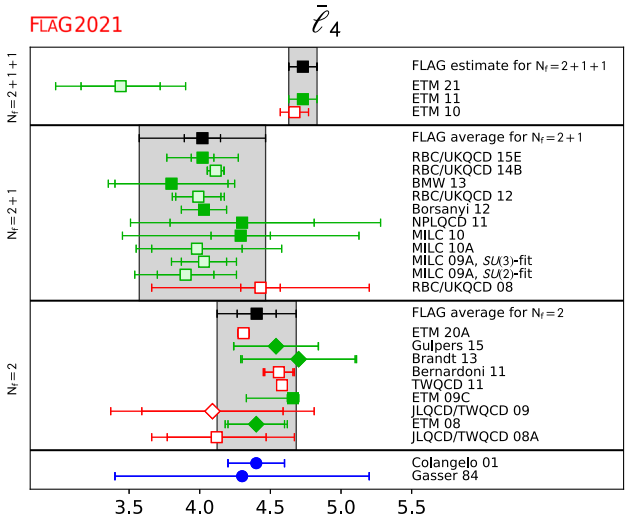

Fig. 16 Effective coupling constant $\bar{\ell}_4$. Squares indicate determinations from correlators in the p-regime, diamonds refer to determinations from the pion form factor

Table 24 Vector form factor of the pion: Lattice results for the charge radius $\langle r^2\rangle_V^\pi$ and the chiral coupling constant $\bar{\ell}_6$ are compared with the experimental value, as obtained by NA7, and some phenomenological estimates. The publication status of χQCD 20 [376] changed from "preprint" to "accepted" after our closing date

Collaboration	Refs.	N_f	Publication status	Chiral extrapolation	Continuum extrapolation	Finite volume	$\langle r^2\rangle_V^\pi$ [fm^2]	$\bar{\ell}_6$
HPQCD 15B	[374]	2+1+1	A	★	○	★	0.403(18)(6)	
Gao 21	[375]	2+1	P	○	■	★	$0.42(2)_{\text{tot}}$	
χQCD 20	[376]	2+1	A	★	○	★	0.430(5)(13)	17.1(1.4)
Feng 19	[377]	2+1	A	★	■	★	0.434(20)(13)	
JLQCD 15A, $SU(2)$-fit	[378]	2+1	A	○	■	○	0.395(26)(32)	13.49(89)(82)
JLQCD 14	[379]	2+1	A	★	■	■	0.49(4)(4)	7.5(1.3)(1.5)
PACS-CS 11A	[380]	2+1	A	○	■	○	0.441(46)	
RBC/UKQCD 08A	[381]	2+1	A	■	■	○	0.418(31)	12.2(9)
LHP 04	[382]	2+1	A	■	■	■	0.310(46)	
ETM 17F	[383]	2	A	★	■	★	0.443(21)(20)	16.21(76)(70)
Brandt 13	[88]	2	A	○	★	○	0.481(33)(13)	15.5(1.7)(1.3)
JLQCD/TWQCD 09	[372]	2	A	○	■	■	0.409(23)(37)	11.9(0.7)(1.0)
ETM 08	[92]	2	A	○	○	○	0.456(30)(24)	14.9(1.2)(0.7)
QCDSF/UKQCD 06A	[384]	2	A	○	★	■	0.441(19)(63)	
Bijnens 98	[385]						0.437(16)	16.0(0.5)(0.7)
NA7 86	[386]						0.439(8)	
Gasser 84	[320]							16.5(1.1)

extrapolation is performed; they quote the result from the $a \simeq 0.076$fm physical pion mass ensemble as listed in Table 24. The error quoted is a total error, comprising systematic uncertainties unrelated to cut-off effects.

The available information on $\langle r^2\rangle_V^\pi$ is summarized in Fig. 17. It is obvious that the lattice computations for this quantity do not achieve the precision of the experimental result (NA 7) yet.

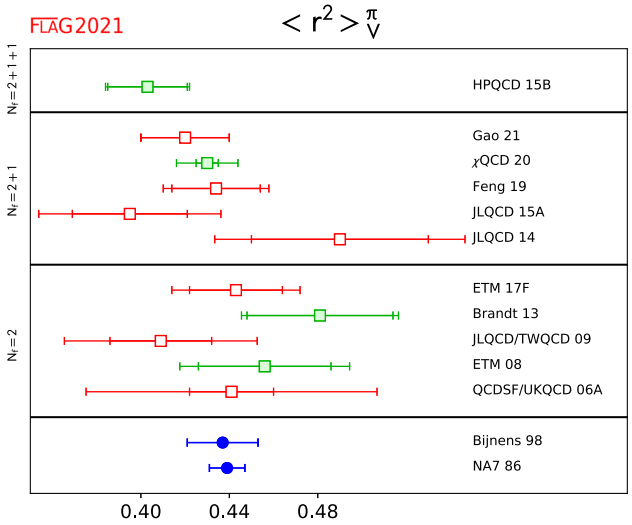

Fig. 17 Summary of the pion form factor $\langle r^2 \rangle^{\pi}_{V}$. The publication status of χQCD 20 [376] changed from "preprint" to "accepted" after our closing date

5.2.3 New results for an SU(2) linear combination linked to $\pi\pi$ scattering

We are aware of four new papers on $\pi\pi$ scattering (in the isospin $I = 2$ and/or $I = 0$ state). As before, we begin with a brief description of their specifics.

Reference [387] by Hörz and Hanlon uses one CLS ensemble of $N_f = 2 + 1$ nonperturbatively improved Wilson (clover) fermions. Since it is away from the physical mass point and no extrapolation to the latter is attempted, we refrain from applying the FLAG criteria, and there will be no listing in tables and/or plots. We add that this procedure is in strict analogy to our treatment of Ref. [388] in FLAG 19. A sequel publication, based on the same data, is Ref. [389]. They find that the $\pi\pi$ ($I = 2$) spectrum is fit well by an S-wave phase shift that incorporates the expected Adler zero. Obviously, the same comment regarding the applicability of the FLAG criteria applies.

The paper Culver 19 [390] uses $N_f = 2$ flavours of nHYP clover fermions at $a = 0.12$fm, $M_\pi = 315$ MeV on $48 \times 24^2 \times \{24, 30, 48\}$ and $M_\pi = 226$ MeV on $64 \times 24^2 \times \{24, 28, 32\}$. With a conventional analysis technique they find $a_0^2 M_\pi = -0.0455(16)$, after extrapolation to physical pion mass. From an inverse amplitude method, they obtain $a_0^2 M_\pi = -0.0436\binom{+0.0013}{-0.0012}$, again at the physical pion mass. Since the paper does not give preference to one of the analysis methods, we take the liberty to condense the two numbers into the result $a_0^2 M_\pi = -0.0445(14)(19)$, as shown in Table 25. Here, the systematic error reflects the full difference between the two central values given in the paper.

The paper Mai 19 [391] employs $N_f = 2$ nHYP clover fermions at a single lattice spacing ($a = 0.12$fm), with $M_\pi = 315$ MeV on $48 \times 24^2 \times \{24, 30, 48\}$ lattices and $M_\pi = 224$ MeV on $64 \times 24^2 \times \{24, 28, 32\}$ lattices. They quote, extrapolated to the physical pion mass, $a_0^0 M_\pi = 0.2132\binom{+0.0008}{-0.0009}$ and $a_0^2 M_\pi = -0.0433 \pm 0.0002$ for $I = 0$ and $I = 2$, respectively. With statistical error only, these results go into Table 25, but not into a plot.

The paper ETM 20B [392] is based on $N_f = 2$ QCD with twisted mass fermions at $a = 0.0914(15)$fm, and with $c_{\rm SW} = 1.57551$. They have three pion masses ($M_\pi = 340$ MeV on $32^3 \times 64$ and $M_\pi = 242$ MeV and $M_\pi = 134$ MeV on $48^3 \times 96$). They find, for $I = 2$, at the pion masses considered, $a_0^2 M_\pi = -0.2061(49), -0.156(15), -0.0481(86)$, with the last being at physical pion mass, but finite a. Accordingly, we take $a_0^2 M_\pi = -0.0481(86)$ with unknown systematic error. With statistical error only, this result goes into Table 25, but not into a plot.

These four works, when combined with the information listed in FLAG 19, represent the information from the lattice on the $\pi\pi$ scattering lengths a_0^0 and a_0^2 in the isospin channels $I = 0$ and $I = 2$, respectively. As can be seen from Eqs. (93, 95), the $I = 0$ scattering length carries information about $\frac{20}{21}\bar{\ell}_1 + \frac{40}{21}\bar{\ell}_2 - \frac{5}{14}\bar{\ell}_3 + 2\bar{\ell}_4$. And from Eqs. (94, 96) it follows that the $I = 2$ counterpart carries information about the linear combination $\frac{4}{3}\bar{\ell}_1 + \frac{8}{3}\bar{\ell}_2 - \frac{1}{2}\bar{\ell}_3 - 2\bar{\ell}_4$. Still, we prefer quoting the dimensionless products $a_0^I M_\pi$ (at the physical mass point) over the aforementioned linear combinations to ease comparison with phenomenology.

The updated Table 25 summarizes the present lattice information on $a_0^{I=0} M_\pi$ and $a_0^{I=2} M_\pi$ at the physical mass point, and the results are displayed in Fig. 18. We remind the reader that a lattice computation of $a_0^{I=0} M_\pi$ involves quark-loop

Table 25 Summary of $\pi\pi$ scattering data in the $I = 0$ (top) and $I = 2$ (bottom) channels. Some of the results have been adapted to our sign convention. The results of Refs. [324,333] allow for a cross-check with phenomenology

Collaboration	Refs.	N_f	Publication status	Chiral extrapolation	Cont. extrapolation	Finite volume	$a_0^0 M_\pi$	$\ell^0_{\pi\pi}$
Fu 17	[393]	2+1	A	■	○	★	0.217(9)(5)	45.6(7.6)(3.8)
Fu 13	[335]	2+1	A	■	■	★	0.214(4)(7)	43.2(3.5)(5.6)
Fu 11	[394]	2+1	A	■	■	★	0.186(2)	18.7(1.2)
Mai 19	[391]	2	P	■	■	○	0.2132(9)	
ETM 16C	[336]	2	A	★	■	★	0.198(9)(6)	30(8)(6)
Caprini 11	[333]						0.2198(46)(16)(64)	
Colangelo 01	[324]						$0.220(5)_{\text{tot}}$	

Collaboration	Refs.	N_f	Publication status	Chiral extrapolation	Cont. extrapolation	Finite volume	$a_0^2 M_\pi$	$\ell^2_{\pi\pi}$
ETM 15E	[94]	2+1+1	A	○	★	★	$-0.0442(2)\binom{4}{0}$	$3.79(0.61)\binom{+1.34}{-0.11}$
PACS-CS 13	[344]	2+1	A	★	■	■	−0.04243(22)(43)	
Fu 13	[335]	2+1	A	■	■	★	−0.04430(25)(40)	3.27(0.77)(1.12)
Fu 11	[394]	2+1	A	■	■	★	−0.0416(2)	11.6(9)
NPLQCD 11A	[395]	2+1	A	■	■	★	−0.0417(07)(02)(16)	
NPLQCD 07	[334]	2+1	A	■	■	■	$-0.04330(42)_{\text{tot}}$	
NPLQCD 05	[396]	2+1	A	■	■	■	−0.0426(06)(03)(18)	
ETM 20B	[392]	2	A	○	■	○	−0.0481(86)	
Mai 19	[391]	2	P	■	■	○	−0.0433(2)	
Culver 19	[390]	2	P	■	■	○	−0.0445(14)(19)	
Yagi 11	[397]	2	P	○	■	■	−0.04410(69)(18)	
ETM 09G	[95]	2	A	○	○	○	−0.04385(28)(38)	4.65(0.85)(1.07)
CP-PACS 04	[398]	2	A	■	■	★	−0.0413(29)	
Caprini 11	[333]						−0.0445(11)(4)(8)	
Colangelo 01	[324]						$-0.0444(10)_{\text{tot}}$	

disconnected contributions, which tend to be very noisy and thus require large statistics. Compared to the situation in FLAG 19 the number of computations has increased from three to five, but still none of them is free of red tags. The situation is somewhat better for $a_0^{I=2} M_\pi$ which is computed from quark-line connected contributions only. In this case there is one computation at $N_f = 2$ and one at $N_f = 2+1+1$ that qualifies for a FLAG average. We quote these numbers in Sect. 5.2.4 below.

The available information on $a_0^{I=0} M_\pi$ and $a_0^{I=2} M_\pi$ is summarized in Fig. 18. It is obvious that the former quantity (due to quark-loop disconnected contributions) is much harder to calculate on the lattice than the latter one. Nonetheless, the good news is that in both cases the lattice determinations are in reasonable agreement with EFT results.

5.2.4 LO and NLO SU(2) estimates and averages

As promised in an earlier section, here we list our FLAG 19 estimates and averages [4] that all remain unchanged. We refer the reader to that review for details and explanations.

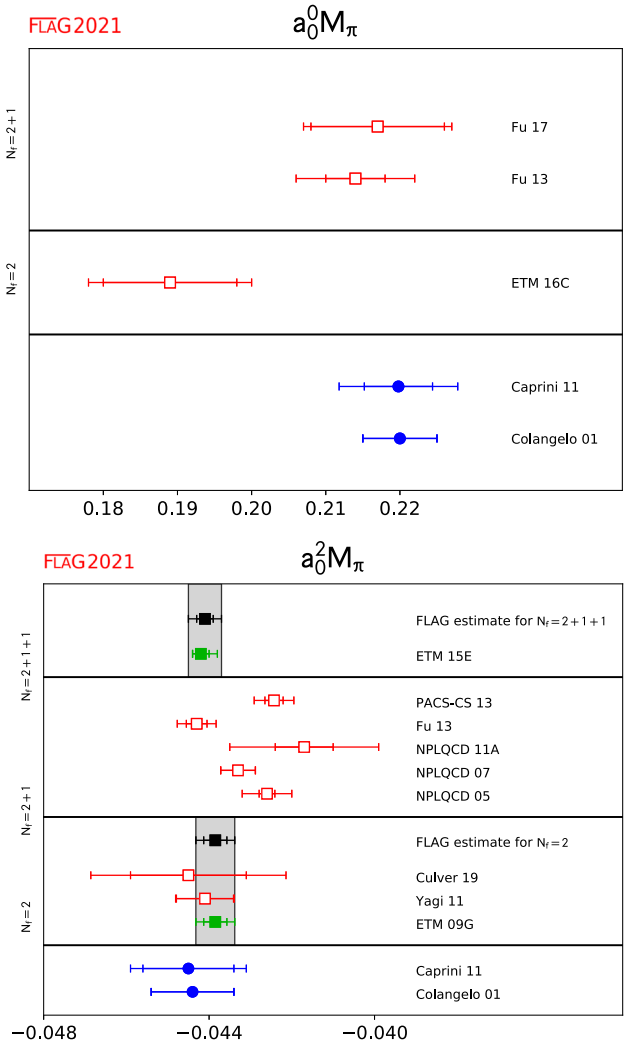

Fig. 18 Summary of the $\pi\pi$ scattering lengths $a_0^0 M_\pi$ (top) and $a_0^2 M_\pi$ (bottom). Results in Table 25 with statistical error only are not shown

For the $SU(2)$ LEC Σ, in the $\overline{\text{MS}}$ scheme, at the renormalization scale $\mu = 2\,\text{GeV}$, we obtained the averages and/or estimate

$$\begin{aligned} N_f = 2+1+1: &\quad \Sigma^{1/3} = 286(23)\,\text{MeV} &&\text{Refs. [80,81]},\\ N_f = 2+1: &\quad \Sigma^{1/3} = 272(5)\,\text{MeV} &&\text{Refs. [12,82–86]},\\ N_f = 2: &\quad \Sigma^{1/3} = 266(10)\,\text{MeV} &&\text{Refs. [80,87–89]}, \end{aligned} \tag{112}$$

where the errors include both statistical and systematic uncertainties.

For the ratio of the pion decay constant at the physical point, F_π, to its value in the $SU(2)$ chiral limit (zero up- and down-quark mass but physical strange-quark mass), F, we obtained the averages and/or estimate

$$\begin{aligned} N_f = 2+1+1: &\quad F_\pi/F = 1.077(3) &&\text{Ref. [90]},\\ N_f = 2+1: &\quad F_\pi/F = 1.062(7) &&\text{Refs. [41,82–84,91]},\\ N_f = 2: &\quad F_\pi/F = 1.073(15) &&\text{Refs. [87–89,92]}. \end{aligned} \tag{113}$$

For $SU(2)$ NLO LECs we obtained the averages and/or estimates

$$\begin{aligned} N_f = 2+1+1: &\quad \bar{\ell}_3 = 3.53(26) &&\text{Ref. [90]},\\ N_f = 2+1: &\quad \bar{\ell}_3 = 3.07(64) &&\text{Refs. [41,82–84,91]},\\ N_f = 2: &\quad \bar{\ell}_3 = 3.41(82) &&\text{Refs. [87,88,92]}, \end{aligned} \tag{114}$$

$$\begin{aligned} N_f = 2+1+1: &\quad \bar{\ell}_4 = 4.73(10) &&\text{Ref. [90]},\\ N_f = 2+1: &\quad \bar{\ell}_4 = 4.02(45) &&\text{Refs. [41,82–84,91]},\\ N_f = 2: &\quad \bar{\ell}_4 = 4.40(28) &&\text{Refs. [87,88,92,93]}, \end{aligned} \tag{115}$$

as well as the estimate

$$N_f = 2: \quad \bar{\ell}_6 = 15.1(1.2) \quad \text{Refs. [88,92]}. \tag{116}$$

For the scattering length extracted from $\pi\pi$ scattering in the $I = 2$ channel we quote

$$\begin{aligned} N_f = 2+1+1: &\quad a_0^2 M_\pi = -0.0441(4) &&\text{Ref. [94]},\\ N_f = 2: &\quad a_0^2 M_\pi = -0.04385(47) &&\text{Ref. [95]}, \end{aligned} \tag{117}$$

where the errors include both statistical and systematic uncertainties. We remark that our preprocessing procedure[23] symmetrizes the asymmetric errors with a slight adjustment of the central value.

In all cases the references shown are the papers with the contributing results, and we ask the readers to cite those papers when quoting these averages.

5.3 Extraction of SU(3) low-energy constants

5.3.1 New results for individual LO SU(3) LECs

We are unaware of any new paper that determines a large number of LECs in the $SU(3)$ framework (as was done, in the past, by the MILC collaboration). However, there is one paper, χQCD 21 [351], with a new result on two $SU(3)$ LECs at LO. They find $F_0 = 67.8(1.2)(3.2)$ and $\Sigma_0 = 232.6(0.9)(2.7)$ in the 3-flavour chiral limit.[24] They also quote $\Sigma/\Sigma_0 = 1.40(2)(2)$ which we consider interesting for reasons detailed in Sect. 5.3.4.

These values are listed, together with those of FLAG 19, in Table 26. The paper has been discussed and color coded in Sect. 5.2. As they are not published yet, there is no update to the FLAG averages/estimates here.

5.3.2 New results for individual NLO SU(3) LECs

There are a number of new results on L_5, for instance in Refs. [349,399,400] to be discussed below in the context of πK scattering. This is not so surprising, since Eqs. (101, 102, 103, 104) indicate that the observables $a_0^2 M_\pi$, $a_0^1 M_K$, $a_0^{3/2}\mu_{\pi K}$, $a_0^{1/2}\mu_{\pi K}$ jointly determine the combination $L_{\rm scat}$ and L_5 (both of which are conventionally quoted at the scale $\mu = 770\,\text{MeV}$). Determining any of these two LECs is afflicted with an extra uncertainty, compared to the four scattering lengths, due to the convergence of the $SU(3)$ chiral series.[25] Therefore we give preference to reviewing the scattering lengths and converting, once they exist, the pertinent FLAG averages into numerical values of $L_{\rm scat}$ and L_5, over collecting values of $L_{\rm scat}$ and L_5 as converted by the individual collaborations.

[23] There are two naive procedures to symmetrize an asymmetric systematic error: (i) keep the central value untouched and enlarge the smaller error, (ii) shift the central value by half of the difference between the two original errors and enlarge/shrink both errors by the same amount. Our procedure (iii) is to average the results of (i) and (ii). In other words a result $c(s)\binom{+u}{-\ell}$ with $\ell > u$ is changed into $c + (u-\ell)/4$ with statistical error s and a symmetric systematic error $(u+3\ell)/4$. The case $\ell < u$ is handled accordingly.

[24] We use $\Sigma = \lim_{m_u,m_d\to 0}\Sigma(m_u,m_d,m_s,m_c,\ldots)$, $\Sigma_0 = \lim_{m_u,m_d,m_s\to 0}\Sigma(m_u,m_d,m_s,m_c,\ldots)$, and likewise for B, B_0, F and F_0. The quantities Σ, Σ_0, B, B_0 are renormalized at the scale $\mu = 2\,\text{GeV}$.

[25] One of the issues is whether the convergence in the LECs pertinent to $a_0^1 M_K$, i.e., with two strange quarks involved, is visibly slower than for $a_0^{3/2}\mu_{\pi K}$ and $a_0^{1/2}\mu_{\pi K}$, where only one strange quark appears.

Table 26 Lattice results for the low-energy constants F_0, B_0 and $\Sigma_0 \equiv F_0^2 B_0$, which specify the effective $SU(3)$ Lagrangian at leading order. The ratios F/F_0, B/B_0, Σ/Σ_0, which compare these with their $SU(2)$ counterparts, indicate the strength of the Zweig-rule violations in these quantities (in the large-N_c limit, they tend to unity). Numbers in slanted fonts are calculated by us, from the information given in the references

Collaboration	Refs.	N_f	Publication status	Chiral extrapolation	Cont. extrapolation	Finite volume	F_0 [MeV]	F/F_0	B/B_0
JLQCD/TWQCD 10A	[354]	3	A	■	■	■	71(3)(8)		
χQCD 21	[351]	2+1	P	★	★	★	67.8(1.2)(3.2)		
MILC 10	[41]	2+1	C	○	★	★	80.3(2.5)(5.4)		
MILC 09A	[15]	2+1	C	○	★	★	78.3(1.4)(2.9)	*1.104(3)(41)*	*1.21(4)*$\binom{+5}{-6}$
MILC 09	[157]	2+1	A	○	★	★		1.15(5)$\binom{+13}{-03}$	*1.15(16)*$\binom{+39}{-13}$
PACS-CS 08	[193]	2+1	A	★	■	■	83.8(6.4)	1.078(44)	1.089(15)
RBC/UKQCD 08	[194]	2+1	A	○	■	○	66.1(5.2)	1.229(59)	1.03(05)

Collaboration	Refs.	N_f	Publication status	Chiral extrapolation	Cont. extrapolation	Finite volume	Renormalization	$\Sigma_0^{1/3}$ [MeV]	Σ/Σ_0
JLQCD/TWQCD 10A	[354]	3	A	■	■	■	★	214(6)(24)	*1.31(13)(52)*
χQCD 21	[351]	2+1	P	★	★	★	★	232.6(0.9)(2.7)	1.40(2)(2)
MILC 09A	[15]	2+1	C	○	★	★	○	245(5)(4)(4)	*1.48(9)(8)(10)*
MILC 09	[157]	2+1	A	○	★	★	○	242(9)$\binom{+05}{-17}$(4)	1.52(17)$\binom{+38}{-15}$
PACS-CS 08	[193]	2+1	A	★	■	■	■	290(15)	1.245(10)
RBC/UKQCD 08	[194]	2+1	A	○	■	○	★		1.55(21)

On the other hand, there is no new result on those LECs at the NLO in the $SU(3)$ expansion which were covered in previous editions of FLAG (L_4, L_6, L_9, L_{10}).

5.3.3 Results for SU(3) linear combinations linked to πK, KK scattering

Since πK, KK scattering were not covered in previous editions of the FLAG report, we list here all works which include such results. Following the example of the section on $\pi\pi$ scattering, where all results were given in the dimensionless variable $a_0^I M_\pi$, we give the results on πK scattering in the form $a_0^I \mu_{\pi K}$, where $\mu_{\pi K}$ is the pertinent reduced mass, and the results on KK scattering are given in the form $a_0^I M_K$. We start with a brief mentioning of all papers we are aware of.

The paper NPLQCD 06B [349] uses asqtad (staggered) sea quarks with $N_f = 2+1$ at a single lattice spacing ($a = 0.125$fm with $L \simeq 2.5$fm) with $M_\pi = [290, 350, 490, 600]$ MeV. The domain-wall valence fermions come with quark masses such that the resulting pion masses match the aforementioned Nambu–Goldstone boson masses. After chiral extrapolation they find $a_0^{1/2}\mu_{\pi K} = 0.1346(13)\binom{+18}{-122}$ and $a_0^{3/2}\mu_{\pi K} = -0.0448(12)\binom{+19}{-45}$, with L_5 pinned down at a value extracted from the analysis of the quark mass dependence of f_K/f_π. The color coding in Table 27 is based on $M_{\pi,\min}(\mathrm{RMS}) = 488$ MeV.

The paper NPLQCD 07B [401] uses asqtad (staggered) sea quarks with $N_f = 2+1$ in conjunction with domain-wall valence quarks. They have two lattice spacings ($a = 0.125$ fm, 0.09 fm) with somewhat unequal span in quark masses. At $a = 0.125$ fm they cover $M_\pi \simeq 290, 350, 490, 590$ MeV with $L \simeq 2.5$fm. At $a = 0.09$ fm they do not quote M_π[MeV], but from $aM_\pi = 0.1453$ in Tab. II and $a \simeq 0.09$ fm one would conclude $M_\pi \simeq 320$ MeV. After chiral extrapolation, they find $a_0^1 M_K = -0.352(16)_{\mathrm{tot}}$. The color coding in Table 27 is based on $M_{\pi,\min}(\mathrm{RMS}) = 413$ MeV.

The paper Fu 11A [399] employs one ensemble of $N_f = 2+1$ asqtad (staggered) quarks at $a \simeq 0.15$ fm, $m_l/m_s = 0.2$, $m_s \simeq m_s^{\mathrm{phys}}$ with $L = 2.5$ fm. It uses six valence pion masses $M_\pi = 334 - 466$ MeV to study S-wave scattering. It quotes,

Table 27 Summary of πK scattering data in the $I = \frac{1}{2}, \frac{3}{2}$ channels, and of KK scattering with $I = 1$. Some of the results have been adapted to our sign convention

Collaboration	Refs.	N_f	Publication status	Chiral extrapolation	Cont. extrapolation	Finite volume	$a_0^{1/2}\mu_{\pi K}$	$a_0^{3/2}\mu_{\pi K}$	$a_0^1 M_K$
ETM 18B	[96]	2+1+1	A	○	★	○	$0.127(2)_{\text{tot}}$	$-0.0463(17)_{\text{tot}}$	
ETM 17G	[97]	2+1+1	A	○	★	○			$-0.385(16)\binom{+4}{-14}$
PACS-CS 13	[344]	2+1	A	★	■	■	0.150(16)(37)	−0.0477(27)(20)	−0.312(17)(31)
Fu 11A	[399]	2+1	A	■	■	★	0.1425(29)	−0.0394(15)	
NPLQCD 07B	[401]	2+1	A	■	○	○			$-0.352(16)_{\text{tot}}$
NPLQCD 06B	[349]	2+1	A	■	■	★	$0.1346(13)\binom{+18}{-122}$	$-0.0448(12)\binom{+19}{-45}$	

after chiral extrapolation, $a_0^{1/2}\mu_{\pi K} = 0.1425(29)$ and $a_0^{3/2}\mu_{\pi K} = -0.0394(15)$. The color coding in Table 27 is based on $M_{\pi,\text{min}}(\text{RMS}) = 590\,\text{MeV}$.

We are also aware of Ref. [402] which is based on a single ensemble of $N_f = 2$ clover quarks. Since it is away from the physical mass point and no extrapolation to the latter is attempted, we feel it would be unfair (or misleading) to quote its results in Table 27.

Reference PACS-CS 13 [344] uses five ensembles of $N_f = 2 + 1$ nonperturbative clover fermions with $a = 0.09$fm, $L = 2.9$fm, and $M_\pi = 166, 297, 414, 575, 707\,\text{MeV}$. They quote, after extrapolation with χPT: $a_0^2 M_\pi = -0.04243(22)(43)$ (see Table 25), $a_0^1 M_K = -0.312(17)(31)$, $a_0^{3/2}\mu_{\pi K} = -0.0477(27)(20)$ and $a_0^{1/2}\mu_{\pi K} = 0.150(16)(37)$ (listed in Table 27). These figures reflect the final numbers quoted in the Erratum of Ref. [344]. The reason for the change is the mishap reported in footnote 21; fortunately it turns out that it affected the final analysis only very mildly. We thank the collaboration for keeping us up-to-date with all aspects of the revision. Since there are no FLAG averages for scattering lengths for $N_f = 2 + 1$, these small changes have no impact on the quoted FLAG averages.

The paper HS 14A [403] is based on $N_f = 2 + 1$ anisotropic clover fermions at $a_s \simeq 0.12\,\text{fm}$, $a_t \simeq 0.035\,\text{fm}$, with $M_\pi = 391\,\text{MeV}$ in $\{16^3, 20^3, 24^3\} \times 128$ boxes, i.e. with $L = 1.9, 2.4, 2.9\,\text{fm}$. These parameters yield $M_K = 549\,\text{MeV}$ thus $\mu_{\pi K} = 228\,\text{MeV}$. They quote various resonance parameters and, in the S-wave $I = 3/2$ channel, $a_0^{3/2} M_\pi = -0.278(15)$ which we convert to $a_0^{3/2}\mu_{\pi K} = -0.161(9)$ at the given M_π. Since this work does not extrapolate to M_π^{phys}, we stay away from color coding.

The paper ETM 17G [97] uses $N_f = 2+1+1$ twisted mass fermions at three lattice spacings, $a = 0.089, 0.082, 0.062\,\text{fm}$, with up to five $M_\pi = 230{-}450\,\text{MeV}$, and $L(M_{\pi,\text{min}}) \simeq 2.8\,\text{fm}$. In the $I = 1$ channel they find $a_0^1 M_K = -0.385(16)\binom{+0}{-12}\binom{+0}{-5}(4)$. We take the liberty to combine the various non-statistical errors in quadrature, using $a_0^1 M_K = -0.385(16)\binom{+4}{-14}$ as quoted in Table 27.

Reference [404] by Brett et al. uses one ensemble of $N_f = 2 + 1$ anisotropic clover fermions with $a_s = 0.115\,\text{fm}$, $M_\pi = 233\,\text{MeV}$, in a $32^3 \times 256$ box, hence $L = 3.7$fm. These parameters yield $M_K = 494\,\text{MeV}$ and thus $\mu_{\pi K} = 158\,\text{MeV}$. Their result for $I = 1/2$ S-wave scattering reads $a_0^{1/2} M_\pi = -0.353(25)$, or $a_0^{1/2}\mu_{\pi K} = -0.240(17)$ in our notation. Since this work does not extrapolate to M_π^{phys}, we stay away from color coding.

The paper ETM 18B [96] uses $N_f = 2+1+1$ twisted mass fermions at three lattice spacings, $a = 0.089, 0.082, 0.062\,\text{fm}$, with up to five pion masses $M_\pi = 230{-}450\,\text{MeV}$ and up to two volumes. From the tables, one finds $M_{\pi,\text{min}} = 276, 302, 311\,\text{MeV}$ at the three lattice spacings. They find, after chiral extrapolation, $a_0^{1/2}\mu_{\pi K} = 0.127(2)_{\text{tot}}$ and $a_0^{3/2}\mu_{\pi K} = -0.0463(17)_{\text{tot}}$ as quoted in Table 27.

An overview of all scattering lengths with at least one kaon involved is shown in Fig. 19. As usual we refrain from displaying data with statistical error only.

In passing, we note that there is an additional paper by Z. Fu, Ref. [400], which deals with $K\bar{K}$ scattering. It employs one ensemble of $N_f = 2 + 1$ asqtad (staggered) quarks at $a \simeq 0.15\,\text{fm}$, $m_l/m_s = 0.2$, $m_s \simeq m_s^{\text{phys}}$ with $L = 2.5\,\text{fm}$ together with six valence pion masses $M_\pi = 334 - 466\,\text{MeV}$. Extrapolating to the physical point, the result for $K\bar{K}$ scattering in

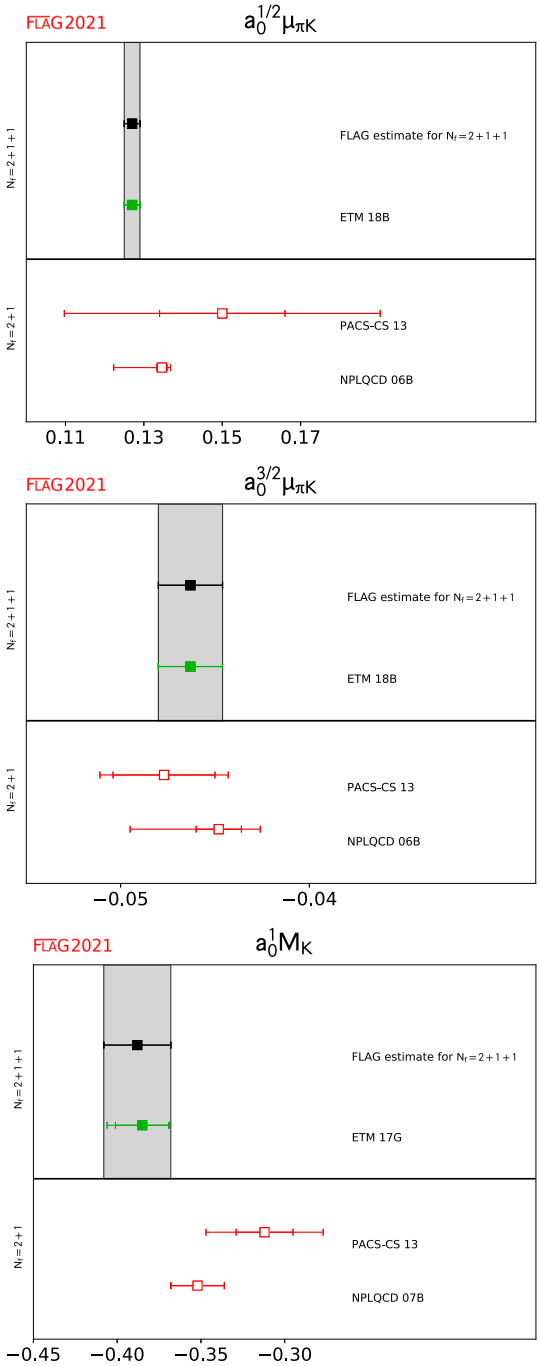

Fig. 19 Summary of the πK scattering lengths $a_0^{1/2}\mu_{\pi K}$ (top), $a_0^{3/2}\mu_{\pi K}$ (middle) and of the KK scattering length $a_0^1 M_K$ (bottom). Results in Table 27 with statistical error only are not shown

the $I = 1$ state is $a_0^1 M_K = 0.211(33)$. Hence the interaction for $K\bar{K}$ in the S-wave $I = 1$ state is found to be attractive, in agreement with LO χPT.

In summary, for the quantities $a_0^{1/2}\mu_{\pi K}$, $a_0^{3/2}\mu_{\pi K}$ and $a_0^1 M_K$ Refs. [96,97] are the only sources without red tags. Since they appeared in refereed journals and no other works qualify, we take the results quoted in the top two lines of Table 27 as the current FLAG averages. For the reader's convenience we list them at the end of Sect. 5.3.5.

Last but not least we like to remind the reader that KK scattering might be outside the validity of $SU(3)$ χPT, since it involves a scale around $2M_K \simeq 1$ GeV. However, our review focuses on the scattering length $a_0^1 M_K$, where this issue does not

feature prominently. But it is a key topic in the subsequent conversion of such a scattering length to the low-energy constants L_i. We hope that forthcoming high-quality data will allow a future edition of FLAG to address this topic.

5.3.4 Implication on Zweig rule violations

Let us spend a minute to explain why we consider the result on Σ/Σ_0 of χQCD 21 [351] particularly interesting. The reason is linked to the question of how close real-world QCD with $N_c = 3$ is to the large-N_c limit of 't Hooft (see also Ref. [405]). In the large-N_c limit the Zweig rule becomes exact, and the NLO LECs L_4 and L_6 tend to zero. As discussed in FLAG 19, the available lattice data are consistent with the view that these two couplings approximately satisfy the Zweig rule. Also the ratios F/F_0, B/B_0 and Σ/Σ_0 (note that they are linearly dependent, since $\Sigma = BF^2$ and $\Sigma_0 = B_0F_0^2$) test the validity of this rule.

The available data seem to confirm the paramagnetic inequalities of Ref. [406], which require $\Sigma/\Sigma_0 > 1$ and $F/F_0 > 1$. There is much less information concerning B/B_0, and this is the point where the new result of χQCD 21 [351] comes in handy. Let us assume, for the sake of an argument, $F/F_0 = 1.15(5)(5)$. Together with $\Sigma/\Sigma_0 = 1.40(2)(2)$ [351], this would imply $B/B_0 = 1.06(9)(9)$. This numerical example illustrates how much precision is lost in forming the ratio $(\Sigma/\Sigma_0)/(F/F_0)^2$; with these numbers it would not be clear whether $B/B_0 > 1$. Therefore we plead with all collaborations to calculate the numbers F/F_0, B/B_0 and Σ/Σ_0 in their analysis framework to take advantage of correlations.

5.3.5 LO and NLO $SU(3)$ estimates

For each of the $SU(3)$ LO and NLO LECs discussed in the 2019 FLAG review [4] exactly one paper contributed and hence constituted the FLAG average. The present status is that this situation is unchanged. For the convenience of the reader, we list the results here but refer to the 2019 FLAG review for the details and explanations.

The LO LECs in the $SU(3)$ chiral limit ($m_u, m_d, m_s \to 0$) are denoted by a subscript 0 to distinguish them from their $SU(2)$ chiral limit counterparts. The parameters Σ_0, B_0 are in the $\overline{\text{MS}}$ scheme at the renormalization scale $\mu = 2\,\text{GeV}$. We quote

$$N_f = 2+1: \quad \Sigma_0^{1/3} = 245(8)\,\text{MeV} \quad \text{Ref. [15]}, \tag{118}$$
$$N_f = 2+1: \quad \Sigma/\Sigma_0 = 1.48(16) \quad \text{Ref. [15]}, \tag{119}$$
$$N_f = 2+1: \quad F_0 = 80.3(6.0)\,\text{MeV} \quad \text{Ref. [41]}, \tag{120}$$
$$N_f = 2+1: \quad F/F_0 = 1.104(41) \quad \text{Ref. [15]}, \tag{121}$$
$$N_f = 2+1: \quad B/B_0 = 1.21(7) \quad \text{Ref. [15]}, \tag{122}$$

where the errors include both statistical and systematic uncertainties. The references shown are the papers from which the results are taken.

For $SU(3)$ NLO LECs we display the results for individual low-energy constants

$$N_f = 2+1+1: \quad L_4 = +0.09(34) \times 10^{-3} \quad \text{Ref. [37]},$$
$$N_f = 2+1: \quad L_4 = -0.02(56) \times 10^{-3} \quad \text{Ref. [41]}, \tag{123}$$
$$N_f = 2+1+1: \quad L_5 = +1.19(25) \times 10^{-3} \quad \text{Ref. [37]},$$
$$N_f = 2+1: \quad L_5 = +0.95(41) \times 10^{-3} \quad \text{Ref. [41]}, \tag{124}$$
$$N_f = 2+1+1: \quad L_6 = +0.16(20) \times 10^{-3} \quad \text{Ref. [37]},$$
$$N_f = 2+1: \quad L_6 = +0.01(34) \times 10^{-3} \quad \text{Ref. [41]}, \tag{125}$$
$$N_f = 2+1+1: \quad L_8 = +0.55(15) \times 10^{-3} \quad \text{Ref. [37]},$$
$$N_f = 2+1: \quad L_8 = +0.43(28) \times 10^{-3} \quad \text{Ref. [41]}, \tag{126}$$

at the chiral scale $\mu = 770\,\text{MeV}$, where again all errors quoted are total errors. For details of the symmetrization of asymmetric error bars see footnote 23.

For the scattering lengths involving at least one kaon

$$N_f = 2+1+1: \qquad a_0^{1/2}\mu_{\pi K} = 0.127(2) \qquad \text{Ref. [96]}, \tag{127}$$

$$N_f = 2+1+1: \qquad a_0^{3/2}\mu_{\pi K} = -0.0463(17) \qquad \text{Ref. [96]}, \tag{128}$$

$$N_f = 2+1+1: \qquad a_0^{1}M_K = -0.388(20) \qquad \text{Ref. [97]}, \tag{129}$$

represent the FLAG estimates with all errors added in quadrature. For details of the symmetrization of asymmetric error bars see footnote 23. Throughout we ask the reader to cite the original references when using these values.

6 Kaon mixing

Authors: P. Dimopoulos, X. Feng, G. Herdoíza

The mixing of neutral pseudoscalar mesons plays an important role in the understanding of the physics of quark-flavour mixing and CP violation. In this section we discuss $K^0 - \bar{K}^0$ oscillations, which probe the physics of indirect CP violation. Extensive reviews on this subject can be found in Refs. [407–412]. With respect to the FLAG 19 report, in the new Sect. 6.2 of the present edition the reader will find an updated discussion regarding the lattice determination of the $K \to \pi\pi$ decay amplitudes and related quantities. Discussions concerning the kaon mixing within the Standard Model (SM) and Beyond the Standard Model (BSM) are presented in Sects. 6.3 and 6.4, respectively. We note that FLAG averages for SM and BSM bag parameters have not changed with respect to the FLAG 19 report.

6.1 Indirect CP violation and ϵ_K in the SM

Indirect CP violation arises in $K_L \to \pi\pi$ transitions through the decay of the CP $= +1$ component of K_L into two pions (which are also in a CP $= +1$ state). Its measure is defined as

$$\epsilon_K = \frac{\mathcal{A}[K_L \to (\pi\pi)_{I=0}]}{\mathcal{A}[K_S \to (\pi\pi)_{I=0}]}, \tag{130}$$

with the final state having total isospin zero. The parameter ϵ_K may also be expressed in terms of $K^0 - \bar{K}^0$ oscillations. In the Standard Model, ϵ_K receives contributions from: (i) short-distance (SD) physics given by $\Delta S = 2$ "box diagrams" involving $W^\pm$ bosons and u, c and t quarks; (ii) the long-distance (LD) physics from light hadrons contributing to the imaginary part of the dispersive amplitude M_{12} used in the two component description of $K^0 - \bar{K}^0$ mixing; (iii) the imaginary part of the absorptive amplitude Γ_{12} from $K^0 - \bar{K}^0$ mixing; and (iv) $\mathrm{Im}(A_0)/\mathrm{Re}(A_0)$, where A_0 is the $K \to (\pi\pi)_{I=0}$ decay amplitude. The various factors in this decomposition can vary with phase conventions. In terms of the $\Delta S = 2$ effective Hamiltonian, $\mathcal{H}_{\mathrm{eff}}^{\Delta S=2}$, it is common to represent contribution (i) by

$$\mathrm{Im}(M_{12}^{\mathrm{SD}}) \equiv \frac{1}{2m_K}\mathrm{Im}[\langle \bar{K}^0|\mathcal{H}_{\mathrm{eff}}^{\Delta S=2}|K^0\rangle], \tag{131}$$

and contribution (ii) by $\mathrm{Im}(M_{12}^{\mathrm{LD}})$. Contribution (iii) can be related to $\mathrm{Im}(A_0)/\mathrm{Re}(A_0)$ since $(\pi\pi)_{I=0}$ states provide the dominant contribution to absorptive part of the integral in Γ_{12}. Collecting the various pieces yields the following expression for the ϵ_K factor [411,413–416]

$$\epsilon_K = \exp(i\phi_\epsilon)\,\sin(\phi_\epsilon)\left[\frac{\mathrm{Im}(M_{12}^{\mathrm{SD}})}{\Delta M_K} + \frac{\mathrm{Im}(M_{12}^{\mathrm{LD}})}{\Delta M_K} + \frac{\mathrm{Im}(A_0)}{\mathrm{Re}(A_0)}\right], \tag{132}$$

where the phase of ϵ_K is given by

$$\phi_\epsilon = \arctan\frac{\Delta M_K}{\Delta\Gamma_K/2}. \tag{133}$$

The quantities ΔM_K and $\Delta\Gamma_K$ are the mass and decay width differences between long- and short-lived neutral kaons. The experimentally known values of the above quantities read [165]:

$$|\epsilon_K| = 2.228(11) \times 10^{-3}, \tag{134}$$
$$\phi_\epsilon = 43.52(5)^\circ, \tag{135}$$
$$\Delta M_K \equiv M_{K_L} - M_{K_S} = 3.484(6) \times 10^{-12}\,\text{MeV}, \tag{136}$$
$$\Delta\Gamma_K \equiv \Gamma_{K_S} - \Gamma_{K_L} = 7.3382(33) \times 10^{-12}\,\text{MeV}, \tag{137}$$

where the latter three measurements have been obtained by imposing CPT symmetry.

We will start by discussing the short-distance effects (i) since they provide the dominant contribution to ϵ_K. To lowest order in the electroweak theory, the contribution to $K^0 - \bar{K}^0$ oscillations arises from the so-called box diagrams, in which two W bosons and two "up-type" quarks (i.e., up, charm, top) are exchanged between the constituent down and strange quarks of the K mesons. The loop integration of the box diagrams can be performed exactly. In the limit of vanishing external momenta and external quark masses, the result can be identified with an effective four-fermion interaction, expressed in terms of the effective Hamiltonian

$$\mathcal{H}_{\text{eff}}^{\Delta S=2} = \frac{G_F^2 M_{\text{W}}^2}{16\pi^2} \mathcal{F}^0 Q^{\Delta S=2} + \text{h.c.} \tag{138}$$

In this expression, G_F is the Fermi coupling, M_{W} the W-boson mass, and

$$Q^{\Delta S=2} = \left[\bar{s}\gamma_\mu(1-\gamma_5)d\right]\left[\bar{s}\gamma_\mu(1-\gamma_5)d\right] \equiv O_{\text{VV+AA}} - O_{\text{VA+AV}}, \tag{139}$$

is a dimension-six, four-fermion operator. The subscripts V and A denote vector ($\bar{s}\gamma_\mu d$) and axial-vector ($\bar{s}\gamma_\mu\gamma_5 d$) bilinears, respectively. The function $\mathcal{F}^0$ is given by

$$\mathcal{F}^0 = \lambda_c^2 S_0(x_c) + \lambda_t^2 S_0(x_t) + 2\lambda_c\lambda_t S_0(x_c, x_t), \tag{140}$$

where $\lambda_a = V_{as}^* V_{ad}$, and $a = c, t$ denotes a flavour index. The quantities $S_0(x_c)$, $S_0(x_t)$ and $S_0(x_c, x_t)$ with $x_c = m_c^2/M_{\text{W}}^2$, $x_t = m_t^2/M_{\text{W}}^2$ are the Inami–Lim functions [417], which express the basic electroweak loop contributions without QCD corrections. The contribution of the up quark, which is taken to be massless in this approach, has been taken into account by imposing the unitarity constraint $\lambda_u + \lambda_c + \lambda_t = 0$.

When strong interactions are included, $\Delta S = 2$ transitions can no longer be discussed at the quark level. Instead, the effective Hamiltonian must be considered between mesonic initial and final states. Since the strong coupling is large at typical hadronic scales, the resulting weak matrix element cannot be calculated in perturbation theory. The operator product expansion (OPE) does, however, factorize long- and short- distance effects. For energy scales below the charm threshold, the $K^0 - \bar{K}^0$ transition amplitude of the effective Hamiltonian can be expressed as

$$\begin{aligned}\langle \bar{K}^0|\mathcal{H}_{\text{eff}}^{\Delta S=2}|K^0\rangle = {} & \frac{G_F^2 M_{\text{W}}^2}{16\pi^2}\left[\lambda_c^2 S_0(x_c)\eta_1 + \lambda_t^2 S_0(x_t)\eta_2 + 2\lambda_c\lambda_t S_0(x_c, x_t)\eta_3\right] \\ & \times \left(\frac{\bar{g}(\mu)^2}{4\pi}\right)^{-\gamma_0/(2\beta_0)} \exp\left\{\int_0^{\bar{g}(\mu)} dg \left(\frac{\gamma(g)}{\beta(g)} + \frac{\gamma_0}{\beta_0 g}\right)\right\} \langle \bar{K}^0|Q_{\text{R}}^{\Delta S=2}(\mu)|K^0\rangle + \text{h.c.},\end{aligned} \tag{141}$$

where $\bar{g}(\mu)$ and $Q_{\text{R}}^{\Delta S=2}(\mu)$ are the renormalized gauge coupling and four-fermion operator in some renormalization scheme. The factors η_1, η_2 and η_3 depend on the renormalized coupling $\bar{g}$, evaluated at the various flavour thresholds m_t, m_b, m_c and M_{W}, as required by the OPE and Renormalization Group (RG) running procedure that separate high- and low-energy contributions. Explicit expressions can be found in Ref. [410] and references therein, except that η_1 and η_3 have been calculated to NNLO in Refs. [418] and [419], respectively. We follow the same conventions for the RG equations as in Ref. [410]. Thus the Callan–Symanzik function and the anomalous dimension $\gamma(\bar{g})$ of $Q^{\Delta S=2}$ are defined by

$$\frac{d\bar{g}}{d\ln\mu} = \beta(\bar{g}), \qquad \frac{dQ_{\text{R}}^{\Delta S=2}}{d\ln\mu} = -\gamma(\bar{g})\, Q_{\text{R}}^{\Delta S=2}, \tag{142}$$

with perturbative expansions

$$\beta(g) = -\beta_0 \frac{g^3}{(4\pi)^2} - \beta_1 \frac{g^5}{(4\pi)^4} - \cdots ,$$
$$\gamma(g) = \gamma_0 \frac{g^2}{(4\pi)^2} + \gamma_1 \frac{g^4}{(4\pi)^4} + \cdots . \tag{143}$$

We stress that β_0, β_1 and γ_0 are universal, i.e., scheme independent. As for $K^0 - \bar{K}^0$ mixing, this is usually considered in the naive dimensional regularization (NDR) scheme of $\overline{\text{MS}}$, and below we specify the perturbative coefficient γ_1 in that scheme:

$$\beta_0 = \left\{ \frac{11}{3} N - \frac{2}{3} N_f \right\}, \qquad \beta_1 = \left\{ \frac{34}{3} N^2 - N_f \left(\frac{13}{3} N - \frac{1}{N} \right) \right\},$$
$$\gamma_0 = \frac{6(N-1)}{N}, \qquad \gamma_1 = \frac{N-1}{2N} \left\{ -21 + \frac{57}{N} - \frac{19}{3} N + \frac{4}{3} N_f \right\}. \tag{144}$$

Note that for QCD the above expressions must be evaluated for $N = 3$ colours, while N_f denotes the number of active quark flavours. As already stated, Eq. (141) is valid at scales below the charm threshold, after all heavier flavours have been integrated out, i.e., $N_f = 3$.

In Eq. (141), the terms proportional to η_1, η_2 and η_3, multiplied by the contributions containing $\bar{g}(\mu)^2$, correspond to the Wilson coefficient of the OPE, computed in perturbation theory. Its dependence on the renormalization scheme and scale μ is canceled by that of the weak matrix element $\langle \bar{K}^0 | Q_{\text{R}}^{\Delta S=2}(\mu) | K^0 \rangle$. The latter corresponds to the long-distance effects of the effective Hamiltonian and must be computed nonperturbatively. For historical, as well as technical reasons, it is convenient to express it in terms of the B-parameter B_K, defined as

$$B_K(\mu) = \frac{\left\langle \bar{K}^0 \left| Q_{\text{R}}^{\Delta S=2}(\mu) \right| K^0 \right\rangle}{\frac{8}{3} f_K^2 m_K^2}. \tag{145}$$

The four-quark operator $Q^{\Delta S=2}(\mu)$ is renormalized at scale μ in some regularization scheme, for instance, NDR-$\overline{\text{MS}}$. Assuming that $B_K(\mu)$ and the anomalous dimension $\gamma(g)$ are both known in that scheme, the renormalization group independent (RGI) B-parameter $\hat{B}_K$ is related to $B_K(\mu)$ by the exact formula

$$\hat{B}_K = \left(\frac{\bar{g}(\mu)^2}{4\pi} \right)^{-\gamma_0/(2\beta_0)} \exp \left\{ \int_0^{\bar{g}(\mu)} dg \left(\frac{\gamma(g)}{\beta(g)} + \frac{\gamma_0}{\beta_0 g} \right) \right\} B_K(\mu). \tag{146}$$

At NLO in perturbation theory the above reduces to

$$\hat{B}_K = \left(\frac{\bar{g}(\mu)^2}{4\pi} \right)^{-\gamma_0/(2\beta_0)} \left\{ 1 + \frac{\bar{g}(\mu)^2}{(4\pi)^2} \left[\frac{\beta_1 \gamma_0 - \beta_0 \gamma_1}{2\beta_0^2} \right] \right\} B_K(\mu). \tag{147}$$

To this order, this is the scale-independent product of all μ-dependent quantities in Eq. (141).

Lattice-QCD calculations provide results for $B_K(\mu)$. However, these results are usually obtained in intermediate schemes other than the continuum $\overline{\text{MS}}$ scheme used to calculate the Wilson coefficients appearing in Eq. (141). Examples of intermediate schemes are the RI/MOM scheme [420] (also dubbed the "Rome–Southampton method") and the Schrödinger functional (SF) scheme [421]. These schemes are used as they allow a nonperturbative renormalization of the four-fermion operator, using an auxiliary lattice simulation. This allows $B_K(\mu)$ to be calculated with percent-level accuracy, as described below.

In order to make contact with phenomenology, however, and in particular to use the results presented above, one must convert from the intermediate scheme to the $\overline{\text{MS}}$ scheme or to the RGI quantity $\hat{B}_K$. This conversion relies on 1- or 2-loop perturbative matching calculations, the truncation errors in which are, for many recent calculations, the dominant source of error in $\hat{B}_K$ (see, for instance, Refs. [8,49,50,188,422]). While this scheme-conversion error is not, strictly speaking, an error of the lattice calculation itself, it must be included in results for the quantities of phenomenological interest, namely, $B_K(\overline{\text{MS}}, 2\,\text{GeV})$ and $\hat{B}_K$. Incidentally, we remark that this truncation error is estimated in different ways and that its relative contribution to the total error can considerably differ among the various lattice calculations. We note that this error can be

minimized by matching between the intermediate scheme and $\overline{\text{MS}}$ at as large a scale μ as possible (so that the coupling which determines the rate of convergence is minimized). Recent calculations have pushed the matching μ up to the range 3–3.5 GeV. This is possible because of the use of nonperturbative RG running determined on the lattice [8,48,188]. The Schrödinger functional offers the possibility to run nonperturbatively to scales $\mu \sim M_{\text{W}}$ where the truncation error can be safely neglected. However, so far this has been applied only for two flavours for B_K in Ref. [423] and for the case of the BSM bag parameters in Ref. [424], see more details in Sect. 6.4.

Perturbative truncation errors in Eq. (141) also affect the Wilson coefficients η_1, η_2 and η_3. It turns out that the largest uncertainty arises from the charm quark contribution $\eta_1 = 1.87(76)$ [418]. Although it is now calculated at NNLO, the series shows poor convergence. The net effect from the uncertainty on η_1 on the amplitude in Eq. (141) is larger than that of present lattice calculations of B_K. Exploiting an idea presented in Ref. [425], it has been recently shown in Ref. [426] that, by using the $u - t$ instead of the usual $c - t$ unitarity in the ϵ_K computation, the perturbative uncertainties associated with residual short-distance quark contributions can be reduced.

We will now proceed to discuss the remaining contributions to ϵ_K in Eq. (132). An analytical estimate of the leading contribution from $\text{Im}(M_{12}^{\text{LD}})$ based on χPT, shows that it is approximately proportional to $\xi \equiv \text{Im}(A_0)/\text{Re}(A_0)$ so that Eq. (132) can be written as follows [415,416]

$$\epsilon_K = \exp(i\phi_\epsilon)\sin(\phi_\epsilon)\left[\frac{\text{Im}(M_{12}^{\text{SD}})}{\Delta M_K} + \rho\,\xi\right], \tag{148}$$

where the deviation of ρ from one parameterizes the long-distance effects in $\text{Im}(M_{12})$.

In order to facilitate the subsequent discussions about the status of the lattice studies of $K \to \pi\pi$ and of the current estimates of ξ, we proceed by providing a brief account of the parameter ϵ' that describes direct CP-violation in the kaon sector. The definition of ϵ' is given by:

$$\epsilon' \equiv \frac{1}{\sqrt{2}}\frac{\mathcal{A}[K_S \to (\pi\pi)_{I=2}]}{\mathcal{A}[K_S \to (\pi\pi)_{I=0}]}\left(\frac{\mathcal{A}[K_L \to (\pi\pi)_{I=2}]}{\mathcal{A}[K_S \to (\pi\pi)_{I=2}]} - \frac{\mathcal{A}[K_L \to (\pi\pi)_{I=0}]}{\mathcal{A}[K_S \to (\pi\pi)_{I=0}]}\right). \tag{149}$$

By selecting appropriate phase conventions for the mixing parameters between K^0 and $\bar{K}^0$ CP-eigenstates (see e.g. Ref. [408] for further details), the expression of ϵ' can be expressed in terms of the real and imaginary parts of the isospin amplitudes, as follows

$$\epsilon' = \frac{i\omega\, e^{i(\delta_2-\delta_0)}}{\sqrt{2}}\left[\frac{\text{Im}(A_2)}{\text{Re}(A_2)} - \xi\right], \tag{150}$$

where $\omega = \text{Re}(A_2)/\text{Re}(A_0)$, A_2 denotes the $\Delta I = 3/2$ $K \to \pi\pi$ decay amplitude, and δ_I denotes the strong scattering phase shifts in the corresponding, $I = 0, 2$, $K \to (\pi\pi)_I$ decays. Given that the phase, $\phi'_\epsilon = \delta_2 - \delta_0 + \pi/2 = 42.3(1.5)^\circ$ [165] is nearly equal to ϕ_ϵ in Eq. (135), the ratio of parameters characterizing the direct and indirect CP-violation in the kaon sector can be approximated in the following way,

$$\epsilon'/\epsilon \approx \text{Re}(\epsilon'/\epsilon) = \frac{\omega}{\sqrt{2}\,|\epsilon_K|}\left[\frac{\text{Im}(A_2)}{\text{Re}(A_2)} - \xi\right], \tag{151}$$

where on the left hand side we have set $\epsilon \equiv \epsilon_K$. The experimentally measured value reads [165],

$$\text{Re}(\epsilon'/\epsilon) = 16.6(2.3) \times 10^{-4}. \tag{152}$$

We remark that isospin breaking and electromagnetic effects (see Refs. [427,428], and the discussion in Ref. [409]) introduce additional correction terms into Eq. (151).

6.2 Lattice-QCD studies of the $K \to (\pi\pi)_I$ decay amplitudes, ξ and ϵ'/ϵ

As a preamble to this section, it should be noted that the study of $K \to \pi\pi$ decay amplitudes requires the development of computational strategies that are at the forefront of lattice QCD techniques. These studies represent a significant advance in

Table 28 Results for the real and imaginary parts of the $K \to \pi\pi$ decay amplitude A_0 from lattice-QCD computations with $N_f = 2+1$ dynamical flavours. Information about the renormalization, running and matching to the $\overline{\text{MS}}$ scheme is indicated in the column "running/matching", with details given at the bottom of the table. We refer to the text for further details about the main differences between the lattice computations in Refs. [429] and [430]

Collaboration	Refs.	N_f	Publication status	Continuum extrapolation	Chiral extrapolation	Finite volume	Renormalization	Running/matching	Re(A_0) [10^{-7} GeV]	Im(A_0) [10^{-11} GeV]
RBC/UKQCD 20	[429]	2+1	A	■	○	○	★	*a*	2.99(0.32)(0.59)	−6.98(0.62)(1.44)
RBC/UKQCD 15G	[430]	2+1	A	■	○	○	★	*b*	4.66(1.00)(1.26)	−1.90(1.23)(1.08)

a Nonperturbative renormalization with the RI/SMOM scheme at a scale of 1.53 GeV and running to 4.01 GeV employing a nonperturbatively determined step-scaling function. Conversion to $\overline{\text{MS}}$ at 1-loop order
b Nonperturbative renormalization with the RI/SMOM scheme at a scale of 1.53 GeV. Conversion to $\overline{\text{MS}}$ at 1-loop order

the study of kaon physics. However, at present, they have not yet reached the same level of maturity of most of the quantities analyzed in the FLAG report, where, for instance, independent results by various lattice collaborations are being compared and averaged. In the present version of this section we will therefore review the current status of $K \to \pi\pi$ lattice computations, but we will provide a FLAG average only for the case of the decay amplitude A_2.

We start by reviewing the determination of the parameter $\xi = \text{Im}(A_0)/\text{Re}(A_0)$. An estimate of ξ has been obtained from a direct evaluation of the ratio of amplitudes $\text{Im}(A_0)/\text{Re}(A_0)$ where $\text{Im}(A_0)$ is determined from a lattice-QCD computation by RBC/UKQCD 20 [429] employing $N_f = 2+1$ Möbius domain wall fermions at a single value of the lattice spacing while $\text{Re}(A_0) \simeq |A_0|$ and the value $|A_0| = 3.320(2) \times 10^{-7}$ GeV are used based on the relevant experimental input [165] from the decay to two pions. This leads to a result for ξ with a rather large relative error,

$$\xi = -2.1(5) \cdot 10^{-4}. \tag{153}$$

Following a similar procedure, an estimate of ξ was obtained through the use of a previous lattice QCD determination of $\text{Im}(A_0)$ by RBC/UKQCD 15G [430]. We refer to Table 28 for further details about these computations of $\text{Im}(A_0)$. The comparison of the estimates of ξ based on lattice QCD input are collected in Table 30.

Another estimate for ξ can be obtained through a lattice-QCD computation of the ratio of amplitudes $\text{Im}(A_2)/\text{Re}(A_2)$ by RBC/UKQCD 15F [46] where the continuum–limit result is based on computations at two values of the lattice spacing employing $N_f = 2+1$ Möbius domain wall fermions. Further details about the lattice computations of A_2 are collected in Table 29. To obtain the value of ξ, the expression in Eq. (151) together with the experimental values of $\text{Re}(\epsilon'/\epsilon)$, $|\epsilon_K|$ and ω are used. In this case we obtain $\xi = -1.6(2) \cdot 10^{-4}$. The use of the updated value of $\text{Im}(A_2) = -8.34(1.03) \times 10^{-13}$ GeV from Ref. [429],[26] in combination with the experimental value of $\text{Re}(A_2) = 1.479(4) \times 10^{-8}$ GeV, introduces a small change with respect to the above result. The value for ξ reads[27]

$$\xi = -1.7(2) \cdot 10^{-4}. \tag{154}$$

A phenomenological estimate can also be obtained from the relationship of ξ to $\text{Re}(\epsilon'/\epsilon)$, using the experimental value of the latter and further assumptions concerning the estimate of hadronic contributions. The corresponding value of ξ reads [415,416]

[26] The update in $\text{Im}(A_2)$ is due to a change in the value of the imaginary part of the ratio of CKM matrix elements, $\tau = -V_{ts}^* V_{td} / V_{us}^* V_{ud}$, as given in Ref. [431]. The lattice QCD input is therefore the one reported in Ref. [46].

[27] The current estimates for the corrections owing to isospin breaking and electromagnetic effects [428] imply a relative change on the theoretical value for ϵ'/ϵ by about -20% with respect to the determination based on Eq. (151). The size of these isospin breaking and electromagnetic corrections is related to the enhancement of the decay amplitudes between the $I = 0$ and the $I = 2$ channels. As a consequence, one obtains a similar reduction on ξ, leading to a value that is close to the result of Eq. (153).

Table 29 Results for the real and the imaginary parts of the $K \to \pi\pi$ decay amplitude A_2 from lattice-QCD computations with $N_f = 2+1$ dynamical flavours. Information about the renormalization and matching to the $\overline{\text{MS}}$ scheme is indicated in the column "running/matching", with details given at the bottom of the table

Collaboration	Refs.	N_f	Publication status	Continuum extrapolation	Chiral extrapolation	Finite volume	Renormalization	Running/matching	$\text{Re}(A_2)$ [10^{-8} GeV]	$\text{Im}(A_2)$ [10^{-13} GeV]
RBC/UKQCD 15F	[46]	2+1	A	○	○	★	★	a	1.50(0.04)(0.14)	$-8.34(1.03)^{\diamond}$

a Nonperturbative renormalization with the RI/SMOM scheme at a scale of 3 GeV. Conversion to $\overline{\text{MS}}$ at 1-loop order
$^{\diamond}$ This value of $\text{Im}(A_2)$ is an update reported in Ref. [429] which is based on the lattice QCD computation in Ref. [46] but where a change in the value of the imaginary part of the ratio of CKM matrix elements $\tau = -V_{ts}^* V_{td} / V_{us}^* V_{ud}$ reported in Ref. [431] has been applied

Table 30 Results for the parameter $\xi = \text{Im}(A_0)/\text{Re}(A_0)$ obtained through the combination of lattice-QCD determinations of $K \to \pi\pi$ decay amplitudes with $N_f = 2+1$ dynamical flavours and experimental inputs

Collaboration	Refs.	N_f	ξ
RBC/UKQCD 20†	[429]	2+1	$-2.1(5) \cdot 10^{-4}$
RBC/UKQCD 15G$^{\diamond}$	[430]	2+1	$-0.6(5) \cdot 10^{-4}$
RBC/UKQCD 15F*	[46]	2+1	$-1.7(2) \cdot 10^{-4}$

†Estimate for ξ obtained from a direct evaluation of the ratio of amplitudes $\text{Im}(A_0)/\text{Re}(A_0)$ where $\text{Im}(A_0)$ is determined from the lattice-QCD computation of Ref. [429] while for $\text{Re}(A_0) \simeq |A_0|$ is taken from the experimental value for $|A_0|$
$^{\diamond}$Estimate for ξ obtained from a direct evaluation of the ratio of amplitudes $\text{Im}(A_0)/\text{Re}(A_0)$ where $\text{Im}(A_0)$ is determined from the lattice-QCD computation of Ref. [430] while for $\text{Re}(A_0) \simeq |A_0|$ is taken from the experimental value for $|A_0|$
*Estimate for ξ based on the use of Eq. (151). The new value of $\text{Im}(A_2)$ reported in Ref. [429] – based on the lattice-QCD computation of Ref. [46] following an update of a nonlattice input – is used in combination with the experimental values for $\text{Re}(A_2)$, $\text{Re}(\epsilon'/\epsilon)$, $|\epsilon_K|$ and ω

$$\xi = -6.0(1.5) \cdot 10^{-2} \sqrt{2}\, |\epsilon_K| = -1.9(5) \cdot 10^{-4}. \tag{155}$$

We note that the use of the experimental value for $\text{Re}(\epsilon'/\epsilon)$ is based on the assumption that it is free from New Physics contributions. The value of ξ can then be combined with a χPT-based estimate for the long-range contribution, $\rho = 0.6(3)$ [416]. Overall, the combination $\rho\xi$ appearing in Eq. (148) leads to a suppression of the SM prediction of $|\epsilon_K|$ by about 3(2)% relative to the experimental measurement of $|\epsilon_K|$ given in Eq. (134), regardless of whether the phenomenological estimate of ξ [see Eq. (155)] or the most precise lattice result [see Eq. (153)] are used. The uncertainty in the suppression factor is dominated by the error on ρ. Although this is a small correction, we note that its contribution to the error of ϵ_K is larger than that arising from the value of B_K reported below.

Efforts are under way to compute the long-distance contributions to ϵ_K [432] and to the $K_L - K_S$ mass difference in lattice QCD [425,433–435]. However, the results are not yet precise enough to improve the accuracy in the determination of the parameter ρ.

The lattice-QCD study of $K \to \pi\pi$ decays provides crucial input to the SM prediction of ϵ_K. We now proceed to describe the current status of these computations. In recent years, the RBC/UKQCD collaboration has undertaken a series of lattice-QCD calculations of $K \to \pi\pi$ decay amplitudes [46,429,430]. In 2015, the first calculation of the $K \to (\pi\pi)_{I=0}$ decay amplitude A_0 was performed using physical kinematics on a $32^3 \times 64$ lattice with an inverse lattice spacing of $a^{-1} = 1.3784(68)$ GeV [430,436]. The main features of the RBC/UKQCD 15G calculation included, fixing the $I = 0$ $\pi\pi$ energy very close to the kaon mass by imposing G-parity boundary conditions, a continuum-like operator mixing pattern through the use of a domain wall fermion action with accurate chiral symmetry, and the construction of the complete set of correlation functions by computing seventy-five distinct diagrams. Results for the real and the imaginary parts of the decay amplitude A_0 from the RBC/UKQCD 15G computation are collected in Table 28, where the first error is statistical and the second one is systematic.

The latest 2020 calculation RBC/UKQCD 20 [429] using the same lattice setup has improved the 2015 calculation RBC/UKQCD 15G [430] in three important aspects: (i) an increase by a factor of 3.4 in statistics; (ii) the inclusion of a scalar two-quark operator and the addition of another pion-pion operator to isolate the ground state, and (iii) the use of step

scaling techniques to raise the renormalization scale from 1.53 to 4.01 GeV. The updated determinations of the real and the imaginary parts of A_0 in Ref. [429] are shown in Table 28.

As previously discussed, the determination of $\mathrm{Im}(A_0)$ from Ref. [429] has been used to obtain the value of the parameter ξ in Eq. (153). A first-principles computation of $\mathrm{Re}(A_0)$ is essential to address the so-called $\Delta I = 1/2$ puzzle associated to the enhancement of $\Delta I = 1/2$ over $\Delta I = 3/2$ transitions owing, crucially, to long distance effects. Indeed, short-distance enhancements in the Wilson coefficients are not large enough to explain the $\Delta I = 1/2$ rule [437,438]. Lattice-QCD calculations do provide a method to study such a long-distance enhancement. The combination of the result for A_0 in Table 28 with the earlier lattice calculation of A_2 in Ref. [46] leads to the ratio, $\mathrm{Re}(A_0)/\mathrm{Re}(A_2) = 19.9(5.0)$, which agrees with the experimentally measured value, $\mathrm{Re}(A_0)/\mathrm{Re}(A_2) = 22.45(6)$. In Ref. [429], the lattice determination of relative size of direct CP violation was updated as follows,

$$\mathrm{Re}(\epsilon'/\epsilon) = 21.7(2.6)(6.2)(5.0) \times 10^{-4}, \tag{156}$$

where the first two errors are statistical and systematic, respectively. The third error arises from the omitted strong and electromagnetic isospin breaking effects. The value of $\mathrm{Re}(\epsilon'/\epsilon)$ in Eq. (156) uses the experimental values of $\mathrm{Re}(A_0)$ and $\mathrm{Re}(A_2)$. The lattice determination of $\mathrm{Re}(\epsilon'/\epsilon)$ is in good agreement with the experimental result in Eq. (152). However, while the result in Eq. (156) represents a significant step forward, it is important to keep in mind that the calculation of A_0 is currently based on a single value of the lattice spacing. It is expected that future work with additional values of the lattice spacing will contribute to improve the precision. For a description of the computation of the $\pi\pi$ scattering phase shifts entering in the determination of $\mathrm{Re}(\epsilon'/\epsilon)$ in Eq. (156), we refer to Ref. [439].

The real and imaginary values of the amplitude A_2 have been determined by RBC/UKQCD 15F [46] employing $N_f = 2+1$ Möbius domain wall fermions at two values of the lattice spacing, namely $a = 0.114\,\mathrm{fm}$ and $0.083\,\mathrm{fm}$, and performing simulations at the physical pion mass with $M_\pi L \approx 3.8$.

A compilation of lattice results for the real and imaginary parts of the $K \to \pi\pi$ decay amplitudes, A_0 and A_2, with $N_f = 2 + 1$ flavours of dynamical quarks is shown in Tables 28 and 29. In Appendix C.4.1 we collect the corresponding information about the lattice QCD simulations, including the values of some of the most relevant parameters. The results for the parameter ξ, determined through the combined use of $K \to \pi\pi$ amplitudes computed on the lattice and experimental inputs, are presented in Table 30. As previously discussed, we remark that the total uncertainty on the reported values of ξ depends on the specific way in which the lattice and experimental inputs are selected.

The determination of the real and imaginary parts of A_2 by RBC/UKQCD 15F shown in Table 29 is free of red tags. We therefore quote the following FLAG averages:

$$N_f = 2+1: \quad \begin{aligned} &\mathrm{Re}(A_2) = 1.50(0.04)(0.14) \times 10^{-8}\ \mathrm{GeV}, \\ &\mathrm{Im}(A_2) = -8.34(1.03) \times 10^{-13}\ \mathrm{GeV}, \end{aligned} \quad \text{Ref. [46].} \tag{157}$$

Besides the RBC/UKQCD collaboration programme [46,429,430] using domain-wall fermions, an approach based on improved Wilson fermions [440,441] has presented a determination of the $K \to \pi\pi$ decay amplitudes, A_0 and A_2, at unphysical quark masses. For an analysis of the scaling with the number of colours of $K \to \pi\pi$ decay amplitudes using lattice-QCD computations, we refer to Refs. [442,443].

Recent proposals aiming at the inclusion of electromagnetism in lattice-QCD calculations of $K \to \pi\pi$ decays are being explored [444,445] in order to reduce the uncertainties associated with isospin breaking effects.

Finally, we notice that ϵ_K receives a contribution from $|V_{cb}|$ through the λ_t parameter in Eq. (140). The present uncertainty on $|V_{cb}|$ has a significant impact on the error of ϵ_K (see, e.g., Refs. [446,447] and the recent update in Ref. [448]).

6.3 Lattice computation of B_K

Lattice calculations of B_K are affected by the same type of systematic effects discussed in previous sections of this review. However, the issue of renormalization merits special attention. The reason is that the multiplicative renormalizability of the relevant operator $Q^{\Delta S=2}$ is lost once the regularized QCD action ceases to be invariant under chiral transformations. As a result, the renormalization pattern of B_K depends on the specific choice of the fermionic discretization.

In the case of Wilson fermions, $Q^{\Delta S=2}$ mixes with four additional dimension-six operators, which belong to different representations of the chiral group, with mixing coefficients that are finite functions of the gauge coupling. This complicated renormalization pattern was identified as the main source of systematic error in earlier, mostly quenched calculations of B_K

with Wilson quarks. It can be bypassed via the implementation of specifically designed methods, which are either based on Ward identities [449] or on a modification of the Wilson quark action, known as twisted-mass QCD [450–452].

An advantage of staggered fermions is the presence of a remnant $U(1)$ chiral symmetry. However, at nonvanishing lattice spacing, the symmetry among the extra unphysical degrees of freedom (tastes) is broken. As a result, mixing with other dimension-six operators cannot be avoided in the staggered formulation, which complicates the determination of the B-parameter. In general, taste conserving mixings are implemented directly in the lattice computation of the matrix element. The effects of the broken taste symmetry are usually treated through an effective field theory, staggered Chiral Perturbation Theory (SχPT) [453,454], parameterizing the quark-mass and lattice-spacing dependences.

Fermionic lattice actions based on the Ginsparg–Wilson relation [455] are invariant under the chiral group, and hence four-quark operators such as $Q^{\Delta S=2}$ renormalize multiplicatively. However, depending on the particular formulation of Ginsparg–Wilson fermions, residual chiral symmetry breaking effects may be present in actual calculations. For instance, in the case of domain-wall fermions, the finiteness of the extra 5th dimension implies that the decoupling of modes with different chirality is not exact, which produces a residual nonzero quark mass in the chiral limit. The mixing with dimension-six operators of different chirality is expected to be an $\mathcal{O}(m_{\rm res}^2)$ suppressed effect [456,457] that should be investigated on a case-by-case basis.

Before proceeding to the description and compilation of the results of B_K, we would like to reiterate a discussion presented in the previous FLAG report about an issue related to the computation of the kaon bag parameters through lattice-QCD simulations with $N_f = 2+1+1$ dynamical quarks. In practice, this only concerns the calculations of the kaon B-parameters including dynamical charm-quark effects in Ref. [47], that were examined in the FLAG 16 report. As described in Sect. 6.1, the effective Hamiltonian in Eq. (138) depends solely on the operator $Q^{\Delta S=2}$ in Eq. (139) – which appears in the definition of B_K in Eq. (145) – at energy scales below the charm threshold where charm-quark contributions are absent. As a result, a computation of B_K based on $N_f = 2+1+1$ dynamical simulations will include an extra sea-quark contribution from charm-quark loop effects for which there is at present no direct evaluation in the literature.

When the matrix element of $Q^{\Delta S=2}$ is evaluated in a theory that contains a dynamical charm quark, the resulting estimate for B_K must then be matched to the three-flavour theory that underlies the effective four-quark interaction.[28] In general, the matching of $2+1$-flavour QCD with the theory containing $2+1+1$ flavours of sea quarks is performed around the charm threshold. It is usually accomplished by requiring that the coupling and quark masses are equal in the two theories at a renormalization scale μ around m_c. In addition, B_K should be renormalized and run, in the four-flavour theory, to the value of μ at which the two theories are matched, as described in Sect. 6.1. The corrections associated with this matching are of order $(E/m_c)^2$, where E is a typical energy in the process under study, since the subleading operators have dimension eight [458].

When the kaon-mixing amplitude is considered, the matching also involves the relation between the relevant box diagrams and the effective four-quark operator. In this case, corrections of order $(E/m_c)^2$ arise not only from the charm quarks in the sea, but also from the valence sector, since the charm quark propagates in the box diagrams. We note that the original derivation of the effective four-quark interaction is valid up to corrections of order $(E/m_c)^2$. The kaon-mixing amplitudes evaluated in the $N_f = 2+1$ and $2+1+1$ theories are thus subject to corrections of the same order in E/m_c as the derivation of the conventional four-quark interaction.

Regarding perturbative QCD corrections at the scale of the charm-quark mass on the amplitude in Eq. (141), the uncertainty on η_1 and η_3 factors is of $\mathcal{O}(\alpha_s(m_c)^3)$ [418,419], while that on η_2 is of $\mathcal{O}(\alpha_s(m_c)^2)$ [459].[29] On the other hand, the corrections of order $(E/m_c)^2$ due to dynamical charm-quark effects in the matching of the amplitudes are further suppressed by powers of $\alpha_s(m_c)$ and by a factor of $1/N_c$, given that they arise from quark-loop diagrams. In order to make progress in resolving this so far uncontrolled systematic uncertainty, it is essential that any future calculation of B_K with $N_f = 2+1+1$ flavours properly addresses the size of these residual dynamical charm effects in a quantitative way.

Another issue in this context is how the lattice scale and the physical values of the quark masses are determined in the $2+1$ and $2+1+1$ flavour theories. Here it is important to consider in which way the quantities used to fix the bare parameters are affected by a dynamical charm quark.

A recent study [167] using three degenerate light quarks, together with a charm quark, indicates that the deviations between the $N_f = 3+1$ and the $N_f = 3$ theories are considerably below the 1% level in dimensionless quantities constructed

[28] We thank Martin Lüscher for an interesting discussion on this issue.

[29] The recent results [426] based on the use of $u-t$ unitarity for the two corresponding perturbative factors, also have an uncertainty of $\mathcal{O}(\alpha_s(m_c)^2)$ and $\mathcal{O}(\alpha_s(m_c)^3)$. The estimates for the missing higher-order contributions are, however, expected to be reduced with respect to the more traditional case where $c-t$ unitarity is used.

Table 31 Results for the kaon B-parameter in QCD with $N_f = 2+1+1$ and $N_f = 2+1$ dynamical flavours, together with a summary of systematic errors. Information about nonperturbative running is indicated in the column "running", with details given at the bottom of the table

Collaboration	Refs.	N_f	Publication status	Continuum extrapolation	Chiral extrapolation	Finite volume	Renormalization	Running	$B_K(\overline{\text{MS}}, 2\,\text{GeV})$	$\hat{B}_K$
ETM 15	[47]	2+1+1	A	★	○	○	★	a	0.524(13)(12)	0.717(18)(16)[1]
RBC/UKQCD 16	[52]	2+1	A	○	○	○	★	b	0.543(9)(13)[2]	0.744(13)(18)[3]
SWME 15A	[50]	2+1	A	★	○	★	○‡	–	0.537(4)(26)	0.735(5)(36)[4]
RBC/UKQCD 14B	[8]	2+1	A	★	★	★	★	b	0.5478(18)(110)[2]	0.7499(24)(150)
SWME 14	[422]	2+1	A	★	○	★	○‡	–	0.5388(34)(266)	0.7379(47)(365)
SWME 13A	[461]	2+1	A	★	○	★	○‡	–	0.537(7)(24)	0.735(10)(33)
SWME 13	[462]	2+1	C	★	○	★	○‡	–	0.539(3)(25)	0.738(5)(34)
RBC/UKQCD 12A	[188]	2+1	A	○	★	○	★	b	0.554(8)(14)[2]	0.758(11)(19)
Laiho 11	[49]	2+1	C	★	○	○	★	–	0.5572(28)(150)	0.7628(38)(205)[4]
SWME 11A	[463]	2+1	A	★	○	○	○‡	–	0.531(3)(27)	0.727(4)(38)
BMW 11	[48]	2+1	A	★	★	★	★	c	0.5644(59)(58)	0.7727(81)(84)
RBC/UKQCD 10B	[464]	2+1	A	○	○	★	★	d	0.549(5)(26)	0.749(7)(26)
SWME 10	[465]	2+1	A	★	○	○	○	–	0.529(9)(32)	0.724(12)(43)
Aubin 09	[466]	2+1	A	○	○	○	★	–	0.527(6)(21)	0.724(8)(29)

‡The renormalization is performed using perturbation theory at 1-loop, with a conservative estimate of the uncertainty

a B_K is renormalized nonperturbatively at scales $1/a \sim 2.2-3.3$ GeV in the $N_f = 4$ RI/MOM scheme using two different lattice momentum scale intervals, the first around $1/a$ while the second around 3.5 GeV. The impact of the two ways to the final result is taken into account in the error budget. Conversion to $\overline{\text{MS}}$ is at 1-loop at 3 GeV

b B_K is renormalized nonperturbatively at a scale of 1.4 GeV in two RI/SMOM schemes for $N_f = 3$, and then run to 3 GeV using a nonperturbatively determined step-scaling function. Conversion to $\overline{\text{MS}}$ is at 1-loop order at 3 GeV

c B_K is renormalized and run nonperturbatively to a scale of 3.5 GeV in the RI/MOM scheme. At the same scale conversion at 1-loop to $\overline{\text{MS}}$ is applied. Nonperturbative and NLO perturbative running agrees down to scales of 1.8 GeV within statistical uncertainties of about 2%

d B_K is renormalized nonperturbatively at a scale of 2 GeV in two RI/SMOM schemes for $N_f = 3$, and then run to 3 GeV using a nonperturbatively determined step-scaling function. Conversion to $\overline{\text{MS}}$ is at 1-loop order at 3 GeV

[1] $B_K(\overline{\text{MS}}, 2\,\text{GeV})$ and $\hat{B}_K$ are related using the conversion factor 1.369, i.e., the one obtained with $N_f = 2+1$

[2] $B_K(\overline{\text{MS}}, 2\,\text{GeV})$ is obtained from the estimate for $\hat{B}_K$ using the conversion factor 1.369

[3] $\hat{B}_K$ is obtained from $B_K(\overline{\text{MS}}, 3\,\text{GeV})$ using the conversion factor employed in Ref. [8]

[4] $\hat{B}_K$ is obtained from the estimate for $B_K(\overline{\text{MS}}, 2\,\text{GeV})$ using the conversion factor 1.369

from ratios of gradient flow observables, such as t_0 and w_0, used for scale setting. This study extends the nonperturbative investigations with two heavy mass-degenerate quarks [158,160] which indicate that dynamical charm-quark effects in low-energy hadronic observables are considerably smaller than the expectation from a naive power counting in terms of $\alpha_s(m_c)$. For an additional discussion on this point, we refer to Ref. [47]. Given the hierarchy of scales between the charm-quark mass and that of B_K, we expect these errors to be modest, but a more quantitative understanding is needed as statistical errors on B_K are reduced. Within this review we will not discuss this issue further. However, we wish to point out that the present discussion also applies to $N_f = 2+1+1$ computations of the kaon BSM B-parameters discussed in Sect. 6.4.

A compilation of results for B_K with $N_f = 2, 2+1$ and $2+1+1$ flavours of dynamical quarks is shown in Tables 31 and 32, as well as Fig. 20. An overview of the quality of systematic error studies is represented by the colour coded entries in Tables 31 and 32. The values of the most relevant lattice parameters, and comparative tables on the various estimates of systematic errors have been collected in the corresponding Appendices of the previous FLAG editions [2–4].

Since the last edition of the FLAG report no new results for B_K have appeared in the bibliography. We mention here an ongoing work related to the B_K computation where the relevant operators are defined in the gradient flow framework. In a first publication [460] the small flow time expansion method is applied in order to compute, to 1-loop approximation, the finite matching coefficients between the gradient flow and the $\overline{\text{MS}}$ schemes for the operators entering the B_K computation.

Table 32 Results for the kaon B-parameter in QCD with $N_f = 2$ dynamical flavours, together with a summary of systematic errors. Information about nonperturbative running is indicated in the column "running", with details given at the bottom of the table

Collaboration	Refs.	N_f	Publication status	Continuum extrapolation	Chiral extrapolation	Finite volume	Renormalization	Running	$B_K(\overline{\text{MS}}, 2\,\text{GeV})$	$\hat{B}_K$
ETM 12D	[51]	2	A	★	○	○	★	e	0.531(16)(9)	0.727(22)(12)[1]
ETM 10A	[467]	2	A	★	○	○	★	f	0.533(18)(12)[1]	0.729(25)(17)

e B_K is renormalized nonperturbatively at scales $1/a \sim 2 - 3.7\,\text{GeV}$ in the $N_f = 2$ RI/MOM scheme. In this scheme, nonperturbative and NLO perturbative running are shown to agree from 4 GeV down to 2 GeV to better than 3% [467,468]
f B_K is renormalized nonperturbatively at scales $1/a \sim 2 - 3\,\text{GeV}$ in the $N_f = 2$ RI/MOM scheme. In this scheme, nonperturbative and NLO perturbative running are shown to agree from 4 GeV down to 2 GeV to better than 3% [467,468]
[1] $B_K(\overline{\text{MS}}, 2\,\text{GeV})$ and $\hat{B}_K$ are related using the conversion factor 1.369, i.e., the one obtained with $N_f = 2 + 1$

For a detailed description of previous B_K calculations – and in particular those considered in the computation of the average values – we refer the reader to the FLAG 19 [4], FLAG 16 [3] and FLAG 13 [2] reports.

We now give the global averages for B_K for $N_f = 2 + 1 + 1, 2 + 1$ and 2 dynamical flavours. The details about the calculation of these averages can be found in FLAG 19 [4].

We begin with the $N_f = 2 + 1$ global average since it is estimated by employing four different B_K results, namely BMW 11 [48], Laiho 11 [49], RBC/UKQCD 14B [8] and SWME 15A [50]. Note also that the expression of ϵ_K in terms of B_K is obtained in the three-flavour theory (see Sect. 6.1). After constructing the global covariance matrix according to Schmelling [163], we arrive at:

$$N_f = 2 + 1: \qquad \hat{B}_K = 0.7625(97) \qquad \text{Refs. [8,48–50]}, \tag{158}$$

with $\chi^2/\text{dof} = 0.675$. After applying the NLO conversion factor $\hat{B}_K / B_K^{\overline{\text{MS}}}(2\,\text{GeV}) = 1.369$,[30] this translates into

$$N_f = 2 + 1: \qquad B_K^{\overline{\text{MS}}}(2\,\text{GeV}) = 0.5570(71) \qquad \text{Refs. [8,48–50]}. \tag{159}$$

Note that the statistical errors of each calculation entering the global average are small enough to make their results statistically incompatible. It is only because of the relatively large systematic errors that the weighted average produces a value of $\mathcal{O}(1)$ for the reduced χ^2.

There is only a single result for $N_f = 2 + 1 + 1$, computed by the ETM collaboration [47]. Since it is free of red tags, it qualifies as the currently best global average, i.e.,

$$N_f = 2 + 1 + 1: \qquad \hat{B}_K = 0.717(18)(16)\,, \qquad B_K^{\overline{\text{MS}}}(2\,\text{GeV}) = 0.524(13)(12) \qquad \text{Ref. [47]}. \tag{160}$$

For $N_f = 2$ flavours the best global average is given by a single result, that of ETM 12D [51]:

$$N_f = 2: \qquad \hat{B}_K = 0.727(22)(12), \qquad B_K^{\overline{\text{MS}}}(2\,\text{GeV}) = 0.531(16)(19) \qquad \text{Ref. [51]}. \tag{161}$$

The result in the $\overline{\text{MS}}$ scheme has been obtained by applying the same conversion factor of 1.369 as in the three-flavour theory.

6.4 Kaon BSM B-parameters

We now report on lattice results concerning the matrix elements of operators that encode the effects of physics beyond the Standard Model (BSM) to the mixing of neutral kaons. In this theoretical framework both the SM and BSM contributions add

[30] We refer to the FLAG 19 report [4] for a discussion about the estimates of these conversion factors.

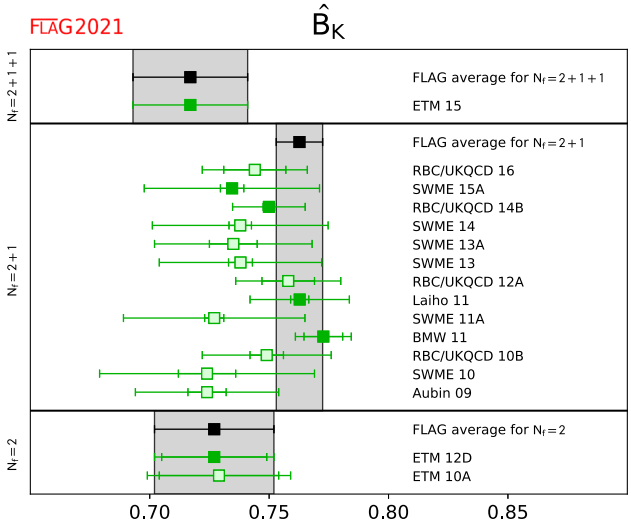

Fig. 20 Recent unquenched lattice results for the RGI B-parameter $\hat{B}_K$. The grey bands indicate our global averages described in the text. For $N_f = 2+1+1$ and $N_f = 2$ the global averages coincide with the results by ETM 15 and ETM 12D, respectively

up to reproduce the experimentally observed value of ϵ_K. Since BSM contributions involve heavy but unobserved particles they are short-distance dominated. The effective Hamiltonian for generic $\Delta S = 2$ processes including BSM contributions reads

$$\mathcal{H}_{\text{eff,BSM}}^{\Delta S=2} = \sum_{i=1}^{5} C_i(\mu) Q_i(\mu), \tag{162}$$

where Q_1 is the four-quark operator of Eq. (139) that gives rise to the SM contribution to ϵ_K. In the so-called SUSY basis introduced by Gabbiani et al. [469] the operators $Q_2, \ldots, Q_5$ read[31]

$$\begin{aligned} Q_2 &= \left(\bar{s}^a(1-\gamma_5)d^a\right)\left(\bar{s}^b(1-\gamma_5)d^b\right), \\ Q_3 &= \left(\bar{s}^a(1-\gamma_5)d^b\right)\left(\bar{s}^b(1-\gamma_5)d^a\right), \\ Q_4 &= \left(\bar{s}^a(1-\gamma_5)d^a\right)\left(\bar{s}^b(1+\gamma_5)d^b\right), \\ Q_5 &= \left(\bar{s}^a(1-\gamma_5)d^b\right)\left(\bar{s}^b(1+\gamma_5)d^a\right), \end{aligned} \tag{163}$$

where a and b denote colour indices. In analogy to the case of B_K one then defines the B-parameters of $Q_2, \ldots, Q_5$ according to

$$B_i(\mu) = \frac{\left\langle \bar{K}^0 \left| Q_i(\mu) \right| K^0 \right\rangle}{N_i \left\langle \bar{K}^0 \left| \bar{s}\gamma_5 d \right| 0 \right\rangle \left\langle 0 \left| \bar{s}\gamma_5 d \right| K^0 \right\rangle}, \quad i = 2, \ldots, 5. \tag{164}$$

The factors $\{N_2, \ldots, N_5\}$ are given by $\{-5/3, 1/3, 2, 2/3\}$, and it is understood that $B_i(\mu)$ is specified in some renormalization scheme, such as $\overline{\text{MS}}$ or a variant of the regularization-independent momentum subtraction (RI-MOM) scheme.

The SUSY basis has been adopted in Refs. [47,51,52,470]. Alternatively, one can employ the chiral basis of Buras, Misiak and Urban [471]. The SWME collaboration prefers the latter since the anomalous dimension that enters the RG running has been calculated to 2-loops in perturbation theory [471]. Results obtained in the chiral basis can be easily converted to the SUSY basis via

$$B_3^{\text{SUSY}} = \tfrac{1}{2}\left(5B_2^{\text{chiral}} - 3B_3^{\text{chiral}}\right). \tag{165}$$

The remaining B-parameters are the same in both bases. In the following we adopt the SUSY basis and drop the superscript.

[31] Thanks to QCD parity invariance lattice computations for three more dimension-six operators, whose parity conserving parts coincide with the corresponding parity conserving contributions of the operators Q_1, Q_2 and Q_3, can be ignored.

Table 33 Results for the BSM B-parameters $B_2, \ldots, B_5$ in the $\overline{\text{MS}}$ scheme at a reference scale of 3 GeV. Information about nonperturbative running is indicated in the column "running", with details given at the bottom of the table.

Collaboration	Refs.	N_f	Publication status	Continuum extrapolation	Chiral extrapolation	Finite volume	Renormalization	Running	B_2	B_3	B_4	B_5
ETM 15	[47]	2+1+1	A	★	○	○	★	a	0.46(1)(3)	0.79(2)(5)	0.78(2)(4)	0.49(3)(3)
RBC/UKQCD 16	[52]	2+1	A	○	○	○	★	b	0.488(7)(17)	0.743(14)(65)	0.920(12)(16)	0.707(8)(44)
SWME 15A	[50]	2+1	A	★	○	★	○†	–	0.525(1)(23)	0.773(6)(35)	0.981(3)(62)	0.751(7)(68)
SWME 14C	[476]	2+1	C	★	○	★	○†	–	0.525(1)(23)	0.774(6)(64)	0.981(3)(61)	0.748(9)(79)
SWME 13A‡	[461]	2+1	A	★	○	★	○†	–	0.549(3)(28)	0.790(30)	1.033(6)(46)	0.855(6)(43)
RBC/UKQCD 12E	[470]	2+1	A	■	○	★	★	b	0.43(1)(5)	0.75(2)(9)	0.69(1)(7)	0.47(1)(6)
ETM 12D	[51]	2	A	★	○	○	★	c	0.47(2)(1)	0.78(4)(2)	0.76(2)(2)	0.58(2)(2)

†The renormalization is performed using perturbation theory at 1-loop, with a conservative estimate of the uncertainty

a B_i are renormalized nonperturbatively at scales $1/a \sim 2.2{-}3.3$ GeV in the $N_f = 4$ RI/MOM scheme using two different lattice momentum scale intervals, with values around $1/a$ for the first and around 3.5 GeV for the second one. The impact of these two ways to the final result is taken into account in the error budget. Conversion to $\overline{\text{MS}}$ is at 1-loop at 3 GeV

b The B-parameters are renormalized nonperturbatively at a scale of 3 GeV

c B_i are renormalized nonperturbatively at scales $1/a \sim 2 - 3.7$ GeV in the $N_f = 2$ RI/MOM scheme using two different lattice momentum scale intervals, with values around $1/a$ for the first and around 3 GeV for the second one

‡The computation of B_4 and B_5 has been revised in Refs. [50] and [476]

Older quenched results for the BSM B-parameters can be found in Refs. [472–474]. For a nonlattice approach to get estimates for the BSM B-parameters see Ref. [475].

Estimates for $B_2, \ldots, B_5$ have been reported for QCD with $N_f = 2$ (ETM 12D [51]), $N_f = 2 + 1$ (RBC/UKQCD 12E [470], SWME 13A [461], SWME 14C [476], SWME 15A [50], RBC/UKQCD 16 [52,477]) and $N_f = 2 + 1 + 1$ (ETM 15 [47]) flavours of dynamical quarks. Since the publication of the FLAG 19 report [4] no new results for the BSM B-parameters have appeared in the bibliography. The available results are listed and compared in Table 33 and Fig. 21. In general one finds that the BSM B-parameters computed by different collaborations do not show the same level of consistency as the SM kaon-mixing parameter B_K discussed previously. Control over the systematic uncertainties from chiral and continuum extrapolations as well as finite-volume effects in $B_2, \ldots, B_5$ is expected to be at a commensurate level as for B_K, as far as the results by ETM 12D, ETM 15, SWME 15A and RBC/UKQCD 16 are concerned, since the set of gauge ensembles employed in both kinds of computations is the same. The calculation by RBC/UKQCD 12E has been performed at a single value of the lattice spacing and a minimum pion mass of 290 MeV.

Let us notice that as reported in RBC/UKQCD 16 [52] the comparison of results obtained in the conventional RI-MOM and two RI-SMOM schemes shows significant discrepancies for B_4 and B_5 in the $\overline{\text{MS}}$ scheme at the scale of 3 GeV, which amount up to 2.8σ in the case of B_5. By contrast, the agreement for B_2 and B_3 determined for different intermediate scheme is much better. The RBC/UKQCD collaboration has presented an ongoing study [478] in which simulations with two values of the lattice spacing at the physical point and with a third finer lattice spacing at $M_\pi = 234$ MeV are employed in order to obtain the BSM matrix elements in the continuum limit. Results are still preliminary.

The findings by RBC/UKQCD 16 [52,477] provide evidence that the nonperturbative determination of the matching factors depends strongly on the details of the implementation of the Rome–Southampton method. The use of nonexceptional momentum configurations in the calculation of the vertex functions produces a significant modification of the renormalization factors, which affects the matching between $\overline{\text{MS}}$ and the intermediate momentum subtraction scheme. This effect is most pronounced in B_4 and B_5. Furthermore, it can be noticed that the estimates for B_4 and B_5 from RBC/UKQCD 16 are much closer to those of SWME 15A. At the same time, the results for B_2 and B_3 obtained by ETM 15, SWME 15A and RBC/UKQCD 16 are in good agreement within errors.

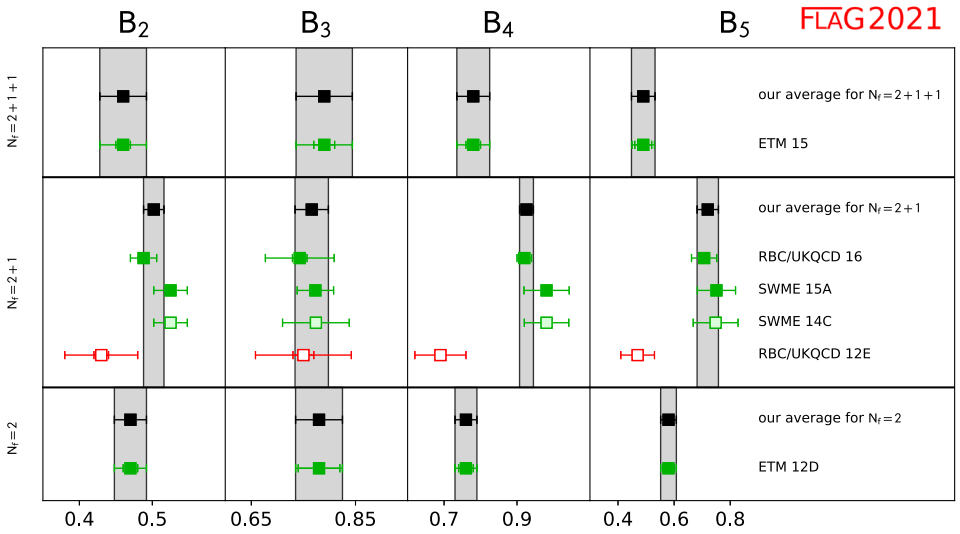

Fig. 21 Lattice results for the BSM B-parameters defined in the $\overline{\text{MS}}$ scheme at a reference scale of 3 GeV, see Table 33

A nonperturbative computation of the running of the four-fermion operators contributing to the $B_2, \ldots, B_5$ parameters has been carried out with two dynamical flavours using the Schrödinger functional renormalization scheme [424]. Renormalization matrices of the operator basis are used to build step-scaling functions governing the continuum-limit running between hadronic and electroweak scales. A comparison to perturbative results using NLO (2-loops) for the four-fermion operator anomalous dimensions indicates that, at scales of about 3 GeV, nonperturbative effects can induce a sizeable contribution to the running.

A detailed look at the calculations reported in the works of ETM 15 [47], SWME 15A [50] and RBC/UKQCD 16 [52] reveals that cutoff effects appear to be larger for the BSM B-parameters compared to B_K. Depending on the details of the renormalization procedure and/or the fit ansatz for the combined chiral and continuum extrapolation, the results obtained at the coarsest lattice spacing differ by 15–30%. At the same time the available range of lattice spacings is typically much reduced compared to the corresponding calculations of B_K, as can be seen by comparing the quality criteria in Tables 31 and 33. Hence, the impact of the renormalization procedure and the continuum limit on the BSM B-parameters certainly requires further investigation.

Finally we present our estimates for the BSM B-parameters, quoted in the $\overline{\text{MS}}$-scheme at scale 3 GeV. For $N_f = 2+1$ our estimate is given by the average between the results from SWME 15A and RBC/UKQCD 16, i.e.,

$$\begin{aligned} &N_f = 2+1: \\ &B_2 = 0.502(14), \quad B_3 = 0.766(32), \quad B_4 = 0.926(19), \quad B_5 = 0.720(38), \quad \text{Refs. [50,52]}. \end{aligned} \tag{166}$$

For $N_f = 2+1+1$ and $N_f = 2$, our estimates coincide with the ones by ETM 15 and ETM 12D, respectively, since there is only one computation for each case. Thus we quote

$$\begin{aligned} &N_f = 2+1+1: \\ &B_2 = 0.46(1)(3), \quad B_3 = 0.79(2)(5), \quad B_4 = 0.78(2)(4), \quad B_5 = 0.49(3)(3), \quad \text{Ref. [47]}, \end{aligned} \tag{167}$$

$$\begin{aligned} &N_f = 2: \\ &B_2 = 0.47(2)(1), \quad B_3 = 0.78(4)(2), \quad B_4 = 0.76(2)(2), \quad B_5 = 0.58(2)(2), \quad \text{Ref. [51]}. \end{aligned} \tag{168}$$

Based on the above discussion on the effects of employing different intermediate momentum subtraction schemes in the nonperturbative renormalization of the operators, the discrepancy for B_4 and B_5 results between $N_f = 2, 2+1+1$ and $N_f = 2+1$ computations should not be considered an effect associated with the number of dynamical flavours. To clarify the present situation, it would be important to perform a direct comparison of results by the ETM collaboration obtained both with RI-MOM and RI-SMOM methods. Furthermore, extending the computation of the BSM-B parameters to include physical point simulations with improved continuum-limit extrapolations would also provide valuable information. As a closing remark, we encourage authors to provide the correlation matrix of the B_i parameters since this information is required in phenomenological studies of New Physics scenarios.

7 Charm hadron decay constants and form factors

Authors: Y. Aoki, M. Della Morte, E. Lunghi, S. Meinel, C. Monahan, C. Pena

Leptonic and semileptonic decays of charmed D and D_s mesons or Λ_c and other charm baryons occur via charged W-boson exchange, and are sensitive probes of $c \to d$ and $c \to s$ quark flavour-changing transitions. Given experimental measurements of the branching fractions combined with sufficiently precise theoretical calculations of the hadronic matrix elements, they enable the determination of the CKM matrix elements $|V_{cd}|$ and $|V_{cs}|$ (within the Standard Model) and a precise test of the unitarity of the second row of the CKM matrix. Here, we summarize the status of lattice-QCD calculations of the charmed leptonic decay constants. Significant progress has been made in charm physics on the lattice in recent years, largely due to the availability of gauge configurations produced using highly-improved lattice-fermion actions that enable treating the c quark with the same action as for the u, d, and s quarks.

This section updates the corresponding one in the last FLAG review [4] for results that appeared before April 30, 2021. As already done in Ref. [4], we limit our review to results based on modern simulations with reasonably light pion masses (below approximately 500 MeV).

Following our review of lattice-QCD calculations of $D_{(s)}$-meson leptonic decay constants and charm-hadron semileptonic form factors, we then interpret our results within the context of the Standard Model. We combine our best-determined values of the hadronic matrix elements with the most recent experimentally-measured branching fractions to obtain $|V_{cd(s)}|$ and test the unitarity of the second row of the CKM matrix.

7.1 Leptonic decay constants f_D and f_{D_s}

In the Standard Model, and up to electromagnetic corrections, the decay constant $f_{D_{(s)}}$ of a pseudoscalar D or D_s meson is related to the branching ratio for leptonic decays mediated by a W boson through the formula

$$\mathcal{B}(D_{(s)} \to \ell\nu_\ell) = \frac{G_F^2 |V_{cq}|^2 \tau_{D_{(s)}}}{8\pi} f_{D_{(s)}}^2 m_\ell^2 m_{D_{(s)}} \left(1 - \frac{m_\ell^2}{m_{D_{(s)}}^2}\right)^2, \tag{169}$$

where q is d or s and V_{cd} (V_{cs}) is the appropriate CKM matrix element for a D (D_s) meson. The branching fractions have been experimentally measured by CLEO, Belle, Babar and BES with a precision around 4–5% for both the D and the D_s-meson decay modes [164]. When combined with lattice results for the decay constants, they allow for determinations of $|V_{cs}|$ and $|V_{cd}|$.

In lattice-QCD calculations, the decay constants $f_{D_{(s)}}$ are extracted from Euclidean matrix elements of the axial current

$$\langle 0|A_{cq}^\mu|D_q(p)\rangle = i f_{D_q}\ p_{D_q}^\mu, \tag{170}$$

with $q = d, s$ and $A_{cq}^\mu = \bar{c}\gamma_\mu\gamma_5 q$. Results for $N_f = 2,\ 2+1$ and $2+1+1$ dynamical flavours are summarized in Table 34 and Fig. 22. Since the publication of the last FLAG review, a handful of results for f_D and f_{D_s} have appeared, as described below. We consider isospin-averaged quantities, although, in a few cases, results for f_{D^+} are quoted (see, for example, the FNAL/MILC 11,14A and 17 computations, where the difference between f_D and f_{D^+} has been estimated to be around 0.5 MeV).

Only one new computation appeared for $N_f = 2$. Reference [58], Balasubramanian 19, updates the result for f_{D_s} in Blossier 18 [479] (discussed in the previous review) by including in the analysis two additional ensembles at a coarser lattice spacing ($a = 0.075$ fm, compared to 0.065 fm and 0.048 fm used in Ref. [479]). Pion masses at this coarser resolution reach 282 MeV and $M_\pi L$ is always kept larger than 4.

The $N_f = 2$ averages for f_D and f_{D_s}/f_D coincide with those in the previous FLAG review and are given by the values in ETM 13B [56], while the estimate for f_{D_s} is the result of the weighted average of the numbers in ETM 13B [56] and Balasubramanian 19 [58]. They read

$$N_f = 2: \qquad f_D = 208(7)\ \text{MeV} \qquad \text{Ref. [56]}, \tag{171}$$

$$N_f = 2: \qquad f_{D_s} = 246(4)\ \text{MeV} \qquad \text{Refs. [56,58]}, \tag{172}$$

$$N_f = 2: \qquad \frac{f_{D_s}}{f_D} = 1.20(0.02) \qquad \text{Ref. [56]}. \tag{173}$$

Table 34 Decay constants of the D and D_s mesons (in MeV) and their ratio

Collaboration	Refs.	N_f	Publication status	Continuum extrapolation	Chiral extrapolation	Finite volume	Renormalization/matching	Heavy-quark treatment	f_D	f_{D_s}	f_{D_s}/f_D
FNAL/MILC 17 $^{\nabla\nabla}$	[16]	2+1+1	A	★	★	★	★	✓	212.1(0.6)	249.9(0.5)	1.1782(16)
FNAL/MILC 14A**	[17]	2+1+1	A	★	★	★	★	✓	212.6(0.4) $(^{+1.0}_{-1.2})$	249.0(0.3)$(^{+1.1}_{-1.5})$	1.1745(10)$(^{+29}_{-32})$
ETM 14E†	[38]	2+1+1	A	★	○	○	★	✓	207.4(3.8)	247.2(4.1)	1.192(22)
ETM 13F	[306]	2+1+1	C	○	○	○	★	✓	202(8)	242(8)	1.199(25)
FNAL/MILC 13$^{\nabla}$	[480]	2+1+1	C	★	★	★	★	✓	212.3(0.3)(1.0)	248.7(0.2)(1.0)	1.1714(10)(25)
FNAL/MILC 12B	[481]	2+1+1	C	★	★	★	★	✓	209.2(3.0)(3.6)	246.4(0.5)(3.6)	1.175(16)(11)
χQCD 20A††	[482]	2+1	A	■	★	★	★	✓	213(5)	249(7)	1.16(3)
RBC/UKQCD 18A$^{\square\nabla}$	[70]	2+1	P	★	★	★	★	✓			1.1740(51)$(^{+68}_{-68})$
RBC/UKQCD 17	[55]	2+1	A	★	★	○	★	✓	208.7(2.8)$(^{+2.1}_{-1.8})$	246.4(1.3)$(^{+1.3}_{-1.9})$	1.1667(77)$(^{+57}_{-43})$
χQCD 14$^{\dagger\square}$	[24]	2+1	A	○	○	○	★	✓		254(2)(4)	
HPQCD 12A	[53]	2+1	A	○	○	○	★	✓	208.3(1.0)(3.3)	246.0(0.7)(3.5)	1.187(4)(12)
FNAL/MILC 11	[54]	2+1	A	○	○	○	○	✓	218.9(11.3)	260.1(10.8)	1.188(25)
PACS-CS 11	[483]	2+1	A	■	★	■	○	✓	226(6)(1)(5)	257(2)(1)(5)	1.14(3)
HPQCD 10A	[57]	2+1	A	★	○	★	★	✓	213(4)*	248.0(2.5)	
HPQCD/UKQCD 07	[40]	2+1	A	○	○	○	★	✓	207(4)	241 (3)	1.164(11)
FNAL/MILC 05	[484]	2+1	A	○	○	■	○	✓	201(3)(17)	249(3)(16)	1.24(1)(7)
Balasubramanian 19	[58]	2	A	★	★	★	★	✓		244(4)(2)	
Blossier 18	[479]	2	A	○	★	○	★	✓		238(5)(2)	
TWQCD 14$^{\square\square}$	[485]	2	A	■	○	■	★	✓	202.3(2.2)(2.6)	258.7(1.1)(2.9)	1.2788(264)
ALPHA 13B	[486]	2	C	○	★	○	★	✓	216(7)(5)	247(5)(5)	1.14(2)(3)
ETM 13B$^{\square}$	[56]	2	A	★	○	○	★	✓	208(7)	250(7)	1.20(2)
ETM 11A	[231]	2	A	★	○	○	★	✓	212(8)	248(6)	1.17(5)
ETM 09	[45]	2	A	○	○	○	★	✓	197(9)	244(8)	1.24(3)

†Update of ETM 13F
$^{\nabla}$Update of FNAL/MILC 12B
*This result is obtained by using the central value for f_{D_s}/f_D from HPQCD/UKQCD 07 and increasing the error to account for the effects from the change in the physical value of r_1
$^{\square}$Update of ETM 11A and ETM 09
$^{\square\square}$One lattice spacing $\simeq 0.1$ fm only. $m_{\pi,\min}L = 1.93$
**At $\beta = 5.8$, $m_{\pi,\min}L = 3.2$ but this lattice spacing is not used in the final cont./chiral extrapolations
$^{\nabla\nabla}$Update of FNAL/MILC 14A. The ratio quoted is $f_{D_s}/f_{D^+} = 1.1749(16)$. In order to compare with results from other collaborations, we rescale the number by the ratio of central values for f_{D+} and f_D. We use the same rescaling in FNAL/MILC 14A. At the finest lattice spacing the finite-volume criterium would produce an empty green circle, however, as checked by the authors, results would not significantly change by excluding this ensemble, which instead sharpens the continuum limit extrapolation
$^{\square\nabla}$Update of RBC/UKQCD 17
$^{\dagger\square}$Two values of sea pion masses
††Four valence pion masses between 208 and 114 MeV have been used at one value of the sea pion mass of 139 MeV

Turning to $N_f = 2 + 1$ results, the χQCD collaboration presented in χQCD 20A [482] a calculation of the $D_s^{(*)}$, $D^{(*)}$ and ϕ meson decay constants. The couplings of the vector mesons to the tensor current are also computed. The computation is performed at a single lattice spacing with $a^{-1} \approx 1.7$ GeV on a $2 + 1$ domain wall fermion ensemble generated by the RBC/UKQCD Collaboration. The sea pion mass is at its physical value and the spatial extension is 5.5 fm. Overlap valence fermions are used with different values of the light, strange and (quenched) charm quark masses. For the light quarks the corresponding pion masses range between 114 and 208 MeV. The setup follows very closely the one in χQCD 14 [24] (presented in the 2016 FLAG review). The decay constants f_D and f_{D_s} are obtained from an exactly conserved PCAC Ward identity so they do not depend on renormalization factors. The results, however, do not enter the FLAG average as the simulations do not meet the quality criteria concerning the number of lattice spacings used in the continuum extrapolation.

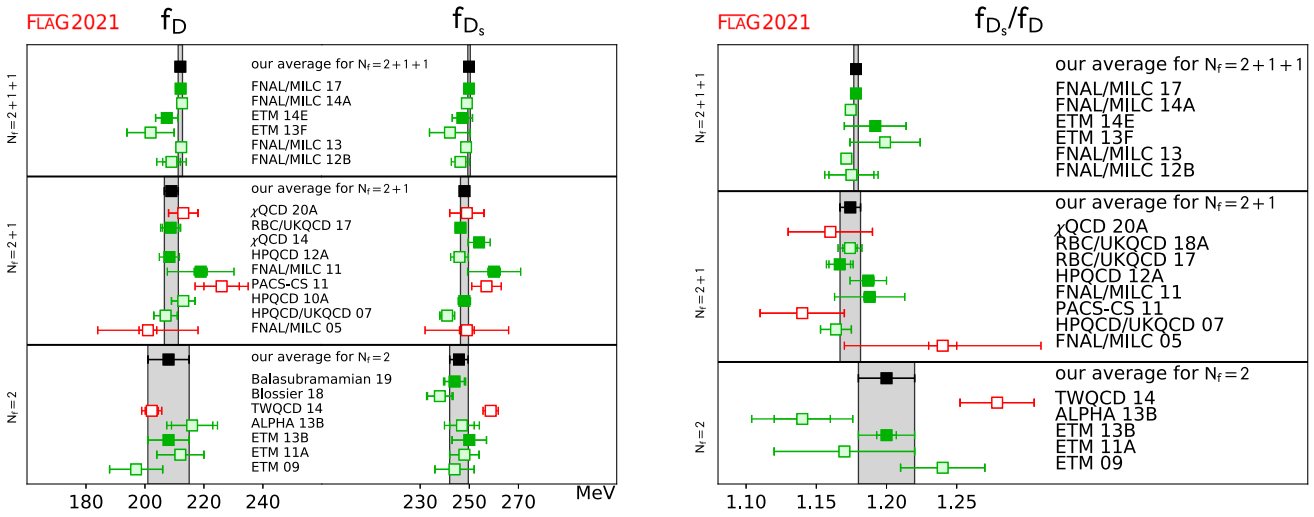

Fig. 22 Decay constants of the D and D_s mesons [values in Table 34 and Eqs. (171–179)]. As usual, full green squares are used in the averaging procedure, pale green squares have been superseded by later determinations, while pale red squares do not satisfy the criteria. The black squares and grey bands indicate our averages

A new result (RBC/UKQCD 18A) for the SU(3)-breaking ratio f_{D_s}/f_D has been reported in Ref. [70]. The setup includes $2+1$ dynamical flavors of Domain Wall fermions. This new result essentially supersedes RBC/UKQCD 17 [55] (discussed in the previous FLAG review) by implementing a number of improvements. One level of stout smearing for the gauge fields has been introduced before performing the charm-quark inversions, which has allowed them to simulate directly at the physical charm mass. At the same time, the valence the strange-quark mass has been tuned to its physical value in order to eliminate a small correction needed previously. Finally, the number of source positions has been doubled on a few ensembles. As of April 30, 2021 the article has not been published in a journal. Therefore, the result does not contribute to the FLAG estimates.

The $N_f = 2+1$ FLAG estimates remain unchanged and read

$$N_f = 2+1: \quad f_D = 209.0(2.4)\ \text{MeV} \quad \text{Refs. [53–55]}, \tag{174}$$

$$N_f = 2+1: \quad f_{D_s} = 248.0(1.6)\ \text{MeV} \quad \text{Refs. [24,54,55,57]}, \tag{175}$$

$$N_f = 2+1: \quad \frac{f_{D_s}}{f_D} = 1.174(0.007) \quad \text{Refs. [53–55]}, \tag{176}$$

where the error on the $N_f = 2+1$ average of f_{D_s} has been rescaled by the factor $\sqrt{\chi^2/\text{dof}} = 1.1$. Those come from the results in HPQCD 12A [53], FNAL/MILC 11 [54] as well as RBC/UKQCD 17 [55] concerning f_D while for f_{D_s} also the χQCD 14 [24] result contributes, and instead of the value in HPQCD 12A [53] the one in HPQCD 10A [57] is used. In addition, the statistical errors between the results of FNAL/MILC and HPQCD have been everywhere treated as 100% correlated since the two collaborations use overlapping sets of configurations. The same procedure had been used in the past reviews.

No new result appeared for $N_f = 2+1+1$ since the last FLAG review. Our estimates, therefore, coincide with those in Ref. [4], namely

$$N_f = 2+1+1: \quad f_D = 212.0(0.7)\ \text{MeV} \quad \text{Refs. [16,38]}, \tag{177}$$

$$N_f = 2+1+1: \quad f_{D_s} = 249.9(0.5)\ \text{MeV} \quad \text{Refs. [16,38]}, \tag{178}$$

$$N_f = 2+1+1: \quad \frac{f_{D_s}}{f_D} = 1.1783(0.0016) \quad \text{Refs. [16,38]}, \tag{179}$$

where the error on the average of f_D has been rescaled by the factor $\sqrt{\chi^2/\text{dof}} = 1.22$.

On a general note, an important recent theoretical development is represented by the nonperturbative calculation of the form factors F_A and F_V contributing to the radiative leptonic decays of a charged pseudoscalar meson P. As discussed in Ref. [238], those appear in the decomposition of the hadronic matrix element

$$H_W^{\alpha r}(k,\mathbf{p}) = \epsilon_\mu^r(k) \int d^4y\, e^{iky}\, \mathrm{T}\langle 0|j_W^\alpha(0) j_{em}^\mu(y)|P(\mathbf{p})\rangle, \tag{180}$$

with $\epsilon_\mu^r(k)$ the polarisation vector of the outgoing photon (with momentum k) and j_W^α and j_{em}^μ the weak and electromagnetic currents, respectively. With general kinematics four form factors together with the pseudoscalar decay constant f_P are needed; however, for $k^2 = 0$, by choosing in addition a physical basis for the polarisation such that $\epsilon_r(\mathbf{k}) \cdot k = 0$, the decay rate can be calculated once F_A, F_V, and f_P are known. A preliminary study has been presented in Ref. [487] in the theory with $2+1$ dynamical flavors. While a more complete calculation at three different lattice spacings (in the range 0.09–0.06 fm) and for $N_f = 2+1+1$ appeared in Ref. [488]. The form factors, once used in combination with the nonperturbative calculation of the corrections to $P \to \ell\bar{\nu}_\ell$ due to the exchange of a virtual photon, allow for a complete determination of the QED corrections to semileptonic decays of mesons. In Ref. [488] the form factors are defined after removing the point-like, infrared divergent contribution, in order to highlight the interesting structure dependent part. Restricting attention to on-shell photons, the behaviour of discretisation effects is studied in Ref. [488] as the photon momentum is changed and heavy quarks are considered. A prescription is also given to nonperturbatively subtract infrared divergent cutoff effects. Still, for charmed mesons discretization effects turned out to be rather large, relative to the size of the form factors, suggesting that very fine lattice spacings will be needed in the case of B mesons.

7.2 Form factors for $D \to \pi\ell\nu$ and $D \to K\ell\nu$ semileptonic decays

The SM prediction for the differential decay rate of the semileptonic processes $D \to \pi\ell\nu$ and $D \to K\ell\nu$ can be written as

$$\frac{d\Gamma(D \to P\ell\nu)}{dq^2} = \frac{G_F^2|V_{cx}|^2}{24\pi^3} \frac{(q^2-m_\ell^2)^2\sqrt{E_P^2-m_P^2}}{q^4 m_D^2} \times \left[\left(1+\frac{m_\ell^2}{2q^2}\right) m_D^2(E_P^2-m_P^2)|f_+(q^2)|^2 + \frac{3m_\ell^2}{8q^2}(m_D^2-m_P^2)^2|f_0(q^2)|^2\right] \tag{181}$$

where $x = d, s$ is the daughter light quark, $P = \pi, K$ is the daughter light-pseudoscalar meson, E_P is the light-pseudoscalar meson energy in the rest frame of the decaying D, and $q = (p_D - p_P)$ is the momentum of the outgoing lepton pair; in this section, the charged lepton ℓ will either be an electron (resp. positron) or (anti)muon. The vector and scalar form factors $f_+(q^2)$ and $f_0(q^2)$ parameterize the hadronic matrix element of the heavy-to-light quark flavour-changing vector current $V_\mu = \bar{x}\gamma_\mu c$,

$$\langle P|V_\mu|D\rangle = f_+(q^2)\left(p_{D\mu} + p_{P\mu} - \frac{m_D^2-m_P^2}{q^2}q_\mu\right) + f_0(q^2)\frac{m_D^2-m_P^2}{q^2}q_\mu, \tag{182}$$

and satisfy the kinematic constraint $f_+(0) = f_0(0)$. Because the contribution to the decay width from the scalar form factor is proportional to m_ℓ^2, within current precision standards it can be neglected for $\ell = e, \mu$, and Eq. (181) simplifies to

$$\frac{d\Gamma\,(D \to P\ell\nu)}{dq^2} = \frac{G_F^2}{24\pi^3}|\vec{p}_P|^3|V_{cx}|^2|f_+(q^2)|^2. \tag{183}$$

In models of new physics, decay rates may also receive contributions from matrix elements of other parity-even currents. In the case of the scalar density, partial vector current conservation allows one to write matrix elements of the latter in terms of f_+ and f_0, while for tensor currents $T_{\mu\nu} = \bar{x}\sigma_{\mu\nu}c$ a new form factor has to be introduced, viz.,

$$\langle P|T_{\mu\nu}|D\rangle = \frac{2}{m_D+m_P}\left[p_{P\mu}p_{D\nu} - p_{P\nu}p_{D\mu}\right] f_T(q^2). \tag{184}$$

Recall that, unlike the Noether current V_μ, the operator $T_{\mu\nu}$ requires a scale-dependent renormalization.

Lattice-QCD computations of $f_{+,0}$ allow for comparisons to experiment to ascertain whether the SM provides the correct prediction for the q^2-dependence of $d\Gamma(D \to P\ell\nu)/dq^2$; and, subsequently, to determine the CKM matrix elements $|V_{cd}|$ and $|V_{cs}|$ from Eq. (181). The inclusion of f_T allows for analyses to constrain new physics. Currently, state-of-the-art experimental results by CLEO-c [489] and BESIII [490,491] provide data for the differential rates in the whole q^2 range available, with a precision of order 2–3% for the total branching fractions in both the electron and muon final channels.

Calculations of the $D \to \pi \ell \nu$ and $D \to K \ell \nu$ form factors typically use the same light-quark and charm-quark actions as those of the leptonic decay constants f_D and f_{D_s}. Therefore, many of the same issues arise; in particular, considerations about cutoff effects coming from the large charm-quark mass, or the normalization of weak currents, apply. Additional complications arise, however, due to the necessity of covering a sizeable range of values in q^2:

- Lattice kinematics imposes restrictions on the values of the hadron momenta. Because lattice calculations are performed in a finite spatial volume, the pion or kaon three-momentum can only take discrete values in units of $2\pi/L$ when periodic boundary conditions are used. For typical box sizes in recent lattice D- and B-meson form-factor calculations, $L \sim 2.5$–3 fm; thus, the smallest nonzero momentum in most of these analyses lies in the range $|\vec{p}_P| \sim 400$–500 MeV. The largest momentum in lattice heavy-light form-factor calculations is typically restricted to $|\vec{p}_P| \leq 4\pi/L$. For $D \to \pi \ell \nu$ and $D \to K \ell \nu$, $q^2 = 0$ corresponds to $|\vec{p}_\pi| \sim 940$ MeV and $|\vec{p}_K| \sim 1$ GeV, respectively, and the full recoil-momentum region is within the range of accessible lattice momenta. This has implications for both the accuracy of the study of the q^2-dependence, and the precision of the computation, since statistical errors and cutoff effects tend to increase at larger meson momenta. As a consequence, many recent studies have incorporated the use of nonperiodic ("twisted") boundary conditions (tbc) [492,493] in the valence fields used for the computation of observables, as a means to alleviate some of these difficulties. In particular, while they will not necessarily lead to a decrease of numerical noise or cutoff effects, the use of tbc allows not only for a better momentum resolution, but also to better control the $q^2 = 0$ endpoint [59,494–498].
- Final-state pions and kaons can have energies $\gtrsim 1$ GeV, given the available kinematical range $0 \lesssim q^2 \leq q^2_{\rm max} = (m_D - m_P)^2$. This makes the use of (heavy-meson) chiral perturbation theory to extrapolate to physical light-quark masses potentially problematic.
- Accurate comparisons to experiment, including the determination of CKM parameters, requires good control of systematic uncertainties in the parameterization of the q^2-dependence of form factors. While this issue is far more important for semileptonic B decays, where existing lattice computations cover just a fraction of the kinematic range, the increase in experimental precision requires accurate work in the charm sector as well. The parameterization of semileptonic form factors is discussed in detail in Appendix B.1.

The most advanced $N_f = 2$ lattice-QCD calculation of the $D \to \pi \ell \nu$ and $D \to K \ell \nu$ form factors is by the ETM collaboration [494]. This work, which did not proceed beyond the preliminary stage, uses the twisted-mass Wilson action for both the light and charm quarks, with three lattice spacings down to $a \approx 0.068$ fm and (charged) pion masses down to $m_\pi \approx 270$ MeV. The calculation employs the method of Ref. [499] to avoid the need to renormalize the vector current, by introducing double-ratios of lattice three-point correlation functions in which the vector current renormalization cancels. Discretization errors in the double ratio are of $\mathcal{O}((am_c)^2)$, due to the automatic $\mathcal{O}(a)$ improvement at maximal twist. The vector and scalar form factors $f_+(q^2)$ and $f_0(q^2)$ are obtained by taking suitable linear combinations of these double ratios. Extrapolation to physical light-quark masses is performed using $SU(2)$ heavy-light meson χPT. The ETM collaboration simulates with twisted boundary conditions for the valence quarks to access arbitrary momentum values over the full physical q^2 range, and interpolate to $q^2 = 0$ using the Bečirević–Kaidalov ansatz [500]. The statistical errors in $f_+^{D\pi}(0)$ and $f_+^{DK}(0)$ are 9% and 7%, respectively, and lead to rather large systematic uncertainties in the fits to the light-quark mass and energy dependence (7% and 5%, respectively). Another significant source of uncertainty is from discretization errors (5% and 3%, respectively). On the finest lattice spacing used in this analysis $am_c \sim 0.17$, so $\mathcal{O}((am_c)^2)$ cutoff errors are expected to be about 5%. This can be reduced by including the existing $N_f = 2$ twisted-mass ensembles with $a \approx 0.051$ fm discussed in Ref. [87].

The first published $N_f = 2 + 1$ lattice-QCD calculation of the $D \to \pi \ell \nu$ and $D \to K \ell \nu$ form factors came from the Fermilab Lattice, MILC, and HPQCD collaborations [501].[32] This work uses asqtad-improved staggered sea quarks and light (u, d, s) valence quarks and the Fermilab action for the charm quarks, with a single lattice spacing of $a \approx 0.12$ fm, and a minimum RMS-pion mass of ≈ 510 MeV, dictated by the presence of fairly large staggered taste splittings. The vector current is normalized using a mostly nonperturbative approach, such that the perturbative truncation error is expected to be negligible compared to other systematics. Results for the form factors are provided over the full kinematic range, rather than focusing just at $q^2 = 0$ as was customary in previous work, and fitted to a Bečirević–Kaidalov ansatz. In fact, the publication of this result predated the precise measurements of the $D \to K \ell \nu$ decay width by the FOCUS [502] and Belle experiments [503], and showed good agreement with the experimental determination of the shape of $f_+^{DK}(q^2)$. Progress on extending this work

[32] Because only two of the authors of this work are members of HPQCD, and to distinguish it from other more recent works on the same topic by HPQCD, we hereafter refer to this work as "FNAL/MILC."

was reported in [504]; efforts are aimed at reducing both the statistical and systematic errors in $f_+^{D\pi}(q^2)$ and $f_+^{DK}(q^2)$ by increasing the number of configurations analyzed, simulating with lighter pions, and adding lattice spacings as fine as $a \approx 0.045$ fm.

The most precise published calculations of the $D \to \pi \ell \nu$ [60] and $D \to K \ell \nu$ [62] form factors in $N_f = 2+1$ QCD are by the HPQCD collaboration. They are also based on $N_f = 2+1$ asqtad-improved staggered MILC configurations, but use two lattice spacings $a \approx 0.09$ and 0.12 fm, and a HISQ action for the valence u, d, s, and c quarks. In these mixed-action calculations, the HISQ valence light-quark masses are tuned so that the ratio m_l/m_s is approximately the same as for the sea quarks; the minimum RMS sea-pion mass ≈ 390 MeV. Form factors are determined only at $q^2 = 0$, by using a Ward identity to relate matrix elements of vector currents to matrix elements of the absolutely normalized quantity $(m_c - m_x)\langle P|\bar{x}c|D\rangle$ (where $x = u, d, s$), and exploiting the kinematic identity $f_+(0) = f_0(0)$ to yield $f_+(q^2 = 0) = (m_c - m_x)\langle P|\bar{x}c|D\rangle/(m_D^2 - m_P^2)$. A modified z-expansion (cf. Appendix B.1) is employed to simultaneously extrapolate to the physical light-quark masses and the continuum and to interpolate to $q^2 = 0$, and allow the coefficients of the series expansion to vary with the light- and charm-quark masses. The form of the light-quark dependence is inspired by χPT, and includes logarithms of the form $m_\pi^2 \log(m_\pi^2)$ as well as polynomials in the valence-, sea-, and charm-quark masses. Polynomials in $E_{\pi(K)}$ are also included to parameterize momentum-dependent discretization errors. The number of terms is increased until the result for $f_+(0)$ stabilizes, such that the quoted fit error for $f_+(0)$ not only contains statistical uncertainties, but also reflects relevant systematics. The largest quoted uncertainties in these calculations are from statistics and charm-quark discretization errors. Progress towards extending the computation to the full q^2 range have been reported in Refs. [495,496]; however, the information contained in these conference proceedings is not enough to establish an updated value of $f_+(0)$ with respect to the previous journal publications.

The most recent $N_f = 2+1$ computation of D semileptonic form factors has been carried out by the JLQCD collaboration, and so far only published in conference proceedings; most recently in Ref. [505]. They use their own Möbius domain-wall configurations at three values of the lattice spacing $a = 0.080, 0.055, 0.044$ fm, with several pion masses ranging from 226 to 501 MeV (though there is so far only one ensemble, with $m_\pi = 284$ MeV, at the finest lattice spacing). The vector and scalar form factors are computed at four values of the momentum transfer for each ensemble. The computed form factors are observed to depend mildly on both the lattice spacing and the pion mass. The momentum dependence of the form factors is fitted to a BCL z-parameterization (see Appendix B.1) with a Blaschke factor that contains the measured value of the $D_{(s)}^*$ mass in the vector channel, and a trivial Blaschke factor in the scalar channel. The systematics of this latter fit is assessed by a BCL fit with the experimental value of the scalar resonance mass in the Blaschke factor. Continuum and chiral extrapolations are carried out through a linear fit in the squared lattice spacing and the squared pion and η_c masses. A global fit that uses hard-pion HMχPT to model the mass dependence is furthermore used for a comparison of the form factor shapes with experimental data.[33] Since the computation is only published in proceedings so far, it will not enter our $N_f = 2+1$ average.[34]

The first full computation of both the vector and scalar form factors in $N_f = 2+1+1$ QCD was achieved by the ETM collaboration [59]. Furthermore, they have provided a separate determination of the tensor form factor, relevant for new physics analyses [498]. Both works use the available $N_f = 2+1+1$ twisted-mass Wilson lattices [218], totaling three lattice spacings down to $a \approx 0.06$ fm, and a minimal pion mass of 220 MeV. Matrix elements are extracted from suitable double ratios of correlation functions that avoid the need of nontrivial current normalizations. The use of twisted boundary conditions allows both for imposing several kinematical conditions, and considering arbitrary frames that include moving initial mesons. After interpolation to the physical strange- and charm-quark masses, the results for form factors are fitted to a modified z-expansion that takes into account both the light-quark mass dependence through hard-pion $SU(2)$ χPT [507], and the lattice-spacing dependence. In the latter case, a detailed study of Lorentz-breaking effects due to the breaking of rotational invariance down to the hypercubic subgroup is performed, leading to a nontrivial momentum-dependent parameterization of cutoff effects. The z-parameterization (see Appendix B.1) itself includes a single-pole Blaschke factor (save for the scalar channel in $D \to K$, where the Blaschke factor is trivial), with pole masses treated as free parameters. The final quoted uncertainty on the form factors is about 5–6% for $D \to \pi$, and 4% for $D \to K$. The dominant source of uncertainty is quoted as statistical+fitting procedure+input parameters – the latter referring to the values of quark masses, the lattice spacing (i.e., scale setting), and the LO $SU(2)$ LECs.

[33] It is important to stress the finding in Ref. [506] that the factorization of chiral logs in hard-pion χPT breaks down, implying that it does not fulfill the expected requisites for a proper effective field theory. Its use to model the mass dependence of form factors can thus be questioned.

[34] The ensemble parameters quoted in Ref. [505] appear to show that the volumes employed at the lightest pion masses are insufficient to meet our criteria for finite-volume effects. There is, however, a typo in the table which results in a wrong assignment of lattice sizes, whereupon the criteria are indeed met. We thank T. Kaneko for correspondence on this issue.

Table 35 Summary of computations of charmed-meson semileptonic form factors. Note that HPQCD 20 (discussed in Sect. 7.4) addresses the $B_c \to B_s$ and $B_c \to B_d$ transitions – hence the absence of quoted values for $f_+^{D\pi}(0)$ and $f_+^{DK}(0)$ – while ETM 18 provides a computation of tensor form factors

Collaboration	Refs.	N_f	Publication status	Continuum extrapolation	Chiral extrapolation	Finite volume	Renormalization	Heavy-quark treatment	$f_+^{D\pi}(0)$	$f_+^{DK}(0)$
HPQCD 21A	[61]	2+1+1	P	★	★	○†	★	✓	n/a	0.7380(44)
HPQCD 20	[510]	2+1+1	A	★	○	★	★	✓	n/a	n/a
ETM 17D, 18	[59,498]	2+1+1	A	★	○	○	★	✓	0.612(35)	0.765(31)
JLQCD 17B	[505]	2+1	C	★	★	○	★	✓	$0.615(31)(^{+17}_{-16})(^{+28}_{-7})$*	$0.698(29)(18)(^{+32}_{-12})$*
HPQCD 11	[60]	2+1	A	○	○	○	★	✓	0.666(29)	
HPQCD 10B	[62]	2+1	A	○	○	○	★	✓		0.747(19)
FNAL/MILC 04	[501]	2+1	A	■	■	○	○	✓	0.64(3)(6)	0.73(3)(7)
ETM 11B	[494]	2	C	○	○	★	★	✓	0.65(6)(6)	0.76(5)(5)

*The first error is statistical, the second from the $q^2 \to 0$ extrapolation, the third from the chiral-continuum extrapolation

†The volumes used in the computation satisfy the nominal criterion for finite-volume effects. However, the impact of the topologically frozen ensemble at $a \simeq 0.044$ fm is neglected. We therefore assign a ○ rating here, as a mark of caution

Another $N_f = 2+1+1$ computation of f_+ and f_0 in the full kinematical range for the $D \to Kl\nu$ mode, performed by HPQCD, has recently been published – HPQCD 21A (Ref. [61]). This work uses MILC's HISQ ensembles at five values of the lattice spacing, and pion masses reaching to the physical point for the three coarsest values of a. Vector currents are normalized nonperturbatively by imposing that form factors satisfy Ward identities exactly at zero recoil. Results for the form factors are fitted to a modified z-expansion ansatz, with all sub-threshold poles removed by using the experimental value of the mass shifted by a factor that matches the corresponding result at finite lattice spacing. The accuracy of the description of the q^2 dependence is crosschecked by comparing to a fit based on cubic splines. Finite-volume effects are expected to be small, and chiral-perturbation-theory-based estimates for them are included in the chiral fit. However, the impact of frozen topology at the finest lattice spacing is neglected. The final uncertainty from the form factors in the determination of $|V_{cs}|$ quoted in HPQCD 21A is at the 0.5% level, and comparable to the rest of the uncertainty (due to the experimental error, as well as weak and electromagnetic corrections); in particular, the precision of the form factors is around seven times higher than that of the other existing $N_f = 2+1+1$ determination by ETMC. The work also provides an accurate prediction for the lepton flavour universality ratio between the muon and electron modes, where the uncertainty is overwhelmingly dominated by the electromagnetic corrections.

The FNAL/MILC collaboration has also reported ongoing work on extending their computation to $N_f = 2+1+1$, using MILC HISQ ensembles at four values of the lattice spacing down to $a = 0.042$ fm and pion masses down to the physical point. The latest updates on this computation, focusing on the form factors at $q^2 = 0$, but without explicit values of the latter yet, can be found in Refs. [508,509].

Table 35 contains our summary of the existing calculations of the $D \to \pi\ell\nu$ and $D \to K\ell\nu$ semileptonic form factors. Additional tables in Appendix C.5.1 provide further details on the simulation parameters and comparisons of the error estimates. Recall that only calculations without red tags that are published in a refereed journal are included in the FLAG average. We will quote no FLAG estimate for $N_f = 2$, since the results by ETM have only appeared in conference proceedings. For $N_f = 2+1$, only HPQCD 10B,11 qualify, which provides our estimate for $f_+(q^2 = 0) = f_0(q^2 = 0)$. For $N_f = 2+1+1$, we quote as the FLAG estimate for $f_+^{D\pi}(0)$ the only published result by ETM 17D, while for $f_+^{DK}(0)$ we quote the weighted average of the values published by ETM 17D and HPQCD 21A:

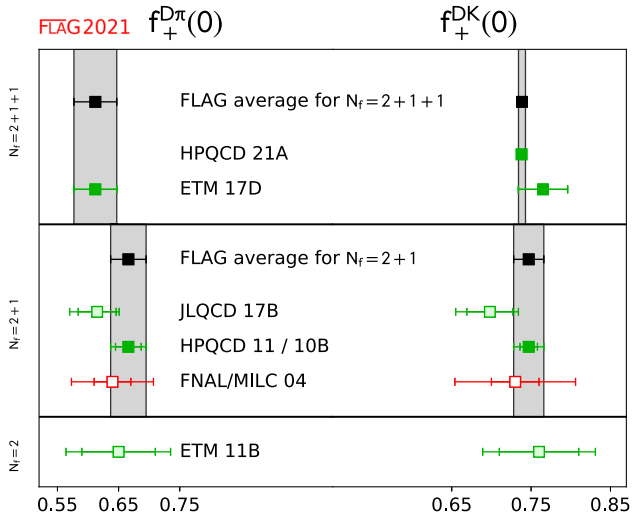

Fig. 23 $D \to \pi \ell \nu$ and $D \to K \ell \nu$ semileptonic form factors at $q^2 = 0$. The $N_f = 2 + 1$ HPQCD result for $f_+^{D\pi}(0)$ is from HPQCD 11, the one for $f_+^{DK}(0)$ represents HPQCD 10B (see Table 35)

$$N_f = 2 + 1: \quad \begin{array}{ll} f_+^{D\pi}(0) = 0.666(29) & \text{Ref. [60]}, \\ f_+^{DK}(0) = 0.747(19) & \text{Ref. [62]}, \end{array} \tag{185}$$

$$N_f = 2 + 1 + 1: \quad \begin{array}{ll} f_+^{D\pi}(0) = 0.612(35) & \text{Ref. [59]}, \\ f_+^{DK}(0) = 0.7385(44) & \text{Refs. [59,61]}. \end{array} \tag{186}$$

It is worth noting that, at the current level of precision, no significant effect of the dynamical charm quark is observed. However, given the paucity of results, it is premature to infer strong conclusions on this point.

In Fig. 23, we display the existing $N_f = 2$, $N_f = 2 + 1$, and $N_f = 2 + 1 + 1$ results for $f_+^{D\pi}(0)$ and $f_+^{DK}(0)$; the grey bands show our estimates of these quantities. Section 7.5 discusses the implications of these results for determinations of the CKM matrix elements $|V_{cd}|$ and $|V_{cs}|$ and tests of unitarity of the second row of the CKM matrix.

In the case of $N_f = 2 + 1 + 1$, we can also provide a complete result for the q^2 dependence of f_+ and f_0. In the case of the $D \to \pi \ell \nu$ channel, the latter is provided by the fit given in ETM 17D (Ref. [59]), to which we refer the reader. For $D \to K \ell \nu$, we can average the results in ETM 17D (Ref. [59]), and HPQCD 21A (Ref. [61]). To that purpose, we use the parameterizations provided in the papers to produce synthetic data for both $f_+(q^2)$ and $f_0(q^2)$ at a number of values of q^2. The large correlations involved make covariance matrices ill-behaved as the number of values of q^2 considered increases; we have settled for two q^2 values for ETM 17D and three q^2 values for HPQCD 21A, in both cases including the kinematical endpoints $q^2 = 0$ and $q^2 = (m_D - m_K)^2$ of the semileptonic interval. This choice allows us to obtain well-behaved covariance matrices. We fit the resulting dataset to a BCL ansatz (cf. Eqs. (532, 533)) for a number of combinations of the highest orders N_+ and N_0 considered for either form factor; the constraint $f_+(0) = f_0(0)$ is used to rewrite the highest-order coefficient $a^0_{N_0-1}$ in f_0 in terms of the other $N_+ + N_0 - 1$ coefficients. In both form factors, we include non-trivial Blaschke factors, with pole masses set to the experimental values of the D_s^* (for the vector channel) and D_{s0} (scalar channel) masses found in the PDG [165]. We take flavour averages of charged and neutral states for the D and K masses. Our external input is thus $m_D = 1.87265$ GeV, $m_K = 495.644$ MeV, $m_{D_s^*} = 2.1122$ GeV, and $m_{D_{s0}} = 2.317$ GeV. With this setup, we observe stable fits beyond the linear approximation in z for the form factors, although precision is rapidly lost for coefficients of terms of $\mathcal{O}(z^3)$ and higher. We quote as our preferred fit, and, therefore, FLAG average, the $N_+ = N_0 = 3$ result, quoted in full in Table 36, and illustrated in Fig. 24. As clearly shown in the figure, there is some tension between the two datasets, that grows with q^2 to reach the $\sim 2\sigma$ level. This results in a relatively poor $\chi^2/\text{d.o.f.} = 9.17/3$, which has resulted in our rescaling the errors of our average fit accordingly.

Table 36 Coefficients for the $N^+ = 3$, $N^0 = 3$ z-expansion of the $N_f = 2+1+1$ FLAG average for the $D \to K$ form factors f_+ and f_0, and their correlation matrix

$D \to K\ell\nu$ ($N_f = 2+1+1$)						
	Values	Correlation matrix				
a_0^+	0.7877(87)	1.000000	−0.498440	0.073805	0.687417	0.363513
a_1^+	−0.97(18)	−0.498440	1.000000	−0.609159	−0.063023	0.309377
a_2^+	−0.3(2.0)	0.073805	−0.609159	1.000000	0.020575	0.007175
a_0^0	0.6959(47)	0.687417	−0.063023	0.020575	1.000000	0.273019
a_1^0	0.775(69)	0.363513	0.309377	0.007175	0.273019	1.000000

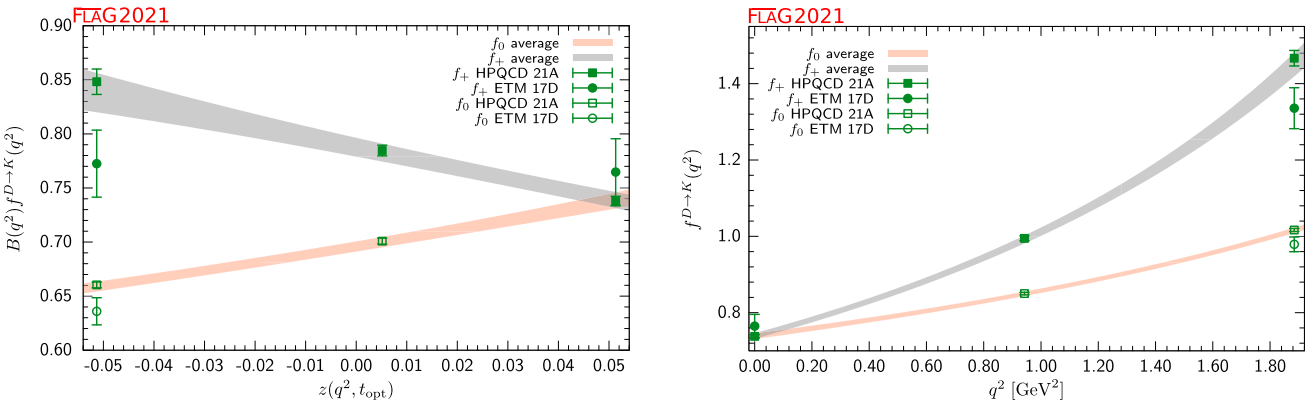

Fig. 24 The form factors $f_+(q^2)$ and $f_0(q^2)$ for $D \to K\ell\nu$ plotted versus z (left panel) and q^2 (right panel). In the left plot, we removed the Blaschke factors. See text for a discussion of the data set. The grey and salmon bands display our preferred $N^+ = N^0 = 3$ BCL fit (five parameters)

7.3 Form factors for Λ_c and Ξ_c semileptonic decays

The motivation for studying charm-baryon semileptonic decays is two-fold. First, these decays allow for independent determinations of $|V_{cs}|$. Second, given that possible new-physics contributions to the $c \to s\ell\nu$ weak effective Hamiltonian are already constrained to be much smaller compared to $b \to u\ell\bar{\nu}$ and $b \to s\ell\ell$, charm-baryon semileptonic decays allow testing the lattice techniques for baryons that are also employed for bottom-baryon semileptonic decays (see Sect. 8.6) in a better-controlled environment.

The amplitudes of the decays $\Lambda_c \to \Lambda\ell\nu$ receive contributions from both the vector and the axial components of the current in the matrix element $\langle\Lambda|\bar{s}\gamma^\mu(\mathbf{1}-\gamma_5)c|\Lambda_c\rangle$, and can be parameterized in terms of six different form factors f_+, f_0, $f_\perp$, g_+, g_0, $g_\perp$ – see, e.g., Ref. [511] for a complete description.

The computation in Meinel 16 [512] uses RBC/UKQCD $N_f = 2+1$ DWF ensembles, and treats the c quarks within the Columbia RHQ approach. Two values of the lattice spacing ($a \approx 0.11,\ 0.085$ fm) are considered, with the absolute scale set from the $\Upsilon(2S)$–$\Upsilon(1S)$ splitting. In one ensemble, the pion mass $m_\pi \approx 139$ MeV is at the physical point, while for other ensembles it ranges from 295 to 352 MeV. Results for the form factors are obtained from suitable three-point functions, and fitted to a modified z-expansion ansatz that combines the q^2-dependence with the chiral and continuum extrapolations. The paper predicts for the total rates in the e and μ channels

$$\begin{aligned} \frac{\Gamma(\Lambda_c \to \Lambda e^+ \nu_e)}{|V_{cs}|^2} &= 0.2007(71)(74)\ \text{ps}^{-1}, \\ \frac{\Gamma(\Lambda_c \to \Lambda \mu^+ \nu_\mu)}{|V_{cs}|^2} &= 0.1945(69)(72)\ \text{ps}^{-1}, \end{aligned} \tag{187}$$

where the uncertainties are statistical and systematic, respectively. In combination with the recent experimental determination of the total branching fractions by BESIII [513,514], it is possible to extract $|V_{cs}|$ as discussed in Sect. 7.5 below.

Lattice results are also available for the $\Lambda_c \to N$ form factors, where N is a neutron or proton [515]. This calculation uses the same lattice actions but a different set of ensembles with parameters matching those used in the 2015 calculation of the $\Lambda_b \to p$ form factors in Ref. [516] (cf. Sect. 8.6). Predictions are given for the rates of the $c \to d$ semileptonic

Table 37 Summary of computations of charmed-baryon semileptonic form factors

Process	Collaboration	Refs.	N_f	Publication status	Continuum extrapolation	Chiral extrapolation	Finite volume	Renormalization	Heavy-quark treatment
$\Xi_c \to \Xi \ell \nu$	Zhang 21	[517]	2+1	P	○	■	○	★	■
$\Lambda_c \to n \ell \nu$	Meinel 17	[515]	2+1	A	○	○	■	○	✓
$\Lambda_c \to \Lambda \ell \nu$	Meinel 16	[512]	2+1	A	○	★	★	○	✓

decays $\Lambda_c \to n\ell^+\nu_\ell$; these modes have not yet been observed. Reference [515] also studies the phenomenology of the flavour-changing neutral-current decay $\Lambda_c \to p\mu^+\mu^-$. As is typical for rare charm decays to charged leptons, this mode is dominated by long-distance effects that have not yet been calculated on the lattice and whose description is model-dependent.

Recently, the authors of Zhang 21 [517] also performed a first lattice calculation of the $\Xi_c \to \Xi$ form factors and extracted $|V_{cs}|$, with still large uncertainties, from the recent Belle measurement of the $\Xi_c \to \Xi \ell^+ \nu_\ell$ branching fractions [518]. This calculation uses only two ensembles with $2+1$ flavours of clover fermions, with lattice spacings of 0.108 and 0.080 fm and nearly identical pion masses of 290 and 300 MeV. The results are extrapolated to the continuum limit but are not extrapolated to the physical pion mass. No systematic uncertainty is estimated for the effect of the missing chiral extrapolation.

A summary of the lattice calculations of charm-baryon semileptonic decay form factors is given in Table 37.

7.4 Form factors for charm semileptonic decays with heavy spectator quarks

Two other decays mediated by the $c \to s\ell\nu$ and $c \to d\ell\nu$ transitions are $B_c \to B_s \ell \nu$ and $B_c \to B^0 \ell \nu$, respectively. At present, there are no experimental results for these processes, but it may be possible to produce them at LHCb in the future. The HPQCD Collaboration has recently computed the form factors for both of these B_c decay modes with $N_f = 2+1+1$ [510]. The calculation uses six different MILC ensembles with HISQ light, strange, and charm quarks, and employs the PCAC Ward identity to nonperturbatively renormalize the $c \to s$ and $c \to d$ currents. Data were generated for two different choices of lattice action for the spectator b quark: lattice NRQCD on five of the six ensembles, and HISQ on three of the six ensembles (cf. Sect. 8 for a discussion of different lattice approaches used for the b quark). For the NRQCD calculation, two of the ensembles have a physical light-quark mass, and the lattice spacings are 0.15 fm, 0.12 fm, and 0.09 fm. The heavy-HISQ calculation is performed only at $m_l/m_s = 0.2$, and at lattice spacings of 0.12 fm, 0.09 fm, and 0.06 fm. The largest value of the heavy-HISQ mass used is 0.8 in lattice units on all three ensembles, which does not reach the physical b-quark mass even at the finest lattice spacing.

Form-factor fits are performed using z-expansions (see Appendix B.1) modified to include dependence on the lattice spacing and quark masses, including an expansion in the inverse heavy quark mass in the case of the heavy-HISQ approach. The parameters t_+ are set to $(m_{B_c} + m_{B_{(s)}})^2$ even though the branch cuts start at $(m_D + m_K)^2$ or $(m_D + m_\pi)^2$, as also noted by the authors. The variable z is rescaled by a constant. The lowest charmed-meson poles are removed before the z-expansion, but this still leaves the branch cuts and higher poles below t_+. As a consequence of this structure, the good convergence properties of the z-expansion are not necessarily expected to apply. Fits are performed (i) using the NRQCD data only, (ii) using the HISQ data only, and (iii) using the NRQCD data, but with priors on the continuum-limit form-factor parameters equal to the results of the HISQ fit. The results from fits (i) and (ii) are mostly consistent, with the NRQCD fit having smaller uncertainties than the HISQ fit. Case (iii) then results in the smallest uncertainties and gives the predictions (for massless leptons)

$$\begin{aligned} \frac{\Gamma(B_c \to B_s \ell^+ \nu_\ell)}{|V_{cs}|^2} &= 1.738(55) \times 10^{-11}\ \text{MeV}, \\ \frac{\Gamma(B_c \to B^0 \ell^+ \nu_\ell)}{|V_{cd}|^2} &= 2.29(12) \times 10^{-11}\ \text{MeV}. \end{aligned} \tag{188}$$

Table 38 Determinations of $|V_{cd}|$ (upper panel) and $|V_{cs}|$ (lower panel) obtained from lattice calculations of D-meson leptonic decay constants and semileptonic form factors. The errors shown are from the lattice calculation and experiment (plus nonlattice theory), respectively, save for ETM 17D/Riggio 17, where the joint fit to lattice and experimental data does not provide a separation of the two sources of error (although the latter is largely theory dominated, like other results using $D \to \pi$ and $D \to K$ decays)

Collaboration	Refs.	N_f	From	$\|V_{cd}\|$ or $\|V_{cs}\|$
FNAL/MILC 17	[16]	2+1+1	f_D	0.2179(6)(57)
ETM 17D/Riggio 17	[59,521]	2+1+1	$D \to \pi \ell \nu$	0.2341(74)
ETM 14E	[38]	2+1+1	f_D	0.2228(41)(57)
RBC/UKQCD 17	[55]	2+1	f_D	0.2214(36)(57)
HPQCD 12A	[53]	2+1	f_D	0.2218(36)(57)
HPQCD 11	[60]	2+1	$D \to \pi \ell \nu$	0.2140(93)(29)
FNAL/MILC 11	[54]	2+1	f_D	0.2110(108)(55)
ETM 13B	[56]	2	f_D	0.2221(74)(57)
HPQCD 21A	[61]	2+1+1	$D \to K \ell \nu$	0.9750(54)(45)[†]
FNAL/MILC 17	[16]	2+1+1	f_{D_s}	0.983(2)(18)
ETM 17D/Riggio 17	[59,521]	2+1+1	$D \to K \ell \nu$	0.970(33)
ETM 17D ($q^2 = 0$)	[59]	2+1+1	$D \to K \ell \nu$	0.939(38)
ETM 14E	[38]	2+1+1	f_{D_s}	0.994(17)(19)
RBC/UKQCD 17	[55]	2+1	f_{D_s}	0.997(9)(19)
Meinel 16	[512]	2+1	$\Lambda_c \to \Lambda \ell \nu$	0.949(24)(51)
χQCD 14	[24]	2+1	f_{D_s}	0.968(17)(19)
FNAL/MILC 11	[54]	2+1	f_{D_s}	0.945(40)(19)
HPQCD 10A	[57]	2+1	f_{D_s}	0.991(10)(19)
HPQCD 10B	[62]	2+1	$D \to K \ell \nu$	0.975(25)(7)
Balasubramanian 19	[58]	2	f_{D_s}	1.007(18)(19)
ETM 13B	[56]	2	f_{D_s}	0.983(28)(19)

[†]The value quoted in HPQCD 21A is actually $|V_{cs}| = 0.9663(53)_{\text{latt}}(39)_{\text{exp}}(19)_{\eta_{EW}}(40)_{\text{EM}}$, and takes into account an electroweak correction $\eta_{EW} = 1.009(2)$ that we have eliminated to allow for a straight comparison with the other results. The three remaining errors have been combined in quadrature. Note also that the other computations in the table do not incorporate estimates of electroweak and soft electromagnetic corrections. HPQCD 21A also quotes a value for $|V_{cs}|$ obtained from the total branching fraction that results in a very small decrease in the total error due to a reduction in the estimate of electromagnetic corrections

We note that there is a discrepancy between the NRQCD and HISQ results in the case of $f_0(B_c \to B^0)$, and the uncertainty quoted for method (iii) does not cover this discrepancy. However, this form factor does not enter in the decay rate for massless leptons.

7.5 Determinations of $|V_{cd}|$ and $|V_{cs}|$ and test of second-row CKM unitarity

We now interpret the lattice-QCD results for the $D_{(s)}$ meson decays as determinations of the CKM matrix elements $|V_{cd}|$ and $|V_{cs}|$ in the Standard Model.

For the leptonic decays, we use the latest experimental averages from the Particle Data Group [165, see Sec. 71.3.1]

$$f_D|V_{cd}| = 46.2(1.2)\ \text{MeV}, \qquad f_{D_s}|V_{cs}| = 245.7(4.6)\ \text{MeV}, \tag{189}$$

where the errors include those from nonlattice theory, e.g., estimates of radiative corrections to lifetimes [519]. By combining these with the average values of f_D and f_{D_s} from the individual $N_f = 2$, $N_f = 2+1$ and $N_f = 2+1+1$ lattice-QCD calculations that satisfy the FLAG criteria, we obtain the results for the CKM matrix elements $|V_{cd}|$ and $|V_{cs}|$ in Table 38. For our preferred values we use the averaged $N_f = 2, 2+1$, and $2+1+1$ results for f_D and f_{D_s} in Eqs. (171–179). We obtain

$$\text{leptonic decays, } N_f = 2+1+1: \qquad |V_{cd}| = 0.2179(7)(57), \qquad |V_{cs}| = 0.983(2)(18), \tag{190}$$

Refs. [16,38],

leptonic decays, $N_f = 2+1$: $|V_{cd}| = 0.2211(25)(57)$, $|V_{cs}| = 0.991(7)(19)$, (191)
Refs. [24,53–55,57],

leptonic decays, $N_f = 2$: $|V_{cd}| = 0.2221(74)(57)$, $|V_{cs}| = 0.998(16)(19)$, (192)
Refs. [56,58],

where the errors shown are from the lattice calculation and experiment (plus nonlattice theory), respectively. For the $N_f = 2+1$ and the $N_f = 2+1+1$ determinations, the uncertainties from the lattice-QCD calculations of the decay constants are significantly smaller than the experimental uncertainties in the branching fractions.

The leptonic determinations of these CKM matrix elements have uncertainties that are reaching the few-percent level. However, higher-order electroweak and hadronic-structure dependent corrections to the rate have not been computed for the case of $D_{(s)}$ mesons, whereas they have been estimated to be around 1–2% for pion and kaon decays [520]. Therefore, it is important that such theoretical calculations are tackled soon, perhaps directly on the lattice, as proposed in Ref. [238].

For D meson semileptonic decays, there are still no $N_f = 2$ results, and for $N_f = 2+1$ the only works entering the FLAG averages are still HPQCD 10B/11 [60,62]. For $N_f = 2+1+1$, on the other hand, there is a new work that enters FLAG averages, HPQCD 21A (Ref. [61]). There is also a new experimental result by BESIII [522], in which the muon mode $D^0 \to K^-\mu^+\nu_\mu$ has been measured for the first time. This has two consequences. First, HFLAV has updated their averages for the combinations $f_+(0)|V_{cx}|$ [261]. They now find

$$f_+^{D\pi}(0)|V_{cd}| = 0.1426(18), \qquad f_+^{DK}(0)|V_{cs}| = 0.7180(33) \tag{193}$$

The previous HFLAV average $f_+^{DK}(0)|V_{cs}| = 0.7226(34)$ differed from the new one by 1.4 standard deviations. Second, we now determine $|V_{cs}|$ using the full q^2 dependence of the form factors provided by both HPQCD 21A and ETM 17D (Ref. [59]). Using both the new lattice and new experimental input, we perform a joint lattice+experimental fit to determine the CKM matrix elements. This reduces the error on the CKM matrix elements significantly compared with just using the form factor at $q^2 = 0$, especially for $|V_{cd}|$ (cf. Fig. 26). This was, indeed, the strategy to extract $|V_{cd}|$ and $|V_{cs}|$ pursued in a companion paper to ETM 17D, Ref. [521], as as well as in HPQCD 21A (for $|V_{cs}|$ only).[35]

The result for $|V_{cd}|$ in Ref. [521] is still state-of-the-art, and we will quote it as the FLAG estimate. In the case of $|V_{cs}|$, we have performed joint lattice+experiment fits using the same ansatz as described for the lattice average of form factors in Sect. 7.2, including $|V_{cs}|^2$ as an additional coefficient that provides the normalization of the experimental data. The experimental datasets we include are three different measurements of the $D^0 \to K^-e^+\nu_e$ mode by BaBar (BaBar 07, Ref. [523]), CLEO-c (CLEO 09/0, Ref. [489]), and BESIII (BESIII 15, Ref. [524]); CLEO-c (CLEO 09/+, Ref. [489]) and BESIII measurements of the $D^+ \to \bar{K}^0e^+\nu_e$ mode (BESIII 17, Ref. [525]); and the recent first measurement of the $D^0 \to K^-\mu^+\nu_\mu$ mode by BESIII, Ref. [522]. There is also a Belle dataset available in Ref. [526], but it provides results for parameterized form factors rather than partial widths, which implies that reverse modeling of the q^2 dependence of the form factor would be needed to add them to the fit, which involves an extra source of systematic uncertainty; it is, furthermore, the measurement with the largest error. Thus, we will drop it. The CLEO collaboration provides correlation matrices for the systematic uncertainties across the channels in their two measurements; the latter are, however, not available for BESIII, and, therefore, we will conservatively treat their systematics with a 100% correlation, following the same prescription as in the HFLAV review [261]. Since all lattice results have been obtained in the isospin limit, we will average over the D^0 and D^+ electronic modes.

We observe that the error of the final result for $|V_{cs}|$ is independent of the specific ansatz, while the central values differ by at most one standard deviation. From the lattice point of view, HPQCD 21A dominates the result completely, because of its much smaller uncertainties than in ETM 17D. The precision of the data does not allow us to consistently resolve the higher-order coefficients of the z-expansion beyond $N_+ = N_0 = 3$, at which point the result for $|V_{cs}|$ becomes insensitive to increasing the order. Thus, we quote the result from the latter fit, provided in full detail in Table 39 and illustrated in Fig. 25, as the $N_f = 2+1+1$ FLAG average. The χ^2/d.o.f. of our preferred fit is 1.46, and we have rescaled the full covariance matrix with that value to obtain conservative error estimates.

Notice that, notwithstanding the fact that HPQCD 21A dominates the fit, our final value $|V_{cs}| = 0.9714(69)$ is slightly higher than their quoted value $|V_{cs}| = 0.9663(66)$ (where for the error we have combined in quadrature their lattice and

[35] Notice that the estimate for $|V_{cs}|$ in Ref. [521] does not include the later experimental result in Ref. [522]. The value obtained in Ref. [521] is however completely dominated by the uncertainty of the lattice form factors, and changes very little once the full experimental information is incorporated into the determination.

Table 39 Coefficients for the $N^+ = N^0 = 3$ z-expansion of the $D \to K$ form factors f_+ and f_0, $|V_{cs}|$, and their correlation matrix

$D \to K\ell\nu$ ($N_f = 2+1+1$)							
	Values	Correlation matrix					
a_0^+	0.7864(54)	1	−0.282248	−0.052775	0.760032	0.631483	−0.899274
a_1^+	−0.849(68)	−0.282248	1	−0.640953	−0.088377	0.041977	0.128087
a_2^+	−1.5(1.1)	−0.052775	−0.640953	1	0.018139	0.115382	0.020790
a_0^0	0.6958(32)	0.760032	−0.088377	0.018139	1	0.300343	−0.734376
a_1^0	0.781(45)	0.631483	0.041977	0.115382	0.300343	1	−0.664113
$\|V_{cs}\|$	0.9714(69)	−0.899274	0.128087	0.020790	−0.734376	−0.664113	1

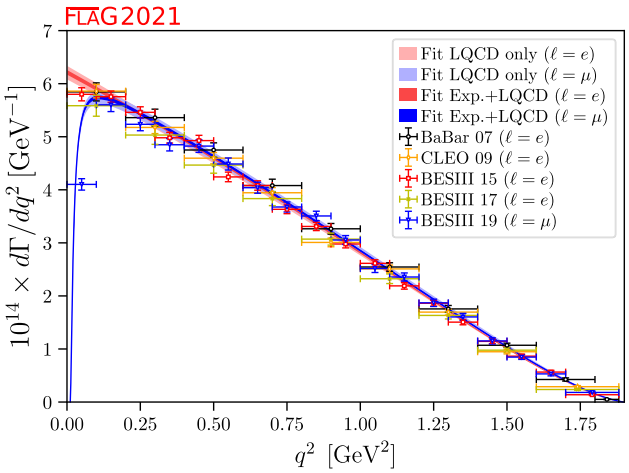

Fig. 25 The $D \to K\ell\nu$ differential decay rates

experiment error, in order to allow for a direct comparison, and dropped the estimated systematic uncertainties due to electroweak and electromagnetic corrections also provided in HPQCD 21A). This is due to the fact that HPQCD 21A has applied the structure-independent electroweak correction factor $\eta_{EW} = 1.009(2)$ in their analysis, which we are not doing for consistency with other determinations in this review; if we had applied the same procedure, our final result would be $|V_{cs}| = 0.9628(68)$.

Meinel 16 has also determined the form factors for $\Lambda_c \to \Lambda\ell\nu$ decays for $N_f = 2+1$, which results in a determination of $|V_{cs}|$ in combination with the experimental measurement of the branching fractions for the e^+ and μ^+ channels in Refs. [513,514]. In Ref. [512] the value $|V_{cs}| = 0.949(24)(14)(49)$ is quoted, where the first error comes from the lattice computation, the second from the Λ_c lifetime, and the third from the branching fraction of the decay. While the lattice uncertainty is competitive with meson channels (for $N_f = 2+1$), the experimental uncertainty is far larger.

Our estimates for $|V_{cd}|$ and $|V_{cs}|$ from semileptonic decay are

$$\text{SL averages for } N_f = 2+1: \quad \begin{array}{ll} |V_{cd}| = 0.2141(93)(29) & \text{Ref. [60]}, \\ |V_{cs}| = 0.967(25)(5) & \text{Ref. [62]}, \\ |V_{cs}|(\Lambda_c) = 0.949(24)(51) & \text{Ref. [512]}, \end{array} \tag{194}$$

$$\text{SL averages for } N_f = 2+1+1: \quad \begin{array}{ll} |V_{cd}| = 0.2341(74) & \text{Refs. [59,521]}, \\ |V_{cs}| = 0.9714(69) & \text{Refs. [59,61]}, \end{array} \tag{195}$$

where the errors for $N_f = 2+1$ are lattice and experimental (plus nonlattice theory), respectively. It has to be stressed that for meson decay errors are largely theory-dominated, save for the $D \to K$ mode for $N_f = 2+1+1$ where the lattice contribution to the error is only slightly larger than the experimental one; while in the baryon mode for $|V_{cs}|$ the dominant error is experimental. The above values are compared with individual leptonic determinations in Table 38.

Table 40 Comparison of determinations of $|V_{cd}|$ and $|V_{cs}|$ obtained from lattice methods with nonlattice determinations and the Standard Model prediction from global fits assuming CKM unitarity. Experimental and lattice errors have been combined in quadrature. The PDG figures quoted are taken from the "CKM Quark-Mixing Matrix" review

	From	Refs.	$\|V_{cd}\|$	$\|V_{cs}\|$
$N_f = 2+1+1$	f_D & f_{D_s}	[16,38]	0.2179(57)	0.983(18)
$N_f = 2+1$	f_D & f_{D_s}	[24,53–55,57]	0.2211(62)	0.991(20)
$N_f = 2$	f_D & f_{D_s}	[56,58]	0.2220(93)	0.999(25)
$N_f = 2+1+1$	$D \to \pi\ell\nu$ and $D \to K\ell\nu$	[59,61,521]	0.2341(74)	0.9714(69)
$N_f = 2+1$	$D \to \pi\ell\nu$ and $D \to K\ell\nu$	[60,62]	0.2141(97)	0.967(25)
$N_f = 2+1$	$\Lambda_c \to \Lambda\ell\nu$	[512]	n/a	0.949(56)
PDG	Neutrino scattering	[165]	0.230(11)	
PDG	CKM unitarity	[165]	0.2265(5)	0.9732(1)

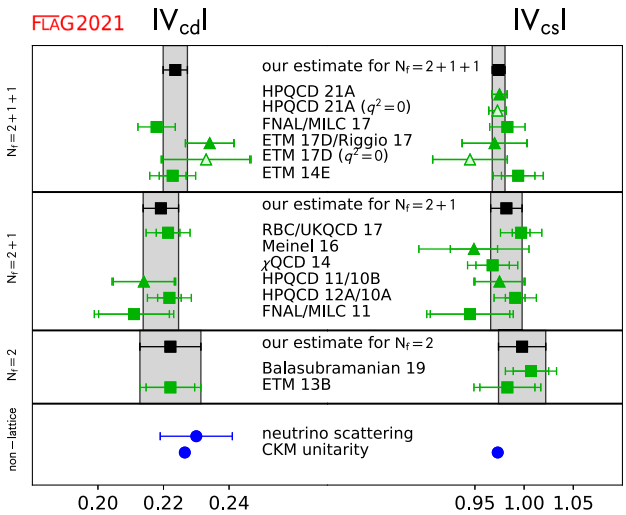

Fig. 26 Comparison of determinations of $|V_{cd}|$ and $|V_{cs}|$ obtained from lattice methods with nonlattice determinations and the Standard Model prediction based on CKM unitarity. When two references are listed on a single row, the first corresponds to the lattice input for $|V_{cd}|$ and the second to that for $|V_{cs}|$. The results denoted by squares are from leptonic decays, while those denoted by triangles are from semileptonic decays. The points indicated as $(q^2 = 0)$ do not contribute to the average, and are shown to stress the decrease in the final uncertainty obtained by considering the full q^2 dependence. Notice that the HPQCD 21A point includes estimates of the electroweak and soft electromagnetic uncertainties that we have not incorporated into our average

In Table 40, we summarize the results for $|V_{cd}|$ and $|V_{cs}|$ from leptonic and semileptonic decays, and compare them to determinations from neutrino scattering (for $|V_{cd}|$ only) and global fits assuming CKM unitarity. These results are also plotted in Fig. 26. For both $|V_{cd}|$ and $|V_{cs}|$, the errors in the direct determinations from leptonic and semileptonic decays are approximately one order of magnitude larger than the indirect determination from CKM unitarity. The direct and indirect determinations are still always compatible within at most 1.2σ, save for the leptonic determinations of $|V_{cs}|$ – that show a $\sim 2\sigma$ deviation for all values of N_f – and $|V_{cd}|$ using the $N_f = 2+1+1$ lattice result, where the difference is 1.8σ.

In order to provide final estimates, we average all the available results separately for each value of N_f. Whenever two results share ensembles, we have conservatively fully correlated their statistical uncertainties. This is a particularly sensitive issue in the average for $|V_{cs}|$, that is dominated by the FNAL/MILC 17 and HPQCD 21A results, and for which precision has been greatly improved by the latter; however, the uncertainty of the leptonic determination is completely dominated by the experimental uncertainty, and therefore the impact of the statistical correlation is all but negligible. We have also 100% correlated the errors from the heavy-quark discretization and scale setting in HPQCD's $N_f = 2+1$ results. Finally, we include a 100% correlation in the fraction of the error of $|V_{cd(s)}|$ leptonic determinations that comes from the experimental input, to avoid an artificial reduction of the experimental uncertainty in the averages. Our results thus are

$$\text{our average, } N_f = 2+1+1 \qquad |V_{cd}| = 0.2236(37), \qquad |V_{cs}| = 0.9741(65), \qquad (196)$$
$$\text{Refs. [16,38,59,61,521]},$$

$$\text{our average, } N_f = 2+1: \quad |V_{cd}| = 0.2192(54), \quad |V_{cs}| = 0.982(16), \tag{197}$$

Refs. [24,53–55,57,60,62,512] ,

$$\text{our average, } N_f = 2: \quad |V_{cd}| = 0.2221(93), \quad |V_{cs}| = 0.998(24), \tag{198}$$

Refs. [56,58],

where the errors include both theoretical and experimental uncertainties. These averages also appear in Fig. 26. The mutual consistency between the various lattice results is good except for the case of $|V_{cd}|$ with $N_f = 2+1+1$, where a $\sim 2\sigma$ tension between the leptonic and semileptonic determinations is observed. Currently, the leptonic and semileptonic determinations of V_{cd} are controlled by experimental and lattice uncertainties, respectively. The leptonic error will be reduced by Belle II and BES III. It would be valuable to have other lattice calculations of the semileptonic form factors.

Using the lattice determinations of $|V_{cd}|$ and $|V_{cs}|$ in Table 40, we can test the unitarity of the second row of the CKM matrix. We obtain

$$N_f = 2+1+1: \quad |V_{cd}|^2 + |V_{cs}|^2 + |V_{cb}|^2 - 1 = -0.001(8), \tag{199}$$

$$N_f = 2+1: \quad |V_{cd}|^2 + |V_{cs}|^2 + |V_{cb}|^2 - 1 = 0.01(3), \tag{200}$$

$$N_f = 2: \quad |V_{cd}|^2 + |V_{cs}|^2 + |V_{cb}|^2 - 1 = 0.05(6). \tag{201}$$

The much-improved precision in $|V_{cs}|$ – cf. the value 0.025(22) quoted in the latest PDG review, Ref. [165] – has thus not resulted in any tension with CKM unitarity. Note that, given the current level of precision, this result does not depend on $|V_{cb}|$, which is of $\mathcal{O}(10^{-2})$. Notice, on the other hand, that the final quoted precision of 0.7% makes the incorporation of electromagnetic corrections from first principles a necessary step for the near future, similarly to the ongoing developments in the light-meson sector.

8 Bottom hadron decays and mixings

Authors: Y. Aoki, M. Della Morte, E. Lunghi, S. Meinel, C. Monahan, C. Pena

The (semi)leptonic decay and mixing processes of $B_{(s)}$ mesons have been playing a crucial role in flavour physics. In particular, they contain important information for the investigation of the $b-d$ unitarity triangle in the Cabibbo–Kobayashi–Maskawa (CKM) matrix, and can be ideal probes of physics beyond the Standard Model. The charged-current decay channels $B^+ \to l^+ \nu_l$ and $B^0 \to \pi^- l^+ \nu_l$, where l^+ is a charged lepton with ν_l being the corresponding neutrino, are essential in extracting the CKM matrix element $|V_{ub}|$. Similarly, the B to $D^{(*)}$ semileptonic transitions can be used to determine $|V_{cb}|$. The flavour-changing neutral current (FCNC) processes, such as $B \to K^{(*)} \ell^+ \ell^-$ and $B_{d(s)} \to \ell^+ \ell^-$, occur only beyond the tree level in weak interactions and are suppressed in the Standard Model. Therefore, these processes can be sensitive to new physics, since heavy particles can contribute to the loop diagrams. They are also suitable channels for the extraction of the CKM matrix elements involving the top quark that can appear in the loop. The decays $B \to D^{(*)} \ell \nu$ and $B \to K^{(*)} \ell \ell$ can also be used to test lepton flavour universality by comparing results for $\ell = e, \mu$ and τ. In particular, anomalies have been seen in the ratios $R(D^{(*)}) = \mathcal{B}(B \to D^{(*)} \tau \nu)/\mathcal{B}(B \to D^{(*)} \ell \nu)_{\ell = e,\mu}$ and $R(K^{(*)}) = \mathcal{B}(B \to K^{(*)} \mu\mu)/\mathcal{B}(B \to K^{(*)} ee)$. In addition, the neutral $B_{d(s)}$-meson mixings are FCNC processes and are dominated by the 1-loop "box" diagrams containing the top quark and the W bosons. Thus, using the experimentally measured neutral $B^0_{d(s)}$-meson oscillation frequencies, $\Delta M_{d(s)}$, and the theoretical calculations for the relevant hadronic mixing matrix elements, one can obtain $|V_{td}|$ and $|V_{ts}|$ in the Standard Model.

At the Large Hadron Collider, decays of b quarks can also be probed with Λ_b and other bottom baryons, which can provide complementary constraints on physics beyond the Standard Model. The most important processes are the charged-current decays $\Lambda_b \to p \ell \bar{\nu}$ and $\Lambda_b \to \Lambda_c \ell \bar{\nu}$, and the neutral-current decay $\Lambda_b \to \Lambda \ell^+ \ell^-$.

Accommodating the light quarks and the b quark simultaneously in lattice-QCD computations is a challenging endeavour. To incorporate the pion and the b hadrons with their physical masses, the simulations have to be performed using the lattice size $\hat{L} = L/a \sim \mathcal{O}(10^2)$, where a is the lattice spacing and L is the physical (dimensionful) box size. The most ambitious calculations are now using such volumes; however, many ensembles are smaller. Therefore, in addition to employing Chiral Perturbation Theory for the extrapolations in the light-quark mass, current lattice calculations for quantities involving b hadrons often make use of effective theories that allow one to expand in inverse powers of m_b. In this regard, two general

approaches are widely adopted. On the one hand, effective field theories such as Heavy-Quark Effective Theory (HQET) and Nonrelativistic QCD (NRQCD) can be directly implemented in numerical computations. On the other hand, a relativistic quark action can be improved *à la* Symanzik to suppress cutoff errors, and then re-interpreted in a manner that is suitable for heavy-quark physics calculations. This latter strategy is often referred to as the method of the Relativistic Heavy-Quark Action (RHQA). The utilization of such effective theories inevitably introduces systematic uncertainties that are not present in light-quark calculations. These uncertainties can arise from the truncation of the expansion in constructing the effective theories (as in HQET and NRQCD), or from more intricate cutoff effects (as in NRQCD and RHQA). They can also be introduced through more complicated renormalization procedures which often lead to significant systematic effects in matching the lattice operators to their continuum counterparts. For instance, due to the use of different actions for the heavy and the light quarks, it is more difficult to construct absolutely normalized bottom-light currents.

Complementary to the above "effective theory approaches", another popular method is to simulate the heavy and the light quarks using the same (normally improved) lattice action at several values of the heavy-quark mass m_h with $am_h < 1$ and $m_h < m_b$. This enables one to employ HQET-inspired relations to extrapolate the computed quantities to the physical b mass. When combined with results obtained in the static heavy-quark limit, this approach can be rendered into an interpolation, instead of extrapolation, in m_h. The discretization errors are the main source of the systematic effects in this method, and very small lattice spacings are needed to keep such errors under control.

In recent years, it has also been possible to perform lattice simulations at very fine lattice spacings and treat heavy quarks as fully relativistic fermions without resorting to effective field theories. Such simulations are, of course, very demanding in computing resources.

Because of the challenge described above, the efforts that have been made to obtain reliable, accurate lattice-QCD results for physics of the b quark have been enormous. These efforts include significant theoretical progress in formulating QCD with heavy quarks on the lattice. This aspect is briefly reviewed in Appendix A.1.3 of FLAG 19 [4].

In this section, we summarize the results of the B-meson leptonic decay constants, the neutral B-mixing parameters, and the semileptonic form factors of B mesons and Λ_b baryons, from lattice QCD. To focus on the calculations that have strong phenomenological impact, we limit the review to results based on modern simulations containing dynamical fermions with reasonably light pion masses (below approximately 500 MeV).

Following our review of $B_{(s)}$-meson leptonic decay constants, the neutral B-meson mixing parameters, and semileptonic form factors, we then interpret our results within the context of the Standard Model. We combine our best-determined values of the hadronic matrix elements with the most recent experimentally-measured branching fractions to obtain $|V_{ub}|$ and $|V_{cb}|$, and compare these results to those obtained from inclusive semileptonic B decays.

8.1 Leptonic decay constants f_B and f_{B_s}

The B- and B_s-meson decay constants are crucial inputs for extracting information from leptonic B decays. Charged B mesons can decay to a lepton-neutrino final state through the charged-current weak interaction. On the other hand, neutral $B_{d(s)}$ mesons can decay to a charged-lepton pair via a flavour-changing neutral current (FCNC) process.

In the Standard Model, the decay rate for $B^+ \to \ell^+\nu_\ell$ is described by a formula identical to Eq. (169), with $D_{(s)}$ replaced by B, and the relevant CKM matrix element V_{cq} replaced by V_{ub},

$$\Gamma(B \to \ell\nu_\ell) = \frac{m_B}{8\pi} G_F^2 f_B^2 |V_{ub}|^2 m_\ell^2 \left(1 - \frac{m_\ell^2}{m_B^2}\right)^2 . \tag{202}$$

The only two-body charged-current B-meson decay that has been observed so far is $B^+ \to \tau^+\nu_\tau$, which has been measured by the Belle and Babar collaborations [527,528]. Both collaborations have reported results with errors around 20%. These measurements can be used to determine $|V_{ub}|$ when combined with lattice-QCD predictions of the corresponding decay constant.

Neutral $B_{d(s)}$-meson decays to a charged-lepton pair $B_{d(s)} \to l^+l^-$ is a FCNC process, and can only occur at one loop in the Standard Model. Hence these processes are expected to be rare, and are sensitive to physics beyond the Standard Model. The corresponding expression for the branching fraction has the form

$$B(B_q \to \ell^+\ell^-) = \tau_{B_q} \frac{G_F^2}{\pi} Y \left(\frac{\alpha}{4\pi \sin^2\Theta_W}\right)^2 m_{B_q} f_{B_q}^2 |V_{tb}^* V_{tq}|^2 m_\ell^2 \sqrt{1 - 4\frac{m_\ell^2}{m_B^2}}, \tag{203}$$

where the light quark $q = s$ or d, and the function Y includes NLO QCD and electro-weak corrections [417,529]. Evidence for the $B_s \to \mu^+\mu^-$ decay was first observed by the CMS and the LHCb collaborations, and a combined analysis was presented in 2014 in Ref. [530]. In 2020, the ATLAS, CMS and LHCb collaborations reported their measurements from a preliminary combined analysis as [531]

$$\begin{aligned} B(B_d \to \mu^+\mu^-) &< (1.9) \times 10^{-10} \text{ at } 95\% \text{ CL}, \\ B(B_s \to \mu^+\mu^-) &= (2.69^{+0.37}_{-0.35}) \times 10^{-9}, \end{aligned} \tag{204}$$

which are compatible with the Standard Model predictions within approximately 2 standard deviations [532]. We note that the errors of these results are currently too large to enable a precise determination of $|V_{td}|$ and $|V_{ts}|$.

The decay constants f_{B_q} (with $q = u, d, s$) parameterize the matrix elements of the corresponding axial-vector currents $A^\mu_{bq} = \bar{b}\gamma^\mu\gamma^5 q$ analogously to the definition of f_{D_q} in Sect. 7.1:

$$\langle 0|A^\mu|B_q(p)\rangle = ip^\mu_B f_{B_q}. \tag{205}$$

For heavy-light mesons, it is convenient to define and analyse the quantity

$$\Phi_{B_q} \equiv f_{B_q}\sqrt{m_{B_q}}, \tag{206}$$

which approaches a constant (up to logarithmic corrections) in the $m_B \to \infty$ limit, because of heavy-quark symmetry. In the following discussion, we denote lattice data for Φ, and the corresponding decay constant f, obtained at a heavy-quark mass m_h and light valence-quark mass m_ℓ as $\Phi_{h\ell}$ and f_{hl}, to differentiate them from the corresponding quantities at the physical b- and light-quark masses.

The $SU(3)$-breaking ratio f_{B_s}/f_B is of phenomenological interest, because many systematic effects can be partially reduced in lattice-QCD calculations of this ratio. The discretization errors, heavy-quark mass tuning effects, and renormalization/matching errors may all be partially reduced. This $SU(3)$-breaking ratio is, however, still sensitive to the chiral extrapolation. Provided the chiral extrapolation is under control, one can then adopt f_{B_s}/f_B as an input in extracting phenomenologically-interesting quantities. In addition, it often happens to be easier to obtain lattice results for f_{B_s} with smaller errors than direct calculations of f_B. Therefore, one can combine the B_s-meson decay constant with the $SU(3)$-breaking ratio to calculate f_B. Such a strategy can lead to better precision in the computation of the B-meson decay constant, and has been adopted by the ETM [30,56] and the HPQCD collaborations [66]. An alternative strategy, used in Ref. [58], is to obtain the B_s-meson decay constant by combining the D_s-meson decay constant with the ratio f_{B_s}/f_{D_s}.

It is clear that the decay constants for charged and neutral B mesons play different roles in flavour-physics phenomenology. Knowledge of the B^+-meson decay constant f_{B^+} is essential for extracting $|V_{ub}|$ from leptonic B^+ decays. The neutral B-meson decay constants f_{B^0} and f_{B_s} are inputs to searches for new physics in rare leptonic B^0 decays. In view of this, it is desirable to include isospin-breaking effects in lattice computations for these quantities, and have results for f_{B^+} and f_{B^0}. With the increasing precision of recent lattice calculations, isospin splittings for B-meson decay constants can be significant, and will play an important role in the foreseeable future. A few collaborations have reported f_{B^+} and f_{B^0} separately by taking into account strong isospin effects in the valence sector, and estimated the corrections from electromagnetism. The $N_f = 2+1+1$ strong isospin-breaking effect was computed in HPQCD 13 [63] (see Table 41 in this subsection). However, since only unitary points (with equal sea- and valence-quark masses) were considered in HPQCD 13 [63], this procedure only correctly accounts for the effect from the valence-quark masses, while introducing a spurious sea-quark contribution. The decay constants f_{B^+} and f_{B^0} are also separately reported in FNAL/MILC 17 [16] by taking into account the strong-isospin effect. The new FNAL/MILC results were obtained by keeping the averaged light sea-quark mass fixed when varying the quark masses in their analysis procedure. Their finding indicates that the strong isospin-breaking effects, $f_{B^+} - f_B \sim 0.5$ MeV, could be smaller than those suggested by previous computations. One would have to take into account QED effects in the B-meson leptonic decay rates to properly use these results for extracting phenomenologically relevant information.[36] Currently, errors on the experimental measurements on these decay rates are still very large. In this review, we will therefore concentrate on the isospin-averaged result f_B and the B_s-meson decay constant, as well as the $SU(3)$-breaking ratio f_{B_s}/f_B.

The status of lattice-QCD computations for B-meson decay constants and the $SU(3)$-breaking ratio, using gauge-field ensembles with light dynamical fermions, is summarized in Tables 41 and 42, while Figs. 27 and 28 contain the graphical

[36] See Ref. [238] for a strategy that has been proposed to account for QED effects.

Table 41 Decay constants of the B, B^+, B^0 and B_s mesons (in MeV). Here f_B stands for the mean value of f_{B^+} and f_{B^0}, extrapolated (or interpolated) in the mass of the light valence-quark to the physical value of m_{ud}

Collaboration	Refs.	N_f	Publication status	Continuum extrapolation	Chiral extrapolation	Finite volume	Renormalization/matching	Heavy-quark treatment	f_{B^+}	f_{B^0}	f_B	f_{B_s}
FNAL/MILC 17	[16]	2+1+1	A	★	★	★	★	✓	189.4(1.4)	190.5(1.3)	189.9(1.4)	230.7(1.2)
HPQCD 17A	[64]	2+1+1	A	○	★	★	○	✓	–	–	196(6)	236(7)
ETM 16B	[30]	2+1+1	A	★	○	○	○	✓	–	–	193(6)	229(5)
ETM 13E	[533]	2+1+1	C	★	○	○	○	✓	–	–	196(9)	235(9)
HPQCD 13	[63]	2+1+1	A	○	★	★	○	✓	184(4)	188(4)	186(4)	224(5)
RBC/UKQCD 14	[68]	2+1	A	○	○	○	○	✓	195.6(14.9)	199.5(12.6)	–	235.4(12.2)
RBC/UKQCD 14A	[67]	2+1	A	○	○	○	○	✓	–	–	219(31)	264(37)
RBC/UKQCD 13A	[534]	2+1	C	○	○	○	○	✓	–	–	$191(6)^{\diamond}_{\text{stat}}$	$233(5)^{\diamond}_{\text{stat}}$
HPQCD 12	[66]	2+1	A	○	○	○	○	✓	–	–	191(9)	228(10)
HPQCD 12	[66]	2+1	A	○	○	○	○	✓	–	–	$189(4)^{\triangle}$	–
HPQCD 11A	[65]	2+1	A	★	○	★	★	✓	–	–	–	$225(4)^{\nabla}$
FNAL/MILC 11	[54]	2+1	A	○	○	★	○	✓	197(9)	–	–	242(10)
HPQCD 09	[72]	2+1	A	○	○	○	○	✓	–	–	$190(13)^{\bullet}$	$231(15)^{\bullet}$
Balasubramamian 19†	[58]	2	A	★	★	★	○	✓	–	–	–	$215(10)(2)(^{+2}_{-5})$
ALPHA 14	[69]	2	A	★	★	★	★	✓	–	–	186(13)	224(14)
ALPHA 13	[535]	2	C	★	★	★	★	✓	–	–	187(12)(2)	224(13)
ETM 13B, 13C‡	[56,536]	2	A	★	○	★	○	✓	–	–	189(8)	228(8)
ALPHA 12A	[537]	2	C	★	★	★	★	✓	–	–	193(9)(4)	219(12)
ETM 12B	[538]	2	C	★	○	★	○	✓	–	–	197(10)	234(6)
ALPHA 11	[539]	2	C	★	○	★	★	✓	–	–	174(11)(2)	–
ETM 11A	[231]	2	A	★	○	★	○	✓	–	–	195(12)	232(10)
ETM 09D	[540]	2	A	★	○	○	○	✓	–	–	194(16)	235(12)

$^{\diamond}$Statistical errors only
$^{\triangle}$Obtained by combining f_{B_s} from HPQCD 11A with f_{B_s}/f_B calculated in this work
$^{\nabla}$This result uses one ensemble per lattice spacing with light to strange sea-quark mass ratio $m_\ell/m_s \approx 0.2$
$^{\bullet}$This result uses an old determination of $r_1 = 0.321(5)$ fm from Ref. [118] that has since been superseded
‡Obtained by combining f_{D_s}, updated in this work, with f_{B_s}/f_{D_s}, calculated in this work
‡Update of ETM 11A and 12B

presentation of the collected results and our averages. Most results in these tables and plots have been reviewed in detail in FLAG 19 [4]. Here, we only describe the new results published after January 2019.

One new $N_f = 2$ calculation of f_{B_s} has appeared after the publication of the previous FLAG review [4]. In Table 41, this result is labelled Balasubramamian 19 [58].

In Balasubramamian 19 [58], simulations at three values of the lattice spacing, $a = 0.0751$, 0.0653 and 0.0483 fm were performed with nonperturbatively $\mathcal{O}(a)$-improved Wilson-clover fermions and the Wilson plaquette gauge action. The pion masses in this work range from 194 to 439 MeV, and the lattice sizes are between 2.09 and 4.18 fm. A key feature of this calculation is the use of a variant of the ratio method [540], applied for the first time to Wilson-clover fermions. This variant is required because, in contrast to twisted-mass Wilson fermions, there is no simple relationship between the heavy quark pole mass and the bare quark mass. In the application of this approach to the B_s-decay constant, one first computes the quantity $\mathcal{F}_{hq} \equiv f_{hq}/M_{hq}$, where f_{hq} and M_{hq} are the decay constant and mass of the pseudoscalar meson composed of valence (relativistic) heavy quark h and light (or strange) quark q. The matching between the lattice and the continuum heavy-light currents for extracting the above f_{hq} is straightforward because the valence heavy quark is also described by

Table 42 Ratios of decay constants of the B and B_s mesons (for details see Table 41)

Collaboration	Refs.	N_f	Publication status	Continuum extrapolation	Chiral extrapolation	Finite volume	Renormalization/matching	Heavy-quark treatment	f_{B_s}/f_{B^+}	f_{B_s}/f_{B^0}	f_{B_s}/f_B
FNAL/MILC 17	[16]	2+1+1	A	★	★	★	★	✓	1.2180(49)	1.2109(41)	–
HPQCD 17A	[64]	2+1+1	A	○	★	★	○	✓	–	–	1.207(7)
ETM 16B	[30]	2+1+1	A	★	○	○	○	✓	–	–	1.184(25)
ETM 13E	[533]	2+1+1	C	★	○	○	○	✓	–	–	1.201(25)
HPQCD 13	[63]	2+1+1	A	○	★	★	○	✓	1.217(8)	1.194(7)	1.205(7)
RBC/UKQCD 18A	[70]	2+1	P	★	★	★	★	✓	–	–	$1.1949(60)(^{+95}_{-175})$
RBC/UKQCD 14	[68]	2+1	A	○	○	○	○	✓	1.223(71)	1.197(50)	–
RBC/UKQCD 14A	[67]	2+1	A	○	○	○	○	✓	–	–	1.193(48)
RBC/UKQCD 13A	[534]	2+1	C	○	○	○	○	✓	–	–	$1.20(2)^{\diamond}_{\text{stat}}$
HPQCD 12	[66]	2+1	A	○	○	○	○	✓	–	–	1.188(18)
FNAL/MILC 11	[54]	2+1	A	○	○	★	○	✓	1.229(26)	–	–
RBC/UKQCD 10C	[541]	2+1	A	■	■	■	○	✓	–	–	1.15(12)
HPQCD 09	[72]	2+1	A	○	○	○	○	✓	–	–	1.226(26)
ALPHA 14	[69]	2	A	★	★	★	★	✓	–	–	1.203(65)
ALPHA 13	[535]	2	C	★	★	★	★	✓	–	–	1.195(61)(20)
ETM 13B, 13C†	[56,536]	2	A	★	○	★	○	✓	–	–	1.206(24)
ALPHA 12A	[537]	2	C	★	★	★	★	✓	–	–	1.13(6)
ETM 12B	[538]	2	C	★	○	★	○	✓	–	–	1.19(5)
ETM 11A	[231]	2	A	○	○	★	○	✓	–	–	1.19(5)

$^{\diamond}$Statistical errors only
†Update of ETM 11A and 12B

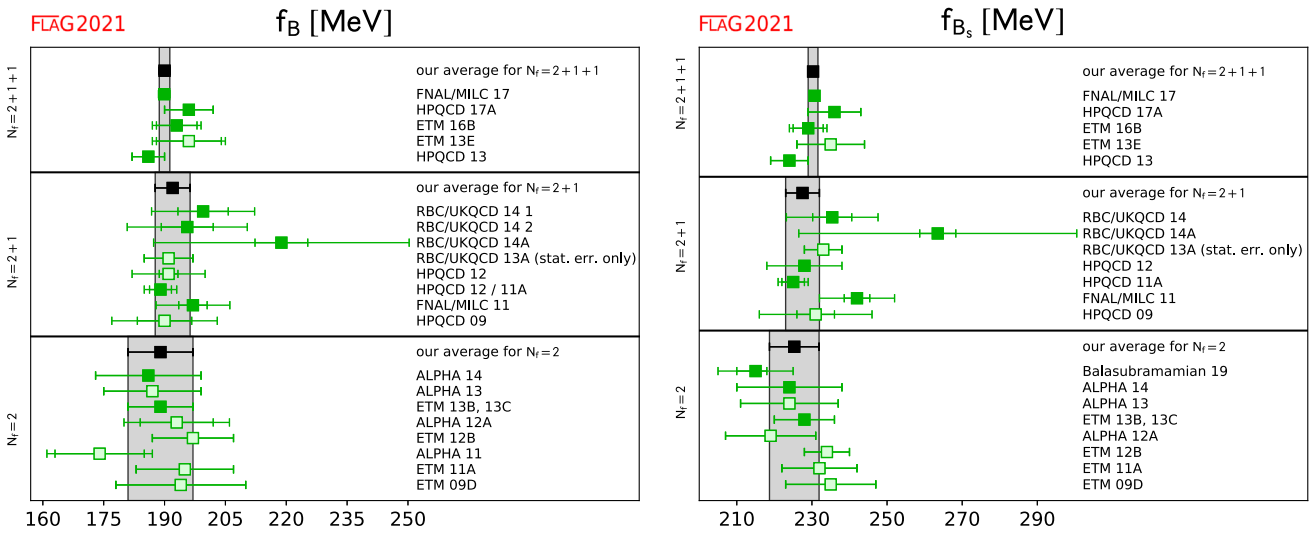

Fig. 27 Decay constants of the B and B_s mesons. The values are taken from Table 41 (the f_B entry for FNAL/MILC 11 represents f_{B^+}). The significance of the colours is explained in Sect. 2. The black squares and grey bands indicate our averages in Eqs. (207), (210), (213), (208), (211) and (214)

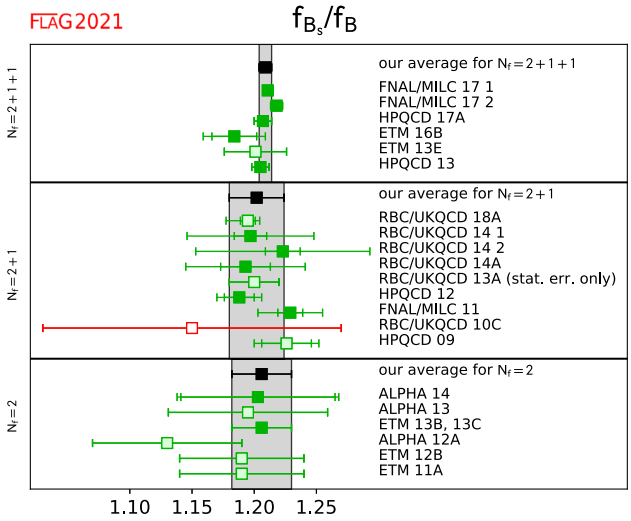

Fig. 28 Ratio of the decay constants of the B and B_s mesons. The values are taken from Table 42. Results labelled as FNAL/MILC 17 1 and FNAL/MILC 17 2 correspond to those for f_{B_s}/f_{B^0} and f_{B_s}/f_{B^+} reported in FNAL/MILC 17. The significance of the colours is explained in Sect. 2. The black squares and grey bands indicate our averages in Eqs. (209), (212), and (215)

Wilson-clover fermions. In the second step, the ratio $z_q(M_{hq}, \lambda) \equiv [\mathcal{F}_{hq} C_A^{\rm stat}(M_{h'q}) M_{hq}^{3/2}]/[\mathcal{F}_{h'q} C_A^{\rm stat}(M_{hq}) M_{h'q}^{3/2}]$ is calculated, where $C_A^{\rm stat}(M_{hq})$ is the matching coefficient for the (hq)-meson decay constant in QCD and its counterpart in HQET, and $M_{hq} = \lambda M_{h'q}$. The authors of Balasubramamian 19 [58] use the NNLO perturbative result of $C_A^{\rm stat}(M_{hq})$ [542–544] and $\lambda = 1.18$. By starting from a "triggering" point with the heavy-meson mass around that of the D_s meson, one can proceed with the calculations in steps, such that M_{hq} is increased by a factor of λ at each step. The authors simulate up to heavy-quark mass around 4.5 GeV, but observed significant $(aM_{H_s})^2$ cutoff effects on ensembles with lattice spacings $a = 0.0751$ and 0.0653 fm and so simulate up to 3.2 GeV on these lattices. In this formulation of the ratio method, the ratio obeys $z_q(M_{hq}, \lambda) \to 1/\sqrt{\lambda}$ in the limit $M_{hq} \to \infty$. Designing the computations in such a way that in the last step M_{hq} is equal to the physical B_s mass, one obtains $f_{B_{(s)}}/f_{D_{(s)}}$. Combining this ratio with results for $f_{D_{(s)}}$, updated with a third lattice spacing, the decay constant of the B_s meson can be extracted. The authors estimated the systematic uncertainty associated with their generic fit form, which combines chiral-continuum extrapolation with heavy quark discretization effects, and quote a single systematic uncertainty. The systematic uncertainty associated with scale-setting is estimated from f_{D_s}.

There have been no new $N_f = 2$ calculations of f_B or f_{B_s}/f_B. Therefore, our averages for these two cases stay the same as those in Ref. [4]. We update our average of f_{B_s} to include the new calculation of Balasubramamian 19 [58]:

$$N_f = 2: \quad f_B = 188(7)\ \text{MeV} \quad \text{Refs. [56,69]}, \tag{207}$$

$$N_f = 2: \quad f_{B_s} = 225.3(6.6)\ \text{MeV} \quad \text{Refs. [56,58,69]}, \tag{208}$$

$$N_f = 2: \quad \frac{f_{B_s}}{f_B} = 1.206(0.023) \quad \text{Refs. [56,69]}. \tag{209}$$

One new $N_f = 2 + 1$ calculation of f_{B_s}/f_B was completed after the publication of the previous FLAG review [4]. In Table 42, this result is labelled RBC/UKQCD 18A [70].

The RBC/UKQCD collaboration presented in RBC/UKQCD 18A [70] the ratio of decay constants, f_{B_s}/f_B, using $N_f = 2 + 1$ dynamical ensembles generated using Domain Wall Fermions (DWF). Three lattice spacings, of $a = 0.114$, 0.0835 and 0.0727 fm, were used, with pion masses ranging from 139 to 431 MeV, and lattice sizes between 2.65 and 5.47 fm. Two different Domain Wall discretizations (Möbius and Shamir) have been used for both valence and sea quarks. These discretizations correspond to two different choices for the DWF kernel. The Möbius DWF are loosely equivalent to Shamir DWF at twice the extension in the fifth dimension [8]. The bare parameters for these discretizations were chosen to lie on the same scaling trajectory, to enable a combined continuum extrapolation. Heavy quark masses between the charm and approximately half the bottom quark mass were used, with a linear extrapolation in $1/m_H$ applied to reach the physical B_s mass, where m_H is the mass of the heavy meson used to set the heavy quark mass. For the central fit, the

authors set the heavy quark mass through the pseudoscalar heavy-strange meson H_s, and estimate systematic uncertainties by comparing these results to those obtained with H a heavy-light meson or a heavy-heavy meson. For the quenched heavy quark Möbius DWF are always used, with a domain-wall height slightly different from the one adopted for light valence quarks. The choice helps to keep cutoff effects under control, according to the study in Ref. [545]. The chiral-continuum extrapolations are performed with a Taylor expansion in a^2 and $m_\pi^2 - (m_\pi^{\rm phys})^2$ and the associated systematic error is estimated by varying the fit function to apply cuts in the pion mass. The corresponding systematic error is estimated as approximately 0.5%, which is roughly equal to the statistical uncertainty and to the systematic uncertainties associated with extrapolation to the physical m_{B_s} mass and with higher-order corrections to the static limit. These latter corrections take the form $\mathcal{O}(\Lambda^2/m_{B_s}^2)$. The error estimate comes from assuming the coefficient of such terms is up to five times larger than the fitted $\mathcal{O}(\Lambda/m_{B_s})$ coefficient. Isospin corrections and heavy-quark discretization effects are estimated to be less than 0.1%.

At time of writing, RBC/UKQCD 18A [70] has not been published and therefore is not included in our average. Thus, our averages for these quantities remain the same as in Ref. [4],

$$N_f = 2+1: \qquad f_B = 192.0(4.3)\ \text{MeV} \qquad \text{Refs. [54,65–68]}, \tag{210}$$

$$N_f = 2+1: \qquad f_{B_s} = 228.4(3.7)\ \text{MeV} \qquad \text{Refs. [54,65–68]}, \tag{211}$$

$$N_f = 2+1: \qquad \frac{f_{B_s}}{f_B} = 1.201(0.016) \qquad \text{Refs. [54,66–68,70]}. \tag{212}$$

No new $N_f = 2+1+1$ calculations of f_B, f_{B_s}/f_B or $f_{B_{(s)}}$ have appeared since the last FLAG review. Therefore, our averages for these quantities remain the same as in Ref. [4],

$$N_f = 2+1+1: \qquad f_B = 190.0(1.3)\ \text{MeV} \qquad \text{Refs. [16,30,63,64]}, \tag{213}$$

$$N_f = 2+1+1: \qquad f_{B_s} = 230.3(1.3)\ \text{MeV} \qquad \text{Refs. [16,30,63,64]}, \tag{214}$$

$$N_f = 2+1+1: \qquad \frac{f_{B_s}}{f_B} = 1.209(0.005) \qquad \text{Refs. [16,30,63,64]}. \tag{215}$$

The PDG presented averages for the $N_f = 2+1$ and $N_f = 2+1+1$ lattice-QCD determinations of the isospin-averaged f_B, f_{B_s} and f_{B_s}/f_B in 2020 [165]. The $N_f = 2+1$ and $N_f = 2+1+1$ lattice-computation results used in Ref. [165] are identical to those included in our current work, and the averages quoted in Ref. [165] are those determined in [4].

8.2 Neutral B-meson mixing matrix elements

Neutral B-meson mixing is induced in the Standard Model through 1-loop box diagrams to lowest order in the electroweak theory, similar to those for short-distance effects in neutral kaon mixing. The effective Hamiltonian is given by

$$\mathcal{H}_{\rm eff}^{\Delta B=2,\rm SM} = \frac{G_F^2 M_{\rm W}^2}{16\pi^2}(\mathcal{F}_d^0 \mathcal{Q}_1^d + \mathcal{F}_s^0 \mathcal{Q}_1^s) + \text{h.c.}, \tag{216}$$

with

$$\mathcal{Q}_1^q = \left[\bar{b}\gamma_\mu(1-\gamma_5)q\right]\left[\bar{b}\gamma_\mu(1-\gamma_5)q\right], \tag{217}$$

where $q = d$ or s. The short-distance function $\mathcal{F}_q^0$ in Eq. (216) is much simpler compared to the kaon mixing case due to the hierarchy in the CKM matrix elements. Here, only one term is relevant,

$$\mathcal{F}_q^0 = \lambda_{tq}^2 S_0(x_t) \tag{218}$$

where

$$\lambda_{tq} = V_{tq}^* V_{tb}, \tag{219}$$

and where $S_0(x_t)$ is an Inami–Lim function with $x_t = m_t^2/M_W^2$, which describes the basic electroweak loop contributions without QCD [417]. The transition amplitude for B_q^0 with $q = d$ or s can be written as

$$\begin{aligned}\langle \bar{B}_q^0 | \mathcal{H}_{\text{eff}}^{\Delta B=2} | B_q^0 \rangle = \frac{G_F^2 M_W^2}{16\pi^2} \left[\lambda_{tq}^2 S_0(x_t) \eta_{2B} \right] \\ \times \left(\frac{\bar{g}(\mu)^2}{4\pi} \right)^{-\gamma_0/(2\beta_0)} \exp\left\{ \int_0^{\bar{g}(\mu)} dg \left(\frac{\gamma(g)}{\beta(g)} + \frac{\gamma_0}{\beta_0 g} \right) \right\} \\ \times \langle \bar{B}_q^0 | Q_{\text{R}}^q(\mu) | B_q^0 \rangle + \text{h.c.},\end{aligned} \tag{220}$$

where $Q_{\text{R}}^q(\mu)$ is the renormalized four-fermion operator (usually in the NDR scheme of $\overline{\text{MS}}$). The running coupling $\bar{g}$, the β-function $\beta(g)$, and the anomalous dimension of the four-quark operator $\gamma(g)$ are defined in Eqs. (142) and (143). The product of μ-dependent terms on the second line of Eq. (220) is, of course, μ-independent (up to truncation errors arising from the use of perturbation theory). The explicit expression for the short-distance QCD correction factor η_{2B} (calculated to NLO) can be found in Ref. [410].

For historical reasons the B-meson mixing matrix elements are often parameterized in terms of bag parameters defined as

$$B_{B_q}(\mu) = \frac{\left\langle \bar{B}_q^0 \left| Q_{\text{R}}^q(\mu) \right| B_q^0 \right\rangle}{\frac{8}{3} f_{B_q}^2 m_{\text{B}}^2}. \tag{221}$$

The renormalization group independent (RGI) B parameter $\hat{B}$ is defined as in the case of the kaon, and expressed to 2-loop order as

$$\hat{B}_{B_q} = \left(\frac{\bar{g}(\mu)^2}{4\pi} \right)^{-\gamma_0/(2\beta_0)} \left\{ 1 + \frac{\bar{g}(\mu)^2}{(4\pi)^2} \left[\frac{\beta_1\gamma_0 - \beta_0\gamma_1}{2\beta_0^2} \right] \right\} B_{B_q}(\mu), \tag{222}$$

with β_0, β_1, γ_0, and γ_1 defined in Eq. (144). Note, as Eq. (220) is evaluated above the bottom threshold ($m_b < \mu < m_t$), the active number of flavours here is $N_f = 5$.

Nonzero transition amplitudes result in a mass difference between the CP eigenstates of the neutral B-meson system. Writing the mass difference for a B_q^0 meson as Δm_q, its Standard Model prediction is

$$\Delta m_q = \frac{G_F^2 m_W^2 m_{B_q}}{6\pi^2} |\lambda_{tq}|^2 S_0(x_t) \eta_{2B} f_{B_q}^2 \hat{B}_{B_q}. \tag{223}$$

Experimentally, the mass difference is determined from the oscillation frequency of the CP eigenstates. The frequencies are measured precisely with an error of less than a percent. Many different experiments have measured Δm_d, but the current average [165] is dominated by the LHCb experiment. For Δm_s the experimental average is again dominated by results from LHCb [165] and the precision reached is about one per mille. With these experimental results and lattice-QCD calculations of $f_{B_q}^2 \hat{B}_{B_q}$, λ_{tq} can be determined. In lattice-QCD calculations the flavour $SU(3)$-breaking ratio

$$\xi^2 = \frac{f_{B_s}^2 B_{B_s}}{f_{B_d}^2 B_{B_d}} \tag{224}$$

can be obtained more precisely than the individual B_q-mixing matrix elements because statistical and systematic errors cancel in part. From ξ^2, the ratio $|V_{td}/V_{ts}|$ can be determined and used to constrain the apex of the CKM triangle.

Neutral B-meson mixing, being loop-induced in the Standard Model, is also a sensitive probe of new physics. The most general $\Delta B = 2$ effective Hamiltonian that describes contributions to B-meson mixing in the Standard Model and beyond is given in terms of five local four-fermion operators:

$$\mathcal{H}_{\text{eff,BSM}}^{\Delta B=2} = \sum_{q=d,s} \sum_{i=1}^{5} C_i \mathcal{Q}_i^q, \tag{225}$$

Table 43 Neutral B- and B_s-meson mixing matrix elements (in MeV) and bag parameters

Collaboration	Refs.	N_f	Publication status	Continuum extrapolation	Chiral extrapolation	Finite volume	Renormalization/matching	Heavy-quark treatment	$f_{B_d}\sqrt{\hat{B}_{B_d}}$	$f_{B_s}\sqrt{\hat{B}_{B_s}}$	$\hat{B}_{B_d}$	$\hat{B}_{B_s}$
HPQCD 19A	[71]	2+1+1	A	○	○	★	○	✓	210.6(5.5)	256.1(5.7)	1.222(61)	1.232(53)
FNAL/MILC 16	[73]	2+1	A	★	○	★	○	✓	227.7(9.5)	274.6(8.4)	1.38(12)(6)$^{\odot}$	1.443(88)(48)$^{\odot}$
RBC/UKQCD 14A	[67]	2+1	A	○	○	○	○	✓	240(15)(33)	290(09)(40)	1.17(11)(24)	1.22(06)(19)
FNAL/MILC 11A	[548]	2+1	C	★	○	★	○	✓	250(23)†	291(18)†	–	–
HPQCD 09	[72]	2+1	A	○	○$^{\nabla}$	○	○	✓	216(15)*	266(18)*	1.27(10)*	1.33(6)*
HPQCD 06A	[549]	2+1	A	■	■	★	○	✓	–	281(21)	–	1.17(17)
ETM 13B	[56]	2	A	★	○	○	★	✓	216(6)(8)	262(6)(8)	1.30(5)(3)	1.32(5)(2)
ETM 12A, 12B	[538,550]	2	C	★	○	○	★	✓	–	–	1.32(8)$^{\diamond}$	1.36(8)$^{\diamond}$

$^{\odot}$PDG averages of decay constant f_{B^0} and f_{B_s} [164] are used to obtain these values
†Reported $f_B^2 B$ at $\mu = m_b$ is converted to RGI by multiplying the 2-loop factor 1.517
$^{\nabla}$While wrong-spin contributions are not included in the HMrSχPT fits, the effect is expected to be small for these quantities (see description in FLAG 13 [2])
*This result uses an old determination of $r_1 = 0.321(5)$ fm from Ref. [118] that has since been superseded, which however has only a small effect in the total error budget (see description in FLAG 13 [2])
$^{\diamond}$Reported B at $\mu = m_b = 4.35$ GeV is converted to RGI by multiplying the 2-loop factor 1.521

where $\mathcal{Q}_1$ is defined in Eq. (217) and where

$$\begin{aligned} \mathcal{Q}_2^q &= \left[\bar{b}(1-\gamma_5)q\right]\left[\bar{b}(1-\gamma_5)q\right], \qquad \mathcal{Q}_3^q = \left[\bar{b}^\alpha(1-\gamma_5)q^\beta\right]\left[\bar{b}^\beta(1-\gamma_5)q^\alpha\right], \\ \mathcal{Q}_4^q &= \left[\bar{b}(1-\gamma_5)q\right]\left[\bar{b}(1+\gamma_5)q\right], \qquad \mathcal{Q}_5^q = \left[\bar{b}^\alpha(1-\gamma_5)q^\beta\right]\left[\bar{b}^\beta(1+\gamma_5)q^\alpha\right], \end{aligned} \tag{226}$$

with the superscripts α, β denoting colour indices, which are shown only when they are contracted across the two bilinears. There are three other basis operators in the $\Delta B = 2$ effective Hamiltonian. When evaluated in QCD, however, they give identical matrix elements to the ones already listed due to parity invariance in QCD. The short-distance Wilson coefficients $\mathcal{C}_i$ depend on the underlying theory and can be calculated perturbatively. In the Standard Model only matrix elements of $\mathcal{Q}_1^q$ contribute to Δm_q, while all operators do, for example, for general SUSY extensions of the Standard Model [469]. The matrix elements or bag parameters for the non-SM operators are also useful to estimate the width difference $\Delta\Gamma_q$ between the CP eigenstates of the neutral B meson in the Standard Model, where combinations of matrix elements of $\mathcal{Q}_1^q$, $\mathcal{Q}_2^q$, and $\mathcal{Q}_3^q$ contribute to $\Delta\Gamma_q$ at $\mathcal{O}(1/m_b)$ [546,547].

In this section, we report on results from lattice-QCD calculations for the neutral B-meson mixing parameters $\hat{B}_{B_d}$, $\hat{B}_{B_s}$, $f_{B_d}\sqrt{\hat{B}_{B_d}}$, $f_{B_s}\sqrt{\hat{B}_{B_s}}$ and the $SU(3)$-breaking ratios B_{B_s}/B_{B_d} and ξ defined in Eqs. (221), (222), and (224). The results are summarized in Tables 43 and 44 and in Figs. 29 and 30. Additional details about the underlying simulations and systematic error estimates are given in Appendix C.6.2. Some collaborations do not provide the RGI quantities $\hat{B}_{B_q}$, but quote instead $B_B(\mu)^{\overline{MS},NDR}$. In such cases, we convert the results using Eq. (222) to the RGI quantities quoted in Table 43 with a brief description for each case. More detailed descriptions for these cases are provided in FLAG13 [2]. We do not provide the B-meson matrix elements of the other operators $\mathcal{Q}_{2-5}$ in this report. They have been calculated in Ref. [56] for the $N_f = 2$ case and in Refs. [73,548] for $N_f = 2+1$.

There are no new results for $N_f = 2$ reported after the previous FLAG review. In this category, one work (ETM 13B) [56] passes the quality criteria. A description of this work can be found in the FLAG 13 review [2] where it did not enter the average as it had not appeared in a journal. Because this is the only result available for $N_f = 2$, we quote their values as our estimates

$$f_{B_d}\sqrt{\hat{B}_{b_d}} = 216(10)\ \text{MeV} \qquad f_{B_s}\sqrt{\hat{B}_{B_s}} = 262(10)\ \text{MeV} \qquad \text{Ref. [56]}, \tag{227}$$

Table 44 Results for $SU(3)$-breaking ratios of neutral B_d- and B_s-meson mixing matrix elements and bag parameters

Collaboration	Refs.	N_f	Publication status	Continuum extrapolation	Chiral extrapolation	Finite volume	Renormalization/matching	Heavy-quark treatment	ξ	B_{B_s}/B_{B_d}
HPQCD 19A	[71]	2+1+1	A	○	○	★	○	✓	1.216(16)	1.008(25)
RBC/UKQCD 18A	[70]	2+1	P	★	★	★	★	✓	$1.1939(67)(^{+95}_{-177})$	$0.9984(45)(^{+80}_{-63})$
FNAL/MILC 16	[73]	2+1	A	★	○	★	○	✓	1.206(18)	1.033(31)(26)$^{\odot}$
RBC/UKQCD 14A	[67]	2+1	A	○	○	○	○	✓	1.208(41)(52)	1.028(60)(49)
FNAL/MILC 12	[551]	2+1	A	○	○	★	○	✓	1.268(63)	1.06(11)
RBC/UKQCD 10C	[541]	2+1	A	■	■	■	○	✓	1.13(12)	–
HPQCD 09	[72]	2+1	A	○	○$^{\nabla}$	○	○	✓	1.258(33)	1.05(7)
ETM 13B	[56]	2	A	★	○	○	★	✓	1.225(16)(14)(22)	1.007(15)(14)
ETM 12A, 12B	[538,550]	2	C	★	○	○	★	✓	1.21(6)	1.03(2)

$^{\odot}$PDG average of the ratio of decay constants f_{B_s}/f_{B^0} [164] is used to obtain the value
$^{\nabla}$Wrong-spin contributions are not included in the HMrSχPT fits. As the effect may not be negligible, these results are excluded from the average (see description in FLAG 13 [2])

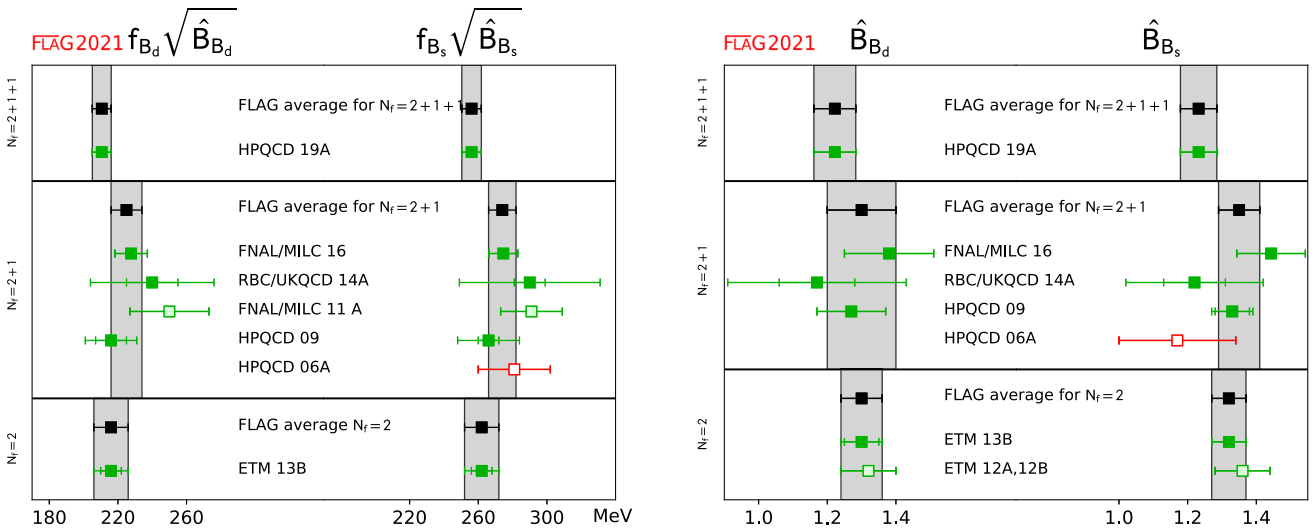

Fig. 29 Neutral B- and B_s-meson mixing matrix elements and bag parameters [values in Table 43 and Eqs. (227), (230), (233), (228), (231), (234)]

$$N_f = 2: \quad \hat{B}_{B_d} = 1.30(6) \quad \hat{B}_{B_s} = 1.32(5) \quad \text{Ref. [56]}, \tag{228}$$
$$\xi = 1.225(31) \quad B_{B_s}/B_{B_d} = 1.007(21) \quad \text{Ref. [56]}. \tag{229}$$

For the $N_f = 2+1$ case the RBC/UKQCD collaboration reported their new results on the flavour SU(3) breaking ratio of neutral B-meson mixing parameters in 2018. Their paper [70] has not been published yet, thus the results will not be included in our averages presented here. Their computation uses ensembles generated by the $2+1$ flavour domain-wall fermion (DWF) formulation. The use of the DWFs also for the heavy quarks makes the renormalization structure simple. Because of the chiral symmetry, the mixing is the same as in the continuum theory. The operators for standard model mixing matrix elements are multiplicatively renormalized. Since they only report the SU(3) breaking ratio, the renormalization of the operators is not needed. The lattice spacings employed are not as fine as some of the recent results reported here. But, by applying successive

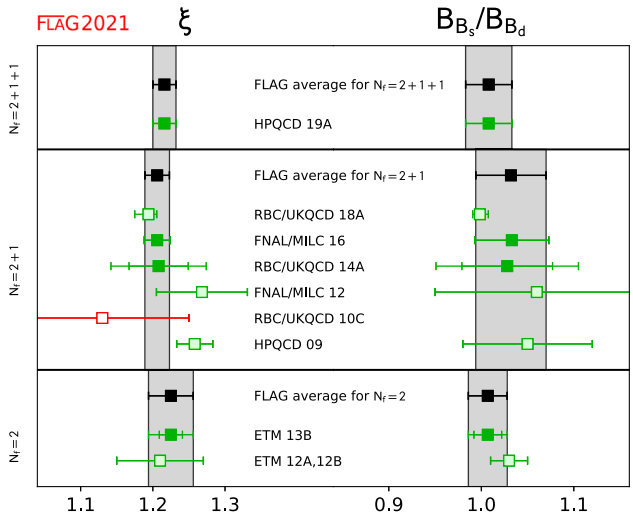

Fig. 30 The $SU(3)$-breaking quantities ξ and B_{B_s}/B_{B_d} [values in Table 44 and Eqs. (229), (232), (235)]

stout link smearings in the heavy DWF, the reach to heavy mass is improved, which allows them to simulate up to half of the physical bottom mass. Two ensembles are of physical ud quark mass at $a = 0.11$ and 0.09 fm, and there is yet another ensemble off the physical point but with finer lattice spacing, $a = 0.07$ fm. This is the first computation using physical light-quark mass for these quantities, which yields a drastic reduction of the chiral extrapolation error.

The results that enter our averages for $N_f = 2 + 1$ are FNAL/MILC 16 [73], which had been included in the averages at FLAG 19 [4], RBC/UKQCD 14A [67], included in the averages at FLAG 16 [3], and HPQCD 09 [72] for which a description is available in FLAG 13 [2]. Thus, the averages for $N_f = 2 + 1$ are unchanged:

$$N_f = 2 + 1:$$

$$f_{B_d}\sqrt{\hat{B}_{B_d}} = 225(9)\,\text{MeV} \qquad f_{B_s}\sqrt{\hat{B}_{B_s}} = 274(8)\,\text{MeV} \qquad \text{Refs. [67,72,73]}, \tag{230}$$

$$\hat{B}_{B_d} = 1.30(10) \qquad \hat{B}_{B_s} = 1.35(6) \qquad \text{Refs. [67,72,73]}, \tag{231}$$

$$\xi = 1.206(17) \qquad B_{B_s}/B_{B_d} = 1.032(38) \qquad \text{Refs. [67,73]}. \tag{232}$$

Here all the above equations have not been changed from the FLAG 19. The averages were obtained using the nested averaging scheme described in Sect. 2.3.2, due to a nested correlation structure among the results. Details are discussed in the FLAG 19 report [4].

We have the first $N_f = 2 + 1 + 1$ calculation for these quantities by the HPQCD collaboration HPQCD 19A [71], using the MILC collaboration's HISQ ensembles. The lattice spacings used are 0.15, 0.12 and 0.09 fm, among which the mass of the Nambu–Goldstone pion (lightest in the staggered taste multiplets) is as small as 130 MeV for two coarser lattices. However, the smallest root-mean-squared pion mass through all taste multiplets is 241 MeV, which is a similar size as the FNAL/MILC 16 result [73] with $N_f = 2 + 1$ and makes the rating on the chiral extrapolation a green circle. The heavy quark formulation used is non-relativistic QCD (NRQCD). The NRQCD action employed is improved from that used in older calculations, especially by including one-loop radiative corrections to most of the coefficients of the $\mathcal{O}(v_b^4)$ terms [552]. The b-quark mass is pre-tuned with the spin-averaged kinetic mass of the Υ and η_b states. Therefore, there is no need for extrapolation or interpolation on the b-quark mass. The HISQ-NRQCD four-quark operators are matched through $\mathcal{O}(1/M)$ and renormalized to one-loop, which includes the effects of $\mathcal{O}(\alpha_s)$, $\mathcal{O}(\Lambda_{\text{QCD}}/M)$, $\mathcal{O}(\alpha_s/aM)$, and $\mathcal{O}(\alpha_s\,\Lambda_{\text{QCD}}/M)$. The remaining error is dominated by $\mathcal{O}(\alpha_s\Lambda_{\text{QCD}}/M)$ 2.9% and $\mathcal{O}(\alpha_s^2)$ 2.1% for individual bag parameters. The bag parameters are the primary quantities calculated in this work. The mixing matrix elements are obtained by combining the so-obtained bag parameters with the B-meson decay constants calculated by Fermilab-MILC collaboration (FNAL/MILC 17 [16]).

Because this is the only result available for $N_f = 2 + 1 + 1$, we quote their values as the FLAG estimates

$N_f = 2+1+1$:

$$f_{B_d}\sqrt{\hat{B}_{B_d}} = 210.6(5.5)\ \text{MeV} \qquad f_{B_s}\sqrt{\hat{B}_{B_s}} = 256.1(5.7)\ \text{MeV} \qquad \text{Ref. [71]}, \tag{233}$$

$$\hat{B}_{B_d} = 1.222(61) \qquad \hat{B}_{B_s} = 1.232(53) \qquad \text{Ref. [71]}, \tag{234}$$

$$\xi = 1.216(16) \qquad B_{B_s}/B_{B_d} = 1.008(25) \qquad \text{Ref. [71]}. \tag{235}$$

We note that the above results within same N_f (e.g., those in Eqs. (233–235)) are all correlated with each other, due to the use of the same gauge field ensembles for different quantities. The results are also correlated with the averages obtained in Sect. 8.1 and shown in Eqs. (207)–(209) for $N_f = 2$, Eqs. (210)–(212) for $N_f = 2+1$ and Eqs. (213)–(215) for $N_f = 2+1+1$. This is because the calculations of B-meson decay constants and mixing quantities are performed on the same (or on similar) sets of ensembles, and results obtained by a given collaboration use the same actions and setups. These correlations must be considered when using our averages as inputs to unitarity triangle (UT) fits. For this reason, if one were for example to estimate $f_{B_s}\sqrt{\hat{B}_s}$ from the separate averages of f_{B_s} (Eq. (211)) and $\hat{B}_s$ (Eq. (231)) for $N_f = 2+1$, one would obtain a value about one standard deviation below the one quoted above in Eq. (230). While these two estimates lead to compatible results, giving us confidence that all uncertainties have been properly addressed, we do not recommend combining averages this way, as many correlations would have to be taken into account to properly assess the errors. We recommend instead using the numbers quoted above. In the future, as more independent calculations enter the averages, correlations between the lattice-QCD inputs to UT fits will become less significant.

8.3 Semileptonic form factors for B decays to light flavours

The Standard Model differential rate for the decay $B_{(s)} \to P\ell\nu$ involving a quark-level $b \to u$ transition is given, at leading order in the weak interaction, by a formula analogous to the one for D decays in Eq. (181), but with $D \to B_{(s)}$ and the relevant CKM matrix element $|V_{cq}| \to |V_{ub}|$:

$$\frac{d\Gamma(B_{(s)} \to P\ell\nu)}{dq^2} = \frac{G_F^2|V_{ub}|^2}{24\pi^3}\frac{(q^2-m_\ell^2)^2\sqrt{E_P^2-m_P^2}}{q^4 m_{B_{(s)}}^2} \times\left[\left(1+\frac{m_\ell^2}{2q^2}\right)m_{B_{(s)}}^2(E_P^2-m_P^2)|f_+(q^2)|^2 + \frac{3m_\ell^2}{8q^2}(m_{B_{(s)}}^2-m_P^2)^2|f_0(q^2)|^2\right]. \tag{236}$$

Again, for $\ell = e, \mu$ the contribution from the scalar form factor f_0 can be neglected, and one has a similar expression to Eq. (183), which, in principle, allows for a direct extraction of $|V_{ub}|$ by matching theoretical predictions to experimental data. However, while for D (or K) decays the entire physical range $0 \le q^2 \le q^2_{\text{max}}$ can be covered with moderate momenta accessible to lattice simulations, in $B \to \pi\ell\nu$ decays one has $q^2_{\text{max}} \sim 26\ \text{GeV}^2$ and only part of the full kinematic range is reachable. As a consequence, obtaining $|V_{ub}|$ from $B \to \pi\ell\nu$ is more complicated than obtaining $|V_{cd(s)}|$ from semileptonic D-meson decays.

In practice, lattice computations are restricted to large values of the momentum transfer q^2 (see Sect. 7.2) where statistical and momentum-dependent discretization errors can be controlled,[37] which in existing calculations roughly cover the upper third of the kinematically allowed q^2 range. Since, on the other hand, the decay rate is suppressed by phase space at large q^2, most of the semileptonic $B \to \pi$ events are observed in experiment at lower values of q^2, leading to more accurate experimental results for the binned differential rate in that region.[38] It is, therefore, a challenge to find a window of intermediate values of q^2 at which both the experimental and lattice results can be reliably evaluated.

State-of-the-art determinations of CKM matrix elements, say, e.g., $|V_{ub}|$, are obtained from joint fits to lattice and experimental results, keeping the relative normalization $|V_{ub}|^2$ as a free parameter. This requires, in particular, that both experimental and lattice data for the q^2-dependence be parameterized by fitting data to specific ansätze, with the ultimate aim of minimizing the systematic uncertainties involved. This plays a key role in assessing the systematic uncertainties of CKM determinations,

[37] The variance of hadron correlation functions at nonzero three-momentum is dominated at large Euclidean times by zero-momentum multiparticle states [553]; therefore the noise-to-signal grows more rapidly than for the vanishing three-momentum case.

[38] Upcoming data from Belle II are expected to significantly improve the precision of experimental results, in particular, for larger values of q^2.

and will be discussed extensively in this section. A detailed discussion of the parameterization of form factors as a function of q^2 can be found in Appendix B.1.

8.3.1 Form factors for $B \to \pi \ell \nu$

The semileptonic decay process $B \to \pi \ell \nu$ enables determination of the CKM matrix element $|V_{ub}|$ within the Standard Model via Eq. (236). Early results for $B \to \pi \ell \nu$ form factors came from the HPQCD [554] and FNAL/MILC [555] collaborations. Only HPQCD provided results for the scalar form factor f_0. Our 2016 review featured a significantly extended calculation of $B \to \pi \ell \nu$ from FNAL/MILC [556] and a new computation from RBC/UKQCD [557]. All the above computations employ $N_f = 2 + 1$ dynamical configurations, and provide values for both form factors f_+ and f_0. In addition, HPQCD using MILC ensembles had published the first $N_f = 2 + 1 + 1$ results for the $B \to \pi \ell \nu$ scalar form factor, working at zero recoil ($q^2 = q^2_{\rm max}$) and pion masses down to the physical value [558]; this adds to previous reports on ongoing work to upgrade their 2006 computation [559,560]. Since this latter result has no immediate impact on current $|V_{ub}|$ determinations, which come from the vector-form-factor-dominated decay channels into light leptons, we will from now on concentrate on the $N_f = 2+1$ determinations of the q^2-dependence of $B \to \pi$ form factors.

Several groups are working on new calculations of the $B \to \pi$ form factors and have reported on their progress at the annual Lattice conferences and the 2020 Asia-Pacific Symposium for Lattice Field Theory. The results are preliminary or blinded, so not yet ready for inclusion in this review. The JLQCD collaboration is using Möbius Domain Wall fermions (including for the heavy quark) with $a \approx 0.08$, 0.055, and 0.044 fm and pion masses down to 225 MeV to study this process [561–563]. FNAL/MILC is using $N_f = 2 + 1 + 1$ HISQ ensembles with $a \approx 0.15$, 0.12, 0.088 fm, 0.057 fm, with Goldstone pion mass down to its physical value [564,565]. The RBC/UKQCD Collaborations have added a new Möbius-domain-wall-fermion ensemble with $a \approx 0.07$ fm and $m_\pi \approx 230$ MeV to their analysis [566].

Returning to the calculations that contribute to our averages (with no new results since FLAG 19), both the HPQCD and the FNAL/MILC computations of $B \to \pi \ell \nu$ amplitudes use ensembles of gauge configurations with $N_f = 2 + 1$ flavours of rooted staggered quarks produced by the MILC collaboration; however, the latest FNAL/MILC work makes a much more extensive use of the currently available ensembles, both in terms of lattice spacings and light-quark masses. HPQCD have results at two values of the lattice spacing ($a \approx 0.12,\ 0.09$ fm), while FNAL/MILC employs four values ($a \approx 0.12,\ 0.09,\ 0.06,\ 0.045$ fm). Lattice-discretization effects are estimated within heavy-meson rooted staggered chiral perturbation theory (HMrSχPT) in the FNAL/MILC computation, while HPQCD quotes the results at $a \approx 0.12$ fm as central values and uses the $a \approx 0.09$ fm results to quote an uncertainty. The relative scale is fixed in both cases through the quark–antiquark potential-derived ratio r_1/a. HPQCD set the absolute scale through the Υ $2S$–$1S$ splitting, while FNAL/MILC uses a combination of f_π and the same Υ splitting, as described in Ref. [54]. The spatial extent of the lattices employed by HPQCD is $L \simeq 2.4$ fm, save for the lightest mass point (at $a \approx 0.09$ fm) for which $L \simeq 2.9$ fm. FNAL/MILC, on the other hand, uses extents up to $L \simeq 5.8$ fm, in order to allow for light-pion masses while keeping finite-volume effects under control. Indeed, while in the 2006 HPQCD work the lightest RMS pion mass is 400 MeV, the latest FNAL/MILC work includes pions as light as 165 MeV – in both cases the bound $m_\pi L \gtrsim 3.8$ is kept. Other than the qualitatively different range of MILC ensembles used in the two computations, the main difference between HPQCD and FNAL/MILC lies in the treatment of heavy quarks. HPQCD uses the NRQCD formalism, with a 1-loop matching of the relevant currents to the ones in the relativistic theory. FNAL/MILC employs the clover action with the Fermilab interpretation, with a mostly nonperturbative renormalization of the relevant currents, within which the overall renormalization factor of the heavy-light current is written as a product of the square roots of the renormalization factors of the light-light and heavy-heavy temporal vector currents (which are determined nonperturbatively) and a residual factor that is computed using 1-loop perturbation theory. (See Table 45; full details about the computations are provided in tables in Appendix C.6.3.)

The RBC/UKQCD computation is based on $N_f = 2 + 1$ DWF ensembles at two values of the lattice spacing ($a \approx 0.12,\ 0.09$ fm), and pion masses in a narrow interval ranging from slightly above 400 MeV to slightly below 300 MeV, keeping $m_\pi L \gtrsim 4$. The scale is set using the Ω^- baryon mass. Discretization effects coming from the light sector are estimated in the 1% ballpark using HMχPT supplemented with effective higher-order interactions to describe cutoff effects. The b quark is treated using the Columbia RHQ action, with a mostly nonperturbative renormalization of the relevant currents. Discretization effects coming from the heavy sector are estimated with power-counting arguments to be below 2%.

Given the large kinematical range available in the $B \to \pi$ transition, chiral extrapolations are an important source of systematic uncertainty: apart from the eventual need to reach physical pion masses in the extrapolation, the applicability of χPT is not guaranteed for large values of the pion energy E_π. Indeed, in all computations E_π reaches values in the 1 GeV ballpark, and chiral extrapolation systematics is the dominant source of errors. FNAL/MILC uses $SU(2)$ NLO HMrSχPT

Table 45 Results for the $B \to \pi \ell \nu$ semileptonic form factor

Collaboration	Refs.	N_f	Publication status	Continuum extrapolation	Chiral extrapolation	Finite volume	Renormalization	Heavy-quark treatment	z-parameterization
FNAL/MILC 15	[556]	2+1	A	★	○	★	○	✓	BCL
RBC/UKQCD 15	[557]	2+1	A	○	○	○	○	✓	BCL
HPQCD 06	[554]	2+1	A	○	○	○	○	✓	n/a

for the continuum-chiral extrapolation, supplemented by NNLO analytic terms and hard-pion χPT terms [507];[39] systematic uncertainties are estimated through an extensive study of the effects of varying the specific fit ansatz and/or data range. RBC/UKQCD uses $SU(2)$ hard-pion HMχPT to perform its combined continuum-chiral extrapolation, and obtains estimates for systematic uncertainties by varying the ansätze and ranges used in fits. HPQCD performs chiral extrapolations using HMrSχPT formulae, and estimates systematic uncertainties by comparing the result with the ones from fits to a linear behaviour in the light-quark mass, continuum HMχPT, and partially quenched HMrSχPT formulae (including also data with different sea and valence light-quark masses).

FNAL/MILC and RBC/UKQCD describe the q^2-dependence of f_+ and f_0 by applying a BCL parameterization to the form factors extrapolated to the continuum limit, within the range of values of q^2 covered by data. (A discussion of the various parameterizations can be found in Appendix B.1.) RBC/UKQCD generate synthetic data for the form factors at some values of q^2 (evenly spaced in z) from the continuous function of q^2 obtained from the joint chiral-continuum extrapolation, which are then used as input for the fits. After having checked that the kinematical constraint $f_+(0) = f_0(0)$ is satisfied within errors by the extrapolation to $q^2 = 0$ of the results of separate fits, this constraint is imposed to improve fit quality. In the case of FNAL/MILC, rather than producing synthetic data a functional method is used to extract the z-parameterization directly from the fit functions employed in the continuum-chiral extrapolation. In the case of HPQCD, the parameterization of the q^2-dependence of form factors is somewhat intertwined with chiral extrapolations: a set of fiducial values $\{E_\pi^{(n)}\}$ is fixed for each value of the light-quark mass, and $f_{+,0}$ are interpolated to each of the $E_\pi^{(n)}$; chiral extrapolations are then performed at fixed E_π (i.e., m_π and q^2 are varied subject to E_π = constant). The interpolation is performed using a Ball–Zwicky (BZ) ansatz [567]. The q^2-dependence of the resulting form factors in the chiral limit is then described by means of a BZ ansatz, which is cross-checked against Becirevic–Kaidalov (BK) [500], Richard Hill (RH) [568], and Boyd–Grinstein–Lebed (BGL) [569] parameterizations (see Appendix B.1), finding agreement within the quoted uncertainties. Unfortunately, the correlation matrix for the values of the form factors at different q^2 is not provided, which severely limits the possibilities of combining them with other computations into a global z-parameterization.

The different ways in which the current results are presented do not allow a straightforward averaging procedure. RBC/UKQCD only provides synthetic values of f_+ and f_0 at a few values of q^2 as an illustration of their results, and FNAL/MILC does not quote synthetic values at all. In both cases, full results for BCL z-parameterizations defined by Eq. (532) are quoted. In the case of HPQCD 06, unfortunately, a fit to a BCL z-parameterization is not possible, as discussed above.

In order to combine these form factor calculations, we start from sets of synthetic data for several q^2 values. HPQCD and RBC/UKQCD directly provide this information; FNAL/MILC present only fits to a BCL z-parameterization from which we can easily generate an equivalent set of form factor values. It is important to note that in both the RBC/UKQCD synthetic data and the FNAL/MILC z-parameterization fits the kinematic constraint at $q^2 = 0$ is automatically included (in the FNAL/MILC case the constraint is manifest in an exact degeneracy of the (a_n^+, a_n^0) covariance matrix). Due to these considerations, in our opinion, the most accurate procedure is to perform a simultaneous fit to all synthetic data for the vector and scalar form factors. Unfortunately, the absence of information on the correlation in the HPQCD result between the vector and scalar form factors even at a single q^2 point makes it impossible to include consistently this calculation in the overall fit.

[39] It is important to stress the finding in Ref. [506] that the factorization of chiral logs in hard-pion χPT breaks down, implying that it does not fulfill the expected requisites for a proper effective field theory. Its use to model the mass dependence of form factors can thus be questioned.

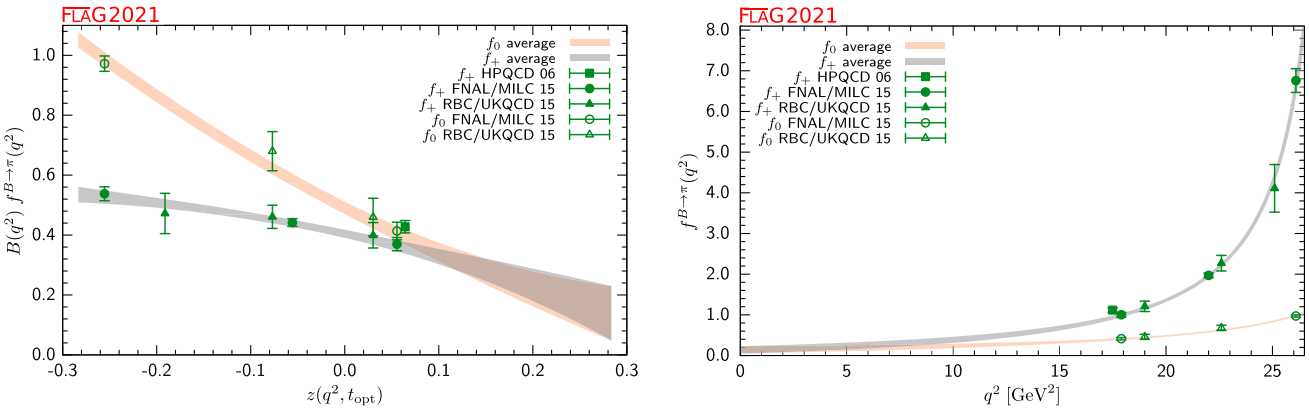

Fig. 31 The form factors $f_+(q^2)$ and $f_0(q^2)$ for $B \to \pi\ell\nu$ plotted versus z (left panel) and q^2 (right panel). In the left plot, we removed the Blaschke factors. See text for a discussion of the data set. The grey and salmon bands display our preferred $N^+ = N^0 = 3$ BCL fit (five parameters)

Table 46 Coefficients and correlation matrix for the $N^+ = N^0 = 3$ z-expansion fit of the $B \to \pi$ form factors f_+ and f_0. The coefficient a_2^0 is fixed by the $f_+(q^2 = 0) = f_0(q^2 = 0)$ constraint. The chi-square per degree of freedom is $\chi^2/\text{dof} = 0.82$. The lattice calculations that enter this fit are taken from FNAL/MILC 15 [556] and RBC/UKQCD 15 [557]. The parameterizations are defined in Eqs. (532) and (533)

$B \to \pi$ ($N_f = 2+1$)						
	Central values	Correlation matrix				
a_0^+	0.404 (13)	1	0.404	0.118	0.327	0.344
a_1^+	−0.68 (13)	0.404	1	0.741	0.310	0.900
a_2^+	−0.86 (61)	0.118	0.741	1	0.363	0.886
a_0^0	0.490 (21)	0.327	0.310	0.363	1	0.233
a_1^0	−1.61 (16)	0.344	0.900	0.886	0.233	1

In fact, the HPQCD and FNAL/MILC statistical uncertainties are highly correlated (because they are based on overlapping subsets of MILC $N_f = 2+1$ ensembles) and, without knowledge of the $f_+ - f_0$ correlation we are unable to construct the HPQCD-FNAL/MILC off-diagonal entries of the overall covariance matrix.

In conclusion, we will present as our best result a combined vector and scalar form factor fit to the FNAL/MILC and RBC/UKQCD results that we treat as completely uncorrelated. For sake of completeness, we will also show the results of a vector form factor fit alone in which we include one HPQCD datum at $q^2 = 17.34$ GeV^2 assuming conservatively a 100% correlation between the statistical error of this point and of all FNAL/MILC synthetic data. In spite of contributing just one point, the HPQCD datum has a significant weight in the fit due to its small overall uncertainty. We stress again that this procedure is slightly inconsistent because FNAL/MILC and RBC/UKQCD include information on the kinematic constraint at $q^2 = 0$ in their f_+ results.

The resulting data set is then fitted to the BCL parameterization in Eqs. (532) and (533). We assess the systematic uncertainty due to truncating the series expansion by considering fits to different orders in z. In Fig. 31, we show the FNAL/MILC, RBC/UKQCD, and HPQCD data points for $(1 - q^2/m_{B^*}^2) f_+(q^2)$ and $f_0(q^2)$ versus z. The data is highly linear and we get $\chi^2/\text{dof} = 0.82$ with $N^+ = N^0 = 3$. Note that this implies three independent parameters for f_+ corresponding to a polynomial through $\mathcal{O}(z^3)$ and two independent parameters for f_0 corresponding to a polynomial through $\mathcal{O}(z^2)$ (the coefficient a_2^0 is fixed using the $q^2 = 0$ kinematic constraint). We cannot constrain the coefficients of the z-expansion beyond this order; for instance, including a fourth parameter in f_+ results in 100% uncertainties on a_2^+ and a_3^+. The outcome of the five-parameter $N^+ = N^0 = 3$ BCL fit to the FNAL/MILC and RBC/UKQCD calculations is shown in Table 46. The uncertainties on $a_0^{+,0}$, $a_1^{+,0}$ and a_2^+ encompass the central values obtained from $N^+ = 2, 4$ and $N^0 = 2, 4, 5$ fits and thus adequately reflect the systematic uncertainty on those series coefficients. The fit shown in Table 46 can therefore be used as the averaged FLAG result for the lattice-computed form factor $f_+(q^2)$. The coefficient a_3^+ can be obtained from the values for a_0^+–a_2^+ using Eq. (531). The coefficient a_2^0 can be obtained from all other coefficients imposing the $f_+(q^2 = 0) = f_0(q^2 = 0)$ constraint. The fit is illustrated in Fig. 31.

We emphasize that future lattice-QCD calculations of semileptonic form factors should publish their full statistical and systematic correlation matrices to enable others to use the data. It is also preferable to present a set of synthetic form factors data equivalent to the z-fit results, since this allows for an independent analysis that avoids further assumptions about the compatibility of the procedures to arrive at a given z-parameterization.[40] It is also preferable to present covariance/correlation matrices with enough significant digits to calculate correctly all their eigenvalues.

For the sake of completeness, we present also a standalone z-fit to the vector form factor. In this fit, we are able to include the single f_+ point at $q^2 = 17.34$ GeV^2 that we mentioned above. This fit uses the FNAL/MILC and RBC/UKQCD results that do make use of the kinematic constraint at $q^2 = 0$, but is otherwise unbiased. The results of the three-parameter BCL fit to the HPQCD, FNAL/MILC and RBC/UKQCD calculations of the vector form factor are:

$$N_f = 2+1: \quad a_0^+ = 0.421(13), \quad a_1^+ = -0.35(10), \quad a_2^+ = -0.41(64)\,;$$
$$\mathrm{corr}(a_i, a_j) = \begin{pmatrix} 1.000 & 0.306 & 0.084 \\ 0.306 & 1.000 & 0.856 \\ 0.084 & 0.856 & 1.000 \end{pmatrix}. \tag{237}$$

Note that the a_0^+ coefficient, that is the most relevant for input to the extraction of V_{ub} from semileptonic $B \to \pi \ell \nu_\ell (\ell = e, \mu)$ decays, shifts by about a standard deviation.

8.3.2 *Form factors for $B_s \to K \ell \nu$*

Similar to $B \to \pi \ell \nu$, measurements of $B_s \to K \ell \nu$ decay rates enable determinations of the CKM matrix element $|V_{ub}|$ within the Standard Model via Eq. (236). From the lattice point of view, the two channels are very similar. As a matter of fact, $B_s \to K \ell \nu$ is actually somewhat simpler, in that the kaon mass region is easily accessed by all simulations making the systematic uncertainties related to chiral extrapolation smaller.

At the time of our FLAG 19 review [4], results for $B_s \to K \ell \nu$ form factors were provided by HPQCD [570] and RBC/UKQCD [557] for both form factors f_+ and f_0, in both cases using $N_f = 2+1$ dynamical configurations. HPQCD has recently emphasized the value of using ratios of form factors for the processes $B_s \to K \ell \nu$ and $B_s \to D_s \ell \nu$ for the determination of $|V_{ub}/V_{cb}|$ [571]. In the FLAG Review 19 [4], FNAL/MILC preliminary results had been reported for both $N_f = 2+1$ [572] and $N_f = 2+1+1$ [564], but were not included in the average due to their non-final status. The $N_f = 2+1$ results have since been published [573]; we will, therefore, include them in the average here.

The RBC/UKQCD computation has been published together with the $B \to \pi \ell \nu$ computation discussed in Sect. 8.3.1, all technical details being practically identical. The main difference is that errors are significantly smaller, mostly due to the reduction of systematic uncertainties due to the chiral extrapolation. Detailed information is provided in Appendix C.6.3. The RBC/UKQCD collaboration is also working on an improved determination of $B_s \to K$ form factors that includes a finer lattice spacing, with preliminary results shown in Ref. [566], but these results cannot yet be included in the average. The HPQCD computation uses ensembles of gauge configurations with $N_f = 2+1$ flavours of asqtad rooted staggered quarks produced by the MILC collaboration at two values of the lattice spacing ($a \approx 0.12,\ 0.09$ fm), for three and two different sea-pion masses, respectively, down to a value of 260 MeV. The b quark is treated within the NRQCD formalism, with a 1-loop matching of the relevant currents to the ones in the relativistic theory, omitting terms of $\mathcal{O}(\alpha_s \Lambda_{\mathrm{QCD}}/m_b)$. The HISQ action is used for the valence s quark. The continuum-chiral extrapolation is combined with the description of the q^2-dependence of the form factors into a modified z-expansion (cf. Appendix B.1) that formally coincides in the continuum with the BCL ansatz. The dependence of form factors on the pion energy and quark masses is fitted to a 1-loop ansatz inspired by hard-pion χPT [507], that factorizes out the chiral logarithms describing soft physics. The FNAL/MILC computation coincides with HPQCD's in using ensembles of gauge configurations with $N_f = 2+1$ flavours of asqtad rooted staggered quarks produced by the MILC collaboration, but only one ensemble is shared, and a different valence regularization is employed; we will thus treat the two results as fully independent from the statistics point of view. FNAL/MILC uses three values of the lattice spacing ($a \approx 0.12,\ 0.09,\ 0.06$ fm); only one value of the sea pion mass and the volume is available at the extreme values of the lattice spacing, while four different masses and volumes are considered at $a = 0.09$ fm. Heavy quarks are treated within the Fermilab approach. HMrSχPT expansion is used at next-to-leading order in $SU(2)$ and leading order in $1/M_B$, including next-to-next-to-leading-order (NNLO) analytic and generic discretization terms, to perform continuum-chiral extrapolations.

[40] Note that generating synthetic data is a trivial task, but less so is choosing the number of required points and the q^2 values that lead to an optimal description of the form factors.

Table 47 Summary of lattice calculations of the $B_s \to K\ell\nu$ semileptonic form factors

Collaboration	Refs.	N_f	Publication status	Continuum extrapolation	Chiral extrapolation	Finite volume	Renormalization	Heavy-quark treatment	z-parameterization
FNAL/MILC 19	[573]	2+1	A	★	○	★	○	✓	BCL
RBC/UKQCD 15	[557]	2+1	A	○	○	○	○	✓	BCL
HPQCD 14	[570]	2+1	A	○	○	○	○	✓	BCL†

†Results from modified z-expansion

Table 48 Coefficients and correlation matrix for the $N^+ = N^0 = 4$ z-expansion of the $B_s \to K$ form factors f_+ and f_0. The coefficient a_3^0 is fixed by the $f_+(q^2 = 0) = f_0(q^2 = 0)$ constrain. The chi-square per degree of freedom is $\chi^2/\text{dof} = 1.54$ and the errors on the z-parameters have been rescaled by $\sqrt{\chi^2/\text{dof}} = 1.24$

$B_s \to K$ $(N_f = 2+1)$								
	Central values	Correlation matrix						
a_0^+	0.374 (12)	1	0.2471	−0.1715	−0.2396	0.6445	0.3791	0.2857
a_1^+	−0.672 (64)	0.2471	1	0.4198	0.1724	0.4626	0.8183	0.7948
a_2^+	0.07 (31)	−0.1715	0.4198	1	0.8136	0.3804	0.7293	0.7481
a_3^+	1.34 (52)	−0.2396	0.1724	0.8136	1	0.2823	0.5120	0.5529
a_0^0	0.2203 (68)	0.6445	0.4626	0.3804	0.2823	1	0.6570	0.4837
a_1^0	0.089 (57)	0.3791	0.8183	0.7293	0.5120	0.6570	1	0.9220
a_2^0	0.24 (23)	0.2857	0.7948	0.7481	0.5529	0.4837	0.9220	1

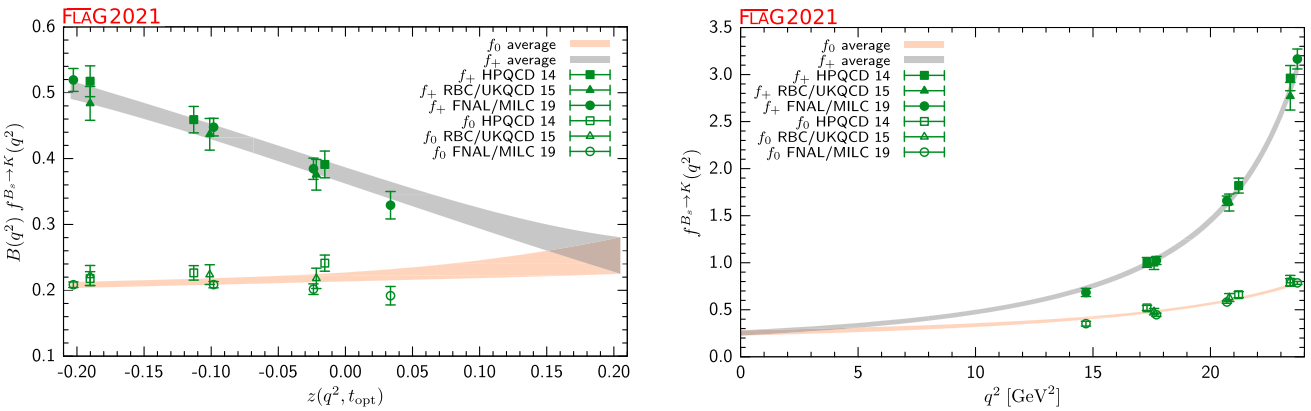

Fig. 32 The form factors $f_+(q^2)$ and $f_0(q^2)$ for $B_s \to K\ell\nu$ plotted versus z (left panel) and q^2 (right panel). In the left plot, we remove the Blaschke factors. See text for a discussion of the data sets. The grey and salmon bands display our preferred $N^+ = N^0 = 4$ BCL fit (seven parameters)

Hard kaons are assumed to decouple, i.e., their effect is reabsorbed in the $SU(2)$ LECs. Continuum- and chiral-extrapolated values of the form factors are fitted to a z-parametrization imposing the kinematical constraint $f_+(0) = f_0(0)$. See Table 47 and the tables in Appendix C.6.3 for full details.

In order to combine the results for the q^2 dependence of the form factors from the three collaborations, we will follow a similar approach to the one adopted above for $B \to \pi\ell\nu$, and produce synthetic data from the preferred fits quoted in the papers, to obtain a dataset to which a joint fit can be performed. Note that the kinematic constraint at $q^2 = 0$ is included in all three cases; we will impose it in our fit as well, since the synthetic data will implicitly depend on that fitting choice. However, it is worth mentioning that the systematic uncertainty of the resulting extrapolated value $f_+(0) = f_0(0)$ can be fairly large, the main reason being the required long extrapolation from the high-q^2 region covered by lattice data. While we stress that the average far away from the high-q^2 region has to be used carefully, it is possible that increasing the number of

z coefficients beyond what is sufficient for a good description of the lattice data and using unitarity constraints to control the size of additional terms, might yield fits with a more stable extrapolation at very low q^2. We plan to include said unitarity analysis into the next edition of the FLAG review. It is, however, important to emphasize that joint fits with experimental data, where the latter accurately map the q^2 region, are expected to be safe.

Our fits employ a BCL ansatz with $t_+ = (M_B + M_\pi)^2$ and $t_0 = t_+ - \sqrt{t_+(t_+ - t_-)}$, with $t_- = (M_{B_s} - M_K)^2$. Our pole factors will contain a single pole in both the vector and scalar channels, for which we take the mass values $M_{B^*} = 5.32465$ GeV and $M_{B^*(0^+)} = 5.68$ GeV.[41] The constraint $f_+(0) = f_0(0)$ is imposed by expressing the coefficient $b^0_{N^0-1}$ in terms of all others. The outcome of the seven-parameter $N^+ = N^0 = 4$ BCL fit, which we quote as our preferred result, is shown in Table 48. The fit has a chi-square per degree of freedom $\chi^2/\text{dof} = 1.54$. Following the PDG recommendation, we rescale the whole covariance matrix by χ^2/dof: the errors on the z-parameters are increased by $\sqrt{\chi^2/\text{dof}} = 1.24$ and the correlation matrix is unaffected. The parameters shown in Table 48 provide the averaged FLAG results for the lattice-computed form factors $f_+(q^2)$ and $f_0(q^2)$. The coefficient a_4^+ can be obtained from the values for a_0^+–a_3^+ using Eq. (531). The fit is illustrated in Fig. 32.[42]

We will conclude by pointing out progress in the application of the npHQET method to the extraction of semileptonic form factors, reported for $B_s \to K$ transitions in Ref. [574], which extends the work of Ref. [575]. This is a methodological study based on CLS $N_f = 2$ ensembles at two different values of the lattice spacing and pion masses, and full $1/m_b$ corrections are incorporated within the npHQET framework. Emphasis is on the role of excited states in the extraction of the bare form factors, which are shown to pose an impediment to reaching precisions better than a few percent.

8.3.3 Form factors for rare and radiative B-semileptonic decays to light flavours

Lattice-QCD input is also available for some exclusive semileptonic decay channels involving neutral-current $b \to q$ transitions at the quark level, where $q = d, s$. Being forbidden at tree level in the SM, these processes allow for stringent tests of potential new physics; simple examples are $B \to K^*\gamma$, $B \to K^{(*)}\ell^+\ell^-$, or $B \to \pi\ell^+\ell^-$ where the B meson (and therefore the light meson in the final state) can be either neutral or charged.

The corresponding SM effective weak Hamiltonian is considerably more complicated than the one for the tree-level processes discussed above: after integrating out the top quark and the W boson, as many as ten dimension-six operators formed by the product of two hadronic currents or one hadronic and one leptonic current appear.[43] Three of the latter, coming from penguin and box diagrams, dominate at short distances and have matrix elements that, up to small QED corrections, are given entirely in terms of $B \to (\pi, K, K^*)$ form factors. The matrix elements of the remaining seven operators can be expressed, up to power corrections whose size is still unclear, in terms of form factors, decay constants and light-cone distribution amplitudes (for the π, K, K^* and B mesons) by employing OPE arguments (at large di-lepton invariant mass) and results from Soft Collinear Effective Theory (at small di-lepton invariant mass). In conclusion, the most important contributions to all of these decays are expected to come from matrix elements of current operators (vector, tensor, and axial-vector) between one-hadron states, which in turn can be parameterized in terms of a number of form factors (see Ref. [577] for a complete description).

In channels with pseudoscalar mesons in the final state, the level of sophistication of lattice calculations is similar to the $B \to \pi$ case and there are results for the vector, scalar, and tensor form factors for $B \to K\ell^+\ell^-$ decays by HPQCD [579], and more recent results for both $B \to \pi\ell^+\ell^-$ [580] and $B \to K\ell^+\ell^-$ [578] from FNAL/MILC. Full details about these two calculations are provided in Table 49 and in Appendix C.6.4. Both computations employ MILC $N_f = 2 + 1$ asqtad ensembles. HPQCD [581] and FNAL/MILC [582] have also companion papers in which they calculate the Standard Model predictions for the differential branching fractions and other observables and compare to experiment. The HPQCD computation employs NRQCD b quarks and HISQ valence light quarks, and parameterizes the form factors over the full kinematic range using a model-independent z-expansion as in Appendix B.1, including the covariance matrix of the fit coefficients. In the case of the (separate) FNAL/MILC computations, both of them use Fermilab b quarks and asqtad light quarks, and a BCL z-parameterization of the form factors.

[41] These are the values used in the FNAL/MILC determination, while HPQCD and RBC/UKQCD use $M_{B^*(0+)} = 5.6794(10)$ GeV and $M_{B^*(0+)} = 5.63$ GeV, respectively. They also employ different values of t_+ and t_0 than employed here, which again coincide with FNAL/MILC's choice.

[42] Note that in FLAG 19 [4] we had adopted the threshold $t_+ = (M_{B_s} + M_K)^2$ rather than $t_+ = (M_B + M_\pi)^2$. This change impacted the z-range which the physical q^2 interval maps onto. We also point out that, in the FLAG 19 version of Fig. 32, the three synthetic f_0 data points from HPQCD were plotted incorrectly, but this did not affect the fit.

[43] See, e.g., Ref. [576] and references therein.

Table 49 Summary of lattice calculations of the $B \to K$ semileptonic form factors

Collaboration	Refs.	N_f	Publication status	Continuum extrapolation	Chiral extrapolation	Finite volume	Renormalization	Heavy-quark treatment	z-parameterization
FNAL/MILC 15D	[578]	2+1	A	★	○	★	○	✓	BCL
HPQCD 13E	[579]	2+1	A	○	○	○	○	✓	BCL

Table 50 Coefficients and correlation matrix for the $N^+ = N^0 = 3$ z-expansion of the $B \to \pi$ form factor f_T

$B \to \pi$ ($N_f = 2+1$)					
	Central values	Correlation matrix			
a_0^T	0.393(17)	1.000	0.400	0.204	0.166
a_1^T	−0.65(23)	0.400	1.000	0.862	0.806
a_2^T	−0.6(1.5)	0.204	0.862	1.000	0.989
a_3^T	0.1(2.8)	0.166	0.806	0.989	1.000

Reference [580] includes results for the tensor form factor for $B \to \pi \ell^+ \ell^-$ not included in previous publications on the vector and scalar form factors [556]. Nineteen ensembles from four lattice spacings are used to control continuum and chiral extrapolations. The results for $N_z = 4$ z-expansion of the tensor form factor and its correlations with the expansions for the vector and scalar form factors, which we consider the FLAG estimate, are shown in Table 50. Partial decay widths for decay into light leptons or $\tau^+\tau^-$ are presented as a function of q^2. The former is compared with results from LHCb [583], while the latter is a prediction.

The averaging of the HPQCD and FNAL/MILC results for the $B \to K$ form factors is similar to our treatment of the $B \to \pi$ and $B_s \to K$ form factors. In this case, even though the statistical uncertainties are partially correlated because of some overlap between the adopted sets of MILC ensembles, we choose to treat the two calculations as independent. The reason is that, in $B \to K$, statistical uncertainties are subdominant and cannot be easily extracted from the results presented by HPQCD and FNAL/MILC. Both collaborations provide only the outcome of a simultaneous z-fit to the vector, scalar and tensor form factors, that we use to generate appropriate synthetic data. We then impose the kinematic constraint $f_+(q^2 = 0) = f_0(q^2 = 0)$ and fit to ($N^+ = N^0 = N^T = 3$) BCL parameterization. The functional forms of the form factors that we use are identical to those adopted in Ref. [582].[44] The results of the fit are presented in Table 51. The fit is illustrated in Fig. 33. Note that the average for the f_T form factor appears to prefer the FNAL/MILC synthetic data. This happens because we perform a correlated fit of the three form factors simultaneously (both FNAL/MILC and HPQCD present covariance matrices that include correlations between all form factors). We checked that the average for the f_T form factor, obtained neglecting correlations with f_0 and f_+, is a little lower and lies in between the two data sets. There is still a noticeable tension between the FNAL/MILC and HPQCD data for the tensor form factor; indeed, a standalone fit to these data results in $\chi^2_{\rm red} = 7.2/3 = 2.4$, while a similar standalone joint fit to f_+ and f_0 has $\chi^2_{\rm red} = 9.2/7 = 1.3$. Finally, the global fit that is shown in the figure has $\chi^2_{\rm red} = 18.6/10 = 1.86$.

Lattice computations of form factors in channels with a vector meson in the final state face extra challenges with respect to the case of a pseudoscalar meson: the state is unstable, and the extraction of the relevant matrix element from correlation functions is significantly more complicated; χPT cannot be used as a guide to extrapolate results at unphysically heavy pion masses to the chiral limit. While field-theory procedures to take resonance effects into account are available [328–330,585–592], they have not yet been implemented in the existing preliminary computations, which therefore suffer from uncontrolled systematic errors in calculations of weak decay form factors into unstable vector meson final states, such as the K^* or ρ mesons.[45]

[44] Note in particular that not much is known about the sub-threshold poles for the scalar form factor. FNAL/MILC includes one pole at the B^*_{s0} mass as taken from the calculation in Ref. [584].

[45] In cases such as $B \to D^*$ transitions, that will be discussed below, this is much less of a practical problem due to the very narrow nature of the resonance.

Table 51 Coefficients and correlation matrix for the $N^+ = N^0 = N^T = 3$ z-expansion of the $B \to K$ form factors f_+, f_0 and f_T. The coefficient a_2^0 is fixed by the $f_+(q^2 = 0) = f_0(q^2 = 0)$ constraint. The chi-square per degree of freedom is $\chi^2/\text{dof} = 1.86$ and the errors on the z-parameters have been rescaled by $\sqrt{\chi^2/\text{dof}} = 1.36$

$B \to K$ ($N_f = 2+1$)									
	Central values	Correlation matrix							
a_0^+	0.471 (14)	1	0.513	0.128	0.773	0.594	0.613	0.267	0.118
a_1^+	−0.74 (16)	0.513	1	0.668	0.795	0.966	0.212	0.396	0.263
a_2^+	0.32 (71)	0.128	0.668	1	0.632	0.768	−0.104	0.0440	0.187
a_0^0	0.301 (10)	0.773	0.795	0.632	1	0.864	0.393	0.244	0.200
a_1^0	0.40 (15)	0.594	0.966	0.768	0.864	1	0.235	0.333	0.253
a_0^T	0.455 (21)	0.613	0.212	−0.104	0.393	0.235	1	0.711	0.608
a_1^T	−1.00 (31)	0.267	0.396	0.0440	0.244	0.333	0.711	1	0.903
a_2^T	−0.9 (1.3)	0.118	0.263	0.187	0.200	0.253	0.608	0.903	1

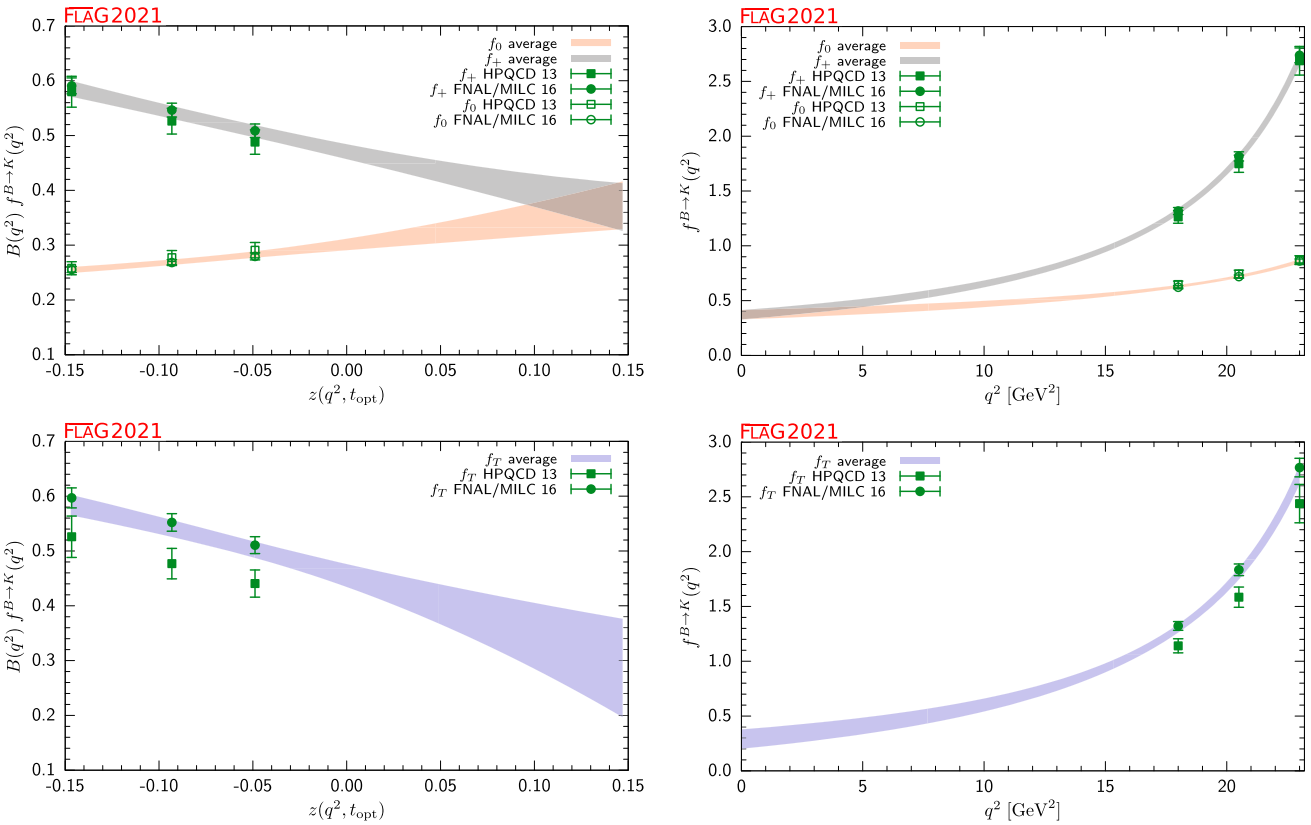

Fig. 33 The $B \to K$ form factors $f_+(q^2)$, $f_0(q^2)$ and $f_T(q^2)$ plotted versus z (left panels) and q^2 (right panels). In the plots as a function of z, we remove the Blaschke factors. See text for a discussion of the data sets. The grey, salmon and blue bands display our preferred $N^+ = N^0 = N^T = 3$ BCL fit (eight parameters)

As a consequence of the complexity of the problem, the level of maturity of these computations is significantly below the one present for pseudoscalar form factors. Therefore, we only provide a short guide to the existing results. Horgan et al. have obtained the seven form factors governing $B \to K^* \ell^+ \ell^-$ (as well as those for $B_s \to \phi\, \ell^+ \ell^-$ and for the charged-current decay $B_s \to K^* \ell \nu$) in Ref. [593] using NRQCD b quarks and asqtad staggered light quarks. In this work, they use a modified z-expansion to simultaneously extrapolate to the physical light-quark masses and fit the q^2-dependence. As discussed above, the unstable nature of the vector mesons was not taken into account. Horgan et al. use their form-factor results to calculate the differential branching fractions and angular distributions and discuss the implications for phenomenology in a companion paper [594]. An update of the form factor fits that enforces endpoint relations and also provides the full correlation matrices can be found in Ref. [595]. Finally, preliminary results on $B \to K^* \ell^+ \ell^-$ and $B_s \to \phi \ell^+ \ell^-$ by RBC/UKQCD have been reported in Refs. [596–598].

8.4 Semileptonic form factors for $B_{(s)} \to D_{(s)}\ell\nu$ and $B_{(s)} \to D^*_{(s)}\ell\nu$

The semileptonic processes $B_{(s)} \to D_{(s)}\ell\nu$ and $B_{(s)} \to D^*_{(s)}\ell\nu$ have been studied extensively by experimentalists and theorists over the years. They allow for the determination of the CKM matrix element $|V_{cb}|$, an extremely important parameter of the Standard Model. The matrix element V_{cb} appears in many quantities that serve as inputs to CKM unitarity triangle analyses and reducing its uncertainties is of paramount importance. For example, when ϵ_K, the measure of indirect CP violation in the neutral kaon system, is written in terms of the parameters ρ and η that specify the apex of the unitarity triangle, a factor of $|V_{cb}|^4$ multiplies the dominant term. As a result, the errors coming from $|V_{cb}|$ (and not those from B_K) are now the dominant uncertainty in the Standard Model (SM) prediction for this quantity.

The decay rate for $B \to D\ell\nu$ can be parameterized in terms of vector and scalar form factors in the same way as, e.g., $B \to \pi\ell\nu$ (see Sect. 8.3). The decay rate for $B \to D^*\ell\nu$ is different because the final-state hadron is spin-1. There are four form factors used to describe the vector and axial-vector current matrix elements that are needed to calculate this decay. We define the 4-velocity of the meson P as $v_P = p_P/m_P$ and the polarization vector of the D^* as ϵ. When the light lepton $\ell = e$, or μ, it is traditional to use $w = v_B \cdot v_{D^{(*)}}$ rather than q^2 as the variable upon which the form factors depend. Then, the form factors h_V and h_{A_i}, with $i = 1$, 2 or 3 are defined by

$$\langle D^*|V_\mu|B\rangle = \sqrt{m_B m_{D^*}}\, h_V(w)\varepsilon_{\mu\nu\alpha\beta}\epsilon^{*\nu}v^\alpha_{D^*}v^\beta_B, \tag{238}$$

$$\langle D^*|A_\mu|B\rangle = i\sqrt{m_B m_{D^*}}\left[h_{A_1}(w)(1+w)\epsilon^{*\mu} - h_{A_2}(w)\epsilon^*\cdot v_B v_{B\mu} - h_{A_3}(w)\epsilon^*\cdot v_B v_{D^*\mu}\right]. \tag{239}$$

The differential decay rates can then be written as[46]

$$\frac{d\Gamma_{B^-\to D^0\ell^-\bar\nu}}{dw} = \frac{G_F^2 m_D^3}{48\pi^3}(m_B + m_D)^2(w^2-1)^{3/2}|\eta_{\rm EW}|^2|V_{cb}|^2|\mathcal{G}(w)|^2, \tag{240}$$

$$\frac{d\Gamma_{B^-\to D^{0*}\ell^-\bar\nu}}{dw} = \frac{G_F^2 m_{D^*}^3}{4\pi^3}(m_B - m_{D^*})^2(w^2-1)^{1/2}|\eta_{\rm EW}|^2|V_{cb}|^2\chi(w)|\mathcal{F}(w)|^2, \tag{241}$$

where $w = v_B \cdot v_{D^{(*)}}$ (depending on whether the final-state meson is D or D^*) and $\eta_{\rm EW} = 1.0066$ is the 1-loop electroweak correction [599]. The function $\chi(w)$ in Eq. (241) depends on the recoil w and the meson masses, and reduces to unity at zero recoil [576].[47] These formulas do not include terms that are proportional to the lepton mass squared, which can be neglected for $\ell = e, \mu$. Further details of the definitions of $\mathcal{F}$ and $\mathcal{G}$ (which can be expressed in terms of the form factors h_V and h_{A_i}) may be found, e.g., in Ref. [576]. Until recently, most unquenched lattice calculations for $B \to D^*\ell\nu$ and $B \to D\ell\nu$ decays focused on the form factors at zero recoil $\mathcal{F}^{B\to D^*}(1)$ and $\mathcal{G}^{B\to D}(1)$; these can then be combined with experimental input to extract $|V_{cb}|$. The main reasons for concentrating on the zero recoil point are that (i) the decay rate then depends on a single form factor, and (ii) for $B \to D^*\ell\nu$, there are no $\mathcal{O}(\Lambda_{QCD}/m_Q)$ contributions due to Luke's theorem [600]. Further, the zero recoil form factor can be computed via a double ratio in which most of the current renormalization cancels and heavy-quark discretization errors are suppressed by an additional power of Λ_{QCD}/m_Q. Recent work on $B \to D^{(*)}\ell\nu$ transitions has started to explore the dependence of the relevant form factors on the momentum transfer, using a similar methodology to the one employed in $B \to \pi\ell\nu$ transitions; see Sect. 8.3 for a detailed discussion.

Early computations of the form factors for $B \to D\ell\nu$ decays include $N_f = 2+1$ results by FNAL/MILC [601,602] for $\mathcal{G}^{B\to D}(1)$ and the $N_f = 2$ study by Atoui et al. [603], that in addition to providing $\mathcal{G}^{B\to D}(1)$ explored the $w > 1$ region. This latter work also provided the first results for $B_s \to D_s\ell\nu$ amplitudes, again including information about the momentum-transfer dependence. The first published unquenched results for $\mathcal{F}^{B\to D^*}(1)$, obtained by FNAL/MILC, date from 2008 [604]. In 2014 and 2015, significant progress was achieved in $N_f = 2+1$ computations: the FNAL/MILC value for $\mathcal{F}^{B\to D^*}(1)$ was updated in Ref. [605], and full results for $B \to D\ell\nu$ at $w \geq 1$ were published by FNAL/MILC [606]

[46] These are the only meson decay channels dealt with in this review where we apply the Sirlin correction factor η_{EW}, that incorporates leading-order, structure-independent corrections. This is in keeping with common practice. While including η_{EW} in the analysis of $b \to c$ transitions is nearly universal in the literature, this is not so in other flavour-changing decays. It is worth stressing that this is just part of the expected corrections – cf. the discussion of QED corrections in the sections of this review dealing with light meson decay – and therefore its inclusion is largely arbitrary, insofar as a precise control of the full corrections, including the structure-dependent ones, is unavailable for a given channel. It is also necessary to remark, on the other hand, that different practices contribute to a small ambiguity in the comparison of CKM matrix elements determined from different decays, precisely of the order of the typically neglected electromagnetic corrections.

[47] The reason to keep the factor $\chi(w)$ outside the combination of form factors that defines $\mathcal{F}(w)$ is conventional, and inspired by the heavy-quark limit. One particular consequence of this notation is that at zero recoil $\mathcal{F}(1) = h_{A_1}(1)$.

and HPQCD [607]. These works also provided full results for the scalar form factor, allowing analysis of the decay with a final-state τ. In the FLAG 19 review [4], we included new results for $B_s \to D_s \ell\nu$ form factors over the full kinematic range for $N_f = 2+1$ from HPQCD [608,609], and for $B_{(s)} \to D^*_{(s)} \ell\nu$ form factors at zero recoil with $N_f = 2+1+1$ also from HPQCD [610,611]. Most recently, HPQCD published further new calculations of the $B_s \to D_s^*$ form factor at zero recoil [612] and of the $B_s \to D_s$ form factors in the full kinematic range [613], now using MILC's HISQ $N_f = 2+1+1$ ensembles and using the HISQ action also for the b quark. Both of these calculations have recently been used by LHCb to determine $|V_{cb}|$ [614,615], as discussed further in Sect. 8.9. Improved calculations of the $B \to D$ and $B_s \to D_s$ form factors are also underway by RBC/UKQCD [566], and the Fermilab/MILC computation of the $B \to D^*$ form factors at nonzero recoil is nearing completion [616]. The JLQCD collaboration also presented preliminary results for the $B \to D$ and $B \to D^*$ form factors, both at nonzero recoil [617].

In the discussion below, we mainly concentrate on the latest generation of results, which supersedes previous $N_f = 2+1$ determinations and allows for an extraction of $|V_{cb}|$ that incorporates information about the q^2-dependence of the decay rate (cf. Sect. 8.9).

8.4.1 $B_{(s)} \to D_{(s)}$ decays

We will first discuss the $N_f = 2+1$ computations of $B \to D\ell\nu$ by FNAL/MILC and HPQCD mentioned above, both based on MILC asqtad ensembles. Full details about all the computations are provided in Table 54 and in the tables in Appendix C.6.5.

The FNAL/MILC study [606] employs ensembles at four values of the lattice spacing ranging between approximately 0.045 fm and 0.12 fm, and several values of the light-quark mass corresponding to pions with RMS masses ranging between 260 MeV and 670 MeV (with just one ensemble with $M_\pi^{\rm RMS} \simeq 330$ MeV at the finest lattice spacing). The b and c quarks are treated using the Fermilab approach. The quantities directly studied are the form factors $h_\pm$ defined by

$$\frac{\langle D(p_D)|i\bar{c}\gamma_\mu b|B(p_B)\rangle}{\sqrt{m_D m_B}} = h_+(w)(v_B + v_D)_\mu + h_-(w)(v_B - v_D)_\mu, \tag{242}$$

which are related to the standard vector and scalar form factors by

$$f_+(q^2) = \frac{1}{2\sqrt{r}}\left[(1+r)h_+(w) - (1-r)h_-(w)\right], \tag{243}$$

$$f_0(q^2) = \sqrt{r}\left[\frac{1+w}{1+r}h_+(w) + \frac{1-w}{1-r}h_-(w)\right], \tag{244}$$

with $r = m_D/m_B$. (Recall that $q^2 = (p_B - p_D)^2 = m_B^2 + m_D^2 - 2wm_B m_D$.) The hadronic form factor relevant for experiment, $\mathcal{G}(w)$, is then obtained from the relation $\mathcal{G}(w) = \sqrt{4r}\, f_+(q^2)/(1+r)$. The form factors are obtained from double ratios of three-point functions in which the flavour-conserving current renormalization factors cancel. The remaining matching factor to the flavour-changing normalized current is estimated with 1-loop lattice perturbation theory. In order to obtain $h_\pm(w)$, a joint continuum-chiral fit is performed to an ansatz that contains the light-quark mass and lattice-spacing dependence predicted by next-to-leading order HMrSχPT, and the leading dependence on m_c predicted by the heavy-quark expansion ($1/m_c^2$ for h_+ and $1/m_c$ for h_-). The w-dependence, which allows for an interpolation in w, is given by analytic terms up to $(1-w)^2$, as well as a contribution from the logarithm proportional to $g^2_{D^*D\pi}$. The total resulting systematic error, determined as a function of w and quoted at the representative point $w = 1.16$ as 1.2% for f_+ and 1.1% for f_0, dominates the final error budget for the form factors. After f_+ and f_0 have been determined as functions of w within the interval of values of q^2 covered by the computation, synthetic data points are generated to be subsequently fitted to a z-expansion of the BGL form, cf. Sect. 8.3, with pole factors set to unity. This in turn enables one to determine $|V_{cb}|$ from a joint fit of this z-expansion and experimental data. The value of the zero-recoil form factor resulting from the z-expansion is

$$\mathcal{G}^{B\to D}(1) = 1.054(4)_{\rm stat}(8)_{\rm sys}. \tag{245}$$

The HPQCD computations [607,609] use ensembles at two values of the lattice spacing, $a = 0.09,\ 0.12$ fm, and two and three values of light-quark masses, respectively. The b quark is treated using NRQCD, while for the c quark the HISQ action is used. The form factors studied, extracted from suitable three-point functions, are

$$\langle D_{(s)}(p_{D_{(s)}})|V^0|B_{(s)}\rangle = \sqrt{2M_{B_{(s)}}}\, f_\parallel^{(s)}, \qquad \langle D_{(s)}(p_{D_{(s)}})|V^k|B_{(s)}\rangle = \sqrt{2M_{B_{(s)}}}\, p^k_{D_{(s)}} f_\perp^{(s)}, \tag{246}$$

where V_μ is the relevant vector current and the $B_{(s)}$ rest frame is chosen. The standard vector and scalar form factors are retrieved as

$$f_+^{(s)} = \frac{1}{\sqrt{2M_{B_{(s)}}}}\left[f_\parallel^{(s)} + (M_{B_{(s)}} - E_{D_{(s)}}) f_\perp^{(s)}\right], \tag{247}$$

$$f_0^{(s)} = \frac{\sqrt{2M_{B_{(s)}}}}{M^2_{B_{(s)}} - M^2_{D_{(s)}}}\left[(M_{B_{(s)}} - E_{D_{(s)}}) f_\parallel^{(s)} + (M^2_{B_{(s)}} - E^2_{D_{(s)}}) f_\perp^{(s)}\right]. \tag{248}$$

The currents in the effective theory are matched at 1-loop to their continuum counterparts. Results for the form factors are then fitted to a modified BCL z-expansion ansatz, that takes into account simultaneously the lattice spacing, light-quark masses, and q^2-dependence. For the mass dependence, NLO chiral logarithms are included, in the form obtained in hard-pion χPT (see footnote 33). As in the case of the FNAL/MILC computation, once f_+ and f_0 have been determined as functions of q^2, $|V_{cb}|$ can be determined from a joint fit of this z-expansion and experimental data. The papers quote for the zero-recoil vector form factor the result

$$\mathcal{G}^{B\to D}(1) = 1.035(40) \quad \mathcal{G}^{B_s\to D_s}(1) = 1.068(40). \tag{249}$$

The HPQCD and FNAL/MILC results for $B \to D$ differ by less than half a standard deviation (assuming they are uncorrelated, which they are not as some of the ensembles are common) primarily because of lower precision of the former result. The HPQCD central value is smaller by 1.8 of the FNAL/MILC standard deviations than the FNAL/MILC value. The dominant source of errors in the $|V_{cb}|$ determination by HPQCD are discretization effects and the systematic uncertainty associated with the perturbative matching.

In order to combine the form factor determinations of HPQCD and FNAL/MILC into a lattice average, we proceed in a similar way as with $B \to \pi\ell\nu$ and $B_s \to K\ell\nu$ above. FNAL/MILC quotes synthetic values for each form factor at three values of w (or, alternatively, q^2) with a full correlation matrix, which we take directly as input. In the case of HPQCD, we use their preferred modified z-expansion parameterization to produce synthetic values of the form factors at five different values of q^2 (three for f_+ and two for f_0). This leaves us with a total of six (five) data points in the kinematical range $w \in [1.00, 1.11]$ for the form factor f_+ (f_0). As in the case of $B \to \pi\ell\nu$, we conservatively assume a 100% correlation of statistical uncertainties between HPQCD and FNAL/MILC. We then fit this data set to a BCL ansatz, using $t_+ = (M_{B^0} + M_{D^\pm})^2 \simeq 51.12\ \text{GeV}^2$ and $t_0 = (M_{B^0} + M_{D^\pm})(\sqrt{M_{B^0}} - \sqrt{M_{D^\pm}})^2 \simeq 6.19\ \text{GeV}^2$. In our fits, pole factors have been set to unity, i.e., we do not take into account the effect of sub-threshold poles, which is then implicitly absorbed into the series coefficients. The reason for this is our imperfect knowledge of the relevant resonance spectrum in this channel, which does not allow us to decide the precise number of poles needed.[48] This, in turn, implies that unitarity bounds do not rigorously apply, which has to be taken into account when interpreting the results (cf. Appendix B.1).

With a procedure similar to what we adopted for the $B \to \pi$ and $B_s \to K$ cases, we impose the kinematic constraint at $q^2 = 0$ by expressing the $a^0_{N^0-1}$ coefficient in the z-expansion of f_0 in terms of all the other coefficients. As mentioned above, FNAL/MILC provides synthetic data for f_+ and f_0 including correlations; HPQCD presents the result of simultaneous z-fits to the two form factors including all correlations, thus enabling us to generate a complete set of synthetic data for f_+ and f_0. Since both calculations are based on MILC ensembles, we then reconstruct the off-diagonal HPQCD-FNAL/MILC entries of the covariance matrix by conservatively assuming that statistical uncertainties are 100% correlated. The Fermilab/MILC (HPQCD) statistical error is 58% (31%) of the total error for every f_+ value, and 64% (49%) for every f_0 one. Using this information we can easily build the off-diagonal block of the overall covariance matrix (e.g., the covariance between $[f_+(q_1^2)]_{\text{FNAL}}$ and $[f_0(q_2^2)]_{\text{HPQCD}}$ is $(\delta[f_+(q_1^2)]_{\text{FNAL}} \times 0.58)$ $(\delta[f_0(q_2^2)]_{\text{HPQCD}} \times 0.49)$, where δf is the total error).

For our central value, we choose an $N^+ = N^0 = 3$ BCL fit, shown in Table 52. The coefficient a_3^+ can be obtained from the values for a_0^+–a_2^+ using Eq. (531). We find $\chi^2/\text{dof} = 4.6/6 = 0.77$. The fit, which is dominated by the FNAL/MILC calculation, is illustrated in Fig. 34.

Reference [603] is the only existing $N_f = 2$ work on $B \to D\ell\nu$ transitions, that furthermore provided the first available results for $B_s \to D_s\ell\nu$. This computation uses the publicly available ETM configurations obtained with the twisted-mass QCD action at maximal twist. Four values of the lattice spacing, ranging between 0.054 and 0.098 fm, are considered, with

[48] As noted above, this is the same approach adopted by FNAL/MILC in their fits to a BGL ansatz. HPQCD, meanwhile, uses one single pole in the pole factors that enter their modified z-expansion, using their spectral studies to fix the value of the relevant resonance masses.

Table 52 Coefficients and correlation matrix for the $N^+ = N^0 = 3$ z-expansion of the $B \to D$ form factors f_+ and f_0. The chi-square per degree of freedom is $\chi^2/\text{dof} = 4.6/6 = 0.77$. The lattice calculations that enter this fit are taken from FNAL/MILC [606] and HPQCD [607]

$B \to D$ ($N_f = 2+1$)						
a_n^i	Central values	Correlation matrix				
a_0^+	0.896 (10)	1	0.423	−0.231	0.958	0.596
a_1^+	−7.94 (20)	0.423	1	0.325	0.498	0.919
a_2^+	51.4 (3.2)	−0.231	0.325	1	−0.146	0.317
a_0^0	0.7821 (81)	0.958	0.498	−0.146	1	0.593
a_1^0	−3.28 (20)	0.596	0.919	0.317	0.593	1

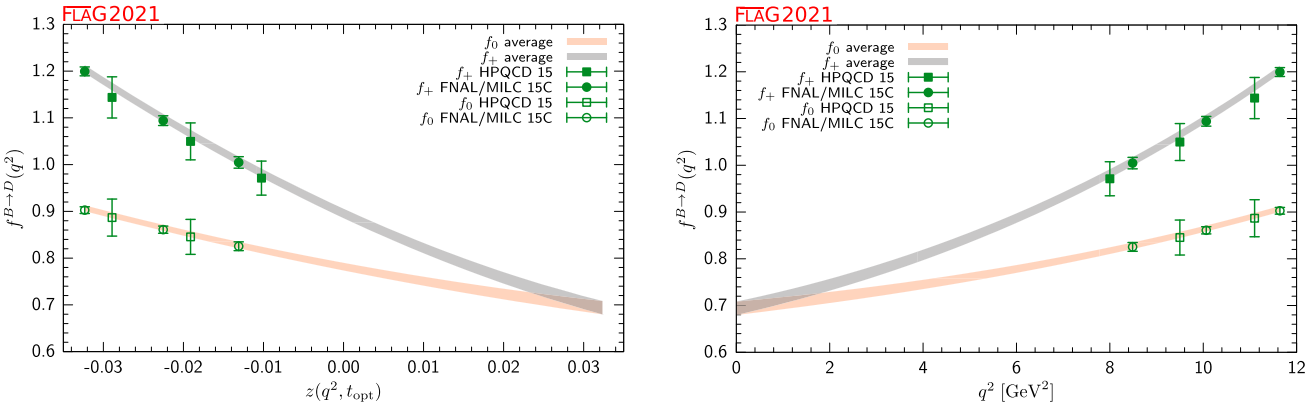

Fig. 34 The form factors $f_+(q^2)$ and $f_0(q^2)$ for $B \to D\ell\nu$ plotted versus z (left panel) and q^2 (right panel). See text for a discussion of the data sets. The grey and salmon bands display our preferred $N^+ = N^0 = 3$ BCL fit (five parameters)

physical box lengths ranging between 1.7 and 2.7 fm. At two values of the lattice spacing two different physical volumes are available. Charged-pion masses range between ≈ 270 and ≈ 490 MeV, with two or three masses available per lattice spacing and volume, save for the $a \approx 0.054$ fm point at which only one light mass is available for each of the two volumes. The strange- and heavy-valence quarks are also treated with maximally twisted-mass QCD.

The quantities of interest are again the form factors $h_\pm$ defined above. In order to control discretization effects from the heavy quarks, a strategy similar to the one employed by the ETM collaboration in their studies of B-meson decay constants (cf. Sect. 8.1) is employed: the value of $\mathcal{G}(w)$ is computed at a fixed value of m_c and several values of a heavier quark mass $m_h^{(k)} = \lambda^k m_c$, where λ is a fixed scaling parameter, and step-scaling functions are built as

$$\Sigma_k(w) = \frac{\mathcal{G}(w, \lambda^{k+1} m_c, m_c, a^2)}{\mathcal{G}(w, \lambda^k m_c, m_c, a^2)}. \tag{250}$$

Each ratio is extrapolated to the continuum limit, $\sigma_k(w) = \lim_{a\to 0} \Sigma_k(w)$. One then exploits the fact that the $m_h \to \infty$ limit of the step-scaling is fixed. In particular, it is easy to find from the heavy-quark expansion that $\lim_{m_h\to\infty} \sigma(1) = 1$. In this way, the physical result at the b-quark mass can be reached by interpolating $\sigma(w)$ between the charm region (where the computation can be carried out with controlled systematics) and the known static limit value.

In practice, the values of m_c and m_s are fixed at each value of the lattice spacing such that the experimental kaon and D_s masses are reached at the physical point, as determined in Ref. [618]. For the scaling parameter, $\lambda = 1.176$ is chosen, and eight scaling steps are performed, reaching $m_h/m_c = 1.176^9 \simeq 4.30$, approximately corresponding to the ratio of the physical b- and c-masses in the $\overline{\text{MS}}$ scheme at 2 GeV. All observables are obtained from ratios that do not require (re)normalization. The ansatz for the continuum and chiral extrapolation of Σ_k contains a constant and linear terms in $m_{\rm sea}$ and a^2. Twisted boundary conditions in space are used for valence-quark fields for better momentum resolution. Applying this strategy, the form factors are finally obtained at four reference values of w between 1.004 and 1.062, and, after a slight extrapolation to $w = 1$, the result is

$$\mathcal{G}^{B_s\to D_s}(1) = 1.052(46). \tag{251}$$

The authors also provide values for the form factor relevant for the meson states with light-valence quarks, obtained from a similar analysis to the one described above for the $B_s \to D_s$ case. Values are quoted from fits with and without a linear $m_{\rm sea}/m_s$ term in the chiral extrapolation. The result in the former case, which safely covers systematic uncertainties, is

$$\mathcal{G}^{B\to D}(1) = 1.033(95). \tag{252}$$

Given the identical strategy, and the small sensitivity of the ratios used in their method to the light valence- and sea-quark masses, we assign this result the same ratings in Table 54 as those for their calculation of $\mathcal{G}^{B_s\to D_s}(1)$. Currently, the precision of this calculation is not competitive with that of $N_f = 2+1$ works, but this is due largely to the small number of configurations analyzed by Atoui et al. The viability of their method has been clearly demonstrated, however, which leaves significant room for improvement on the errors of both the $B \to D$ and $B_s \to D_s$ form factors with this approach by including either additional two-flavour data or analysing more recent ensembles with $N_f > 2$.

Atoui et al. also study the scalar and tensor form factors, as well as the momentum-transfer dependence of $f_{+,0}$. The value of the ratio $f_0(q^2)/f_+(q^2)$ is provided at a reference value of q^2 as a proxy for the slope of $\mathcal{G}(w)$ around the zero-recoil limit.

Let us finally discuss the most recent results for $B_s \to D_s$ form factors, obtained by the HPQCD collaboration using MILC's $N_f = 2+1+1$ ensembles in Ref. [613]. Three values of the lattice spacing are used, including a very fine ensemble at $a \simeq 0.044$ fm; the pion mass is kept fixed at around 300 MeV, and in addition at the coarser $a \simeq 0.09$ fm lattice an ensemble with the physical pion mass is included. The scalar current needs no renormalization because of the PCVC relation, while the vector current is nonperturbatively normalized by imposing a condition based on the PCVC relation at zero recoil. Heavy quarks are treated in a fully relativistic fashion through the use of the HISQ regularization, employing bare values of the quark mass up to $am_h = 0.8$ for the extrapolation to the physical b point.

Results for the form factors are fitted to a modified z-expansion ansatz, based on a BCL ansatz with a Blaschke factor containing one sub-threshold pole, tuned to reproduce the lattice-spacing and heavy-quark-mass-dependent mass of the corresponding resonance. The final error budget is equally dominated by statistics and the combined effect of the continuum and heavy quark mass extrapolations, which correspond to 1.1% and 1.2% uncertainties, respectively, for the scalar form factor at zero recoil. The total uncertainty of the latter is thus below 2%, which remains true in the whole q^2 range. The uncertainty of f_+ is somewhat larger, starting at around 2% at $q^2 = 0$ and increasing up to around 3.5% at zero recoil.

One important matter of concern with this computation is the use of the $a \simeq 0.044$ fm ensemble with periodic boundary conditions, which suffers from severe topology freezing. Other than possible implications for statistical uncertainties, the lack of topology fluctuations are expected to significantly enhance finite-volume effects, which are no longer exponential in $m_\pi L$, but become power-like in the spatial volume. The authors neglect the impact of finite-volume effects in the computation, with a twofold argument: for the two coarser lattice spacings, the impact of pion-mass-related corrections on the heavy-meson states involved is presumably negligible; and, for the finest ensemble, the estimate of finite-volume effects on the D_s decay constant obtained in Ref. [142] turns out to be very small, a result which is presumed to extend to form factors. It is however unclear whether the latter argument would really hold, since the computation in Ref. [142] does show that the expected effect is heavily observable-dependent, reaching, e.g., more than 1% for f_D. We have, therefore, concluded that our standard criteria for finite-volume effects cannot be applied at the finest lattice spacing, and opted to assign ○ rating to them.

We thus proceed to quote the final result of HPQCD 19 as the FLAG estimate for the $N_f = 2+1+1$ $B_s \to D_s$ form factors. The preferred fit is a constrained BCL form with the imposition of the kinematical constraint $f_+(0) = f_0(0)$, carried through z^2 for f_0 and z^3 for f_+. Both form factors contain just one sub-threshold pole, to which the masses $M_{B_c^*} = 6.329$ GeV and $M_{B_{c0}} = 6.704$ GeV, respectively, have been assigned. The fit parameters and covariance matrix, quoted in Table VIII of Ref. [613], are reproduced in Table 53.

8.4.2 Lepton-flavour-universality ratios $R(D)$ and $R(D_s)$

The availability of results for the scalar form factor f_0 for $B \to D\ell\nu$ amplitudes allows us to study interesting observables that involve the decay in the τ channel. One such quantity is the ratio

$$R(D) = \frac{\mathcal{B}(B \to D\tau\nu)}{\mathcal{B}(B \to D\ell\nu)} \quad \text{with} \quad \ell = e, \mu, \tag{253}$$

which, in the Standard Model, depends only on the form factors and hadron and lepton masses. Indeed, the recent availability of experimental results for $R(D)$ has made this quantity particularly relevant in the search for possible physics beyond the

Table 53 Coefficients and correlation matrix for the z-expansion of the $B_s \to D_s$ form factors f_+ and f_0

$B_s \to D_s$ ($N_f = 2+1+1$)							
a_n^i	Central values	Correlation matrix					
a_0^0	0.666(12)	1	0.62004	0.03149	1	0.03973	0.00122
a_1^0	−0.26(25)	0.62004	1	0.36842	0.62004	0.12945	0.00002
a_2^0	−0.1(1.8)	0.03149	0.36842	1	0.03149	0.22854	-0.00168
a_0^+	−0.075(12)	1	0.62004	0.03149	1	0.03973	0.00122
a_1^+	−3.24(45)	0.03973	0.12945	0.22854	0.03973	1	0.11086
a_2^+	0.7(2.0)	0.00122	0.00002	−0.00168	0.00122	0.11086	1

Standard Model. The most recent HFLAV average reads [619]:

$$R(D)_{\text{exp}} = 0.340(27)(13). \tag{254}$$

HPQCD provides a Standard-Model prediction for $R(D)$ using the form factors from their 2015 lattice computation [607],

$$R(D)_{\text{lat}} = 0.300(8) \quad \text{Ref. [607]}. \tag{255}$$

The FNAL/MILC collaboration computed $R(D)$ using form factors from a combined fit of their lattice data and $B \to D\ell\nu$ experimental data:

$$R(D)_{\text{lat+exp}} = 0.299(11) \quad \text{Ref. [606]}. \tag{256}$$

Note that other authors have obtained even smaller uncertainties from fits including $B \to D\ell\nu$ experimental data, cf. the value $R(D)_{\text{lat+exp}} = 0.299(3)$ quoted in Ref. [620]. One important reason for this is that, while Refs. [606,607] only use the 2009 BaBar data in Refs. [620,621] also incorporates the more precise Belle 2015 data in Ref. [622].

If instead we take the lattice-only form factors from FNAL/MILC, we obtain

$$R(D)_{\text{lat}} = 0.285(15) \quad \text{Ref. [606]}. \tag{257}$$

(We average over electrons and muons in the denominator, which only affects the last digit.)

Finally, using the FLAG average of the $B \to D$ form factors discussed above, we find $R(D)_{\text{lat}}^{\text{FLAG}} = 0.2934(38)$. The ratio $R(D)$ requires the integral of the branching ratios for $\ell = e, \mu, \tau$ over the whole phase space. Since lattice simulations are sensitive mostly to relatively large q^2 values, lattice-only calculations of $R(D)$ rely on the extrapolation of the form factors to low q^2 and are especially sensitive to the choice of parameterization. In order to estimate this source of systematics, we repeated the fit using the parameterization adopted by HPQCD in Ref. [607]. The main difference with respect to our default paremeterization is the inclusion of Blaschke factors for the form factors f_+ and f_0 located at $M_+ = M_{B_c^*} = 6.330(9)$ GeV and $M_0 = 6.420(9)$ GeV; additionally, the parameter t_0 is set to $(m_B - m_D)^2$. Using five coefficients ($a_{1,2,3}^+$ and $a_{1,2}^0$ with a_3^0 fixed by the $f_+(q^2 = 0) = f_0(q^2 = 0)$ condition) we find $R(D)_{\text{lat}}^{\text{HPQCD}} = 0.3009(38)$ which deviates from $R(D)_{\text{lat}}^{\text{FLAG}}$ by $1.4\,\sigma$. To take this potential source of systematic uncertainty into account we rescale accordingly the uncertainty of our default fit and obtain:

$$R(D)_{\text{lat}} = 0.2934(53), \quad \text{our average}. \tag{258}$$

This result is about 1.5σ lower than the current experimental average [261] for this quantity. It has to be stressed that achieving this level of precision critically depends on the reliability with which the low-q^2 region is controlled by the parameterizations of the form factors.

After including the $B \to D\ell\nu$ ($\ell = e, \mu$) data in the fit, as discussed at the end of Sect. 8.9, we obtain the following combined lattice plus experiment result:

$$R(D)_{\text{lat+exp}} = 0.2951(31), \quad \text{our average}. \tag{259}$$

HPQCD also computes values for $R(D_s)$, the analog of $R(D)$ with both heavy-light mesons containing a strange quark. The earlier calculation using NRQCD b quarks gives

$$R(D_s)_{\text{lat}} = 0.301(6), \qquad N_f = 2+1 \ [609]. \tag{260}$$

The newer calculation with HISQ b quarks yields the somewhat more precise value

$$R(D_s)_{\text{lat}} = 0.2987(46), \qquad N_f = 2+1+1 \ [613]. \tag{261}$$

A similar ratio $R(D^*)$ can be considered for $B \to D^*$ transitions. As a matter of fact, the experimental value of $R(D^*)$ is significantly more accurate than the one of $R(D)$. A preliminary lattice-QCD-only prediction of $R(D^*)$ was shown by A. Vaquero [623].

8.4.3 Fragmentation fraction ratio f_s/f_d

Another area of immediate interest in searches for physics beyond the Standard Model is the measurement of $B_s \to \mu^+\mu^-$ decays, recently studied at the LHC. One of the inputs required by the LHCb analysis is the ratio of B_q meson ($q = d, s$) fragmentation fractions f_s/f_d, where f_q is the probability that a q quark hadronizes into a B_q. This ratio can be measured by writing it as a product of ratios that involve experimentally measurable quantities, cf. Refs. [624,625]. One of the factors is the ratio $f_0^{(s)}(M_\pi^2)/f_0^{(d)}(M_K^2)$ of scalar form factors for the corresponding semileptonic meson decay, which is where lattice input becomes useful.

A dedicated $N_f = 2+1$ study by FNAL/MILC[49] [626] addresses the ratios of scalar form factors $f_0^{(q)}(q^2)$, and quotes:

$$f_0^{(s)}(M_\pi^2)/f_0^{(d)}(M_K^2) = 1.046(44)(15), \qquad f_0^{(s)}(M_\pi^2)/f_0^{(d)}(M_\pi^2) = 1.054(47)(17), \tag{262}$$

where the first error is statistical and the second systematic. The more recent results from HPQCD [609] are:

$$f_0^{(s)}(M_\pi^2)/f_0^{(d)}(M_K^2) = 1.000(62), \qquad f_0^{(s)}(M_\pi^2)/f_0^{(d)}(M_\pi^2) = 1.006(62). \tag{263}$$

Results from both groups lead to fragmentation fraction ratios f_s/f_d that are consistent with LHCb's measurements via other methods [625].

8.4.4 $B_{(s)} \to D^*_{(s)}$ decays

The most precise computation of the zero-recoil form factors needed for the determination of $|V_{cb}|$ from exclusive B semileptonic decays comes from the $B \to D^*\ell\nu$ form factor at zero recoil $\mathcal{F}^{B\to D^*}(1)$, calculated by the FNAL/MILC collaboration. The original computation, published in Ref. [604], has been updated [605] by employing a much more extensive set of gauge ensembles and increasing the statistics of the ensembles originally considered, while preserving the analysis strategy. There are currently no final unquenched results for the relevant form factors at nonzero recoil, but work is in progress by FNAL/MILC [616] and JLQCD [617].

Reference [605] uses the MILC $N_f = 2+1$ ensembles. The bottom and charm quarks are simulated using the clover action with the Fermilab interpretation and light quarks are treated via the asqtad staggered fermion action. Recalling the definition of the form factors in Eq. (239), at zero recoil $\mathcal{F}^{B\to D^*}(1)$ reduces to a single form factor $h_{A_1}(1)$ coming from the axial-vector current

$$\langle D^*(v,\epsilon')|\mathcal{A}_\mu|\overline{B}(v)\rangle = i\sqrt{2m_B 2m_{D^*}}\ \epsilon'^*_\mu h_{A_1}(1), \tag{264}$$

where ϵ' is the polarization of the D^*. The form factor is accessed through a ratio of three-point correlators, viz.,

$$\mathcal{R}_{A_1} = \frac{\langle D^*|\bar{c}\gamma_j\gamma_5 b|\overline{B}\rangle\ \langle\overline{B}|\bar{b}\gamma_j\gamma_5 c|D^*\rangle}{\langle D^*|\bar{c}\gamma_4 c|D^*\rangle\ \langle\overline{B}|\bar{b}\gamma_4 b|\overline{B}\rangle} = |h_{A_1}(1)|^2. \tag{265}$$

[49] This work also provided a value for $R(D)$, now superseded by Ref. [606].

Simulation data is obtained on MILC ensembles with five lattice spacings, ranging from $a \approx 0.15$ fm to $a \approx 0.045$ fm, and as many as five values of the light-quark masses per ensemble (though just one at the finest lattice spacing). Results are then extrapolated to the physical, continuum/chiral, limit employing staggered χPT.

The D^* meson is not a stable particle in QCD and decays predominantly into a D plus a pion. Nevertheless, heavy-light meson χPT can be applied to extrapolate lattice simulation results for the $B \to D^* \ell\nu$ form factor to the physical light-quark mass. The D^* width is quite narrow, 0.096 MeV for the $D^{*\pm}(2010)$ and less than 2.1 MeV for the $D^{*0}(2007)$, making this system much more stable and long lived than the ρ or the K^* systems. The fact that the $D^* - D$ mass difference is close to the pion mass leads to the well-known "cusp" in $\mathcal{R}_{A_1}$ just above the physical pion mass [627–629]. This cusp makes the chiral extrapolation sensitive to values used in the χPT formulas for the $D^* D\pi$ coupling $g_{D^* D\pi}$. The error budget in Ref. [605] includes a separate error of 0.3% coming from the uncertainty in $g_{D^* D\pi}$ in addition to general chiral extrapolation errors in order to take this sensitivity into account.

The final value presented in Ref. [605] is

$$N_f = 2+1: \quad \mathcal{F}^{B\to D^*}(1) = 0.906(4)(12), \tag{266}$$

where the first error is statistical, and the second the sum of systematic errors added in quadrature, making up a total error of 1.4% (down from the original 2.6% of Ref. [604]). The largest systematic uncertainty comes from discretization errors followed by effects of higher-order corrections in the chiral perturbation theory ansatz.

In 2017, the HPQCD collaboration has published the first study of $B_{(s)} \to D^*_{(s)} \ell\nu$ form factors at zero recoil for $N_f = 2+1+1$ using eight MILC ensembles with lattice spacing $a \approx 0.15$ fm, 0.12 fm, and 0.09 fm [611]. There are three ensembles with varying light-quark masses for the two coarser lattice spacings and two choices of light-quark mass for the finest lattice spacing. In each case, there is one ensemble for which the light-quark mass is very close to the physical value. The b quark is treated using NRQCD and the light quarks are treated using the HISQ action. The resulting zero-recoil form factors are:

$$N_f = 2+1+1: \quad \mathcal{F}^{B\to D^*}(1) = 0.895(10)(24), \quad \mathcal{F}^{B_s\to D_s^*}(1) = 0.883(12)(28). \tag{267}$$

In 2019, the HPQCD collaboration published a new $N_f = 2+1+1$ calculation of the $B_s \to D_s^*$ form factor at zero recoil, now using the HISQ action also for the b quark [612]. The lattice methodology and ensembles used are the same as in their 2019 calculation of the $B_s \to D_s$ form factors [613], which was discussed in detail in Sect. 8.4.1. The resulting form factor is:

$$N_f = 2+1+1: \quad \mathcal{F}^{B_s\to D_s^*}(1) = 0.9020(96)(90). \tag{268}$$

The calculations in Refs. [611,612] use different b-quark actions and share only two ensambles at $a = 0.09$ fm and can be considered essentially independent, yielding the average:

$$N_f = 2+1+1: \quad \mathcal{F}^{B_s\to D_s^*}(1) = 0.899(12), \quad \text{our average.} \tag{269}$$

In recent years, the FNAL/MILC, HPQCD, and JLQCD collaborations have periodically reported about their efforts to determine the full momentum dependence of $B_{(s)} \to D^*_{(s)} \ell\nu$ form factors at Lattice conferences. JLQCD efforts are based on $N_f = 2+1$ Möbius domain-wall ensembles and a relativistic heavy quark action. The latest status update published in conference proceedings can be found in Ref. [617]. At the time of finalizing this review, FNAL/MILC and HPQCD have produced preprints with their final results for $B \to D^*$ and $B_s \to D_s^*$ form factors, respectively. The FNAL/MILC computation, Ref. [630] is based on $N_f = 2+1$ asqtad sea-quark ensembles with lattice spacing between approximately 0.15 and 0.045 fm, and uses a relativistic heavy-quark action with the Fermilab interpretation. The HPQCD computation, Ref. [631], is based on $N_f = 2+1+1$ HISQ ensembles, and uses the same regularization for heavy quarks. Upon publication of both works, we intend to include full details for them in an upcoming intermediate update of this section (Table 54).

8.5 Semileptonic form factors for $B_c \to (\eta_c, J/\psi)\ell\nu$ decays

In a recent publication, HPQCD 20B [632] provided the first full determination of $B_c \to J/\psi$ form factors, extending earlier preliminary work that also covered $B_c \to \eta_c$, Refs. [633,634]. While the latter employed both NRQCD and HISQ actions for the valence b quark, and the HISQ action for the c quark, in HPQCD 20B the HISQ action is used throughout for all flavors. The setup is the same as for the $B_s \to D_s$ computation discussed above, HPQCD 19; we refer to the entries for the

Table 54 Lattice results for mesonic processes involving $b \to c$ transitions

Collaboration	Refs.	N_f	Publication status	Continuum extrapolation	Chiral extrapolation	Finite volume	Renormalization	Heavy-quark treatment	$w = 1$ form factor/ratio	
HPQCD 15, HPQCD 17	[607,609]	2+1	A	○	○	○	○	✓	$\mathcal{G}^{B\to D}(1)$	1.035(40)
FNAL/MILC 15C	[606]	2+1	A	★	○	★	○	✓	$\mathcal{G}^{B\to D}(1)$	1.054(4)(8)
Atoui 13	[603]	2	A	★	○	★	–	✓	$\mathcal{G}^{B\to D}(1)$	1.033(95)
HPQCD 19	[613]	2+1+1	A	★	○	○*	✓	✓	$\mathcal{G}^{B_s\to D_s}(1)$	1.071(37)
HPQCD 15, HPQCD 17	[607,609]	2+1	A	○	○	○	○	✓	$\mathcal{G}^{B_s\to D_s}(1)$	1.068(40)
Atoui 13	[603]	2	A	★	○	★	–	✓	$\mathcal{G}^{B_s\to D_s}(1)$	1.052(46)
HPQCD 17B	[611]	2+1+1	A	○	★	★	○	✓	$\mathcal{F}^{B\to D^*}(1)$	0.895(10)(24)
FNAL/MILC 14	[605]	2+1	A	★	○	★	○	✓	$\mathcal{F}^{B\to D^*}(1)$	0.906(4)(12)
HPQCD 17B	[611]	2+1+1	A	○	★	★	○	✓	$\mathcal{F}^{B_s\to D_s^*}(1)$	0.883(12)(28)
HPQCD 19B	[612]	2+1+1	A	★	○	○*	✓	✓	$\mathcal{F}^{B_s\to D_s^*}(1)$	0.9020(96)(90)
HPQCD 15, HPQCD 17	[607,609]	2+1	A	○	○	○	○	✓	$\mathcal{G}^{B_s\to D_s}(1)$	1.068(40)
HPQCD 20B	[632]	2+1+1	A	★	○	○*	✓	✓	n/a	n/a
HPQCD 15, HPQCD 17	[607,609]	2+1	A	○	○	○	○	✓	$R(D)$	0.300(8)
FNAL/MILC 15C	[606]	2+1	A	★	○	★	○	✓	$R(D)$	0.299(11)

*The rationale for assigning a ○ rating is discussed in the text

latter paper in summary tables for details. The flavor singlet nature of the final state means that there are contributions to the relevant three-point functions from disconnected Wick contractions, which are not discussed in the paper.

There are however some relevant differences with $B_s \to D_s$ decays. In the J/ψ case, since the hadron in the final state has vector quantum numbers, the description of the hadronic amplitude requires four independent form factors V, A_0, A_1, A_2. Specifically,

$$\begin{aligned}
\langle J/\psi(p',\lambda)|\bar{c}\gamma^\mu b|B_c^-(p)\rangle &= \frac{2iV(q^2)}{M_{B_c}+M_{J/\psi}}\varepsilon^{\mu\nu\rho\sigma}\epsilon_\nu^*(p',\lambda)p'_\rho p_\sigma,\\
\langle J/\psi(p',\lambda)|\bar{c}\gamma^\mu\gamma^5 b|B_c^-(p)\rangle &= 2M_{J/\psi}A_0(q^2)\frac{\epsilon^*(p',\lambda)\cdot q}{q^2}q^\mu + (M_{B_c}+M_{J/\psi})A_1(q^2)\left[\epsilon^{*\mu}(p',\lambda) - \frac{\epsilon^*(p',\lambda)\cdot q}{q^2}q^\mu\right]\\
&\quad - A_2(q^2)\frac{\epsilon^*(p',\lambda)\cdot q}{M_{B_c}+M_{J/\psi}}\left[p^\mu + p'^\mu - \frac{M_{B_c}^2 - M_{J/\psi}^2}{q^2}q^\mu\right],
\end{aligned} \tag{270}$$

where ϵ_μ is the polarization vector of the J/ψ state. The computed form factors are fitted to a z-parameterization-inspired ansatz, where coefficients are modified to model the lattice-spacing and the heavy- and light-mass dependences, for a total of 280 fit parameters. In the continuum and at physical kinematics only 16 parameters survive, as each form factor is parameterized by an expression of the form

$$F(q^2) = \frac{1}{P(q^2)}\sum_{n=0}^{3} a_n z^n, \tag{271}$$

where the pole factor is given by

$$P(q^2) = \prod_k z(q^2, M_k^2) \tag{272}$$

with $\{M_k\}$ a different set of pole energies below the BD^* threshold for each set of J^P quantum numbers, taken from a mixture of experimental results, lattice determinations, and model estimates. The values used (in GeV) are

$$\begin{aligned} 0^- &: \ 6.275,\ 6.872,\ 7.25; \\ 1^- &: \ 6.335,\ 6.926,\ 7.02,\ 7.28; \\ 1^+ &: \ 6.745,\ 6.75,\ 7.15,\ 7.15. \end{aligned} \tag{273}$$

The outcome of the fit, that we quote as a FLAG estimate, is

	a_0	a_1	a_2	a_3
V	0.1057(55)	−0.746(92)	0.10(98)	0.006(1.000)
$A0$	0.1006(37)	−0.731(72)	0.30(90)	−0.02(1.00)
$A1$	0.0553(19)	−0.266(40)	0.31(70)	0.11(99)
$A2$	0.0511(91)	−0.22(19)	−0.36(82)	−0.05(1.00)

The correlation matrix for the coefficients is provided in Tables XIX–XXVII of Ref. [632]

8.6 Semileptonic form factors for $\Lambda_b \to (p, \Lambda_c^{(*)})\ell\bar{\nu}$ decays

The $b \to c\ell\bar{\nu}$ and $b \to u\ell\bar{\nu}$ transitions can also be probed in decays of Λ_b baryons. With the LHCb experiment, the final state of $\Lambda_b \to p\mu\bar{\nu}$ is easier to identify than that of $B \to \pi\mu\bar{\nu}$ [635], and the first determination of $|V_{ub}|/|V_{cb}|$ at the Large Hadron Collider was performed using a ratio of $\Lambda_b \to p\mu\bar{\nu}$ and $\Lambda_b \to \Lambda_c\mu\bar{\nu}$ decay rates [636] (cf. Sect. 8.10).

The amplitudes of the decays $\Lambda_b \to p\ell\bar{\nu}$ and $\Lambda_b \to \Lambda_c\ell\bar{\nu}$ receive contributions from both the vector and the axial-vector components of the current in the matrix elements $\langle p|\bar{u}\gamma^\mu(\mathbf{1}-\gamma_5)b|\Lambda_b\rangle$ and $\langle\Lambda_c|\bar{c}\gamma^\mu(\mathbf{1}-\gamma_5)b|\Lambda_b\rangle$. The matrix elements split into three form factors f_+, f_0, $f_\perp$ mediated by the vector component of the current, and another three form factors g_+, g_0, $g_\perp$ mediated by the axial-vector component – see, e.g., Ref. [511] for a complete description. Given the sensitivity to all Dirac structures, measurements of the baryonic decay rates also provides useful complementary constraints on right-handed couplings beyond the Standard Model [636].

To date, only one unquenched lattice-QCD computation of the $\Lambda_b \to p$ and $\Lambda_b \to \Lambda_c$ form factors with physical heavy-quark masses has been published: Detmold 15 [516]. This computation uses RBC/UKQCD $N_f = 2+1$ DWF ensembles, and treats the b and c quarks within the Columbia RHQ approach. The renormalization of the currents is carried out using a mostly nonperturbative method, with residual matching factors computed at one loop. Two values of the lattice spacing ($a \approx 0.11,\ 0.085$ fm) are considered, with the absolute scale set from the $\Upsilon(2S)$–$\Upsilon(1S)$ splitting. Sea pion masses lie in a narrow interval ranging from slightly above 400 MeV to slightly below 300 MeV, keeping $m_\pi L \gtrsim 4$; however, lighter pion masses are considered in the valence DWF action for the u, d quarks. The lowest valence-valence pion mass is 227(3) MeV, which leads to a ■ rating of finite-volume effects. Results for the form factors are obtained from suitable three-point functions, and fitted to a modified z-expansion ansatz that combines the q^2-dependence with the chiral and continuum extrapolations. The main results of the paper are the predictions (errors are statistical and systematic, respectively)

$$\zeta_{p\mu\bar{\nu}}(15\text{GeV}^2) \equiv \frac{1}{|V_{ub}|^2}\int_{15\ \text{GeV}^2}^{q^2_{\max}} \frac{\mathrm{d}\Gamma(\Lambda_b \to p\mu^-\bar{\nu}_\mu)}{\mathrm{d}q^2}\,\mathrm{d}q^2 = 12.31(76)(77)\ \text{ps}^{-1}, \tag{274}$$

$$\zeta_{\Lambda_c\mu\bar{\nu}}(7\text{GeV}^2) \equiv \frac{1}{|V_{cb}|^2}\int_{7\ \text{GeV}^2}^{q^2_{\max}} \frac{\mathrm{d}\Gamma(\Lambda_b \to \Lambda_c\mu^-\bar{\nu}_\mu)}{\mathrm{d}q^2}\,\mathrm{d}q^2 = 8.37(16)(34)\ \text{ps}^{-1}, \tag{275}$$

$$\frac{\zeta_{p\mu\bar{\nu}}(15\text{GeV}^2)}{\zeta_{\Lambda_c\mu\bar{\nu}}(7\text{GeV}^2)} = 1.471(95)(109), \tag{276}$$

which are the input for the LHCb analysis. Predictions for the total rates in all possible lepton channels, as well as for ratios similar to $R(D)$ (cf. Sect. 8.4) between the τ and light-lepton channels are also available, in particular,

$$R(\Lambda_c) = \frac{\Gamma(\Lambda_b \to \Lambda_c\,\tau^-\bar{\nu}_\tau)}{\Gamma(\Lambda_b \to \Lambda_c\,\mu^-\bar{\nu}_\mu)} = 0.3328(74)(70). \tag{277}$$

Datta 2017 [637] additionally includes results for the $\Lambda_b \to \Lambda_c$ tensor form factors $h_+, h_\perp, \widetilde{h}_+, \widetilde{h}_\perp$, based on the same lattice computation as Detmold 15 [516]. The main focus of Datta 2017 is the phenomenology of the $\Lambda_b \to \Lambda_c \tau \bar{\nu}_\tau$ decay and how it can be used to constrain contributions from beyond the Standard Model physics. Unlike in the case of the vector and axial-vector currents, the residual matching factors of the tensor currents are set to their tree-level value. While the matching systematic uncertainty is augmented to take this fact into account, the procedure implies that the tensor current retains an uncanceled logarithmic divergence at $\mathcal{O}(\alpha_s)$.

Recently, first lattice calculations have also been completed for Λ_b semileptonic decays to negative-parity baryons in the final state. Such calculations are substantially more challenging and have not yet reached the same level of precision. Meinel 21 [638] considers the decays $\Lambda_b \to \Lambda_c^*(2595)\ell\bar{\nu}$ and $\Lambda_b \to \Lambda_c^*(2625)\ell\bar{\nu}$, where the $\Lambda_c^*(2595)$ and $\Lambda_c^*(2625)$ are the lightest charm baryons with isospin 0 and $J^P = \frac{1}{2}^-$ and $J^P = \frac{3}{2}^-$, respectively. These decay modes may eventually provide new opportunities to test lepton-flavor universality at the LHC, but are also very interesting from a theoretical point of view. The lattice results for the form factors may help tighten dispersive constraints in global analyses of $b \to c$ semileptonic decays [639], and may provide new insights into the internal structure of the negative-parity heavy baryons and their description in heavy-quark-effective-theory. The $\Lambda_c^*(2595)$ and $\Lambda_c^*(2625)$ are very narrow resonances decaying through the strong interaction into $\Lambda_c\pi\pi$. The strong decays are neglected in Meinel 21 [638]. The calculation was performed using the same lattice actions as previously for $\Lambda_b \to \Lambda_c$, albeit with newly tuned RHQ parameters. Only three ensembles are used, with $a \approx 0.11,\ 0.08$ fm and pion masses in the range from approximately 300–430 MeV, with valence-quark masses equal to the sea-quark masses. Chiral-continuum extrapolations linear in m_π^2 and a^2 are performed, with systematic uncertainties estimated using higher-order fits. Finite-volume effects and effects associated with the strong decays of the Λ_c^*'s are not quantified. The calculation is done in the Λ_c^* rest frame, where the cubic symmetry is sufficient to avoid mixing with unwanted lower-mass states. As a consequence, the calculation is limited to a small kinematic region near the zero-recoil point $w = 1$. On each ensemble, lattice data were produced for two values of $w - 1$ of approximately 0.01 and 0.03. The final results for the form factors are parameterized as linear functions of $w - 1$ and can be found in Meinel 21 [638] and associated supplemental files.

8.7 Semileptonic form factors for $\Lambda_b \to \Lambda^{(*)}\ell\ell$

The decays $\Lambda_b \to \Lambda\ell^+\ell^-$ are mediated by the same underlying $b \to s\ell^+\ell^-$ FCNC transition as, for example, $B \to K\ell^+\ell^-$ and $B \to K^*\ell^+\ell^-$, and can therefore provide additional information on the hints for physics beyond the Standard Model seen in the meson decays. The Λ baryon in the final state decays through the weak interaction into $p\pi^-$ (or $n\pi^0$), leading to a wealth of angular observables even for unpolarized Λ_b. When including the effects of a nonzero Λ_b polarization, $\Lambda_b \to \Lambda(\to p\pi^-)\ell^+\ell^-$ decays are characterized by five angles leading to 34 angular observables [640], which have been measured by LHCb in the bin $q^2 \in [15, 20]\,\text{GeV}^2$ [641]. Given that the Λ is stable under the strong interactions, the $\Lambda_b \to \Lambda$ form factors parametrizing the matrix elements of local $\bar{s}\Gamma b$ currents can be calculated on the lattice with high precision using standard methods. Of course, the process $\Lambda_b \to \Lambda\ell^+\ell^-$ also receives contributions from nonlocal matrix elements of four-quark and quark-gluon operators in the weak effective Hamiltonian combined with the electromagnetic current. As with the mesonic $b \to s\ell^+\ell^-$ decays, these contributions cannot easily be calculated on the lattice and one relies on other theoretical tools for them, including the local OPE at high q^2 and a light-cone OPE/QCD factorization at low q^2.

Following an early calculation with static b quarks [642], Detmold 16 [643] provides results for all ten relativistic $\Lambda_b \to \Lambda$ form factors parametrizing the matrix elements of the local vector, axial-vector and tensor $b \to s$ currents. The lattice setup is identical to that used in the 2015 calculation of the $\Lambda_b \to p$ form factors in Detmold 15 [516], and similar considerations as in the previous section thus apply. The lattice data cover the upper 60% of the q^2 range, and the form factors are extrapolated to the full q^2 range using BCL z-expansion fits. This extrapolation is done simultaneously with the chiral and continuum extrapolations. The caveat regarding the renormalization of the tensor currents also applies here.

Reference [644] uses the lattice results for the $\Lambda_b \to \Lambda$ form factors together with the experimental results for $\Lambda_b \to \Lambda(\to p\pi^-)\mu^+\mu^-$ from LHCb [641,645] to perform fits of the $b \to s\mu^+\mu^-$ Wilson coefficients and of the Λ_b polarization parameter. Given the uncertainties (which are still dominated by experiment), the results for the Wilson coefficients are presently consistent both with the Standard-Model values and with the deviations seen in global fits that include all mesonic decays [646,647].

As with the $b \to c$ semileptonic form factors, a first lattice calculation, Meinel 2020 [648], was also recently completed for a $b \to s$ transition to a negative-parity baryon in the final state, in this case the $\Lambda^*(1520)$ with $J^P = \frac{3}{2}^-$ (no calculation has yet been published for the strange $J^P = \frac{1}{2}^-$ final states, which would be the broader and even more challenging $\Lambda^*(1405)/\Lambda^*(1380)$ [165]). The $\Lambda^*(1520)$ decays primarily to $pK^-/n\bar{K}^0$, $\Sigma\pi$, and $\Lambda\pi\pi$ with a total width of 15.6 ± 1.0

Table 55 Summary of computations of bottom baryon semileptonic form factors (see also Refs. [642,649] for calculations with static b quarks). The rationale for the ■ rating of finite-volume effects in Meinel 20 and 21 (despite meeting the ○ criterion based on the minimum pion mass) is that the unstable nature of the final-state baryons was neglected in the analysis

Process	Collaboration	Refs.	N_f	Publication status	Continuum extrapolation	Chiral extrapolation	Finite volume	Renormalization	Heavy-quark treatment
$\Lambda_b \to \Lambda_c^*(2625)\,\ell^-\bar{\nu}_\ell$	Meinel 21	[638]	2+1	A	○	○	■	○	✓
$\Lambda_b \to \Lambda_c^*(2595)\,\ell^-\bar{\nu}_\ell$	Meinel 21	[638]	2+1	A	○	○	■	○	✓
$\Lambda_b \to \Lambda^*(1520)\,\ell^+\ell^-$	Meinel 20	[648]	2+1	A	○	○	■	○	✓
$\Lambda_b \to \Lambda\,\ell^+\ell^-$	Detmold 16	[643]	2+1	A	○	○	■	○	✓
$\Lambda_b \to p\,\ell^-\bar{\nu}_\ell$	Detmold 15	[516]	2+1	A	○	○	■	○	✓
$\Lambda_b \to \Lambda_c\,\ell^-\bar{\nu}_\ell$	Detmold 15, Datta 17	[516,637]	2+1	A	○	○	■	○	✓

Table 56 Experimental measurements for $B(B^- \to \tau^-\bar{\nu})$. The first error on each result is statistical, while the second error is systematic

Collaboration	Tagging method	$B(B^- \to \tau^-\bar{\nu}) \times 10^4$
Belle [650]	Hadronic	$0.72^{+0.27}_{-0.25} \pm 0.11$
Belle [528]	Semileptonic	$1.25 \pm 0.28 \pm 0.27$
BaBar [527]	Hadronic	$1.83^{+0.53}_{-0.49} \pm 0.24$
BaBar [651]	Semileptonic	$1.7 \pm 0.8 \pm 0.2$

MeV [165] . The analysis of the lattice data again neglects the strong decays and does not quantify finite-volume effects, and is again limited to a small kinematic region near $q^2_{\max}$ (Table 55).

8.8 Determination of $|V_{ub}|$

We now use the lattice-determined Standard Model transition amplitudes for leptonic (Sect. 8.1) and semileptonic (Sect. 8.3) B-meson decays to obtain exclusive determinations of the CKM matrix element $|V_{ub}|$. In this section, we describe the aspect of our work that involves experimental input for the relevant charged-current exclusive decay processes. The relevant formulae are Eqs. (202) and (236). Among leptonic channels the only input comes from $B \to \tau\nu_\tau$, since the rates for decays to e and μ have not yet been measured. In the semileptonic case, we only consider $B \to \pi\ell\nu$ transitions (experimentally measured for $\ell = e, \mu$).

We first investigate the determination of $|V_{ub}|$ through the $B \to \tau\nu_\tau$ transition. This is the only experimentally measured leptonic decay channel of the charged B meson. The experimental measurements of the branching fraction of this channel, $B(B^- \to \tau^-\bar{\nu})$, have not been updated since the publication of the FLAG Review in 2016 [3]. The status of the experimental results for this branching fraction, summarized in Table 56, is unchanged from FLAG Review 16 [3]. Our corresponding values of $|V_{ub}|$ are unchanged from FLAG Review 19 [4].

It is obvious that all the measurements listed in Table 56 have significance smaller than 5σ, and the large uncertainties are dominated by statistical errors. These measurements lead to the averages of experimental measurements for $B(B^- \to \tau\bar{\nu})$ [527,528],

$$B(B^- \to \tau\bar{\nu}) \times 10^4 = 0.91 \pm 0.22 \quad \text{from Belle}, \tag{278}$$

$$= 1.79 \pm 0.48 \text{ from BaBar}, \tag{279}$$

$$= 1.06 \pm 0.33 \text{ average}, \tag{280}$$

where, following our standard procedure we perform a weighted average and rescale the uncertainty by the square root of the reduced chi-squared. Note that the Particle Data Group [164] did not inflate the uncertainty in the calculation of the averaged branching ratio.

Combining the results in Eqs. (278–280) with the experimental measurements of the mass of the τ-lepton and the B-meson lifetime and mass we get

$$|V_{ub}| f_B = 0.72 \pm 0.09 \text{ MeV from Belle}, \tag{281}$$
$$= 1.01 \pm 0.14 \text{ MeV from BaBar}, \tag{282}$$
$$= 0.77 \pm 0.12 \text{ MeV average}, \tag{283}$$

which can be used to extract $|V_{ub}|$, viz.,

$$N_f = 2 \quad \text{Belle } B \to \tau \nu_\tau : \quad |V_{ub}| = 3.83(14)(48) \times 10^{-3}, \tag{284}$$
$$N_f = 2+1 \quad \text{Belle } B \to \tau \nu_\tau : \quad |V_{ub}| = 3.75(8)(47) \times 10^{-3}, \tag{285}$$
$$N_f = 2+1+1 \quad \text{Belle } B \to \tau \nu_\tau : \quad |V_{ub}| = 3.79(3)(47) \times 10^{-3}; \tag{286}$$
$$N_f = 2 \quad \text{Babar } B \to \tau \nu_\tau : \quad |V_{ub}| = 5.37(20)(74) \times 10^{-3}, \tag{287}$$
$$N_f = 2+1 \quad \text{Babar } B \to \tau \nu_\tau : \quad |V_{ub}| = 5.26(12)(73) \times 10^{-3}, \tag{288}$$
$$N_f = 2+1+1 \quad \text{Babar } B \to \tau \nu_\tau : \quad |V_{ub}| = 5.32(4)(74) \times 10^{-3}, \tag{289}$$
$$N_f = 2 \quad \text{average } B \to \tau \nu_\tau : \quad |V_{ub}| = 4.10(15)(64) \times 10^{-3}, \tag{290}$$
$$N_f = 2+1 \quad \text{average } B \to \tau \nu_\tau : \quad |V_{ub}| = 4.01(9)(63) \times 10^{-3}, \tag{291}$$
$$N_f = 2+1+1 \quad \text{average } B \to \tau \nu_\tau : \quad |V_{ub}| = 4.05(3)(64) \times 10^{-3}, \tag{292}$$

where the first error comes from the uncertainty in f_B and the second comes from experiment.

Let us now turn our attention to semileptonic decays. The experimental value of $|V_{ub}| f_+(q^2)$ can be extracted from the measured branching fractions for $B^0 \to \pi^\pm \ell \nu$ and/or $B^\pm \to \pi^0 \ell \nu$ applying Eq. (236);[50] $|V_{ub}|$ can then be determined by performing fits to the constrained BCL z-parameterization of the form factor $f_+(q^2)$ given in Eq. (532). This can be done in two ways: one option is to perform separate fits to lattice and experimental results, and extract the value of $|V_{ub}|$ from the ratio of the respective a_0 coefficients; a second option is to perform a simultaneous fit to lattice and experimental data, leaving their relative normalization $|V_{ub}|$ as a free parameter. We adopt the second strategy, because it combines the lattice and experimental input in a more efficient way, leading to a smaller uncertainty on $|V_{ub}|$.

The available state-of-the-art experimental input consists of five data sets: three untagged measurements by BaBar (6-bin [652] and 12-bin [653]) and Belle [654], all of which assume isospin symmetry and provide combined $B^0 \to \pi^-$ and $B^+ \to \pi^0$ data; and the two tagged Belle measurements of $\bar{B}^0 \to \pi^+$ (13-bin) and $B^- \to \pi^0$ (7-bin) [655]. Including all of them, along with the available information about cross-correlations, will allow us to obtain a meaningful final error estimate.[51] The lattice input data set will be the same discussed in Sect. 8.3.

We perform a constrained BCL fit of the vector and scalar form factors (this is necessary in order to take into account the $f_+(q^2 = 0) = f_0(q^2 = 0)$ constraint) together with the combined experimental data sets. We find that the error on $|V_{ub}|$ stabilizes for $N^+ = N^0 = 3$. The result of the combined fit is presented in Table 57. The fit has a chi-square per degree of freedom $\chi^2/\text{dof} = 78.7/56 = 1.41$. Following the PDG recommendation we rescale the whole covariance matrix by χ^2/dof: the errors on the z-parameters are increased by $\sqrt{\chi^2/\text{dof}} = 1.19$ and the correlation matrix is unaffected.

In Fig. 35, we show both the lattice and experimental data for $(1 - q^2/m^2_{B^*}) f_+(q^2)$ as a function of $z(q^2)$, together with our preferred fit; experimental data has been rescaled by the resulting value for $|V_{ub}|^2$. It is worth noting the good consistency between the form factor shapes from lattice and experimental data. This can be quantified, e.g., by computing the ratio of the two leading coefficients in the constrained BCL parameterization: the fit to lattice form factors yields $a_1^+/a_0^+ = -1.67(35)$ (cf. the results presented in Sect. 8.3.1), while the above lattice+experiment fit yields $a_1^+/a_0^+ = -1.19(13)$.

[50] Since $\ell = e, \mu$ the contribution from the scalar form factor in Eq. (236) is negligible.

[51] See, e.g., Sec. V.D of Ref. [556] for a detailed discussion.

Table 57 $|V_{ub}|$, coefficients for the $N^+ = N^0 = N^T = 3$ z-expansion of the $B \to \pi$ form factors f_+ and f_0, and their correlation matrix. The chi-square per degree of freedom is $\chi^2/\text{dof} = 78.7/56 = 1.41$ and the errorson the fit parameters have been rescaled by $\sqrt{\chi^2/\text{dof}} = 1.19$. The lattice calculations that enter this fit are taken from FNAL/MILC [556] and RBC/UKQCD [557]. The experimental inputs are taken from BaBar [652,653] and Belle [654,655]

$B \to \pi\ell\nu$ ($N_f = 2+1$)							
	Central values	Correlation matrix					
$V_{ub} \times 10^3$	3.74 (17)	1	−0.851	−0.349	0.375	−0.211	−0.246
a_0^+	0.415 (14)	−0.851	1	0.155	−0.454	0.260	0.144
a_1^+	−0.488 (53)	−0.349	0.155	1	−0.802	−0.0962	0.220
a_2^+	−0.31 (18)	0.375	−0.454	−0.802	1	0.0131	−0.100
a_0^0	0.500 (23)	−0.211	0.260	−0.0962	0.0131	1	−0.453
a_1^0	−1.424 (54)	−0.246	0.144	0.220	−0.100	−0.453	1

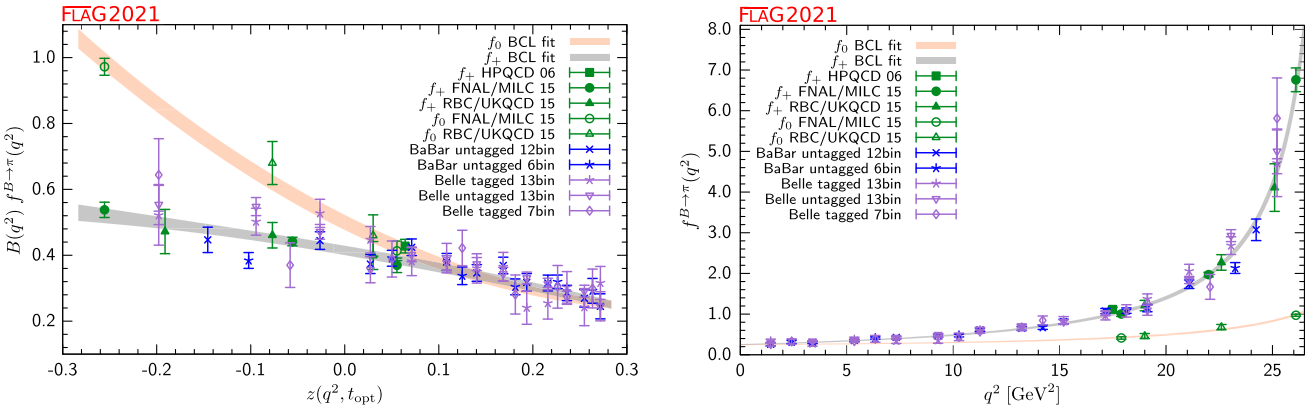

Fig. 35 Lattice and experimental data for $f_+^{B\to\pi}(q^2)$ and $f_0^{B\to\pi}(q^2)$ versus z (left panel) and q^2 (right panel). Experimental data has been rescaled by the value for $|V_{ub}|$ found from the joint fit. Green symbols denote lattice-QCD points included in the fit, while blue and indigo points show experimental data divided by the value of $|V_{ub}|$ obtained from the fit. The grey and orange bands display the preferred $N^+ = N^0 = 3$ BCL fit (five z-parameters and $|V_{ub}|$)

We plot the values of $|V_{ub}|$ we have obtained in Fig. 37, where the GGOU [656] determination through inclusive decays, $|V_{ub}|_{\rm incl} = (4.32 \pm 0.12_{\rm exp} \pm 0.13_{\rm theo} \pm 0.23_{\Delta BF}) \times 10^{-3}$ [165,261] (the ΔBF error has been added in Ref. [165] to account for the spread in results obtained using different theoretical models), is also shown for comparison.[52] In this plot the tension between the BaBar and the Belle measurements of $B(B^- \to \tau^-\bar\nu)$ is manifest. As discussed above, it is for this reason that we do not extract $|V_{ub}|$ through the average of results for this branching fraction from these two collaborations. In fact this means that a reliable determination of $|V_{ub}|$ using information from leptonic B-meson decays is still absent; the situation will only clearly improve with the more precise experimental data expected from Belle II [657,658]. The value for $|V_{ub}|$ obtained from semileptonic B decays for $N_f = 2+1$, on the other hand, is significantly more precise than both the leptonic and the inclusive determinations, and exhibits a $\sim 1.7\sigma$ tension with the latter.

8.9 Determination of $|V_{cb}|$

We will now use the lattice-QCD results for the $B \to D^{(*)}\ell\nu$ form factors in order to obtain determinations of the CKM matrix element $|V_{cb}|$ in the Standard Model. The relevant formulae are given in Eq. (241).

Let us summarize the lattice input that satisfies FLAG requirements for the control of systematic uncertainties, discussed in Sect. 8.4. In the (experimentally more precise) $B \to D^*\ell\nu$ channel, there is only one $N_f = 2+1$ lattice computation of the relevant form factor $\mathcal{F}^{B\to D^*}$ at zero recoil. Concerning the $B \to D\ell\nu$ channel, for $N_f = 2$ there is one determination of the relevant form factor $\mathcal{G}^{B\to D}$ at zero recoil, while for $N_f = 2+1$ there are two determinations of the $B \to D$ form

[52] Note that a recent Belle measurement of partial $B \to X_u\ell^+\nu_\ell$ branching fractions which superseeds their previous result and which yields the somewhat lower value $|V_{ub}| = 4.10(9)(22)(15) \times 10^{-3}$, has not been included in the HFLAV average yet.

factor as a function of the recoil parameter in roughly the lowest third of the kinematically allowed region. In this latter case, it is possible to replicate the analysis carried out for $|V_{ub}|$ in Sect. 8.8, and perform a joint fit to lattice and experimental data; in the former, the value of $|V_{cb}|$ has to be extracted by matching to the experimental value for $\mathcal{F}^{B\to D^*}(1)\eta_{\rm EW}|V_{cb}|$ and $\mathcal{G}^{B\to D}(1)\eta_{\rm EW}|V_{cb}|$.

The latest experimental average by HFLAV [619] for the $B \to D^*$ form factor at zero recoil makes use of the CLN [659] parameterization of the $B \to D^*$ form factor and is

$$[\mathcal{F}^{B\to D^*}(1)\eta_{\rm EW}|V_{cb}|]_{\rm CLN,HFLAV} = 35.61(43) \times 10^{-3}. \tag{293}$$

Recently the Belle collaboration presented an updated measurement of the $B \to D^*\ell\nu$ branching ratio [660] in which, as suggested in Refs. [661–663], the impact of the form factor parameterization has been studied by comparing the CLN [659] and BGL [569,664] ansätze. The fit results using the two parameterizations are now consistent. In light of the fact that the BGL parameterization has a much stronger theoretical standing than the CLN one and that it imposes less stringent constraints on the shape of the form factors, we do not consider the CLN determination any further and focus on the BGL fit:

$$[\mathcal{F}^{B\to D^*}(1)\eta_{\rm EW}|V_{cb}|]_{\rm BGL,\ Belle} = 35.44(23)(60) \times 10^{-3}, \tag{294}$$

where the first error is statistical and the second is systematic.[53] Given the fact that the two determinations in Eqs. (293) and (294) are quite compatible and that the BGL parameterization is on firmer theoretical ground, in the following we present the determination of $|V_{cb}|$ obtained from Eq. (294). We refer to the discussion presented at the end of Sec. 8.8 of the previous edition of this review [4] for further comments on the CLN and BGL parameterizations.

By using $\eta_{\rm EW} = 1.00662$[54] and the $N_f = 2+1$ lattice value for $\mathcal{F}^{B\to D^*}(1)$ in Eq. (266)[55], we thus extract the average

$$N_f = 2+1 [B \to D^*\ell\nu]_{\rm BGL,Belle}: \qquad |V_{cb}| = 38.86(54)(70) \times 10^{-3}, \tag{295}$$

where the first uncertainty comes from the lattice computation and the second from the experimental input.

For the zero-recoil $B \to D$ form factor, HFLAV [619] quotes

$$\text{HFLAV:} \quad \mathcal{G}^{B\to D}(1)\eta_{\rm EW}|V_{cb}| = 41.57(45)(89) \times 10^{-3}, \tag{296}$$

yielding the following average for $N_f = 2$:

$$N_f = 2 \qquad B \to D\ell\nu: \qquad |V_{cb}| = 40.0(3.7)(1.0) \times 10^{-3}, \tag{297}$$

where the first uncertainty comes from the lattice computation and the second from the experimental input.

Finally, for $N_f = 2+1$ we perform, as discussed above, a joint fit to the available lattice data, discussed in Sect. 8.4, and state-of-the-art experimental determinations. In this case, we will combine the aforementioned Belle measurement [666], which provides partial integrated decay rates in 10 bins in the recoil parameter w, with the 2010 BaBar data set in Ref. [667], which quotes the value of $\mathcal{G}^{B\to D}(w)\eta_{\rm EW}|V_{cb}|$ for ten values of w.[56] The fit is dominated by the more precise Belle data; given this, and the fact that only partial correlations among systematic uncertainties are to be expected, we will treat both data sets as uncorrelated.[57]

A constrained ($N^+ = N^0 = 3$) BCL fit using the same ansatz as for lattice-only data in Sect. 8.4, yields our average, which we present in Table 58. The chi-square per degree of freedom is $\chi^2/\text{dof} = 20.0/25 = 0.80$. The fit is illustrated in

[53] Note that the BGL fit employed by Belle uses very few z parameters and that this could lead to an underestimation of the error on $[\mathcal{F}^{B\to D^*}(1)\eta_{\rm EW}|V_{cb}|]$. See Ref. [665] for a through review of this point.

[54] Note that this determination does not include the electromagnetic Coulomb correction roughly estimated in Ref. [605]. Currently the numerical impact of this correction is negligible.

[55] In light of our policy not to average $N_f = 2+1$ and $N_f = 2+1+1$ calculations and of the controversy over the use of the CLN vs. BGL parameterizations, we prefer to simply use only the more precise $N_f = 2+1$ determination of $\mathcal{F}^{B\to D^*}(1)$ in Eq. (266) for the extraction of V_{cb}.

[56] We thank Marcello Rotondo for providing the ten bins result of the BaBar analysis.

[57] We have checked that results using just one experimental data set are compatible within 1σ. In the case of BaBar, we have taken into account the introduction of some EW corrections in the data.

Table 58 $|V_{cb}|$, coefficients for the $N^+ = N^0$ z-expansion of the $B \to D$ form factors f_+ and f_0, and their correlation matrix. The coefficient a_2^0 is fixed by the $f_+(q^2 = 0) = f_0(q^2 = 0)$ constrain. The chi-square per degree offreedom is $\chi^2/\text{dof} = 20.0/25 = 0.80$. The lattice calculations that enter this fit are taken from FNAL/MILC [606] and HPQCD [607]. The experimental inputs are taken from BaBar [667] and Belle [666]

$B \to D\ell\nu$ ($N_f = 2+1$)							
	Central values	Correlation matrix					
$\|V_{cb}\| \times 10^3$	40.0 (1.0)	1.00	−0.525	−0.339	0.0487	−0.521	−0.433
a_0^+	0.8946 (94)	−0.525	1.00	0.303	−0.351	0.953	0.529
a_1^+	−8.03 (16)	−0.339	0.303	1.00	0.203	0.375	0.876
a_2^+	50.1 (3.1)	0.0487	−0.351	0.203	1.00	−0.276	0.196
a_0^0	0.7804 (75)	−0.521	0.953	0.375	−0.276	1.0	0.502
a_1^0	−3.38 (16)	−0.433	0.529	0.876	0.196	0.502	1.0

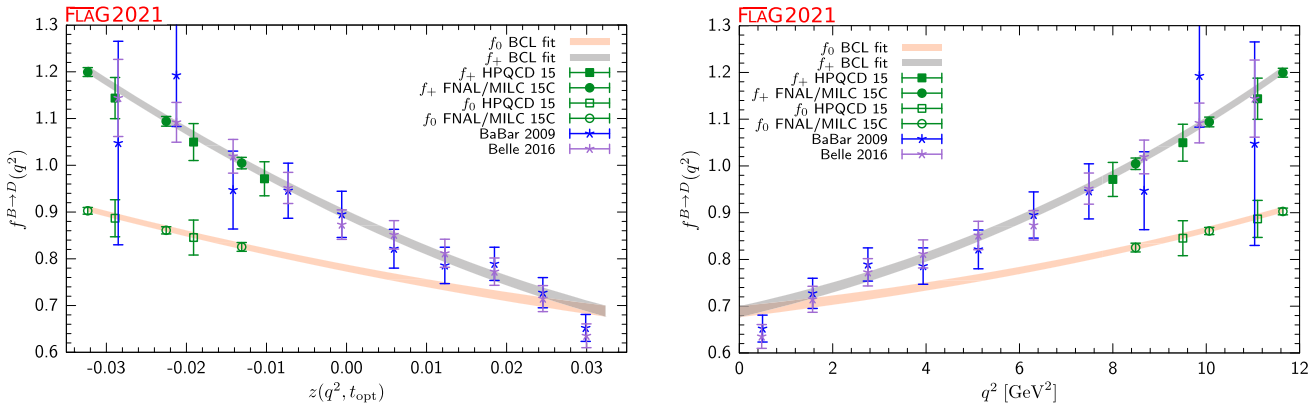

Fig. 36 Lattice and experimental data for $f_+^{B\to D}(q^2)$ and $f_0^{B\to D}(q^2)$ versus z (left panel) and q^2 (right panel). Green symbols denote lattice-QCD points included in the fit, while blue and indigo points show experimental data divided by the value of $|V_{cb}|$ obtained from the fit. The grey and orange bands display the preferred $N^+ = N^0 = 3$ BCL fit (five z-parameters and $|V_{cb}|$)

Fig. 36. In passing, we note that, if correlations between the FNAL/MILC and HPQCD calculations are neglected, the $|V_{cb}|$ central value rises to 40.3×10^{-3} in nice agreement with the results presented in Ref. [620].

Before discussing the combination of the above $|V_{cb}|$ results, we note that the LHCb Collaboration recently reported the first determination of $|V_{cb}|$ at the Large Hadron Collider using $B_s \to D_s^- \mu^+ \nu_\mu$ and $B_s \to D_s^{*-} \mu^+ \nu_\mu$ decays [614,615]. The differential decay rates, in combination with the $N_f = 2+1+1$ HPQCD 19 [613] and HPQCD 19B [612] lattice results for $f_+^{B_s\to D_s}$ and $\mathcal{F}^{B_s\to D_s^*}(1)$, were analyzed using either the CLN or BGL form-factor parameterizations. The result for $|V_{cb}|$ from the BGL fit is [615]

$$|V_{cb}| \times 10^3 = (41.7 \pm 0.8 \pm 0.9 \pm 1.1) \quad B_s \to D_s^{(*)-} \mu^+ \nu_\mu, \text{ BGL, LHCb.} \tag{298}$$

The LHCb analysis used ratios to the reference decay modes $B^0 \to D^- \mu^+ \nu_\mu$ and $B^0 \to D^{*-} \mu^+ \nu_\mu$, whose branching fractions are used as input in the form of the Particle Data Group averages of measurements by other experiments [431]. The result (298) is therefore correlated with the determinations of $|V_{cb}|$ from $B \to D$ and $B \to D^*$ semileptonic decays. Given the challenges involved in performing our own fit to the LHCb data, we do not, at present, include the LHCb results for $B_s \to D_s^- \mu^+ \nu_\mu$ and $B_s \to D_s^{*-} \mu^+ \nu_\mu$ in our combination of $|V_{cb}|$.

We now proceed to combine the determinations of $|V_{cb}|$ from exclusive $B \to D$ and $B \to D^*$ semileptonic decays. To this end, we need to estimate the correlation between the lattice uncertainties in the two modes. We assume conservatively that the statistical component of the lattice error in both determinations are 100% correlated because they are based on the same MILC configurations (albeit on different subsets). We obtain:

$$|V_{cb}| \times 10^3 = 39.36(68) \quad \text{BGL, Belle.} \tag{299}$$

Table 59 Results for $|V_{cb}|$. When two errors are quoted in our averages, the first one comes from the lattice form factor, and the second from the experimental measurement. The LHCb result using $B_s \to D_s^{(*)}\ell\nu$ decays [612–615], as well as the inclusive average obtained in the kinetic scheme from Ref. [668] are shown for comparison

	From	$\|V_{cb}\| \times 10^3$
Our average for $N_f = 2+1$ (BGL)	$B \to D^*\ell\nu$	38.86(54)(70)
Our average for $N_f = 2+1$	$B \to D\ell\nu$	40.0(1.0)
Our average for $N_f = 2+1$ (BGL)	$B \to (D, D^*)\ell\nu$	39.36(68)
Our average for $N_f = 2$	$B \to D\ell\nu$	40.0(3.7)(1.0)
LHCb result for $N_f = 2+1+1$ (BGL)	$B_s \to D_s^{(*)}\ell\nu$	41.7(0.8)(0.9)(1.1)
Gambino et al.	$B \to X_c\ell\nu$	42.00(64)

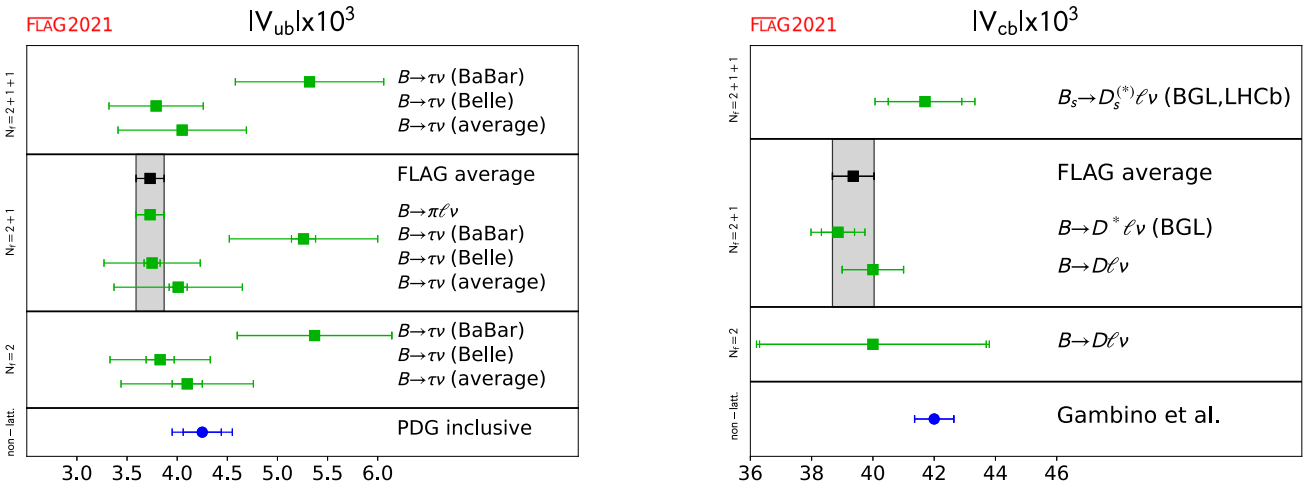

Fig. 37 Left: Summary of $|V_{ub}|$ determined using: i) the B-meson leptonic decay branching fraction, $B(B^- \to \tau^-\bar{\nu})$, measured at the Belle and BaBar experiments, and our averages for f_B from lattice QCD; and ii) the various measurements of the $B \to \pi\ell\nu$ decay rates by Belle and BaBar, and our averages for lattice determinations of the relevant vector form factor $f_+(q^2)$. Right: Same for determinations of $|V_{cb}|$ using semileptonic decays. The inclusive results are taken from Refs. [619,668]

Our results are summarized in Table 59, which also shows the HFLAV inclusive determination of $|V_{cb}| = 42.00(64) \times 10^{-3}$ [668] for comparison, and illustrated in Fig. 37. Finally, using the fit results in Table 59, we extract a value for $R(D)$ which includes both lattice and experimental information:

$$R(D)_{\text{lat+exp}} = 0.2951(31), \quad \text{our average.} \tag{300}$$

Note that we do not need to rescale the uncertainty on $R(D)_{\text{lat+exp}}$ because, after the inclusion of experimental $B \to D\ell\nu$ ($\ell = e, \mu$) results, the shift in central value caused by using a different parameterization is negligible (see the discussion above Eq. (258)).

8.10 Determination of $|V_{ub}/V_{cb}|$ from Λ_b decays

In 2015, the LHCb Collaboration reported a measurement of the ratio [636]

$$R_{\text{BF}}(\Lambda_b) = \frac{\displaystyle\int_{15\ \text{GeV}^2}^{q^2_{\text{max}}} \frac{\mathrm{d}\mathcal{B}(\Lambda_b \to p\mu^-\bar{\nu}_\mu)}{\mathrm{d}q^2}\,\mathrm{d}q^2}{\displaystyle\int_{7\ \text{GeV}^2}^{q^2_{\text{max}}} \frac{\mathrm{d}\mathcal{B}(\Lambda_b \to \Lambda_c\mu^-\bar{\nu}_\mu)}{\mathrm{d}q^2}\,\mathrm{d}q^2}, \tag{301}$$

which, combined with the lattice QCD prediction [516] discussed in Sect. 8.6 yields a determination of $|V_{ub}/V_{cb}|$. The LHCb analysis uses the decay $\Lambda_c \to pK\pi$ to reconstruct the Λ_c and requires the branching fraction $\mathcal{B}(\Lambda_c \to pK\pi)$ of this decay as an external input. Using the latest world average of $\mathcal{B}(\Lambda_c \to pK\pi) = (6.28 \pm 0.32)\%$ [165] to update the LHCb measurement gives [261]

$$R_{\rm BF}(\Lambda_b) = (0.92 \pm 0.04 \pm 0.07) \times 10^{-2}, \tag{302}$$

and, combined with the lattice QCD prediction for $\frac{\zeta_{p\mu\bar{\nu}}(15\text{GeV}^2)}{\zeta_{\Lambda_c\mu\bar{\nu}}(7\text{GeV}^2)}$ discussed in Sect. 8.6,

$$|V_{ub}/V_{cb}| = 0.079 \pm 0.004_{\rm lat.} \pm 0.004_{\rm exp.}. \tag{303}$$

8.11 Determination of $|V_{ub}/V_{cb}|$ from B_s decays

More recently, LHCb reported the measurements [669]

$$R_{\rm BF}(B_s, \text{low}) = \frac{\displaystyle\int_{q^2_{\rm min}=m^2_\mu}^{7\,\text{GeV}^2} \frac{\mathrm{d}\mathcal{B}(B_s \to K^-\mu^+\nu_\mu)}{\mathrm{d}q^2}\,\mathrm{d}q^2}{\mathcal{B}(B_s \to D_s^-\mu^+\nu_\mu)} = (1.66 \pm 0.12) \times 10^{-3}, \tag{304}$$

$$R_{\rm BF}(B_s, \text{high}) = \frac{\displaystyle\int_{7\,\text{GeV}^2}^{q^2_{\rm max}=(m_{B_s}-m_K)^2} \frac{\mathrm{d}\mathcal{B}(B_s \to K^-\mu^+\nu_\mu)}{\mathrm{d}q^2}\,\mathrm{d}q^2}{\mathcal{B}(B_s \to D_s^-\mu^+\nu_\mu)} = (3.25 \pm 0.28) \times 10^{-3}, \tag{305}$$

$$R_{\rm BF}(B_s, \text{all}) = \frac{\mathcal{B}(B_s \to K^-\mu^+\nu_\mu)}{\mathcal{B}(B_s \to D_s^-\mu^+\nu_\mu)} = (4.89 \pm 0.33) \times 10^{-3}. \tag{306}$$

Using our average of the $B_s \to K$ form factors from lattice QCD as discussed in Sect. 8.3.2, we obtain the Standard-Model predictions

$$\frac{1}{|V_{ub}|^2}\int_{q^2_{\rm min}=m^2_\mu}^{7\,\text{GeV}^2} \frac{\mathrm{d}\Gamma(B_s \to K^-\mu^+\nu_\mu)}{\mathrm{d}q^2} = (2.26 \pm 0.38)\ \text{ps}^{-1}, \tag{307}$$

$$\frac{1}{|V_{ub}|^2}\int_{7\,\text{GeV}^2}^{q^2_{\rm max}=(m_{B_s}-m_K)^2} \frac{\mathrm{d}\Gamma(B_s \to K^-\mu^+\nu_\mu)}{\mathrm{d}q^2} = (4.02 \pm 0.31)\ \text{ps}^{-1}, \tag{308}$$

$$\frac{1}{|V_{ub}|^2}\Gamma(B_s \to K^-\mu^+\nu_\mu) = (6.28 \pm 0.67)\ \text{ps}^{-1}. \tag{309}$$

For the denominator, we use the $B_s \to D_s$ form factors from Ref. [613], which yields

$$\frac{1}{|V_{cb}|^2}\Gamma(B_s \to D_s^-\mu^+\nu_\mu) = (9.15 \pm 0.37)\ \text{ps}^{-1}. \tag{310}$$

Combined with the LHCb measurements we obtain

$$\frac{|V_{ub}|}{|V_{cb}|}(\text{low}) = 0.0819 \pm 0.0072_{\rm lat.} \pm 0.0029_{\rm exp.}, \tag{311}$$

$$\frac{|V_{ub}|}{|V_{cb}|}(\text{high}) = 0.0860 \pm 0.0037_{\rm lat.} \pm 0.0038_{\rm exp.}, \tag{312}$$

$$\frac{|V_{ub}|}{|V_{cb}|}(\text{all}) = 0.0844 \pm 0.0048_{\rm lat.} \pm 0.0028_{\rm exp.}. \tag{313}$$

We note the excellent compatibility of the results in the high and low q^2 regions. Nevertheless, we will use the result from the high-q^2 region in our combination in Sect. 8.12, as this is the region in which the form factor shape is most reliably constrained by the lattice data.

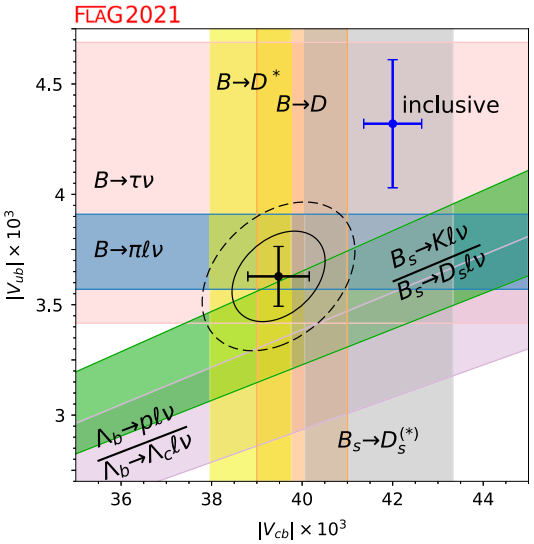

Fig. 38 Summary of $|V_{ub}|$ and $|V_{cb}|$ determinations. The black solid and dashed lines correspond to 68% and 95% C.L. contours, respectively. The result of the global fit (which does not include $\left|V_{ub}/V_{cb}\right|$ from baryon modes or $|V_{cb}|$ from $B_s \to D_s^{(*)}\ell\nu$) is $(|V_{cb}|, |V_{ub}|) = (39.48 \pm 0.68, 3.63 \pm 0.14) \times 10^{-3}$ with a p-value of 0.39. The lattice and experimental results that contribute to the various contours are the following. $B \to \pi\ell\nu$: lattice (FNAL/MILC [556] and RBC/UKQCD [557]) and experiment (BaBar [652,653] and Belle [654,655]). $B \to D\ell\nu$: lattice (FNAL/MILC [606] and HPQCD [607]) and experiment (BaBar [667] and Belle [666]). $B \to D^*\ell\nu$: lattice (FNAL/MILC [605]) and experiment (Belle [660]). $B \to \tau\nu$: lattice (f_B determinations in Fig 27) and experiment (BaBar [528] and Belle [527]). $B_s \to K\ell\nu/B_s \to D_s\ell\nu$: lattice (HPQCD [570], RBC/UKQCD [556], FNAL/MILC [573], HPQCD [613]) and experiment (LHCb [669]). $\Lambda_b \to p\ell\nu/\Lambda_b \to \Lambda_c\ell\nu$: lattice (Detmold 15 [516]) and experiment (LHCb [636]). $B_s \to D_s^*\ell\nu/B_s \to D_s\ell\nu$: lattice (HPQCD 19 [613] and HPQCD 19B [612]) and experiment (LHCb [614,615]). The inclusive determinations are taken from Refs. [165,261,668] and read $(|V_{cb}|, |V_{ub}|)_{\text{incl}} = (42.00 \pm 0.64, 4.32 \pm 0.29) \times 10^{-3}$

8.12 Summary: $|V_{ub}|$ and $|V_{cb}|$

In Fig. 38, we present a summary of determinations of $|V_{ub}|$ and $|V_{cb}|$ from $B \to (\pi, D^{(*)})\ell\nu$, $B_s \to (K, D_s)\ell\nu$ (high q^2 only), $B \to \tau\nu$ and $\Lambda_b \to (p, \Lambda_c)\ell\nu$, as well as the results from inclusive $B \to X_{u,c}\ell\nu$ decays. Note that constraints on $\left|V_{ub}/V_{cb}\right|$ from baryon modes are displayed but, in view of the rating in Table 55, are not included in the global fit. As discussed in Sect. 8.9, experimental inputs used in the extraction of $|V_{cb}|$ from $B_s \to D_s^{(*)}\ell\nu$ decays [614,615] given in Eq. (298) are highly correlated with those entering the global $(|V_{ub}|, |V_{cb}|)$ fit described in this section. Given these correlations and the challenges in reproducing the LHCb analysis, for the time being we do not include the result Eq. (298) into the global fit.

Currently, the determinations of V_{cb} from $B \to D^*$ and $B \to D$ decays are quite compatible; however, a sizeable tension involving the extraction of V_{cb} from inclusive decays remains. In the determination of the 1σ and 2σ contours for our average, we have included an estimate of the correlation between $|V_{ub}|$ and $|V_{cb}|$ from semileptonic B decays: the lattice inputs to these quantities are dominated by results from the Fermilab/MILC and HPQCD collaborations that are both based on MILC $N_f = 2 + 1$ ensembles, leading to our conservatively introducing a 100% correlation between the lattice statistical uncertainties of the three computations involved. The results of the fit are

$$|V_{cb}| = 39.48(68) \times 10^{-3}, \tag{314}$$

$$|V_{ub}| = 3.63(14) \times 10^{-3}, \tag{315}$$

$$p\text{-value} = 0.39. \tag{316}$$

For reference, the inclusive determinations read $|V_{cb}|_{\text{incl}} = (42.00 \pm 0.64) \times 10^{-3}$ [668] and $|V_{ub}|_{\text{incl}} = (4.32 \pm 0.12_{\text{exp}} \pm 0.13_{\text{theo}} \pm 0.23_{\Delta BF}) \times 10^{-3}$ [165,261] (the ΔBF error has been added in Ref. [165] to account for the spread in results obtained using different theoretical models). Note that a recent Belle analysis [670] of partial $B \to X_u\ell^+\nu_\ell$ branching fractions finds a slightly lower central value $|V_{ub}|_{\text{incl,Belle}} = (4.10 \pm 0.09_{\text{stat}} \pm 0.22_{\text{syst}} \pm 0.15_{\text{theo}}) \times 10^{-3}$.

9 The strong coupling α_s

Authors[58] : R. Horsley, P. Petreczky, S. Sint

9.1 Introduction

The strong coupling $\bar{g}_s(\mu)$ defined at scale μ, plays a key role in the understanding of QCD and in its application to collider physics. For example, the parametric uncertainty from α_s is one of the dominant sources of uncertainty in the Standard-Model prediction for the $H \to b\bar{b}$ partial width, and the largest source of uncertainty for $H \to gg$. Thus higher precision determinations of α_s are needed to maximize the potential of experimental measurements at the LHC, and for high-precision Higgs studies at future colliders and the study of the stability of the vacuum [671–678]. The value of α_s also yields one of the essential boundary conditions for completions of the Standard Model at high energies.

In order to determine the running coupling at scale μ

$$\alpha_s(\mu) = \frac{\bar{g}_s^2(\mu)}{4\pi}, \tag{317}$$

we should first "measure" a short-distance quantity $\mathcal{Q}$ at scale μ either experimentally or by lattice calculations, and then match it to a perturbative expansion in terms of a running coupling, conventionally taken as $\alpha_{\overline{\rm MS}}(\mu)$,

$$\mathcal{Q}(\mu) = c_1\alpha_{\overline{\rm MS}}(\mu) + c_2\alpha_{\overline{\rm MS}}(\mu)^2 + \cdots . \tag{318}$$

The essential difference between continuum determinations of α_s and lattice determinations is the origin of the values of $\mathcal{Q}$ in Eq. (318).

The basis of continuum determinations are experimentally measurable cross sections or decay widths from which $\mathcal{Q}$ is defined. These cross sections have to be sufficiently inclusive and at sufficiently high scales such that perturbation theory can be applied. Often hadronization corrections have to be used to connect the observed hadronic cross sections to the perturbative ones. Experimental data at high μ, where perturbation theory is progressively more precise, usually have increasing experimental errors, and it is not easy to find processes that allow one to follow the μ-dependence of a single $\mathcal{Q}(\mu)$ over a range where $\alpha_s(\mu)$ changes significantly and precision is maintained.

In contrast, in lattice gauge theory, one can design $\mathcal{Q}(\mu)$ as Euclidean short-distance quantities that are not directly related to experimental observables. This allows us to follow the μ-dependence until the perturbative regime is reached and nonperturbative "corrections" are negligible. The only experimental input for lattice computations of α_s is the hadron spectrum which fixes the overall energy scale of the theory and the quark masses. Therefore experimental errors are completely negligible and issues such as hadronization do not occur. We can construct many short-distance quantities that are easy to calculate nonperturbatively in lattice simulations with small statistical uncertainties. We can also simulate at parameter values that do not exist in nature (for example, with unphysical quark masses between bottom and charm) to help control systematic uncertainties. These features mean that precise results for α_s can be achieved with lattice-gauge-theory computations. Further, as in the continuum, the different methods available to determine α_s in lattice calculations with different associated systematic uncertainties enable valuable cross-checks. Practical limitations are discussed in the next section, but a simple one is worth mentioning here. Experimental results (and therefore the continuum determinations) of course have all quarks present, while in lattice gauge theories in practice only the lighter ones are included and one is then forced to use the matching at thresholds, as discussed in the following subsection.

It is important to keep in mind that the dominant source of uncertainty in most present day lattice-QCD calculations of α_s are from the truncation of continuum/lattice perturbation theory and from discretization errors. Perturbative truncation errors are of particular concern because they often cannot easily be estimated from studying the data itself. Further, the size of higher-order coefficients in the perturbative series can sometimes turn out to be larger than naive expectations based on power counting from the behaviour of lower-order terms. We note that perturbative truncation errors are also the dominant source of uncertainty in several of the phenomenological determinations of α_s.

The various phenomenological approaches to determining the running coupling constant, $\alpha^{(5)}_{\overline{\rm MS}}(M_Z)$ are summarized by the Particle Data Group [165]. The PDG review lists five categories of phenomenological results used to obtain the running

[58] There is a strong overlap with the FLAG 19 report's section on α_s, authored by Horsley, Onogi and Sommer [4]. In particular the introduction, and the description of methods without new data have been taken over almost unchanged.

coupling: using hadronic τ decays, hadronic final states of e^+e^- annihilation, deep inelastic lepton–nucleon scattering, electroweak precision data, and high energy hadron collider data. Excluding lattice results, the PDG quotes the weighted average as

$$\alpha_{\overline{\rm MS}}^{(5)}(M_Z) = 0.1176(11), \quad \text{PDG 20 [165]} \tag{319}$$

compared to $\alpha_{\overline{\rm MS}}^{(5)}(M_Z) = 0.1174(16)$ of the older PDG 2018 [431]. For a general overview of the various phenomenological and lattice approaches see, e.g., Ref. [679]. The extraction of α_s from τ data, which is one of the most precise and thus has a large impact on the nonlattice average in Eq. (319), is especially sensitive to the treatment of higher-order perturbative terms as well as the treatment of nonperturbative effects. This is important to keep in mind when comparing our chosen range for $\alpha_{\overline{\rm MS}}^{(5)}(M_Z)$ from lattice determinations in Eq. (396) with the nonlattice average from the PDG.

9.1.1 Scheme and scale dependence of α_s and $\Lambda_{\rm QCD}$

Despite the fact that the notion of the QCD coupling is initially a perturbative concept, the associated Λ parameter is nonperturbatively defined

$$\begin{aligned} \Lambda &\equiv \mu\, \varphi_s(\bar{g}_s(\mu)), \\ \varphi_s(\bar{g}_s) &= (b_0\bar{g}_s^2)^{-b_1/(2b_0^2)} e^{-1/(2b_0\bar{g}_s^2)} \exp\left[-\int_0^{\bar{g}_s} dx \left(\frac{1}{\beta(x)} + \frac{1}{b_0 x^3} - \frac{b_1}{b_0^2 x}\right)\right], \end{aligned} \tag{320}$$

where $\beta(\bar{g}_s) = \mu \frac{\partial \bar{g}_s(\mu)}{\partial \mu}$ is the full renormalization group function in the scheme which defines $\bar{g}_s$, and b_0 and b_1 are the first two scheme-independent coefficients of the perturbative expansion

$$\beta(x) \sim -b_0 x^3 - b_1 x^5 + \cdots, \tag{321}$$

with

$$b_0 = \frac{1}{(4\pi)^2}\left(11 - \frac{2}{3}N_f\right), \qquad b_1 = \frac{1}{(4\pi)^4}\left(102 - \frac{38}{3}N_f\right). \tag{322}$$

Thus the Λ parameter is renormalization-scheme-dependent but in an exactly computable way, and lattice gauge theory is an ideal method to relate it to the low-energy properties of QCD. In the $\overline{\rm MS}$ scheme presently b_{n_l} up to $n_l = 4$ are known [199,680–683].

The change in the coupling from one scheme S to another (taken here to be the $\overline{\rm MS}$ scheme) is perturbative,

$$g^2_{\overline{\rm MS}}(\mu) = g^2_{\rm S}(\mu)(1 + c_g^{(1)} g^2_{\rm S}(\mu) + \cdots), \tag{323}$$

where $c_g^{(i)}$, $i \geq 1$ are finite renormalization coefficients. The scale μ must be taken high enough for the error in keeping only the first few terms in the expansion to be small. On the other hand, the conversion to the Λ parameter in the $\overline{\rm MS}$ scheme is given exactly by

$$\Lambda_{\overline{\rm MS}} = \Lambda_{\rm S} \exp\left[c_g^{(1)}/(2b_0)\right]. \tag{324}$$

The fact that $\Lambda_{\overline{\rm MS}}$ can be obtained exactly from Λ_S in any scheme S where $c_g^{(1)}$ is known together with the high-order knowledge (5-loop by now) of $\beta_{\overline{\rm MS}}$ means that the errors in $\alpha_{\overline{\rm MS}}(m_Z)$ are dominantly due to the errors of Λ_S. We will therefore mostly discuss them in that way. Starting from Eq. (320), we have to consider (i) the error of $\bar{g}^2_S(\mu)$ (denoted as $\left(\frac{\Delta\Lambda}{\Lambda}\right)_{\Delta\alpha_S}$) and (ii) the truncation error in β_S (denoted as $\left(\frac{\Delta\Lambda}{\Lambda}\right)_{\rm trunc}$). Concerning (ii), note that knowledge of $c_g^{(n_l)}$ for the scheme S means that β_S is known to $n_l + 1$ loop order; b_{n_l} is known. We thus see that in the region where perturbation theory can be applied, the following errors of Λ_S (or consequently $\Lambda_{\overline{\rm MS}}$) have to be considered

$$\left(\frac{\Delta\Lambda}{\Lambda}\right)_{\Delta\alpha_S} = \frac{\Delta\alpha_S(\mu)}{8\pi b_0 \alpha_S^2(\mu)} \times [1 + \mathcal{O}(\alpha_S(\mu))]\,, \tag{325}$$

$$\left(\frac{\Delta\Lambda}{\Lambda}\right)_{\text{trunc}} = k\alpha_S^{n_l}(\mu) + \mathcal{O}(\alpha_S^{n_l+1}(\mu)), \tag{326}$$

where k depends on b_{n_l+1} and in typical good schemes such as $\overline{\text{MS}}$ it is numerically of order one. Statistical and systematic errors such as discretization effects contribute to $\Delta\alpha_S(\mu)$. In the above we dropped a scheme subscript for the Λ-parameters because of Eq. (324).

By convention $\alpha_{\overline{\text{MS}}}$ is usually quoted at a scale $\mu = M_Z$ where the appropriate effective coupling is the one in the 5-flavour theory: $\alpha^{(5)}_{\overline{\text{MS}}}(M_Z)$. In order to obtain it from a result with fewer flavours, one connects effective theories with different number of flavours as discussed by Bernreuther and Wetzel [684]. For example, one considers the $\overline{\text{MS}}$ scheme, matches the 3-flavour theory to the 4-flavour theory at a scale given by the charm-quark mass [685–687], runs with the 5-loop β-function [199,680–683] of the 4-flavour theory to a scale given by the b-quark mass, and there matches to the 5-flavour theory, after which one runs up to $\mu = M_Z$ with the 5-loop β function. For the matching relation at a given quark threshold we use the mass $m_\star$ which satisfies $m_\star = \overline{m}_{\overline{\text{MS}}}(m_\star)$, where $\overline{m}$ is the running mass (analogous to the running coupling). Then

$$\bar{g}^2_{N_f-1}(m_\star) = \bar{g}^2_{N_f}(m_\star) \times [1 + 0 \times \bar{g}^2_{N_f}(m_\star) + \sum_{n\geq 2} t_n\, \bar{g}^{2n}_{N_f}(m_\star)] \tag{327}$$

with [685,687,688]

$$t_2 = \frac{1}{(4\pi^2)^2}\frac{11}{72}, \tag{328}$$

$$t_3 = \frac{1}{(4\pi^2)^3}\left[-\frac{82043}{27648}\zeta_3 + \frac{564731}{124416} - \frac{2633}{31104}(N_f - 1)\right], \tag{329}$$

$$t_4 = \frac{1}{(4\pi^2)^4}\left[5.170347 - 1.009932(N_f - 1) - 0.021978\,(N_f - 1)^2\right], \tag{330}$$

(where ζ_3 is the Riemann zeta-function) provides the matching at the thresholds in the $\overline{\text{MS}}$ scheme. Often the package `RunDec` is used for quark-threshold matching and running in the $\overline{\text{MS}}$-scheme [689,690].

While t_2, t_3, t_4 are numerically small coefficients, the charm-threshold scale is also relatively low and so there are nonperturbative uncertainties in the matching procedure, which are difficult to estimate but which we assume here to be negligible. Obviously there is no perturbative matching formula across the strange "threshold"; here matching is entirely nonperturbative. Model dependent extrapolations of $\bar{g}^2_{N_f}$ from $N_f = 0, 2$ to $N_f = 3$ were done in the early days of lattice gauge theory. We will include these in our listings of results but not in our estimates, since such extrapolations are based on untestable assumptions.

9.1.2 Overview of the review of α_s

We begin by explaining lattice-specific difficulties in Sect. 9.2.1 and the FLAG criteria designed to assess whether the associated systematic uncertainties can be controlled and estimated in a reasonable manner. These criteria are taken over unchanged from the FLAG 19 report, as there has not yet been sufficiently broad progress to make these criteria more stringent. We would also like to point to a recent review [691] of lattice methodology and systematic uncertainties for α_s. There, a systematic scale variation is advocated to assess systematic errors due to the truncation of the perturbative series and such a procedure may indeed be incorporated into future FLAG criteria, as it can be applied without change to most lattice approaches.

We then discuss, in Sects. 9.3–9.9, the various lattice approaches and results from calculations with $N_f = 0$, 2, 2+1, and 2+1+1 flavours.

Besides new results and upgrades of previous works, a new strategy of nonperturbative renormalization by decoupling has been proposed by the ALPHA collaboration [692], which shifts the perspective on results with unphysical flavour numbers, in particular for $N_f = 0$. As these can be nonperturbatively related to $N_f > 0$ results by a nonperturbative matching calculation,

it becomes very important to obtain precise and controlled $N_f = 0$ results, with obvious implications for this and future FLAG reports. A short account of the decoupling strategy is given in Sect. 9.4.

In Sect. 9.11, we present averages together with our best estimates for $\alpha^{(5)}_{\overline{\rm MS}}$. These are currently determined from 3- and 4-flavour QCD simulations only, however, in the near future the decoupling strategy is expected to link e.g. 3-flavour simulations with the pure gauge theory simulations. Therefore, for the Λ parameter, we also give results for other numbers of flavours, including $N_f = 0$ and $N_f = 2$.

9.1.3 Additions with respect to the FLAG 19 report

The additional papers since the FLAG 19 report are:

Dalla Brida 19 [693] and Nada 20 [694] from step-scaling methods (Sect. 9.3).
ALPHA 19A [692] from the decoupling method (Sect. 9.4).
TUMQCD 19 [75] and Ayala 20 [74] and Husung 20 [695] from the static quark potential (Sect. 9.5).
Cali 20 [76] from (light-quark) vacuum polarization in position space (Sect. 9.6).
Petreczky 20 [696], Petreczky 19 [26], and Boito 20 [697,698] from heavy-quark current two-point functions (Sect. 9.8).
Zafeiropoulos 19 [699] from QCD vertices (Sect. 9.9).

9.2 General issues

9.2.1 Discussion of criteria for computations entering the averages

As in the PDG review, we only use calculations of α_s published in peer-reviewed journals, and that use NNLO or higher-order perturbative expansions, to obtain our final range in Sect. 9.11. We also, however, introduce further criteria designed to assess the ability to control important systematics, which we describe here. Some of these criteria, e.g., that for the continuum extrapolation, are associated with lattice-specific systematics and have no continuum analogue. Other criteria, e.g., that for the renormalization scale, could in principle be applied to nonlattice determinations. Expecting that lattice calculations will continue to improve significantly in the near future, our goal in reviewing the state-of-the-art here is to be conservative and avoid prematurely choosing an overly small range.

In lattice calculations, we generally take $\mathcal{Q}$ to be some combination of physical amplitudes or Euclidean correlation functions which are free from UV and IR divergences and have a well-defined continuum limit. Examples include the force between static quarks and two-point functions of quark-bilinear currents.

In comparison to values of observables $\mathcal{Q}$ determined experimentally, those from lattice calculations require two more steps. The first step concerns setting the scale μ in GeV, where one needs to use some experimentally measurable low-energy scale as input. Ideally one employs a hadron mass. Alternatively convenient intermediate scales such as $\sqrt{t_0}$, w_0, r_0, r_1, [114,317,700,701] can be used if their relation to an experimental dimensionful observable is established. The low-energy scale needs to be computed at the same bare parameters where $\mathcal{Q}$ is determined, at least as long as one does not use the step-scaling method (see below). This induces a practical difficulty given present computing resources. In the determination of the low-energy reference scale the volume needs to be large enough to avoid finite-size effects. On the other hand, in order for the perturbative expansion of Eq. (318) to be reliable, one has to reach sufficiently high values of μ, i.e., short enough distances. To avoid uncontrollable discretization effects the lattice spacing a has to be accordingly small. This means

$$L \gg \text{hadron size} \sim \Lambda^{-1}_{\rm QCD} \quad \text{and} \quad 1/a \gg \mu, \tag{331}$$

(where L is the box size) and therefore

$$L/a \ggg \mu/\Lambda_{\rm QCD}. \tag{332}$$

The currently available computer power, however, limits L/a, typically to $L/a = 32{-}96$. Unless one accepts compromises in controlling discretization errors or finite-size effects, this means one needs to set the scale μ according to

$$\mu \lll L/a \times \Lambda_{\rm QCD} \sim 10{-}30\,\text{GeV}. \tag{333}$$

(Here $\lll$ or $\ggg$ means at least one order of magnitude smaller or larger.) Therefore, μ can be $1-3$ GeV at most. This raises the concern whether the asymptotic perturbative expansion truncated at 1-loop, 2-loop, or 3-loop in Eq. (318) is sufficiently accurate. There is a finite-size scaling method, usually called step-scaling method, which solves this problem by identifying $\mu = 1/L$ in the definition of $\mathcal{Q}(\mu)$, see Sect. 9.3.

For the second step after setting the scale μ in physical units (GeV), one should compute $\mathcal{Q}$ on the lattice, $\mathcal{Q}_{\rm lat}(a, \mu)$ for several lattice spacings and take the continuum limit to obtain the left hand side of Eq. (318) as

$$\mathcal{Q}(\mu) \equiv \lim_{a\to 0} \mathcal{Q}_{\rm lat}(a, \mu) \text{ with } \mu \text{ fixed.} \tag{334}$$

This is necessary to remove the discretization error.

Here it is assumed that the quantity $\mathcal{Q}$ has a continuum limit, which is regularization-independent. The method discussed in Sect. 9.7, which is based on the perturbative expansion of a lattice-regulated, divergent short-distance quantity $W_{\rm lat}(a)$ differs in this respect and must be treated separately.

In summary, a controlled determination of α_s needs to satisfy the following:

1. The determination of α_s is based on a comparison of a short-distance quantity $\mathcal{Q}$ at scale μ with a well-defined continuum limit without UV and IR divergences to a perturbative expansion formula in Eq. (318).
2. The scale μ is large enough so that the perturbative expansion in Eq. (318) is precise to the order at which it is truncated, i.e., it has good *asymptotic* convergence.
3. If $\mathcal{Q}$ is defined by physical quantities in infinite volume, one needs to satisfy Eq. (332).
   Nonuniversal quantities need a separate discussion, see Sect. 9.7.

Conditions 2. and 3. give approximate lower and upper bounds for μ respectively. It is important to see whether there is a window to satisfy 2. and 3. at the same time. If it exists, it remains to examine whether a particular lattice calculation is done inside the window or not.

Obviously, an important issue for the reliability of a calculation is whether the scale μ that can be reached lies in a regime where perturbation theory can be applied with confidence. However, the value of μ does not provide an unambiguous criterion. For instance, the Schrödinger Functional, or SF-coupling (Sect. 9.3) is conventionally taken at the scale $\mu = 1/L$, but one could also choose $\mu = 2/L$. Instead of μ we therefore define an effective $\alpha_{\rm eff}$. For schemes such as SF (see Sect. 9.3) or qq (see Sect. 9.5) this is directly the coupling of the scheme. For other schemes such as the vacuum polarization we use the perturbative expansion Eq. (318) for the observable $\mathcal{Q}$ to define

$$\alpha_{\rm eff} = \mathcal{Q}/c_1. \tag{335}$$

If there is an α_s-independent term it should first be subtracted. Note that this is nothing but defining an effective, regularization-independent coupling, a physical renormalization scheme.

Let us now comment further on the use of the perturbative series. Since it is only an asymptotic expansion, the remainder $R_n(\mathcal{Q}) = \mathcal{Q} - \sum_{i\le n} c_i\alpha_s^i$ of a truncated perturbative expression $\mathcal{Q} \sim \sum_{i\le n} c_i\alpha_s^i$ cannot just be estimated as a perturbative error $k\,\alpha_s^{n+1}$. The error is nonperturbative. Often one speaks of "nonperturbative contributions", but nonperturbative and perturbative cannot be strictly separated due to the asymptotic nature of the series (see, e.g., Ref. [702]).

Still, we do have some general ideas concerning the size of nonperturbative effects. The known ones such as instantons or renormalons decay for large μ like inverse powers of μ and are thus roughly of the form

$$\exp(-\gamma/\alpha_s), \tag{336}$$

with some positive constant γ. Thus we have, loosely speaking,

$$\mathcal{Q} = c_1\alpha_s + c_2\alpha_s^2 + \cdots + c_n\alpha_s^n + \mathcal{O}(\alpha_s^{n+1}) + \mathcal{O}(\exp(-\gamma/\alpha_s)). \tag{337}$$

For small α_s, the $\exp(-\gamma/\alpha_s)$ is negligible. Similarly the perturbative estimate for the magnitude of relative errors in Eq. (337) is small; as an illustration for $n = 3$ and $\alpha_s = 0.2$ the relative error is $\sim 0.8\%$ (assuming coefficients $|c_{n+1}/c_1| \sim 1$).

For larger values of α_s nonperturbative effects can become significant in Eq. (337). An instructive example comes from the values obtained from τ decays, for which $\alpha_s \approx 0.3$. Here, different applications of perturbation theory (fixed order and

contour improved) each look reasonably asymptotically convergent[59] but the difference does not seem to decrease much with the order (see, e.g., the contribution of Pich in Ref. [704]). In addition nonperturbative terms in the spectral function may be nonnegligible even after the integration up to m_τ (see, e.g., Refs. [705,706]). All of this is because α_s is not really small.

Since the size of the nonperturbative effects is very hard to estimate one should try to avoid such regions of the coupling. In a fully controlled computation one would like to verify the perturbative behaviour by changing α_s over a significant range instead of estimating the errors as $\sim \alpha_s^{n+1}$. Some computations try to take nonperturbative power 'corrections' to the perturbative series into account by including such terms in a fit to the μ-dependence. We note that this is a delicate procedure, both because the separation of nonperturbative and perturbative is theoretically not well defined and because in practice a term like, e.g., $\alpha_s(\mu)^3$ is hard to distinguish from a $1/\mu^2$ term when the μ-range is restricted and statistical and systematic errors are present. We consider it safer to restrict the fit range to the region where the power corrections are negligible compared to the estimated perturbative error.

The above considerations lead us to the following special criteria for the determination of α_s:

- Renormalization scale
  - ★ all points relevant in the analysis have $\alpha_{\rm eff} < 0.2$
  - ○ all points have $\alpha_{\rm eff} < 0.4$ and at least one $\alpha_{\rm eff} \leq 0.25$
  - ■ otherwise
- Perturbative behaviour
  - ★ verified over a range of a factor 4 change in $\alpha_{\rm eff}^{n_l}$ without power corrections or alternatively $\alpha_{\rm eff}^{n_l} \leq \frac{1}{2}\Delta\alpha_{\rm eff}/(8\pi b_0\alpha_{\rm eff}^2)$ is reached
  - ○ agreement with perturbation theory over a range of a factor $(3/2)^2$ in $\alpha_{\rm eff}^{n_l}$ possibly fitting with power corrections or alternatively $\alpha_{\rm eff}^{n_l} \leq \Delta\alpha_{\rm eff}/(8\pi b_0\alpha_{\rm eff}^2)$ is reached
  - ■ otherwise

Here $\Delta\alpha_{\rm eff}$ is the accuracy cited for the determination of $\alpha_{\rm eff}$ and n_l is the loop order to which the connection of $\alpha_{\rm eff}$ to the $\overline{\rm MS}$ scheme is known. Recall the discussion around Eqs. (325,326); the β-function of $\alpha_{\rm eff}$ is then known to $n_l + 1$ loop order.[60]

- Continuum extrapolation
  At a reference point of $\alpha_{\rm eff} = 0.3$ (or less) we require
  - ★ three lattice spacings with $\mu a < 1/2$ and full $\mathcal{O}(a)$ improvement,
    or three lattice spacings with $\mu a \leq 1/4$ and 2-loop $\mathcal{O}(a)$ improvement,
    or $\mu a \leq 1/8$ and 1-loop $\mathcal{O}(a)$ improvement
  - ○ three lattice spacings with $\mu a < 3/2$ reaching down to $\mu a = 1$ and full $\mathcal{O}(a)$ improvement,
    or three lattice spacings with $\mu a \leq 1/4$ and 1-loop $\mathcal{O}(a)$ improvement
  - ■ otherwise

We also need to specify what is meant by μ. Here are our choices:

$$\begin{aligned}
\text{step-scaling} &: \mu = 1/L,\\
\text{heavy quark–antiquark potential} &: \mu = 2/r,\\
\text{observables in position space} &: \mu = 1/|x|,\\
\text{observables in momentum space} &: \mu = q,\\
\text{moments of heavy-quark currents} &: \mu = 2\bar{m}_{\rm c},\\
\text{eigenvalues of the Dirac operator} &: \mu = \lambda_{\overline{\rm MS}}
\end{aligned} \tag{338}$$

[59] See, however, the recent discussion in [703].

[60] Once one is in the perturbative region with $\alpha_{\rm eff}$, the error in extracting the Λ parameter due to the truncation of perturbation theory scales like $\alpha_{\rm eff}^{n_l}$, as discussed around Eq. (326). In order to detect/control such corrections properly, one needs to change the correction term significantly; we require a factor of four for a ★ and a factor $(3/2)^2$ for a ○. An exception to the above is the situation where the correction terms are small anyway, i.e., $\alpha_{\rm eff}^{n_l} \approx (\Delta\Lambda/\Lambda)_{\rm trunc} < (\Delta\Lambda/\Lambda)_{\Delta\alpha} \approx \Delta\alpha_{\rm eff}/(8\pi b_0\alpha_{\rm eff}^2)$ is reached.

where $|x|$ is the Euclidean norm of the 4-vector x, q is the magnitude of the momentum, $\bar{m}_c$ is the heavy-quark mass (in the $\overline{\rm MS}$ scheme) and usually taken around the charm-quark mass and $\lambda_{\overline{\rm MS}}$ is the eigenvalue of the Dirac operator, see Sect. 9.10. We note again that the above criteria cannot be applied when regularization dependent quantities $W_{\rm lat}(a)$ are used instead of $\mathcal{Q}(\mu)$. These cases are specifically discussed in Sect. 9.7.

In principle one should also account for electro-weak radiative corrections. However, both in the determination of α_s at intermediate scales μ and in the running to high scales, we expect electro-weak effects to be much smaller than the presently reached precision. Such effects are therefore not further discussed.

The attentive reader will have noticed that bounds such as $\mu a < 3/2$ or at least one value of $\alpha_{\rm eff} \leq 0.25$ which we require for a ○ are not very stringent. There is a considerable difference between ○ and ★. We have chosen the above bounds, unchanged as compared to FLAG 16 and FLAG 19, since not too many computations would satisfy more stringent ones at present. Nevertheless, we believe that the ○ criteria already give reasonable bases for estimates of systematic errors. An exception may be Cali 20, which is discussed in detail in Sect. 9.6. In the future, we expect that we will be able to tighten our criteria for inclusion in the average, and that many more computations will reach the present ★ rating in one or more categories.

In addition to our explicit criteria, the following effects may influence the precision of results:

Topology sampling: In principle a good way to improve the quality of determinations of α_s is to push to very small lattice spacings thus enabling large μ. It is known that the sampling of field space becomes very difficult for the HMC algorithm when the lattice spacing is small and one has the standard periodic boundary conditions. In practice, for all known discretizations the topological charge slows down dramatically for $a \approx 0.05$ fm and smaller [116,125,128–132]. Open boundary conditions solve the problem [133] but are not frequently used. Since the effect of the freezing on short distance observables is not known, we also do need to pay attention to this issue. Remarks are added in the text when appropriate.

Quark-mass effects: We assume that effects of the finite masses of the light quarks (including strange) are negligible in the effective coupling itself where large, perturbative, μ is considered.

Scale setting: The scale does not need to be very precise, since using the lowest-order β-function shows that a 3% error in the scale determination corresponds to a $\sim$ 0.5% error in $\alpha_s(M_Z)$. As long as systematic errors from chiral extrapolation and finite-volume effects are well below 3% we do not need to be concerned about those at the present level of precision in $\alpha_s(M_Z)$. This may change in the future.

9.2.2 Physical scale

Since FLAG 19, a new FLAG working group on scale setting has been established. We refer to Sect. 11 for definitions and the current status. Note that the error from scale setting is sub-dominant for current α_s determinations.

A popular scale choice has been the intermediate r_0 scale, and its variant r_1, which both derive from the force between static quarks, see Eq. (358). One should bear in mind that their determination from physical observables also has to be taken into account. The phenomenological value of r_0 was originally determined as $r_0 \approx 0.49$ fm through potential models describing quarkonia [700]. Of course the quantity is precisely defined, independently of such model considerations. But a lattice computation with the correct sea-quark content is needed to determine a completely sharp value. When the quark content is not quite realistic, the value of r_0 may depend to some extent on which experimental input is used to determine (actually define) it.

The latest determinations from two-flavour QCD are $r_0 = 0.420(14)$–$0.450(14)$ fm by the ETM collaboration [45,87], using as input f_π and f_K and carrying out various continuum extrapolations. On the other hand, the ALPHA collaboration [707] determined $r_0 = 0.503(10)$ fm with input from f_K, and the QCDSF collaboration [107] cites 0.501(10)(11) fm from the mass of the nucleon (no continuum limit). Recent determinations from three-flavour QCD are consistent with $r_1 = 0.313(3)$ fm and $r_0 = 0.472(5)$ fm [41,120,708]. Due to the uncertainty in these estimates, and as many results are based directly on r_0 to set the scale, we shall often give both the dimensionless number $r_0\Lambda_{\overline{\rm MS}}$, as well as $\Lambda_{\overline{\rm MS}}$. In the cases where no physical r_0 scale is given in the original papers or we convert to the r_0 scale, we use the value $r_0 = 0.472$ fm. In case $r_1\Lambda_{\overline{\rm MS}}$ is given in the publications, we use $r_0/r_1 = 1.508$ [708], to convert, which remains well consistent with the update [116] neglecting the error on this ratio. In some, mostly early, computations the string tension, $\sqrt{\sigma}$ was used. We convert to r_0 using $r_0^2\sigma = 1.65 - \pi/12$, which has been shown to be an excellent approximation in the relevant pure gauge theory [709,710].

The new scales t_0, w_0 based on the gradient flow are very attractive alternatives to r_0 but their discretization errors are still under discussion [112,711–713] and their values at the physical point are not yet determined with great precision. We

remain with r_0 as our main reference scale for now. A general discussion of the various scales is given in [714] and in the scale-setting section of this FLAG report, cf. Sect. 11.

9.2.3 Studies of truncation errors of perturbation theory

As discussed previously, we have to determine α_s in a region where the perturbative expansion for the β-function, Eq. (321) in the integral Eq. (320), is reliable. In principle this must be checked, however, this is difficult to achieve as we need to reach up to a sufficiently high scale. A frequently used recipe to estimate the size of truncation errors of the perturbative series is to vary the renormalization-scale dependence around the chosen 'optimal' scale μ_*, of an observable evaluated at a fixed order in the coupling from $\mu = \mu_*/2$ to $2\mu_*$. For examples, see Ref. [691].

Alternatively, or in addition, the renormalization scheme chosen can be varied, which investigates the perturbative conversion of the chosen scheme to the perturbatively defined $\overline{\text{MS}}$ scheme and in particular 'fastest apparent convergence' when the 'optimal' scale is chosen so that the $\mathcal{O}(\alpha_s^2)$ coefficient vanishes.

The ALPHA collaboration in Ref. [715] and ALPHA 17 [716], within the SF approach defined a set of ν-schemes for which the 3-loop (scheme-dependent) coefficient of the β-function for $N_f = 2 + 1$ flavours was computed to be $b_2^\nu = -(0.064(27) + 1.259(1)\nu)/(4\pi)^3$. The standard SF scheme has $\nu = 0$. For comparison, $b_2^{\overline{\text{MS}}} = 0.324/(4\pi)^3$. A range of scales from about 4 GeV to 128 GeV was investigated. It was found that while the procedure of varying the scale by a factor 2 up and down gave a correct estimate of the residual perturbative error for $\nu \approx 0 \ldots 0.3$, for negative values, e.g., $\nu = -0.5$, the estimated perturbative error is much too small to account for the mismatch in the Λ-parameter of $\approx 8\%$ at $\alpha_s = 0.15$. This mismatch, however, did, as expected, still scale with $\alpha_s^{n_l}$ with $n_l = 2$. In the schemes with negative ν, the coupling α_s has to be quite small for scale-variations of a factor 2 to correctly signal the perturbative errors.

For a systematic study of renormalization scale variations as a measure of perturbative truncation errors in various lattice determinations of α_s we refer to the recent review by Del Debbio and Ramos [691].

9.3 α_s from step-scaling methods

9.3.1 General considerations

The method of step-scaling functions avoids the scale problem, Eq. (331). It is in principle independent of the particular boundary conditions used and was first developed with periodic boundary conditions in a two-dimensional model [717].

The essential idea of the step-scaling strategy is to split the determination of the running coupling at large μ and of a hadronic scale into two lattice calculations and connect them by 'step-scaling'. In the former part, we determine the running coupling constant in a finite-volume scheme in which the renormalization scale is set by the inverse lattice size $\mu = 1/L$. In this calculation, one takes a high renormalization scale while keeping the lattice spacing sufficiently small as

$$\mu \equiv 1/L \sim 10 \ldots 100\,\text{GeV}, \qquad a/L \ll 1. \tag{339}$$

In the latter part, one chooses a certain $\bar{g}^2_{\text{max}} = \bar{g}^2(1/L_{\text{max}})$, typically such that L_{max} is around 0.5–1 fm. With a common discretization, one then determines L_{max}/a and (in a large volume $L \geq$ 2–3 fm) a hadronic scale such as a hadron mass, $\sqrt{t_0}/a$ or r_0/a at the same bare parameters. In this way one gets numbers for, e.g., L_{max}/r_0 and by changing the lattice spacing a carries out a continuum limit extrapolation of that ratio.

In order to connect $\bar{g}^2(1/L_{\text{max}})$ to $\bar{g}^2(\mu)$ at high μ, one determines the change of the coupling in the continuum limit when the scale changes from L to L/s, starting from $L = L_{\text{max}}$ and arriving at $\mu = s^k/L_{\text{max}}$. This part of the strategy is called step-scaling. Combining these results yields $\bar{g}^2(\mu)$ at $\mu = s^k\,(r_0/L_{\text{max}})\,r_0^{-1}$, where r_0 stands for the particular chosen hadronic scale. Most applications use a scale factor $s = 2$.

At present most applications in QCD use Schrödinger functional boundary conditions [421,718] and we discuss this below in a little more detail. (However, other boundary conditions are also possible, such as twisted boundary conditions and the discussion also applies to them.) An important reason is that these boundary conditions avoid zero modes for the quark fields and quartic modes [719] in the perturbative expansion in the gauge fields. Furthermore the corresponding renormalization scheme is well studied in perturbation theory [720–722] with the 3-loop β-function and 2-loop cutoff effects (for the standard Wilson regularization) known.

In order to have a perturbatively well-defined scheme, the SF scheme uses Dirichlet boundary conditions at time $t = 0$ and $t = T$. These break translation invariance and permit $\mathcal{O}(a)$ counter terms at the boundary through quantum corrections.

Table 60 Results for the Λ parameter from computations using step-scaling of the SF-coupling. Entries without values for Λ computed the running and established perturbative behaviour at large μ

Collaboration	Refs.	N_f	Publication status	Renormalization scale	Perturbative behaviour	Continuum extrapolation	Scale	$\Lambda_{\overline{\text{MS}}}$ [MeV]	$r_0\Lambda_{\overline{\text{MS}}}$
ALPHA 10A	[735]	4	A	★	★	★	Only running of α_s in Fig. 4		
Perez 10	[736]	4	C	★	★	○	Only step-scaling function in Fig. 4		
ALPHA 17	[77]	2+1	A	★	★	★	$\sqrt{8t_0} = 0.415$ fm	341(12)	0.816(29)
PACS-CS 09A	[78]	2+1	A	★	★	○	m_ρ	$371(13)(8)(^{+0}_{-27})^{\#}$	$0.888(30)(18)(^{+0}_{-65})^{\dagger}$
			A	★	★	○	m_ρ	$345(59)^{\#\#}$	$0.824(141)^{\dagger}$
ALPHA 12*	[707]	2	A	★	★	★	f_K	310(20)	0.789(52)
ALPHA 04	[737]	2	A	■	★	★	$r_0 = 0.5$ fm§	$245(16)(16)^{\S}$	$0.62(2)(2)^{\S}$
ALPHA 01A	[738]	2	A	★	★	★	Only running of α_s in Fig. 5		
Nada 20	[694]	0	A	★	★	★	Consistency checks for [693], same gauge configurations		
Dalla Brida 19	[693]	0	A	★	★	★	$r_0 = 0.5$fm	260.5(4.4)	0.660(11)
Ishikawa 17	[732]	0	A	★	★	★	r_0, $[\sqrt{\sigma}]$	$253(4)(^{+13}_{-2})^{\dagger}$	$0.606(9)(^{+31}_{-5})^{+}$
CP-PACS 04$^{\&}$	[723]	0	A	★	★	○	Only tables of g^2_{SF}		
ALPHA 98††	[739]	0	A	★	★	○	$r_0 = 0.5$fm	238(19)	0.602(48)
Lüscher 93	[720]	0	A	★	○	○	$r_0 = 0.5$fm	233(23)	$0.590(60)^{\S\S}$

$^{\#}$Result with a constant (in a) continuum extrapolation of the combination $L_{\max}m_\rho$
†In conversion from $\Lambda_{\overline{\text{MS}}}$ to $r_0\Lambda_{\overline{\text{MS}}}$ and vice versa, r_0 is taken to be 0.472 fm
$^{\#\#}$Result with a linear continuum extrapolation in a of the combination $L_{\max}m_\rho$
*Supersedes ALPHA 04
§The $N_f = 2$ results were based on values for r_0/a which have later been found to be too small by [707]. The effect will be of the order of 10–15%, presumably an increase in Λr_0. We have taken this into account by a ■ in the renormalization scale
$^{\&}$This investigation was a precursor for PACS-CS 09A and confirmed two step-scaling functions as well as the scale setting of ALPHA 98
††Uses data of Lüscher 93 and therefore supersedes it
§§Converted from $\alpha_{\overline{\text{MS}}}(37r_0^{-1}) = 0.1108(25)$
$^{+}$Also $\Lambda_{\overline{\text{MS}}}/\sqrt{\sigma} = 0.532(8)(^{+27}_{-5})$ is quoted

Therefore, the leading discretization error is $\mathcal{O}(a)$. Improving the lattice action is achieved by adding counter terms at the boundaries whose coefficients are denoted as $c_t, \tilde{c}_t$. In practice, these coefficients are computed with 1-loop or 2-loop perturbative accuracy. A better precision in this step yields a better control over discretization errors, which is important, as can be seen, e.g., in Refs. [709,723].

Also computations with Dirichlet boundary conditions do in principle suffer from the insufficient change of topology in the HMC algorithm at small lattice spacing. However, in a small volume the weight of nonzero charge sectors in the path integral is exponentially suppressed [724][61] and in a Monte Carlo run of typical length very few configurations with nontrivial topology should appear. Considering the issue quantitatively Ref. [725] finds a strong suppression below $L \approx 0.8$ fm. Therefore the lack of topology change of the HMC is not a serious issue for the high energy regime in step-scaling studies. However, the matching to hadronic observables requires volumes where the problem cannot be ignored. Therefore, Ref. [726] includes a projection to zero topology into the *definition* of the coupling. We note also that a mix of Dirichlet and open boundary conditions is expected to remove the topology issue entirely [727] and may be considered in the future.

Apart from the boundary conditions, the very definition of the coupling needs to be chosen. We briefly discuss in turn, the two schemes used at present, namely, the 'Schrödinger Functional' (SF) and 'Gradient Flow' (GF) schemes.

[61] We simplify here and assume that the classical solution associated with the used boundary conditions has charge zero. In practice this is the case.

The SF scheme is the first one, which was used in step-scaling studies in gauge theories [421]. Inhomogeneous Dirichlet boundary conditions are imposed in time,

$$A_k(x)|_{x_0=0} = C_k, \quad A_k(x)|_{x_0=L} = C'_k, \tag{340}$$

for $k = 1, 2, 3$. Periodic boundary conditions (up to a phase for the fermion fields) with period L are imposed in space. The matrices

$$\begin{aligned} LC_k &= i\,\mathrm{diag}\big(\eta - \pi/3, -\eta/2, -\eta/2 + \pi/3\big), \\ LC'_k &= i\,\mathrm{diag}\big(-(\eta + \pi), \eta/2 + \pi/3, \eta/2 + 2\pi/3\big), \end{aligned}$$

just depend on the dimensionless parameter η. The coupling $\bar{g}_{\mathrm{SF}}$ is obtained from the η-derivative of the effective action,

$$\langle \partial_\eta S|_{\eta=0}\rangle = \frac{12\pi}{\bar{g}^2_{\mathrm{SF}}}. \tag{341}$$

For this scheme, the finite $c_g^{(i)}$, Eq. (323), are known for $i = 1, 2$ [721,722].

More recently, gradient-flow couplings have been used frequently because of their small statistical errors at large couplings (in contrast to $\bar{g}_{\mathrm{SF}}$, which has small statistical errors at small couplings). The gradient flow is introduced as follows [317,728]. Consider the flow gauge field $B_\mu(t, x)$ with the flow time t, which is a one parameter deformation of the bare gauge field $A_\mu(x)$, where $B_\mu(t, x)$ is the solution to the gradient-flow equation

$$\begin{aligned} \partial_t B_\mu(t, x) &= D_\nu G_{\nu\mu}(t, x), \\ G_{\mu\nu} &= \partial_\mu B_\nu - \partial_\nu B_\mu + [B_\mu, B_\nu], \end{aligned} \tag{342}$$

with initial condition $B_\mu(0, x) = A_\mu(x)$. The renormalized coupling is defined by [317]

$$\bar{g}^2_{\mathrm{GF}}(\mu) = \mathcal{N} t^2 \langle E(t, x)\rangle\Big|_{\mu=1/\sqrt{8t}}, \tag{343}$$

with $\mathcal{N} = 16\pi^2/3 + \mathcal{O}((a/L)^2)$ and where $E(t, x)$ is the action density given by

$$E(t, x) = \frac{1}{4} G^a_{\mu\nu}(t, x) G^a_{\mu\nu}(t, x). \tag{344}$$

In a finite volume, one needs to specify additional conditions. In order not to introduce two independent scales one sets

$$\sqrt{8t} = cL, \tag{345}$$

for some fixed number c [729]. Schrödinger functional boundary conditions [730] or twisted boundary conditions [731,732] have been employed. Matching of the GF coupling to the $\overline{\mathrm{MS}}$-scheme coupling is known to 1-loop for twisted boundary conditions with zero quark flavours and $SU(3)$ group [732] and to 2-loop with SF boundary conditions with zero quark flavours [733]. The former is based on a MC evaluation at small couplings[62] and the latter on numerical stochastic perturbation theory.

9.3.2 Discussion of computations

In Table 60 we give results from various determinations of the Λ parameter. For a clear assessment of the N_f-dependence, the last column also shows results that refer to a common hadronic scale, r_0. As discussed above, the renormalization scale can be chosen large enough such that $\alpha_s < 0.2$ and the perturbative behaviour can be verified. Consequently only ★ is present for these criteria except for early work where the $n_l = 2$ loop correction to $\overline{\mathrm{MS}}$ was not yet known and we assigned a ■

[62] For a variant of the twisted periodic finite volume scheme the 1-loop matching has been computed analytically [734].

concerning the renormalization scale. With dynamical fermions, results for the step-scaling functions are always available for at least $a/L = \mu a = 1/4, 1/6, 1/8$. All calculations have a nonperturbatively $\mathcal{O}(a)$ improved action in the bulk. For the discussed boundary $\mathcal{O}(a)$ terms this is not so. In most recent calculations 2-loop $\mathcal{O}(a)$ improvement is employed together with at least three lattice spacings.[63] This means a ★ for the continuum extrapolation. In other computations only 1-loop c_t was available and we arrive at ○. We note that the discretization errors in the step-scaling functions of the SF coupling are usually found to be very small, at the percent level or below. However, the overall desired precision is very high as well, and the results in CP-PACS 04 [723] show that discretization errors at the below percent level cannot be taken for granted. In particular with staggered fermions (unimproved except for boundary terms) few percent effects are seen in Perez 10 [736].

In the work by PACS-CS 09A [78], the continuum extrapolation in the scale setting is performed using a constant function in a and with a linear function. Potentially the former leaves a considerable residual discretization error. We here use, as discussed with the collaboration, the continuum extrapolation linear in a, as given in the second line of PACS-CS 09A [78] results in Table 60. After perturbative conversion from a three-flavour result to five flavours (see Sect. 9.2.1), they obtain

$$\alpha^{(5)}_{\overline{\rm MS}}(M_Z) = 0.118(3). \tag{346}$$

In Ref. [77], the ALPHA collaboration determined $\Lambda^{(3)}_{\overline{\rm MS}}$ combining step-scaling in $\bar{g}^2_{\rm GF}$ in the lower scale region $\mu_{\rm had} \le \mu \le \mu_0$, and step-scaling in $\bar{g}^2_{\rm SF}$ for higher scales $\mu_0 \le \mu \le \mu_{\rm PT}$. Both schemes are defined with SF boundary conditions. For $\bar{g}^2_{\rm GF}$ a projection to the sector of zero topological charge is included, Eq. (344) is restricted to the magnetic components, and $c = 0.3$. The scales $\mu_{\rm had}$, μ_0, and $\mu_{\rm PT}$ are defined by $\bar{g}^2_{\rm GF}(\mu_{\rm had}) = 11.3$, $\bar{g}^2_{\rm SF}(\mu_0) = 2.012$, and $\mu_{\rm PT} = 16\mu_0$ which are roughly estimated as

$$1/L_{\rm max} \equiv \mu_{\rm had} \approx 0.2\ {\rm GeV},\ \mu_0 \approx 4\ {\rm GeV},\ \mu_{\rm PT} \approx 70\ {\rm GeV}. \tag{347}$$

Step-scaling is carried out with an $\mathcal{O}(a)$-improved Wilson quark action [740] and Lüscher–Weisz gauge action [741] in the low-scale region and an $\mathcal{O}(a)$-improved Wilson quark action [742] and Wilson gauge action in the high-energy part. For the step-scaling using steps of $L/a \to 2L/a$, three lattice sizes $L/a = 8, 12, 16$ were simulated for $\bar{g}^2_{\rm GF}$ and four lattice sizes $L/a = (4,)\,6, 8, 12$ for $\bar{g}^2_{\rm SF}$. The final results do not use the small lattices given in parenthesis. The parameter $\Lambda^{(3)}_{\overline{\rm MS}}$ is then obtained via

$$\Lambda^{(3)}_{\overline{\rm MS}} = \underbrace{\frac{\Lambda^{(3)}_{\overline{\rm MS}}}{\mu_{\rm PT}}}_{\text{perturbation theory}} \times \underbrace{\frac{\mu_{\rm PT}}{\mu_{\rm had}}}_{\text{step-scaling}} \times \underbrace{\frac{\mu_{\rm had}}{f_{\pi K}}}_{\text{large volume simulation}} \times \underbrace{f_{\pi K}}_{\text{experimental data}}, \tag{348}$$

where the hadronic scale $f_{\pi K}$ is $f_{\pi K} = \frac{1}{3}(2f_K + f_\pi) = 147.6(5)$ MeV. The first factor on the right hand side of Eq. (348) is obtained from $\alpha_{\rm SF}(\mu_{\rm PT})$ which is the output from SF step-scaling using Eq. (320) with $\alpha_{\rm SF}(\mu_{\rm PT}) \approx 0.1$ and the 3-loop β-function and the exact conversion to the $\overline{\rm MS}$-scheme. The second factor is essentially obtained from step-scaling in the GF scheme and the measurement of $\bar{g}^2_{\rm SF}(\mu_0)$ (except for the trivial scaling factor of 16 in the SF running). The third factor is obtained from a measurement of the hadronic quantity at large volume.

A large-volume simulation is done for three lattice spacings with sufficiently large volume and reasonable control over the chiral extrapolation so that the scale determination is precise enough. The step-scaling results in both schemes satisfy renormalization criteria, perturbation theory criteria, and continuum limit criteria just as previous studies using step-scaling. So we assign green stars for these criteria.

The dependence of Λ, Eq. (320) with 3-loop β-function, on α_s and on the chosen scheme is discussed in [715]. This investigation provides a warning on estimating the truncation error of perturbative series. Details are explained in Sect. 9.2.3.

The result for the Λ parameter is $\Lambda^{(3)}_{\overline{\rm MS}} = 341(12)$ MeV, where the dominant error comes from the error of $\alpha_{\rm SF}(\mu_{\rm PT})$ after step-scaling in the SF scheme. Using 4-loop matching at the charm and bottom thresholds and 5-loop running one finally obtains

$$\alpha^{(5)}_{\overline{\rm MS}}(M_Z) = 0.11852(84). \tag{349}$$

[63] With 2-loop $\mathcal{O}(a)$ improvement we here mean c_t including the g_0^4 term and $\tilde{c}_{\rm t}$ with the g_0^2 term. For gluonic observables such as the running coupling this is sufficient for cutoff effects being suppressed to $\mathcal{O}(g^6 a)$.

Several other results do not have a sufficient number of quark flavours or do not yet contain the conversion of the scale to physical units (ALPHA 10A [735], Perez 10 [736]). Thus no value for $\alpha^{(5)}_{\overline{\rm MS}}(M_Z)$ is quoted.

The computation of Ishikawa et al. [732] is based on the gradient flow coupling with twisted boundary conditions [731] (TGF coupling) in the pure gauge theory. Again they use $c = 0.3$. Step-scaling with a scale factor $s = 3/2$ is employed, covering a large range of couplings from $\alpha_s \approx 0.5$ to $\alpha_s \approx 0.1$ and taking the continuum limit through global fits to the step-scaling function on $L/a = 12, 16, 18$ lattices with between 6 and 8 parameters. Systematic errors due to variations of the fit functions are estimated. Two physical scales are considered: r_0/a is taken from [709] and σa^2 from [194] and [743]. As the ratio $\Lambda_{\rm TGF}/\Lambda_{\overline{\rm MS}}$ has not yet been computed analytically, Ref. [732] determines the 1-loop relation between $\bar{g}_{\rm SF}$ and $\bar{g}_{\rm TGF}$ from MC simulations performed in the weak coupling region and then uses the known $\Lambda_{\rm SF}/\Lambda_{\overline{\rm MS}}$. Systematic errors due to variations of the fit functions dominate the overall uncertainty.

Since FLAG 19 two new and quite extensive $N_f = 0$ step-scaling studies have been carried out in Dalla Brida 19 [693] and by Nada and Ramos [694]. They use different strategies for the running from mid to high energies, but use the same gauge configurations and share the running at low energies and matching to the hadronic scales. These results are therefore correlated. However, given the comparatively high value for $r_0\Lambda_{\overline{\rm MS}}$, it is re-assuring that these conceptually different approaches yield perfectly compatible results within errors of similar size of around 1.5% for $\sqrt{8t_0}\Lambda_{\overline{\rm MS}} = 0.6227(98)$, or, alternatively $r_0\Lambda_{\overline{\rm MS}} = 0.660(11)$.

In Dalla Brida 19 [693] two GF-coupling definitions with SF-boundary conditions are considered, corresponding to (colour-) magnetic and electric components of the action density respectively. The coupling definitions include the projection to $Q = 0$, as was also done in [77]. The flow time parameter is set to $c = 0.3$, and both Zeuthen and Wilson flow are measured. Lattice sizes range from $L/a = 8$ to $L/a = 48$, covering up to a factor of 3 in lattice spacings for the step-scaling function, where both L/a and $2L/a$ are needed. Lattice effects in the step-scaling function are visible but can be extrapolated using global fits with a^2 errors. Some remnant $\mathcal{O}(a)$ effects from the boundaries are expected, as their perturbative cancellation is incomplete. These $\mathcal{O}(a)$ contaminations are treated as a systematic error on the data, following [77] and are found to be subdominant. An intermediate reference scale $\mu_{\rm ref}$ is defined where $\alpha = 0.2$, and the scales above and below are analyzed separately. Again this is similar to [77], except that here GF coupling data is available also at high energy scales. The GF β-functions are then obtained by fitting to the continuum extrapolated data for the step-scaling functions. In addition, a nonperturbative matching to the standard SF coupling is performed above $\mu_{\rm ref}$ for a range of couplings covering a factor 2. The nonperturbative β-function for the SF scheme can thus be inferred from the GF β-function. It turns out that GF schemes are very slow to reach the perturbative regime. Particularly the Λ-parameter for the magnetic GF coupling shows a large slope in α^2, which is the parametric uncertainty with known 3-loop β-function. Also, convincing contact with the 3-loop β-function is barely seen down to $\alpha = 0.08$. This is likely to be related to the rather large 3-loop β-function coefficients, especially for the magnetic GF scheme [733]. In contrast, once the GF couplings are matched nonperturbatively to the SF scheme the contact to perturbative running can be safely made. It is also re-assuring that in all cases the extrapolations (linear in α^2) to $\alpha = 0$ for the Λ-parameters agree very well, and the authors argue in favour of such extrapolations. Their data confirms that this procedure yields consistent results with the SF scheme for $\nu = 0$, where such an extrapolation is not required.

The low energy regime between $\mu_{\rm ref}$ and a hadronic scale $\mu_{\rm had}$ is covered again using the nonperturbative step-scaling function and the derived β-function. Finally, contact between $\mu_{\rm had}$ and hadronic scales t_0 and r_0 is established using 5 lattice spacings covering a factor up to 2.7. The multitude of cross checks of both continuum limit and perturbative truncation errors make this a study which passes all current FLAG criteria by some margin. The comparatively high value for $r_0\Lambda_{\overline{\rm MS}}$ found in this study must therefore be taken very seriously.

In Nada 20 [694], Nada and Ramos provide further consistency checks of [693] for scales larger than $\mu_{\rm ref}$. The step scaling function for $c = 0.2$ is constructed in 2 steps, by determining first the relation between couplings for $c = 0.2$ and $c = 0.4$ at the same L and then increasing L to $2L$ keeping the flow time fixed (in units of the lattice spacing), so that one arrives again at $c = 0.2$ on the $2L$ volume. The authors demonstrate that the direct construction of the step-scaling function for $c = 0.2$ would require much larger lattices in order to control the continuum limit at the same level of precision. The consistency with [693] for the Λ-parameter is therefore a highly non-trivial check on the systematic effects of the continuum extrapolations. The study obtains results for the Λ-parameter (again extrapolating to $\alpha = 0$) with a similar error as in [693]. using the low-energy running and matching to the hadronic scale from that reference. For this reason and since gauge configurations are shared between both papers, these results are not independent of [693], so Dalla Brida 19 will be taken as representative for both works.

9.4 The decoupling method

The ALPHA collaboration has proposed a new strategy to compute the Λ parameter in QCD with $N_f \geq 3$ flavours based on simultaneous decoupling of $N_f \geq 3$ heavy quarks with RGI mass M [692]. We refer to [744] for a pedagogical introduction and to [745] for recent results. Generically, a running coupling in a mass-dependent renormalization scheme

$$\bar{g}^2(\mu, M)^{(N_f)} = \bar{g}^2(\mu)^{(N_f=0)} + O(M^{-k}) \tag{350}$$

can be represented by the corresponding $N_f = 0$ coupling, up to power corrections in $1/M$. The leading power is usually $k = 2$, however renormalization schemes in finite volume may have $k = 1$, depending on the set-up. For example, this is the case with standard SF or open boundary conditions in combination with a standard mass term. In practice one may try to render such boundary contributions numerically small by a careful choice of the scheme's parameters. In principle, power corrections can be either $(\mu/M)^k$ or $(\Lambda/M)^k$. Fixing $\mu = \mu_{\rm dec}$, e.g. by prescribing a value for the mass-independent coupling, such that $\mu_{\rm dec}/\Lambda = \mathcal{O}(1)$ thus helps to reduce the need for very large M. Defining $\bar{g}^2(\mu_{\rm dec}, M) = u_M$ at fixed $\bar{g}^2(\mu_{\rm dec}, M = 0)$, Eq. (350) translates to a relation between Λ-parameters, which can be cast in the form,

$$\frac{\Lambda_{\overline{\rm MS}}^{(N_f)}}{\mu_{\rm dec}}\, P\left(\frac{M}{\mu_{\rm dec}}\frac{\mu_{\rm dec}}{\Lambda_{\overline{\rm MS}}^{(N_f)}}\right) = \frac{\Lambda_{\overline{\rm MS}}^{(0)}}{\Lambda_s^{(0)}}\,\varphi_s^{(N_f=0)}\left(\sqrt{u_{\rm M}}\right) + \mathcal{O}(M^{-k}), \tag{351}$$

with the function φ_s as defined in Eq. (320), for scheme s and $N_f = 0$. A crucial observation is that the function P, which gives the ratios of Λ-parameters $\Lambda_{\overline{\rm MS}}^{(0)}/\Lambda_{\overline{\rm MS}}^{(N_f)}$, can be evaluated perturbatively to a very good approximation [158,160]. Eq. (350) also implies a relation between the couplings in mass-independent schemes, in the theories with N_f and zero flavours, respectively. In the $\overline{\rm MS}$ scheme this relation is analogous to Eq. (327),

$$\bar{g}^2_{\overline{\rm MS}}(m_\star)^{(N_f=0)} = \bar{g}^2_{\overline{\rm MS}}(m_\star)^{(N_f)} \times C\left(\bar{g}_{\overline{\rm MS}}(m_\star)^{(N_f)}\right) \tag{352}$$

and the function $C(g)$ is also known up to to 4-loop order [685–688,746]. The function $P(y)$, with $y \equiv M/\Lambda_{\overline{\rm MS}}^{(N_f)}$ can therefore be evaluated perturbatively in the $\overline{\rm MS}$ scheme, as the ratio

$$P(y) = \frac{\varphi_{\overline{\rm MS}}^{(N_f=0)}\left(g^\star(y)\sqrt{C(g^\star(y))}\right)}{\varphi_{\overline{\rm MS}}^{(N_f)}(g^\star(y))}, \qquad g^\star(y) = \bar{g}_{\overline{\rm MS}}^{(N_f)}(m_\star). \tag{353}$$

Hence, perturbation theory is only required at the scale set by the heavy-quark mass, which works the better the larger M can be chosen. Once P is known, the LHS of (351) can be inferred from a $N_f = 0$ computation of the RHS in the scheme s, assuming the ratio $\Lambda_{\overline{\rm MS}}/\Lambda_s$ is known from a 1-loop calculation.

To put the decoupling strategy into practice, the ALPHA collaboration uses $N_f = 3$, so that information from [77] can be used. Using the massless GF coupling in finite volume from this project, $\mu_{\rm dec}$ is defined through $\bar{g}^2_{\rm GF}(\mu_{\rm dec}) = 3.95$, and thus known in physical units, $\mu_{\rm dec} = 789(15)$ MeV. Varying L/a between 12 and 32 (five lattice spacings) defines a range of values for the bare coupling along a line of constant $\mu_{\rm dec}$ and for vanishing quark mass. Next, a mass-dependent GF coupling is defined at constant $\mu_{\rm dec}$, using the available information on nonperturbative mass renormalization [203] and $\mathcal{O}(a)$ improvement. In order to obtain a larger suppression of the leading $1/M$ boundary correction term, the time extent T is here set to $2L$, so as to maximize the distance to the time boundaries. Choosing 4 values of $z = M/\mu_{\rm dec}$ within the range from 2 to 8, with up to 5 lattice spacings[64] and using precision results for $N_f = 0$ from [693] then leads to the result for $\Lambda_{\overline{\rm MS}}^{(N_f=3)}$, up to power corrections in $1/z$, expected to be predominantly of order $1/z^2$. Figure 39, taken from [692] shows the continuum extrapolated results obtained for $\Lambda_{\overline{\rm MS}}^{(3)}/\mu_{\rm dec}$ at different values of z, together with the FLAG 19 average for three-flavour QCD. While the authors of [692] stopped short of quoting an extrapolated value for the three-flavour Λ-parameter, the result $\Lambda_{\overline{\rm MS}}^{(3)} = 332(10)(2)$ MeV is now given in the 2021 lattice conference proceedings [745], compatible with ALPHA 17 albeit with a somewhat smaller error. Despite some common elements with ALPHA 17, the authors emphasize that the decoupling

[64] At the largest mass, $z = 8$, only the 2-3 finest lattice spacings are useful in a linear extrapolation in a^2.

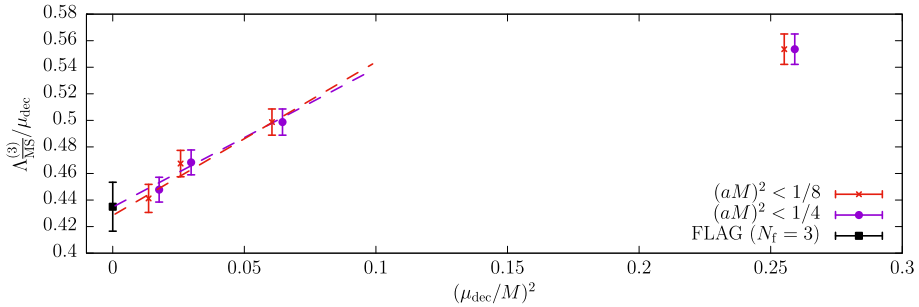

Fig. 39 Illustration of the decoupling method, taken from Ref. [692]

method is largely independent, with the overlap in squared error amounting to ca. 40 percent. This is due to the fact that the error in ALPHA 17 is dominated by the $N_f = 3$ step scaling procedure at *high* energy, and this part is completely replaced by the $N_f = 0$ result by Dalla Brida 19 [693]. The decoupling method thus seems to offer scope for a further error reduction, the major challenges being the continuum extrapolation for the GF coupling at fixed and large RGI masses, followed by the large M limit.

It is important to note that this new method relies on new precision results for $N_f = 0$ which have appeared in the last two years [693,694]. Therefore, the pure gauge theory acquires new relevance for α_s results, beyond its traditional rôle as a test bed for the study of systematic errors. FLAG will take account of this development by continuing to carefully monitor $N_f = 0$ results. It is hoped that this will encourage more groups to undertake precision studies with $N_f = 0$.

9.5 α_s from the potential at short distances

9.5.1 General considerations

The basic method was introduced in Ref. [747] and developed in Ref. [748]. The force or potential between an infinitely massive quark and antiquark pair defines an effective coupling constant via

$$F(r) = \frac{dV(r)}{dr} = C_F \frac{\alpha_{\rm qq}(r)}{r^2}. \tag{354}$$

The coupling can be evaluated nonperturbatively from the potential through a numerical differentiation, see below. In perturbation theory one also defines couplings in different schemes $\alpha_{\bar{V}}, \alpha_V$ via

$$V(r) = -C_F \frac{\alpha_{\bar{V}}(r)}{r}, \quad \text{or} \quad \tilde{V}(Q) = -C_F \frac{\alpha_V(Q)}{Q^2}, \tag{355}$$

where one fixes the unphysical constant in the potential by $\lim_{r\to\infty} V(r) = 0$ and $\tilde{V}(Q)$ is the Fourier transform of $V(r)$. Nonperturbatively, the subtraction of a constant in the potential introduces an additional renormalization constant, the value of $V(r_{\rm ref})$ at some distance $r_{\rm ref}$. Perturbatively, it is believed to entail a renormalon ambiguity. In perturbation theory, the different definitions are all simply related to each other, and their perturbative expansions are known including the α_s^4, $\alpha_s^4 \log \alpha_s$ and $\alpha_s^5 \log \alpha_s$, $\alpha_s^5 (\log \alpha_s)^2$ terms [749–756].

The potential $V(r)$ is determined from ratios of Wilson loops, $W(r,t)$, which behave as

$$\langle W(r,t) \rangle = |c_0|^2 e^{-V(r)t} + \sum_{n\neq 0} |c_n|^2 e^{-V_n(r)t}, \tag{356}$$

where t is taken as the temporal extension of the loop, r is the spatial one and V_n are excited-state potentials. To improve the overlap with the ground state, and to suppress the effects of excited states, t is taken large. Also various additional techniques are used, such as a variational basis of operators (spatial paths) to help in projecting out the ground state. Furthermore some lattice-discretization effects can be reduced by averaging over Wilson loops related by rotational symmetry in the continuum.

In order to reduce discretization errors it is of advantage to define the numerical derivative giving the force as

$$F(r_{\rm I}) = \frac{V(r) - V(r-a)}{a}, \tag{357}$$

Table 61 Short-distance potential results

Collaboration	Refs.	N_f	Publication status	Renormalization scale	Perturbative behaviour	Continuum extrapolation	Scale	$\Lambda_{\overline{\text{MS}}}$ [MeV]	$r_0\Lambda_{\overline{\text{MS}}}$
Ayala 20	[74]	2+1	A	○	★	○	$r_1 = 0.3106(17)$ fm[c]	338(13)	0.802(31)
TUMQCD 19	[75]	2+1	A	○	★	○	$r_1 = 0.3106(17)$ fm[c]	314^{+16}_{-8}	$0.745(^{+38}_{-19})$
Takaura 18	[758,759]	2+1	A	■	○	○	$\sqrt{t_0} = 0.1465(25)$fm[a]	$334(10)(^{+20}_{-18})$[b]	$0.799(51)^{+}$
Bazavov 14	[760]	2+1	A	○	★	○	$r_1 = 0.3106(17)$ fm[c]	$315(^{+18}_{-12})$[d]	$0.746(^{+42}_{-27})$
Bazavov 12	[761]	2+1	A	○[†]	○	○[#]	$r_0 = 0.468$ fm	295(30)[⋆]	0.70(7)[⋆⋆]
Karbstein 18	[762]	2	A	○	○	○	$r_0 = 0.420(14)$ fm[e]	302(16)	0.643(34)
Karbstein 14	[763]	2	A	○	○	○	$r_0 = 0.42$ fm	331(21)	0.692(31)
ETM 11C	[764]	2	A	○	○	○	$r_0 = 0.42$ fm	315(30)[§]	0.658(55)
Husung 20	[695]	0	C	○	★	★	No quoted value for $\Lambda_{\overline{\text{MS}}}$		
Husung 17	[765]	0	C	○	★	★	$r_0 = 0.50$ fm	232(6)	0.590(16)
Brambilla 10	[766]	0	A	○	★	○[††]		$266(13)^{+}$	$0.637(^{+32}_{-30})$[††]
UKQCD 92	[748]	0	A	★	○[++]	■	$\sqrt{\sigma} = 0.44$ GeV	256(20)	0.686(54)
Bali 92	[767]	0	A	★	○[++]	■	$\sqrt{\sigma} = 0.44$ GeV	247(10)	0.661(27)

[a] Scale determined from t_0 in Ref. [114]
[b] $\alpha^{(5)}_{\overline{\text{MS}}}(M_Z) = 0.1179(7)(^{+13}_{-12})$
[c] Determination on lattices with $m_\pi L = 2.2 - 2.6$. Scale from r_1 [116] as determined from f_π in Ref. [41]
[d] $\alpha^{(3)}_{\overline{\text{MS}}}(1.5\,\text{GeV}) = 0.336(^{+12}_{-8})$, $\alpha^{(5)}_{\overline{\text{MS}}}(M_Z) = 0.1166(^{+12}_{-8})$
[e] Scale determined from f_π, see [87]
[†] Since values of α_{eff} within our designated range are used, we assign a ○ despite values of α_{eff} up to $\alpha_{\text{eff}} = 0.5$ being used
[#] Since values of $2a/r$ within our designated range are used, we assign a ○ although only values of $2a/r \geq 1.14$ are used at $\alpha_{\text{eff}} = 0.3$
[⋆] Using results from Ref. [708]
[⋆⋆] $\alpha^{(3)}_{\overline{\text{MS}}}(1.5\,\text{GeV}) = 0.326(19)$, $\alpha^{(5)}_{\overline{\text{MS}}}(M_Z) = 0.1156(^{+21}_{-22})$
[§] Both potential and r_0/a are determined on a small ($L = 3.2r_0$) lattice
[††] Uses lattice results of Ref. [709], some of which have very small lattice spacings where according to more recent investigations a bias due to the freezing of topology may be present
[+] Our conversion using $r_0 = 0.472$ fm
[++] We give a ○ because only a NLO formula is used and the error bars are very large; our criterion does not apply well to these very early calculations

where r_1 is chosen so that at tree level the force is the continuum force. $F(r_1)$ is then a 'tree-level improved' quantity and similarly the tree-level improved potential can be defined [757].

Lattice potential results are in position space, while perturbation theory is naturally computed in momentum space at large momentum. Usually, the Fourier transform of the perturbative expansion is then matched to lattice data.

Finally, as was noted in Sect. 9.2.1, a determination of the force can also be used to determine the scales r_0, r_1, by defining them from the static force by

$$r_0^2 F(r_0) = 1.65, \quad r_1^2 F(r_1) = 1. \tag{358}$$

9.5.2 *Discussion of computations*

In Table 61, we list results of determinations of $r_0\Lambda_{\overline{\text{MS}}}$ (together with $\Lambda_{\overline{\text{MS}}}$ using the scale determination of the authors).

Since the last review, FLAG 19, there have been three new publications, namely, TUMQCD 19 [75], Ayala 20 [74] and Husung 20 [695].

The first determinations in the three-colour Yang Mills theory are by UKQCD 92 [748] and Bali 92 [767] who used α_{qq} as explained above, but not in the tree-level improved form. Rather a phenomenologically determined lattice-artifact correction

was subtracted from the lattice potentials. The comparison with perturbation theory was on a more qualitative level on the basis of a 2-loop β-function ($n_l = 1$) and a continuum extrapolation could not be performed as yet. A much more precise computation of $\alpha_{\rm qq}$ with continuum extrapolation was performed in Refs. [709,757]. Satisfactory agreement with perturbation theory was found [757] but the stability of the perturbative prediction was not considered sufficient to be able to extract a Λ parameter.

In Brambilla 10 [766] the same quenched lattice results of Ref. [757] were used and a fit was performed to the continuum potential, instead of the force. Perturbation theory to $n_l = 3$ loop was used including a resummation of terms $\alpha_s^3(\alpha_s \ln \alpha_s)^n$ and $\alpha_s^4(\alpha_s \ln \alpha_s)^n$. Close agreement with perturbation theory was found when a renormalon subtraction was performed. Note that the renormalon subtraction introduces a second scale into the perturbative formula which is absent when the force is considered.

Bazavov 14 [760] updates Bazavov 12 [761] and modifies this procedure somewhat. They consider the perturbative expansion for the force. They set $\mu = 1/r$ to eliminate logarithms and then integrate the force to obtain an expression for the potential. The resulting integration constant is fixed by requiring the perturbative potential to be equal to the nonperturbative one exactly at a reference distance $r_{\rm ref}$ and the two are then compared at other values of r. As a further check, the force is also used directly.

For the quenched calculation of Brambilla 10 [766] very small lattice spacings, $a \sim 0.025\,\text{fm}$, were available from Ref. [757]. For ETM 11C [764], Bazavov 12 [761], Karbstein 14 [763] and Bazavov 14 [760] using dynamical fermions such small lattice spacings are not yet realized (Bazavov 14 reaches down to $a \sim 0.041\,\text{fm}$). They all use the tree-level improved potential as described above. We note that the value of $\Lambda_{\overline{\rm MS}}$ in physical units by ETM 11C [764] is based on a value of $r_0 = 0.42$ fm. This is at least 10% smaller than the large majority of other values of r_0. Also the values of r_0/a on the finest lattices in ETM 11C [764] and r_1/a for Bazavov 14 [760] come from rather small lattices with $m_\pi L \approx 2.4, 2.2$ respectively.

Instead of the procedure discussed previously, Karbstein 14 [763] reanalyzes the data of ETM 11C [764] by first estimating the Fourier transform $\tilde{V}(p)$ of $V(r)$ and then fitting the perturbative expansion of $\tilde{V}(p)$ in terms of $\alpha_{\overline{\rm MS}}(p)$. Of course, the Fourier transform requires some modelling of the r-dependence of $V(r)$ at short and at large distances. The authors fit a linearly rising potential at large distances together with string-like corrections of order r^{-n} and define the potential at large distances by this fit.[65] Recall that for observables in momentum space we take the renormalization scale entering our criteria as $\mu = q$, Eq. (338). The analysis (as in ETM 11C [764]) is dominated by the data at the smallest lattice spacing, where a controlled determination of the overall scale is difficult due to possible finite-size effects. Karbstein 18 [762] is a reanalysis of Karbstein 14 and supersedes it. Some data with a different discretization of the static quark is added (on the same configurations) and the discrete lattice results for the static potential in position space are first parameterized by a continuous function, which then allows for an analytical Fourier transformation to momentum space.

Similarly also for Takaura 18 [758,759] the momentum space potential $\tilde{V}(Q)$ is the central object. Namely, they assume that renormalon/power-law effects are absent in $\tilde{V}(Q)$ and only come in through the Fourier transformation. They provide evidence that renormalon effects (both $u = 1/2$ and $u = 3/2$) can be subtracted and arrive at a nonperturbative term $k\,\Lambda^3_{\overline{\rm MS}} r^2$. Two different analyses are carried out with the final result taken from "Analysis II". Our numbers including the evaluation of the criteria refer to it. Together with the perturbative 3-loop (including the $\alpha_s^4 \log \alpha_s$ term) expression, this term is fitted to the nonperturbative results for the potential in the region $0.04\,\text{fm} \le r \le 0.35\,\text{fm}$, where 0.04 fm is $r = a$ on the finest lattice. The nonperturbative potential data originates from JLQCD ensembles (Symanzik-improved gauge action and Möbius domain-wall quarks) at three lattice spacings with a pion mass around 300 MeV. Since at the maximal distance in the analysis we find $\alpha_{\overline{\rm MS}}(2/r) = 0.43$, the renormalization scale criterion yields a ■. The perturbative behaviour is ○ because of the high orders in perturbation theory known. The continuum-limit criterion yields a ○.

One of the main issues for all these computations is whether the perturbative running of the coupling constant has been reached. While for $N_f = 0$ fermions Brambilla 10 [766] reports agreement with perturbative behaviour at the smallest distances, Husung 17 (which goes to shorter distances) finds relatively large corrections beyond the 3-loop $\alpha_{\rm qq}$. For dynamical fermions, Bazavov 12 [761] and Bazavov 14 [760] report good agreement with perturbation theory after the renormalon is subtracted or eliminated.

A second issue is the coverage of configuration space in some of the simulations, which use very small lattice spacings with periodic boundary conditions. Affected are the smallest two lattice spacings of Bazavov 14 [760] where very few tunnelings of the topological charge occur [116]. With present knowledge, it also seems possible that the older data by Refs. [709,757] used by Brambilla 10 [766] are partially obtained with (close to) frozen topology.

[65] Note that at large distances, where string breaking is known to occur, this is not any more the ground state potential defined by Eq. (356).

The computation in Husung 17 [765], for $N_f = 0$ flavours, first determines the coupling $\bar{g}^2_{\rm qq}(r,a)$ from the force and then performs a continuum extrapolation on lattices down to $a \approx 0.015$ fm, using a step-scaling method at short distances, $r/r_0 \lesssim 0.5$. Using the 4-loop $\beta^{\rm qq}$ function this allows $r_0\Lambda_{\rm qq}$ to be estimated, which is then converted to the $\overline{\rm MS}$ scheme. $\alpha_{\rm eff} = \alpha_{\rm qq}$ ranges from ~ 0.17 to large values; we give ○ for renormalization scale and ★ for perturbative behaviour. The range $a\mu = 2a/r \approx 0.37$–0.14 leads to a ★ in the continuum extrapolation. Recently these calculations have been extended in Husung 20 [695]. A finer lattice spacing of $a = 0.01$ fm (scale from $r_0 = 0.5$ fm) is reached and lattice volumes up to $L/a = 192$ are simulated (in Ref. [765] the smallest lattice spacing is 0.015 fm). The Wilson action is used despite its significantly larger cutoff effects compared to Symanzik-improved actions; this avoids unitarity violations, thus allowing for a clean ground state extraction via a generalized eigenvalue problem. Open boundary conditions are used to avoid the topology-freezing problem. Furthermore, new results for the continuum approach are employed, which determine the cutoff dependence at $\mathcal{O}(a^2)$ including the exact coupling-dependent terms, in the asymptotic region where the Symanzik effective theory is applicable [768]. An ansatz for the remaining higher order cutoff effects at $\mathcal{O}(a^4)$ is propagated as a systematic error to the data, which effectively discards data for $r/a < 3.5$. The large volume step-scaling function with step factor 3/4 is computed and compared to perturbation theory. For $\alpha_{qq} > 0.2$ there is a noticeable difference between the 2-loop and 3-loop results. Furthermore, the ultra-soft contributions at 4-loop level give a significant contribution to the static $Q\bar{Q}$ force. While this study is for $N_f = 0$ flavours it does raise the question whether the weak coupling expansion for the range of r-values used in present analyses of α_s is sufficiently reliable. Around $\alpha_{\rm qq} \approx 0.21$ the differences get smaller but the error increases significantly, mainly due to the propagated lattice artifacts. The dependence of $\Lambda^{n_f=0}_{\overline{\rm MS}}\sqrt{8t_0}$ on $\alpha^3_{\rm qq}$ is very similar to the one observed in the previous study but no value for its $\alpha_{qq} \to 0$ limit is quoted. Husung 20 [695] is more pessimistic about the error on the Λ parameter stating the relative error has to be 5% or larger, while Husung 17 quotes a relative error of 3%.

In 2+1-flavor QCD two new papers appeared on the determination of the strong coupling constant from the static quark anti-quark potential after the FLAG 19 report [74,75]. In TUMQCD 19 [75][66] the 2014 analysis of Bazavov 14 [760] has been extended by including three finer lattices with lattice spacing $a = 0.035$, 0.030 and 0.025 fm as well as lattice results on the free energy of static quark anti-quark pair at non-zero temperature. On the new fine lattices the effect of freezing topology has been observed, however, it was verified that this does not affect the potential within the estimated errors [769,770]. The comparison of the lattice result on the static potential has been performed in the interval $r = [r_{\rm min}, r_{\rm max}]$, with $r_{\rm max} = 0.131$, 0.121, 0.098, 0.073 and 0.055 fm. The main result quoted in the paper is based on the analysis with $r_{\rm max} = 0.073$ fm [75]. Since the new study employs a much wider range in r than the previous one [760] we give it a ★ for the perturbative behaviour. Since $\alpha_{\rm eff} = \alpha_{qq}$ varies in the range 0.2–0.4 for the r values used in the main analysis we give ○ for the renormalization scale. Several values of $r_{\rm min}$ have been used in the analysis, the largest being $r_{\rm min}/a = \sqrt{8} \simeq 2.82$, which corresponds to $a\mu \simeq 0.71$. Therefore, we give a ○ for continuum extrapolation in this case. An important difference compared to the previous study [760] is the variation of the renormalization scale. In Ref. [760] the renormalization scale was varied by a factor of $\sqrt{2}$ around the nominal value of $\mu = 1/r$, in order to exclude very low scales, for which the running of the strong coupling constant is no longer perturbative. In the new analysis the renormalization scale was varied by a factor of two. As the result, despite the extended data set and shorter distances used in the new study the perturbative error did not decrease [75]. We also note that the scale dependence turned out to be non-monotonic in the range $\mu = 1/(2r)$–$2/r$ [75]. The final result reads ("us" stands for "ultra-soft"),

$$\Lambda^{N_f=3}_{\overline{\rm MS}} = 314.0 \pm 5.8({\rm stat}) \pm 3.0({\rm lat}) \pm 1.7({\rm scale})^{+13.4}_{-1.8}({\rm pert}) \pm 4.0({\rm pert.\ us})\ {\rm MeV} = 314^{+16}_{-08}\ {\rm MeV}, \tag{359}$$

where all errors were combined in quadrature. This is in very good agreement with the previous determination [760].

The analysis was also applied to the singlet static quark anti-quark free energy at short distances. At short distances the free energy is expected to be the same as the static potential. This is verified numerically in the lattice calculations TUMQCD 19 [75] for $rT < 1/4$ with T being the temperature. Furthermore, this is confirmed by the perturbative calculations at $T > 0$ at NLO [771]. The advantage of using the free energy is that it gives access to much shorter distances. On the other hand, one has fewer data points because the condition $rT < 1/4$ has to be satisfied. The analysis based on the free energy gives

$$\Lambda^{N_f=3}_{\overline{\rm MS}} = 310.9 \pm 11.3({\rm stat}) \pm 3.0({\rm lat}) \pm 1.7({\rm scale})^{+5.6}_{-0.8}({\rm pert}) \pm 2.1({\rm pert.\ us})\ {\rm MeV} = 311(13)\ {\rm MeV}, \tag{360}$$

in good agreement with the above result and thus, providing additional confirmation of it.

[66] The majority of authors are the same as in [760].

The analysis of Ayala 20 [74] uses a subset of data presented in TUMQCD 19 [75] with the same correction of the lattice effects. For this reason the continuum extrapolation gets ○, too. They match to perturbation theory for $1/r > 2$ GeV, which corresponds to $\alpha_{\rm eff} = \alpha_{qq} = 0.2$–$0.4$. Therefore, we give ○ for the renormalization scale. They verify the perturbative behaviour in the region 1 GeV $< 1/r <$ 2.9 GeV, which corresponds to variation of $\alpha^3_{\rm eff}$ by a factor of 3.34. However, the relative error on the final result has $\delta\Lambda/\Lambda \simeq 0.035$ which is larger than $\alpha^3_{\rm eff} = 0.011$. Therefore, we give a ★ for the perturbative behaviour in this case. The final result for the Λ-parameter reads:

$$\Lambda^{N_f=3}_{\overline{\rm MS}} = 338 \pm 2({\rm stat}) \pm 8({\rm matching}) \pm 10({\rm pert})\ \ {\rm MeV} = 338(13)\,{\rm MeV}. \tag{361}$$

This is quite different from the above result. This difference is mostly due to the organization of the perturbative series. The authors use ultra-soft (log) resummation, i.e. they resum the terms $\alpha_s^{3+n} \ln^n \alpha_s$ to all orders instead of using fixed-order perturbation theory. They also include what is called the terminant of the perturbative series associated to the leading renormalon of the force [74]. When they use fixed order perturbation theory they obtain very similar results to Refs. [75,760]. It has been argued that log resummation cannot be justified since for the distance range available in the lattice studies α_s is not small enough and the logarithmic and non-logarithmic higher-order terms are of a similar size [760]. On the other hand, the resummation of ultra-soft logs does not lead to any anomalous behaviour of the perturbative expansion like large scale dependence or bad convergence [74].

To obtain the value of $\Lambda^{N_f=3}_{\overline{\rm MS}}$ from the static potential we combine the results in Eqs. (359) and (361) using the weighted average with the weight given by the perturbative error and using the difference in the central value as the error estimate. This leads to

$$\Lambda^{N_f=3}_{\overline{\rm MS}} = 330(24)\ \ {\rm MeV}. \tag{362}$$

from the static potential determination. In the case of TUMQCD 19, where the perturbative error is very asymmetric we used the larger upper error for the calculation of the corresponding weight.

9.6 α_s from the light-quark vacuum polarization in momentum/position space

9.6.1 General considerations

Except for the new calculation Cali 20 [76], where position space is used (see below), the light-flavour-current 2-point function is usually evaluated in momentum space, in terms of the vacuum-polarization function. For the flavour-nonsinglet currents J^a_μ ($a = 1, 2, 3$) in the momentum representation this is parametrized as

$$\langle J^a_\mu J^b_\nu \rangle = \delta^{ab}[(\delta_{\mu\nu} Q^2 - Q_\mu Q_\nu)\Pi^{(1)}_J(Q) - Q_\mu Q_\nu \Pi^{(0)}_J(Q)], \tag{363}$$

where Q_μ is a space-like momentum and $J_\mu \equiv V_\mu$ for a vector current and $J_\mu \equiv A_\mu$ for an axial-vector current. Defining $\Pi_J(Q) \equiv \Pi^{(0)}_J(Q) + \Pi^{(1)}_J(Q)$, the operator product expansion (OPE) of $\Pi_{V/A}(Q)$ is given by

$$\begin{aligned}\Pi_{V/A}|_{\rm OPE}(Q^2, \alpha_s) = c + C_1^{V/A}(Q^2) + C_m^{V/A}(Q^2)\frac{\bar m^2(Q)}{Q^2} + \sum_{q=u,d,s} C^{V/A}_{\bar qq}(Q^2)\frac{\langle m_q \bar q q\rangle}{Q^4} \\ + C^{V/A}_{GG}(Q^2)\frac{\langle \alpha_s GG\rangle}{Q^4} + \mathcal{O}(Q^{-6}),\end{aligned} \tag{364}$$

for large Q^2. The perturbative coefficient functions $C_X^{V/A}(Q^2)$ for the operators X ($X = 1, \bar qq, GG$) are given as $C_X^{V/A}(Q^2) = \sum_{i\geq 0}\left(C_X^{V/A}\right)^{(i)} \alpha_s^i(Q^2)$ and $\bar m$ is the running mass of the mass-degenerate up and down quarks. $C_1^{V/A}$ is known including α_s^4 in a continuum renormalization scheme such as the $\overline{\rm MS}$ scheme [772–775]. Nonperturbatively, there are terms in $C_X^{V/A}$ that do not have a series expansion in α_s. For an example for the unit operator see Ref. [776]. The term c is Q-independent and divergent in the limit of infinite ultraviolet cutoff. However the Adler function defined as

$$D(Q^2) \equiv -Q^2\frac{d\Pi(Q^2)}{dQ^2}, \tag{365}$$

is a scheme-independent finite quantity. Therefore one can determine the running-coupling constant in the $\overline{\text{MS}}$ scheme from the vacuum-polarization function computed by a lattice-QCD simulation. Of course, there is the choice whether to use the vector or the axial vector channel, or both, the canonical choice being $\Pi_{V+A} = \Pi_V + \Pi_A$. While perturbation theory does not distinguish between these channels, the nonperturbative contributions are different, and the quality of lattice data may differ, too. For a given choice, the lattice data of the vacuum polarization is fitted with the perturbative formula Eq. (364) with fit parameter $\Lambda_{\overline{\text{MS}}}$ parameterizing the running coupling $\alpha_{\overline{\text{MS}}}(Q^2)$.

While there is no problem in discussing the OPE at the nonperturbative level, the 'condensates' such as $\langle\alpha_s GG\rangle$ are ambiguous, since they mix with lower-dimensional operators including the unity operator. Therefore one should work in the high-Q^2 regime where power corrections are negligible within the given accuracy. Thus setting the renormalization scale as $\mu \equiv \sqrt{Q^2}$, one should seek, as always, the window $\Lambda_{\text{QCD}} \ll \mu \ll a^{-1}$.

9.6.2 Definitions in position space

The 2-point current correlation functions in position space contain the same physical information as in momentum space, but the technical details are sufficiently different to warrant a separate discussion. The (Euclidean) current-current correlation function for $J^\mu_{ff'}$ (with flavour indices f, f') is taken to be either the flavour non-diagonal vector or axial vector current, with the Lorentz indices contracted,

$$C_{\text{A,V}}(x) = -\sum_\mu \left\langle J^\mu_{ff'\text{A,V}}(x) J^\mu_{f'f\text{A,V}}(0)\right\rangle = \frac{6}{\pi^4 (x^2)^3}\left(1 + \frac{\alpha_s}{\pi} + \mathcal{O}(\alpha^2)\right). \tag{366}$$

In the chiral limit, the perturbative expansion is known to α_s^4 [777], and is identical for vector and axial vector correlators. The only scale is set by the Euclidean distance $\mu = 1/|x|$ and the effective coupling can thus be defined as

$$\alpha_{\text{eff}}(\mu = 1/|x|) = \pi\left[(x^2)^3(\pi^4/6)C_{\text{A,V}}(x) - 1\right]. \tag{367}$$

As communicated to us by the authors of [76], there is a typo in Eq. (35) of [777]. For future reference, the numerical coefficients for the 3-loop conversion

$$\alpha_{\text{eff}}(\mu) = \alpha_{\overline{\text{MS}}}(\mu) + c_1\alpha^2_{\overline{\text{MS}}}(\mu) + c_2\alpha^3_{\overline{\text{MS}}}(\mu) + c_3\alpha^4_{\overline{\text{MS}}}(\mu), \tag{368}$$

should read

$$c_1 = -1.4346, \qquad c_2 = 0.16979, \qquad c_3 = 3.21120. \tag{369}$$

9.6.3 Discussion of computations

Results using this method in momentum space are, to date, only available using overlap fermions or domain-wall fermions. Since the last review, FLAG 19, there has been one new computation, Cali 20 [76], which uses the vacuum polarization in position space, using $\mathcal{O}(a)$ improved Wilson fermions. The results are collected in Table 62 for $N_f = 2$, JLQCD/TWQCD 08C [778] and for $N_f = 2+1$, JLQCD 10 [779], Hudspith 18 [780] and Cali 20 [76].

We first discuss the results of JLQCD/TWQCD 08C [778] and JLQCD 10 [779]. The fit to Eq. (364) is done with the 4-loop relation between the running coupling and $\Lambda_{\overline{\text{MS}}}$. It is found that without introducing condensate contributions, the momentum scale where the perturbative formula gives good agreement with the lattice results is very narrow, $aQ \simeq 0.8$–1.0. When a condensate contribution is included the perturbative formula gives good agreement with the lattice results for the extended range $aQ \simeq 0.6$–1.0. Since there is only a single lattice spacing $a \approx 0.11$ fm there is a ■ for the continuum limit. The renormalization scale μ is in the range of $Q = 1.6$–2 GeV. Approximating $\alpha_{\text{eff}} \approx \alpha_{\overline{\text{MS}}}(Q)$, we estimate that $\alpha_{\text{eff}} = 0.25$–$0.30$ for $N_f = 2$ and $\alpha_{\text{eff}} = 0.29$–$0.33$ for $N_f = 2+1$. Thus we give a ○ and ■ for $N_f = 2$ and $N_f = 2+1$, respectively, for the renormalization scale and a ■ for the perturbative behaviour.

A further investigation of this method was initiated in Hudspith 15 [781] and completed by Hudspith 18 [780] (see also [782]) based on domain-wall fermion configurations at three lattice spacings, $a^{-1} = 1.78, 2.38, 3.15$ GeV, with three different light-quark masses on the two coarser lattices and one on the fine lattice. An extensive discussion of condensates, using continuum finite-energy sum rules was employed to estimate where their contributions might be negligible. It was found that

Table 62 Results from the vacuum polarization in both momentum and position space

Collaboration	Ref.	N_f	Publication status	Renormalization scale	Perturbative behaviour	Continuum extrapolation	Scale	$\Lambda_{\overline{\text{MS}}}$ [MeV]	$r_0\Lambda_{\overline{\text{MS}}}$
Cali 20	[76]	2+1	A	○	★	★	$m_\Upsilon^{\S}$	342(17)	0.818(41)[a]
Hudspith 18	[780]	2+1	P	○	○	■	$m_\Omega^\star$	337(40)	0.806(96)[b]
Hudspith 15	[781]	2+1	C	○	○	■	$m_\Omega^\star$	300(24)$^+$	0.717(58)
JLQCD 10	[779]	2+1	A	■	○	■	$r_0 = 0.472$ fm	247(5)†	0.591(12)
JLQCD/TWQCD 08C	[778]	2	A	○	○	■	$r_0 = 0.49$ fm	234(9)$(^{+16}_{-0})$	0.581(22)$(^{+40}_{-0})$

[§] Via t_0/a^2, still unpublished. We use $r_0 = 0.472$ fm

[⋆] Determined in [8]

[a] Evaluates to $\alpha^{(5)}_{\overline{\text{MS}}}(M_Z) = 0.11864(114)$
In conversion to $r_0\Lambda$ we used $r_0 = 0.472$ fm.

[b] $\alpha^{(5)}_{\overline{\text{MS}}}(M_Z) = 0.1181(27)(^{+8}_{-22})$. $\Lambda_{\overline{\text{MS}}}$ determined by us from $\alpha^{(3)}_{\overline{\text{MS}}}(2\,\text{GeV}) = 0.2961(185)$. In conversion to $r_0\Lambda$ we used $r_0 = 0.472$ fm

[+] Determined by us from $\alpha^{(3)}_{\overline{\text{MS}}}(2\text{ GeV}) = 0.279(11)$. Evaluates to $\alpha^{(5)}_{\overline{\text{MS}}}(M_Z) = 0.1155(18)$

[†] $\alpha^{(5)}_{\overline{\text{MS}}}(M_Z) = 0.1118(3)(^{+16}_{-17})$

even up to terms of $O((1/Q^2)^8)$ (a higher order than depicted in Eq. (364) but with constant coefficients) no single condensate dominates and apparent convergence was poor for low Q^2 due to cancellations between contributions of similar size with alternating signs. (See, e.g., the list given by Hudspith 15 [781].) Choosing Q^2 to be at least $\sim 3.8\,\text{GeV}^2$ mitigated the problem, but then the coarsest lattice had to be discarded, due to large lattice artefacts. So this gives a ■ for continuum extrapolation. With the higher Q^2 the quark-mass dependence of the results was negligible, so ensembles with different quark masses were averaged over. A range of Q^2 from 3.8–16 GeV^2 gives $\alpha_{\text{eff}} = 0.31$–$0.22$, so there is a ○ for the renormalization scale. The value of α^3_{eff} reaches $\Delta\alpha_{\text{eff}}/(8\pi b_0\alpha_{\text{eff}})$ and thus gives a ○ for perturbative behaviour. In Hudspith 15 [781] (superseded by Hudspith 18 [780]) about a 20% difference in $\Pi_V(Q^2)$ was seen between the two lattice spacings and a result is quoted only for the smaller a.

9.6.4 Vacuum polarization in position space

Cali 20 [76] evaluate the light-current 2-point function in position space. The 2-point functions for the nonperturbatively renormalized (non-singlet) flavour currents is computed for distances $|x|$ between 0.1 and 0.25 fm and extrapolated to the chiral limit. The available CLS configurations are used for this work, with lattice spacings between 0.039 and 0.086 fm. Despite fully nonperturbative renormalization and $\mathcal{O}(a)$ improvement, the remaining $\mathcal{O}(a^2)$ effects, as measured by $O(4)$ symmetry violations, are very large, even after subtraction of tree-level lattice effects. Therefore the authors performed a numerical stochastic perturbation theory (NSPT) simulation in order to determine the lattice artifacts at $\mathcal{O}(g^2)$. Only after subtraction of these effects the constrained continuum extrapolations from 3 different lattice directions to the same continuum limit are characterized by reasonable χ^2-values, so the feasibility of the study crucially depends on this step. Interestingly, there is no subtraction performed of nonperturbative effects. For instance, chiral-symmetry breaking would manifest itself in a difference between the vector and the axial vector 2-point functions, and is invisible to perturbation theory, where these 2-point functions are known to α_s^4 [777]. According to the authors, phenomenological estimates suggest that a difference of 1.5% between the continuum correlators would occur around 0.3 fm and this difference would not be resolvable by their lattice data. Equality within their errors is confirmed for shorter distances. We note, however, that chiral symmetry breaking effects are but one class of nonperturbative effects, and their smallness does not allow for the conclusion that such effects are generally small. In fact, the need for explicit subtractions in momentum space analyses may lead one to suspect that such effects are not negligible at the available distance scales. For the determination of $\Lambda^{N_f=3}_{\overline{\text{MS}}}$ the authors limit the range of distances to 0.13–0.19 fm, where $\alpha_{\text{eff}} \in [0.2354, 0.3075]$ (private communication by the authors). These effective couplings are converted

to $\overline{\text{MS}}$ couplings at the same scales $\mu = 1/|x|$ by solving Eq. (368) numerically. Central values for the Λ-parameter thus obtained are in the range 325–370 MeV (using the β-function at 5-loop order) and a weighted average yields the quoted result 342(17) MeV, where the average emphasizes the data around $|x| = 0.16$ fm, or $\mu = 1.3$ GeV.

Applying the FLAG criteria the range of lattice spacings yields ★ for the continuum extrapolation. However, the FLAG criterion implicitly assumes that the remaining cutoff effects after non-perturbative $\mathcal{O}(a)$ improvement are small, which is not the case here. Some hypercubic lattice artefacts are still rather large even after 1-loop subtraction, but these are not used for the analysis. As for the renormalization scale, the lowest effective coupling entering the analysis is $0.235 < 0.25$, so we give ○. As for perturbative behaviour, for the range of couplings in the above interval α^3_{eff} changes by $(0.308/0.235)^3 \approx 2.2$, marginally reaching $(3/2)^2 = 2.25$. The errors $\Delta\alpha_{\text{eff}}$ after continuum and chiral extrapolations are 4–6% (private communication by the authors) and the induced uncertainty in Λ is comfortably above $2\alpha^3_{\text{eff}}$, which gives a ★ according to FLAG criteria.

Although the current FLAG criteria are formally passed by this result, the quoted error of 5% for Λ seems very optimistic. We have performed a simple test, converting to the $\overline{\text{MS}}$ scheme by inverting Eq. (368) perturbatively (instead of solving the fixed-order equation numerically). The differences between the couplings are of order α_s^5 and thus indicative of the sensitivity to perturbative truncation errors. The resulting Λ-parameter estimates are now in the range 409–468 MeV, i.e. ca. 15–30% larger than before. While the difference between both estimates decreases proportionally to the expected α^3_{eff}, an extraction of the Λ-parameter in this energy range is a priori affected by systematic uncertainties corresponding to such differences. The FLAG criterion might fail to capture this e.g. if the assumption of an $\mathcal{O}(1)$ coefficient for the asymptotic α^3_{eff} behaviour is not correct. Some indication for a problematic behaviour is indeed seen when perturbatively inverting Eq. (368) to order α_s^3. The resulting $\overline{\text{MS}}$ couplings are then closer to the values used in Cali 20, although the difference is formally $\mathcal{O}(\alpha_s^4)$ rather than $\mathcal{O}(\alpha_s^5)$.

9.7 α_s from observables at the lattice spacing scale

9.7.1 General considerations

The general method is to evaluate a short-distance quantity $\mathcal{Q}$ at the scale of the lattice spacing $\sim 1/a$ and then determine its relationship to $\alpha_{\overline{\text{MS}}}$ via a perturbative expansion.

This is epitomized by the strategy of the HPQCD collaboration [783,784], discussed here for illustration, which computes and then fits to a variety of short-distance quantities

$$Y = \sum_{n=1}^{n_{\max}} c_n \alpha^n_{\text{V}'}(q^*). \tag{370}$$

The quantity Y is taken as the logarithm of small Wilson loops (including some nonplanar ones), Creutz ratios, 'tadpole-improved' Wilson loops and the tadpole-improved or 'boosted' bare coupling ($\mathcal{O}(20)$ quantities in total). The perturbative coefficients c_n (each depending on the choice of Y) are known to $n = 3$ with additional coefficients up to $n_{\max}$ being fitted numerically. The running coupling $\alpha_{\text{V}'}$ is related to α_{V} from the static-quark potential (see Sect. 9.5).[67]

The coupling constant is fixed at a scale $q^* = d/a$. The latter is chosen as the mean value of $\ln q$ with the one-gluon loop as measure [785,786]. (Thus a different result for d is found for every short-distance quantity.) A rough estimate yields $d \approx \pi$, and in general the renormalization scale is always found to lie in this region.

For example, for the Wilson loop $W_{mn} \equiv \langle W(ma, na)\rangle$ we have

$$\ln\left(\frac{W_{mn}}{u_0^{2(m+n)}}\right) = c_1\alpha_{\text{V}'}(q^*) + c_2\alpha^2_{\text{V}'}(q^*) + c_3\alpha^3_{\text{V}'}(q^*) + \cdots, \tag{371}$$

for the tadpole-improved version, where $c_1, c_2, \ldots$ are the appropriate perturbative coefficients and $u_0 = W_{11}^{1/4}$. Substituting the nonperturbative simulation value in the left hand side, we can determine $\alpha_{\text{V}'}(q^*)$, at the scale q^*. Note that one finds empirically that perturbation theory for these tadpole-improved quantities have smaller c_n coefficients and so the series has a faster apparent convergence compared to the case without tadpole improvement.

[67] $\alpha_{\text{V}'}$ is defined by $\Lambda_{\text{V}'} = \Lambda_{\text{V}}$ and $b_i^{\text{V}'} = b_i^{\text{V}}$ for $i = 0, 1, 2$ but $b_i^{\text{V}'} = 0$ for $i \geq 3$.

Using the β-function in the V′ scheme, results can be run to a reference value, chosen as $\alpha_0 \equiv \alpha_{V'}(q_0)$, $q_0 = 7.5\,\text{GeV}$. This is then converted perturbatively to the continuum $\overline{\text{MS}}$ scheme

$$\alpha_{\overline{\text{MS}}}(q_0) = \alpha_0 + d_1\alpha_0^2 + d_2\alpha_0^3 + \cdots, \tag{372}$$

where d_1, d_2 are known 1-and 2-loop coefficients.

Other collaborations have focused more on the bare 'boosted' coupling constant and directly determined its relationship to $\alpha_{\overline{\text{MS}}}$. Specifically, the boosted coupling is defined by

$$\alpha_{\text{P}}(1/a) = \frac{1}{4\pi}\frac{g_0^2}{u_0^4}, \tag{373}$$

again determined at a scale $\sim 1/a$. As discussed previously, since the plaquette expectation value in the boosted coupling contains the tadpole-diagram contributions to all orders, which are dominant contributions in perturbation theory, there is an expectation that the perturbation theory using the boosted coupling has smaller perturbative coefficients [785], and hence smaller perturbative errors.

9.7.2 Continuum limit

Lattice results always come along with discretization errors, which one needs to remove by a continuum extrapolation. As mentioned previously, in this respect the present method differs in principle from those in which α_s is determined from physical observables. In the general case, the numerical results of the lattice simulations at a value of μ fixed in physical units can be extrapolated to the continuum limit, and the result can be analyzed as to whether it shows perturbative running as a function of μ in the continuum. For observables at the cutoff-scale ($q^* = d/a$), discretization effects cannot easily be separated out from perturbation theory, as the scale for the coupling comes from the lattice spacing. Therefore the restriction $a\mu \ll 1$ (the 'continuum-extrapolation' criterion) is not applicable here. Discretization errors of order a^2 are, however, present. Since $a \sim \exp(-1/(2b_0 g_0^2)) \sim \exp(-1/(8\pi b_0 \alpha(q^*))$, these errors now appear as power corrections to the perturbative running, and have to be taken into account in the study of the perturbative behaviour, which is to be verified by changing a. One thus usually fits with power corrections in this method.

In order to keep a symmetry with the 'continuum-extrapolation' criterion for physical observables and to remember that discretization errors are, of course, relevant, we replace it here by one for the lattice spacings used:

- Lattice spacings
  - ★ 3 or more lattice spacings, at least 2 points below $a = 0.1$ fm
  - ○ 2 lattice spacings, at least 1 point below $a = 0.1$ fm
  - ■ otherwise

9.7.3 Discussion of computations

Note that due to $\mu \sim 1/a$ being relatively large the results easily have a ★ or ○ in the rating on renormalization scale.

The work of El-Khadra 92 [794] employs a 1-loop formula to relate $\alpha_{\overline{\text{MS}}}^{(0)}(\pi/a)$ to the boosted coupling for three lattice spacings $a^{-1} = 1.15, 1.78, 2.43\,\text{GeV}$. (The lattice spacing is determined from the charmonium 1S-1P splitting.) They obtain $\Lambda_{\overline{\text{MS}}}^{(0)} = 234\,\text{MeV}$, corresponding to $\alpha_{\text{eff}} = \alpha_{\overline{\text{MS}}}^{(0)}(\pi/a) \approx 0.15$–$0.2$. The work of Aoki 94 [791] calculates $\alpha_V^{(2)}$ and $\alpha_{\overline{\text{MS}}}^{(2)}$ for a single lattice spacing $a^{-1} \sim 2\,\text{GeV}$, again determined from charmonium 1S-1P splitting in two-flavour QCD. Using 1-loop perturbation theory with boosted coupling, they obtain $\alpha_V^{(2)} = 0.169$ and $\alpha_{\overline{\text{MS}}}^{(2)} = 0.142$. Davies 94 [790] gives a determination of α_{V} from the expansion

$$-\ln W_{11} \equiv \frac{4\pi}{3}\alpha_{\text{V}}^{(N_f)}(3.41/a) \times [1 - (1.185 + 0.070N_f)\alpha_{\text{V}}^{(N_f)}], \tag{374}$$

neglecting higher-order terms. They compute the Υ spectrum in $N_f = 0, 2$ QCD for single lattice spacings at $a^{-1} = 2.57$, $2.47\,\text{GeV}$ and obtain $\alpha_{\text{V}}(3.41/a) \simeq 0.15, 0.18$, respectively. Extrapolating the inverse coupling linearly in N_f, a value of

$\alpha_V^{(3)}(8.3\,\text{GeV}) = 0.196(3)$ is obtained. SESAM 99 [788] follows a similar strategy, again for a single lattice spacing. They linearly extrapolated results for $1/\alpha_V^{(0)}$, $1/\alpha_V^{(2)}$ at a fixed scale of 9 GeV to give $\alpha_V^{(3)}$, which is then perturbatively converted to $\alpha_{\overline{\text{MS}}}^{(3)}$. This finally gave $\alpha_{\overline{\text{MS}}}^{(5)}(M_Z) = 0.1118(17)$. Wingate 95 [789] also follows this method. With the scale determined from the charmonium 1S-1P splitting for single lattice spacings in $N_f = 0$, 2 giving $a^{-1} \simeq 1.80\,\text{GeV}$ for $N_f = 0$ and $a^{-1} \simeq 1.66\,\text{GeV}$ for $N_f = 2$, they obtain $\alpha_V^{(0)}(3.41/a) \simeq 0.15$ and $\alpha_V^{(2)} \simeq 0.18$, respectively. Extrapolating the inverse coupling linearly in N_f, they obtain $\alpha_V^{(3)}(6.48\,\text{GeV}) = 0.194(17)$.

The QCDSF/UKQCD collaboration, QCDSF/UKQCD 05 [787,795–797], use the 2-loop relation (re-written here in terms of α)

$$\frac{1}{\alpha_{\overline{\text{MS}}}(\mu)} = \frac{1}{\alpha_{\text{P}}(1/a)} + 4\pi(2b_0 \ln a\mu - t_1^{\text{P}}) + (4\pi)^2(2b_1 \ln a\mu - t_2^{\text{P}})\alpha_{\text{P}}(1/a), \tag{375}$$

where t_1^{P} and t_2^{P} are known. (A 2-loop relation corresponds to a 3-loop lattice β-function.) This was used to directly compute $\alpha_{\overline{\text{MS}}}$, and the scale was chosen so that the $\mathcal{O}(\alpha_{\text{P}}^0)$ term vanishes, i.e.,

$$\mu^* = \frac{1}{a}\exp\left[t_1^{\text{P}}/(2b_0)\right] \approx \begin{cases} 2.63/a & N_f = 0 \\ 1.4/a & N_f = 2 \end{cases}. \tag{376}$$

The method is to first compute $\alpha_{\text{P}}(1/a)$ and from this, using Eq. (375) to find $\alpha_{\overline{\text{MS}}}(\mu^*)$. The RG equation, Eq. (320), then determines $\mu^*/\Lambda_{\overline{\text{MS}}}$ and hence using Eq. (376) leads to the result for $r_0\Lambda_{\overline{\text{MS}}}$. This avoids giving the scale in MeV until the end. In the $N_f = 0$ case seven lattice spacings were used [709], giving a range $\mu^*/\Lambda_{\overline{\text{MS}}} \approx 24$–$72$ (or $a^{-1} \approx 2$–7 GeV) and $\alpha_{\text{eff}} = \alpha_{\overline{\text{MS}}}(\mu^*) \approx 0.15$–$0.10$. Neglecting higher-order perturbative terms (see discussion after Eq. (377) below) in Eq. (375) this is sufficient to allow a continuum extrapolation of $r_0\Lambda_{\overline{\text{MS}}}$. A similar computation for $N_f = 2$ by QCDSF/UKQCD 05 [787] gave $\mu^*/\Lambda_{\overline{\text{MS}}} \approx 12$–$17$ (or roughly $a^{-1} \approx 2$–3 GeV) and $\alpha_{\text{eff}} = \alpha_{\overline{\text{MS}}}(\mu^*) \approx 0.20$–$0.18$. The $N_f = 2$ results of QCDSF/UKQCD 05 [787] are affected by an uncertainty which was not known at the time of publication: It has been realized that the values of r_0/a of Ref. [787] were significantly too low [707]. As this effect is expected to depend on a, it influences the perturbative behaviour leading us to assign a ■ for that criterion.

Since FLAG 13, there has been one new result for $N_f = 0$ by FlowQCD 15 [793], later updated and published in Kitazawa 16 [792]. They also use the techniques as described in Eqs. (375), (376), but together with the gradient flow scale w_0 (rather than the r_0 scale) leading to a determination of $w_0\Lambda_{\overline{\text{MS}}}$. The continuum limit is estimated by extrapolating the data at 6 lattice spacings linearly in a^2. The data range used is $\mu^*/\Lambda_{\overline{\text{MS}}} \approx 50$–$120$ (or $a^{-1} \approx 5$–11 GeV) and $\alpha_{\overline{\text{MS}}}(\mu^*) \approx 0.12$–$0.095$. Since a very small value of $\alpha_{\overline{\text{MS}}}$ is reached, there is a ★ in the perturbative behaviour. Note that our conversion to the common r_0 scale unfortunately leads to a significant increase of the error of the Λ parameter compared to using w_0 directly [714]. Again we note that the results of QCDSF/UKQCD 05 [787] ($N_f = 0$) and Kitazawa 16 [792] may be affected by frozen topology as they have lattice spacings significantly below $a = 0.05$ fm. Kitazawa 16 [792] investigate this by evaluating w_0/a in a fixed topology and estimate any effect at about $\sim 1\%$.

The work of HPQCD 05A [783] (which supersedes the original work [798]) uses three lattice spacings $a^{-1} \approx 1.2$, 1.6, 2.3 GeV for $2+1$ flavour QCD. Typically the renormalization scale $q \approx \pi/a \approx 3.50$–$7.10$ GeV, corresponding to $\alpha_{V'} \approx 0.22$–0.28.

In the later update HPQCD 08A [784] twelve data sets (with six lattice spacings) are now used reaching up to $a^{-1} \approx 4.4$ GeV, corresponding to $\alpha_{V'} \approx 0.18$. The values used for the scale r_1 were further updated in HPQCD 10 [11]. Maltman 08 [79] uses most of the same lattice ensembles as HPQCD 08A [784], but not the one at the smallest lattice spacing, $a \approx 0.045$ fm. Maltman 08 [79] also considers a much smaller set of quantities (three versus 22) that are less sensitive to condensates. They also use different strategies for evaluating the condensates and for the perturbative expansion, and a slightly different value for the scale r_1. The central values of the final results from Maltman 08 [79] and HPQCD 08A [784] differ by 0.0009 (which would be decreased to 0.0007 taking into account a reduction of 0.0002 in the value of the r_1 scale used by Maltman 08 [79]).

As mentioned before, the perturbative coefficients are computed through 3-loop order [799], while the higher-order perturbative coefficients c_n with $n_{\max} \geq n > 3$ (with $n_{\max} = 10$) are numerically fitted using the lattice-simulation data for the lattice spacings with the help of Bayesian methods. It turns out that corrections in Eq. (371) are of order $|c_i/c_1|\alpha^i = 5$–15% and 3–10% for $i = 2$, 3, respectively. The inclusion of a fourth-order term is necessary to obtain a good fit to the data, and leads to a shift of the result by $1-2$ sigma. For all but one of the 22 quantities, central values of $|c_4/c_1| \approx 2$–4 were found, with errors from the fits of ≈ 2. It should be pointed out that the description of lattice results for the short distance quantities

does not require Bayesian priors, once the term proportional to c_4 is included [79]. We also stress that different short distance quantities have quite different nonperturbative contributions [800]. Hence the fact that different observables lead to consistent α_s values is a nontrivial check of the approach.

An important source of uncertainty is the truncation of perturbation theory. In HPQCD 08A [784], 10 [11] it is estimated to be about 0.4% of $\alpha_{\overline{\rm MS}}(M_Z)$. In FLAG 13 we included a rather detailed discussion of the issue with the result that we prefer for the time being a more conservative error based on the above estimate $|c_4/c_1| = 2$. From Eq. (370) this gives an estimate of the uncertainty in $\alpha_{\rm eff}$ of

$$\Delta\alpha_{\rm eff}(\mu_1) = \left|\frac{c_4}{c_1}\right| \alpha^4_{\rm eff}(\mu_1), \tag{377}$$

at the scale μ_1 where $\alpha_{\rm eff}$ is computed from the Wilson loops. This can be used with a variation in Λ at lowest order of perturbation theory and also applied to α_s evolved to a different scale μ_2,[68]

$$\frac{\Delta\Lambda}{\Lambda} = \frac{1}{8\pi b_0 \alpha_s}\frac{\Delta\alpha_s}{\alpha_s}, \qquad \frac{\Delta\alpha_s(\mu_2)}{\Delta\alpha_s(\mu_1)} = \frac{\alpha_s^2(\mu_2)}{\alpha_s^2(\mu_1)}. \tag{378}$$

With $\mu_2 = M_Z$ and $\alpha_s(\mu_1) = 0.2$ (a typical value extracted from Wilson loops in HPQCD 10 [11], HPQCD 08A [784] at $\mu = 5\,\text{GeV}$) we have

$$\Delta\alpha_{\overline{\rm MS}}(m_Z) = 0.0012, \tag{379}$$

which we shall later use as the typical perturbative uncertainty of the method with $2+1$ fermions.

Table 63 summarizes the results. Within the errors of 3–5% $N_f = 3$ determinations of $r_0\Lambda$ nicely agree.

9.8 α_s from heavy-quark current two-point functions

9.8.1 General considerations

The method has been introduced in HPQCD 08, Ref. [202], and updated in HPQCD 10, Ref. [11], see also Ref. [801]. In addition there is a 2+1+1-flavour result, HPQCD 14A [14].

The basic observable is constructed from a current,

$$J(x) = iam_c\overline{\psi}_c(x)\gamma_5\psi_{c'}(x), \tag{380}$$

of two mass-degenerate heavy-valence quarks, c, c', usually taken to be at or around the charm-quark mass. The pre-factor m_c denotes the bare mass of the quark. When the lattice discretization respects chiral symmetry, $J(x)$ is a renormalization group invariant local field, i.e., it requires no renormalization. Staggered fermions and twisted-mass fermions have such a residual chiral symmetry. The (Euclidean) time-slice correlation function

$$G(x_0) = a^6\sum_{\vec{x}}\langle J^\dagger(x)J(0)\rangle, \tag{381}$$

($J^\dagger(x) = iam_c\overline{\psi}_{c'}(x)\gamma_5\psi_c(x)$) has a $\sim x_0^{-3}$ singularity at short distances and moments

$$G_n = a\sum_{x_0=-(T/2-a)}^{T/2-a} x_0^n\, G(x_0) \tag{382}$$

are nonvanishing for even n and furthermore finite for $n \geq 4$. Here T is the time extent of the lattice. The moments are dominated by contributions at x_0 of order $1/m_c$. For large mass m_c these are short distances and the moments become

[68] From Eq. (327) we see that at low order in PT the coupling α_s is continuous and differentiable across the mass thresholds (at the same scale). Therefore to leading order α_s and $\Delta\alpha_s$ are independent of N_f.

Table 63 Wilson loop results. Some early results for $N_f = 0, 2$ did not determine $\Lambda_{\overline{\rm MS}}$

Collaboration	Refs.	N_f	Publication status	Renormalization scale	Perturbative behaviour	Lattice spacings	Scale	$\Lambda_{\overline{\rm MS}}$ [MeV]	$r_0\Lambda_{\overline{\rm MS}}$
HPQCD 10[a,§]	[11]	2+1	A	○	★	★	$r_1 = 0.3133(23)$ fm	340(9)	0.812(22)
HPQCD 08A[a]	[784]	2+1	A	○	★	★	$r_1 = 0.321(5)$ fm[††]	338(12)[⋆]	0.809(29)
Maltman 08[a]	[79]	2+1	A	○	○	★	$r_1 = 0.318$ fm	352(17)[†]	0.841(40)
HPQCD 05A[a]	[783]	2+1	A	○	○	○	r_1[††]	319(17)[⋆⋆]	0.763(42)
QCDSF/UKQCD 05	[787]	2	A	★	■	★	$r_0 = 0.467(33)$ fm	261(17)(26)	0.617(40)(21)[b]
SESAM 99[c]	[788]	2	A	○	■	■	$c\bar{c}$(1S-1P)		
Wingate 95[d]	[789]	2	A	★	■	■	$c\bar{c}$(1S-1P)		
Davies 94[e]	[790]	2	A	★	■	■	Υ		
Aoki 94[f]	[791]	2	A	★	■	■	$c\bar{c}$(1S-1P)		
Kitazawa 16	[792]	0	A	★	★	★	w_0	260(5)[j]	0.621(11)[j]
FlowQCD 15	[793]	0	P	★	★	★	$w^i_{0.4}$	258(6)[i]	0.618(11)[i]
QCDSF/UKQCD 05	[787]	0	A	★	○	★	$r_0 = 0.467(33)$ fm	259(1)(20)	0.614(2)(5)[b]
SESAM 99[c]	[788]	0	A	★	■	■	$c\bar{c}$(1S-1P)		
Wingate 95[d]	[789]	0	A	★	■	■	$c\bar{c}$(1S-1P)		
Davies 94[e]	[790]	0	A	★	■	■	Υ		
El-Khadra 92[g]	[794]	0	A	★	■	○	$c\bar{c}$(1S-1P)	234(10)	0.560(24)[h]

[a] The numbers for Λ have been converted from the values for $\alpha_s^{(5)}(M_Z)$

[§] $\alpha^{(3)}_{\overline{\rm MS}}(5\ {\rm GeV}) = 0.2034(21)$, $\alpha^{(5)}_{\overline{\rm MS}}(M_Z) = 0.1184(6)$, only update of intermediate scale and c-, b-quark masses, supersedes HPQCD 08A

[†] $\alpha^{(5)}_{\overline{\rm MS}}(M_Z) = 0.1192(11)$

[⋆] $\alpha^{(3)}_V(7.5\,{\rm GeV}) = 0.2120(28)$, $\alpha^{(5)}_{\overline{\rm MS}}(M_Z) = 0.1183(8)$, supersedes HPQCD 05

[††] Scale is originally determined from Υ mass splitting. r_1 is used as an intermediate scale. In conversion to $r_0\Lambda_{\overline{\rm MS}}$, r_0 is taken to be 0.472 fm

[⋆⋆] $\alpha^{(3)}_V(7.5\,{\rm GeV}) = 0.2082(40)$, $\alpha^{(5)}_{\overline{\rm MS}}(M_Z) = 0.1170(12)$

[b] This supersedes Refs. [795–797]. $\alpha^{(5)}_{\overline{\rm MS}}(M_Z) = 0.112(1)(2)$. The $N_f = 2$ results were based on values for r_0/a which have later been found to be too small [707]. The effect will be of the order of 10–15%, presumably an increase in Λr_0

[c] $\alpha^{(5)}_{\overline{\rm MS}}(M_Z) = 0.1118(17)$

[d] $\alpha^{(3)}_V(6.48\,{\rm GeV}) = 0.194(7)$ extrapolated from $N_f = 0, 2$. $\alpha^{(5)}_{\overline{\rm MS}}(M_Z) = 0.107(5)$

[e] $\alpha^{(3)}_P(8.2\,{\rm GeV}) = 0.1959(34)$ extrapolated from $N_f = 0, 2$. $\alpha^{(5)}_{\overline{\rm MS}}(M_Z) = 0.115(2)$

[f] Estimated $\alpha^{(5)}_{\overline{\rm MS}}(M_Z) = 0.108(5)(4)$

[g] This early computation violates our requirement that scheme conversions are done at the 2-loop level. $\Lambda^{(4)}_{\overline{\rm MS}} = 160(^{+47}_{-37})$MeV, $\alpha^{(4)}_{\overline{\rm MS}}(5{\rm GeV}) = 0.174(12)$. We converted this number to give $\alpha^{(5)}_{\overline{\rm MS}}(M_Z) = 0.106(4)$

[h] We used $r_0 = 0.472$ fm to convert to $r_0\Lambda_{\overline{\rm MS}}$

[i] Reference scale $w_{0.4}$ where w_x is defined by $t\partial_t[t^2\langle E(t)\rangle]\big|_{t=w_x^2} = x$ in terms of the action density $E(t)$ at positive flow time t [793]. Our conversion to r_0 scale using [793] $r_0/w_{0.4} = 2.587(45)$ and $r_0 = 0.472$ fm

[j] Our conversion from $w_0\Lambda_{\overline{\rm MS}} = 0.2154(12)$ to r_0 scale using $r_0/w_0 = (r_0/w_{0.4})\cdot(w_{0.4}/w_0) = 2.885(50)$ with the factors cited by the collaboration [793] and with $r_0 = 0.472$ fm

increasingly perturbative for decreasing n. Denoting the lowest-order perturbation theory moments by $G_n^{(0)}$, one defines the normalized moments

$$R_n = \begin{cases} G_4/G_4^{(0)} & \text{for } n = 4, \\ \dfrac{am_{\eta_c}}{2am_c}\left(\dfrac{G_n}{G_n^{(0)}}\right)^{1/(n-4)} & \text{for } n \geq 6, \end{cases} \tag{383}$$

of even order n. Note that Eq. (380) contains the variable (bare) heavy-quark mass m_c. The normalization $G_n^{(0)}$ is introduced to help in reducing lattice artifacts. In addition, one can also define moments with different normalizations,

$$\tilde{R}_n = 2R_n/m_{\eta_c} \qquad \text{for } n \geq 6. \tag{384}$$

While $\tilde{R}_n$ also remains renormalization-group invariant, it now also has a scale which might introduce an additional ambiguity [25].

The normalized moments can then be parameterized in terms of functions

$$R_n \equiv \begin{cases} r_4(\alpha_s(\mu)) & \text{for } n = 4, \\ \frac{m_{\eta_c}}{2\bar{m}_c(\mu_m)} r_n(\alpha_s(\mu)) & \text{for } n \geq 6, \end{cases} \tag{385}$$

with $\bar{m}_c(\mu_m)$ being the renormalized heavy-quark mass. The scale μ_m at which the heavy-quark mass is defined could be different from the scale μ at which α_s is defined [802]. The HPQCD collaboration, however, used the choice $\mu = \mu_m = 3m_c(\mu)$. This ensures that the renormalization scale is never too small. The reduced moments r_n have a perturbative expansion

$$r_n = 1 + r_{n,1}\alpha_s + r_{n,2}\alpha_s^2 + r_{n,3}\alpha_s^3 + \ldots, \tag{386}$$

where the written terms $r_{n,i}(\mu/\bar{m}_c(\mu))$, $i \leq 3$ are known for low n from Refs. [803–807]. In practice, the expansion is performed in the $\overline{\text{MS}}$ scheme. Matching nonperturbative lattice results for the moments to the perturbative expansion, one determines an approximation to $\alpha_{\overline{\text{MS}}}(\mu)$ as well as $\bar{m}_c(\mu)$. With the lattice spacing (scale) determined from some extra physical input, this calibrates μ. As usual suitable pseudoscalar masses determine the bare-quark masses, here in particular the charm mass, and then through Eq. (385) the renormalized charm-quark mass.

A difficulty with this approach is that large masses are needed to enter the perturbative domain. Lattice artifacts can then be sizeable and have a complicated form. The ratios in Eq. (383) use the tree-level lattice results in the usual way for normalization. This results in unity as the leading term in Eq. (386), suppressing some of the kinematical lattice artifacts. We note that in contrast to, e.g., the definition of α_{qq}, here the cutoff effects are of order $a^k\alpha_s$, while there the tree-level term defines α_s and therefore the cutoff effects after tree-level improvement are of order $a^k\alpha_s^2$. To obtain the continuum results for the moments it is important to perform fits with high powers of a. This implies many fit parameters. To deal with this problem the HPQCD collaboration used Bayesian fits of their lattice results. More recent analyses of the moments, however, did not rely on Bayesian fits [25,26,189,696].

Finite-size effects (FSE) due to the omission of $|x_0| > T/2$ in Eq. (382) grow with n as $(m_{\eta_c}T/2)^n \exp(-m_{\eta_c}T/2)$. In practice, however, since the (lower) moments are short-distance dominated, the FSE are expected to be small at the present level of precision. Possible exception could be the ratio R_8/R_{10}, where the finite-volume effects could be significant as discussed below.

Moments of correlation functions of the quark's electromagnetic current can also be obtained from experimental data for e^+e^- annihilation [808,809]. This enables a nonlattice determination of α_s using a similar analysis method. In particular, the same continuum perturbation-theory computation enters both the lattice and the phenomenological determinations.

9.8.2 Discussion of computations

The determination of the strong-coupling constant from the moments of quarkonium correlators by HPQCD collaboration have been discussed in detail in the FLAG 2016 and 2019 reports. Therefore, we only give the summary of these determinations in Table 64.

Two additional computations have appeared between the FLAG 16 and the FLAG 19 reports. We re-discuss them here (see also the summary section), as the assessment in FLAG 19 was partially based on an inconsistent use of the FLAG criteria and has now been changed. Maezawa and Petreczky, [189] computed the two-point functions of the $c\bar{c}$ pseudoscalar operator and obtained R_4, R_6/R_8 and R_8/R_{10} based on the HotQCD collaboration HISQ staggered ensembles, [116]. The scale is set by measuring $r_1 = 0.3106(18)$ fm. Continuum limits are taken fitting the lattice-spacing dependence with $a^2 + a^4$ form as the best fit. For R_4, they also employ other forms for fit functions such as a^2, $\alpha_s^{\text{boosted}}a^2 + a^4$, etc., the results agreeing within errors. Matching R_4 with the 3-loop formula Eq. (386) through order $\alpha_{\overline{\text{MS}}}^3$ [803], where μ is fixed to m_c, they obtain $\alpha_{\overline{\text{MS}}}^{(3)}(\mu = m_c) = 0.3697(54)(64)(15)$. The first error is statistical, the second is the uncertainty in the continuum

Table 64 Heavy-quark current two-point function results. Note that all analysis using 2 + 1 flavour simulations perturbatively add a dynamical charm quark. Partially they then quote results in $N_f = 4$-flavour QCD, which we converted back to $N_f = 3$, corresponding to the nonperturbative sea quark content

Collaboration	Refs.	N_f	Publication status	Renormalization scale	Perturbative behaviour	Continuum extrapolation	Scale	$\Lambda_{\overline{\text{MS}}}$ [MeV]	$r_0\Lambda_{\overline{\text{MS}}}$
HPQCD 14A	[14]	2+1+1	A	○	★	○	$w_0 = 0.1715(9)$ fm[a]	294(11)[bc]	0.703(26)
Petreczky 20	[696]	2+1	P	○	○	★	$r_1 = 0.3106(18)$ fm	332(17)[h]	0.792(41)[g]
Boito 20	[698]	2+1	A	■	■	○	$m_c(m_c) = 1.28(2)$ GeV	328(30)[h]	0.785(72)
Petrezcky 19, $m_h{=}m_c$	[26]	2+1	A	■	■	★	$r_1 = 0.3106(18)$ fm[g]	314(10)	0.751(24)[g]
Petrezcky 19, $\frac{m_h}{m_c}{=}1.5$	[26]	2+1	A	■	■	○	$r_1 = 0.3106(18)$ fm[g]	310(10)	0.742(24)[g]
Maezawa 16	[189]	2+1	A	■	■	○	$r_1 = 0.3106(18)$ fm[d]	309(10)[e]	0.739(24)[e]
JLQCD 16	[25]	2+1	A	■	○	○	$\sqrt{t_0} = 0.1465(25)$ fm	331(38)[f]	0.792(89)[f]
HPQCD 10	[11]	2+1	A	○	★	○	$r_1 = 0.3133(23)$ fm[†]	338(10)[⋆]	0.809(25)
HPQCD 08B	[202]	2+1	A	■	■	■	$r_1 = 0.321(5)$ fm[†]	325(18)[+]	0.777(42)

[a] Scale determined in [37] using f_π
[b] $\alpha^{(4)}_{\overline{\text{MS}}}(5\,\text{GeV}) = 0.2128(25)$, $\alpha^{(5)}_{\overline{\text{MS}}}(M_Z) = 0.11822(74)$
[c] We evaluated $\Lambda^{(4)}_{\overline{\text{MS}}}$ from $\alpha^{(4)}_{\overline{\text{MS}}}$. We also used $r_0 = 0.472$ fm
[d] Scale is determined from f_π
[e] $\alpha^{(3)}_{\overline{\text{MS}}}(m_c = 1.267\,\text{GeV}) = 0.3697(85)$, $\alpha^{(5)}_{\overline{\text{MS}}}(M_Z) = 0.11622(84)$. Our conversion with $r_0 = 0.472$ fm
[f] We evaluated $\Lambda^{(3)}_{\overline{\text{MS}}}$ from the given $\alpha^{(4)}_{\overline{\text{MS}}}(3\,\text{GeV}) = 0.2528(127)$. $\alpha^{(5)}_{\overline{\text{MS}}}(M_Z) = 0.1177(26)$. We also used $r_0 = 0.472$ fm to convert
[g] We used $r_0 = 0.472$ fm to convert
[h] We back-engineered from $\alpha^{(5)}_{\overline{\text{MS}}}(M_Z) = 0.1177(20)$. We used $r_0 = 0.472$ fm to convert
[⋆] $\alpha^{(3)}_{\overline{\text{MS}}}(5\,\text{GeV}) = 0.2034(21)$, $\alpha^{(5)}_{\overline{\text{MS}}}(M_Z) = 0.1183(7)$
[†] Scale is determined from Υ mass splitting
[+] We evaluated $\Lambda^{(3)}_{\overline{\text{MS}}}$ from the given $\alpha^{(4)}_{\overline{\text{MS}}}(3\,\text{GeV}) = 0.251(6)$. $\alpha^{(5)}_{\overline{\text{MS}}}(M_Z) = 0.1174(12)$

extrapolation, and the third is the truncation error in the perturbative approximation of r_4. This last error is estimated by the "typical size" of the missing 4-loop contribution, which they assume to be $\alpha^4_{\overline{\text{MS}}}(\mu)$ multiplied by 2 times the 3-loop coefficient $2 \times r_{4,3} \times \alpha^4_{\overline{\text{MS}}}(\mu) = 0.2364 \times \alpha^4_{\overline{\text{MS}}}(\mu)$. The result is converted to

$$\alpha^{(5)}_{\overline{\text{MS}}}(M_Z) = 0.11622(84). \tag{387}$$

Since $\alpha_{\text{eff}} = 0.38$ we assign ■ for the criterion of the renormalization scale. As $\Delta\Lambda/\Lambda < \alpha^2_{\text{eff}}$, we assign ■ for the criterion of perturbative behaviour. The lattice cutoff ranges as a^{-1} = 1.42–4.89 GeV with $\mu = 2m_c \sim 2.6$ GeV so that we assign ○ for continuum extrapolation.

JLQCD 16 [25] also computed the two-point functions of the $c\bar{c}$ pseudoscalar operator and obtained R_6, R_8, R_{10} and their ratios based on 2+1-flavour QCD with Möbius domain-wall quark for three lattice cutoff a^{-1} = 2.5, 3.6, 4.5 GeV. The scale is set by $\sqrt{t_0} = 0.1465(21)(13)$ fm. The continuum limit is taken assuming linear dependence on a^2. They find a sizeable lattice-spacing dependence of R_4, which is therefore not used in their analysis, but for R_6, R_8, R_{10} the dependence is mild giving reasonable control over the continuum limit. They use the perturbative formulae for the vacuum polarization in the pseudoscalar channel Π_{PS} through order $\alpha^3_{\overline{\text{MS}}}$ in the $\overline{\text{MS}}$ scheme [805,806] to obtain $\alpha^{(4)}_{\overline{\text{MS}}}$. Combining the matching of lattice results with continuum perturbation theory for R_6, R_6/R_8 and R_{10}, they obtain $\alpha^{(4)}_{\overline{\text{MS}}}(\mu = 3\ \text{GeV}) = 0.2528(127)$, where the error is dominated by the perturbative truncation error. To estimate the truncation error they study the dependence of the final result on the choice of the renormalization scales μ, μ_m which are used as renormalization scales for α_s and the quark mass. Independently [802] the two scales are varied in the range of 2 GeV to 4 GeV. The above result is converted to $\alpha^{(5)}_{\overline{\text{MS}}}(M_Z)$ as

$$\alpha^{(5)}_{\overline{\rm MS}}(M_Z) = 0.1177(26). \tag{388}$$

Since $\alpha_{\rm eff} \simeq 0.37$, they have ■ for the renormalization scale criterion. Since $\Delta\Lambda/\Lambda \simeq \alpha^2_{\rm eff}$, we also assign ○ for the criterion of perturbative behaviour. The lattice cutoff ranges over a^{-1} = 2.5–4.5 GeV with $\mu = 3$ GeV so we also give them a ○ for continuum extrapolation. We note, however, that the χ^2/dof of the a^2 extrapolation was quite bad, namely between 2.1 and 5.1 [25]. Please note that the 2019 FLAG review mistakenly took $\alpha_{\overline{\rm MS}}(2m_c)$ for $\alpha_{\rm eff}$. This resulted in a ○ rating for the renormalization scale for both Maezawa 16 and JLQCD 16. With the consistent definition of $\alpha_{\rm eff}$ both determinations now have ■ for the renormalization scale.

Three new determinations of α_s from the moments of quarkonium correlators appeared since the 2019 FLAG review [26,696,698]. Petreczky 19 [26] extended the calculation of [189] by considering heavy-quark masses larger than the charm-quark mass, namely, $m_h = 1.5m_c$, $2m_c$ and $3m_c$. Also three additional lattice spacings, $a = 0.025$, 0.03 and 0.035 fm have been added to the analysis. Another improvement compared to Maezawa 16 was the use of random-colour wall sources which greatly reduced the statistical errors. In fact, the statistical errors on the moments were completely negligible compared to other sources of errors. The lattices corresponding to the three smallest lattice spacings have been generated for the calculations of the QCD equation of state at high temperature [769] at light sea-quark masses corresponding to the pion mass of 300 MeV in the continuum limit, instead of the pion mass of 160 MeV as in the previous calculations. However, it has been checked that the effect of the larger light sea-quark masses is very small, about the size of the statistical errors [26]. Therefore, the calculations at the two light sea-quark masses have been combined into a single analysis [26]. For each value of the heavy-quark mass the continuum extrapolations have been performed using various fit ansätze, some of which included high powers of a. Due to availability of many lattice spacing it was possible to perform such fits without using Bayesian priors. The variation of the continuum-extrapolated values with the variation of the fit range in a^2 and the fit forms has been investigated and included as the systematic error of the continuum results. The renormalization scale μ was fixed to the heavy-quark mass, and $\alpha_s(\mu = m_h)$ and the corresponding $\Lambda^{N_f=3}_{\overline{MS}}$ has been determined for each value of m_h using continuum results for R_4, R_6/R_8 and R_8/R_{10}. The perturbative error was estimated as in Maezawa 16 but with the coefficient of the 4-loop term being 1.6 times the coefficient of the 3-loop term. The values of $\Lambda^{N_f=3}_{\overline{MS}}$ obtained for $m_h = m_c$ and $m_h = 1.5m_c$ were consistent with each other, $\Lambda^{N_f=3}_{\overline{MS}} = 314(10)$ MeV for $m_h = m_c$ and $\Lambda^{N_f=3}_{\overline{MS}} = 310(10)$ MeV for $m_h = 1.5m_c$. However, the $\Lambda^{N_f=3}_{\overline{MS}}$ values turned out to be significantly lower for $m_h = 2m_c$ and $3m_c$. In Petreczky 20 [696], it has been argued that reliable continuum extrapolations of R_4, R_6/R_8 and R_8/R_{10} are not possible for $m_h \geq 2m_c$. Therefore, we only review the results obtained for $m_h = m_c$ and $m_h = 1.5m_c$. There are many lattice spacings available for analysis, including three lattice spacings $a \leq 0.035$ fm, implying that $a\mu < 0.5$. Therefore, we assign ★ for the continuum extrapolation. The value of $\alpha_{\rm eff}$ is 0.38 and 0.31 for $m_h = m_c$ and $m_h = 1.5m_c$, respectively. So we assign ■ for the renormalization scale. Since $(\Delta\Lambda/\Lambda)_{\Delta\alpha} < \alpha^2_{\rm eff}$ we assign ■ for the perturbative behaviour.

Petreczky 20 [696] used the same raw lattice data as Petreczky 19 but a different strategy for continuum extrapolation and α_s extraction. The lattice spacing dependence of the results of R_4 at different quark masses was fitted simultaneously in a similar manner as in the HPQCD 10 and HPQCD 14 analyses, but without using Bayesian priors. In extracting α_s several choices of the renormalization scale μ in the range $2/3m_h$–$3m_h$ have been considered. The perturbative error was estimated as in Petreczky 19 but the variation of the results due to the scale variation was larger than the estimated perturbative error. The final error of the result $\Lambda^{N_f=3}_{\overline{MS}} = 331(17)$ MeV comes mostly from the scale variation [696]. Since there are three lattice spacing available with $a\mu < 0.5$ we give ★ for continuum extrapolation. Because $\alpha_{\rm eff} = 0.22 - 0.38$ we give ○ for the renormalization scale. Finally, since $(\Delta\Lambda/\Lambda)_{\Delta\alpha} > \alpha^2_{\rm eff}$ for the smallest $\alpha_{\rm eff}$ value we give ○ for the perturbative behaviour. In addition to R_4 Petreczky 20 also considered using R_6/R_8 and R_8/R_{10} for the α_s determination. It was pointed out that the lattice spacing dependence of R_6/R_8 is quite subtle and therefore reliable continuum extrapolations for this ratio are not possible for $m_h \geq 2m_c$ [696]. For $m_h = m_c$ and $1.5m_c$ the ratio R_6/R_8 leads to α_s values that are consistent with the ones from R_4. Furthermore, it was argued that finite-volume effects in the case of R_8/R_{10} are large for $m_h = m_c$ and therefore the corresponding data are not suitable for extracting α_s. This observation may explain why the central values of α_s extracted from R_8/R_{10} in some previous studies were systematically lower [26,189,202]. On the other hand for $m_h \geq 1.5m_c$ the finite-volume effects are sufficiently small in the continuum extrapolated results if some small-volume lattice data are excluded from the analysis [696]. The α_s obtained from R_8/R_{10} with $m_h \geq 1.5m_c$ were consistent with the ones obtained from R_4.

Boito 20 [698] use published continuum extrapolated lattice results on R_4, R_6/R_8 and R_8/R_{10} from various groups combined with experimental results on e^+e^- annihilation. They quote a separate result for each lattice determinations of R_4,

Table 65 Moments and the ratios of the moments from $N_f = 3$ simulations at the charm mass

	HPQCD 08	HPQCD 10	Maezawa 16	JLQCD 16	Petreczky 19	Petreczky 20
R_4	1.272(5)	1.282(4)	1.265(7)	–	1.279(4)	1.278(2)
R_6	1.528(11)	1.527(4)	1.520(4)	1.509(7)	1.521(3)	1.522(2)
R_8	1.370(10)	1.373(3)	1.367(8)	1.359(4)	1.369(3)	1.368(3)
R_{10}	1.304(9)	1.304(2)	1.302(8)	1.297(4)	1.311(7)	1.301(3)
R_6/R_8	1.113(2)	–	1.114(2)	1.111(2)	1.1092(6)	1.10895(32)
R_8/R_{10}	1.049(2)	–	1.0495(7)	1.0481(9)	1.0485(8)	–

R_6/R_8 and R_8/R_{10} for $m_h = m_c$ from different lattice groups. They vary the scale μ and μ_m independently in the region between m_c and 4 GeV. As the typical value they quote $\alpha_s(M_Z) = 0.1177(20)$. The error is dominated by the perturbative uncertainty. Since the effective coupling is around 0.38 we give ■ for the renormalization scale. Because $(\Delta\Lambda/\Lambda)_{\Delta\alpha} < \alpha_{\text{eff}}^2$ we give this determination ■ for perturbative behaviour. The continuum results used in the analysis were rated as ○ with the exception of HPQCD 08B, which however, does not affect the quoted α_s value. Therefore we give them ○ for the continuum extrapolation. An interesting point of the Boito 20 analysis is that the α_s values extracted from R_8/R_{10} are systematically lower than the ones extracted from R_4. This confirms the above assertion that finite volume effects are significant for R_8/R_{10} at $m_h = m_c$.

Aside from the final results for $\alpha_s(m_Z)$ obtained by matching with perturbation theory, it is interesting to make a comparison of the short distance quantities in the continuum limit R_n which are available from HPQCD 08 [202], JLQCD 16 [25], Maezawa 16 [189], Petreczky 19 [26] and Petreczky 20 [696] (all using $2 + 1$ flavours). This comparison is shown in Table 65. The results are in quite good agreement with each other. For future studies it is of course interesting to check agreement of these numbers before turning to the more involved determination of α_s.

9.9 α_s from QCD vertices

9.9.1 General considerations

The most intuitive and in principle direct way to determine the coupling constant in QCD is to compute the appropriate three- or four-point gluon vertices or alternatively the quark-quark-gluon vertex or ghost-ghost-gluon vertex (i.e., $q\bar{q}A$ or $c\bar{c}A$ vertex, respectively). A suitable combination of renormalization constants then leads to the relation between the bare (lattice) and renormalized coupling constant. This procedure requires the implementation of a nonperturbative renormalization condition and the fixing of the gauge. For the study of nonperturbative gauge fixing and the associated Gribov ambiguity, we refer to Refs. [810–812] and references therein. In practice the Landau gauge is used and the renormalization constants are defined by requiring that the vertex is equal to the tree-level value at a certain momentum configuration. The resulting renormalization schemes are called 'MOM' scheme (symmetric momentum configuration) or '$\widetilde{\text{MOM}}$' (one momentum vanishes), which are then converted perturbatively to the $\overline{\text{MS}}$ scheme.

A pioneering work to determine the three-gluon vertex in the $N_f = 0$ theory is Alles 96 [813] (which was followed by Ref. [814] for two flavour QCD); a more recent $N_f = 0$ computation was Ref. [815] in which the three-gluon vertex as well as the ghost-ghost-gluon vertex was considered. (This requires a computation of the propagator of the Faddeev–Popov ghost on the lattice.) The latter paper concluded that the resulting $\Lambda_{\overline{\text{MS}}}$ depended strongly on the scheme used, the order of perturbation theory used in the matching and also on nonperturbative corrections [816].

Subsequently in Refs. [817,818] a specific $\widetilde{\text{MOM}}$ scheme with zero ghost momentum for the ghost-ghost-gluon vertex was used. In this scheme, dubbed the 'MM' (Minimal MOM) or 'Taylor' (T) scheme, the vertex is not renormalized, and so the renormalized coupling reduces to

$$\alpha_{\text{T}}(\mu) = D_{\text{lat}}^{\text{gluon}}(\mu, a) D_{\text{lat}}^{\text{ghost}}(\mu, a)^2 \frac{g_0^2}{4\pi}, \tag{389}$$

where $D_{\text{lat}}^{\text{ghost}}$ and $D_{\text{lat}}^{\text{gluon}}$ are the (bare lattice) dressed ghost and gluon 'form factors' of these propagator functions in the Landau gauge,

$$D^{ab}(p) = -\delta^{ab}\,\frac{D^{\text{ghost}}(p)}{p^2}, \qquad D^{ab}_{\mu\nu}(p) = \delta^{ab}\left(\delta_{\mu\nu} - \frac{p_\mu p_\nu}{p^2}\right)\frac{D^{\text{gluon}}(p)}{p^2}, \tag{390}$$

and we have written the formula in the continuum with $D^{\text{ghost/gluon}}(p) = D^{\text{ghost/gluon}}_{\text{lat}}(p,0)$. Thus there is now no need to compute the ghost-ghost-gluon vertex, just the ghost and gluon propagators.

9.9.2 Discussion of computations

For the calculations considered here, to match to perturbative scaling, it was first necessary to reduce lattice artifacts by an $H(4)$ extrapolation procedure (addressing $O(4)$ rotational invariance), e.g., ETM 10F [824] or by lattice perturbation theory, e.g., Sternbeck 12 [822]. To match to perturbation theory, collaborations vary in their approach. In ETM 10F [824], it was necessary to include the operator A^2 in the OPE of the ghost and gluon propagators, while in Sternbeck 12 [822] very large momenta are used and a^2p^2 and a^4p^4 terms are included in their fit to the momentum dependence. A further later refinement was the introduction of higher nonperturbative OPE power corrections in ETM 11D [821] and ETM 12C [820]. Although the expected leading power correction, $1/p^4$, was tried, ETM finds good agreement with their data only when they fit with the next-to-leading-order term, $1/p^6$. The update ETM 13D [819] investigates this point in more detail, using better data with reduced statistical errors. They find that after again including the $1/p^6$ term they can describe their data over a large momentum range from about 1.75 GeV to 7 GeV.

In all calculations except for Sternbeck 10 [823], Sternbeck 12 [822], the matching with the perturbative formula is performed including power corrections in the form of condensates, in particular $\langle A^2\rangle$. Three lattice spacings are present in almost all calculations with $N_f = 0, 2$, but the scales ap are rather large. This mostly results in a ■ on the continuum extrapolation (Sternbeck 10 [823], Boucaud 01B [814] for $N_f = 2$. Ilgenfritz 10 [825], Boucaud 08 [818], Boucaud 05 [815], Becirevic 99B [830], Becirevic 99A [831], Boucaud 98B [832], Boucaud 98A [833], Alles 96 [813] for $N_f = 0$). A ○ is reached in the $N_f = 0$ computations Boucaud 00A [829], 00B [828], 01A [827], Soto 01 [826] due to a rather small lattice spacing, but this is done on a lattice of a small physical size. The $N_f = 2+1+1$ calculation, fitting with condensates, is carried out for two lattice spacings and with $ap > 1.5$, giving ■ for the continuum extrapolation as well. In ETM 10F [824] we have $0.25 < \alpha_{\text{eff}} < 0.4$, while in ETM 11D [821], ETM 12C [820] (and ETM 13 [80]) we find $0.24 < \alpha_{\text{eff}} < 0.38$, which gives a ○ in these cases for the renormalization scale. In ETM 10F [824] the values of ap violate our criterion for a continuum limit only slightly, and we give a ○.

In Sternbeck 10 [823], the coupling ranges over $0.07 \le \alpha_{\text{eff}} \le 0.32$ for $N_f = 0$ and $0.19 \le \alpha_{\text{eff}} \le 0.38$ for $N_f = 2$ giving ★ and ○ for the renormalization scale, respectively. The fit with the perturbative formula is carried out without condensates, giving a satisfactory description of the data. In Boucaud 01A [827], depending on a, a large range of α_{eff} is used which goes down to 0.2 giving a ○ for the renormalization scale and perturbative behaviour, and several lattice spacings are used leading to ○ in the continuum extrapolation. The $N_f = 2$ computation Boucaud 01B [827], fails the continuum limit criterion because both $a\mu$ is too large and an unimproved Wilson fermion action is used. Finally in the conference proceedings Sternbeck 12 [822], the $N_f = 0, 2, 3$ coupling α_{T} is studied. Subtracting 1-loop lattice artifacts and subsequently fitting with a^2p^2 and a^4p^4 additional lattice artifacts, agreement with the perturbative running is found for large momenta ($r_0^2p^2 > 600$) without the need for power corrections. In these comparisons, the values of $r_0\Lambda_{\overline{\text{MS}}}$ from other collaborations are used. As no numbers are given, we have not introduced ratings for this study.

Since the previous FLAG review, there has been one new result, Zafeiropoulos 19 [699], again based on the method described in ETM 10F, [824] but now for $N_f = 3$ flavours rather than two. Again an $\langle A^2\rangle$ condensate is included, but cannot be determined; an estimate is used from ETM 10F ($N_f = 2$) and ETM12C ($N_f = 4$). The scale Λ is determined from the largest momenta available (when a plateau appears), and the error is estimated from the larger range $p \sim 3.0$–3.7 GeV. This is used to determine $\alpha_{\overline{MS}}$. In this work there is also some emphasis on being close to the physical-quark masses, using three domain-wall fermion data sets and careful consideration of discretization effects following [834]. The disadvantage is that a lower upper bound on the momenta is now reached.

The range of effective couplings is $0.35 \lesssim \alpha_{\text{eff}} \lesssim 0.42$, and over this range we have $(\alpha_{\text{eff}}(3.0\ \text{GeV})/\alpha_{\text{eff}}(3.7\ \text{GeV}))^3 \sim 1.7$, which leads to a ■ for perturbative behaviour. With no α_{eff} at or below 0.3 and only two lattice spacings, we also obtain a ■ for both the renormalization scale and the continuum extrapolation.

In Table 66 we summarize the results. Presently there are no $N_f \ge 3$ calculations of α_s from QCD vertices that satisfy the FLAG criteria to be included in the range.

Table 66 Results for the gluon–ghost vertex

Collaboration	Refs.	N_f	Publication status	Renormalization scale	Perturbative behaviour	Continuum extrapolation	Scale	$\Lambda_{\overline{\text{MS}}}$ [MeV]	$r_0\Lambda_{\overline{\text{MS}}}$
ETM 13D	[819]	2+1+1	A	○	○	■	f_π	314(7)(14)(10)[a]	0.752(18)(34)(81)[†]
ETM 12C	[820]	2+1+1	A	○	○	■	f_π	324(17)[§]	0.775(41)[†]
ETM 11D	[821]	2+1+1	A	○	○	■	f_π	316(13)(8)$(^{+0}_{-9})$[⋆]	0.756(31)(19)$(^{+0}_{-22})$[†]
Zafeiropoulos 19	[699]	2+1	A	■	■	■	m_Ω	320(4)(12)[b]	0.766(10)(29)[†]
Sternbeck 12	[822]	2+1	C				Only running of α_s in Fig. 4		
Sternbeck 12	[822]	2	C				Agreement with $r_0\Lambda_{\overline{\text{MS}}}$ value of [707]		
Sternbeck 10	[823]	2	C	○	★	■		251(15)[#]	0.60(3)(2)
ETM 10F	[824]	2	A	○	○	○	f_π	330(23)(22)$(^{+0}_{-33})$	0.72(5)[+]
Boucaud 01B	[814]	2	A	○	○	■	$K^* - K$	264(27)[⋆⋆]	0.669(69)
Sternbeck 12	[822]	0	C				Agreement with $r_0\Lambda_{\overline{\text{MS}}}$ value of [766]		
Sternbeck 10	[823]	0	C	★	★	■		259(4)[#]	0.62(1)
Ilgenfritz 10	[825]	0	A	★	★	■	Only running of α_s in Fig. 13		
Boucaud 08	[818]	0	A	○	★	■	$\sqrt{\sigma} = 445$ MeV	224(3)$(^{+8}_{-5})$	0.59(1)$(^{+2}_{-1})$
Boucaud 05	[815]	0	A	■	★	■	$\sqrt{\sigma} = 445$ MeV	320(32)	0.85(9)
Soto 01	[826]	0	A	○	○	○	$\sqrt{\sigma} = 445$ MeV	260(18)	0.69(5)
Boucaud 01A	[827]	0	A	○	○	○	$\sqrt{\sigma} = 445$ MeV	233(28) MeV	0.62(7)
Boucaud 00B	[828]	0	A	○	○	○		Only running of α_s	
Boucaud 00A	[829]	0	A	○	○	○	$\sqrt{\sigma} = 445$ MeV	237(3)$(^{+\,0}_{-10})$	0.63(1)$(^{+0}_{-3})$
Becirevic 99B	[830]	0	A	○	○	■	$\sqrt{\sigma} = 445$ MeV	319(14)$(^{+10}_{-20})$	0.84(4)$(^{+3}_{-5})$
Becirevic 99A	[831]	0	A	○	○	■	$\sqrt{\sigma} = 445$ MeV	$\lesssim$ 353(2)$(^{+25}_{-15})$	$\lesssim$ 0.93$(^{+7}_{-4})$
Boucaud 98B	[832]	0	A	■	○	■	$\sqrt{\sigma} = 445$ MeV	295(5)(15)	0.78(4)
Boucaud 98A	[833]	0	A	■	○	■	$\sqrt{\sigma} = 445$ MeV	300(5)	0.79(1)
Alles 96	[813]	0	A	■	■	■	$\sqrt{\sigma} = 440$ MeV [++]	340(50)	0.91(13)

[a] $\alpha^{(5)}_{\overline{\text{MS}}}(M_Z) = 0.1196(4)(8)(6)$

[†] We use the 2+1 value $r_0 = 0.472$ fm

[§] $\alpha^{(5)}_{\overline{\text{MS}}}(M_Z) = 0.1200(14)$

[⋆] First error is statistical; second is due to the lattice spacing and third is due to the chiral extrapolation. $\alpha^{(5)}_{\overline{\text{MS}}}(M_Z) = 0.1198(9)(5)(^{+0}_{-5})$

[b] $\alpha^{(5)}_{\overline{\text{MS}}}(M_Z) = 0.1172(3)(9)(5)$. The first error is the uncertainty in the determination of α_T, the second due to the condensate while the third is due to higher order nonperturbative corrections

[#] In the paper only $r_0\Lambda_{\overline{\text{MS}}}$ is given, we converted to MeV with $r_0 = 0.472$ fm

[+] The determination of r_0 from the f_π scale is found in Ref. [87]

[⋆⋆] $\alpha^{(5)}_{\overline{\text{MS}}}(M_Z) = 0.113(3)(4)$

[++] The scale is taken from the string tension computation of Ref. [767]

9.10 α_s from the eigenvalue spectrum of the Dirac operator

9.10.1 General considerations

Consider the spectral density of the continuum Dirac operator

$$\rho(\lambda) = \frac{1}{V}\left\langle \sum_k (\delta(\lambda - i\lambda_k) + \delta(\lambda + i\lambda_k)) \right\rangle, \tag{391}$$

where V is the volume and λ_k are the eigenvalues of the Dirac operator in a gauge background.

Its perturbative expansion

$$\rho(\lambda) = \frac{3}{4\pi^2}\lambda^3(1 - \rho_1\bar{g}^2 - \rho_2\bar{g}^4 - \rho_3\bar{g}^6 + \mathcal{O}(\bar{g}^8)), \tag{392}$$

is known including ρ_3 in the $\overline{\text{MS}}$ scheme [835,836]. In renormalization group improved form one sets the renormalization scale μ to $\mu = s\lambda$ with $s = \mathcal{O}(1)$ and the ρ_i are pure numbers. Nakayama 18 [837] initiated a study of $\rho(\lambda)$ in the perturbative regime. They prefer to consider μ independent from λ. Then ρ_i are polynomials in $\log(\lambda/\mu)$ of degree i. One may consider

$$F(\lambda) \equiv \frac{\partial \log(\rho(\lambda))}{\partial \log(\lambda)} = 3 - F_1\bar{g}^2 - F_2\bar{g}^4 - F_3\bar{g}^6 - F_4\bar{g}^8 + \mathcal{O}(\bar{g}^{10}), \tag{393}$$

where the coefficients, F_i, which are known for $i = 1, \ldots, 4$, are again polynomials of degree i in $\log(\lambda/\mu)$. Choosing the alternate renormalization-group-improved form with $\mu = s\lambda$ in Eq. (392), Eq. (393) would instead lead to

$$F(\lambda) = 3 - \bar{F}_2\bar{g}^4(\lambda) - \bar{F}_3\bar{g}^6(\lambda) - \bar{F}_4\bar{g}^8(\lambda) + \mathcal{O}(\bar{g}^{10}), \tag{394}$$

with pure numbers $\bar{F}_i$ and $\bar{F}_1 = 0$. Determinations of α_s can be carried out by a computation and continuum extrapolation of $\rho(\lambda)$ and/or $F(\lambda)$ at large λ. Such computations are made possible by the techniques of [85,362,837].

We note that according to our general discussions in terms of an effective coupling, we have $n_1 = 2$; the 3-loop β function of a coupling defined from Eq. (392) or Eq. (394) is known.[69]

9.10.2 Discussion of computations

There is one pioneering result to date using this method by Nakayama 18 [837]. They computed the eigenmode distributions of the Hermitian operator $a^2 D_{\text{ov}}^\dagger D_{\text{ov}}$ where $D_{\text{ov}} = D_{\text{ov}}(m_f = 0, am_{\text{PV}})$ is the overlap operator and m_{PV} is the Pauli–Villars regulator on ensembles with 2+1 flavours using Möbius domain-wall quarks for three lattice cutoffs $a^{-1} = 2.5$, 3.6, 4.5 GeV, where $am_{\text{PV}} = 3$ or ∞. The bare eigenvalues are converted to the $\overline{\text{MS}}$ scheme at $\mu = 2$ GeV by multiplying with the renormalization constant $Z_m(2\,\text{GeV})$, which is then transformed to those renormalized at $\mu = 6$ GeV using the renormalization-group equation. The scale is set by $\sqrt{t_0} = 0.1465(21)(13)$ fm. The continuum limit is taken assuming a linear dependence in a^2, while the volume size is kept about constant: 2.6–2.8 fm. Choosing the renormalization scale $\mu = 6$ GeV, Nakayama 18 [837] extracted the strong coupling constant $\alpha_{\overline{\text{MS}}}^{(3)}(6\,\text{GeV}) = 0.204(10)$. The result is converted to

$$\alpha_{\overline{\text{MS}}}^{(5)}(M_Z) = 0.1226(36). \tag{395}$$

Three lattice spacings in the range $a^{-1} = 2.5$–4.5 GeV with $\mu = \lambda = 0.8$–1.25 GeV yield quite small values $a\mu$. However, our continuum-limit criterion does not apply as it requires us to consider $\alpha_s = 0.3$. We thus deviate from the general rule and give a ○ which would result at the smallest value $\alpha_{\overline{\text{MS}}}(\mu) = 0.4$ considered by Nakayama 18 [837]. The values of $\alpha_{\overline{\text{MS}}}$ lead to a ■ for the renormalization scale, while perturbative behaviour is rated ○.

In Table 67 we list this result.

9.11 Summary

After reviewing the individual computations, we are now in a position to discuss the overall result. We first present the current status and for that briefly consider $r_0\Lambda$ with its flavour dependence from $N_f = 0$ to 4 flavours. Then we discuss the central $\alpha_{\overline{\text{MS}}}(M_Z)$ results, which just use $N_f \geq 3$, give ranges for each sub-group discussed previously, and give final FLAG average as well as an overall average together with the current PDG nonlattice numbers. Finally we return to $r_0\Lambda$, presenting our estimates for the various N_f.

[69] In the present situation, Nakayama 18 [837], the effective coupling is defined by $\bar{g}_\lambda^2(\mu) = \bar{F}_2^{-1/2}(3 - F(\lambda))$ with $\mu = \lambda$. The alternative definition, Eq. (394), would give $\bar{g}_\lambda^2(\mu) = \bar{F}_2^{-1/2}(3 - F(\lambda))^{1/2}$.

Table 67 Dirac eigenvalue result

Collaboration	Refs.	N_f	Publication status	Renormalization scale	Perturbative behaviour	Continuum extrapolation	Scale	$\Lambda_{\overline{\rm MS}}$ [MeV]	$r_0\Lambda_{\overline{\rm MS}}$
Nakayama 18	[837]	2+1	A	■	○	○	$\sqrt{t_0}$	409(60) *	0.978(144)

*$\alpha^{(5)}_{\overline{\rm MS}}(M_Z) = 0.1226(36)$. $\Lambda_{\overline{\rm MS}}$ determined by us using $\alpha^{(3)}_{\overline{\rm MS}}(6\,\text{GeV}) = 0.204(10)$. Uses $r_0 = 0.472\,\text{fm}$

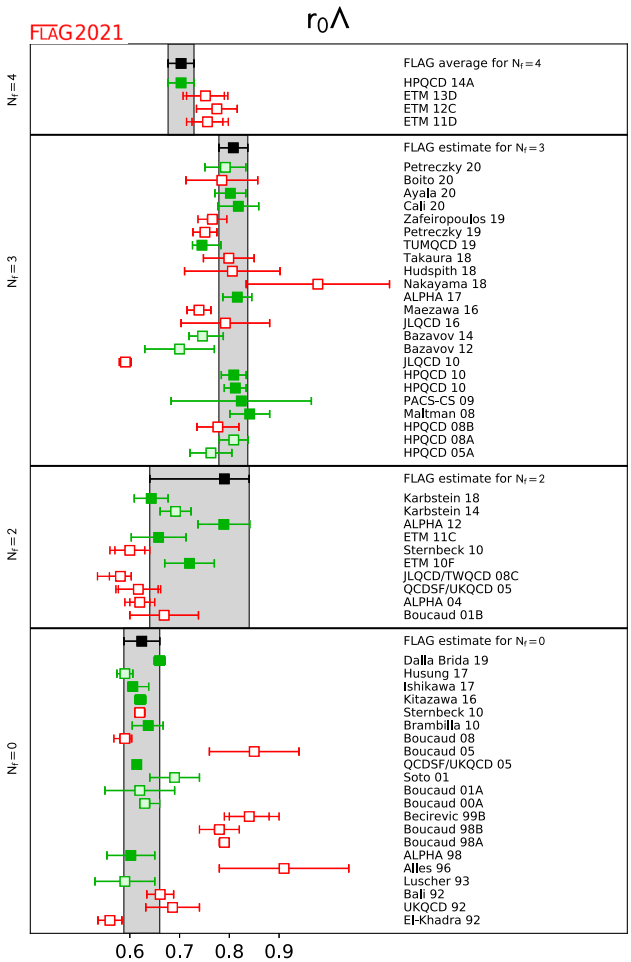

Fig. 40 $r_0\Lambda_{\overline{\rm MS}}$ estimates for $N_f = 0, 2, 3, 4$ flavours. Full green squares are used in our final ranges, pale green squares also indicate that there are no red squares in the colour coding but the computations were superseded by later more complete ones or not published, while red open squares mean that there is at least one red square in the colour coding

9.11.1 The present situation

We first summarize the status of lattice-QCD calculations of the QCD scale $\Lambda_{\overline{\rm MS}}$. Figure 40 shows all the results for $r_0\Lambda_{\overline{\rm MS}}$ discussed in the previous sections.

Many of the numbers are the ones given directly in the papers. However, when only $\Lambda_{\overline{\rm MS}}$ in physical units (MeV) is available, we have converted them by multiplying with the value of r_0 in physical units. The notation used is full green squares for results used in our final average, while a lightly shaded green square indicates that there are no red squares in the

previous colour coding but the computation does not enter the ranges because either it has been superseded by an update or it is not published. Red open squares mean that there is at least one red square in the colour coding.

For $N_f = 0$ there is now some tension: the value of the new result, Dalla Brida 19 [693] is rather high compared to the previous FLAG average and yet it passes the FLAG 19 criteria by some margin.

When two flavours of quarks are included, the numbers extracted by the various groups show a considerable spread, as in particular older computations did not yet control the systematics sufficiently. This illustrates the difficulty of the problem and emphasizes the need for strict criteria. The agreement among the more modern calculations with three or more flavours, however, is quite good.

We now turn to the status of the essential result for phenomenology, $\alpha^{(5)}_{\overline{\rm MS}}(M_Z)$. In Table 68 and the upper plot in Fig. 41 we show all the results for $\alpha^{(5)}_{\overline{\rm MS}}(M_Z)$ (i.e., $\alpha_{\overline{\rm MS}}$ at the Z mass) obtained from $N_f = 2+1$ and $N_f = 2+1+1$ simulations. The conversion from $N_f = 3$ or $N_f = 4$ to $N_f = 5$ is made by matching the coupling constant at the charm and bottom quark thresholds and using the scale as determined or used by the authors.

As can be seen from the tables and figures, at present there are several computations satisfying the criteria to be included in the FLAG average. Since FLAG 19 four new computations of $\alpha^{(5)}_{\overline{\rm MS}}(M_Z)$ pass all our criteria with at least a ○ . The results agree quite well within the stated uncertainties, which vary significantly.

9.11.2 Our range for $\alpha^{(5)}_{\overline{\rm MS}}$

We now explain the determination of our range. We only include those results without a red tag and that are published in a refereed journal. We also do not include any numbers that were obtained by extrapolating from theories with less than three flavours. They are not controlled and can be looked up in the previous FLAG reviews.

A general issue with most determinations of $\alpha_{\overline{\rm MS}}$, both lattice and nonlattice, is that they are dominated by perturbative truncation errors, which are difficult to estimate. Further, all results discussed here except for those of Sects. 9.3, 9.7 are based on extractions of $\alpha_{\overline{\rm MS}}$ that are largely influenced by data with $\alpha_{\rm eff} \geq 0.3$. At smaller α_s the momentum scale μ quickly gets at or above a^{-1}. We have included computations using $a\mu$ up to 1.5 and $\alpha_{\rm eff}$ up to 0.4, but one would ideally like to be significantly below that. Accordingly we choose to not simply perform weighted averages with the individual errors estimated by each group. Rather, we use our own more conservative estimates of the perturbative truncation errors in the weighted average.

In the following we repeat aspects of the methods and calculations that inform our estimates of the perturbative truncation errors. We also provide separate estimates for α_s obtained from step-scaling, the heavy-quark potential, Wilson loops, heavy-quark current two-point functions and vacuum polarization to enable a comparison of the different lattice approaches; these are summarized in Table 68.

- *Step-scaling*
  The step-scaling computations of PACS-CS 09A [78] and ALPHA 17 [77] reach energies around the Z-mass where perturbative uncertainties in the three-flavour theory are negligible. Perturbative errors do enter in the conversion of the Λ-parameters from three to five flavours, but successive order contributions decrease rapidly and can be neglected. We form a weighted average of the two results and obtain $\alpha_{\overline{\rm MS}} = 0.11848(81)$.
- *Static-quark potential computations*
  Brambilla 10 [766], ETM 11C [764] and Bazavov 12 [761] give evidence that they have reached distances where perturbation theory can be used. However, in addition to Λ, a scale is introduced into the perturbative prediction by the process of subtracting the renormalon contribution. This subtraction is avoided in Bazavov 14 [760] by using the force and again agreement with perturbative running is reported. Husung 17 [765] (unpublished) studies the reliability of perturbation theory in the pure gauge theory with lattice spacings down to 0.015 fm and finds that at weak coupling there is a downwards trend in the Λ-parameter with a slope $\Delta\Lambda/\Lambda \approx 9\alpha_s^3$. The downward trend is broadly confirmed in Husung 20 [695] albeit with larger errors.
  Bazavov 14 [760] satisfies all of the criteria to enter the FLAG average for α_s but has been superseded by TUMQCD 19 [75]. Moreover, there is another study, Ayala 20 [74] who use the very same data as TUMQCD 19, but treat perturbation theory differently, resulting in a rather different central value. This shows that perturbative truncation errors are the main source of errors. We combine the results for $\Lambda^{N_f=3}_{\overline{\rm MS}}$ from both groups as a weighted average (with the larger upward error of TUMQCD 19) and take the difference of the central values as the uncertainty of the average. We obtain $\Lambda^{N_f=3}_{\overline{\rm MS}} = 330(24)$ MeV, which translates to $\alpha_s(m_Z) = 0.11782(165)$.

Table 68 Results for $\alpha_{\overline{\rm MS}}(M_Z)$. Different methods are listed separately and they are combined to a pre-range when computations are available without any ■. A weighted average of the pre-ranges gives 0.11843(60), using the smallest pre-range uncertainty gives 0.11843(81) while the average uncertainty of the ranges used as an error gives 0.11843(187). Note that TUMQCD 19 supersedes Bazavov 14/12

Collaboration	Ref.	N_f	Publication status	Renormalization scale	Perturbative behaviour	Continuum extrapolation	$\alpha_{\overline{\rm MS}}(M_Z)$	Remark	Tables
ALPHA 17	[77]	2+1	A	★	★	★	0.11852(84)	Step-scaling	60
PACS-CS 09A	[78]	2+1	A	★	★	○	0.11800(300)	Step-scaling	60
Pre-range (average)							0.11848(81)		
Ayala 20	[74]	2+1	A	○	★	○	0.11836(88)	Q-$\bar{Q}$ potential	61
TUMQCD 19	[75]	2+1	A	○	★	○	$0.11671(^{+110}_{-57})$	Q-$\bar{Q}$ potential (and free energy)	61
Takaura 18	[758,759]	2+1	A	■	○	○	$0.11790(70)(^{+130}_{-120})$	Q-$\bar{Q}$ potential	61
Bazavov 14	[760]	2+1	A	○	★	○	0.11660(100)	Q-$\bar{Q}$ potential	61
Bazavov 12	[761]	2+1	A	○	○	○	$0.11560(^{+210}_{-220})$	Q-$\bar{Q}$ potential	61
Pre-range with estimated pert. error							0.11782(165)		
Cali 20	[76]	2+1	A	○	★	★	0.11863(114)	Vacuum pol. (position space)	62
Hudspith 18	[780]	2+1	P	○	★	■	$0.11810(270)(^{+80}_{-220})$	Vacuum polarization	62
JLQCD 10	[779]	2+1	A	■	○	■	$0.11180(30)(^{+160}_{-170})$	Vacuum polarization	62
Pre-range with estimated pert. error							0.11863(360)		
HPQCD 10	[11]	2+1	A	○	★	★	0.11840(60)	Wilson loops	63
Maltman 08	[79]	2+1	A	○	○	★	0.11920(110)	Wilson loops	63
Pre-range with estimated pert. error							0.11871(128)		
Petreczky 20	[696]	2+1	P	○	○	★	0.11773(119)	Heavy current two points	64
Boito 20	[697,698]	2+1	A	■	■	○	0.1177(20)	Use published lattice data	64
Petreczky 19	[26]	2+1	A	■	■	★	0.1159(12)	Heavy current two points	64
JLQCD 16	[25]	2+1	A	■	○	○	0.11770(260)	Heavy current two points	64
Maezawa 16	[189]	2+1	A	■	■	○	0.11622(84)	Heavy current two points	64
HPQCD 14A	[14]	2+1+1	A	○	★	○	0.11822(74)	Heavy current two points	64
HPQCD 10	[11]	2+1	A	○	★	○	0.11830(70)	Heavy current two points	64
HPQCD 08B	[202]	2+1	A	■	■	■	0.11740(120)	Heavy current two points	64
Pre-range with estimated pert. error							0.11826(200)		
Zafeiropoulos 19	[699]	2+1	A	■	■	■	0.1172(11)	Gluon-ghost vertex	66
ETM 13D	[819]	2+1+1	A	○	○	■	0.11960(40)(80)(60)	Gluon-ghost vertex	66
ETM 12C	[820]	2+1+1	A	○	○	■	0.12000(140)	Gluon-ghost vertex	66
ETM 11D	[821]	2+1+1	A	○	○	■	$0.11980(90)(50)(^{+0}_{-50})$	Gluon-ghost vertex	66
Nakayama 18	[837]	2+1	A	★	○	■	0.12260(360)	Dirac eigenvalues	67

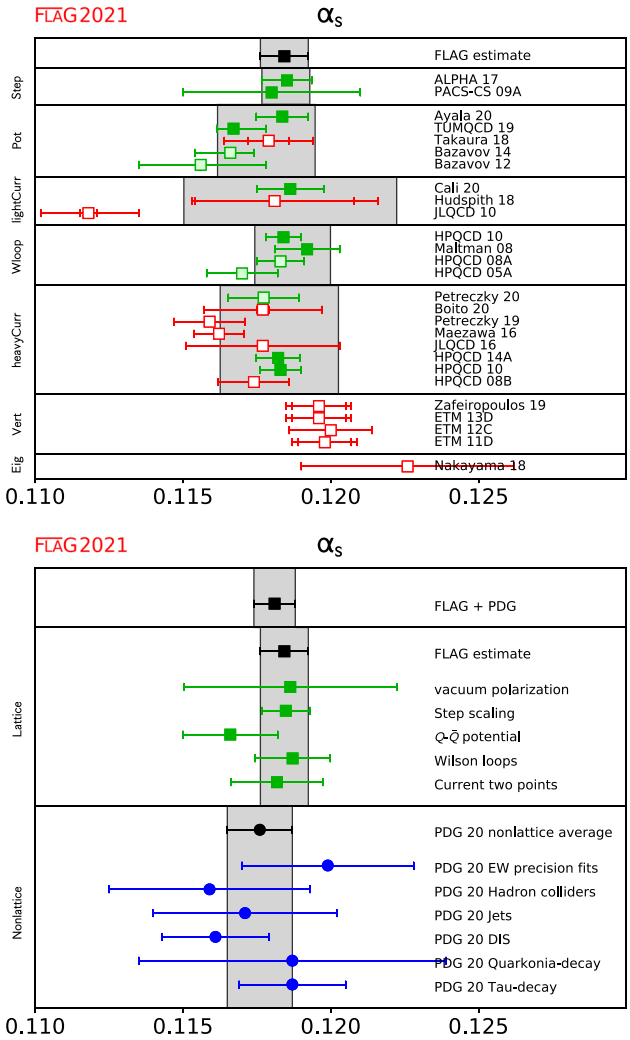

Fig. 41 $\alpha^{(5)}_{\overline{\rm MS}}(M_Z)$, the coupling constant in the $\overline{\rm MS}$ scheme at the Z mass. Top: lattice results, pre-ranges from different calculation methods, and final average. Bottom: Comparison of the lattice pre-ranges and average with the nonlattice ranges and average. The first PDG 20 entry gives the outcome of their analysis excluding lattice results (see Sect. 9.11.4)

- *Small Wilson loops*
  Here the situation is unchanged as compared to FLAG 16. In the determination of α_s from observables at the lattice spacing scale, there is an interplay of higher-order perturbative terms and lattice artifacts. In HPQCD 05A [783], HPQCD 08A [784] and Maltman 08 [79] both lattice artifacts (which are power corrections in this approach) and higher-order perturbative terms are fitted. We note that Maltman 08 [79] and HPQCD 08A [784] analyze largely the same data set but use different versions of the perturbative expansion and treatments of nonperturbative terms. After adjusting for the slightly different lattice scales used, the values of $\alpha_{\overline{\rm MS}}(M_Z)$ differ by 0.0004 to 0.0008 for the three quantities considered. In fact the largest of these differences (0.0008) comes from a tadpole-improved loop, which is expected to be best behaved perturbatively. We therefore replace the perturbative-truncation errors from [79] and [11] with our estimate of the perturbative uncertainty Eq. (379). Taking the perturbative errors to be 100% correlated between the results, we obtain for the weighted average $\alpha_{\overline{\rm MS}} = 0.11871(128)$.
- *Heavy quark current two-point functions*
  Other computations with small errors are HPQCD 10 [11] and HPQCD 14A [14], where correlation functions of heavy valence quarks are used to construct short-distance quantities. Due to the large quark masses needed to reach the region of small coupling, considerable discretization errors are present, see Fig. 30 of FLAG 16. These are treated by fits to the perturbative running (a 5-loop running $\alpha_{\overline{\rm MS}}$ with a fitted 5-loop coefficient in the β-function is used) with high-order terms in a double expansion in $a^2\Lambda^2$ and $a^2 m_{\rm c}^2$ supplemented by priors which limit the size of the coefficients. The priors

play an especially important role in these fits given the much larger number of fit parameters than data points. We note, however, that the size of the coefficients does not prevent high-order terms from contributing significantly, since the data includes values of am_c that are rather close to 1.

We note that the result of JLQCD 16 was classified in FLAG 19 as having passed all FLAG criteria, although the scale is set by the charm-quark mass, implying $\alpha_{\rm eff} \simeq 0.38$. We now assign a red flag for renormalization scale, as we do for Petreczky 19 and Boito 20 (see below). Since FLAG 19, there have been three new studies, Petreczky 19 [26], Petreczky 20 [696] and Boito 20 [698] (Petreczky 19/Petreczky 20 supersede Maezawa 16 [189]). While Petreczky 19/Petreczky 20 share the same lattice data for heavy quark masses in the range $m_h = m_c$–$4m_c$ they use a different strategy for continuum extrapolations and a different treatment of perturbative uncertainties. Petreczky 19 [26] perform continuum extrapolation separately for each value of the valence-quark mass, while Petreczky 20 rely on joint continuum extrapolations of the lattice data at different heavy-quark masses, similar to the analysis of HPQCD, but without Bayesian priors. It is concluded that reliable continuum extrapolations for $m_h \geq 2m_c$ require a joint fit to the data. This limits the eligible α_s determinations in Petreczky 19 [26] to $m_h = m_c$ and $1.5m_c$, for which, however, the FLAG criteria are not satisfied. There is also a difference in the choice of renormalization scale between both analyses: Petreczky 19 [26] uses $\mu = m_h$, while Petreczky 20 [696] considers several choices [Us] of μ in the range $\mu = 2/3m_h$–$3m_h$, which leads to larger perturbative uncertainties in the determination of α_s [696]. Boito 20 [698] use published continuum extrapolated lattice results for $m_h = m_c$ and performs its own extraction of α_s. Limiting the choice of m_h to the charm-quark mass means that the FLAG criteria are not met ($\alpha_{\rm eff} \simeq 0.38$). However, their analysis gives valuable insight into the perturbative error. In addition to the renormalization scale μ, Boito 20 also vary the renormalization scale μ_m at which the charm quark mass is defined. The corresponding result $\alpha_s(M_Z) = 0.1177(20)$ agrees well with previous lattice determination but has a larger error, which is dominated by the perturbative uncertainty due to the variation of both scales. This increased uncertainty suggests that the perturbative error estimated by HPQCD using a fixed scale $\mu = 3m_h$ may be too small. Therefore, we take the average of the HPQCD 10 and HPQCD 14A determinations and assign an error of 0.0020, based on the analysis of Boito 20 [698]. This results in the range $\alpha_s(M_Z) = 0.11826(200)$.

- *Light quark vacuum polarization*
  Since FLAG 19 a new study, Cali 20 [76] appeared, which uses the light current two-point functions in position space, evaluated on a subset of CLS configurations for lattice spacings in the range 0.038–0.076 fm, and for Euclidean distances 0.13–0.19 fm, corresponding to renormalization scales $\mu = 1$–1.5 GeV. Both flavour nonsinglet vector and axial vector currents are considered and their difference is shown to vanish within errors. After continuum and chiral limits are taken, the effective coupling from the axial vector two-point function is converted at 3-loop order to $\alpha_{\overline{\rm MS}}(\mu)$. The authors do this by numerical solution for $\alpha_{\overline{\rm MS}}$ and then perform a weighted average of the Λ-parameter estimates for the available energy range, which yields $\Lambda_{\overline{\rm MS}}^{N_f=3} = 342(17)$ MeV. Note that this is the first calculation in the vacuum polarization category that passes the current FLAG criteria. Yet the renormalization scales are rather low and one might suspect that other nonperturbative (i.e., non chiral-symmetry breaking) effects may still be sizeable. Our main issue is a rather optimistic estimate of perturbative truncation errors, based only on the variation of the Λ-parameter from the range of effective couplings considered. If the solution for the $\overline{\rm MS}$ coupling is done by series expansion in $\alpha_{\rm eff}$, the differences in $\alpha_{\overline{\rm MS}}$, formally of order $\alpha_{\rm eff}^5$, are still large at the scales considered. Hence, as a measure of the systematic uncertainty we take the difference $409 - 355$ MeV between $\Lambda_{\overline{\rm MS}}^{N_f=3}$ estimates at $\mu = 1.5$ GeV as a proxy for the total error, i.e. $\Lambda_{\overline{\rm MS}}^{N_f=3} = 342(54)$ MeV, which translates to our pre-range, $\alpha_s(m_Z) = 0.11863(360)$, from vacuum polarization.
- *Other methods*
  Computations using other methods do not qualify for an average yet, predominantly due to a lacking ○ in the continuum extrapolation.

We obtain the central value for our range of α_s from the weighted average of the five pre-ranges listed in Table 68. The error of this weighted average is 0.0006, which is quite a bit smaller than the most precise entry. Because, however, the errors on almost all of the α_s calculations that enter the average are dominated by perturbative truncation errors, which are especially difficult to estimate, we choose instead to take a larger range for α_s of 0.0008. This is the error on the pre-range for α_s from step-scaling, because perturbative-truncation errors are sub-dominant in this method. Our final range is then given by

$$\alpha_{\overline{\rm MS}}^{(5)}(M_Z) = 0.1184(8). \tag{396}$$

moving up by 2 in the last given digit compared to FLAG 19 and with the same uncertainty. Of the eleven calculations that are included most are within 1σ of this range, an exception being TUMQCD 19 (which supersedes Bazavov 14 and Bazavov 12). Further, the range for $\alpha^{(5)}_{\overline{\rm MS}}(M_Z)$ presented here is based on results with rather different systematics (apart from the matching across the charm threshold). We therefore believe that the true value is very likely to lie within this range.

All computations which enter this range, with the exception of HPQCD 14A [14], rely on a perturbative inclusion of the charm and bottom quarks. Perturbation theory for the matching of $\bar{g}^2_{N_f}$ and $\bar{g}^2_{N_f-1}$ looks very well behaved even at the mass of the charm. Worries that still there may be purely nonperturbative effects at this rather low scale have been removed by nonperturbative studies of the accuracy of perturbation theory. While the original study in Ref. [158] was not precise enough, the extended one in Ref. [160] estimates effects in the Λ-parameter to be significantly below 1% and thus negligible for the present and near future accuracy.

9.11.3 Ranges for $[r_0\Lambda]^{(N_f)}$ *and* $\Lambda_{\overline{\rm MS}}$

In the present situation, we give ranges for $[r_0\Lambda]^{(N_f)}$ and $\Lambda_{\overline{\rm MS}}$, discussing their determination case by case. We include results with $N_f < 3$ because it is interesting to see the N_f-dependence of the connection of low- and high-energy QCD. This aids our understanding of the field theory and helps in finding possible ways to tackle it beyond the lattice approach. It is also of interest in providing an impression on the size of the vacuum-polarization effects of quarks, in particular with an eye on the still difficult-to-treat heavier charm and bottom quarks. Most importantly, however, the decoupling strategy described in Sect. 9.4 means that Λ-parameters at different N_f can be connected by a nonperturbative matching computation. Thus, even results at unphysical flavour numbers, in particular $N_f = 0$, may enter results for the physically interesting case. Rather than phasing out results for "unphysical flavour numbers", continued scrutiny by FLAG will be necessary. Having said this, we emphasize that results for $[r_0\Lambda]^{(0)}$ and $[r_0\Lambda]^{(2)}$ are *not* meant to be used directly for phenomenology.

For the ranges we obtain:

$$[r_0\Lambda_{\overline{\rm MS}}]^{(4)} = 0.70(3), \tag{397}$$
$$[r_0\Lambda_{\overline{\rm MS}}]^{(3)} = 0.808(29), \tag{398}$$
$$[r_0\Lambda_{\overline{\rm MS}}]^{(2)} = 0.79(^{+\,5}_{-15}), \tag{399}$$
$$[r_0\Lambda_{\overline{\rm MS}}]^{(0)} = 0.624(36). \tag{400}$$

No change has occurred since FLAG 19 for $N_f = 2, 4$, so we take over the respective discussion from FLAG 19.

For $N_f = 2{+}1{+}1$, we presently do not quote a range as there is a single result: HPQCD 14A [14] found $[r_0\Lambda]^{(4)} = 0.70(3)$.

For $N_f = 2 + 1$, we take as a central value the weighted average of Cali 20 [76], Ayala 20 [74], TUMQCD 19 [75], ALPHA 17 [77] HPQCD 10 [11] (Wilson loops and current two-point correlators), PACS-CS 09A [78] (with linear continuum extrapolation) and Maltman 08 [79]. Since the uncertainty in r_0 is small compared to that of Λ, we can directly propagate the error from the analog of Eq. (396) with the 2+1+1 number removed and arrive at

$$[r_0\Lambda_{\overline{\rm MS}}]^{(3)} = 0.808(29). \tag{401}$$

(The error of the straight weighted average is 0.012.) It is in good agreement with all 2+1 results without red tags. In physical units, using $r_0 = 0.472$ fm and neglecting its error, this means[70]

$$\Lambda^{(3)}_{\overline{\rm MS}} = 338(12)\,\text{MeV}, \tag{402}$$

where the error of the straight weighted average is less than 5 MeV.

For $N_f = 2$, at present there is one computation with a ★ rating for all criteria, ALPHA 12 [707]. We adopt it as our central value and enlarge the error to cover the central values of the other three results with filled green boxes. This results in an asymmetric error. Our range is unchanged as compared to FLAG 13,

$$[r_0\Lambda_{\overline{\rm MS}}]^{(2)} = 0.79(^{+\,5}_{-15}), \tag{403}$$

[70] In the FLAG 19 report [4], an inaccurate conversion of $[r_0\Lambda_{\overline{\rm MS}}]^{(3)}$ in Eq. (345) to physical units (using $r_0 = 0.472$ fm) led to 343 MeV in Eqs. (346, 353). However, using fm × MeV = 1/197.3 gives 337 MeV (Eqs. (351) and (352) are however correct) (Note: All equation references in this footnote refer to [4]).

and in physical units, using $r_0 = 0.472$ fm,

$$\Lambda^{(2)}_{\overline{\rm MS}} = 330(^{+21}_{-63})\,\text{MeV}. \tag{404}$$

A weighted average of the four eligible numbers would yield $[r_0\Lambda_{\overline{\rm MS}}]^{(2)} = 0.689(23)$, not covering the best result and in particular leading to a smaller error than we feel is justified, given the issues discussed previously in Sect. 9.5.2 (Karbstein 18 [762], ETM 11C [764]) and Sect. 9.9.2 (ETM 10F [824]). Thus we believe that our estimate is a conservative choice; the low values of ETM 11C [764] and Karbstein 18 [762] lead to a large downward error. We note that this can largely be explained by different values of r_0 between ETM 11C [764] and ALPHA 12 [707]. We still hope that future work will improve the situation.

For $N_f = 0$, the new result DallaBrida 19 [693], is quite large compared to the FLAG 19 average. We combine it with those results which entered the FLAG 19 report, namely ALPHA 98 [739], QCDSF/UKQCD 05 [787], Brambilla 10 [766], Kitazawa 16 [792] and Ishikawa 17 [732] for forming a range.[71] Taking a weighted average of the six numbers, we obtain $[r_0\Lambda_{\overline{\rm MS}}]^{(0)} = 0.624(5)$, up from 0.615(5) for FLAG 19.

Clearly the errors are dominantly systematic, mostly due to perturbative truncation errors. Since we do not change the FLAG 19 criteria for this edition, we give a range which encompasses all central values. Unfortunately, this requires to double the error of the FLAG 19 result (which was given by 0.615(18)), due to the large central value of 0.660 by DallaBrida 19. We arrive at our range for $N_f = 0$,

$$[r_0\Lambda_{\overline{\rm MS}}]^{(0)} = 0.624(36). \tag{405}$$

This is clearly not very satisfactory, and, despite this large error, this still means that the high quality, and statistics dominated new step-scaling result Dalla Brida 19 is more than 3 sigma away from the central value of the new FLAG average.

Converting to physical units, again using $r_0 = 0.472$ fm yields

$$\Lambda^{(0)}_{\overline{\rm MS}} = 261(15)\,\text{MeV}. \tag{406}$$

While the conversion of the Λ parameter to physical units is quite unambiguous for $N_f = 2+1$, our choice of $r_0 = 0.472$ fm also for smaller numbers of flavour amounts to a convention, in particular for $N_f = 0$. Indeed, in the Tables 60, 61, 62, 63, 64, 65 and 66 somewhat different numbers in MeV are found.

9.11.4 Conclusions

With the present results our range for the strong coupling is (repeating Eq. (396))

$$\alpha^{(5)}_{\overline{\rm MS}}(M_Z) = 0.1184(8) \qquad \text{Refs. [11,14,74–79]}$$

and the associated Λ parameters

$$\Lambda^{(5)}_{\overline{\rm MS}} = 214(10)\ \text{MeV} \qquad \text{Refs. [11,14,74–79]}, \tag{407}$$

$$\Lambda^{(4)}_{\overline{\rm MS}} = 297(12)\ \text{MeV} \qquad \text{Refs. [11,14,74–79]}, \tag{408}$$

$$\Lambda^{(3)}_{\overline{\rm MS}} = 339(12)\ \text{MeV} \qquad \text{Refs. [11,14,74–79]}. \tag{409}$$

Compared with FLAG 19, the central values have moved slightly, with the errors remaining the same.

It is interesting to compare with the Particle Data Group average of nonlattice determinations of recent years,

$$\alpha^{(5)}_{\overline{\rm MS}}(M_Z) = 0.1176(11), \quad \text{PDG 20, nonlattice [165], also appeared as Eq. (319)},$$

$$\alpha^{(5)}_{\overline{\rm MS}}(M_Z) = 0.1174(16), \quad \text{PDG 18, nonlattice [431]}, \tag{410}$$

$$\alpha^{(5)}_{\overline{\rm MS}}(M_Z) = 0.1174(16), \quad \text{PDG 16, nonlattice [234]}, \tag{411}$$

[71] We have assigned a ○ for the continuum limit, in Boucaud 00A [829], 00B [828], 01A [827], Soto 01 [826] but these results are from lattices of a very small physical size with finite-size effects that are not easily quantified.

$$\alpha^{(5)}_{\overline{\rm MS}}(M_Z) = 0.1175(17), \quad \text{PDG 14, nonlattice [201]}, \tag{412}$$

$$\alpha^{(5)}_{\overline{\rm MS}}(M_Z) = 0.1183(12), \quad \text{PDG 12, nonlattice [838]}, \tag{413}$$

(there was no update in [431]). There is good agreement with Eq. (396). Despite our very conservative error estimate, the FLAG lattice average has an error that is 30% smaller than the PDG 20 nonlattice-world average and a weighted average of the two [Eq. (396) and Eq. (319)] yields

$$\alpha^{(5)}_{\overline{\rm MS}}(M_Z) = 0.1181(7), \quad \text{FLAG 21 + PDG 20}. \tag{414}$$

In the lower plot in Fig. 41 we show as blue circles the various PDG pre-averages which lead to the PDG 20 nonlattice average. They are on a similar level as our pre-ranges (green squares) : each one corresponds to an estimate (by the PDG) of α_s determined from one set of input quantities. Within each pre-average multiple groups did the analysis and published their results as displayed in Ref. [165].

The fact that our range for the lattice determination of $\alpha_{\overline{\rm MS}}(M_Z)$ in Eq. (396) is in excellent agreement with the PDG 20 nonlattice average Eq. (319) is an excellent check for the subtle interplay of theory, phenomenology and experiments in the nonlattice determinations. The work done on the lattice provides an entirely independent determination, with negligible experimental uncertainty, which reaches a better precision even with our quite conservative estimate of its uncertainty.

We finish by commenting on perspectives for the future. The step-scaling methods have been shown to yield a very precise result and to satisfy all criteria easily. A downside is that dedicated simulations have to be done and the method is thus hardly used. It would be desirable to have at least one more such computation by an independent collaboration, as also requested in the review [679].

While this FLAG review does not report an error reduction compared to FLAG 19, the understanding of some systematic errors has improved. With the exception of the step-scaling result, all determinations of α_s, appear to be limited by systematic uncertainties due to perturbative truncation errors. Similar conclusions have been drawn in the recent review article [691]. In order to improve control of systematics it would be necessary to reach higher energy scales without incurring large cutoff effects. This could be achieved by applying step-scaling methods in large (infinite) volume, provided that finite volume effects are carefully controlled. Even a relatively modest increase by a scale factor 2–3 could significantly enhance the scope for some of the current approaches to determine α_s. Another hope for improvement are decoupling strategies, following the recent proposal by the ALPHA collaboration, cf. Sect. 9.4. This in turn motivates further state-of-the-art studies in the pure gauge theory ($N_f = 0$), where it would be important to resolve the current tension between results in the literature.

10 Nucleon matrix elements (NME)

Authors: S. Collins, R. Gupta, A. Nicholson, H. Wittig

A large number of experiments testing the Standard Model (SM) and searching for physics Beyond the Standard Model (BSM) involve either free nucleons (proton and neutron beams) or the scattering of electrons, muons, neutrinos and dark matter off nuclear targets. Necessary ingredients in the analysis of the experimental results are the matrix elements of various probes (fundamental currents or operators in a low energy effective theory) between nucleon or nuclear states. The goal of lattice-QCD calculations in this context is to provide high precision predictions of these matrix elements, the simplest of which give the nucleon charges and form factors. Determinations of the charges are the most mature and in this review we summarize the results for twelve quantities, the isovector and flavour diagonal axial vector, scalar and tensor charges. Other quantities that are not being reviewed but for which significant progress has been made in the last five years are the nucleon axial vector and electromagnetic form factors [839–853] and parton distribution functions [854–858]. The more challenging calculations of nuclear matrix elements, that are needed, for example, to calculate the cross-sections of neutrinos or dark matter scattering off nuclear targets, are proceeding along three paths. First is direct evaluation of matrix elements calculated with initial and final states consisting of multiple nucleons [859,860]. Second, convoluting nucleon matrix elements with nuclear effects [861], and third, determining two and higher body terms in the nuclear potential via the direct or the HAL QCD methods [862,863]. We expect future FLAG reviews to include results on these quantities once a sufficient level of control over all the systematics is reached.

10.1 Isovector and flavour diagonal charges of the nucleon

The simplest nucleon matrix elements are composed of local quark bilinear operators, $\overline{q_i}\Gamma_\alpha q_j$, where Γ_α can be any of the sixteen Dirac matrices. In this report, we consider two types of flavour structures: (a) when $i = u$ and $j = d$. These $\overline{u}\Gamma_\alpha d$ operators arise in $W^\pm$ mediated weak interactions such as in neutron or pion decay. We restrict the discussion to the matrix elements of the axial vector (A), scalar (S) and tensor (T) currents, which give the isovector charges, $g^{u-d}_{A,S,T}$.[72] (b) When $i = j$ for $j \in \{u, d, s\}$, there is no change of flavour, e.g., in processes mediated via the electromagnetic or weak neutral interaction or dark matter. These γ or Z^0 or possible dark matter mediated processes couple to all flavours with their corresponding charges. Since these probes interact with nucleons within nuclear targets, one has to include the effects of QCD (to go from the couplings defined at the quark and gluon level to those for nucleons) and nuclear forces in order to make contact with experiments. The isovector and flavour diagonal charges, given by the matrix elements of the corresponding operators calculated between nucleon states, are these nucleon level couplings. Here we review results for the light and strange flavours, $g^u_{A,S,T}$, $g^d_{A,S,T}$, and $g^s_{A,S,T}$ and the isovector charges $g^{u-d}_{A,S,T}$.

The isovector and flavour diagonal operators also arise in BSM theories due to the exchange of novel force carriers or as effective interactions due to loop effects. The associated couplings are defined at the energy scale $\Lambda_{\rm BSM}$, while lattice-QCD calculations of matrix elements are carried out at a hadronic scale, μ, of a few GeV. The tool for connecting the couplings at the two scales is the renormalization group. Since the operators of interest are composed of quark fields (and more generally also of gluon fields), the predominant change in the corresponding couplings under a scale transformation is due to QCD. To define the operators and their couplings at the hadronic scale μ, one constructs renormalized operators, whose matrix elements are finite in the continuum limit. This requires calculating both multiplicative renormalization factors, including the anomalous dimensions and finite terms, and the mixing with other operators. We discuss the details of the renormalization factors needed for each of the six operators reviewed in this report in Sect. 10.1.3.

Once renormalized operators are defined, the matrix elements of interest are extracted using expectation values of two-point and three-point correlation functions illustrated in Fig. 42, where the latter can have both quark-line connected and disconnected contributions. In order to isolate the ground-state matrix element, these correlation functions are analyzed using their spectral decomposition. The current practice is to fit the n-point correlation functions (or ratios involving three- and two-point functions) including contributions from one or two excited states. In some cases, such as axial and vector operators, Ward identities provide relations between correlation functions, or ground state matrix elements, or facilitate the calculation of renormalization constants. It is important to ensure that all such Ward identities are satisfied in lattice calculations, especially as in the case of axial form factors where they provide checks of whether excited state contamination has been removed in obtaining matrix elements within ground state nucleons [101,850,864].

The ideal situation occurs if the time separation τ between the nucleon source and sink positions, and the distance of the operator insertion time from the source and the sink, t and $\tau - t$, respectively, are large enough such that the contribution of all excited states is negligible. In the limit of large τ, the ratio of noise to signal in the nucleon two- and three-point correlation functions grows exponentially as $e^{(M_N - \frac{3}{2}M_\pi)\tau}$ [865,866], where M_N and M_π are the masses of the nucleon and the pion, respectively. Therefore, in particular at small pion masses, maintaining reasonable errors for large τ is challenging, with current calculations limited to $\tau \lesssim 1.5$ fm. In addition, the mass gap between the ground and excited (including multi-particle) states is smaller than in the meson sector and at these separations, excited-state effects can be significant. The approach commonly taken is to first obtain results with high statistics at multiple values of τ, using the methods described in Sect. 10.1.1. Then, as mentioned above, excited-state contamination is removed by fitting the data using a fit form involving one or two excited states. The different strategies that have been employed to minimize excited-state contamination are discussed in Sect. 10.1.2.

Usually, the quark-connected part of the three-point function (corresponding to the plot in the centre of Fig. 42) is computed via the so-called "sequential propagator method", which uses the product of two quark propagators between the positions of the initial and the final nucleons as a source term for another inversion of the lattice Dirac operator. This implies that the position of the sink timeslice is fixed at some chosen value. Varying the value of the source-sink separation τ then requires the calculation of another sequential propagator.

The evaluation of quark-disconnected contributions is computationally more challenging as the disconnected loop (which contains the operator insertion, as illustrated in Fig. 42, right) is needed at all points on a particular timeslice or, in general, over the whole lattice. The quark loop is computed stochastically and then correlated with the nucleon two-point function before averaging this three-point function over the ensemble of gauge configurations. The associated statistical error, therefore, is a

[72] In the isospin symmetric limit $\langle p|\bar{u}\Gamma d|n\rangle = \langle p|\bar{u}\Gamma u - \bar{d}\Gamma d|p\rangle = \langle n|\bar{d}\Gamma d - \bar{u}\Gamma u|n\rangle$ for nucleon and proton states $|p\rangle$ and $|n\rangle$, respectively. The latter two (equivalent) isovector matrix elements are computed on the lattice.

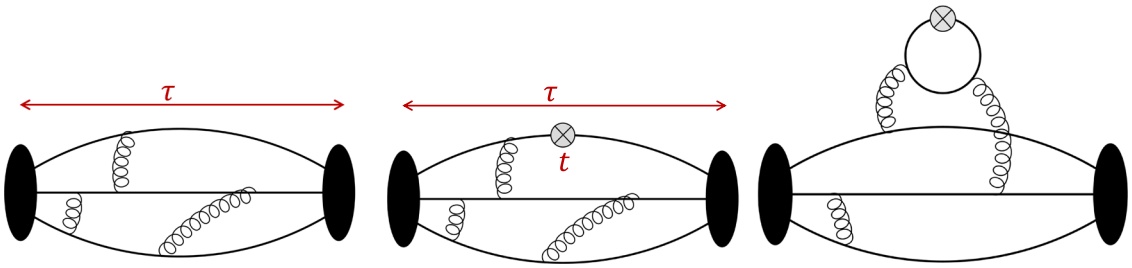

Fig. 42 The two- and three-point correlation functions (illustrated by Feynman diagrams) that need to be calculated to extract the ground state nucleon matrix elements. (Left) the nucleon two-point function. (Middle) the connected three-point function with source-sink separation τ and operator insertion time slice t. (Right) the disconnected three-point function with operator insertion at t

combination of that due to the stochastic evaluation (on each configuration) and that from the gauge average. The number of stochastic sources employed on each configuration is, typically, optimized to reduce the overall error for a given computational cost. The statistical errors of the connected contributions, in contrast, usually come only from the ensemble average since they are often evaluated exactly on each configuration, for a small number of source positions. If these positions are well-separated in space and time, then each measurement is statistically independent. The methodology applied for these calculations and the variance reduction techniques are summarized in Sect. 10.1.1. By construction, arbitrary values of τ across the entire temporal extent of the lattice can be realized when computing the quark-disconnected contribution, since the source-sink separation is determined by the part of the diagram that corresponds to the two-point nucleon correlator. However, in practice statistical fluctuations of both the connected and disconnected contributions increase sharply, so that the signal is lost in the statistical noise for $\tau \gtrsim 1.5\,\text{fm}$.

The lattice calculation is performed for a given number of quark flavours and at a number of values of the lattice spacing a, the pion mass M_π, and the lattice size, represented by $M_\pi L$. The results need to be extrapolated to the physical point defined by $a = 0$, $M_\pi = 135$ MeV and $M_\pi L \to \infty$. This is done by fitting the data simultaneously in these three variables using a theoretically motivated ansatz. The ansätze used and the fitting strategy are described in Sect. 10.1.4.

The procedure for rating the various calculations and the criteria specific to this chapter are discussed in Sect. 10.2, which also includes a brief description of how the final averages are constructed. The physics motivation for computing the isovector charges, $g^{u-d}_{A,S,T}$, and the review of the lattice results are presented in Sect. 10.3. This is followed by a discussion of the relevance of the flavour diagonal charges, $g^{u,d,s}_{A,S,T}$, and a presentation of the lattice results in Sect. 10.4.

10.1.1 Technical aspects of the calculations of nucleon matrix elements

The calculation of n-point functions needed to extract nucleon matrix elements requires making four essential choices. The first involves choosing between the suite of background gauge field ensembles one has access to. The range of lattice parameters should be large enough to facilitate the extrapolation to the continuum and infinite-volume limits, and, ideally, the evaluation at the physical pion mass taken to be $M_\pi = 135$ MeV. Such ensembles have been generated with a variety of discretization schemes for the gauge and fermion actions that have different levels of improvement and preservation of continuum symmetries. The actions employed at present include (i) Wilson gauge with nonperturbatively improved Sheikholeslami–Wohlert fermions (nonperturbatively improved clover fermions) [107,369,867–871], (ii) Iwasaki gauge with nonperturbatively improved clover fermions [847,872], (iii) Iwasaki gauge with twisted-mass fermions with a clover term [873–877], (iv) tadpole Symanzik improved gauge with highly improved staggered quarks (HISQ) [98,99,103,110,878–882], (v) Iwasaki gauge with domain-wall fermions (DW) [101,106,883–887] and (vi) Iwasaki gauge with overlap fermions [888–890]. For details of the lattice actions, see the glossary in the Appendix A.1 of FLAG 19 [4].

The second choice is of the valence quark action. Here there are two choices, to maintain a unitary formulation by choosing exactly the same action as is used in the generation of gauge configurations or to choose a different action and tune the quark masses to match the pseudoscalar meson spectrum in the two theories. Such mixed action formulations are nonunitary but are expected to have the same continuum limit as QCD. The reason for choosing a mixed action approach is expediency. For example, the generation of 2+1+1 flavour HISQ and 2+1 flavour DW ensembles with physical quark masses has been possible even at the coarse lattice spacing of $a = 0.15$ fm and there are indications that cut-off effects are reasonably small. These ensembles have been analyzed using clover-improved Wilson fermions, DW and overlap fermions since the construction of baryon correlation functions with definite spin and parity is much simpler compared to staggered fermions.

The third choice is the combination of the algorithm for inverting the Dirac matrix and variance reduction techniques. Efficient inversion and variance reduction techniques are needed for the calculation of nucleon correlation functions with high precision because the signal-to-noise ratio degrades exponentially as $e^{(\frac{3}{2}M_\pi - M_N)\tau}$ with the source-sink separation τ. Thus, the number of measurements needed for high precision is much larger than in the meson sector. Commonly used inversion algorithms include the multigrid [891] and the deflation-accelerated Krylov solvers [892], which can handle linear systems with large condition numbers very efficiently, thereby enabling calculations of correlation functions at the physical pion mass.

The sampling of the path integral is limited by the number $N_{\rm conf}$ of gauge configurations generated. One requires sufficiently large $N_{\rm conf}$ such that the phase space (for example, different topological sectors) has been adequately sampled and all the correlation functions satisfy the expected lattice symmetries such as C, P, T, momentum and translation invariance. Thus, one needs gauge field generation algorithms that give decorrelated large volume configurations cost-effectively. On such large lattices, to reduce errors one can exploit the fact that the volume is large enough to allow multiple measurements of nucleon correlation functions that are essentially statistically independent. Two other common variance reduction techniques that reduce the cost of multiple measurements on each configuration are: the truncated solver with bias correction method [893] and deflation of the Dirac matrix for the low lying modes followed by sloppy solution with bias correction for the residual matrix consisting predominately of the high frequency modes [893,894].

A number of other variance reduction methods are also being used and developed. These include deflation with hierarchical probing for disconnected diagrams [895,896], the coherent source sequential propagator method [897,898], low-mode averaging [899,900], the hopping-parameter expansion [901,902] and partitioning [903] (also known as dilution [904]).

The final choice is of the interpolating operator used to create and annihilate the nucleon state, and of the operator used to calculate the matrix element. Along with the choice of the interpolating operator (or operators if a variational method is used) one also chooses a "smearing" of the source used to construct the quark propagator. By tuning the width of the smearing, one can optimize the spatial extent of the nucleon interpolating operator to reduce the overlap with the excited states. Two common smearing algorithms are Gaussian (Wuppertal) [905] and Jacobi [906] smearing.

Having made all the above choices, for which a reasonable recipe exists, one calculates a statistical sample of correlation functions from which the desired ground state nucleon matrix element is extracted. Excited states, unfortunately, contribute significantly to nucleon correlation functions in present studies. To remove their contributions, calculations are performed with multiple source-sink separations τ and fits are made to the correlation functions using their spectral decomposition as discussed in the next section.

10.1.2 Controlling excited-state contamination

Nucleon matrix elements are determined from a combination of two- and three-point correlation functions. To be more specific, let $B^\alpha(\vec{x},t)$ denote an interpolating operator for the nucleon. Placing the initial state at time slice $t = 0$, the two-point correlation function of a nucleon with momentum $\vec{p}$ reads

$$C_2(\vec{p};\tau) = \sum_{\vec{x},\vec{y}} e^{i\vec{p}\cdot(\vec{x}-\vec{y})}\, \mathbb{P}_{\beta\alpha} \left\langle B^\alpha(\vec{x},\tau)\, \overline{B}^\beta(\vec{y},0)\right\rangle, \tag{415}$$

where the projector $\mathbb{P}$ selects the polarization, and α, β denote Dirac indices. The three-point function of two nucleons and a quark bilinear operator O_Γ is defined as

$$C_3^\Gamma(\vec{q};t,\tau) = \sum_{\vec{x},\vec{y},\vec{z}} e^{i\vec{p}\,'\cdot(\vec{x}-\vec{z})}\, e^{-i\vec{p}\cdot(\vec{y}-\vec{z})}\, \mathbb{P}_{\beta\alpha} \left\langle B^\alpha(\vec{x},\tau)\, O_\Gamma(\vec{z},t)\, \overline{B}^\beta(\vec{y},0)\right\rangle, \tag{416}$$

where $\vec{p}$, $\vec{p}\,'$ denote the momenta of the nucleons at the source and sink, respectively, and $\vec{q} \equiv \vec{p}\,' - \vec{p}$ is the momentum transfer. The bilinear operator is inserted at time slice t, and τ denotes the source-sink separation. Both C_2 and C_3^Γ can be expressed in terms of the nonperturbative quark propagators, $D^{-1}(y,x)$, where D denotes the lattice Dirac operator.

The framework for the analysis of excited-state contamination is based on spectral decomposition. After inserting complete sets of eigenstates of the transfer matrix, the expressions for the correlators C_2 and C_3^Γ read

$$C_2(\vec{p};\tau) = \frac{1}{L^3} \sum_n \mathbb{P}_{\beta\alpha}\, \langle\Omega|B^\alpha|n\rangle\langle n|\overline{B}^\beta|\Omega\rangle\, e^{-E_n\tau}, \tag{417}$$

$$C_3^{\Gamma}(\vec{q};t,\tau) = \frac{1}{L^3}\sum_{n,m}\mathbb{P}_{\beta\alpha}\,\langle\Omega|B^{\alpha}|n\rangle\,\langle n|O_{\Gamma}|m\rangle\,\langle m|\overline{B}^{\beta}|\Omega\rangle\,e^{-E_n(\tau-t)}\,e^{-E_m t}, \tag{418}$$

where $|\Omega\rangle$ denotes the vacuum state, and E_n represents the energy of the n^{th} eigenstate $|n\rangle$ in the nucleon channel. Here we restrict the discussion to vanishing momentum transfer, i.e., the forward limit $\vec{q} = 0$, and label the ground state by $n = 0$. The matrix element of interest $g_{\Gamma} \equiv \langle 0|O_{\Gamma}|0\rangle$ can, for instance, be obtained from the asymptotic behaviour of the ratio

$$R_{\Gamma}(t,\tau) \equiv \frac{C_3^{\Gamma}(\vec{q}=0;t,\tau)}{C_2(\vec{p}=0;\tau)} \overset{t,(\tau-t)\to\infty}{\longrightarrow} g_{\Gamma} + \mathrm{O}(e^{-\Delta t},\, e^{-\Delta(\tau-t)},\, e^{-\Delta\tau}), \tag{419}$$

where $\Delta \equiv E_1 - E_0$ denotes the energy gap between the ground state and the first excitation. We also assume that the bilinear operator O_{Γ} is appropriately renormalized (see Sect. 10.1.3).

Excited states with the same quantum numbers as the nucleon include resonances such as a Roper-like state with a mass of about 1.5 GeV, or multi-particle states consisting of a nucleon and one or more pions [907,908]. The latter can provide significant contributions to the two- and three-point correlators in Eqs. (415) and (416) or their ratios (419) as the pion mass approaches its physical value. Ignoring the interactions between the individual hadrons, one can easily identify the lowest-lying multi-particle states: they include the $N\pi\pi$ state with all three particles at rest at $\sim$ 1.2 GeV, as well as $N\pi$ states with both hadrons having nonzero and opposite momentum. Depending on the spatial box size L in physical units (with the smallest nonzero momentum equal to $2\pi/L$), there may be a dense spectrum of $N\pi$ states before the first nucleon resonance is encountered. Corrections to nucleon correlation functions due to the pion continuum have been studied using chiral effective theory [907–910] and Lüscher's finite-volume quantization condition [911].

The well-known noise problem of baryonic correlation functions implies that the long-distance regime, $t, (\tau - t) \to \infty$, where the correlators are dominated by the ground state, is difficult to reach. Current lattice calculations of baryonic three-point functions are typically confined to source-sink separations of $\tau \lesssim 1.5$ fm, despite the availability of efficient noise reduction methods. In view of the dense excitation spectrum encountered in the nucleon channel, one has to demonstrate that the contributions from excited states are sufficiently suppressed to guarantee an unbiased determination of nucleon matrix elements. There are several strategies to address this problem:

- Multi-state fits to correlator ratios or individual two- and three-point functions;
- Three-point correlation functions summed over the operator insertion time t;
- Increasing the projection of the interpolator B^{α} onto the ground state.

The first of the above methods includes excited state contributions explicitly when fitting to the spectral decomposition of the correlation functions, Eqs. (417, 418) or, alternatively, their ratio (see Eq. (419)). In its simplest form, the resulting expression for R_{Γ} includes the contributions from the first excited state, i.e.,

$$R_{\Gamma}(t,\tau) = g_{\Gamma} + c_{01}\,e^{-\Delta t} + c_{10}\,e^{-\Delta(\tau-t)} + c_{11}\,e^{-\Delta\tau} + \cdots, \tag{420}$$

where c_{01}, c_{10}, c_{11} and Δ are treated as additional parameters when fitting $R_{\Gamma}(t,\tau)$ simultaneously over intervals in the source-sink separation τ and the operator insertion timeslice t. Multi-exponential fits become more difficult to stabilize for a growing number of excited states, since an increasing number of free parameters must be sufficiently constrained by the data. Therefore, a high level of statistical precision at several source-sink separations is required. One common way to address this issue is to introduce Bayesian constraints, as described in [912]. Alternatively, one may try to reduce the number of free parameters, for instance, by determining the energy gap Δ from nucleon two-point function and/or using a common gap for several different nucleon matrix elements [102].

Ignoring the explicit contributions from excited states and fitting $R_{\Gamma}(t,\tau)$ to a constant in t for fixed τ amounts to applying what is called the "plateau method". The name derives from the ideal situation that sufficiently large source-sink separations τ can be realized, which would cause $R_{\Gamma}(t,\tau)$ to exhibit a plateau in t independent of τ. The ability to control excited-state contamination is rather limited in this approach, since the only option is to check for consistency in the estimate of the plateau as τ is varied. In view of the exponential degradation of the statistical signal for increasing τ, such stability checks are difficult to perform reliably.

Summed operator insertions, originally proposed in Ref. [913], have also emerged as a widely used method to address the problem of excited-state contamination. One way to implement this method [914,915] proceeds by summing $R_{\Gamma}(t,\tau)$ over the insertion time t, resulting in the correlator ratio $S_{\Gamma}(\tau)$,

$$S_\Gamma(\tau) \equiv \sum_{t=a}^{\tau-a} R_\Gamma(t,\tau). \tag{421}$$

The asymptotic behaviour of $S_\Gamma(\tau)$, including sub-leading terms, for large source-sink separations τ can be easily derived from the spectral decomposition of the correlators and is given by [916]

$$S_\Gamma(\tau) \overset{\tau \gg 1/\Delta}{\longrightarrow} K_\Gamma + (\tau - a)\, g_\Gamma + (\tau - a)\, e^{-\Delta\tau} d_\Gamma + e^{-\Delta\tau} f_\Gamma + \cdots, \tag{422}$$

where K_Γ is a constant, and the coefficients d_Γ and f_Γ contain linear combinations of transition matrix elements involving the ground and first excited states. Thus, the matrix element of interest g_Γ is obtained from the linear slope of $S_\Gamma(\tau)$ with respect to the source-sink separation τ. While the leading corrections from excited states $e^{-\Delta\tau}$ are smaller than those of the original ratio $R_\Gamma(t,\tau)$ (see Eq. (419)), extracting the slope from a linear fit to $S_\Gamma(\tau)$ typically results in relatively large statistical errors. In principle, one could include the contributions from excited states explicitly in the expression for $S_\Gamma(\tau)$. However, in practice it is often difficult to constrain an enlarged set of parameters reliably, in particular if one cannot afford to determine $S_\Gamma(\tau)$ except for a handful of source-sink separations.

The original summed operator insertion technique described in Refs. [905,913,917,918] avoids the explicit summation over the operator insertion time t at every fixed value of τ. Instead, one replaces one of the quark propagators that appear in the representation of the two-point correlation function $C_2(t)$ by a "sequential" propagator, according to

$$D^{-1}(y,x) \to D_\Gamma^{-1}(y,x) = \sum_z D^{-1}(y,z)\Gamma D^{-1}(z,x). \tag{423}$$

In this expression, the position $z \equiv (\vec{z},t)$ of the insertion of the quark bilinear operator is implicitly summed over, by inverting the lattice Dirac operator D on the source field $\Gamma D^{-1}(z,x)$. While this gives access to all source-sink separations $0 \le \tau \le T$, where T is the temporal extent of the lattice, the resulting correlator also contains contact terms, as well as contributions from $\tau < t < T$ that must be controlled. This method[73] has been adopted recently by the CalLat collaboration in their calculation of the isovector axial charge [99,882].

As in the case of explicitly summing over the operator insertion time, the matrix element of interest is determined from the slope of the summed correlator. For instance, in Ref. [99], the axial charge was determined from the summed three-point correlation function, by fitting to its asymptotic behaviour [919] including sub-leading terms.

In practice, one often uses several methods simultaneously, e.g., multi-state fits and the summation method based on Eq. (422), in order to check the robustness of the result. All of the approaches for controlling excited-state contributions proceed by fitting data obtained in a finite interval in τ to a function that describes the approach to the asymptotic behaviour derived from the spectral decomposition. Obviously, the accessible values of τ must be large enough so that the model function provides a good representation of the data that enter such a fit. It is then reasonable to impose a lower threshold on τ above which the fit model is deemed reliable. We will return to this issue when explaining our quality criteria in Sect. 10.2.

The third method for controlling excited-state contamination aims at optimizing the projection onto the ground state in the two-point and three-point correlation functions [869,898,922,923]. The RQCD collaboration has chosen to optimize the parameters in the Gaussian smearing procedure, so that the overlap of the nucleon interpolating operator onto the ground state is maximized [869]. In this way it may be possible to use shorter source-sink separations without incurring a bias due to excited states.

The variational method, originally designed to provide detailed information on energy levels of the ground and excited states in a given channel [924–927], has also been adapted to the determination of hadron-to-hadron transition elements [916]. In the case of nucleon matrix elements, the authors of Ref. [922] have employed a basis of operators to construct interpolators that couple to individual eigenstates in the nucleon channel. The method has produced promising results when applied to calculations of the axial and other forward matrix elements at a fixed value of the pion mass [898,922,923, 928]. However, a more comprehensive study aimed at providing an estimate at the physical point has, until now, not been performed.

The investigation of excited-state effects is an active subfield in NME calculations, and many refinements and extensions have been implemented since the previous edition of the FLAG report. For instance, it has been shown that the previously

[73] In Ref. [919] it is shown that the method can be linked to the Feynman–Hellmann theorem. A direct implementation of the Feynman–Hellmann theorem by means of a modification of the lattice action is discussed and applied in Refs. [920,921].

observed failure of the axial and pseudoscalar form factors to satisfy the PCAC relation linking them could be avoided by including the enhanced contribution of $N\pi$ excitations, either by including additional information on the nucleon excitation spectrum extracted from the three-point function of the axial current [864], or with guidance from chiral effective field theory analyses of nucleon three-point functions [850].

The variety of methods that are employed to address the problem of excited-state contamination (ESC) has greatly improved our understanding of and control over excited-state effects in NME calculations. However, there is still room for further improvement: For instance, dedicated calculations of the excitation spectrum using the variational method could replace the often rudimentary spectral information gained from multi-state fits to the two- and three-point functions used primarily for the determination of the matrix elements. In general, the development of methods to explicitly include multi-particle states, such as $N\pi$ and $N\pi\pi$ with appropriate momentum configurations, coupled with the determination of the associated (transition) matrix elements, is needed to significantly enhance the precision of a variety of nucleon matrix elements. Such approaches would, to some extent, eliminate the need to extend the source-sink separation τ into a regime that is currently inaccessible due to the noise problem.

Since the ongoing efforts to study excited-state contamination are producing deeper insights, we have decided to follow a more cautious approach in the assessment of available NME calculations. This is reflected in a modification of the quality criterion for excited-state contamination that is described and discussed in Sect. 10.2.

10.1.3 Renormalization and Symanzik improvement of local currents

In this section we discuss the matching of the normalization of lattice operators to a continuum reference scheme such as $\overline{\text{MS}}$, and the application of Symanzik improvement to remove $\mathcal{O}(a)$ contributions. The relevant operators for this review are the axial (A_μ), tensor ($T_{\mu\nu}$) and scalar (S) local operators of the form $\mathcal{O}_\Gamma = \overline{q}\Gamma q$, with $\Gamma = \gamma_\mu\gamma_5$, $i\sigma_{\mu\nu}$ and $\mathbf{1}$, respectively, whose matrix elements are evaluated in the forward limit. The general form for renormalized operators in the isovector flavour combination, at a scale μ, reads

$$\mathcal{O}_\Gamma^{\overline{\text{MS}}}(\mu) = Z_{\mathcal{O}}^{\overline{\text{MS}},\text{Latt}}(\mu a, g^2)\left[\mathcal{O}_\Gamma(a) + ab_{\mathcal{O}} m\mathcal{O}_\Gamma(a) + ac_{\mathcal{O}}\mathcal{O}_\Gamma^{\text{imp}}(a)\right] + \mathcal{O}(a^2), \tag{424}$$

where $Z_{\mathcal{O}}^{\overline{\text{MS}},\text{Latt}}(\mu a, g^2)$ denotes the multiplicative renormalization factor determined in the chiral limit, $m \to 0$, and the second and third terms represent all possible quark-mass dependent and independent Symanzik improvement terms, respectively, at $\mathcal{O}(a)$.[74] The chiral properties of overlap, domain-wall fermions (with improvement up to $\mathcal{O}(m_{\text{res}}^n)$ where m_{res} is the residual mass) and twisted-mass fermions (at maximal twist [933,934]) mean that the $\mathcal{O}(a)$ improvement terms are absent, while for nonperturbatively improved Sheikholeslami–Wohlert–Wilson (nonperturbatively-improved clover) fermions all terms appear in principle. For the operators of interest here there are several mass dependent terms but at most one dimension-four $\mathcal{O}_\Gamma^{\text{imp}}$; see, e.g., Refs. [935,936]. However, the latter involve external derivatives whose corresponding matrix elements vanish in the forward limit. Note that no mention is made of staggered fermions as they are not, currently, widely employed as valence quarks in nucleon matrix element calculations.

In order to illustrate the above remarks we consider the renormalization and improvement of the isovector axial current. This current has no anomalous dimension and hence the renormalization factor, $Z_A = Z_A^{\overline{\text{MS}},\text{Latt}}(g^2)$, is independent of the scale. The factor is usually computed nonperturbatively via the axial Ward identity [937] or the Rome–Southampton method [420] (see Sec. A.3 of FLAG 19 [4] for details). In some studies, the ratio with the corresponding vector renormalization factor, Z_A/Z_V, is determined for which some of the systematics cancel. In this case, one constructs the combination $Z_A g_A/(Z_V g_V)$, where $Z_V g_V = 1$ and g_A and g_V are the lattice forward matrix elements, to arrive at the renormalized axial charge [881]. For domain-wall fermions the ratio is employed in order to remove $\mathcal{O}(am_{\text{res}})$ terms and achieve leading discretization effects starting at $\mathcal{O}(a^2)$ [8]. Thus, as mentioned above, $\mathcal{O}(a)$ improvement terms are only present for nonperturbatively-improved clover fermions. For the axial current, Eq. (424) takes the explicit form,

$$A_\mu^{\overline{\text{MS}}}(\mu) = Z_A^{\overline{\text{MS}},\text{Latt}}(g^2)\left[\left(1 + ab_A m_{\text{val}} + 3a\tilde{b}_A m_{\text{sea}}\right) A_\mu(a) + ac_A\partial_\mu P(a)\right] + \mathcal{O}(a^2), \tag{425}$$

[74] Here $a(g^2)$ refers to the lattice spacing in the chiral limit, however, lattice simulations are usually carried out by fixing the value of g^2 while varying the quark masses. This means $a = a(\tilde{g}^2)$ where $\tilde{g}^2 = g^2(1 + b_g am_q)$ [929,930] is the improved coupling that varies with the average sea-quark mass m_q. The difference between the Z factors calculated with respect to g^2 and $\tilde{g}^2$ can effectively be absorbed into the $b_{\mathcal{O}}$ coefficients [931,932].

where $m_{\rm val}$ and $m_{\rm sea}$ are the average valence- and sea-quark masses derived from the vector Ward identity [930,936,937], and P is the pseudoscalar operator $\overline{q}\gamma_5 q$. The matrix element of the derivative term is equivalent to $q_\mu \langle N(p')|P|N(p)\rangle$ and hence vanishes in the forward limit when the momentum transfer $q_\mu = 0$. The improvement coefficients b_A and $\tilde{b}_A$ are known perturbatively for a variety of gauge actions [935,938,939] and nonperturbatively for the tree-level Symanzik-improved gauge action for $N_f = 2+1$ [940].

Turning to operators for individual quark flavours, these can mix under renormalization and the singlet and nonsinglet renormalization factors can differ. For the axial current, such mixing occurs for all fermion formulations just like in the continuum, where the singlet combination acquires an anomalous dimension due to the $U_A(1)$ anomaly. The ratio of singlet to nonsinglet renormalization factors, $r_{\mathcal{O}} = Z^{\rm s.}_{\mathcal{O}}/Z^{\rm n.s.}_{\mathcal{O}}$ for $\mathcal{O} = A$ differs from 1 at $\mathcal{O}(\alpha_s^2)$ in perturbation theory (due to quark loops), suggesting that the mixing is a small effect. The nonperturbative determinations performed so far find $r_A \approx 1$ [843,875], supporting this. For the tensor current the disconnected diagram vanishes in the continuum due to chirality and consequently on the lattice $r_T = 1$ holds for overlap and DW fermions (assuming $m_{\rm res} = 0$ for the latter). For twisted-mass and clover fermions the mixing is expected to be small with $r_T = 1 + \mathcal{O}(\alpha_s^3)$ [941] and this is confirmed by the nonperturbative studies of Refs. [877,942].

The scalar operators for the individual quark flavours, $\overline{q}q$, are relevant not only for the corresponding scalar charges, but also for the sigma terms $\sigma_q = m_q \langle N|\overline{q}q|N\rangle$ when combined with the quark masses m_q. For overlap and DW fermions $r_S = 1$, like in the continuum and all $\overline{q}q$ renormalize multiplicatively with the isovector Z_S. The latter is equal to the inverse of the mass renormalization and hence $m_q\overline{q}q$ is renormalization group (RG) invariant. For twisted-mass fermions, through the use of Osterwalder–Seiler valence fermions, the operators $m_{ud}(\overline{u}u + \overline{d}d)$ and $m_s\overline{s}s$ are also invariant [943].[75] In contrast, the lack of good chiral properties leads to significant mixing between quark flavours for clover fermions. Nonperturbative determinations via the axial Ward identity [707,870] have found the ratio r_S to be much larger than the perturbative expectation $1 + \mathcal{O}(\alpha_s^2)$ [941] may suggest. While the sum over the quark flavours which appear in the action $\sum_q^{N_f} m_q\overline{q}q$ is RG invariant, large cancellations between the contributions from individual flavours can occur when evaluating, e.g., the strange sigma term. Note that for twisted-mass and clover fermions there is also an additive contribution $\propto a^{-3}\mathbf{1}$ (or $\propto \mu a^{-2}\mathbf{1}$) to the scalar operator. This contribution is removed from the nucleon scalar matrix elements by working with the subtracted current, $\overline{q}q - \langle\overline{q}q\rangle$, where $\langle\overline{q}q\rangle$ is the vacuum expectation value of the current [936].

Symanzik improvement for the singlet currents follows the same pattern as in the isovector case with $\mathcal{O}(a)$ terms only appearing for nonperturbatively-improved clover fermions. For the axial and tensor operators only mass dependent terms are relevant in the forward limit while for the scalar there is an additional gluonic operator $\mathcal{O}_S^{\rm imp} = {\rm Tr}(F_{\mu\nu}F_{\mu\nu})$ with a coefficient of $\mathcal{O}(\alpha_s)$ in perturbation theory. When constructing the sigma terms from the quark masses and the scalar operator, the improvement terms remain and they must be included to remove all $\mathcal{O}(a)$ effects for nonperturbatively-improved clover fermions, see Ref. [936] for a discussion.

10.1.4 Extrapolations in a, M_π and $M_\pi L$

To obtain physical results that can be used to compare to or make predictions for experiment, all quantities must be extrapolated to the continuum and infinite-volume limits. In general, either a chiral extrapolation or interpolation must also be made to the physical pion mass. These extrapolations need to be performed simultaneously since discretization and finite-volume effects are themselves dependent upon the pion mass. Furthermore, in practice it is not possible to hold the pion mass fixed while the lattice spacing is varied, as some variation in a occurs when tuning the quark masses at fixed gauge coupling. Thus, one performs a simultaneous extrapolation in all three variables using a theoretically motivated formula of the form,

$$g(M_\pi, a, L) = g_{\rm phys} + \delta_{M_\pi} + \delta_a + \delta_L, \tag{426}$$

where $g_{\rm phys}$ is the desired extrapolated result, and $\delta_{M_\pi}, \delta_a, \delta_L$ are the deviations due to the pion mass, the lattice spacing, and the volume, respectively. Below we outline the forms for each of these terms.

[75] Note that for twisted-mass fermions the pseudoscalar renormalization factor is the relevant factor for the scalar operator. The isovector (isosinglet) scalar current in the physical basis becomes the isosinglet (isovector) pseudoscalar current in the twisted basis. Perturbatively $r_P = 1 + \mathcal{O}(\alpha_s^3)$ and nonperturbative determinations have found $r_P \approx 1$ [877].

All observables discussed in this section are dimensionless, therefore the extrapolation formulae may be parameterized by a set of dimensionless variables:

$$\epsilon_\pi = \frac{M_\pi}{\Lambda_\chi}, \qquad M_\pi L, \qquad \epsilon_a = \Lambda_a a. \tag{427}$$

Here, $\Lambda_\chi \sim 1$ GeV is a chiral symmetry breaking scale, which, for example, can be set to $\Lambda_\chi = 4\pi F_\pi$, where $F_\pi = 92.2$ MeV is the pion decay constant, and Λ_a is a discretization scale, e.g., $\Lambda_a = \frac{1}{4\pi w_0}$, where w_0 is a gradient-flow scale [114].

Effective field theory methods may be used to determine the form of each of these extrapolations. For the single nucleon charges, Heavy-Baryon χPT (HBχPT) is a common choice [944,945], however, other variants, such as unitarized [946] or covariant χPT [947,948], are also employed. Various formulations of HBχPT exist, including those for two- and three-flavours, as well as with and without explicit Δ baryon degrees of freedom. Two-flavour HBχPT is typically used due to issues with convergence of the three-flavour theory [872,949–952]. The convergence properties of all known formulations for baryon χPT, even at the physical pion mass, have not been well-established.

To $\mathcal{O}(\epsilon_\pi^2)$, the two-flavour chiral expansion for the nucleon charges is known to be of the form [953],

$$g = g_0 + g_1\epsilon_\pi + g_2\epsilon_\pi^2 + \tilde{g}_2\epsilon_\pi^2 \ln\left(\epsilon_\pi^2\right), \tag{428}$$

where $g_1 = 0$ for all charges g except $g_S^{u,d}$. The dimensionless coefficients $g_{0,1,2}$, $\tilde{g}_2$ are assumed to be different for each of the different charges. The coefficients in front of the logarithms, $\tilde{g}_2$, are known functions of the low-energy constants (LECs), and do not represent new, independent LECs. Mixed action calculations will have further dependence upon the mixed valence-sea pion mass, m_{vs}.

Given the potential difficulties with convergence of the chiral expansion, known values of the $\tilde{g}_2$ in terms of LECs are not typically used, but are left as free fit parameters. Furthermore, many quantities have been found to display mild pion mass dependence, such that Taylor expansions, i.e., neglecting logarithms in the above expressions, are also often employed. The lack of a rigorously established theoretical basis for the extrapolation in the pion mass thus requires data close to the physical pion mass for obtaining high precision extrapolated/interpolated results.

Discretization effects depend upon the lattice action used in a particular calculation, and their form may be determined using the standard Symanzik power counting. In general, for an unimproved action, the corrections due to discretization effects δ_a include terms of the form,

$$\delta_a = c_1\epsilon_a + c_2\epsilon_a^2 + \cdots, \tag{429}$$

where $c_{1,2}$ are dimensionless coefficients. Additional terms of the form $\tilde{c}_n\,(\epsilon_\pi\epsilon_a)^n$, where n is an integer whose lowest value depends on the combined discretization and chiral properties, will also appear. Improved actions systematically remove correction terms, e.g., an $\mathcal{O}(a)$-improved action, combined with a similarly improved operator, will contain terms in the extrapolation ansatz beginning at ϵ_a^2 (see Sect. 10.1.3).

Finite volume corrections δ_L may be determined in the usual way from effective field theory, by replacing loop integrals over continuous momenta with discrete sums. Finite volume effects therefore introduce no new undetermined parameters to the extrapolation. For example, at next-to-leading order, and neglecting contributions from intermediate Δ baryons, the finite-volume corrections for the axial charge in two-flavour HBχPT take the form [954],

$$\delta_L \equiv g_A(L) - g_A(\infty) = \frac{8}{3}\epsilon_\pi^2\left[g_0^3 F_1\left(M_\pi L\right) + g_0 F_3\left(M_\pi L\right)\right], \tag{430}$$

where

$$\begin{aligned} F_1\left(mL\right) &= \sum_{\mathbf{n}\neq\mathbf{0}}\left[K_0\left(mL|\mathbf{n}|\right) - \frac{K_1\left(mL|\mathbf{n}|\right)}{mL|\mathbf{n}|}\right], \\ F_3\left(mL\right) &= -\frac{3}{2}\sum_{\mathbf{n}\neq 0}\frac{K_1\left(mL|\mathbf{n}|\right)}{mL|\mathbf{n}|}, \end{aligned} \tag{431}$$

and $K_\nu(z)$ are the modified Bessel functions of the second kind. Some extrapolations are performed using the form for asymptotically large $M_\pi L$,

$$K_0(z) \to \frac{e^{-z}}{\sqrt{z}}, \tag{432}$$

and neglecting contributions due to K_1. Care must, however, be taken to establish that these corrections are negligible for all included values of $M_\pi L$. The numerical coefficients, for example, 8/3 in Eq. (430), are often taken to be additional free fit parameters, due to the question of convergence of the theory discussed above.

Given the lack of knowledge about the convergence of the expansions and the resulting plethora of possibilities for extrapolation models at differing orders, it is important to include statistical tests of model selection for a given set of data. Bayesian model averaging [955] or use of the Akaike Information Criterion [956] are common choices which penalize over-parameterized models.

10.2 Quality criteria for nucleon matrix elements and averaging procedure

There are two specific issues that call for a modification and extension of the FLAG quality criteria listed in Sect. 2. The first concerns the rating of the chiral extrapolation: The FLAG criteria reflect the ability of χPT to provide accurate descriptions of the pion mass dependence of observables. Clearly, this ability is linked to the convergence properties of χPT in a particular mass range. Quantities extracted from nucleon matrix elements are extrapolated to the physical pion mass using some variant of baryonic χPT, whose convergence is not well established as compared to the mesonic sector. Therefore, we have opted for stricter quality criteria, 200 MeV $\leq M_{\pi,\mathrm{min}} \leq$ 300 MeV, for a green circle in the chiral extrapolation of nucleon matrix elements, i.e.,

- ★ $M_{\pi,\mathrm{min}} <$ 200 MeV with three or more pion masses used in the extrapolation
  or two values of M_π with one lying within 10 MeV of 135 MeV (the physical neutral pion mass) and the other one below 200 MeV
- ○ 200 MeV $\leq M_{\pi,\mathrm{min}} \leq$ 300 MeV with three or more pion masses used in the extrapolation;
  or two values of M_π with $M_{\pi,\mathrm{min}} <$ 200 MeV;
  or a single value of M_π lying within 10 MeV of 135 MeV (the physical neutral pion mass)
- ■ Otherwise

In Sect. 10.1.2 we have discussed that insufficient control over excited-state contributions, arising from the noise problem in baryonic correlation functions, may lead to a systematic bias in the determination of nucleon matrix elements. We therefore introduce an additional criterion that rates the efforts to suppress excited-state contamination in the final result. As described in Sect. 10.1.2, the applied methodology to control excited-state contamination is quite diverse. Since a broad consensus on the question which procedures should be followed has yet to emerge, our criterion is expressed in terms of simulation parameters that can be straightforwardly extracted on the basis of publications. Furthermore, the criterion must also be readily applicable to a variety of different local operators whose matrix elements are discussed in this chapter. These requirements are satisfied by the source-sink separation τ, i.e., the Euclidean distance between the initial and final nucleons. The discussion at the end of Sect. 10.1.2 shows that there is room for improvement in the ability to control excited-state contamination. Hence, we have reverted to a binary system, based on the range of source-sink separations of a given calculations. While we do not award the highest category – a green star – in this edition, we stress that the adoption of the modified ESC criterion has not led to a situation where calculations that were previously rated with a green star are now excluded from FLAG averages. The rating scale concerning control over excited-state contributions is thus

- ○ Three or more source-sink separations τ, at least two of which must be above 1.0 fm.
- ■ Otherwise

We will continue to monitor the situation concerning excited-state contamination and, if necessary, adapt the criteria further in future editions of the FLAG report.

As explained in Sect. 2, FLAG averages are distinguished by the sea-quark content. Hence, for a given configuration of the quark sea (i.e., for $N_f = 2, 2+1, 2+1+1$, or $1+1+1+1$), we first identify those calculations that pass the FLAG

and the additional quality criteria defined in this section, i.e. excluding any calculation that has a red tag in one or more of the categories. We then add statistical and systematic errors in quadrature and perform a weighted average. If the fit is of bad quality (i.e., if $\chi^2_{\rm min}/{\rm dof} > 1$), the errors of the input quantities are scaled by $\sqrt{\chi^2/{\rm dof}}$. In the following step, correlations among different calculations are taken into account in the error estimate by applying Schmelling's procedure [163].

10.3 Isovector charges

The axial, scalar and tensor isovector charges are needed to interpret the results of many experiments and phenomena mediated by weak interactions, including probes of new physics. The most natural process from which isovector charges can be measured is neutron beta decay ($n \to p^+ e^- \bar{\nu}_e$). At the quark level, this process occurs when a down quark in a neutron transforms into an up quark due to weak interactions, in particular due to the axial current interaction. While scalar and tensor currents have not been observed in nature, effective scalar and tensor interactions arise in the SM due to loop effects. At the TeV and higher scales, contributions to these three currents could arise due to new interactions and/or loop effects in BSM theories. These super-weak corrections to standard weak decays can be probed through high precision measurements of the neutron decay distribution by examining deviations from SM predictions as described in Ref. [957]. The lattice-QCD methodology for the calculation of isovector charges is well-established, and the control over statistical and systematic uncertainties is becoming robust.

The axial charge g_A^{u-d} is an important parameter that encapsulates the strength of weak interactions of nucleons. It enters in many analyses of nucleon structure and of SM and BSM physics. For example, it enters in (i) the extraction of V_{ud} and tests of the unitarity of the Cabibbo–Kobayashi–Maskawa (CKM) matrix; (ii) the analysis of neutrinoless double-beta decay, (iii) neutrino-nucleus quasi-elastic scattering cross-section; (iv) the rate of proton-proton fusion, the first step in the thermonuclear reaction chains that power low-mass hydrogen-burning stars like the Sun; (v) solar and reactor neutrino fluxes; (vi) muon capture rates, etc. The current best determination of the ratio of the axial to the vector charge, g_A/g_V, comes from measurement of neutron beta decay using polarized ultracold neutrons by the UCNA collaboration, 1.2772(20) [958,959], and by PERKEO II, 1.2761^{+14}_{-17} [960]. Note that, in the SM, $g_V = 1$ up to second-order corrections in isospin breaking [961,962] as a result of the conservation of the vector current. Given the accuracy with which g_A^{u-d} has been measured in experiments, the goal of lattice-QCD calculations is to calculate it directly with $\mathcal{O}(1\%)$ accuracy.

Isovector scalar or tensor interactions contribute to the helicity-flip parameters, called b and B, in the neutron decay distribution. By combining the calculation of the scalar and tensor charges with the measurements of b and B, one can put constraints on novel scalar and tensor interactions at the TeV scale as described in Ref. [957]. To optimally bound such scalar and tensor interactions using measurements of b and B parameters in planned experiments targeting 10^{-3} precision [963–965], we need to determine g_S^{u-d} and g_T^{u-d} at the 10% level as explained in Refs. [881,957]. Future higher-precision measurements of b and B would require correspondingly higher-precision calculations of the matrix elements to place even more stringent bounds on these couplings at the TeV-scale.

One can estimate g_S^{u-d} using the conserved vector current (CVC) relation, $g_S/g_V = (M_{\rm neutron} - M_{\rm proton})^{\rm QCD}/(m_d - m_u)^{\rm QCD}$, as done by Gonzalez-Alonso et al. [966]. In their analysis, they took estimates of the two mass differences on the right-hand side from the global lattice-QCD data [2] and obtained $g_S^{u-d} = 1.02(8)(7)$.

The tensor charge g_T^{u-d} can be extracted experimentally from semi-inclusive deep-inelastic scattering (SIDIS) data [967–970]. A sample of these phenomenological estimates is shown in Fig. 45, and the noteworthy feature is that the current uncertainty in these phenomenological estimates is large.

10.3.1 Results for g_A^{u-d}

Calculations of the isovector axial charge have a long history, as can be seen from the compilation given in Table 69 and plotted in Fig. 43. The issue of excited-state contamination received little if any attention before 2010. As a consequence, the range of source-sink separations employed in many of the early calculations prior to that year was rather limited, offering little control over this important systematic effect. This concerns, in particular, the calculations by LHPC 05 [974], LHPC 10 [897], RBC 08 [975], RBC/UKQCD 08B [883], RBC/UKQCD 09B [884] and QCDSF 06 [867]. Since the last edition of the FLAG report, no new results in two-flavour QCD have been published. An exception is the calculation ETM 19 [971], which reanalyzed two ensembles with $N_f = 2$ around the physical pion mass to study finite-volume effects, while the main result is quoted from a calculation with $N_f = 2 + 1 + 1$. These two-flavour calculations still do not qualify for inclusion in the FLAG average (see Table 69). We thus refrain from providing a detailed discussion of the results in Refs.

Table 69 Overview of results for g_A^{u-d}

Collaboration	Refs.	N_f	Publication status	Continuum extrapolation	Chiral extrapolation	Finite volume	Renormalization	Excited states	g_A^{u-d}
CalLat 19	[100]	2+1+1	C	○	★	★	★	○	1.2642(93)
ETM 19	[971]	2+1+1	A	■	○	★	★	○	1.286(23)
PNDME 18[a]	[98]	2+1+1	A	★‡	★	★	★	○	1.218(25)(30)
CalLat 18	[99]	2+1+1	A	○	★	★	★	○	1.271(10)(7)
CalLat 17	[882]	2+1+1	P	○	★	★	★	○	1.278(21)(26)
PNDME 16[a]	[881]	2+1+1	A	○‡	★	★	★	○	1.195(33)(20)
NME 21[a]	[972]	2+1	P	○‡	★	★	★	○	1.31(6)(5)
LHPC 19	[851]	2+1	A	■‡	★	★	★	○	1.265(49)
Mainz 19	[102]	2+1	A	★	○	★	★	○	$1.242(25)(^{+0}_{-0.030})$
PACS 18A	[849]	2+1	A	■	★	★	★	○	1.273(24)(5)(9)
PACS 18	[847]	2+1	A	■	■	★	★	■	1.163(75)(14)
χQCD 18	[101]	2+1	A	○	★	★	★	○	1.254(16)(30)[$]
JLQCD 18	[890]	2+1	A	■	○	○	★	○	1.123(28)(29)(90)
LHPC 12A[b]	[973]	2+1	A	■‡	★	★	★	○	0.97(8)
LHPC 10	[897]	2+1	A	■	○	■	★	■	1.21(17)
RBC/UKQCD 09B	[884]	2+1	A	■	■	○	★	■	1.19(6)(4)
RBC/UKQCD 08B	[883]	2+1	A	■	■	○	★	■	1.20(6)(4)
LHPC 05	[974]	2+1	A	■	■	★	★	■	1.226(84)
Mainz 17	[871]	2	A	★	★	★	★	■	$1.278(68)(^{+0}_{-0.087})$
ETM 17B	[875]	2	A	■	○	○	★	○	1.212(33)(22)
ETM 15D	[873]	2	A	■	○	○	★	○	1.242(57)
RQCD 14	[869]	2	A	○	★	★	★	■	1.280(44)(46)
QCDSF 13	[369]	2	A	○	★	■	★	■	1.29(5)(3)
Mainz 12	[868]	2	A	★	○	○	★	■	$1.233(63)(^{+0.035}_{-0.060})$
RBC 08	[975]	2	A	■	■	■	★	■	1.23(12)
QCDSF 06	[867]	2	A	○	■	■	★	■	1.31(9)(7)

[a] The improvement coefficient in the valence quark action is set to its tadpole-improved tree-level value
[b] The quark action is tree-level improved
‡ The rating takes into account that the action is not fully O(a) improved by requiring an additional lattice spacing
[$] For this partially quenched analysis the criteria are applied to the unitary points

[369,867–869,871,873,875,975] and refer the reader to the corresponding chapter in the previous edition of the FLAG report.

Estimates for the axial charge with $N_f = 2+1$ have been published by many collaborations, i.e., LHPC [851,897,973,974], RBC/UKQCD [883,884], JLQCD 18 [890], χQCD 18 [101], PACS 18/PACS 18A [847,849], Mainz 19 [102] (superseding the previously listed result in [976]) and NME 21 [972].

The calculations in LHPC 05 [974] and LHPC 10 [897] were based on a mixed-action setup, combining domain-wall fermions in the valence sector with staggered (asqtad) gauge ensembles generated by MILC. Although the dependence of the results on the source-sink separation was studied to some extent in LHPC 10, excited-state effects are not sufficiently controlled according to our quality criteria described in Sect. 10.2. A different discretization of the quark action was used in their later studies (LHPC 12A [973] and LHPC 19 [851]), employing tree-level improved Wilson fermions with smeared gauge links, both in the sea and valence sectors. While this setup does not realize full $\mathcal{O}(a)$ improvement, it was found

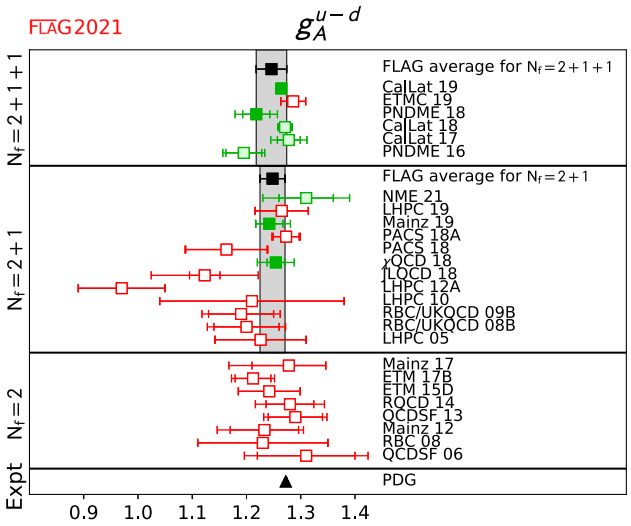

Fig. 43 Lattice results and FLAG averages for the isovector axial charge g_A^{u-d} for $N_f = 2, 2+1$ and $2+1+1$ flavour calculations. Also shown is the experimental result as quoted in the PDG [165]

that smeared gauge links reduce the leading discretization effects of $\mathcal{O}(a)$ substantially. The most recent publication (LHPC 19) is based on two ensembles within 1.5% of the physical pion, at two different values of the lattice spacing. Results for g_A^{u-d} were determined using the summation and ratio methods, with and without including the first excitation in the fit. LHPC quotes the result from the finer lattice spacing, with an error that covers the spread of uncertainties on both ensembles.

The RBC/UKQCD collaboration has employed $N_f = 2+1$ flavours of domain-wall fermions. The results quoted in RBC/UKQCD 08B [883] and RBC/UKQCD 09B [884] were obtained at relatively heavy pion masses at a single value of the lattice spacing, with only limited control over excited-state effects. While systematic investigation of different source-sink separations has been recently performed on two ensembles at the same lattice spacing and pion masses of 250 and 170 MeV, respectively [977], an estimate for g_A^{u-d} at the physical point has not been quoted.

The JLQCD collaboration (JLQCD 18 [890]) has performed a calculation using $N_f = 2+1$ flavours of overlap fermions and the Iwasaki gauge action. Owing to the large numerical cost of overlap fermions, which preserve exact chiral symmetry at nonzero lattice spacing, they have only simulated four light quark masses with $290 < M_\pi < 540$ MeV and at a single lattice spacing so far. Their simultaneous fit to the data for the correlator ratio $R_A(t,\tau)$ computed at six values of τ to a constant, gives a low value for g_A^{u-d} at the physical point. Overlap valence quarks were also used by the χQCD collaboration in their study of various nucleon matrix elements (χQCD 18 [101]), utilizing the gauge ensembles generated by RBC/UKQCD with domain-wall fermions. The quoted estimate for the axial charge was obtained from a combination of two-state fits and the summation method, applied over a range of source-sink separations.

Calculations with $N_f = 2+1$ flavours of $\mathcal{O}(a)$ improved Wilson fermions have been performed by PACS, the Mainz group and NME. The calculations by the PACS collaboration (PACS 18 [847] and PACS 18A [849]) were performed on very large volumes (8.2 fm and 10.8 fm, respectively) at or near the physical pion mass. In PACS 18A, the ratio method without including excited states was used to determine the isovector axial charge, which was found to be in good agreement with the experimental value. However, only a single lattice spacing was used in PACS 18 and PACS 18A, so that these calculations lack control over discretization effects. The Mainz group (Mainz 19 [102]) has presented results for the axial charge, obtained by performing two-state fits to six different nucleon matrix elements (including the scalar and tensor charges), assuming that the mass gap to the excited state can be more reliably constrained in this way. Up to six source-sink separations per ensemble have been studied. The final results are obtained from a combined chiral, continuum and finite-volume extrapolation. The NME collaboration (NME 21 [972]) has recently published the results from a calculation of various nucleon form factors and charges. Results were obtained from multi-state fits, using up to four (three) states in the two-point (three-point) correlation functions. In order to describe and control excited-state effects, $N\pi$ and $N\pi\pi$ states with different relative momenta were included in the analysis. The preferred result for g_A^{u-d} was obtained from the axial form factor $G_A(Q^2)$ extrapolated to $Q^2 = 0$.

Three groups, PNDME, CalLat and ETMC, have published results for $N_f = 2+1+1$, i.e. PNDME 16 [881], PNDME 18 [98], CalLat 17 [882] CalLat 18 [99], CalLat 19 [100]. PNDME and CalLat share the staggered (HISQ) gauge ensembles generated by the MILC collaboration, but employ different discretizations in the valence quark sector: PNDME use $\mathcal{O}(a)$ improved Wilson fermions with the improvement coefficient $c_{\rm sw}$ set to its tadpole-improved tree-level value. By contrast, CalLat use the Möbius variant of domain-wall fermions, which are fully $\mathcal{O}(a)$ improved. The CalLat set of ensembles includes three values of the lattice spacing, i.e. a = 0.09, 0.12, and 0.15 fm, while PNDME added another set of ensembles at the finer lattice spacing of 0.06 fm to this collection. Both groups have included physical pion mass ensembles in their calculations. The operator matrix elements are renormalized nonperturbatively, using the Rome–Southampton method.

In order to control excited-state contamination, PNDME perform multi-state fits, including up to four (three) energy levels in the two-point (three-point) correlation functions. By contrast, CalLat have employed the Feynman–Hellmann-inspired implementation of summed operator insertions described in Sect. 10.1.2. Plotting the summed correlator $S_A(\tau)$ as a function of the source-sink separation, they find that excited-state effects cannot be detected for $\tau \gtrsim 1.0\,\text{fm}$ at their level of statistics. After subtracting the leading contributions from excited states determined from two-state fits, they argue that the data for $S_A(\tau)$ can be described consistently down to $\tau \simeq 0.3\,\text{fm}$.

The recent calculation by ETMC (ETM 19 [971]) with $N_f = 2+1+1$ was performed using a single twisted-mass QCD ensemble with $m_\pi \approx 139\,\text{MeV}$. In order to control excited-state effects, the summation method and multi-state fits were used. No significant finite-volume effects were expected based on a similar analysis of two $N_f = 2$ ensembles with different spatial extents. The quoted estimate is identified with the result obtained from a two-state fit on the single $N_f = 2+1+1$ ensemble, which agrees with the value determined from the summation method.

We now proceed to discuss global averages for the axial charge, in accordance with the procedures in Sect. 10.2. For QCD with $N_f = 2+1+1$, the calculations of PNDME and CalLat pass all our quality criteria, while the result of ETM 19 is excluded due to the fact that it was performed at a single value of the lattice spacing. Hence the results from PNDME 18 [98] and CalLat 19 [100], which is an update of CalLat 18 [99], qualify for being included in a global average. Since both PNDME and CalLat use gauge ensembles produced by MILC, we assume that the quoted errors are 100% correlated, even though the range of pion masses and lattice spacings explored in Refs. [98] and [99,100] is not exactly identical. Performing a weighted average yields $g_A^{u-d} = 1.2617(126)$ with $\chi^2/\text{dof} = 1.33$, where the error has been scaled by about 15% because of the large χ^2/dof. The result by CalLat dominates the weighted average due to its smaller error. Given that the calculations of PNDME 18 and CalLat 19 are correlated, the large value of χ^2/dof indicates a slight tension between the two results. In this situation we adopt a more conservative approach, by requiring that the uncertainty assigned to the FLAG estimate encompasses the central value of PNDME 18. As a result, we choose to represent the axial charge by the interval $1.218 \le g_A^{u-d} \le 1.274$, where the lower bound is identified with the result of PNDME 18, while the upper bound is the weighted average plus the scaled 1σ uncertainty. Hence, for $N_f = 2+1+1$ we quote $g_A^{u-d} = 1.246(28)$ as the FLAG estimate, where the central value marks the mid-point of the interval, and half the width is taken to be the error.

For QCD with $N_f = 2+1$ dynamical quarks, the calculations of χQCD 18 [101], Mainz 19 [102] and NME 21 [972] are free of red tags, while the calculation by PACS 18A [849] and LHPC 19 [851] do not offer enough control over lattice artefacts according to the FLAG criteria. Since the result by NME 21 was published only as a preprint by the FLAG deadline, it does not qualify for being included in a global average. Hence, for $N_f = 2+1$ we compute a weighted average from χQCD 18 [101] and Mainz 19 [102], assuming no correlations between the two calculations. This yields $g_A^{u-d} = 1.248(23)$ with $\chi^2/\text{dof} = 0.07$.

Due to the modified criteria for excited-state contamination, none of the results obtained in two-flavour QCD qualify for a global average. Nonetheless, we find it instructive to show the results for $N_f = 2$ together with the calculations with $N_f = 2+1$ and $2+1+1$ and the respective FLAG estimates in Fig. 43.

To summarize, the FLAG averages for the axial charge read

$$N_f = 2+1+1: \qquad g_A^{u-d} = 1.246(28) \qquad \text{Refs. [98–100]}, \tag{433}$$

$$N_f = 2+1: \qquad g_A^{u-d} = 1.248(23) \qquad \text{Refs. [101,102]}, \tag{434}$$

Within errors, these averages are compatible with the result of $g_A^{u-d} = 1.2724(23)$ quoted by the PDG. While the most recent lattice calculations reproduce the axial charge at the level of a few percent or even better, the experimental result is more precise by an order of magnitude.

Table 70 Overview of results for g_S^{u-d}

Collaboration	Refs.	N_f	Publication status	Continuum extrapolation	Chiral extrapolation	Finite volume	Renormalization	Excited states	g_S^{u-d}
ETM 19	[971]	2+1+1	A	■	○	★	★	○	1.35(17)
PNDME 18	[98]	2+1+1	A	★‡	★	★	★	○	1.022(80)(60)
PNDME 16	[881]	2+1+1	A	○‡	★	★	★	○	0.97(12)(6)
PNDME 13	[878]	2+1+1	A	■‡	■	★	★	○	0.72(32)
NME 21	[972]	2+1	P	○‡	★	★	★	○	1.06(10)(6)
χQCD 21A	[978]	2+1	P	★	★	★	★	○	0.94(10)(6)
RBC/UKQCD 19	[977]	2+1	A	■	○	★	★	■	0.9(3)
Mainz 19	[102]	2+1	A	★	○	★	★	○	$1.13(11)(^{7}_{6})$
LHPC 19	[851]	2+1	A	■‡	★	★	★	○	0.927(303)
JLQCD 18	[890]	2+1	A	■	○	○	★	○	0.88(8)(3)(7)
LHPC 12	[979]	2+1	A	■‡	★	★	★	○	1.08(28)(16)
ETM 17	[877]	2	A	■	○	○	★	○	0.930(252)(48)(204)
RQCD 14	[869]	2	A	○	★	★	★	■	1.02(18)(30)

‡The rating takes into account that the action is not fully O(a) improved by requiring an additional lattice spacing

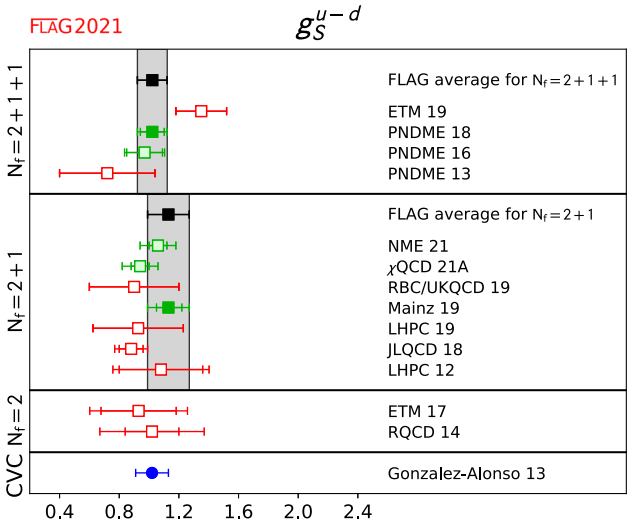

Fig. 44 Lattice results and FLAG averages for the isovector scalar charge g_S^{u-d} for $N_f = 2, 2+1$, and $2+1+1$ flavour calculations. Also shown is a phenomenological result obtained using the conserved vector current (CVC) relation [966] (circle)

10.3.2 Results for g_S^{u-d}

Calculations of the isovector scalar charge have, in general, larger errors than the isovector axial charge as can be seen from the compilation given in Table 70 and plotted in Fig. 44. The isovector scalar charge can also be determined indirectly via the conserved vector current (CVC) relation from results for the neutron-proton mass difference [147,172,221,980–985] and the down and up quark mass difference (see Sect. 3.1.6). For comparison, Fig. 44 also shows an indirect determination obtained using lattice and phenomenological input [966].

As in FLAG 19, for 2+1+1 flavours, only PNDME 18 [98], which supersedes PNDME 16 [881] and PNDME 13 [878], meets all the criteria for inclusion in the average. The discussions for this and other past calculations are repeated from FLAG 19 for completion.

This mixed-action calculation was performed using the MILC HISQ ensembles, with a clover valence action. The 11 ensembles used include three pion mass values, $M_\pi \sim 135$, 225, 320 MeV, and four lattice spacings, $a \sim 0.06$, 0.09, 0.12, 0.15 fm. Note that four lattice spacings are required to meet the green star criteria, as this calculation is not fully $\mathcal{O}(a)$ improved. Lattice size ranges between $3.3 \lesssim M_\pi L \lesssim 5.5$. Physical point extrapolations were performed simultaneously, keeping only the leading-order terms in the various expansion parameters. For the finite-volume extrapolation, the asymptotic limit of the χPT prediction, Eq. (432), was used. Excited-state contamination is controlled using two-state fits to between three and five source-sink time separations between $0.72 \lesssim \tau \lesssim 1.68$ fm. Renormalization was performed nonperturbatively using the RI-SMOM scheme and converted to $\overline{\text{MS}}$ at 2 GeV using 2-loop perturbation theory.

The calculation performed in ETM 19 [971] was generated using twisted-mass fermions with a clover term. The calculation utilized a single 2+1+1-flavour gauge configuration, with a pion mass near the physical point, $m_\pi \sim 139$ MeV, lattice spacing of $a \sim 0.08$ fm, and volume corresponding to $m_\pi L = 3.86$. Seven source-sink separations were used in the analysis, ranging from $t = 0.64$–1.6 fm. Two further two-flavour ensembles were also explored, having the same pion mass, $m_\pi \sim 130$ MeV and lattice spacing $a \sim 0.09$ fm, but with different volumes corresponding to $m_\pi L \sim 3$ and $m_\pi L \sim 4$. The final result is quoted from the single 2+1+1 flavour ensemble and does not include an assessment of discretization systematics, and therefore does not meet the continuum quality criterion for inclusion in the average.

Regarding 2+1-flavour calculations, a single calculation meets all criteria necessary for inclusion in the average. The Mainz 19 [102] calculation was performed on the Wilson CLS ensembles, using four lattice spacings ($a \sim 0.05$ fm to 0.086 fm), several pion masses ranging from ~ 200 to ~ 350 MeV, and volumes corresponding to $m_\pi L \sim 3$ to ~ 5.4. Physical point extrapolations were performed simultaneously in the lattice spacing, pion mass, and volume. Excited states were controlled using two-state simultaneous fits to multiple observables, and included several source-sink separations typically in the range 1-1.5 fm. Renormalization was performed nonperturbatively using the RI-SMOM scheme and converted to $\overline{\text{MS}}$ at 2 GeV using 2-loop perturbation theory.

The 2+1-flavour calculation of χQCD 21A [978] was performed using a mixed-action approach with domain-wall fermion gauge configurations generated by the RBC/UKQCD collaboration and overlap valence quarks. They include five pion masses ranging from $m_\pi \sim 140$ to 370 MeV, four lattice spacings ($a \sim 0.06$, 0.08, 0.11, and 0.14 fm). Three to six different valence-quark masses are computed on each ensemble. The extrapolation to the physical pion mass, continuum and infinite-volume limits is obtained by a global fit of all data to a partially quenched chiral perturbation theory ansatz. Excited-state contamination is assessed using three to five sink-source separations and multi-state fits. Renormalization is performed using RI/MOM and the final result quoted in $\overline{\text{MS}}$ at 2 GeV. At the time of writing of this review, this calculation was unpublished and the results are therefore not included in the average.

The NME 21 [972] 2+1-flavour calculation utilized seven ensembles of Wilson-clover fermions. Three lattice spacings, ranging from $a \sim 0.07$ to 0.13 fm, several pion masses, $m_\pi \sim 165$ to 285 MeV, and volumes corresponding to $m_\pi L \sim 3.75$ to 6.15 were used. Combined continuum, chiral, and infinite-volume extrapolations are performed to the physical point using leading-order fit functions. Several fitting strategies are explored using four to six source-sink separations ranging from 0.7–1.8 fm. Final results are quoted by averaging results from two of these fitting strategies, in which the excited-state energy for the three-point function is fixed using two different prior strategies. Renormalization is non-perturbative (RI-SMOM) using two strategies, and quoted in $\overline{\text{MS}}$ at 2 GeV. This work was also unpublished at the time of writing of this review and is not included in the average.

The RBC/UKQCD 19 [977] calculation employed 2+1 flavours of domain-wall fermions using an Iwasaki and dislocation-suppressing-determinant-ratio gauge action. They utilized two values of the pion mass, $m_\pi \sim 250$ and 170 MeV with volumes corresponding to $m_\pi L \sim 5.8$ and 4.0, respectively. The results are quoted using only one lattice spacing of 0.14 fm, and a single source-sink separation of 1.3 fm and therefore do not meet the criteria for continuum or excited-state contamination. The LHPC 19 [851] calculation used a 2+1 flavour 2-HEX-smeared Wilson-clover action with two ensembles near the physical pion mass, $m_\pi \sim 133$ and 137 MeV. The lattice spacings corresponded to $a \sim 0.09$ and 0.12 fm and volumes $m_\pi L \sim 4$. They used 3 and 8 different time separations for the two ensembles and compare ratio, summation, and multi-state methods to assess excited-state contamination. Because the calculation is not fully $\mathcal{O}(a)$ improved, an additional lattice spacing would be necessary to meet the continuum criterion for inclusion in the average.

The JLQCD 18 [890] calculation, performed using overlap fermions on the Iwasaki gauge action, covered four pion masses down to 290 MeV. The lattice size was adjusted to keep $M_\pi L \geq 4$ in all four cases. However, the single lattice spacing of $a = 0.11$ fm does not meet the criteria for continuum extrapolation. The calculations presented in LHPC 12A used three

Table 71 Overview of results for g_T^{u-d}

Collaboration	Refs.	N_f	Publication status	Continuum extrapolation	Chiral extrapolation	Finite volume	Renormalization	Excited states	g_T^{u-d}
ETM 19	[971]	2+1+1	A	■	○	★	★	○	0.936(25)
PNDME 18	[98]	2+1+1	A	★‡	★	★	★	○	0.989(32)(10)
PNDME 16	[881]	2+1+1	A	○‡	★	★	★	○	0.987(51)(20)
PNDME 15	[879,880]	2+1+1	A	○‡	★	★	★	○	1.020(76)
PNDME 13	[878]	2+1+1	A	■‡	■	★	★	○	1.047(61)
NME 21	[972]	2+1	P	○‡	★	★	★	○	0.95(5)(2)
RBC/UKQCD 19	[977]	2+1	A	■	○	★	★	■	1.04(5)
Mainz 19	[102]	2+1	A	★	○	★	★	○	$0.965(38)(^{13}_{41})$
LHPC 19	[851]	2+1	A	■‡	★	★	★	○	0.972(41)
JLQCD 18	[890]	2+1	A	■	○	○	★	○	1.08(3)(3)(9)
LHPC 12	[979]	2+1	A	■‡	★	★	★	○	1.038(11)(12)
RBC/UKQCD 10D	[885]	2+1	A	■	■	○	★	■	0.9(2)
ETM 17	[877]	2	A	■	○	○	★	○	1.004(21)(2)(19)
ETM 15D	[873]	2	A	■	○	○	★	○	1.027(62)
RQCD 14	[869]	2	A	○	★	★	★	■	1.005(17)(29)
RBC 08	[975]	2	A	■	■	■	★	■	0.93(6)

‡The rating takes into account that the action is not fully O(a) improved by requiring an additional lattice spacing

different lattice actions, Wilson-clover, domain-wall, and mixed action. Pion masses ranged down to near the physical pion mass. Data at two lattice spacings were produced with the domain-wall and Wilson actions, however, the final result utilized only the single lattice spacing of $a = 0.116$ fm from the Wilson action. Because the action is not fully $\mathcal{O}(a)$ improved, two lattice spacings are not sufficient for meeting the quality criteria for the continuum extrapolation.

The two-flavour calculations in Table 70 include ETM 17, which employed twisted-mass fermions on the Iwasaki gauge action.[76] This work utilized a single physical pion mass ensemble with lattice spacing $a \sim 0.09$ fm, and therefore does not meet the criteria for continuum extrapolation. The RQCD 14 calculation included three lattice spacings down to 0.06 fm and several pion masses down to near the physical point. While a study of excited-state contamination was performed on some ensembles using multiple source-sink separations, many ensembles included only a single time separation, so it does not meet the criteria for excited states.

The final FLAG value for g_S^{u-d} is

$$N_f = 2+1+1: \quad g_S^{u-d} = 1.02(10) \quad \text{Ref. [98]}, \tag{435}$$

$$N_f = 2+1: \quad g_S^{u-d} = 1.13(14) \quad \text{Ref. [102]}. \tag{436}$$

10.3.3 Results for g_T^{u-d}

Estimates of the isovector tensor charge are currently the most precise of the isovector charges with values that are stable over time, as can be seen from the compilation given in Table 71 and plotted in Fig. 45. This is a consequence of the smaller statistical fluctuations in the raw data and the very mild dependence on a, M_π, and the lattice size $M_\pi L$. As a result, the

[76] The earlier work, ETM 15D [873], did not give a final value for g_S^{u-d} and is therefore not included in the tables.

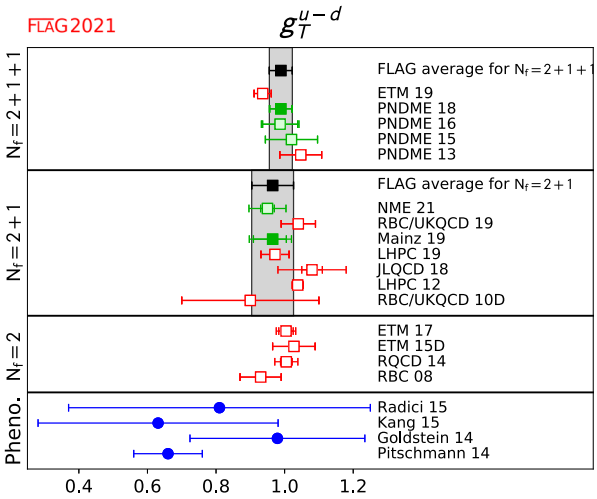

Fig. 45 Lattice results and FLAG averages for the isovector tensor charge g_T^{u-d} for $N_f = 2, 2+1$, and $2+1+1$ flavour calculations. Also shown are phenomenological results using measures of transversity [986–990] (circles)

uncertainty due to the various extrapolations is small. Also shown for comparison in Fig. 45 are phenomenological results using measures of transversity [986–990].

As in FLAG 19, for 2+1+1 flavours, only PNDME 18 [98], which supersedes PNDME 16 [881], PNDME 15 [879] and PNDME 13 [878], meets all the criteria for inclusion in the average. The details for this calculation are the same as those for g_S^{u-d} described in the previous section (Sect. 10.3.2), except that three-state fits were used to remove excited-state effects. The details of the 2+1+1 flavour calculation by ETM 19, which does not meet the criteria for averaging, are also the same as those described in the previous section for g_S^{u-d}.

For 2+1-flavour calculations, only Mainz 19 [102] meets all criteria for inclusion in the averages. Details of this calculation are the same as for g_S^{u-d}, described in the previous section.

Details for the 2+1-flavour NME 21, RBC/UKQCD 19, LHPC 19, Mainz 18, JLQCD 18, and LHPC 12A, calculations are identical to those presented previously in Sect. 10.3.2. The earlier RBC/UKQCD 10 calculation was performed using domain-wall fermions on the Iwasaki gauge action, with two volumes and several pion masses. The lowest pion mass used was $M_\pi \sim 330$ MeV and does not meet the criteria for chiral extrapolation. In addition, the single lattice spacing and single source-sink separation do not meet the criteria for continuum extrapolation and excited states.

Two-flavour calculations include RQCD 14, with details identical to those described in Sect. 10.3.2. There are two calculations, ETM 15D [873] and ETM 17 [877], which employed twisted-mass fermions on the Iwasaki gauge action. The earlier work utilized three ensembles, with three volumes and two pion masses down to the physical point. The more recent work used only the physical pion mass ensemble. Both works used only a single lattice spacing $a \sim 0.09$ fm, and therefore do not meet the criteria for continuum extrapolation. The early work by RBC 08 with domain-wall fermions used three heavy values for the pion mass, and a single value for the lattice spacing, volume, and source-sink separation, and therefore do not meet many of the criteria.

The final FLAG value for g_T^{u-d} is

$$N_f = 2+1+1: \quad g_T^{u-d} = 0.989(34) \quad \text{Ref. [98]}, \tag{437}$$

$$N_f = 2+1: \quad g_T^{u-d} = 0.965(61) \quad \text{Ref. [102]}. \tag{438}$$

10.4 Flavour diagonal charges

Three examples of interactions for which matrix elements of flavour-diagonal operators ($q\Gamma q$ where Γ defines the Lorentz structure of the bilinear quark operator) are needed are the neutral current interactions of neutrinos, elastic scattering of electrons off nuclei, and the scattering of dark matter off nuclei. In addition, these matrix elements also probe intrinsic properties of nucleons (the spin, the nucleon sigma term and strangeness content, and the contribution of the electric dipole moment

(EDM) of the quarks to the nucleon EDM) as explained below. For brevity, all operators are assumed to be appropriately renormalized as discussed in Sect. 10.1.3.

The matrix elements of the scalar operator $\overline{q}q$ with flavour q give the rate of change in the nucleon mass due to nonzero values of the corresponding quark mass. This relationship is given by the Feynman–Hellmann theorem. The quantities of interest are the nucleon σ-term, $\sigma_{\pi N}$, and the strange and charm content of the nucleon, σ_s and σ_c,

$$\sigma_{\pi N} = m_{ud}\langle N|\overline{u}u + \overline{d}d|N\rangle, \tag{439}$$

$$\sigma_s = m_s\langle N|\overline{s}s|N\rangle, \tag{440}$$

$$\sigma_c = m_c\langle N|\overline{c}c|N\rangle. \tag{441}$$

Here m_{ud} is the average of the up and down quark masses and m_s (m_c) is the strange (charm) quark mass. The $\sigma_{\pi N,s,c}$ give the shift in M_N due to nonzero light-, strange- and charm-quark masses. The same matrix elements are also needed to quantify the spin independent interaction of dark matter with nucleons. Note that, while σ_b and σ_t are also phenomenologically interesting, they are unlikely to be calculated on the lattice due to the expected tiny signal in the matrix elements. In principle, the heavy sigma terms can be estimated using $\sigma_{u,d,s}$ by exploiting the heavy-quark limit [991–993].

The matrix elements of the axial operator $\overline{q}\gamma_\mu\gamma_5 q$ give the contribution Δq of quarks of flavour q to the spin of the nucleon:

$$\begin{aligned}\langle N|\overline{q}\gamma_\mu\gamma_5 q|N\rangle &= g_A^q\overline{u}_N\gamma_\mu\gamma_5 u_N,\\ g_A^q \equiv \Delta q &= \int_0^1 dx(\Delta q(x) + \Delta\overline{q}(x)).\end{aligned} \tag{442}$$

The charge g_A^q is thus the contribution of the spin of a quark of flavour q to the spin of the nucleon. It is also related to the first Mellin moment of the polarized parton distribution function (PDF) Δq as shown in the second line in Eq. (442). Measurements by the European Muon collaboration in 1987 of the spin asymmetry in polarized deep inelastic scattering showed that the sum of the spins of the quarks contributes less than half of the total spin of the proton [994]. To understand this unexpected result, called the "proton spin crisis", it is common to start with Ji's sum rule [995], which provides a gauge invariant decomposition of the nucleon's total spin, as

$$\frac{1}{2} = \sum_{q=u,d,s,c,\cdot}\left(\frac{1}{2}\Delta q + L_q\right) + J_g, \tag{443}$$

where $\Delta q/2 \equiv g_A^q/2$ is the contribution of the intrinsic spin of a quark with flavour q; L_q is the orbital angular momentum of that quark; and J_g is the total angular momentum of the gluons. Thus, to obtain the spin of the proton starting from QCD requires calculating the contributions of the three terms: the spin and orbital angular momentum of the quarks, and the angular momentum of the gluons. Lattice-QCD calculations of the various matrix elements needed to extract the three contributions are underway. An alternate decomposition of the spin of the proton has been provided by Jaffe and Manohar [996]. The two formulations differ in the decomposition of the contributions of the quark orbital angular momentum and of the gluons. The contribution of the quark spin, which is the subject of this review and given in Eq. (442), is the same in both formulations.

The tensor charges are defined as the matrix elements of the tensor operator $\overline{q}\sigma^{\mu\nu}q$ with $\sigma^{\mu\nu} = \{\gamma_\mu, \gamma_\nu\}/2$:

$$g_T^q\overline{u}_N\sigma_{\mu\nu}u_N = \langle N|\overline{q}\sigma_{\mu\nu}q|N\rangle. \tag{444}$$

These flavour-diagonal tensor charges $g_T^{u,d,s,c}$ quantify the contributions of the u, d, s, c quark EDM to the neutron electric dipole moment (nEDM) [879,997]. Since particles can have an EDM only due to P and T (or CP assuming CPT is a good symmetry) violating interactions, the nEDM is a very sensitive probe of new sources of CP violation that arise in most extensions of the SM designed to explain nature at the TeV scale. The current experimental bound on the nEDM is $d_n < 2.9\times10^{-26}$ e cm [998], while the known CP violation in the SM implies $d_n < 10^{-31}$ e cm [999]. A nonzero result over the intervening five orders of magnitude would signal new physics. Planned experiments aim to reduce the bound to around 10^{-28} e cm. A discovery or reduction in the bound from these experiments will put stringent constraints on many BSM theories, provided the matrix elements of novel CP-violating interactions, of which the quark EDM is one, are calculated with the required precision.

Table 72 Overview of results for g_A^q

Collaboration	Refs.	N_f	Publication status	Continuum extrapolation	Chiral extrapolation	Finite volume	Renormalization	Excited states	Δu	Δd
PNDME 20	[1000]	2+1+1	C	★‡	★	★	★	○	0.790(23)(30)	−0.425(15)(30)
ETM 19	[971]	2+1+1	A	■	○	★	★	○	0.862(17)	−0.424(16)
PNDME 18A	[103]	2+1+1	A	★‡	★	★	★	○	0.777(25)(30)#	−0.438(18)(30)#
Mainz 19A	[1001]	2+1	C	★	○	★	★	○	0.84(3)(4)	−0.40(3)(4)
χQCD 18	[101]	2+1	A	○	★	★	★	○	0.847(18)(32)$	−0.407(16)(18)$
ETM 17C	[876]	2	A	■	○	○	★	○	0.830(26)(4)	−0.386(16)(6)
									Δs	
PNDME 20	[1000]	2+1+1	C	★‡	★	★	★	○	−0.053(7)	
ETM 19	[971]	2+1+1	A	■	○	★	★	○	−0.0458(73)	
PNDME 18A	[103]	2+1+1	A	★‡	★	★	★	○	−0.053(8)#	
Mainz 19A	[1001]	2+1	C	★	○	★	★	○	−0.044(4)(5)	
χQCD 18	[101]	2+1	A	○	★	★	★	○	−0.035(6)(7)$	
JLQCD 18	[890]	2+1	A	■	○	○	★	○	−0.046(26)(9)#	
χQCD 15	[887]	2+1	A	■	○	■	★	○	−0.0403(44)(78)#	
Engelhardt 12	[1002]	2+1	A	■	○	■	★	○	−0.031(17)#	
ETM 17C	[876]	2	A	■	○	○	★	○	−0.042(10)(2)	

#Assumed that $Z_A^{n,s.} = Z_A^s$
‡The rating takes into account that the action is not fully O(a) improved by requiring an additional lattice spacing
$For this partially quenched analysis the criteria are applied to the unitary points

One can also extract these tensor charges from the zeroth moment of the transversity distributions that are measured in many experiments including Drell–Yan and semi-inclusive deep inelastic scattering (SIDIS). Of particular importance is the active program at Jefferson Lab (JLab) to measure them [967,968]. Transversity distributions describe the net transverse polarization of quarks in a transversely polarized nucleon. Their extraction from the data taken over a limited range of Q^2 and Bjorken x is, however, not straightforward and requires additional phenomenological modeling. At present, lattice-QCD estimates of $g_T^{u,d,s}$ are the most accurate [879,969,970] as can be deduced from Fig. 45. Future experiments will significantly improve the extraction of the transversity distributions. Thus, accurate calculations of the tensor charges using lattice QCD will continue to help elucidate the structure of the nucleon in terms of quarks and gluons and provide a benchmark against which phenomenological estimates utilizing measurements at JLab and other experimental facilities worldwide can be compared.

The methodology for the calculation of flavour-diagonal charges is also well-established. The major challenges are the much larger statistical errors in the disconnected contributions for the same computational cost and the need for the additional calculations of the isosinglet renormalization factors.

10.4.1 Results for $g_A^{u,d,s}$

A compilation of results for the flavour-diagonal axial charges for the proton is given in Table 72 and plotted in Fig. 46. Results for the neutron can be obtained by interchanging the u and d flavour indices. Only two calculations already discussed in FLAG 19 [4] qualify for global averages: the PNDME 18A [103] for 2+1+1 flavours and the χQCD 18 [101] for 2+1 flavours.

The PNDME 18A [103] results were obtained using the 2+1+1 flavour clover-on-HISQ formulation. The connected contributions were obtained on 11 HISQ ensembles generated by the MILC collaboration with $a \approx 0.057$, 0.87, 0.12 and

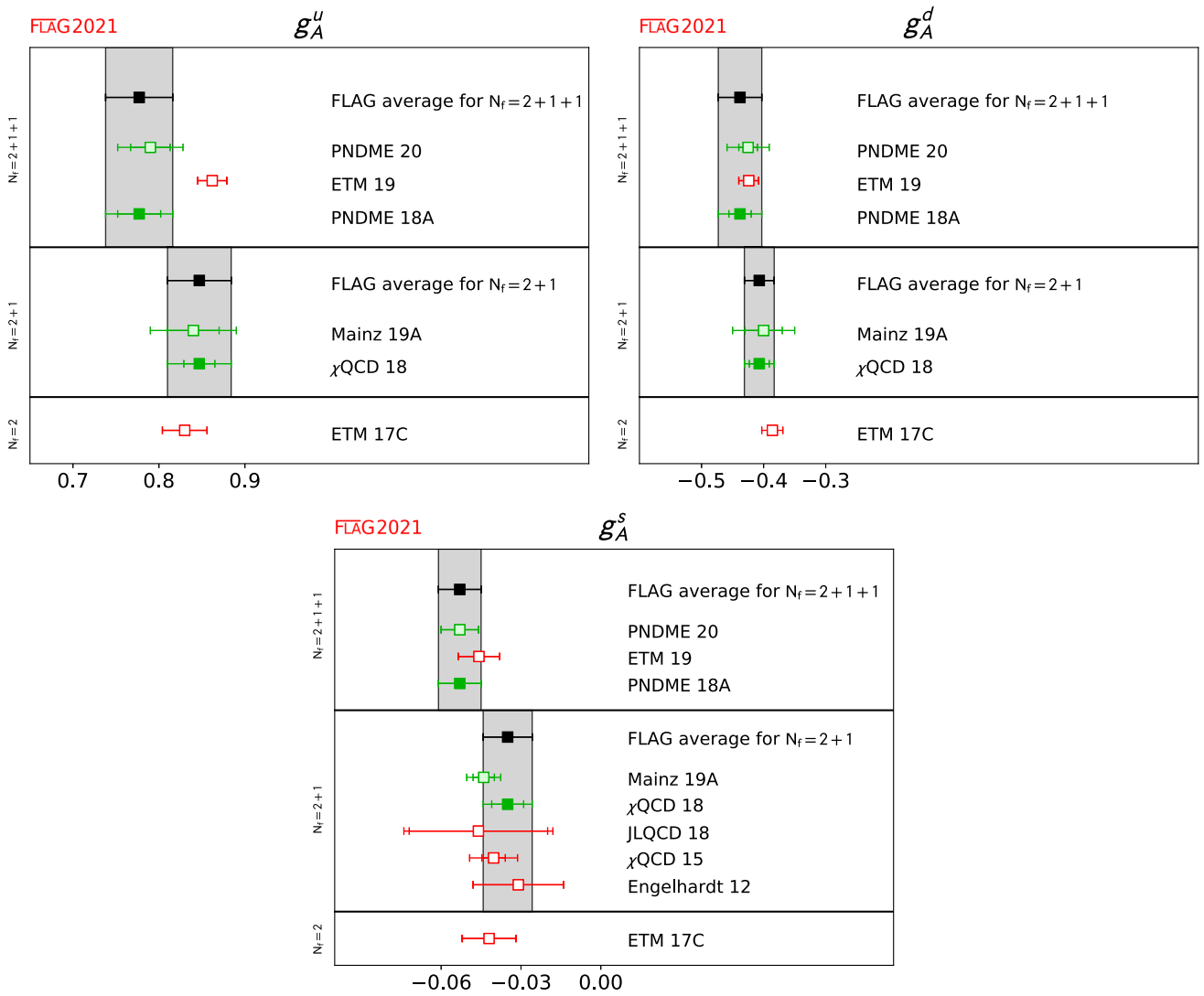

Fig. 46 Lattice results and FLAG averages for $g_A^{u,d,s}$ for the $N_f = 2, 2+1$, and $2+1+1$ flavour calculations

0.15 fm, $M_\pi \approx 135$, 220 and 320 MeV, and $3.3 < M_\pi L < 5.5$. The light disconnected contributions were obtained on six of these ensembles with the lowest pion mass $M_\pi \approx 220$ MeV, while the strange disconnected contributions were obtained on seven ensembles, i.e., including an additional one at $a \approx 0.087$ fm and $M_\pi \approx 135$ MeV. The excited state and the chiral-continuum fits were done separately for the connected and disconnected contributions, which introduces a systematic that is hypothesised to be small as explained in Ref. [103]. The analysis of the excited-state contamination, discussed in Sect. 10.1.2, was done using three-state fits for the connected contribution and two-state fits for the disconnected contributions. The chiral-continuum extrapolation was done keeping the leading correction terms proportional to M_π^2 and a in both cases, and the leading finite-volume correction in $M_\pi L$ was included in the analysis of the connected contributions. Isovector renormalization constants, calculated on the lattice in the RI-SMOM scheme and converted to $\overline{\text{MS}}$, are used for all three flavour diagonal operators.

The PNDME 20 [1000] provided a status update to PNDME 18A [103] and presented results showing that flavour mixing in the calculation of renormalization constants is small, and the isovector renormalization factor is a good approximation for renormalizing flavour diagonal axial charges as discussed in Sect. 10.1.3. It is not considered for the average as it is a conference proceeding.

The ETM 19 [971] presented new results for $g_A^{u,d,s,c}$ from a single ensemble with 2+1+1-flavour twisted-mass fermions with a clover term at $a = 0.0801(4)$ fm and $M_\pi = 139.3(7)$ MeV. These are not considered for the averages as they do not satisfy the criteria for the continuum extrapolation.

The 2+1+1 flavour FLAG values for the axial charges $g_A^{u,d,s}$ of the proton are, therefore, the same as the corresponding results given in Table 72 and unchanged from FLAG 19 [4]:

$$N_f = 2+1+1: \quad g_A^u = 0.777(25)(30) \quad \text{Ref. [103]}, \tag{445}$$
$$N_f = 2+1+1: \quad g_A^d = -0.438(18)(30) \quad \text{Ref. [103]}, \tag{446}$$
$$N_f = 2+1+1: \quad g_A^s = -0.053(8) \quad \text{Ref. [103]}. \tag{447}$$

There are also new results for $g_A^{u,d,s}$ from Mainz 19A [1001] with 2+1-flavour ensembles. While they satisfy all the criteria, they are not included in the averages as [1001] is a conference proceeding.

The 2+1 flavour FLAG results from χQCD 18 [101] were obtained using the overlap-on-domain-wall formalism. Three domain-wall ensembles with lattice spacings 0.143, 0.11 and 0.083 fm and sea-quark pion masses $M_\pi = 171$, 337 and 302 MeV, respectively, were analyzed. In addition to the three approximately unitary points, the paper presents data for an additional 4–5 valence quark masses on each ensemble, i.e., partially quenched data. Separate excited-state fits were done for the connected and disconnected contributions. The continuum, chiral and volume extrapolation to the combined unitary and nonunitary data is made including terms proportional to both $M^2_{\pi,\text{valence}}$ and $M^2_{\pi,\text{sea}}$, and two $\mathcal{O}(a^2)$ discretization terms for the two different domain-wall actions. With just three unitary points, not all the coefficients are well constrained. The $M_{\pi,sea}$ dependence is omitted and considered as a systematic, and a prior is used for the coefficients of the a^2 terms to stabilize the fit. These χQCD 18 2+1 flavour results for the proton, which supersede the χQCD 15 [887] analysis, are

$$N_f = 2+1: \quad g_A^u = 0.847(18)(32) \quad \text{Ref. [101]}, \tag{448}$$
$$N_f = 2+1: \quad g_A^d = -0.407(16)(18) \quad \text{Ref. [101]}, \tag{449}$$
$$N_f = 2+1: \quad g_A^s = -0.035(6)(7) \quad \text{Ref. [101]}. \tag{450}$$

The JLQCD 18 [890], ETM 17C [876] and Engelhardt 12 [1002] calculations were not considered for the averages as they did not satisfy the criteria for the continuum extrapolation. All three calculations were done at a single lattice spacing. The JLQCD 18 calculation used overlap fermions and the Iwasaki gauge action. They perform a chiral fit using data at four pion masses in the range 290–540 MeV. Finite volume corrections are assumed to be negligible since each of the two pairs of points on different lattice volumes satisfy $M_\pi L \geq 4$. The ETM 17C calculation is based on a single twisted-mass ensemble with $M_\pi = 130$ MeV, $a = 0.094$ and a relatively small $M_\pi L = 2.98$. Engelhardt 12 [1002] calculation was done on three asqtad ensembles with $M_\pi = 293$, 356 and 495 MeV, but all at a single lattice spacing $a = 0.124$ fm.

Results for g_A^s were also presented recently by LHPC in Ref. [843]. However, this calculation is not included in Table 72 as it has been performed on a single ensemble with $a = 0.114$ fm and a heavy pion mass value of $M_\pi \approx 317$ MeV.

10.4.2 Results for $g_S^{u,d,s}$ from direct and hybrid calculations of the matrix elements

The sigma terms $\sigma_q = m_q \langle N|\bar{q}q|N\rangle = m_q g_S^q$ or the quark mass fractions $f_{T_q} = \sigma_q / M_N$ are normally computed rather than g_S^q. These combinations have the advantage of being renormalization group invariant in the continuum, and this holds on the lattice for actions with good chiral properties, see Sect. 10.1.3 for a discussion. In order to aid comparison with phenomenological estimates, e.g. from π-N scattering [1003–1005], the light quark sigma terms are usually added to give the πN sigma term, $\sigma_{\pi N} = \sigma_u + \sigma_d$. The direct evaluation of the sigma terms involves the calculation of the corresponding three-point correlation functions for different source-sink separations τ. For $\sigma_{\pi N}$ there are both connected and disconnected contributions, while for most lattice fermion formulations only disconnected contributions are needed for σ_s. The techniques typically employed lead to the availability of a wider range of τ for the disconnected contributions compared to the connected ones (both, however, suffer from signal-to-noise problems for large τ, as discussed in Sect. 10.1) and we only comment on the range of τ computed for the latter in the following.

Recent results for $\sigma_{\pi N}$ and for σ_s from the direct approach are compiled in Table 73. ETM 19 [971] (discussed below) is the only new study included in this table since the last FLAG report. Ref. [1006] is also new, however, it was submitted to the arXiv after the deadline and will be reviewed in the next edition. For completeness, the descriptions of other works are reproduced from FLAG 19.

For both $\sigma_{\pi N}$ and for σ_s, only the results from χQCD 15A [106] qualify for global averaging. In this mixed-action study, three RBC/UKQCD $N_f = 2+1$ domain-wall ensembles are analyzed comprising two lattice spacings, $a = 0.08$ fm with

Table 73 Overview of results for $\sigma_{\pi N}$ and σ_s from the direct approach (above) and σ_s from the hybrid approach (below)

Collaboration	Refs.	N_f	Publication status	Continuum extrapolation	Chiral extrapolation	Finite volume	Renormalization	Excited states	$\sigma_{\pi N}$ [MeV]	σ_s [MeV]
ETM 19	[971]	2+1+1	A	■	○	★	na/na	○	41.6(3.8)	45.6(6.2)
JLQCD 18	[890]	2+1	A	■	○	○	na/na	○	26(3)(5)(2)	17(18)(9)
χQCD 15A	[106]	2+1	A	○	★	★	na/na	○	45.9(7.4)(2.8)$^{\$}$	40.2(11.7)(3.5)$^{\$}$
χQCD 13A	[886]	2+1	A	■	■	○	−/na	○	–	33.3(6.2)$^{\$}$
JLQCD 12A	[889]	2+1	A	■	○	○	−/na	○	–	$0.009(15)(16)\times m_N^{\dagger}$
Engelhardt 12	[1002]	2+1	A	■	○	■	−/na	○	–	$0.046(11)\times m_N^{\dagger}$
ETM 16A	[874]	2	A	■	○	○	na/na	○	$37.2(2.6)(^{4.7}_{2.9})$	$41.1(8.2)(^{7.8}_{5.8})$
RQCD 16	[870]	2	A	○	★	★	na/★	■	35(6)	35(12)
MILC 12C	[108]	2+1+1	A	★	★	★	−/○	○	–	$0.44(8)(5)\times m_s^{\P\S}$
MILC 12C	[108]	2+1	A	★	○	★	−/○	○	–	$0.637(55)(74)\times m_s^{\P\S}$
MILC 09D	[1007]	2+1	A	★	○	★	−/na	○	–	59(6)(8)§

The renormalization criteria is given for $\sigma_{\pi N}$ (first) and σ_s (second). The label 'na' indicates that no renormalization is required
$^{\$}$For this partially quenched analysis the criteria are applied to the unitary points
†This study computes the strange quark fraction f_{T_s}/m_N
§This study employs a hybrid method, see Ref. [1007]
¶The matrix element $\langle N|\bar{s}s|N\rangle$ at the scale $\mu = 2$ GeV in the $\overline{\text{MS}}$ scheme is computed

$M_{\pi,\text{sea}} = 300$ MeV and $a = 0.11$ fm with $M_{\pi,\text{sea}} = 330$ MeV and 139 MeV. Overlap fermions are employed with a number of nonunitary valence quark masses. The connected three-point functions are measured with three values of τ in the range 0.9–1.4 fm. A combined chiral, continuum and volume extrapolation is performed for all data with $M_\pi < 350$ MeV. The leading order expressions are taken for the lattice-spacing and volume dependence while partially quenched $SU(2)$ HBχPT up to M_π^3 terms models the chiral behaviour for $\sigma_{\pi N}$. The strange-quark sigma term has a milder dependence on the pion mass and only the leading-order quadratic terms are included in this case.

The lack of other qualifying studies is an indication of the difficulty and computational expense of performing these calculations. Nonetheless, this situation is likely to improve in the future. We note that although the recent analyses, ETM 16A [874], the new study ETM 19 [971] and JLQCD 18 [890], are at a single lattice spacing ($a = 0.09$ fm, 0.08 fm and 0.11 fm, respectively), they satisfy the criteria for chiral extrapolation, finite volume and excited states. ETM 16A is a single ensemble study with $N_f = 2$ twisted-mass fermions with a pion mass close to the physical point and $M_\pi L = 3.0$. Excited states are investigated utilizing $\tau = 0.9$ fm up to $\tau = 1.7$ fm for the connected three-point functions. In ETM 19 a high statistics analysis was carried out employing a $N_f = 2 + 1 + 1$ physical point ensemble and seven source-sink separations in the range $\tau = 0.6$–1.6 fm, improving the precision they obtain for both $\sigma_{\pi N}$ and σ_s compared to their $N_f = 2$ results. JLQCD in JLQCD 18 utilize $N_f = 2 + 1$ overlap fermion ensembles with pion masses reaching down to 293 MeV ($M_\pi L = 4.0$) and apply techniques which give a wide range of τ for the connected contribution, with the final results extracted from $\tau \geq 1.2$ fm.

RQCD (RQCD 16 [870]) investigates the continuum, physical quark mass and infinite-volume limits, where the lattice spacing spans the range 0.06–0.08 fm, the minimum M_π is 150 MeV and $M_\pi L$ is varied between 3.4 to 6.7 at $M_\pi = 290$ MeV. This $N_f = 2$ study has a red tag for the excited state criterion as multiple source-sink separations for the connected three-point functions are only computed on a subset of the ensembles. Clover fermions are employed and the lack of good chiral properties for this action means that there is mixing between quark flavours under renormalization when determining σ_s and a gluonic term needs to be considered for full $\mathcal{O}(a)$ improvement (which has not been included, see Sect. 10.1.3 for a discussion).

Earlier work focuses only on σ_s. The analysis of JLQCD 12A [889], is performed on the same set of ensembles as the JLQCD 18 study discussed above and in addition includes smaller volumes for the lightest two pion masses.[77] No significant finite-volume effects are observed. Engelhardt 12 [1002] and χQCD 13A [886] have less control over the systematics. The former is a single lattice spacing analysis restricted to small spatial volumes while the latter is a partially quenched study on a single ensemble with unitary $M_\pi > 300$ MeV.

MILC has also computed σ_s using a hybrid method [1007] which makes use of the Feynman–Hellmann (FH) theorem and involves evaluating the nucleon matrix element $\langle N|\int d^4x\, \bar{s}s|N\rangle$.[78] This method is applied in MILC 09D [1007] to the $N_f = 2+1$ asqtad ensembles with lattice spacings $a = 0.06, 0.09, 0.12$ fm and values of M_π ranging down to 224 MeV. A continuum and chiral extrapolation is performed including terms linear in the light-quark mass and quadratic in a. As the coefficient of the discretization term is poorly determined, a Bayesian prior is used, with a width corresponding to a 10% discretization effect between the continuum limit and the coarsest lattice spacing.[79] A similar updated analysis is presented in MILC 12C [108], with an improved evaluation of $\langle N|\int d^4x\, \bar{s}s|N\rangle$ on a subset of the $N_f = 2+1$ asqtad ensembles. The study is also extended to HISQ $N_f = 2+1+1$ ensembles comprising four lattice spacings with $a = 0.06$–0.15 fm and a minimum pion mass of 131 MeV. Results are presented for $g_S^s = \langle N|\bar{s}s|N\rangle$ (in the $\overline{\text{MS}}$ scheme at 2 GeV) rather than for σ_s. The scalar matrix element is renormalized for both three and four flavours using the 2-loop factor for the asqtad action [196]. The error incurred by applying the same factor to the HISQ results is expected to be small.[80]

Both MILC 09D and MILC 12C achieve green tags for all the criteria, see Table 73. As the same set of asqtad ensembles is utilized in both studies we take MILC 12C as superseding MILC 09D for the three-flavour case. The global averaging is discussed in Sect. 10.4.4.

10.4.3 Results for $g_S^{u,d,s}$ using the Feynman–Hellmann theorem

An alternative approach for accessing the sigma terms is to determine the slope of the nucleon mass as a function of the quark masses, or equivalently, the squared pseudoscalar meson masses. The Feynman–Hellman (FH) theorem gives

$$\sigma_{\pi N} = m_u \frac{\partial M_N}{\partial m_u} + m_d \frac{\partial M_N}{\partial m_d} \approx M_\pi^2 \frac{\partial M_N}{\partial M_\pi^2}, \qquad \sigma_s = m_s \frac{\partial M_N}{\partial m_s} \approx M_{\bar{s}s}^2 \frac{\partial M_N}{\partial M_{\bar{s}s}^2}, \tag{451}$$

where the fictitious $\bar{s}s$ meson has a mass squared $M_{\bar{s}s}^2 = 2M_K^2 - M_\pi^2$. In principle this is a straightforward method as the nucleon mass can be extracted from fits to two-point correlation functions, and a further fit to M_N as a function of M_π (and also M_K for σ_s) provides the slope. Nonetheless, this approach presents its own challenges: a functional form for the chiral behaviour of the nucleon mass is needed, and while baryonic χPT (BχPT) is the natural choice, the convergence properties of the different formulations are not well established. Results are sensitive to the formulation chosen and the order of the expansion employed. If there is an insufficient number of data points when implementing higher order terms, the coefficients are sometimes fixed using additional input, e.g. from analyses of experimental data. This may influence the slope extracted. Simulations with pion masses close to or bracketing the physical point can alleviate these difficulties. In some studies the nucleon mass is used to set the lattice spacing. This naturally forces the fit to reproduce the physical nucleon mass at the physical point and may affect the extracted slope. Note that, if the nucleon mass is fitted as a function of the pion and kaon masses, the dependence of the meson masses on the quark masses also, in principle, needs to be considered in order to extract the sigma terms.

An overview of recent determinations of $\sigma_{\pi N}$ and σ_s is given in Table 74. BMW 20A [1010] (discussed below) is the only new study since the last FLAG report. For completeness, the descriptions of other works are reproduced from FLAG 19. Note that the renormalization criterion is not included in Table 74 as renormalization is not normally required when computing the sigma terms in the Feynman–Hellmann approach.[81] At present, a rating indicating control over excited state contamination is also not considered since a wide range of source-sink separations are available for nucleon two-point functions and ground

[77] JLQCD also determine f_{T_s} in Ref. [1008] in a single lattice spacing study on small volumes with heavy pion masses.

[78] Note that in the direct method the matrix element $\langle N|\int d^3x\, \bar{s}s|N\rangle$, involving the spatial volume sum, is evaluated for a fixed timeslice.

[79] This is consistent with discretization effects observed in other quantities at $a = 0.12$ fm.

[80] At least at 1-loop the Z factors for HISQ and asqtad are very similar, cf. Ref. [1009].

[81] An exception to this is when clover fermions are employed. In this case one must take care of the mixing between quark flavours when renormalizing the quark masses that appear in Eq. (451).

Table 74 Overview of results for $\sigma_{\pi N}$ and σ_s from the Feynman–Hellmann approach

Collaboration	Refs.	N_f	Publication status	Continuum extrapolation	Chiral extrapolation	Finite volume	$\sigma_{\pi N}$ [MeV]	σ_s [MeV]
BMW 20A	[1010]	1+1+1+1	P	★‡	★	★	$0.0398(32)(44)\times m_N^{\dagger}$	$0.0577(46)(33)\times m_N^{\dagger}$
ETM 14A	[22]	2+1+1	A	★	○	○	$64.9(1.5)(13.2)^{\triangle}$	–
BMW 15	[105]	2+1	A	★‡	★	★	38(3)(3)	105(41)(37)
Junnarkar 13	[109]	2+1	A	○	○	○	–	48(10)(15)
Shanahan 12	[1011]	2+1	A	■	○	○	45(6)/51(7)⋆	21(6)/59(6)⋆
JLQCD 12A	[889]	2+1	A	■	○	○	–	$0.023(29)(28)\times m_N^{\dagger}$
QCDSF 11	[1012]	2+1	A	■	■	○	31(3)(4)	71(34)(59)
BMW 11A	[104]	2+1	A	○‡	★	○	$39(4)(^{18}_{7})$	$67(27)(^{55}_{47})$
Martin Camalich 10	[1013]	2+1	A	■	★	■	59(2)(17)	−4(23)(25)
PACS-CS 09	[872]	2+1	A	■	★	■	75(15)	–
Walker-Loud 08	[1014]	2+1	A	■	○	■	84(17)(20)/42(14)(9)⋆	–
QCDSF 12	[107]	2	A	○	★	○	37(8)(6)	–
JLQCD 08B	[888]	2	A	■	○	■	$53(2)(^{+21}_{-7})$	–

$^{\triangle}$Two results for $\sigma_{\pi N}$ are quoted arising from different fit ansätze to the nucleon mass. The systematic error is the same as in Ref. [1015] for a combined $N_f = 2$ and $N_f = 2+1+1$ analysis [1016]

‡The rating takes into account that the action is not fully O(a) improved by requiring an additional lattice spacing

⋆Two results are quoted

†The quark fractions $f_{T_{ud}} = f_{T_u} + f_{T_d} = \sigma_{\pi N}/m_N$ and/or $f_{T_s} = \sigma_s/m_N$ are computed

state dominance is normally achieved. This issue may be revisited in the future as statistical precision improves and this systematic is further investigated.

There are several results for $\sigma_{\pi N}$ that can be included in a global average. For $N_f = 2$, one study meets the selection criteria.[82] The analysis of QCDSF 12 [107] employs nonperturbatively improved clover fermions over three lattice spacings ($a =$ 0.06–0.08 fm) with pion masses reaching down to around 160 MeV. Finite volume corrected nucleon masses are extrapolated via $\mathcal{O}(p^4)$ covariant BχPT with three free parameters. The other coefficients are taken from experiment, phenomenology or FLAG, with the corresponding uncertainties accounted for in the fit for those coefficients that are not well known. The nucleon mass is used to set the scale. A novel feature of this study is that a direct determination of $\sigma_{\pi N}$ at around $M_\pi = 290$ MeV was used as an additional constraint on the slope.

Turning to $N_f = 2+1$, two studies performed by the BMW collaboration and one by χQCD are relevant. In BMW 11A [104], stout-smeared tree-level clover fermions are employed on 15 ensembles with simulation parameters encompassing $a = 0.06$–0.12 fm, $M_\pi \sim 190$–550 MeV and $M_\pi L \gtrsim 4$. Taylor, Padé and covariant $SU(3)$ BχPT fit forms are considered. Due to the use of smeared gauge links, discretization effects are found to be mild even though the fermion action is not fully $\mathcal{O}(a)$ improved. Fits are performed including an $\mathcal{O}(a)$ or $\mathcal{O}(a^2)$ term and also without a lattice-spacing dependent term. Finite volume effects were assessed to be small in an earlier work [1018]. The final results are computed considering all combinations of the fit ansatz weighted by the quality of the fit. In BMW 15 [105], a more extensive analysis on 47 ensembles is presented for HEX-smeared clover fermions involving five lattice spacings and pion masses reaching down to 120 MeV. Bracketing the physical point reduces the reliance on a chiral extrapolation. Joint continuum, chiral and infinite-volume extrapolations are carried out for a number of fit parameterisations with the final results determined via the Akaike information criterion procedure [956]. Although only $\sigma_{\pi N}$ is accessible in the FH approach in the isospin limit, the

[82] The ETM collaboration also determine $\sigma_{\pi N}$ in Ref. [1017] as part of an $N_f = 2$ analysis to determine the lattice spacing from the nucleon mass. However, no final result is given.

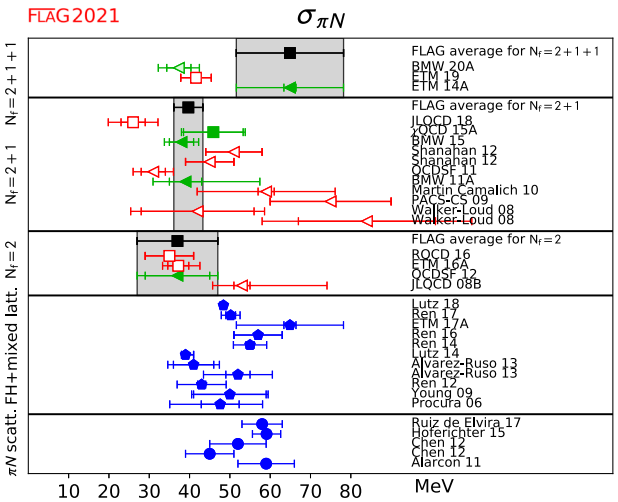

Fig. 47 Lattice results and FLAG averages for the nucleon sigma term, $\sigma_{\pi N}$, for the $N_f = 2$, $2+1$, and $2+1+1$ flavour calculations. Determinations via the direct approach are indicated by squares and the Feynman–Hellmann method by triangles. Results from calculations which analyze more than one lattice data set within the Feynman–Hellmann approach [1015,1021–1029] are shown for comparison (pentagons) along with those from recent analyses of π-N scattering [1003–1005,1030] (circles)

individual quark fractions $f_{T_q} = \sigma_q / M_N$ for $q = u, d$ for the proton and the neutron are also quoted in BMW 15, using isospin relations.[83]

Regarding $N_f = 2+1+1$, there is only one recent study. In ETM 14A [22], fits are performed to the nucleon mass utilizing $SU(2)$ χPT for data with $M_\pi \geq 213$ MeV as part of an analysis to set the lattice spacing. The expansion is considered to $\mathcal{O}(p^3)$ and $\mathcal{O}(p^4)$, with two and three of the coefficients as free parameters, respectively. The difference between the two fits is taken as the systematic error. No discernable discretization or finite-volume effects are observed where the lattice spacing is varied over the range $a = 0.06$–0.09 fm and the spatial volumes cover $M_\pi L = 3.4$ up to $M_\pi L > 5$. The results are unchanged when a near physical point $N_f = 2$ ensemble is added to the analysis in Ref. [1015].

Since FLAG 19, BMW have performed a new $N_f = 1+1+1+1$ study BMW 20A [1010]. A two step analysis is followed: the dependence of the nucleon mass on the pion and kaon masses is determined on HEX-smeared clover ensembles with $a = 0.06$–0.1 fm and pion masses in the range $M_\pi = 195$–420 MeV. The meson masses as a function of the quark masses are evaluated on stout-staggered ensembles with a similar range in a and quark masses which bracket their physical values. As [1010] is a preprint, the result is not considered for the average.

We note that the $N_f = 2+1$ study by χQCD [1020] based on overlap valence fermions on four domain-wall fermion ensembles with $a = 0.08$–0.14 fm and M_π down to the physical point is also new. However, since $\sigma_{\pi N}$ is determined from a single fit and the systematic uncertainties are not estimated, we do not present the result in the table.

Other determinations of $\sigma_{\pi N}$ in Table 74 receive one or more red tags. Walker-Loud 08 [1014], JLQCD 08B [888], PACS-CS 09 [872] and QCDSF 11 [1012] are single lattice spacing studies. In addition, the volume for the minimum pion mass is rather small for Walker-Loud 08, JLQCD 08B and PACS-CS 09, while QCDSF 11 is restricted to heavier pion masses.

We also consider publications that are based on results for baryon masses found in the literature. As different lattice setups (in terms of N_f, lattice actions, etc.) will lead to different systematics, we only include works in Table 74 which utilize a single setup. These correspond to Shanahan 12 [1011] and Martin Camalich 10 [1013], which fit PACS-CS data [193] (the PACS-CS 09 study is also based on these results). Note that Shanahan 12 avoids a red tag for the volume criterion as the lightest pion mass ensemble is omitted. Recent studies which combine data from different setups/collaborations are displayed for comparison in Figs. 47 and 48 in the next section.

Several of the above studies have also determined the strange quark sigma term. This quantity is difficult to access via the Feynman–Hellmann method since in most simulations the physical point is approached by varying the light-quark mass, keeping m_s approximately constant. While additional ensembles can be generated, it is hard to resolve a small slope with respect to m_s. Such problems are illustrated by the large uncertainties in the results from BMW 11A and BMW 15. Alternative approaches have been pursued in QCDSF 11, where the physical point is approached along a trajectory keeping the average

[83] These isospin relations were also derived in Ref. [1019].

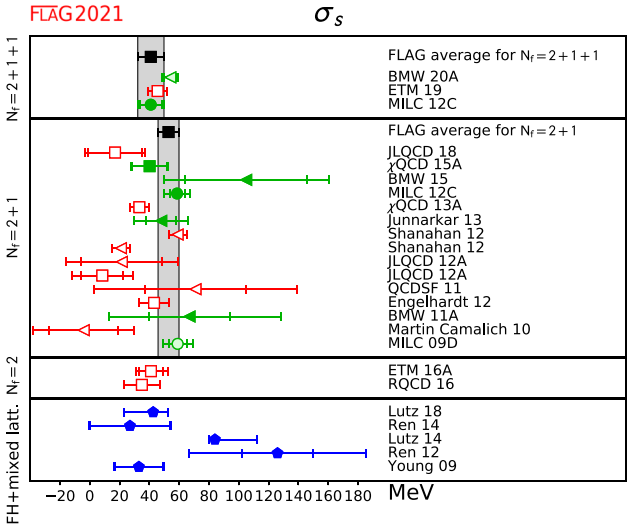

Fig. 48 Lattice results and FLAG averages for σ_s for the $N_f = 2, 2+1$, and $2+1+1$ flavour calculations. Determinations via the direct approach are indicated by squares, the Feynman–Hellmann method by triangles and the hybrid approach by circles. Results from calculations which analyze more than one lattice data set within the Feynman–Hellmann approach [1022,1023,1025,1026,1029] are shown for comparison (pentagons)

of the light- and strange-quark masses fixed, and JLQCD 12A [889], where quark mass reweighting is applied. The latter is a single lattice spacing study. One can also fit to the whole baryon octet and apply $SU(3)$ flavour symmetry constraints as investigated in, e.g. Martin Camalich 10, Shanahan 12, QCDSF 11 and BMW 11A.

The determinations of σ_s in BMW 11A and BMW 15 qualify for averaging. The mixed action study of Junnarkar 13 [109] with domain-wall valence fermions on MILC $N_f = 2+1$ asqtad ensembles also passes the FLAG criteria. The derivative $\partial M_N/\partial m_s$ is determined from simulations above and below the physical strange quark mass for M_π around 240–675 MeV. The resulting values of σ_s are extrapolated quadratically in M_π. The quark fraction $f_{T_s} = \sigma_s/M_N$ exhibits a milder pion-mass dependence and extrapolations of this quantity were also performed using ansätze linear and quadratic in M_π. A weighted average of all three fits was used to form the final result. Two lattice spacings were analyzed, with a around 0.09 fm and 0.12 fm, however, discretization effects could not be resolved. We note that BMW in their $N_f = 1+1+1+1$ study [1010] significantly improve the precision of their estimate of σ_s. Even though all the criteria are satisfied, it is not considered for the average as Ref. [1010] is a preprint. The global averaging of all calculations that qualify is discussed in the next section.

10.4.4 Summary of results for $g_S^{u,d,s}$

We consider computing global averages of results determined via the direct, hybrid and Feynman–Hellmann (FH) methods. These are unchanged from FLAG 19. Beginning with $\sigma_{\pi N}$, Tables 73 and 74 show that for $N_f = 2+1+1$ only ETM 14A (FH) satisfies the selection criteria. We take this value as our FLAG result for the four-flavour case.

$$N_f = 2+1+1: \qquad \sigma_{\pi N} = 64.9(1.5)(13.2)\ \text{MeV} \qquad \text{Ref. [22].} \tag{452}$$

We remark that although the $N_f = 1+1+1+1$ BMW 20A study also satisfies the criteria, as Ref. [1010] is a preprint this work is not considered for averaging. For $N_f = 2+1$ we form an average from the BMW 11A (FH), BMW 15 (FH) and χQCD 15A (direct) results, yielding

$$N_f = 2+1: \qquad \sigma_{\pi N} = 39.7(3.6)\ \text{MeV} \qquad \text{Refs. [104–106].} \tag{453}$$

Note that both BMW results are included as they were obtained on independent sets of ensembles (employing different fermion actions). The average is dominated by the BMW 15 calculation, which has much smaller overall errors compared to the other two studies.

Turning to the results for $N_f = 2$, only QCDSF 12 (FH) qualifies. This is taken as the FLAG result

$$N_f = 2: \qquad \sigma_{\pi N} = 37(8)(6)\ \text{MeV} \qquad \text{Ref. [107].} \tag{454}$$

Moving on to σ_s and the calculations detailed in Table 73, for $N_f = 2+1+1$ MILC 12C (hybrid) and BMW 20A satisfy the quality criteria, however, the latter is a preprint and is not considered for averaging. In order to convert the result for $\langle N|\bar{s}s|N\rangle$ given in MILC 12C to a value for σ_s, we multiply by the appropriate FLAG average for m_s given in Eq. (35) of FLAG 19. This gives our result for four flavours.

$$N_f = 2+1+1: \qquad \sigma_s = 41.0(8.8)\ \text{MeV} \qquad \text{Ref. [108].} \tag{455}$$

For $N_f = 2+1$ we perform a weighted average of BMW 11A (FH), MILC 12C (hybrid), Junnarkar 13 (FH), BMW 15 (FH) and χQCD 15A (direct). MILC 09D [1007] also passes the FLAG selection rules, however, this calculation is superseded by MILC 12C. As for Eq. (455), the strangeness scalar matrix element determined in the latter study is multiplied by the three flavour FLAG average for m_s given in Eq. (33) of FLAG 19. There are correlations between the MILC 12C and Junnarkar 13 results as there is some overlap between the sets of asqtad ensembles used in both cases. To be conservative we take the statistical errors for these two studies to be 100% correlated. The global average is

$$N_f = 2+1: \qquad \sigma_s = 52.9(7.0)\ \text{MeV} \qquad \text{Refs. [104–106,108,109].} \tag{456}$$

Given that all of the $N_f = 2$ studies have at least one red tag we are not able to give an average in this case.

All the results for $\sigma_{\pi N}$ and σ_s are displayed in Figs. 47 and 48 along with the averages given above. Note that where $f_{T_{ud}} = f_{T_u} + f_{T_d}$ or f_{T_s} is quoted in Tables 73 and 74, we multiply by the experimental proton mass in order to include the results in the figures. Those results which pass the FLAG criteria, shown in green, are reasonably consistent. However, there is some fluctuation in the central values, in particular, when taking the lattice results as a whole into account, and we caution the reader that the averages may change as new results become available.

Also shown for comparison in the figures are determinations from the FH method which utilize more than one lattice data set [1015,1021–1029] as well as results for $\sigma_{\pi N}$ obtained from recent analyses of π-N scattering [1003–1005,1030]. There is some tension, at the level of three to four standard deviations, between the lattice average for $N_f = 2+1$ and Hoferichter et al. [1005] (Hoferichter 15 in Fig. 47), who quote a precision similar to that of the average.

Finally we remark that, by exploiting the heavy-quark limit, the light- and strange-quark sigma terms can be used to estimate σ_q for the charm, bottom and top quarks [991–993]. The resulting estimate for the charm quark, see, e.g. the RQCD 16 $N_f = 2$ analysis of Ref. [870] that reports $f_{T_c} = 0.075(4)$ or $\sigma_c = 70(4)$ MeV is consistent with the direct determinations of ETM 19 [971] for $N_f = 2+1+1$ of $\sigma_c = 107(22)$ MeV, ETM 16A [874] for $N_f = 2$ of $\sigma_c = 79(21)(^{12}_{8})$ MeV and χQCD 13A [886] for $N_f = 2+1$ of $\sigma_c = 94(31)$ MeV. BMW in BMW 20A [1010] employing the Feynman–Hellmann approach obtain $f_{T_c} = \sigma_c/m_N = 0.0734(45)(55)$ for $N_f = 1+1+1+1$. MILC in MILC 12C [108] find $\langle N|\bar{c}c|N\rangle = 0.056(27)$ in the $\overline{\text{MS}}$ scheme at a scale of 2 GeV for $N_f = 2+1+1$ via the hybrid method. Considering the large uncertainty, this is consistent with the other results once multiplied by the charm quark mass.

10.4.5 Results for $g_T^{u,d,s}$

A compilation of recent results for the flavour-diagonal tensor charges $g_T^{u,d,s}$ for the proton in the $\overline{\text{MS}}$ scheme at 2 GeV is given in Table 75 and plotted in Fig. 49. Results for the neutron can be obtained by interchanging the u and d flavour indices. Only the PNDME 2+1+1 flavour calculations qualify for the global average.

The FLAG values remain the same as in FLAG 19, i.e., the PNDME 18B [110] results, which supersede the PNDME 16 [881] and the PNDME 15 [879] results:

$$N_f = 2+1+1: \qquad g_T^u = 0.784(28)(10) \qquad \text{Ref. [110],} \tag{457}$$

$$N_f = 2+1+1: \qquad g_T^d = -0.204(11)(10) \qquad \text{Ref. [110],} \tag{458}$$

$$N_f = 2+1+1: \qquad g_T^s = -0.0027(16) \qquad \text{Ref. [110].} \tag{459}$$

Table 75 Overview of results for g_T^q

Collaboration	Refs.	N_f	Publication status	Continuum extrapolation	Chiral extrapolation	Finite volume	Renormalization	Excited states	g_T^u	g_T^d
PNDME 20	[1000]	2+1+1	C	★‡	★	★	★	○	0.783(27)(10)	−0.205(10)(10)
ETM 19	[971]	2+1+1	A	■	○	★	★	○	0.729(22)	−0.2075(75)
PNDME 18B	[110]	2+1+1	A	★‡	★	★	★	○	0.784(28)(10)[#]	−0.204(11)(10)[#]
PNDME 16	[881]	2+1+1	A	○‡	★	★	★	○	0.792(42)[#&]	−0.194(14)[#&]
PNDME 15	[879,880]	2+1+1	A	○‡	★	★	★	○	0.774(66)[#]	−0.233(28)[#]
Mainz 19A	[1001]	2+1	C	★	○	★	★	○	0.77(4)(6)	−0.19(4)(6)
JLQCD 18	[890]	2+1	A	■	○	○	★	○	0.85(3)(2)(7)	−0.24(2)(0)(2)
ETM 17	[877]	2	A	■	○	○	★	○	0.782(16)(2)(13)	−0.219(10)(2)(13)
									g_T^s	
PNDME 20	[1000]	2+1+1	C	★‡	★	★	★	○	−0.0022(12)	
ETM 19	[971]	2+1+1	A	■	○	★	★	○	−0.00268(58)	
PNDME 18B	[110]	2+1+1	A	★‡	★	★	★	○	−0.0027(16)[#]	
PNDME 15	[879,880]	2+1+1	A	○‡	★	★	★	○	0.008(9)[#]	
Mainz 19A	[1001]	2+1	C	★	○	★	★	○	−0.0026(73)(42)	
JLQCD 18	[890]	2+1	A	■	○	○	★	○	−0.012(16)(8)	
ETM 17	[877]	2	A	■	○	○	★	○	−0.00319(69)(2)(22)	

[‡]The rating takes into account that the action is not fully O(a) improved by requiring an additional lattice spacing
[#]Assumed that $Z_T^{n.s.} = Z_T^s$
[&]Disconnected terms omitted

The ensembles and the analysis strategy used in PNDME 18B is the same as described in Sect. 10.4.1 for $g_A^{u,d,s}$. The only difference for the tensor charges was that a one-state (constant) fit was used for the disconnected contributions as the data did not show significant excited-state contamination. The isovector renormalization constant, used for all three flavour-diagonal tensor operators, was calculated on the lattice in the RI-SMOM scheme and converted to $\overline{\text{MS}}$ at 2 GeV using 2-loop perturbation theory.

The PNDME 20 [1000] provided a status update on $g_T^{u,d,s}$ to PNDME 18B [103] but is not considered for the average as it is a conference proceeding. It also presented results showing that flavour mixing in the calculation of tensor renormalization constants is small, and the isovector renormalization factor is a good approximation for renormalizing flavour-diagonal tensor charges as discussed in Sect. 10.1.3.

The ETM 19 [971] presented new results for $g_T^{u,d,s,c}$ from a single ensemble with 2+1+1-flavour twisted-mass fermions with a clover term at $a = 0.0801(4)$ fm and $M_\pi = 139.3(7)$ MeV. It was not considered for the final averages because it did not satisfy the criteria for the continuum extrapolation as already discussed in Sect. 10.4.1. The same applies to the JLQCD 18 [890] and ETM 17 [877] calculations. The Mainz 19A [1001] results with 2+1-flavour ensembles of clover fermions are not included in the averages as Ref. [1001] is a conference proceeding.

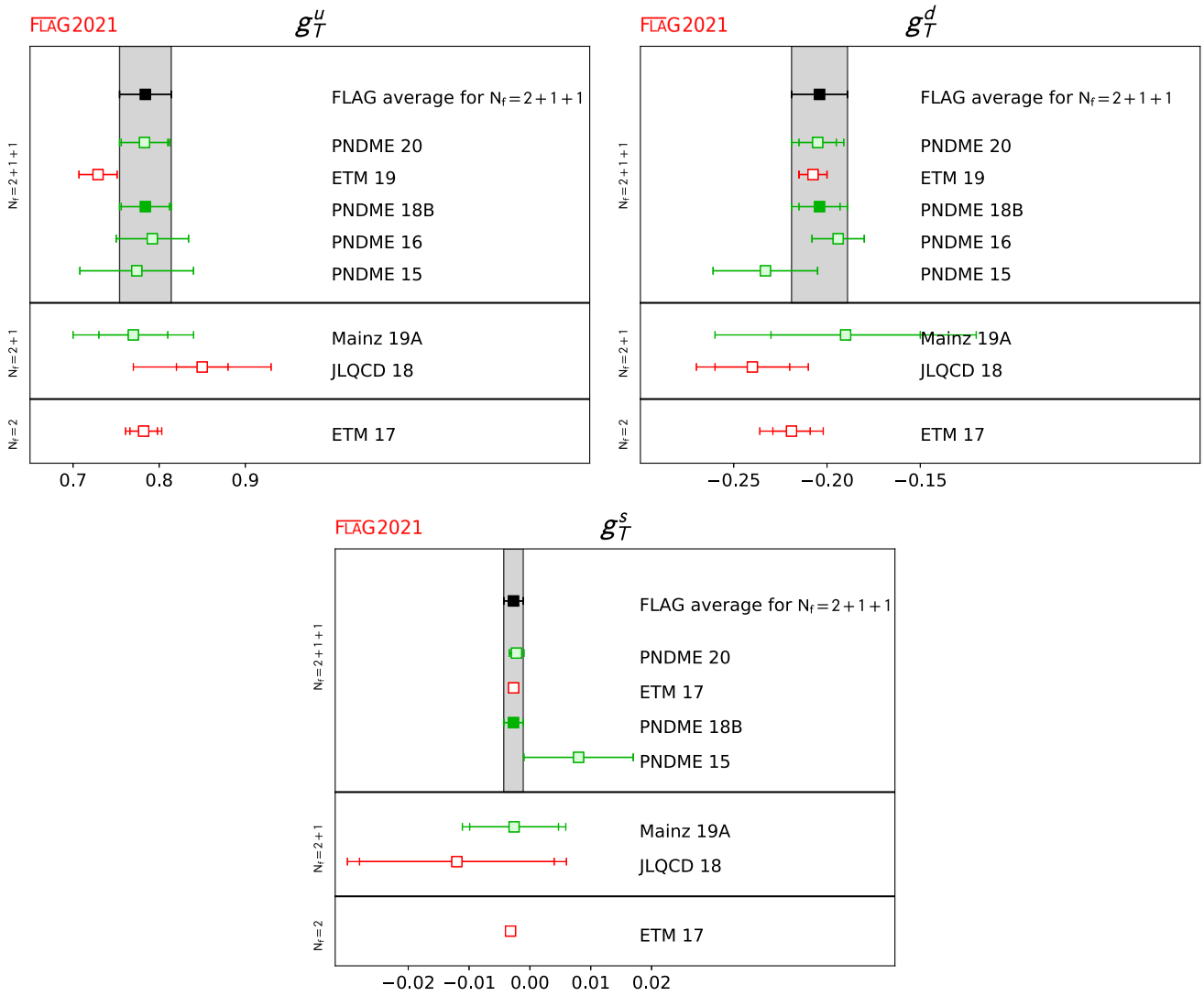

Fig. 49 Lattice results and FLAG averages for $g_T^{u,d,s}$ for the $N_f = 2, 2+1$, and $2+1+1$ flavour calculations

11 Scale setting

Authors: R. Sommer, N. Tantalo, U. Wenger

Matching QCD to Nature requires fixing the quark masses and matching an overall scale to experiment. That overall energy scale $\mathcal{S}$ may be taken, for example, as the nucleon mass. This process is referred to as scale setting.

11.1 Impact

The scale setting procedure, described in some detail below, is a rather technical step necessary to obtain predictions from QCD. What may easily be overlooked is that the exact predictions obtained may depend rather sensitively on the scale.

As long as the theory is incomplete, e.g., because we have predictions from $N_f = 2+1$ QCD, results will depend on which physics scale is used. Whenever a theory scale (see Sect. 11.5) is used, it matters which value one imposes. Thus, to know whether computations of a particular quantity agree or not, one should check which (value for a) scale was used.

The sensitivity of predictions to the scale vary with the observable. For example, the Λ parameter of the theory has a linear dependence,

$$\frac{\delta\Lambda}{\Lambda} \approx \frac{\delta\mathcal{S}}{\mathcal{S}}, \tag{460}$$

because Λ has mass dimension one and other hidden dependences on the scale are (usually) suppressed. Let us preview the results. The present precision on the most popular theory scale, w_0 in Eq. (510) is about 0.4% and for $\sqrt{t_0}$ it is 0.6%. On the Λ parameter it is about 3%. Thus, we would think that the scale uncertainty is irrelevant. However, in Sect. 11.8 we will discuss that differences between $N_f = 2 + 1$ and 2+1+1 numbers for $\sqrt{t_0}$ are at around 2% which *does matter*.

Also, light-quark masses have an approximatively linear dependence on the scale (roughly speaking one determines, e.g., $m_{ud} = \frac{1}{\mathcal{S}} \times [m_\pi^2]_{\rm exp} \times [\frac{m_{ud}\mathcal{S}}{m_\pi^2}]_{\rm lat}$) and scale uncertainties may play an important rôle in the discussion of agreement vs. disagreement of computations within their error budget.

The list of quantities where scale setting is very important may be continued; we just want to mention an observable very much discussed at present, the hadronic vacuum polarisation contribution to the anomalous magnetic moment of the muon [1031]. It is easily seen that the dependence on the scale is about quadratic in that case [1032],

$$\frac{\delta a_\mu^{\rm HVP}}{a_\mu^{\rm HVP}} \approx 2\frac{\delta\mathcal{S}}{\mathcal{S}}. \tag{461}$$

This fact means that scale setting has to be precise at the few per-mille precision to have an impact [115] on the discussion whether or not a_μ computed in the standard model shows a deviation from experiment.

11.2 Scale setting as part of hadronic renormalization schemes

We consider QCD with N_f quarks and without a θ-parameter. This theory is completely defined by its coupling constant as well as N_f quark masses. After these parameters are specified all other properties of the theory are predictions. Coupling and quark masses depend on a renormalization scale μ as well as on a renormalization scheme. The most popular scheme in the framework of perturbative computations is the $\overline{\rm MS}$ scheme, but one may also define nonperturbative renormalization schemes, see Sects. 3 and 9.

In principle, a lattice computation may, therefore, use these $N_f + 1$ parameters as input together with the renormalization scale μ to fix the bare quark masses and coupling of the discretized Lagrangian, perform continuum and infinite volume limit and obtain desired results, e.g., for decay rates.[84] However, there are various reasons why this strategy is inefficient. The most relevant one is that coupling and quark masses cannot be obtained from experiments without invoking perturbation theory and thus necessarily truncation errors. Moreover, these parameters are naturally short distance quantities, since this is where perturbation theory applies. Lattice QCD on the other hand is most effective at long distances, where the lattice spacing plays a minor role. Therefore, it is more natural to proceed differently.

Namely, we may fix $N_f + 1$ nonperturbative, long-distance observables to have the values found in Nature. An obvious choice are $N_f + 1$ hadron masses that are stable in the absence of weak interactions. This hadronic renormalization scheme is defined by

$$\frac{M_i(g_0, \{am_{0,\rm j}\})}{M_1(g_0, \{am_{0,\rm j}\})} = \frac{M_i^{\rm exp}}{M_1^{\rm exp}}, \quad i = 2 \ldots N_f + 1, \quad j = 1 \ldots N_f. \tag{462}$$

Here, M_i are the chosen hadron masses, g_0 is the bare coupling, and $am_{0,j}$ are the bare quark masses in lattice units. The ratio M_i/M_1 is, precisely speaking, defined through the hadron masses in lattice units, but in infinite volume. In QCD (without QED), all particles are massive. Therefore, the infinite volume limit of the properties of stable particles is approached with exponentially small corrections which are assumed to be estimated reliably. The power-like finite-volume corrections in QCD + QED are discussed in subsection 11.3. For fixed g_0, Eq. (462) needs to be solved for the bare quark masses,

$$am_{0,\rm j} = \mu_j(g_0). \tag{463}$$

The functions μ_j define a line in the bare parameter space, called the line of constant physics. Its dependence on the set of masses $\{M_i\}$ is suppressed. The continuum limit is obtained as $g_0 \to 0$ with the lattice spacing shrinking roughly as $aM_1 \sim {\rm e}^{-1/(2b_0 g_0^2)}$. More precisely, consider observables $\mathcal{O}$ with mass dimension $d_\mathcal{O}$. One defines their dimensionless ratio

[84] At first sight this seems like too many inputs, but note that it is the scale μ, at which $\alpha(\mu)$ has a particular value, which is the input. The coupling α by itself can have any (small) value as it runs.

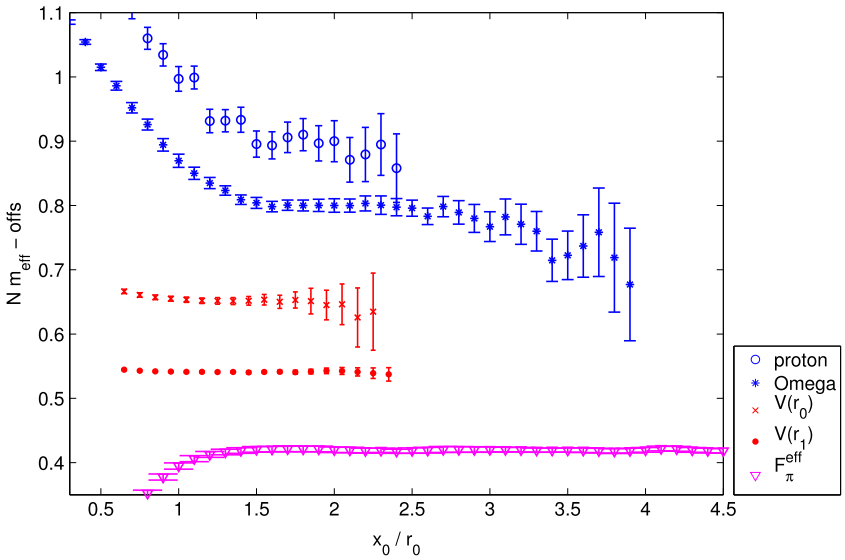

Fig. 50 Effective masses for M_{proton} [1034], M_Ω [1035], $V(\approx r_0)$, $V(\approx r_1)$ [707] and f_π [314] on $N_f = 2$ CLS ensemble N6 with $a = 0.045\,\text{fm}$, $M_\pi = 340$ MeV on a $48^3\,96$ lattice [314]. All effective "masses" have been scaled such that the errors in the graph reflect directly the errors of the determined scales. They are shifted vertically by arbitrary amounts. Figure from Ref. [714]. Note that this example is at still favourably large quark masses. The situation for M_{proton} becomes worse closer to the physical point, but may be changed by algorithmic improvements

$$\hat{\mathcal{O}}(aM_1) = \left.\frac{\mathcal{O}}{M_1^{d_\mathcal{O}}}\right|_{am_{0,j}=\mu_j(g_0)}, \tag{464}$$

and obtains the continuum prediction as

$$\mathcal{O}^{\text{cont}} = \left(M_1^{\text{exp}}\right)^{d_\mathcal{O}} \lim_{aM_1\to 0} \hat{\mathcal{O}}(aM_1) \tag{465}$$

which explains why the determination and use of aM_1 is referred to as scale setting.

Equation (463) has to be obtained from numerical results. Therefore, it is easiest and most transparent if the i-th mass ratio depends predominantly on the i-th quark mass. Remaining for a while in the isospin-symmetric theory with $m_{0,1} = m_{0,2}$ (we enumerate the quark masses in the order up, down, strange, charm, bottom and ignore the top quark), we have natural candidates for the numerators as the pseudoscalar masses in the associated flavour sectors, i.e., π, K, D, B. The desired strong dependence on light- (strange-)quark masses of π- (K-)meson masses derives from their pseudo-Goldstone nature of the approximate $SU(3)_\text{L} \times SU(3)_\text{R}$ symmetry of the massless QCD Lagrangian which predicts that M_π^2 is roughly proportional to the light-quark mass and M_K^2 to the sum of light- and strange-quark masses. For D and B mesons approximate heavy-quark symmetry predicts M_D and M_B to be proportional to charm- and bottom-quark masses. Also other heavy-light bound states have this property. There is another important feature which singles out pseudoscalar masses. Because they are the lightest particles with the given flavour quantum numbers, their correlation functions have the least signal/noise problem in the Monte Carlo evaluation of the path integral [866,1033].

Still restricting ourselves to isospin-symmetric QCD (isoQCD), we thus take it for granted that the choice M_i, $i \geq 2$ is easy, and we do not need to discuss it in detail: the pseudoscalar meson masses are very good choices, and some variations for heavy quarks may provide further improvements.

The choice of M_1 is more difficult. From the point of view of physics, a natural choice is the nucleon mass, $M_1 = M_\text{nucl}$. Unfortunately it has a rather bad signal/noise problem when quark masses are close to their physical values. The ratio of signal to noise of the correlation function at time x_0 from N measurements behaves as [866]

$$R_{S/N}^\text{nucl} \overset{x_0 \text{ large}}{\sim} \sqrt{N}\,\exp\left(-\left(m_\text{nucl} - \frac{3}{2}m_\pi\right)x_0\right) \approx \sqrt{N}\,\exp(-x_0/0.27\,\text{fm}), \tag{466}$$

where the numerical value of 0.27 fm uses the experimental masses. The behaviour in practice, but at still favourably large quark masses, is illustrated in Fig. 50.

Because this property leads to large statistical errors and it is further difficult to control excited-state contaminations when statistical errors are large, it is useful to search for alternative physics scales. The community has gone this way, and we discuss some of them below. For illustration, here we just give one example: the decay constants of leptonic π or K decays have mass dimension one and can directly replace M_1 above. Figure 50 demonstrates their long and precise plateaux as a function of the Euclidean time. Advantages and disadvantages of this choice and others are discussed more systematically in Sect. 11.4.

11.2.1 Theory scales

Since the signal/noise problem of physics scales is rather severe, they were already replaced by theory scales in the very first days of lattice QCD. These scales cannot be determined from experiment alone. Rather, their values have to be computed by lattice QCD using a physics scale as input.

Creutz already used the string tension in his seminal paper on $SU(2)$ Yang Mills theory [1036], because it is by far easier to determine than glueball masses. A further step was made by the potential scale r_0, defined in terms of the static force $F(r)$ as [700]

$$r_0^2 F(r_0) = 1.65. \tag{467}$$

Even though r_0 can vaguely be related to the phenomenology of charmonium and bottomonium states, its precise definition is in terms of $F(r)$ which can be obtained accurately from Monte Carlo lattice computations with (improvable) control over the uncertainties, but not from experiment. In that sense, it is a prototype of a theory scale.
Useful properties of a good theory scale are high statistical accuracy, easy to control systematics (also large volume), quark mass dependence only due to the fermion determinant, and low numerical cost for its evaluation. These properties are realized to varying degrees by the different theory scales covered in this section and, in this respect, they are much preferred compared to physics scales. Consequently, the physics scale M_1 has often been replaced by a theory scale as, e.g., $\mathcal{S} = r_0^{-1}$ in the form

$$\mathcal{O}^{\text{cont}} = \left(\mathcal{S}^{\text{phys}}\right)^{d_\mathcal{O}} \lim_{a\mathcal{S}\to 0} \hat{\mathcal{O}}_\mathcal{S}(a\mathcal{S}) \;\text{ with }\; \hat{\mathcal{O}}_\mathcal{S}(a\mathcal{S}) = \left[\mathcal{S}^{-d_\mathcal{O}}\,\mathcal{O}\right]_{am_{0,j}=\mu_j(g_0)}, \tag{468}$$

and

$$\mathcal{S}^{\text{phys}} = \left(M_1^{\text{exp}}\right) \lim_{aM_1\to 0} \hat{\mathcal{S}}_{M_1}(aM_1). \tag{469}$$

In this section, we review the determination of numerical results for the values of various theory scales in physical units, Eq. (469). The main difficulty is that a physics scale M_1 has to be determined first in order to connect to Nature and, in particular, that the continuum limit of the theory scale in units of the physics scale has to be taken.

11.3 Isospin breaking, electromagnetism, and definition of hadronic schemes

11.3.1 The approximate nature of QCD

For simplicity and because it is a very good approximation, we have assumed above that all other interactions except for QCD can be ignored when hadron masses and many other properties of hadrons are considered. This is a natural point of view because QCD is a renormalizable field theory and thus provides unique results.

However, we must be aware that while it is true that the predictions (e.g., for hadron masses M_i, $i > N_f + 1$) are unique once Eq. (462) is specified, they will change when we change the inputs M_i^{exp}. These ambiguities are due to the neglected electroweak and gravitational interactions, namely because QCD is only an approximate – even if precise – theory of hadrons. At the sub-percent level, QED effects and isospin violations due to $m_u \neq m_d$ must be included. At that level one has a very precise description of Nature, where weak decays or weak effects, in general, can be included perturbatively and systematically in an effective field theory description through the weak effective interaction Hamiltonian, while gravity may be ignored.

We now discuss how to handle the scale setting as part of the renormalization of QCD+QED. Note that a similar discussion with emphasis on quark masses can be found in Sect. 3. In the following discussion, we focus more on the issues related to the scale setting (see also Ref. [240]). In this connection, triviality of QED does not play a rôle at small enough α: we may think of replacing the continuum limit $a \to 0$ by a limit $a \to a_{\text{w}}$ with a_{w} nonzero but very far below all QCD + QED scales.

11.3.2 Hadronic renormalization of QCD + QED

The definition and implementation of a hadronic renormalization scheme of QCD+QED defined on the lattice needs some additions to Sect. 11.2 which we now discuss.

In addition to the $N_f + 1$ parameters of the QCD action (without isospin symmetry), one now also has the elementary electric charge e. This requires $N_f + 2$ experimentally measurable observables to fix the bare parameters of the theory. A natural choice for the experimental inputs are again hadron masses. Indeed, hadron masses are infrared safe quantities also in QCD + QED, while in the cases of cross sections and decay rates, infrared divergences appear at intermediate stages of the calculations (see below). Therefore, we consider the generalization

$$\frac{M_i(g_0, e_0, \{am_{0,\mathrm{j}}\})}{M_1(g_0, e_0, \{am_{0,\mathrm{j}}\})} = \frac{M_i^{\mathrm{exp}}}{M_1^{\mathrm{exp}}}, \quad i = 2 \dots N_f + 2, \quad j = 1 \dots N_f \tag{470}$$

of Eq. (462). Here, M_i are the chosen hadron masses, g_0 the bare strong coupling, e_0 the bare electric charge, and $am_{0,j}$ are the bare quark masses in lattice units. For fixed g_0, the system of equations (470) now needs to be solved for the bare quark masses and the bare electric charge,

$$am_{0,\mathrm{j}} = \mu_j(g_0), \qquad e_0 = \mathrm{e}(g_0), \tag{471}$$

to obtain the line of constant physics of the theory. Some observations are in order.

So far, we have assumed that QCD + QED is simulated nonperturbatively in the electromagnetic coupling constant α_{em}. In this case, the bare electric charge can be conveniently fixed by considering among the experimental inputs both the charged and neutral pion masses. Indeed, by neglecting terms of $\mathcal{O}((m_u - m_d)^2)$ [216] one has that $m_{\pi^+}^2 - m_{\pi^0}^2 \sim \alpha_{\mathrm{em}}$. If the theory is instead treated neglecting $\mathcal{O}(\alpha_{\mathrm{em}}^2)$ contributions, the electric charge does not renormalize and it is consistent and convenient to fix it by the condition [165]

$$\frac{4\pi}{e_0^2} = \frac{1}{\alpha_{\mathrm{em}}^{\mathrm{Thomson}}} = 137.035999084(21)\,. \tag{472}$$

Another important difference from pure QCD concerns finite-volume effects. In contrast to the exponentially suppressed finite-volume effects of stable hadron masses at $\alpha_{\mathrm{em}} = 0$, in QCD + QED with $\alpha_{\mathrm{em}} > 0$ finite-volume effects are

$$\frac{M_i(g_0, e_0, am_{0,\mathrm{j}}; L)}{M_i(g_0, e_0, am_{0,\mathrm{j}}; \infty)} = 1 + \frac{\alpha_{\mathrm{em}} q_i^2 \xi(1)}{L M_i(g_0, e_0, am_{0,\mathrm{j}}; \infty)} + \frac{\alpha_{\mathrm{em}} q_i^2 \xi(2)}{\left[L M_i(g_0, e_0, am_{0,\mathrm{j}}; \infty)\right]^2} + O\left(L^{-n}, \alpha_{\mathrm{em}}^2\right), \tag{473}$$

where q_i is the electric charge of the hadron in units of the charge of the positron, the $\xi(i)$ are known numerical constants that depend on the spatial boundary conditions, and the remainder terms start with a power $n = 3$ in the $\mathrm{QED_L}$ formulation[147,148] and with $n = 4$ in $\mathrm{QED_C}$ [177]. These two definitions of QED in a finite volume are discussed in Refs. [170,179,180] and Refs. [177,185,186], respectively. For other formulations [178,183,184], we refer to Sect. 3 and for a discussion on open problems to Ref. [1037]. Since the bare parameters need to be fixed through experimental observables, finite volume effects have to be removed from the M_i and the behaviour Eq. (473) is crucial in this respect.

Another important observation concerns the use of observables associated with decay rates or cross sections in setting the scale. The issue is particularly subtle in QCD + QED because of the well known problem associated with the appearance of infrared divergences at intermediate stages of the calculations. The solution requires a proper definition of infrared-safe observables, according to the Bloch–Nordsieck mechanism [1038]. These measurable observables are obtained by including in the final state of a process any number of soft photons with total energy up to a given physical threshold. Once the infrared-safe measurable observable has been constructed, it can be used in the scale setting as any other measurable quantity. A particularly relevant example is the leptonic decay rate of the pion,

$$\Gamma^{\mathrm{QCD+QED}}[\pi^- \mapsto \mu \bar{\nu}_\mu(\gamma), E_\gamma]. \tag{474}$$

Here, phase space is integrated over with the constraint that the total energy of the photons is below E_γ. The feasibility of using such an observable in place of a stable hadron mass has to be judged on the basis of the overall precision, statistical plus systematics, that is achievable in the lattice calculation (see Refs. [239,240]).

11.3.3 Hadronic definition of QCD and of QED corrections

Under the assumption of negligible weak (and gravity) corrections QCD + QED is the complete theory and, therefore, the predictions obtained from lattice simulations for any observable $\mathcal{O}^{\rm QCD+QED}$, that has not already been used in the scale setting, are unambiguous. On the contrary, what we call the QCD contribution $\mathcal{O}^{\rm QCD}$ and the associated radiative corrections,

$$\delta\mathcal{O}^{\rm QCD} = \frac{\mathcal{O}^{\rm QCD+QED}}{\mathcal{O}^{\rm QCD}} - 1, \tag{475}$$

do depend upon the inputs used to define QCD.

Going back to Eq. (462), different hadronic definitions of QCD can be obtained by choosing different hadron masses and/or different values for the "physical" inputs. Once we have chosen which hadron masses to use, the different hadronic schemes can be identified by writing

$$\frac{M_i(g_0, \{am_{0,\rm j}\})}{M_1(g_0, \{am_{0,\rm j}\})} = \frac{M_i^{\rm QCD}}{M_1^{\rm QCD}}, \quad i = 2 \ldots N_f + 1, \quad j = 1 \ldots N_f, \tag{476}$$

and by specifying the values of the external inputs, for example parameterized by $\varepsilon_i^{\rm QCD}$ in[85]

$$M_i^{\rm QCD} = M_i^{\rm exp}\left(1 + \varepsilon_i^{\rm QCD}\right). \tag{477}$$

A "natural" choice is to set $\varepsilon_i^{\rm QCD} = 0$, i.e., to define QCD by using exactly the experimental values for the stable hadron masses entering the calibration procedure. In this case, if the same hadron mass is used in the definition of the full theory, Eq. (470), and in the definition of QCD, then the radiative corrections on these quantities are zero by construction. Radiative corrections on any other predictable quantity are well defined and nonvanishing.

In light of this observation, the introduction of the $\varepsilon_i^{\rm QCD}$ parameters might appear unnecessary. However, this is not the case for the following reasons. Isosymmetric QCD (isoQCD), already introduced in Sect. 11.2, is another good approximation of the real world. Due to $m_u = m_d = m_{ud}$, the theory only depends on N_f parameters. In order to set the masses of the light and strange quarks in isoQCD the options of using the charged or the neutral pion and kaon masses are equally valid from the physical point of view. If one picks, e.g., the neutral meson masses, then one has nonzero ε_i when the right hand side of Eq. (477) is written in terms of the charged ones. Furthermore, on the basis of symmetry arguments and/or (chiral) effective theory calculations one may argue that certain linear combinations of charged and neutral meson masses are more "natural" than others (see the discussion in the quark-mass section, Sect. 3) because the resulting radiative corrections are smaller.

As a matter of fact, many of the existing lattice calculations have been performed in the isospin-symmetric limit, but not all the results considered in this review correspond to the very same definition of QCD. The commonly adopted values for the pion and Ω masses in isoQCD are

$$M_\pi^{\rm isoQCD} = M_{\pi^0}^{\rm exp}, \qquad M_\Omega^{\rm isoQCD} = M_{\Omega^-}^{\rm exp} \quad \text{in Refs. [8,111,193].}$$

For the kaon mass in isoQCD different collaborations made different choices, e.g., the values

$$\begin{aligned} M_K^{\rm isoQCD} &= 494.2(4)\ \text{MeV} \quad \text{in Refs. [7,15,111]},\\ M_K^{\rm isoQCD} &= 495.7\ \text{MeV} \quad \text{in Ref. [8]},\\ M_K^{\rm isoQCD} &= 497.6\ \text{MeV} \quad \text{in Ref. [193]}. \end{aligned}$$

The different choices of experimental inputs are perfectly legitimate if QED radiative corrections are neglected, but in principle predictions of isoQCD do depend on these choices, and it is not meaningful to average numbers obtained with different inputs.

[85] After having calibrated the full theory (QCD + QED) with physical hadronic inputs, one can compute the strong coupling constant and the quark masses in a given renormalization scheme. These can then be used to define QCD by matching the corresponding renormalized quantities. This is the so-called GRS approach originally introduced in Ref. [235]. We refer to Ref. [240] for a discussion concerning the connection of the ε-language used here and the GRS scheme, and to Sect. 3 for a detailed discussion of the different schemes that have been used in the literature to define (iso)QCD including the original references on the subject.

However, at the present level of precision the sub-percent differences in the inputs are most likely not relevant, and we will average and compare isoQCD results irrespective of these differences. The issue will become important when results become significantly more precise. Of course, it may not be ignored, when radiative corrections, Eq. (475), are directly compared between collaborations. In this case, we strongly suggest to compare results for the unambiguous full theory observable or to stick to a standard.

Indeed, for the future, it is highly desirable to define such a standard for the parameters used to define (iso)QCD. We suggest using[86]

$$\begin{aligned} M_\pi^{\text{isoQCD}} &= M_{\pi^0}^{\text{exp}}, \\ M_K^{\text{isoQCD}} &= M_{K^0}^{\text{exp}}, \end{aligned} \tag{478}$$

while it is difficult to define a standard scale M_1 right now. Going by the majority of the large-scale computations, the two options m_Ω and pion leptonic decay rate are equally popular at the moment (see Sect. 11.4).

Since leptonic decay rates of pion and kaon play a prominent rôle in scale setting, we discuss the (pure) QCD definition of these quantities and of the associated radiative corrections in some detail. There are no ambiguities in the definition of the physical observable in QCD + QED that, in this case, is the decay rate introduced in Eq. (474) above. We now assume that (iso)QCD has been *already defined* by using as hadronic inputs hadron masses. It is then possible to compute the leptonic decay rate in QCD,

$$\Gamma^{\text{QCD}}[\pi \mapsto \mu\bar{\nu}_\mu] = \frac{G_F^2}{8\pi}|V_{ud}|^2\, M_{\pi^-}^{\text{exp}} \left(m_\mu^{\text{exp}}\right)^2 \left[1 - \frac{\left(m_\mu^{\text{exp}}\right)^2}{\left(M_{\pi^-}^{\text{exp}}\right)^2}\right] \left(f_\pi^{\text{QCD}}\right)^2 \tag{479}$$

where the so-called decay constant of the pion is given by

$$f_\pi^{\text{QCD}} = \frac{\langle 0|\, \bar{u}\gamma^0\gamma^5 d\, |\pi\rangle^{\text{QCD}}}{M_\pi^{\text{QCD}}}. \tag{480}$$

Radiative corrections to f_π^{QCD} are then defined by

$$\delta f_\pi^{\text{QCD}}(E_\gamma) = \sqrt{\frac{\Gamma^{\text{QCD+QED}}[\pi^- \mapsto \mu\bar{\nu}_\mu(\gamma), E_\gamma]}{\Gamma^{\text{QCD}}[\pi \mapsto \mu\bar{\nu}_\mu]}} - 1, \tag{481}$$

such that

$$\Gamma^{\text{QCD+QED}}[\pi^- \mapsto \mu\bar{\nu}_\mu(\gamma), E_\gamma] = \Gamma^{\text{QCD}}[\pi \mapsto \mu\bar{\nu}_\mu]\left[1 + \delta f_\pi^{\text{QCD}}(E_\gamma)\right]^2. \tag{482}$$

We want to stress once again that the definition of $\delta f_\pi^{\text{QCD}}(E_\gamma)$ is not unique. As in the case of any other observable, different values of $\delta f_\pi^{\text{QCD}}(E_\gamma)$ are obtained if one changes the prescription used to define QCD. In this case, in addition, one has to specify the photon energy threshold E_γ and, moreover, the exact expression used to define Γ^{QCD}. Indeed, it would be perfectly legitimate to replace $M_{\pi^-}^{\text{exp}}$ appearing in the kinematical factors of Eq. (479) with M_π^{QCD}. The effect of such a different definition of Γ^{QCD} would be compensated by a change in $\delta f_\pi^{\text{QCD}}(E_\gamma)$ with no ambiguities in the full theory observable $\Gamma^{\text{QCD+QED}}$.

We mentioned in Sect. 11.2 that there are advantages from the numerical point of view in using the leptonic decay constants of the mesons in the QCD scale setting procedure. That observation can now be made more precise in light of the discussion of the previous paragraph. When we say that we use f_π to calibrate QCD, we mean that we choose a value for the $\delta f_\pi^{\text{QCD}}(E_\gamma)$ and we *define*

[86] We note that the π^0 is unstable in QCD + QED and, therefore, it is much more convenient to use $M_{\pi^+}^{\text{exp}}$ to calibrate the full theory. Although it is perfectly consistent to use different observables in the calibration of the full theory and of isoQCD, in the specific case one can write $M_\pi^{\text{isoQCD}} = M_{\pi^+}^{\text{exp}}(1 + \varepsilon_\pi^{\text{isoQCD}})$ with $\varepsilon_\pi^{\text{isoQCD}} = (M_{\pi^0}^{\text{exp}} - M_{\pi^+}^{\text{exp}})/M_{\pi^+}^{\text{exp}}$. In that language, the same observable is used in both theories but with a nonvanishing ε.

$$f_\pi^{\mathrm{QCD}} = \frac{1}{1+\delta f_\pi^{\mathrm{QCD}}(E_\gamma)} \sqrt{\frac{\Gamma^{\mathrm{exp}}[\pi^- \mapsto \mu \bar{\nu}_\mu(\gamma), E_\gamma]}{\frac{G_F^2}{8\pi}|V_{ud}|^2 M_{\pi^-}^{\mathrm{exp}} \left(m_\mu^{\mathrm{exp}}\right)^2 \left[1 - \frac{\left(m_\mu^{\mathrm{exp}}\right)^2}{\left(M_{\pi^-}^{\mathrm{exp}}\right)^2}\right]}}. \tag{483}$$

In the notation of the ε parameters introduced above, one has

$$1 + \varepsilon_{f_\pi}^{\mathrm{QCD}} = \frac{1}{1+\delta f_\pi^{\mathrm{QCD}}(E_\gamma)}. \tag{484}$$

Again, a possible choice would be to set $\varepsilon_{f_\pi}^{\mathrm{QCD}}$ to zero and to use directly the experimentally measured decay rate at a given value of E_γ.[87] Common practice among the different lattice collaborations is to set

$$E_\gamma = E_\gamma^{\mathrm{max}} = \frac{M_{\pi^-}^{\mathrm{exp}}}{2}\left[1 - \frac{\left(m_\mu^{\mathrm{exp}}\right)^2}{\left(M_{\pi^-}^{\mathrm{exp}}\right)^2}\right], \tag{485}$$

the maximum energy allowed to a single photon in the case of negligible $\mathcal{O}(\alpha_{\mathrm{em}}^2)$ corrections, and to use the value

$$\delta f_\pi^{\mathrm{isoQCD}}(E_\gamma^{\mathrm{max}}) = 0.0088(11) \tag{486}$$

obtained in Refs. [241,520,1039] in chiral perturbation theory and using the standard definition Eq. (478). The corresponding number for kaon decays is

$$\delta f_K^{\mathrm{isoQCD}}(E_\gamma^{\mathrm{max}}) = 0.0053(11). \tag{487}$$

A recent lattice determination in the electro-quenched approximation [240]

$$\delta f_\pi^{\mathrm{isoQCD}}(E_\gamma^{\mathrm{max}}) = 0.0076(9), \tag{488}$$

agrees well with Eq. (486), while the number for Kaon decays,

$$\delta f_K^{\mathrm{isoQCD}}(E_\gamma^{\mathrm{max}}) = 0.0012(5), \tag{489}$$

differs by more than three (quadratically combined) error bars from Eq. (487). The scheme dependence can be neglected at the present level of accuracy.

11.4 Physical scales

The purpose of this short section is to summarize the most popular scales and give a short discussion of their advantages and disadvantages. We restrict ourselves to those used in more recent computations and thus have a rather short list.

11.4.1 The mass of the Ω baryon

As already discussed, masses of hadrons that are stable in QCD + QED and have a small width, in general, are very good candidates for physical scales since there are no QED infrared divergences to be discussed. Furthermore, remaining within this class, the radiative corrections $\delta M_i^{\mathrm{QCD}}$, Eq. (475), are expected to be small. Furthermore, the Ω baryon has a significantly better noise/signal ratio than the nucleon (see Fig. 50). It also has little dependence on up- and down-quark masses, since it is composed entirely of strange valence quarks.

Still, one has to be aware that the mass is not extracted from the plateau region but from a modelling of the approach to a plateau in the form of fits [8,111,114,115,117,193]. In this sense, the noise/signal ratio problem may persist. The use of various interpolating fields for the Ω helps in constraining such analyses, but it would be desirable to have a theoretical

[87] This procedure unavoidably requires that one provides a value for the CKM matrix element V_{ud} that has then to be considered an input of the lattice calculation and not a predictable quantity.

understanding of multi-hadron (or in QCD + QED multi-hadron + photon) contributions as it exists for the nucleon [1040] as discussed in Sect. 10. In the present review, we take the estimates of the collaborations at face value and do not try to apply a rating or an estimate of systematic error due to excited-state contributions.

11.4.2 Pion and kaon leptonic decay rates

These decay rates have been discussed above. Here, we just summarize the main issues. In QCD+QED there is so far only one computation of the decay rate in the electro-quenched approximation [240]. The derived estimate for the radiative corrections agrees with the estimates from chiral perturbation theory (see Eqs. (486) and (487)). The quoted uncertainties are at the level of 0.001. This directly sets a limit to the achievable precision on the scale in isoQCD. At present, this limit is not yet relevant. A second source of uncertainty is due to the knowledge of V_{ud} and V_{us}. For convenience, we summarize the isoQCD values

$$f_\pi^{\text{isoQCD}}\,|V_{ud}| = 127.13(2)_{\text{exp}}(13)_{\text{QED}}\,\text{MeV}, \tag{490}$$

$$f_\pi^{\text{isoQCD}} = 130.56(2)_{\text{exp}}(13)_{\text{QED}}(2)_{V_{ud}}\,\text{MeV}, \tag{491}$$

$$f_K^{\text{isoQCD}}\,|V_{us}| = 35.09(4)_{\text{exp}}(4)_{\text{QED}}\,\text{MeV}, \tag{492}$$

$$f_K^{\text{isoQCD}} = 157.2(2)_{\text{exp}}(2)_{\text{QED}}(4)_{V_{us}}\,\text{MeV}, \tag{493}$$

where we have used the PDG values [165] for $f_x|V_y|$ (equivalent to Eqs. (486) and (487)), and the values

$$V_{ud} = 0.97370(14), \quad V_{us} = 0.2232(6).$$

Here, V_{ud} is from the PDG [165] (beta decays) and the latter from Sect. 4 ($f_+(0)$ for $N_f = 2+1+1$). Of course, the information on pion and kaon leptonic decays do not enter the determinations of V_{ud} and V_{us} used here. The uncertainties in the above values are in the following assumed to have been considered in the estimates of the scale given by the collaborations. This is analogous to the systematics due to excited-state contaminations in hadron masses, an issue which is irrelevant in the pseudoscalar channel (see Fig. 50).

Depending on the lattice formulation, there is also a nontrivial renormalization of the axial current. Since it is easily determined from a chiral Ward identity, it does not play an important rôle. When it is present, it is assumed to be accounted for in the statistical errors.

11.4.3 Other physics scales

Scales derived from bottomonium have been used in the past, in particular, the splitting $\Delta m_\Upsilon = m_{\Upsilon(2s)} - m_{\Upsilon(1s)}$. They have very little dependence on the light-quark masses, but need an input for the b-quark mass. In all relevant cases, the b quark is treated by NRQCD.

11.5 Theory scales

In the following, we consider in more detail the two classes of theory scales that are most commonly used in typical lattice computations. The first class consists of scales related to the static quark–antiquark potential [700]. The second class is related to the action density renormalized through the gradient flow [317].

11.5.1 Potential scales

In this approach, lattice scales are derived from the properties of the static quark–antiquark potential. In particular, a scale can be defined by fixing the force $F(r)$ between a static quark and antiquark separated by the distance r in physical units [700]. Advantages of using the potential include the ease and accuracy of its computation, and its mild dependence on the valence-quark mass. In general, a potential scale r_c can be fixed through the condition that the static force takes a predescribed value, i.e.,

$$r_c^2 F(r_c) = X_c \tag{494}$$

where X_c is a suitably chosen number. Phenomenological and computational considerations suggest that the optimal choice for X_c is in the region where the static force turns over from Coulomb-like to linear behaviour and before string breaking occurs. In the original work [700], it was suggested to use $X_0 = 1.65$ leading to the condition

$$r_0^2 F(r_0) = 1.65. \tag{495}$$

In Ref. [701], the value $X_1 = 1.0$ was proposed yielding the scale r_1.

The static force is the derivative of the static quark–antiquark potential $V(r)$ which can be determined through the calculation of Wilson loops. More specifically, the potential at distance r is extracted from the asymptotic time dependence of the $r \times t$-sized Wilson loops $W(r, t)$,

$$V(r) = -\lim_{t\to\infty} \frac{d}{dt} \log\langle W(r, t)\rangle. \tag{496}$$

The derivative of the potential needed for the force is then determined through the derivative of a suitable local parameterization of the potential as a function of r, e.g.,

$$V(r) = C_- \frac{1}{r} + C_0 + C_+ r, \tag{497}$$

estimating uncertainties due to the parameterization. In some calculations, the gauge field is fixed to Coulomb or temporal gauge in order to ease the computation of the potential at arbitrary distances.

In order to optimize the overlap of the Wilson loops with the ground state of the potential, one can use different types and levels of spatial gauge field smearing and extract the ground state energy from the corresponding correlation matrix by solving a generalized eigenvalue problem [925,926,1041]. Finally, one can also make use of the noise reduction proposed in Refs. [1042,1043]. It changes the definition of the discretized loops by a smearing of the temporal parallel transporter [1044] and thus yields a different discretization of the continuum force.

11.5.2 Gradient flow scales

The gradient flow $B_\mu(t, x)$ of gauge fields is defined in the continuum by the flow equation

$$\dot{B}_\mu = D_\nu G_{\nu\mu}, \quad B_\mu\big|_{t=0} = A_\mu\,, \tag{498}$$

$$G_{\mu\nu} = \partial_\mu B_\nu - \partial_\nu B_\mu + [B_\mu, B_\nu], \quad D_\mu = \partial_\mu + [B_\mu, \cdot\,], \tag{499}$$

where A_μ is the fundamental gauge field, $G_{\mu\nu}$ the field strength tensor, and D_μ the covariant derivative [317]. At finite lattice spacing, a possible form of Eqs. (498) and (499) is

$$a^2 \frac{d}{dt} V_t(x, \mu) = -g_0^2 \cdot \partial_{x,\mu} S_G(V_t) \cdot V_t(x, \mu), \tag{500}$$

where $V_t(x, \mu)$ is the flow of the original gauge field $U(x, \mu)$ at flow time t, S_G is an arbitrary lattice discretization of the gauge action, and $\partial_{x,\mu}$ denotes the su(3)-valued differential operator with respect to $V_t(x, \mu)$. An important point to note is that the flow time t has the dimension of a length squared, i.e., $t \sim a^2$, and hence provides a means for setting the scale.

One crucial property of the gradient flow is that any function of the gauge fields evaluated at flow times $t > 0$ is renormalized [1045] by just renormalizing the gauge coupling. Therefore, one can define a scale by keeping a suitable gluonic observable defined at constant flow time t, e.g., the action density $E = -\frac{1}{2}\,\mathrm{Tr}\, G_{\mu\nu} G_{\mu\nu}$ [317], fixed in physical units. This can, for example, be achieved through the condition

$$t_c^2 \langle E(t_c, x)\rangle = c, \quad E(t, x) = -\frac{1}{2}\,\mathrm{Tr}\, G_{\mu\nu}(t, x) G_{\mu\nu}(t, x) \tag{501}$$

where $G_{\mu\nu}(t, x)$ is the field strength tensor evaluated on the flown gauge field V_t. Then, the lattice scale a can be determined from the dimensionless flow time in lattice units, $\hat{t}_c = a^2 t_c$. The original proposal in [317] was to use $c = 0.3$ yielding the scale t_0,

$$t_0^2 \langle E(t_0)\rangle = 0.3\,. \tag{502}$$

For convenience one sometimes also defines $s_0 = \sqrt{t_0}$.

An alternative scale w_0 has been introduced in Ref. [114]. It is defined by fixing a suitable derivative of the action density,

$$W(t_c) = t_c \cdot \partial_t \left(t^2 \langle E(t) \rangle \right)_{t=t_c} = c \,. \tag{503}$$

Setting $c = 0.3$ yields the scale w_0 through

$$W(w_0^2) = 0.3 \,. \tag{504}$$

In addition to the lattice scales from t_0 and w_0, one can also consider the scale from the dimensionful combination t_0/w_0. This combination has been found to have a very weak dependence on the quark mass [305,368,1046].

A useful property of the gradient flow scales is the fact that their quark-mass dependence is known from χPT [1047].

Since the action density at $t \sim t_0 \sim w_0^2$ usually suffers from large autocorrelation [1046,1048], the calculation of the statistical error needs special care.

Lattice artefacts in the gradient flow scales originate from different sources [1049], which are systematically discussed by considering t as a coordinate in a fifth dimension. First, there is the choice of the action S_G for $t > 0$. Second, there is the discretization of $E(t, x)$. Third, there is the discretization of the 4-dimensional quantum action, which is always there, and fourth, there are also terms localized at the boundary $t = 0_+$. The interplay between the different sources of lattice artefacts turns out to be rather subtle [1049].

Removing discretization errors due to the first two sources requires only classical (g_0-independent) improvement. Those due to the quantum action are common to all $t = 0$ observables, but the effects of the boundary terms are not easily removed in practice. At tree level, the Zeuthen flow [1049] does the complete job, but none of the computations reviewed here have used it. Discretization effects due to S_G can be removed by using an improved action such as the tree-level Symanzik-improved gauge action [114,1050]. More phenomenological attempts of improving the gradient flow scales consist of applying a t-shift [1051], or tree-level improvement [712].

11.5.3 Other theory scales

The MILC collaboration has been using another set of scales, the partially quenched pseudoscalar decay constant f_{p4s} with degenerate valence quarks with a mass $m_q = 0.4 \cdot m_{\text{strange}}$, and the corresponding partially quenched pseudoscalar mass M_{p4s}. So far it has been a quantity only used by the MILC collaboration [16,17,145]. We do not perform an in-depth discussion or an average but will list numbers in the results section.

Yet another scale that has been used is the leptonic decay constant of the η_s. This fictitious particle is a pseudoscalar made of a valence quark–antiquark pair with different (fictitious) flavours which are mass-degenerate with the strange quark [118,120,552].

11.6 List of computations and results

11.6.1 Gradient flow scales

We now turn to a review of the calculations of the gradient flow scales $\sqrt{t_0}$ and w_0. The results are compiled in Table 76 and shown in Fig. 51. In the following, we briefly discuss the calculations in the order that they appear in the table and figure.

ETM 21 [305] finalizes and supersedes ETM 20 discussed below. It determines the scales $\sqrt{t_0}$, w_0, also $t_0/w_0 = 0.11969(62)$ fm, and the ratio $\sqrt{t_0}/w_0 = 0.82930(65)$, cf. also HPQCD 13A [37].

CalLat 20A [111] use Möbius Domain-Wall valence fermions on HISQ ensembles generated by the MILC and CalLat collaborations. The gauge fields entering the Möbius Domain-Wall operator are gradient-flow smeared with $t = a^2$. They compute the Ω mass and the scales w_0, t_0 and perform global fits to determine $w_0 M_\Omega$ and $\sqrt{t_0} M_\Omega$ at the physical point. The flow is discretized with the Symanzik tree-level improved action and the clover discretization of $E(t)$ is used. A global fit with Bayesian priors is performed including terms derived from χPT for finite volume and quark-mass dependences, as well as a^2 and $a^2\alpha_s(1.5/a)$ terms for discretization errors. Also, a tree-level improved definition of the GF scales is used where the leading-in-g^2 cutoff effects are removed up to and including $\mathcal{O}(a^8/t^4)$.

BMW 20 [115] presents a result for w_0 in the context of their staggered fermion calculation of the muon anomalous magnetic moment. It is the first computation that takes QED and isospin-breaking corrections into account. The simulations are performed by using staggered fermions with stout gauge field smearing with six lattice spacings and several pion masses around the physical point with M_π between 110 and 140 MeV. Volumes are around $L = 6$ fm. At the largest lattice spacing,

Table 76 Results for gradient flow scales at the physical point, cf. Eq. (469). Note that BMW 20 [115] take IB and QED corrections into account. Some additional results for ratios of scales are: ETM 21 [305]: $t_0/w_0 = 0.11969(62)$ fm

Collaboration	Refs.	N_f	Publication status	Chiral extrapolation	Continuum extrapolation	Finite volume	Physical scale	$\sqrt{t_0}$ [fm]	w_0 [fm]
ETM 21	[305]	2+1+1	P	★	★	★	f_π	0.14436(61)	0.17383(63)
CalLat 20A	[111]	2+1+1	A	★	★	★	m_Ω	0.1422(14)	0.1709(11)
BMW 20	[115]	1+1+1+1	A	★	★	★	m_Ω		0.17236(29)(63)[70]
ETM 20	[1052]	2+1+1	C	★	★	★	f_π		0.1706(18)
MILC 15	[112]	2+1+1	A	★	★	★	$F_{p4s}(f_\pi)^\#$	0.1416(+8/-5)	0.1714(+15/-12)
HPQCD 13A	[37]	2+1+1	A	★	○	★	f_π	0.1420(8)	0.1715(9)
CLS 16	[113]	2+1	A	○	★	★	f_π, f_K	0.1467(14)(7)	
QCDSF/UKQCD 15B	[713]	2+1	P	○	○	○	$m_P^{SU(3)}$	0.1511(22)(6)(5)(3)	0.1808(23)(5)(6)(4)
RBC/UKQCD 14B	[8]	2+1	A	★	★	★	m_Ω	0.14389(81)	0.17250(91)
HotQCD 14	[116]	2+1	A	★	★	★	$r_1(f_\pi)^\#$		0.1749(14)
BMW 12A	[114]	2+1	A	★	★	★	m_Ω	0.1465(21)(13)	0.1755(18)(4)

$^\#$ These scales are not physical scales and have been determined from f_π

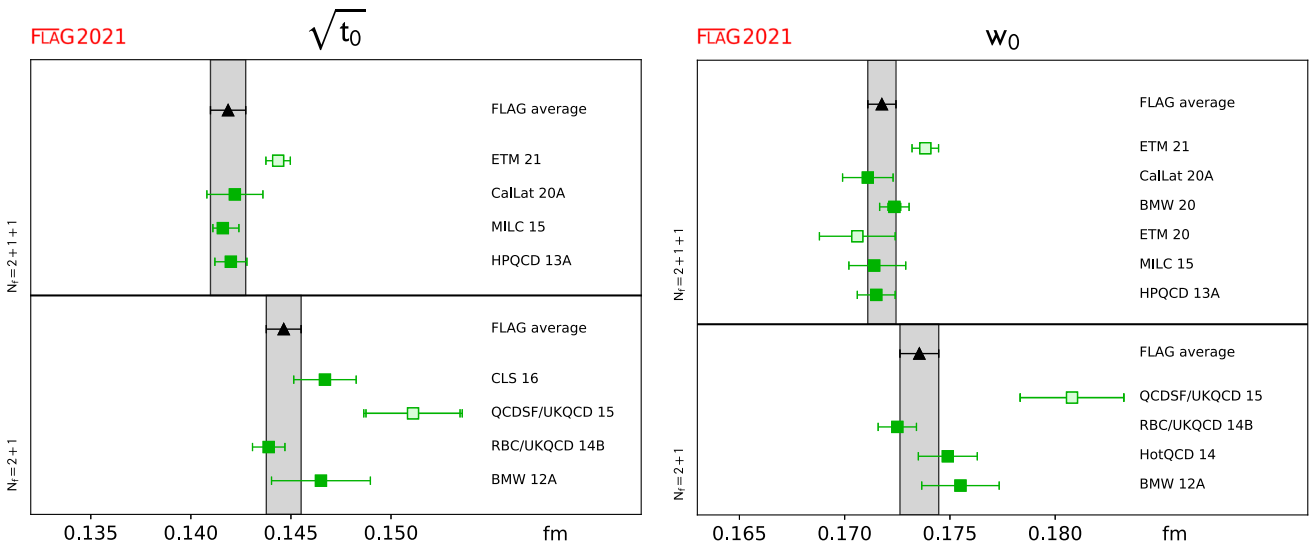

Fig. 51 Results for gradient flow scales

it is demonstrated how the effective masses of the Ω correlator almost reach the plateau value extracted from a four-state fit (two states per parity). Within the range where the data is fitted, the deviation of data points from the estimated plateau is less than a percent. Isospin-breaking corrections are computed by Taylor expansion around isoQCD with QED treated as QED_L. Finite volume effects in QED are taken from the $1/L$, $1/L^2$ universal corrections and $\mathcal{O}(1/L^3)$ effects are neglected. The results for $M_\Omega w_0$ are extrapolated to the continuum by a fit with a^2 and a^4 terms.

ETM 20 [1052] presents in their proceedings contribution a preliminary analysis of their $N_f = 2+1+1$ Wilson twisted-mass fermion simulations at maximal twist (i.e., automatic $\mathcal{O}(a)$ improved), at three lattice spacings and pion masses at the physical point. Their determination of $w_0 = 0.1706(18)$ fm from f_π using an analysis in terms of M_π is the value quoted above. They obtain the consistent value $w_0 = 0.1703(18)$ fm from an analysis in terms of the renormalized light quark mass.

MILC 15 [112] sets the physical scale using the fictitious pseudoscalar decay constant $F_{p4s=}153.90(9)(+21/-28)$ MeV with degenerate valence quarks of mass $m_v = 0.4m_s$ and physical sea-quark masses [145]. (F_{p4s} has strong dependence on the valence-quark mass and is determined from f_π.) They use a definition of the flow scales where the tree-level lattice artefacts up to $\mathcal{O}(a^4/t^2)$ are divided out. Charm-quark mass mistunings are between 1 and 11%. They are taken into account at leading order in $1/m_c$ through $\Lambda^{(3)}_{\rm QCD}$ applied directly to F_{p4s} and $1/m_c$ corrections are included as terms in the fits. They use elaborate variations of fits in order to estimate extrapolation errors (both in GF scales and F_{p4s}). They include errors from FV effects and experimental errors in f_π in F_{p4s}.

HPQCD 13A [37] uses eight MILC-HISQ ensembles with lattice spacings $a = 0.088, 0.121, 0.151$ fm. Values of L are between 2.5 fm and 5.8 fm with $M_\pi L = 3.3$–4.6. Pion masses range between 128 and 306 MeV. QCD is defined by using the inputs $M_\pi = 134.98(32)$ MeV, $M_K = 494.6(3)$ MeV, $f_{\pi^+} = 130.4(2)$ MeV derived by model subtractions of IB effects. Additional scale ratios are given: $\sqrt{t_0}/w_0 = 0.835(8)$, $r_1/w_0 = 1.789(26)$.

CLS 13 [113] uses CLS configurations of 2+1 nonperturbatively $\mathcal{O}(a)$-improved Wilson fermions. There are a few pion masses with the strange mass adjusted along a line of $m_u + m_d + m_s = \text{const}$. Three different lattice spacings are used. They determine t_0 at the physical point defined by π and K masses and the linear combination $f_K + \frac{1}{2} f_\pi$. They use the Wilson flow with the clover definition of $E(t)$.

QCDSF 15B [713,1053] results, unpublished, are obtained by simulating $N_f = 2 + 1$ QCD with the tree-level Symanzik improved gauge action and clover Wilson fermions with single level stout smearing for the hopping terms together with unsmeared links for the clover term (SLiNC action). Simulations are performed at four different lattice spacings, in the range [0.06, 0.08] fm, with $M_{\pi,\rm min} = 228$ MeV and $M_{\pi,\rm min} L = 4.1$. The results for the gradient flow scales have been obtained by relying on the observation that flavour-symmetric quantities get corrections of $\mathcal{O}((\Delta m_q)^2)$ where Δm_q is the difference of the quark mass from the $SU(3)$-symmetric value. The $\mathcal{O}(\Delta m_q^2)$ terms are not detected in the data and subsequently neglected.

RBC/UKQCD 14B [8] presents results for $\sqrt{t_0}$ and w_0 obtained in QCD with $2 + 1$ dynamical flavours. The simulations are performed by using domain-wall fermions on six ensembles with lattice spacing $a^{-1} = 1.38, 1.73, 1.78, 2.36, 2.38,$ and 3.15 GeV, pion masses in the range $M_\pi^{unitary} \in [139, 360]$ MeV. The simulated volumes are such that $M_\pi L > 3.9$. The effective masses of the Ω correlator are extracted with two-state fits and it is shown, by using two different nonlocal interpolating operators at the source, that the correlators almost reach a plateau. In the calculation of $\sqrt{t_0}$ and w_0, the clover definition of $E(t)$ is used. The values given are $\sqrt{t_0} = 0.7292(41)\,\text{GeV}^{-1}$ and $w_0 = 0.8742(46)\,\text{GeV}^{-1}$ which we converted to the values in Table 76.

HotQCD 14 [116] determines the equation of state with $N_f = 2 + 1$ flavours using highly improved staggered quarks (HISQ/tree). As a byproduct, they update the results of HotQCD 11 [708] by adding simulations at four new values of β, for a total of 24 ensembles, with lattice spacings in the range [0.04, 0.25] fm and volumes in the range [2.6, 6.1] fm with $M_\pi = 160$ MeV. They obtain values for the scale parameters r_0 and w_0, via the ratios r_0/r_1, w_0/r_1 and using $r_1 = 0.3106(14)(8)(4)$ fm from MILC 10 [41]. They obtain for the ratios $(r_0/r_1)_{cont} = 1.5092(39)$ and $(w_0/r_1)_{cont} = 0.5619(21)$ in the continuum. They crosscheck their determination of the scale r_1 using the hadronic quantities f_K, f_η from HPQCD 09B [120] and the experimental value of M_φ, and find good agreement.

BMW 12A [114] is the work in which w_0 was introduced. Simulations with 2HEX smeared Wilson fermions and two-level stout-smeared rooted staggered fermions are done. The Wilson flow with clover $E(t)$ is used, and a test of the Symanzik flow is carried out. They take the results with Wilson fermions as their central value, because those "do not rely on the 'rooting' of the fermion determinant". Staggered fermion results agree within uncertainties.

11.6.2 Potential scales

We now turn to a review of the calculations of the potential scales r_0 and r_1. The results are compiled in Table 77 and shown in Fig. 52. The most recent calculations date back to 2014, and we discuss them in the order that they appear in the table and the figure.

ETM 14 [7] uses $N_f = 2 + 1 + 1$ Wilson twisted-mass fermions at maximal twist (i.e., automatic $\mathcal{O}(a)$-improved), three lattice spacings and pion masses reaching down to $M_\pi = 211$ MeV. They determine the scale r_0 through $f_\pi = f_{\pi^+} = 130.41$ MeV. A crosscheck of the so obtained lattice spacings with the ones obtained via the fictitious pseudoscalar meson $M_{s's'}$ made of two strange-like quarks gives consistent results. The crosscheck is done using the dimensionless combinations $r_0 M_{s's'}$ (with r_0 in the chiral limit) and $f_\pi/M_{s's'}$ determined in the continuum, and then using r_0/a and the value of $M_{s's'}$ obtained from the experimental value of f_π. We also note that in Ref. [1046] using the same ensembles the preliminary value $w_0 = 0.1782$ fm is determined, however, without error due to the missing or incomplete investigation of the systematic effects.

HPQCD 13A [37] was already discussed above in connection with the gradient flow scales.

Table 77 Results for potential scales at the physical point, cf. Eq. (469). $\Delta M_\Upsilon = M_{\Upsilon(2s)} - M_{\Upsilon(1s)}$

Collaboration	Ref.	N_f	Publication status	Chiral extrapolation	Continuum extrapolation	Finite volume	Physical scale	r_0 [fm]	r_1 [fm]
ETM 14	[7]	2+1+1	A	○	★	★	f_π	0.474(14)	
HPQCD 13A	[37]	2+1+1	A	★	○	★	f_π		0.3112(30)
HPQCD 11B	[552]	2+1+1	A	○	○	○	ΔM_Υ, f_{η_s}		0.3209(26)
HotQCD 14	[116]	2+1	A	★	★	★	r_1([41])[#]	0.4688(41)	
χQCD 14	[24]	2+1	A	○	○	○	Three inputs[a]	0.465(4)(9)	
HotQCD 11	[708]	2+1	A	★	★	★	f_π	0.468(4)	
RBC/UKQCD 10A	[117]	2+1	A	○	○	○	M_Ω	0.487(9)	0.333(9)
MILC 10	[41]	2+1	C	○	★	★	f_π		0.3106(8)(14)(4)
MILC 09	[157]	2+1	A	○	★	★	f_π		$0.3108(15)(^{+26}_{-79})$
MILC 09A	[15]	2+1	C	○	★	★	f_π		$0.3117(6)(^{+12}_{-31})$
HPQCD 09B	[120]	2+1	A	○	★	○	Three inputs		0.3133(23)(3)
PACS-CS 08	[193]	2+1	A	★	■	■	M_Ω	$0.4921(64)(^{+74}_{-2})$	
HPQCD 05B	[118]	2+1	A	○	○	○	ΔM_Υ	0.469(7)	0.321(5)
Aubin 04	[119]	2+1	A	○	○	○	ΔM_Υ	0.462(11)(4)	0.317(7)(3)

[#]This theory scale was determined in turn from r_1 [41]
[a] $M_{D_s^*}$, $M_{D_s^*} - M_{D_s}$, $M_{J/\psi}$

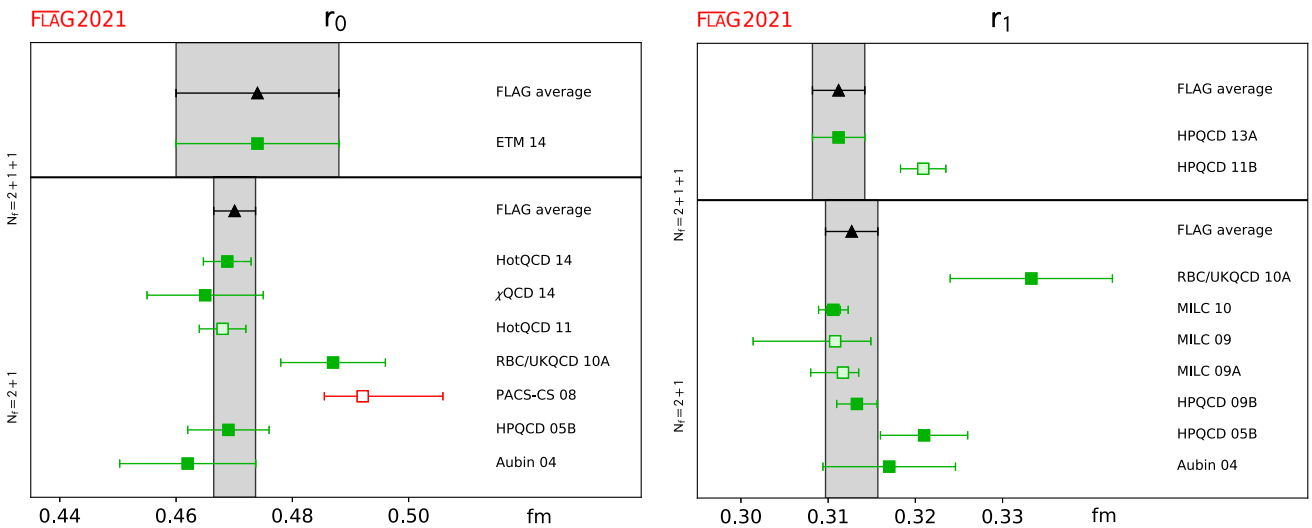

Fig. 52 Results for potential scales

HPQCD 11B [552] uses five MILC-HISQ ensembles and determines r_1 from $M_{\Upsilon(2s)} - M_{\Upsilon(1s)}$ and the decay constant f_{η_s} (see HPQCD 09B). The valence b quark is treated by NRQCD, while the light valence quarks have the HISQ discretization, identical to the sea quarks.

HotQCD 14 [116] was already discussed in connection with the gradient flow scales.

χQCD 14 [24] uses overlap fermions as valence quarks on $N_f = 2 + 1$ domain-wall fermion gauge configurations generated by the RBC/UKQCD collaboration [117]. Using the physical masses of D_s, D_s^* and J/ψ as inputs, the strange and charm quark masses and the decay constant f_{D_s} are determined as well as the scale r_0.

HotQCD 11 [708] uses configurations with tree-level improved Symanzik gauge action and HISQ staggered quarks in addition to previously generated ensembles with p4 and asqtad staggered quarks. In this calculation, QCD is defined by generating lines of constant physics with $m_l/m_s = \{0.2, 0.1, 0.05, 0.025\}$ and setting the strange quark mass by requiring that the mass of a fictitious $\eta_{s\bar{s}}$ meson is $M_{\eta_{s\bar{s}}} = \sqrt{2M_K^2 - M_\pi^2}$. The physical point is taken to be at $m_l/m_s = 0.037$. The physical scale is set by using the value $r_1 = 0.3106(8)(18)(4)$ fm obtained in Ref. [41] by using f_π as physical input. In the paper, this result is shown to be consistent within the statistical and systematic errors with the choice of f_K as physical input. The result $r_0/r_1 = 1.508(5)$ is obtained by averaging over 12 ensembles at $m_l/m_s = 0.05$ with lattice spacings in the range [0.066, 0.14] fm. This result is then used to get $r_0 = 0.468(4)$ fm. Finite volume effects have been monitored with 20 ensembles in the range [3.2, 6.1]fm with $M_\pi L > 2.6$.

RBC/UKQCD 10A [117] uses $N_f = 2 + 1$ flavours of domain-wall quarks and the Iwasaki gauge action at two values of the lattice spacing with unitary pion masses in the approximate range [290, 420] MeV. They use the masses of π and K meson and of the Ω baryon to determine the physical quark masses and the lattice spacings, and so obtain estimates of the scales r_0, r_1 and the ratio r_1/r_0 from a combined chiral and continuum extrapolation.

MILC 10 [41] presents a further update of r_1 with asqtad staggered quark ensembles with $a \in \{0.045, 0.06, 0.09\}$ fm. It supersedes MILC 09 [15,157,1054].

MILC 09 [157] presents an $N_f = 2 + 1$ calculation of the potential scales on asqtad staggered quark ensembles with $a \in \{0.045, 0.06, 0.09, 0.12, 0.15, 0.18\}$ fm. The continuum extrapolation is performed by using Goldstone boson pions as light as $M_\pi = 224$ MeV (RMS pion mass of 258 MeV). The physical scale is set from f_π. The result for r_1 obtained in the published paper [157] is then updated and, therefore, superseded by the conference proceedings MILC 09A and 09B [15,1054].

HPQCD 09B [120] is an extension of HPQCD 05B [118] and uses HISQ valence quarks instead of asqtad quarks. The scale r_1 is obtained from three different inputs. First $r_1 = 0.309(4)$ fm from the splitting of 2S and 1S Υ states as in Ref. [118], second $r_1 = 0.316(5)$ fm from $M_{D_s} - M_{\eta_s}/2$ and third $r_1 = 0.315(3)$ fm from the decay constant of the η_s. The fictitious η_s state is operationally defined by setting quark masses to the s-quark mass and dropping disconnected diagrams. Its mass and decay constant are obtained from a partially quenched chiral perturbation theory analysis using the pion and kaon states from experiment together with various partially quenched lattice data. The three results are combined to $r_1 = 0.3133(23)(3)$ fm.

PACS-CS 08 [193] presents a calculation of r_0 in $N_f = 2 + 1$ QCD by using NP $\mathcal{O}(a)$-improved clover Wilson quarks and Iwasaki gauge action. The calculation is done at fixed lattice spacing $a = 0.09$ fm and is extrapolated to the physical point from (unitary) pion masses in the range [156, 702] MeV. The $N_f = 2 + 1$ theory is defined by fixing M_π, M_K, and M_Ω to 135.0, 497.6, and 1672.25 MeV, respectively. The effective masses of smeared-local Ω correlators averaged over the four spin polarizations show quite good plateaux.

HPQCD 05B [118] performed the first bottomonium spectrum calculation in full QCD with $N_f = 2 + 1$ on MILC asqtad configurations and the b quark treated by NRQCD. They find agreement of the low lying Υ states with experiment and also compare to quenched and $N_f = 2$ results. They determined r_0 and r_1 from the splitting of 2S and 1S states.

Aubin 04 [119] presents an $N_f = 2 + 1$ calculation of the potential scales by using asqtad staggered quark ensembles with $a = 0.09$ and $0.12\}$ fm. The continuum extrapolation is performed by using Goldstone boson pions as light as $m_\pi = 250$ MeV. The physical scale is set from the Υ 2S-1S and 1P-1S splittings computed with NRQCD by HPQCD [1055].

11.6.3 Ratios of scales

It is convenient in many cases to also have ratios of scales at hand. In addition to translating from one scale to another, the ratios provide important crosschecks between different determinations. Results on ratios provided by the collaborations are compiled in Table 78 and Fig. 53. The details of the computations were already discussed in the previous sections.

11.7 Averages

Gradient flow scale $\sqrt{t_0}$

For $N_f = 2 + 1 + 1$, we have two very recent calculations from ETM 21 [305], CalLat 20A [111], and two less recent ones from MILC 15 [112], and HPQCD 13A [37] fulfilling the FLAG criteria to enter the average. The latter two and CalLat 20A are based on the same MILC-HISQ gauge field ensembles, hence we consider their statistical errors to be 100% correlated. ETM 21 is not published, and, hence, does not enter the FLAG average.

Table 78 Results for dimensionless ratios of scales

Collaboration	Refs.	N_f	Publication status	Chiral extrapolation	Continuum extrapolation	Finite volume	$\sqrt{t_0}/w_0$	r_0/r_1	r_1/w_0
ETM 21	[305]	2+1+1	P	★	★	★	0.82930(65)		
HPQCD 13A	[37]	2+1+1	A	★	○	★	0.835(8)		1.789(26)
HotQCD 14	[116]	2+1	A	★	★	★			1.7797(67)
HotQCD 11	[708]	2+1	A	★	★	★		1.508(5)	
RBC/UKQCD 10A	[117]	2+1	A	○	○	○		1.462(32)[#]	
Aubin 04	[119]	2+1	A	○	○	○		1.474(7)(18)	

[#]This value is obtained from $r_1/r_0 = 0.684(15)(0)(0)$

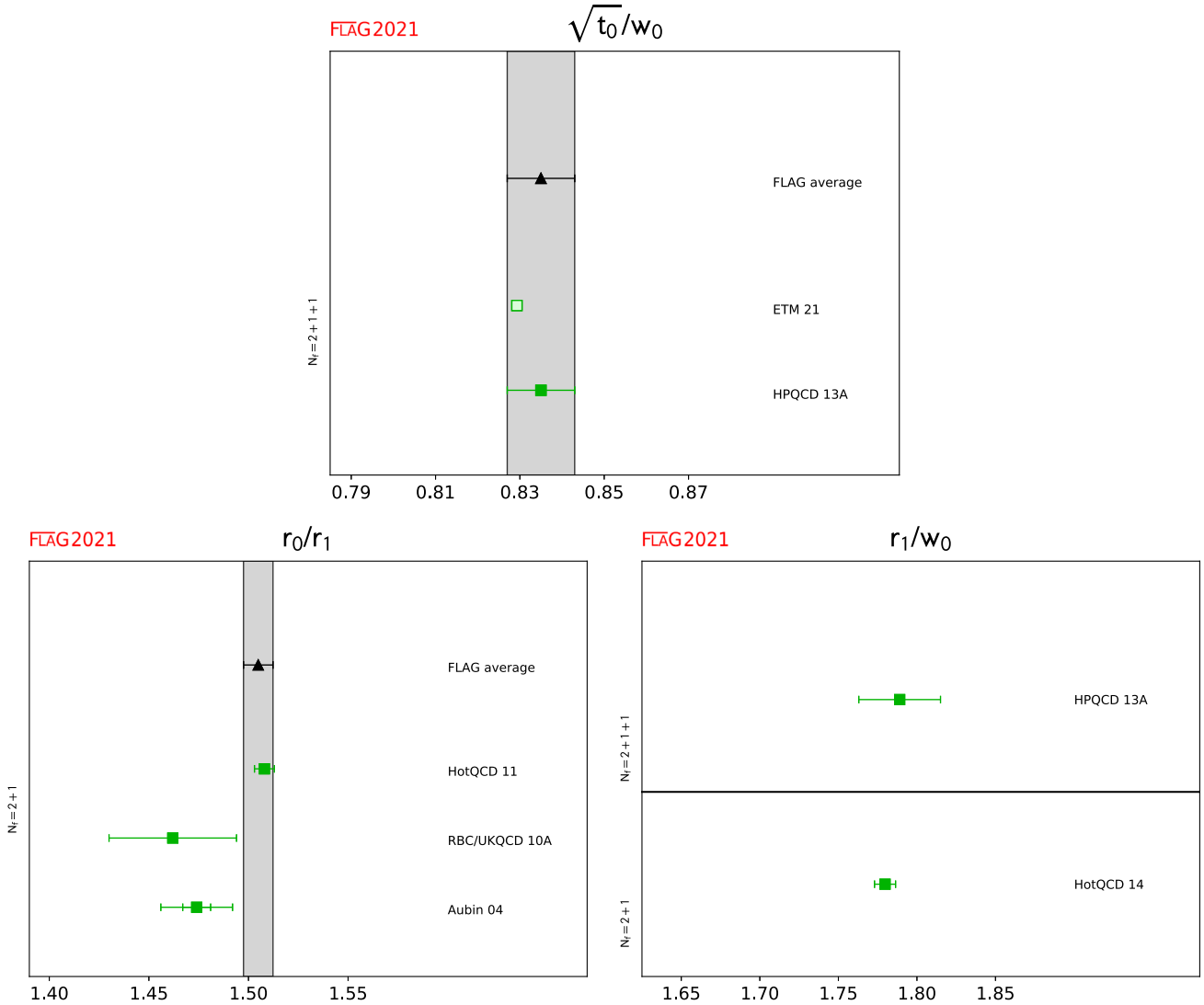

Fig. 53 Results for dimensionless ratios of scales

For $N_f = 2+1$, we have three calculations from CLS 16 [113], RBC/UKQCD 14B [8], and BMW 12A [114] which all enter the FLAG average. They are all independent computations, so there is no correlation to be taken into account. QCDSF/UKQCD 15B [713] does not contribute to the average, because it is not published.

Performing the weighted and correlated average we obtain

$$N_f = 2+1+1: \quad \sqrt{t_0} = 0.14186(88)\ \text{fm} \quad \text{Refs. [37,111,112]}, \tag{505}$$
$$N_f = 2+1: \quad \sqrt{t_0} = 0.14464(87)\ \text{fm} \quad \text{Refs. [8,113,114]}. \tag{506}$$

We note that for the $N_f = 2+1$ average the stretching factor based on the χ^2-value from the weighted average is 1.25.

Gradient flow scale w_0

For $N_f = 1+1+1+1$, including QED, there is a single calculation, BMW 20 [115] with the result

$$N_f = 1+1+1+1+\text{QED}: \quad w_0 = 0.17236(70)\ \text{fm} \quad \text{Ref. [115]}. \tag{507}$$

For $N_f = 2+1+1$, we have four calculations ETM 21 [305], CalLat 20A [111], MILC 15 [112], and HPQCD 13A [37] fulfilling the FLAG criteria to enter the average. However, ETM 20 is a proceedings contribution, while ETM 21 is not published, hence, they do not contribute to the FLAG average. As discussed above in connection with $\sqrt{t_0}$ we correlate the statistical errors of CalLat 20A, MILC 15, and HPQCD 13A.

For $N_f = 2+1$, we have three calculations RBC/UKQCD 14B [8], HotQCD 14 [116], and BMW 12A [114] that enter the FLAG average. These calculations are independent, and no correlation needs to be taken into account. QCDSF/UKQCD 15B [713] does not contribute to the average, because it is not published.

Performing the weighted and correlated average, we obtain

$$N_f = 2+1+1: \quad w_0 = 0.17128(107)\ \text{fm} \quad \text{Refs. [37,111,112]}, \tag{508}$$
$$N_f = 2+1: \quad w_0 = 0.17355(92)\ \text{fm} \quad \text{Refs. [8,114,116]}. \tag{509}$$

We note that for the $N_f = 2+1$ average, the stretching factor based on the χ^2-value from the weighted average is 1.23.

Isospin-breaking and electromagnetic corrections are expected to be small at the level of present uncertainties. This is also confirmed by the explicit computation by BMW 12A. Therefore, we also perform an average over all $N_f > 2+1$ computations and obtain

$$N_f > 2+1: \quad w_0 = 0.17177(67)\ \text{fm} \quad \text{Refs. [37,111,112,115]}. \tag{510}$$

Potential scale r_0

For $N_f = 2+1+1$, there is currently only one determination of r_0 from ETM 14 [7], namely $r_0 = 0.474(14)$ fm, which, therefore, represents the FLAG average.

For $N_f = 2+1$, all but one calculation fulfill all the criteria to enter the FLAG average. HotQCD 14 [116] is essentially an update of HotQCD 11 [708] by enlarging the set of ensembles used in the computation. Therefore, the result from HotQCD 14 supersedes the one from HotQCD 11 and, hence, we only use the former in the average. The computation of χQCD [24] is based on the configurations produced by RBC/UKQCD 10A [117], and we, therefore, assume a 100% correlation between the statistical errors of the two calculations. HPQCD 05B [118] enhances the calculation of Aubin 04 [119] by adding ensembles at a coarser lattice spacing and using the same discretization for the valence fermion. Therefore, we consider the full errors (statistical and systematic) on the results from Aubin 04 and HPQCD 05B to be 100% correlated.

Performing the weighted and correlated average, we obtain

$$N_f = 2+1+1: \quad r_0 = 0.474(14)\ \text{fm} \quad \text{Ref. [7]}, \tag{511}$$
$$N_f = 2+1: \quad r_0 = 0.4701(36)\ \text{fm} \quad \text{Refs. [24,116–119]}. \tag{512}$$

We note that for the $N_f = 2+1$ average, the stretching factor based on the χ^2-value from the weighted average is 1.14.

Potential scale r_1

For $N_f = 2+1+1$, there are two works that fulfill the criteria to enter the FLAG average, namely HPQCD 13A [37] and HPQCD 11B [552]. Both are based on MILC-HISQ ensembles, the former uses eight, the latter only five. The result from HPQCD 13A supersedes the result from HPQCD 11B (in line with a corresponding statement in HPQCD 13A) and forms the FLAG average.

For $N_f = 2+1$, all the results quoted in Table 77 fulfill the FLAG criteria, but not all of them enter the average. The published result from MILC 09 [157] is superseded by the result in the proceedings MILC 10 [41], while MILC 09A [15] is a proceedings contribution and does not enter the average. HPQCD 09B [120] uses HISQ valence quarks instead of asqtad valence quarks as in HPQCD 05B [118]. Therefore, we have RBC/UKQCD 10A [117], MILC 10, HPQCD 09B, HPQCD 05B, and Aubin 04 entering the average. However, since the latter four calculations are based on the aqtad MILC ensembles, we attribute 100% correlation on the statistical error between them and 100% correlation on the systematic error between HPQCD 05B and Aubin 04 as discussed above in connection with r_0.

Performing the weighted and correlated average, we obtain

$$N_f = 2+1+1: \qquad r_1 = 0.3112(30)\ \text{fm} \qquad \text{Ref. [37]}, \tag{513}$$

$$N_f = 2+1: \qquad r_1 = 0.3127(30)\ \text{fm} \qquad \text{Refs. [41,117–120]}. \tag{514}$$

We note that for the $N_f = 2+1$ average the stretching factor based on the χ^2-value from the weighted average is 1.57.

The scales M_{p4s} and f_{p4s}

As mentioned in Sect. 11.5.3, these scales have been used only by the MILC and FNAL/MILC collaborations [16,17,145]. The latest numbers from Ref. [16] are $f_{4ps} = 153.98(11)(^{+2}_{-12})(12)[4]$ MeV and $M_{p4s} = 433.12(14)(^{+17}_{-6})(4)[40]$ MeV and, hence, we have

$$N_f = 2+1+1: \qquad f_{4ps} = 153.98(20)\ \text{MeV} \qquad \text{Ref. [16]}, \tag{515}$$

$$N_f = 2+1+1: \qquad M_{4ps} = 433.12(30)\ \text{MeV} \qquad \text{Ref. [16]}. \tag{516}$$

Dimensionless ratios of scales

We start with the ratio $\sqrt{t_0}/w_0$ for which two $N_f = 2+1+1$ calculations from ETM 21 [305] and HPQCD 13A [37] are available. Since the former is not published, HPQCD 13A forms the FLAG value,

$$N_f = 2+1+1: \qquad \sqrt{t_0}/w_0 = 0.835(8) \qquad \text{Ref. [37]}. \tag{517}$$

For the ratio r_0/r_1 there are three calculations from HotQCD 11 [708], RBC/UKQCD 10A [117], and Aubin 04 [119] available. They all fulfill the FLAG criteria and enter the FLAG average of this ratio,

$$N_f = 2+1: \qquad r_0/r_1 = 1.5049(74) \qquad \text{Refs. [117,119,708]}. \tag{518}$$

We note that the stretching factor based on the χ^2-value from the weighted average is 1.54.

Finally, for the ratio r_1/w_0 there is one computation from HotQCD 14 [116] for $N_f = 2+1+1$, and one from HPQCD 13A [37] for $N_f = 2+1$ fulfilling the FLAG criteria, and, hence, forming the FLAG values

$$N_f = 2+1+1: \qquad r_1/w_0 = 1.789(26) \qquad \text{Ref. [37]}, \tag{519}$$

$$N_f = 2+1: \qquad r_1/w_0 = 1.7797(67) \qquad \text{Ref. [116]}. \tag{520}$$

11.8 Observations and conclusions

The different computations for theory scales reported here are generally in good agreement within each set of 2+1+1 and 2+1 flavour content. Quantitatively, the computed stretching factors are almost all below 1.3, a value which is insignificant considering the small number of computations that enter the averages. The only exception are the potential scales, where the domain-wall fermion results of RBC/UKQCD 10A are above the staggered fermion results, and also the ratio r_0/r_1 needs a stretching factor of 1.54. Of course, the limited number of large-scale QCD simulations that are available means that we

have only a small number of truly independent determinations of the scales. For example, three out of the four computations entering our average for w_0 are based on the same HISQ rooted staggered fermion configurations and thus those differences are only due to the choice of the physical scale (m_Ω vs. f_π), the valence quark action (Möbius domain-wall valence fermions vs. staggered fermions) employed to compute it and different analysis of continuum limit, etc.

Differences between $N_f = 2+1$ and 2+1+1 QCD are small but still larger than expectations [158,159]. A marginally significant difference is indicated by the figure and numbers on w_0 and a larger one by the ones for $\sqrt{t_0}$. The effect of the charm quark is $-1.0(7)\%$ on w_0 and $-1.9(9)\%$ on $\sqrt{t_0}$ as computed from the FLAG averages. In contrast, precision studies of the decoupling of charm quarks predict generic effects of a magnitude of only $\approx 0.2\%$ [158,159] for low energy quantities. We are looking forward to further and more precise results for clarifying whether these $-1.9(9)\%$ hold up over time. In this respect, it is highly desirable for future computations to also publish ratios such as $\sqrt{t_0}/w_0$ where numbers are rare so far.

Such ratios of gradient flow scales are also of high interest in order to better understand the specific discretization errors of gradient flow observables. So far, systematic studies and information on the different contributions (see Sect. 11.5.2 and Ref. [1049]) are missing. A worrying result is, for example, the scale-setting study of Ref. [167] on ratios of scales. The authors find indications that the asymptotic $\sim a^2$ scaling does not set in before $a \approx 0.05$ fm and the $a = 0.04$ fm data has a relevant influence on their continuum extrapolations.

A final word concerns the physics scales that all results depend on. While the mass of the Ω baryon is more popular than the leptonic decay rate of the pion, both have systematics which are difficult to estimate. For the Ω baryon it is the contaminations by excited states and for the decay rates it is the QED effects $\delta f_\pi^{\text{isoQCD}}$. The uncertainty in V_{ud} is *not* relevant at this stage, but means that one is relying more on the standard model being an accurate low energy theory than in the case of the Ω mass. In principle, excited state effects are controlled by just going to large Euclidean time, but, in practice, this yields errors that are too large. One, therefore, performs fits with a very small number of excitations while theoretically there is a multitude of multi-hadron states that are expected to contribute. For the leptonic decay rate of the pion, the situation is quite reversed, namely, the problematic QED contributions have a well-motivated theory: chiral perturbation theory. The needed combination of low-energy constants is not accessible from experiment but its large-N estimate [520] has been (indirectly) confirmed by the recent computation of $\delta f_\pi^{\text{isoQCD}}$ [240]. Unfortunately the same comparison is not so favourable for the leptonic Kaon decay.

Acknowledgements We are very grateful to the external reviewers for providing detailed comments and suggestions on the draft of this review. These reviewers were Gunnar Bali, Claude Bernard, Johann Bijnens, Jérôme Charles, Luigi Del Debbio, Paolo Gambino, Elvira Gámiz, Christian Hoelbling, Marc Knecht, Bira van Kolck, Laurent Lellouch, Zoltan Ligeti, Kim Maltman, Emilie Passemar, Chris Sachrajda, Tilo Wettig, and Takeshi Yamazaki.

The kick-off meeting for the present review was held in February 2020 at the University of Bern and was supported by the Albert Einstein Center for fundamental physics. The mid-review meeting was held virtually in December 2020. We thank our hosts for their hospitality and financial support is gratefully acknowledged.

Members of FLAG were supported by funding agencies; in particular: • Y.A. was supported by JSPS KAKENHI Grant No. 16K05320.
• S.C. acknowledges the support of the European Union's Horizon 2020 research and innovation programme under the Marie Skłodowska-Curie grant agreement no. 813942 (ITN EuroPLEx).
• M.D.M. was supported by DFF Research project 1. Grant n. 8021-00122B.
• P.D. acknowledges support from the European Unions Horizon 2020 research and innovation programme under the Marie Skłodowska-Curie grant agreement No. 813942 (EuroPLEx) and from INFN under the research project INFN-QCDLAT.
• X.F. is supported in part by NSFC of China under Grant No. 11775002, 12070131001, 12125501 and National Key Research and Development Program of China under Contracts No. 2020YFA0406400.
• S.G. acknowledges support from the U.S. Department of Energy through grant DE-SC0010120.
• G.H. and C.P. acknowledge support from the EU H2020-MSCA-ITN-2018-813942 (EuroPLEx), Spanish MICINN grant PGC2018-094857-B-I00, Spanish Agencia Estatal de Investigación through the grant "IFT Centro de Excelencia Severo Ochoa" SEV-2016-0597 and CEX2020-001007-S.
• S.H. is supported in part by JSPS KAKENHI Grant Number 18H03710. S.H. is supported in part by MEXT as "Program for Promoting Researches on the Supercomputer Fugaku" (Simulation for basic science: from fundamental laws of particles to creation of nuclei, JPMXP1020200105) through the Joint Institute for Computational Fundamental Science (JICFuS).
• A.J. received funding from the STFC consolidated grant ST/P000711/1 and ST/ T000775/1.
• T.K. is supported in part by JSPS KAKENHI Grant Number 21H01085. T.K. is supported in part by MEXT as "Program for Promoting Researches on the Supercomputer Fugaku" (Simulation for basic science: from fundamental laws of particles to creation of nuclei, JPMXP1020200105) through the Joint Institute for Computational Fundamental Science (JICFuS).
• S.M. is supported by the U.S. Department of Energy, Office of Science, Office of High Energy Physics under Award Number DE-SC0009913.
• C.J.M. is supported in part by USDOE grant No. DE-AC05-06OR23177, under which Jefferson Science Associates, LLC, manages and operates Jefferson Lab.
• A.P. is supported in part by UK STFC grant ST/P000630/1 and also received funding from the European Research Council (ERC) under the European Union's Horizon 2020 research and innovation programme under grant agreements No 757646 & 813942.
• A.R. is supported by the Generalitat Valenciana through the plan GenT program (CIDEGENT/2019/040) and the Ministerio de Ciencia e Innovacion (PID2020-113644GB-I00).

• S.R.S. is supported in part by the U.S. Department of Energy (grant DE-SC0011637).
• S.S. acknowledges support from the EU H2020-MSCA-ITN-2018-813942 (EuroPLEx).

Data Availability Statement This manuscript has no associated data or the data will not be deposited. [Authors' comment: There is no data.]

Funded by SCOAP^3. SCOAP^3 supports the goals of the International Year of Basic Sciences for Sustainable Development.

A List of acronyms

BχPT	Baryonic chiral perturbation theory
BCL	Bourrely–Caprini–Lellouch
BGL	Boyd–Grinstein–Lebed
BK	Becirevic–Kaidalov
BSM	Beyond standard model
BZ	Ball–Zwicky
χPT	Chiral perturbation theory
CKM	Cabibbo–Kobayashi–Maskawa
CLN	Caprini–Lellouch–Neubert
CP	Charge-parity
CPT	Charge-parity-time reversal
CVC	Conserved vector current
DSDR	Dislocation suppressing determinant ratio
DW	Domain wall
DWF	Domain wall fermion
EDM	Electric dipole moment
EFT	Effective field theory
EM	Electromagnetic
ESC	Excited state contributions
EW	Electroweak
FCNC	Flavor-changing neutral current
FH	Feynman–Hellman
FSE	Finite-size effects
FV	Finite volume
GF	Gradient flow
GGOU	Gambino–Giordano–Ossola–Uraltsev
GRS	Gasser–Rusetsky–Scimemi
HEX	Hypercubic stout
HISQ	Highly-improved staggered quarks
HMχPT	Heavy-meson chiral perturbation theory
HMC	Hybrid Monte Carlo
HMrSχPT	Heavy-meson rooted staggered chiral perturbation theory
HQET	Heavy-quark effective theory
IR	Infrared
isoQCD	Isospin-symmetric QCD
LD	Long distance
LEC	Low-energy constant
LO	Leading order

LW	Lüscher–Weisz
MC	Monte Carlo
MM	Minimal MOM
MOM	Momentum subtraction
$\overline{\text{MS}}$	Modified minimal substraction scheme
NDR	Naive dimensional regularization
nEDM	Nucleon electric dipole moment
NGB	Nambu–Goldstone bosons
NLO	Next-to-leading order
NME	Nucleon matrix elements
NNLO	Next-to-next-to-leading order
NP	Nonperturbative
npHQET	Nonperturbative heavy-quark effective theory
NRQCD	Nonrelativistic QCD
NSPT	Numerical stochastic perturbation theory
OPE	Operator product expansion
PCAC	Partially-conserved axial current
PDF	Parton distribution function
PDG	Particle data group
QCD	Quantum chromodynamics
QED	Quantum electrodynamics
QED_L	Formulation of QED in finite volume (see [179])
QED_TL	Formulation of QED in finite volume (see [1056])
RG	Renormalization group
RGI	Renormalization group invariant
RH	R. Hill
RHQ	Relativistic heavy-quark
RHQA	Relativistic heavy-quark action
RI-MOM	Regularization-independent momentum subtraction (also RI/MOM)
RI-SMOM	Regularization-independent symmetric momentum (also RI/SMOM)
RMS	Root mean square
SχPT	Staggered chiral perturbation theory
SD	Short distance
SF	Schrödinger functional
SIDIS	Semi-inclusive deep-inelastic scattering
SM	Standard model
SSF	Step-scaling function
SUSY	Supersymmetric
SW	Sheikholeslami–Wohlert
UT	Unitarity triangle
UV	Ultraviolet

B Appendix

B.1 Parameterizations of semileptonic form factors

In this section, we discuss the description of the q^2-dependence of form factors, using the vector form factor f_+ of $B \to \pi \ell \nu$ decays as a benchmark case. Since in this channel the parameterization of the q^2-dependence is crucial for the extraction of $|V_{ub}|$ from the existing measurements (involving decays to light leptons), as explained above, it has been studied in great detail in the literature. Some comments about the generalization of the techniques involved will follow.

The vector form factor for $B \to \pi\ell\nu$ All form factors are analytic functions of q^2 outside physical poles and inelastic threshold branch points; in the case of $B \to \pi\ell\nu$, the only pole expected below the $B\pi$ production region, starting at $q^2 = t_+ = (m_B + m_\pi)^2$, is the B^*. A simple ansatz for the q^2-dependence of the $B \to \pi\ell\nu$ semileptonic form factors that incorporates vector-meson dominance is the Bečirević–Kaidalov (BK) parameterization [500], which for the vector form factor reads:

$$f_+(q^2) = \frac{f(0)}{(1 - q^2/m_{B^*}^2)(1 - \alpha q^2/m_{B^*}^2)}. \tag{521}$$

Because the BK ansatz has few free parameters, it has been used extensively to parameterize the shape of experimental branching-fraction measurements and theoretical form-factor calculations. A variant of this parameterization proposed by Ball and Zwicky (BZ) adds extra pole factors to the expressions in Eq. (521) in order to mimic the effect of multiparticle states [1057]. A similar idea, extending the use of effective poles also to $D \to \pi\ell\nu$ decays, is explored in Ref. [1058]. Finally, yet another variant (RH) has been proposed by Hill in Ref. [568]. Although all of these parameterizations capture some known properties of form factors, they do not manifestly satisfy others. For example, perturbative QCD scaling constrains the behaviour of f_+ in the deep Euclidean region [1059–1061], and angular momentum conservation constrains the asymptotic behaviour near thresholds – e.g., Im $f_+(q^2) \sim (q^2 - t_+)^{3/2}$ (see, e.g., Ref. [1062]). Most importantly, these parameterizations do not allow for an easy quantification of systematic uncertainties.

A more systematic approach that improves upon the use of simple models for the q^2 behaviour exploits the positivity and analyticity properties of two-point functions of vector currents to obtain optimal parameterizations of form factors [569,664, 1061,1063–1066]. Any form factor f can be shown to admit a series expansion of the form

$$f(q^2) = \frac{1}{B(q^2)\phi(q^2, t_0)} \sum_{n=0}^{\infty} a_n(t_0)\, z(q^2, t_0)^n, \tag{522}$$

where the squared momentum transfer is replaced by the variable

$$z(q^2, t_0) = \frac{\sqrt{t_+ - q^2} - \sqrt{t_+ - t_0}}{\sqrt{t_+ - q^2} + \sqrt{t_+ - t_0}}. \tag{523}$$

This is a conformal transformation, depending on an arbitrary real parameter $t_0 < t_+$, that maps the q^2 plane cut for $q^2 \geq t_+$ onto the disk $|z(q^2, t_0)| < 1$ in the z complex plane. The function $B(q^2)$ is called the *Blaschke factor*, and contains poles and cuts below t_+ – for instance, in the case of $B \to \pi$ decays,

$$B(q^2) = \frac{z(q^2, t_0) - z(m_{B^*}^2, t_0)}{1 - z(q^2, t_0) z(m_{B^*}^2, t_0)} = z(q^2, m_{B^*}^2). \tag{524}$$

Finally, the quantity $\phi(q^2, t_0)$, called the *outer function*, is some otherwise arbitrary function that does not introduce further poles or branch cuts. The crucial property of this series expansion is that the sum of the squares of the coefficients

$$\sum_{n=0}^{\infty} a_n^2 = \frac{1}{2\pi i} \oint \frac{dz}{z} |B(z)\phi(z) f(z)|^2, \tag{525}$$

is a finite quantity. Therefore, by using this parameterization an absolute bound to the uncertainty induced by truncating the series can be obtained. The aim in choosing ϕ is to obtain a bound that is useful in practice, while (ideally) preserving the correct behaviour of the form factor at high q^2 and around thresholds.

The simplest form of the bound would correspond to $\sum_{n=0}^{\infty} a_n^2 = 1$. *Imposing* this bound yields the following "standard" choice for the outer function

$$\begin{aligned} \phi(q^2, t_0) = &\sqrt{\frac{1}{32\pi\, \chi_{1^-}(0)}} \left(\sqrt{t_+ - q^2} + \sqrt{t_+ - t_0}\right) \\ &\times \left(\sqrt{t_+ - q^2} + \sqrt{t_+ - t_-}\right)^{3/2} \left(\sqrt{t_+ - q^2} + \sqrt{t_+}\right)^{-5} \frac{t_+ - q^2}{(t_+ - t_0)^{1/4}}, \end{aligned} \tag{526}$$

where $t_- = (m_B - m_\pi)^2$, and $\chi_{1^-}(0)$ is the derivative of the transverse component of the polarization function (i.e., the Fourier transform of the vector two-point function) $\Pi_{\mu\nu}(q)$ at Euclidean momentum $Q^2 = -q^2 = 0$. It is computed perturbatively, using operator product expansion techniques, by relating the $B \to \pi\ell\nu$ decay amplitude to $\ell\nu \to B\pi$ inelastic scattering via crossing symmetry and reproducing the correct value of the inclusive $\ell\nu \to X_b$ amplitude. We will refer to the series parameterization with the outer function in Eq. (526) as Boyd, Grinstein, and Lebed (BGL). The perturbative and OPE truncations imply that the bound is not strict, and one should take it as

$$\sum_{n=0}^{N} a_n^2 \lesssim 1, \tag{527}$$

where this holds for any choice of N. Since the values of $|z|$ in the kinematical region of interest are well below 1 for judicious choices of t_0, this provides a very stringent bound on systematic uncertainties related to truncation for $N \geq 2$. On the other hand, the outer function in Eq. (526) is somewhat unwieldy and, more relevantly, spoils the correct large q^2 behaviour and induces an unphysical singularity at the $B\pi$ threshold.

A simpler choice of outer function has been proposed by Bourrely, Caprini and Lellouch (BCL) in Ref. [1062], which leads to a parameterization of the form

$$f_+(q^2) = \frac{1}{1 - q^2/m_{B^*}^2} \sum_{n=0}^{N} a_n^+(t_0) z(q^2, t_0)^n. \tag{528}$$

This satisfies all the basic properties of the form factor, at the price of changing the expression for the bound to

$$\sum_{j,k=0}^{N} B_{jk}(t_0) a_j^+(t_0) a_k^+(t_0) \leq 1. \tag{529}$$

The constants B_{jk} can be computed and shown to be $|B_{jk}| \lesssim \mathcal{O}(10^{-2})$ for judicious choices of t_0; therefore, one again finds that truncating at $N \geq 2$ provides sufficiently stringent bounds for the current level of experimental and theoretical precision. It is actually possible to optimize the properties of the expansion by taking

$$t_0 = t_{\text{opt}} = (m_B + m_\pi)(\sqrt{m_B} - \sqrt{m_\pi})^2, \tag{530}$$

which for physical values of the masses results in the semileptonic domain being mapped onto the symmetric interval $|z| \lesssim 0.279$ (where this range differs slightly for the $B^\pm$ and B^0 decay channels), minimizing the maximum truncation error. If one also imposes that the asymptotic behaviour $\text{Im}\, f_+(q^2) \sim (q^2 - t_+)^{3/2}$ near threshold is satisfied, then the highest-order coefficient is further constrained as

$$a_N^+ = -\frac{(-1)^N}{N} \sum_{n=0}^{N-1} (-1)^n\, n\, a_n^+. \tag{531}$$

Substituting the above constraint on a_N^+ into Eq. (528) leads to the constrained BCL parameterization

$$f_+(q^2) = \frac{1}{1 - q^2/m_{B^*}^2} \sum_{n=0}^{N-1} a_n^+ \left[z^n - (-1)^{n-N} \frac{n}{N} z^N \right], \tag{532}$$

which is the standard implementation of the BCL parameterization used in the literature.

Parameterizations of the BGL and BCL kind, to which we will refer collectively as "z-parameterizations", have already been adopted by the BaBar and Belle collaborations to report their results, and also by the Heavy Flavour Averaging Group (HFAG, later renamed HFLAV). Some lattice collaborations, such as FNAL/MILC and ALPHA, have already started to report their results for form factors in this way. The emerging trend is to use the BCL parameterization as a standard way of presenting results for the q^2-dependence of semileptonic form factors. Our policy will be to quote results for z-parameterizations when the latter are provided in the paper (including the covariance matrix of the fits); when this is not the case, but the published form factors include the full correlation matrix for values at different q^2, we will perform our own fit to the constrained BCL ansatz in Eq. (532); otherwise no fit will be quoted. We however stress the importance of providing, apart from parameterization

coefficients, values for the form factors themselves (in the continuum limit and at physical quark masses) for a number of values of q^2, so that the results can be independently parameterized by the readers if so wished.

The scalar form factor for $B \to \pi \ell \nu$ The discussion of the scalar $B \to \pi$ form factor is very similar. The main differences are the absence of a constraint analogue to Eq. (531) and the choice of the overall pole function. In our fits we adopt the simple expansion:

$$f_0(q^2) = \sum_{n=0}^{N-1} a_n^0 \, z^n \,. \tag{533}$$

We do impose the exact kinematical constraint $f_+(0) = f_0(0)$ by expressing the a_{N-1}^0 coefficient in terms of all remaining a_n^+ and a_n^0 coefficients. This constraint introduces important correlations between the a_n^+ and a_n^0 coefficients; thus only lattice calculations that present the correlations between the vector and scalar form factors can be used in an average that takes into account the constraint at $q^2 = 0$.

Finally we point out that we do not need to use the same number of parameters for the vector and scalar form factors. For instance, with $(N^+ = 3, N^0 = 3)$ we have $a_{0,1,2}^+$ and $a_{0,1}^0$, while with $(N^+ = 3, N^0 = 4)$ we have $a_{0,1,2}^+$ and $a_{0,1,2}^0$ as independent fit parameters. In our average we will choose the combination that optimizes uncertainties.

Extension to other form factors The discussion above largely extends to form factors for other semileptonic transitions (e.g., $B_s \to K$ and $B_{(s)} \to D_{(s)}^{(*)}$, and semileptonic D and K decays). Details are discussed in the relevant sections.

A general discussion of semileptonic meson decay in this context can be found, e.g., in Ref. [1067]. Extending what has been discussed above for $B \to \pi$, the form factors for a generic $H \to L$ transition will display a cut starting at the production threshold t_+, and the optimal value of t_0 required in z-parameterizations is $t_0 = t_+(1 - \sqrt{1 - t_-/t_+})$ (where $t_\pm = (m_H \pm m_L)^2$). For unitarity bounds to apply, the Blaschke factor has to include all sub-threshold poles with the quantum numbers of the hadronic current – i.e., vector (resp. scalar) resonances in $B\pi$ scattering for the vector (resp. scalar) form factors of $B \to \pi$, $B_s \to K$, or $\Lambda_b \to p$; and vector (resp. scalar) resonances in $B_c\pi$ scattering for the vector (resp. scalar) form factors of $B \to D$ or $\Lambda_b \to \Lambda_c$.[88] Thus, as emphasized above, the control over systematic uncertainties brought in by using z-parameterizations strongly depends on implementation details. This has practical consequences, in particular, when the resonance spectrum in a given channel is not sufficiently well-known. Caveats may also apply for channels where resonances with a nonnegligible width appear. A further issue is whether $t_+ = (m_H + m_L)^2$ is the proper choice for the start of the cut in cases such as $B_s \to K \ell \nu$ and $B \to D \ell \nu$, where there are lighter two-particle states that project on the current (B,π and B_c,π for the two processes, respectively).[89] In any such situation, it is not clear a priori that a given z-parameterization will satisfy strict bounds, as has been seen, e.g., in determinations of the proton charge radius from electron-proton scattering [1068–1070].

The HPQCD collaboration pioneered a variation on the z-parameterization approach, which they refer to as a "modified z-expansion," that is used to simultaneously extrapolate their lattice simulation data to the physical light-quark masses and the continuum limit, and to interpolate/extrapolate their lattice data in q^2. This entails allowing the coefficients a_n to depend on the light-quark masses, squared lattice spacing, and, in some cases the charm-quark mass and pion or kaon energy. Because the modified z-expansion is not derived from an underlying effective field theory, there are several potential concerns with this approach that have yet to be studied. The most significant is that there is no theoretical derivation relating the coefficients of the modified z-expansion to those of the physical coefficients measured in experiment; it therefore introduces an unquantified model dependence in the form-factor shape. As a result, the applicability of unitarity bounds has to be examined carefully. Related to this, z-parameterization coefficients implicitly depend on quark masses, and particular care should be taken in the event that some state can move across the inelastic threshold as quark masses are changed (which would in turn also affect the form of the Blaschke factor). Also, the lattice-spacing dependence of form factors provided by Symanzik effective theory techniques may not extend trivially to z-parameterization coefficients. The modified z-expansion is now being utilized by collaborations other than HPQCD and for quantities other than $D \to \pi \ell \nu$ and $D \to K \ell \nu$, where it was originally employed. We advise treating results that utilize the modified z-expansion to obtain form-factor shapes and CKM matrix elements with caution, however, since the systematics of this approach warrant further study.

[88] A more complicated analytic structure may arise in other cases, such as channels with vector mesons in the final state. We will however not discuss form-factor parameterizations for any such process.

[89] We are grateful to G. Herdoíza, R.J. Hill, A. Kronfeld and A. Szczepaniak for illuminating discussions on this issue.

C Notes

In the following Appendices we provide more detailed information on the simulations used to calculate the quantities discussed in Sects. 3–10. We present this information only for results that are new w.r.t. FLAG 19. For all other results the information is available in the corresponding Appendices B.1–8 in FLAG 19 [4] and B.1–7 of FLAG 16 [3]. The complete information is available on the FLAG website http://flag.unibe.ch [5].

C.1 Notes to Sect. 3 on quark masses

See Tables 79, 80, 81, 82, 83, 84, 85, 86, 87, 88, 89, 90, 91, 92, 93, 94, 95, 96, 97, 98, 99, 100, 101, 102.

Table 79 Continuum extrapolations/estimation of lattice artifacts in determinations of m_{ud}, m_s and, in some cases m_u and m_d, with $N_f = 2+1+1$ quark flavours

Collab.	Ref.	N_f	a [fm]	Description
ETM 21A	[204]	2+1+1	0.07, 0.08, 0.09	Scale set from w_0

Table 80 Continuum extrapolations/estimation of lattice artifacts in determinations of m_{ud}, m_s and, in some cases m_u and m_d, with $N_f = 2+1$ quark flavours

Collab.	Ref.	N_f	a [fm]	Description
ALPHA 19	[18]	2+1	0.05, 0.064, 0.076, 0.086	

Table 81 Chiral extrapolation/minimum pion mass in determinations of m_{ud}, m_s and, in some cases, m_u and m_d, with $N_f = 2+1+1$ quark flavours

Collab.	Ref.	N_f	$M_{\pi,\min}$ [MeV]	Description
ETM 21A	[204]	2+1+1	Physical	

Table 82 Chiral extrapolation/minimum pion mass in determinations of m_{ud}, m_s and, in some cases m_u and m_d, with $N_f = 2+1$ quark flavours

Collab.	Ref.	N_f	$M_{\pi,\min}$ [MeV]	Description
ALPHA 19	[18]	2+1	198	

Table 83 Finite-volume effects in determinations of m_{ud}, m_s and, in some cases m_u and m_d, with $N_f = 2+1+1$ quark flavours

Collab.	Ref.	N_f	L [fm]	$M_{\pi,\min}L$	Description
ETM 21A	[204]	2+1+1	2.5–5.6	3.6	

Table 84 Finite-volume effects in determinations of m_{ud}, m_s and, in some cases m_u and m_d, with $N_f = 2+1$ quark flavours

Collab.	Ref.	N_f	L [fm]	$M_{\pi,\min}L$	Description
ALPHA 19	[18]	2+1	2.4–4.1	$\gtrsim 4.0$	

Table 85 Renormalization in determinations of m_{ud}, m_s and, in some cases m_u and m_d, with $N_f = 2+1+1$ quark flavours

Collab.	Ref.	N_f	Description
ETM 21A	[204]	2+1+1	Nonperturbative (RI/MOM)

Table 86 Renormalization in determinations of m_{ud}, m_s and, in some cases m_u and m_d, with $N_f = 2+1$ quark flavours

Collab.	Ref.	N_f	Description
ALPHA 19	[18]	2+1	Schrödinger functional.

Table 87 Continuum extrapolations/estimation of lattice artifacts in the determinations of m_c with $N_f = 2+1+1$ quark flavours

Collab.	Refs.	N_f	a [fm]	Description
ETM 21A	[204]	2+1+1	0.07, 0.08, 0.09	Scale set from w_0. Twisted mass action for charm quarks
HPQCD 20A	[23]	2+1+1	0.03, 0.042,0.06, 0.09, 0.12	Scale set from w_0 and f_π. HISQ action for charm quarks

Table 88 Continuum extrapolations/estimation of lattice artifacts in the determinations of m_c with $N_f = 2+1$ quark flavours

Collab.	Ref.	N_f	a [fm]	Description
ALPHA 21	[227]	2+1	0.039–0.087 fm	Wilson-clover action for the charm quark
Petreczky 19	[26]	2+1	0.025–0.11 fm	HISQ action for the charm quark. Scale set from r_1 parameter of heavy quark potential and f_π

Table 89 Chiral extrapolation/minimum pion mass in the determinations of m_c with $N_f = 2+1+1$ quark flavours

Collab.	Refs.	N_f	$M_{\pi,\min}$ [MeV]	Description
ETM 21A	[204]	2+1+1	Physical	
HPQCD 20A	[23]	2+1+1	Physical	

Table 90 Chiral extrapolation/minimum pion mass in the determinations of m_c with $N_f = 2+1$ quark flavours

Collab.	Refs.	N_f	$M_{\pi,\min}$ [MeV]	Description
ALPHA 21	[227]	2+1	198	
Petreczky 19	[26]	2+1	161	

Table 91 Finite-volume effects in the determinations of m_c with $N_f = 2+1+1$ quark flavours

Collab.	Refs.	N_f	L [fm]	$M_{\pi,\min}L$	Description
ETM 21A	[204]	2+1+1	2.5–5.6	3.6	
HPQCD 20A	[23]	2+1+1	1.9–5.76	3.8	

Table 92 Finite-volume effects in the determinations of m_c with $N_f = 2+1$ quark flavours

Collab.	Refs.	N_f	L [fm]	$M_{\pi,\min}L$	Description
ALPHA 21	[227]	2+1	2.5–4.0	4.2	
Petreczky 19	[26]	2+1	1.6–5.2	4.2	

Table 93 Renormalization in the determinations of m_c with $N_f = 2+1+1$ quark flavours

Collab.	Refs.	N_f	Description
ETM 21A	[204]	2+1+1	Nonperturbative (RI/MOM)
HPQCD 20A	[23]	2+1+1	Nonperturbative (RI/SMOM)

Table 94 Renormalization in the determinations of m_c with $N_f = 2 + 1$ quark flavours

Collab.	Refs.	N_f	Description
ALPHA 21	[227]	2+1	Schrödinger functional
Petreczky 19	[26]	2+1	Not required

Table 95 Continuum extrapolations/estimation of lattice artifacts in the determinations of m_b with $N_f = 2 + 1 + 1$ quark flavours

Collab.	Ref.	N_f	a [fm]	Description
HPQCD 21	[28]	2+1+1	0.03, 0.042, 0.06, 0.09	Scale set from w_0 and f_π. HISQ action for charm quarks

Table 96 Continuum extrapolations/estimation of lattice artifacts in the determinations of m_b with $N_f = 2 + 1$ quark flavours

Collab.	Ref.	N_f	a [fm]	Description
Petreczky 19	[26]	2+1	0.025–0.11 fm	HISQ action for the charm quark. Scale set from r_1 parameter of heavy quark potential and f_π

Table 97 Chiral extrapolation/minimum pion mass in the determinations of m_b with $N_f = 2 + 1 + 1$ quark flavours

Collab.	Ref.	N_f	$M_{\pi,\min}$ [MeV]
HPQCD 21	[28]	2+1+1	Physical

Table 98 Chiral extrapolation/minimum pion mass in the determinations of m_b with $N_f = 2 + 1$ quark flavours

Collab.	Ref.	N_f	$M_{\pi,\min}$ [MeV]
Petreczky 19	[26]	2+1	161

Table 99 Finite-volume effects in the determinations of m_b with $N_f = 2 + 1 + 1$ quark flavours

Collab.	Ref.	N_f	L [fm]	$M_{\pi,\min}L$
HPQCD 21	[28]	2+1+1	1.9–5.76	3.8

Table 100 Finite-volume effects in the determinations of m_b with $N_f = 2 + 1$ quark flavours

Collab.	Ref.	N_f	L [fm]	$M_{\pi,\min}L$
Petreczky 19	[26]	2+1	1.6–5.2	4.2

Table 101 Lattice renormalization in the determinations of m_b with $N_f = 2 + 1 + 1$ flavours

Collab.	Ref.	N_f	Description
ETM 21A	[204]	2+1+1	Nonperturbative (RI/MOM)

Table 102 Lattice renormalization in the determinations of m_b with $N_f = 2 + 1$ flavours

Collab.	Ref.	N_f	Description
Petreczky 19	[26]	2+1	Not required

C.2 Notes to Sect. 4 on $|V_{ud}|$ and $|V_{us}|$

See Tables 103, 104, 105, 106, 107, 108.

Table 103 Continuum extrapolations/estimation of lattice artifacts in the determinations of $f_+(0)$

Collab.	Refs.	N_f	a [fm]	Description
FNAL/MILC 18	[33]	2+1+1	0.042, 0.06, 0.09, 0.12, 0.15	HISQ quark action. Relative scale through r_1
PACS 19	[294]	2+1	0.085	Nonperturbative $\mathcal{O}(a)$ clover quark action. Scale set from Ξ-baryon mass

Table 104 Chiral extrapolation/minimum pion mass in determinations of $f_+(0)$. The subscripts RMS and $\pi, 5$ in the case of staggered fermions indicate the root-mean-square mass and the Nambu–Goldstone boson mass, respectively

Collab.	Refs.	N_f	$M_{\pi,\min}$ [MeV]	Description
FNAL/MILC 18	[33]	2+1+1	$144_{\mathrm{RMS}}(135_{\pi,5})$	Chiral interpolation through NLO $SU(3)$ PQ staggered χPT with continuum χPT at NNLO. Lightest Nambu–Goldstone mass is 135 MeV and lightest RMS mass is 144 MeV at the same gauge ensemble with $a \simeq 0.06$ fm
PACS 19	[294]	2+1	135	Physical point simulation at a single pion mass 135 MeV

Table 105 Finite-volume effects in determinations of $f_+(0)$. The subscripts RMS and $\pi, 5$ in the case of staggered fermions indicate the root-mean-square mass and the Nambu–Goldstone boson mass, respectively

Collab.	Refs.	N_f	L [fm]	$M_{\pi,\min}L$	Description
FNAL/MILC 18	[33]	2+1+1	2.6–5.8	$4.2_{\mathrm{RMS}}(3.9_{\pi,5})$	The values correspond to $M_{\pi,\mathrm{RMS}} = 144$ MeV and $M_{\pi,5} = 135$ MeV, respectively
PACS 19	[294]	2+1	10.9	7.5	

Table 106 Continuum extrapolations/estimation of lattice artifacts in determinations of f_K/f_π for $N_f = 2+1+1$ simulations

Collab.	Refs.	N_f	a [fm]	Description
ETM 21	[305]	2+1+1	0.07, 0.08, 0.09	Wilson-clover twisted mass quark action. Relative scale through gradient flow scale w_0 and absolute scale trough f_π
CalLat 20	[39]	2+1+1	0.06, 0.09, 0.12, 0.15	Möbius domain-wall valence quarks on gradient-flowed HISQ ensembles. Relative scale through the gradient flow scale w_0

Table 107 Chiral extrapolation/minimum pion mass in determinations of f_K/f_π for $N_f = 2+1+1$ simulations

Collab.	Refs.	N_f	$M_{\pi,\min}$ [MeV]	Description
ETM 21	[305]	2+1+1	134	Chiral extrapolation based on NLO $SU(2)$ χPT
CalLat 20	[39]	2+1+1	157	Chiral extrapolation based on NNLO $SU(3)$ χPT. We quote the root-mean-square (RMS) mass of the valence and valence-sea pions as $M_{\pi,\min}$. The smallest mass is 176 MeV for the HISQ sea pions, which do not enter until NNLO in the χPT expression

Table 108 Finite-volume effects in determinations of f_K/f_π for $N_f = 2+1+1$

Collab.	Refs.	N_f	L [fm]	$M_{\pi,\min}L$	Description
ETM 21	[305]	2+1+1	2.0–5.6	3.8	Three different volumes at $M_\pi = 253$ MeV and $a = 0.08$ fm
CalLat 20	[39]	2+1+1	2.4–7.2	3.8	Three different volumes at $M_\pi = 220$ MeV and $a = 0.12$ fm

C.3 Notes to Sect. 5 on low-energy constants

See Tables 109, 110, 111, 112, 113, 114, 115, 116, 117, 118, 119, 120.

Table 109 Continuum extrapolations/estimation of lattice artifacts in determinations of the $SU(2)$ low-energy constants Σ, F, $\bar{\ell}_4$, $\bar{\ell}_6$, and $SU(3)$ low-energy constants Σ_0, F_0

Collab.	Refs.	N_f	a [fm]	Description
ETM 21A	[204]	2+1+1	0.095, 0.082, 0.069	Scale set by f_π = 130.4(2) MeV
ETM 21	[305]	2+1+1	0.092, 0.080, 0.068	Scale set by f_π = 130.4(2) MeV
χQCD 21	[351]	2+1	0.063, 0.071, 0.084, 0.114	Same configs. as RBC/UKQCD 15E
Wang 16	[353]	2+1	0.113	Same configs. as RBC/UKQCD 08A
ETM 20A	[350]	2	0.0914(15)	Single lattice spacing

Table 110 Continuum extrapolations/estimation of lattice artifacts in determinations of the low-energy constants related to the vector form factor of the pion

Collab.	Refs.	N_f	a [fm] or a^{-1} [GeV]	Description
Gao 21	[375]	2+1	0.04, 0.06, 0.076	One lattice spacing at phys. pt
χQCD 20	[376]	2+1	0.083–0.195	One lattice spacing below 0.1 fm
Feng 19	[377]	2+1	1.015, 1.378, 1.730	$a > 0.1$ fm

Table 111 Continuum extrapolations/estimation of lattice artifacts in determinations of the low-energy constants related to $\pi\pi$ scattering

Collab.	Refs.	N_f	a [fm]	Description
ETM 20B	[392]	2	0.0914(15)	Single lattice spacing
Mai 19	[391]	2	0.12	Single lattice spacing
Culver 19	[390]	2	0.12	Single lattice spacing

Table 112 Continuum extrapolations/estimation of lattice artifacts in determinations of the low-energy constants related to πK scattering

Collab.	Refs.	N_f	a [fm]	Description
ETM 18B	[96]	2+1+1	0.089, 0.082, 0.062	Same configuration with ETM 17G
ETM 17G	[97]	2+1+1	0.089, 0.082, 0.062	Scale set by the Sommer parameter r_0
PACS-CS 13	[344]	2+1	0.09	Single lattice spacing
Fu 11A	[399]	2+1	0.15	Single lattice spacing
NPLQCD 07B	[401]	2+1	0.09, 0.125	Configurations generated by MILC
NPLQCD 06B	[349]	2+1	0.125	Single lattice spacing

Table 113 Chiral extrapolation/minimum pion mass in determinations of the $SU(2)$ low-energy constants Σ, F, $\bar{\ell}_4$, $\bar{\ell}_6$, and $SU(3)$ low-energy constants Σ_0, F_0

Collab.	Refs.	N_f	$M_{\pi,\text{min}}$ [MeV]	Description
ETM 21A	[204]	2+1+1	134	4 pion masses in [134, 346] MeV
ETM 21	[305]	2+1+1	135	4 pion masses in [134, 346] MeV
χQCD 21	[351]	2+1	139	3 pion masses with different a
Wang 16	[353]	2+1	220	8 (3) pion masses in val (sea) sector
ETM 20A	[350]	2	132	

Table 114 Chiral extrapolation/minimum pion mass in determinations of the low-energy constants related to the vector form factor of the pion

Collab.	Refs.	N_f	$M_{\pi,\min}$ [MeV]	Description
Gao 21	[375]	2+1	140	
χQCD 20	[376]	2+1	139	
Feng 19	[377]	2+1	$\sim$ 135	

Table 115 Chiral extrapolation/minimum pion mass in determinations of the low-energy constants related to $\pi\pi$ scattering

Collab.	Refs.	N_f	$M_{\pi,\min}$ [MeV]	Description
ETM 20B	[392]	2	134	2 pion masses
Mai 19	[391]	2	224	
Culver 19	[390]	2	226	2 pion masses

Table 116 Chiral extrapolation/minimum pion mass in determinations of the low-energy constants related to πK scattering

Collab.	Refs.	N_f	$M_{\pi,\min}$ [MeV]	Description
ETM 18B	[96]	2+1+1	276	5 pion masses in [230, 450] MeV
ETM 17G	[97]	2+1+1	276	5 pion masses in [230, 450] MeV
PACS-CS 13	[344]	2+1	166	5 pion masses in [166, 707] MeV
Fu 11A	[399]	2+1	590 (RMS)	6 valence pion masses
NPLQCD 07B	[401]	2+1	413 (RMS)	4 pion masses
NPLQCD 06B	[349]	2+1	488 (RMS)	4 pion masses

Table 117 Finite-volume effects in determinations of the $SU(2)$ low-energy constants Σ, F, $\bar{\ell}_4$, $\bar{\ell}_6$, and $SU(3)$ low-energy constants Σ_0, F_0

Collab.	Refs.	N_f	L [fm]	#V
ETM 21A	[204]	2+1+1	5.52	2
ETM 21	[305]	2+1+1	5.55	2
χQCD 21	[351]	2+1	5.4	2 at physical point.
Wang 16	[353]	2+1	2.7	1
ETM 20A	[350]	2	4.39	2

Table 118 Finite-volume effects in determinations of the low-energy constants related to the vector form factor of the pion

Collab.	Refs.	N_f	L [fm]	#V
Gao 21	[375]	2+1	4.86	1
χQCD 20	[376]	2+1	6.24	3
Feng 19	[377]	2+1	6.22	3

Table 119 Finite-volume effects in determinations of the low-energy constants related to $\pi\pi$ scattering

Collab.	Refs.	N_f	L [fm]	#V
ETM 20B	[392]	2	2.92	2
Mai 19	[391]	2	2.88	1
Culver 19	[390]	2	2.88	3

Table 120 Finite-volume effects in determinations of the low-energy constants related to πK scattering

Collab.	Refs.	N_f	L [fm]	#V
ETM 18B	[96]	2+1+1	2.832	2
ETM 17G	[97]	2+1+1	2.832	2
PACS-CS 13	[344]	2+1	2.9	1
Fu 11A	[399]	2+1	2.4	1
NPLQCD 07B	[401]	2+1	2.52	2
NPLQCD 06B	[349]	2+1	2.5	2

C.4 Notes to Sect. 6 on kaon mixing

C.4.1 $K \to \pi\pi$ decay amplitudes

See Tables 121, 122, 123, 124.

Table 121 Continuum extrapolations/estimation of lattice artifacts in determinations of the $K \to \pi\pi$ decay amplitudes

Collab.	Refs.	N_f	a [fm]	Description
RBC/UKQCD 20	[429]	2+1	0.143	Single lattice spacing
RBC/UKQCD 15G	[430]	2+1	0.143	Single lattice spacing
RBC/UKQCD 15F	[46]	2+1	0.114, 0.084	Combined chiral-continuum fit based on two values of the lattice spacing. Systematic error associated with the extrapolation to the continuum limit is negligible with respect to the statistical errors

Table 122 Chiral extrapolation/minimum pion mass in determinations of the $K \to \pi\pi$ decay amplitudes

Collab.	Refs.	N_f	$M_{\pi,\mathrm{min}}$ [MeV]	Description
RBC/UKQCD 20	[429]	2+1	142.3	Single pion mass value, close to the physical point
RBC/UKQCD 15G	[430]	2+1	143.1	Single pion mass value, close to the physical point
RBC/UKQCD 15F	[46]	2+1	139.1, 139.2	Single pion mass value – close to the physical point – at each of the two values of the lattice spacing

Table 123 Finite volume effects in determinations of the $K \to \pi\pi$ decay amplitudes

Collab.	Refs.	N_f	L [fm]	$M_{\pi,\mathrm{min}} L$	Description
RBC/UKQCD 20	[429]	2+1	4.6	3.3	Finite volume effects amount to a 7% systematic error contribution to the final error budget of A_0
RBC/UKQCD 15G	[430]	2+1	4.6	3.3	Finite volume effects amount to a 7% systematic error contribution to the final error budget of A_0
RBC/UKQCD 15F	[46]	2+1	5.5, 5.4	3.8	Finite volume effects amount to a 3.5% systematic error contribution to the error budget of $\mathrm{Im}(A_2)/\mathrm{Re}(A_2)$

Table 124 Running and matching in determinations of the $K \to \pi\pi$ decay amplitudes

Collab.	Refs.	N_f	Ren.	Running match	Description
RBC/UKQCD 20	[429]	2+1	RI	PT1ℓ	Two different RI-SMOM schemes are used. The relative systematic errors due to the renormalisation of the relevant operators amount to 4%, while those arising from the computation of the Wilson coefficients in the $\overline{\text{MS}}$ scheme correspond to 12%
RBC/UKQCD 15G	[430]	2+1	RI	PT1ℓ	Two different RI-SMOM schemes are used. The relative systematic errors due to the renormalisation of the relevant operators amount to 15%, while those arising from the computation of the Wilson coefficients in the $\overline{\text{MS}}$ scheme correspond to 12%
RBC/UKQCD 15F	[46]	2+1	RI	PT1ℓ	Two different RI-SMOM schemes are used. The relative systematic errors for the conversion to $\overline{\text{MS}}$ are 2.9% for ReA_0 and 7% for ImA_0

C.4.2 Kaon B-parameter B_K

No new calculations w.r.t. the previous FLAG report.

C.4.3 Kaon BSM B-parameters

No new calculations w.r.t. the previous FLAG report.

C.5 Notes to Sect. 7 on D-meson decay constants and form factors

See Tables 125, 126, 127, 128, 129, 130, 131, 132, 133, 134.

Table 125 Chiral extrapolation/minimum pion mass in $N_f = 2 + 1$ determinations of the D- and D_s-meson decay constants. For actions with multiple species of pions, masses quoted are the RMS pion masses. The different $M_{\pi,\text{min}}$ entries correspond to the different lattice spacings

Collab.	Refs.	N_f	$M_{\pi,\text{min}}$ [MeV]	Description
χQCD 20A	[482]	2+1	114	Simulations are performed very close to the physical point and linear interpolations/extrapolations are used to correct for mismatches
RBC/UKQCD 17, RBC/UKQCD 18A	[55,70]	2+1	139, 139, 232	The lattice spacing, pion-mass and charm-quark mass dependences are fit simultaneously through a Taylor expansion in a^2, $(m_\pi^2 - m_\pi^{2phys})$ and $1/m_H - 1/m_{D_{(s)}}$

Table 126 Chiral extrapolation/minimum pion mass in $N_f = 2$ determinations of the D- and D_s-meson decay constants. For actions with multiple species of pions, masses quoted are the RMS pion masses. The different $M_{\pi,\text{min}}$ entries correspond to the different lattice spacings

Collab.	Refs.	N_f	$M_{\pi,\text{min}}$ [MeV]	Description
Blossier 18, Balasubramanian 19	[58,479]	2	282, 194, 269	Linear fits (in m_π^2 and in a^2) are used in the combined chiral/continuum extrapolation. NLO HMχPT expressions are used for a cross-check, concluding however that there are not enough data points to be sensitive to the NLO terms

Table 127 Finite-volume effects in $N_f = 2+1$ determinations of the D- and D_s-meson decay constants. Each L-entry corresponds to a different lattice spacing, with multiple spatial volumes at some lattice spacings. For actions with multiple species of pions, the lightest masses are quoted

Collab.	Refs.	N_f	L [fm]	$M_{\pi,\min}L$	Description
χQCD 20A	[482]	2+1	5.5	3.2	No explicit discussion of FSE
RBC/UKQCD 17, RBC/UKQCD 18A	[55,70]	2+1	5.5/2.7, 5.4/2.7, 3.4	3.86, 3.78, 4.11	FV errors estimated to be at the permille level by either comparing values of $m_\pi L$ to the study of FSE by MILC in [17] or by 1-loop HMχPT

Table 128 Finite-volume effects in $N_f = 2$ determinations of the D- and D_s-meson decay constants. Each L-entry corresponds to a different lattice spacing, with multiple spatial volumes at some lattice spacings. For actions with multiple species of pions, the lightest masses are quoted

Collab.	Refs.	N_f	L [fm]	$M_{\pi,\min}L$	Description
Blossier 18, Balasubramanian 19	[58,479]	2	2.4/3.6, 2.1/3.1/4.2, 2.3/3.1	5.2, 4.1, 4.2	No explicit discussion of FV effects, but $m_\pi L > 4$ always

Table 129 Lattice spacings and description of actions used in $N_f = 2+1$ determinations of the D- and D_s-meson decay constants

Collab.	Refs.	N_f	a [fm]	Continuum extrapolation	Scale Setting
χQCD 20A	[482]	2+1	0.115	Cutoff effects are estimated to be 2% by comparing the result for f_{D_s} with the one obtained in [24]	m_Ω used for scale setting by RBC/UKQCD, which produced the ensemble
RBC/UKQCD 17, RBC/UKQCD 18A	[55,70]	2+1	0.11, 0.08, 0.07	The lattice spacing, pion-mass and charm-quark mass dependences are fit simultaneously through a Taylor expansion in a^2, $(m_\pi^2 - m_\pi^{2phys})$ and $1/m_H - 1/m_{D_{(s)}}$	The lattice scale and physical light-quark masses have been determined using m_π, m_K and m_Ω as inputs

Table 130 Lattice spacings and description of actions used in $N_f = 2$ determinations of the D- and D_s-meson decay constants

Collab.	Refs.	N_f	a [fm]	Continuum extrapolation	Scale Setting
Blossier 18, Balasubramanian 19	[58,479]	2	0.075, 0.065, 0.048	Linear fits (in m_π^2 and in a^2) are used in the combined chiral/continuum extrapolation	Scale set through f_K

Table 131 Operator renormalization in $N_f = 2+1$ determinations of the D- and D_s-meson decay constants

Collab.	Refs.	N_f	Ren.	Description
χQCD 20A	[482]	2+1	RI	The decay constants are extracted from an exact lattice Ward identity or from NP renormalized operators
RBC/UKQCD 17, RBC/UKQCD 18A	[55,70]	2+1	mNPR	The local current is renormalized nonperturbatively for the case of the unmixed action; however in the actual computation the domain wall height is chosen differently in the valence than in the sea and the effect of that on the renormalization constant is estimated to be 0.4% through a study in the RI/SMOM scheme

Table 132 Operator renormalization in $N_f = 2$ determinations of the D- and D_s-meson decay constants

Collab.	Refs.	N_f	Ren.	Description
Blossier 18, Balasubramanian 19	[58,479]	2	SF	NP renormalization and improvement of the axial current (am terms included at 1-loop)

Table 133 Heavy-quark treatment in $N_f = 2 + 1$ determinations of the D- and D_s-meson decay constants

Collab.	Refs.	N_f	Action	Description
χQCD 20A	[482]	2+1	Overlap on DW	$am_c \approx 0.73$ set by using m_{D_s}
RBC/UKQCD 17, RBC/UKQCD 18A	[55,70]	2+1	Möbius-DWF on Shamir-DWF or Möbius-DWF	$0.18 < am_h < 0.4$. Charm discretization errors estimated using different ways to define the charm quark mass (through D, D_s or η_c) in the global fits

Table 134 Heavy-quark treatment in $N_f = 2$ determinations of the D- and D_s-meson decay constants

Collab.	Refs.	N_f	Action	Description
Blossier 18, Balasubramanian 19	[58,479]	2	npSW	$am_c \leq 0.32$. Axial current nonperturbatively improved (O(am) at 1-loop)

C.5.1 Form factors for semileptonic decays of charmed hadrons

See Tables 135, 136, 137, 138, 139.

Table 135 Continuum extrapolations/estimation of lattice artifacts in $N_f = 2 + 1 + 1$ determinations of form factors for semileptonic decays of charmed hadrons

Collab.	Refs.	N_f	a [fm]	Continuum extrapolation	Scale setting
HPQCD 21A	[61]	2+1+1	0.042, 0.06, 0.09, 0.12, 0.15	Modified z-expansion fit combining the continuum and chiral extrapolations and the momentum-transfer dependence. Discretization effects assumed dominated by the charm scale. Discretization errors on form factors between 0.4 and 1.2% as a function of the momentum transfer	Scale setting from f_π via the flow quantity w_0 [14,37,1071]
Zhang 21	[517]	2+1	0.080, 0.11	Continuum extrapolation combined with fit to q^2-dependence of form factors in a "modified" z-expansion. Systematics estimated from difference between extrapolated results and results at smallest lattice spacing, and difference between two current renormalization methods	Set from Wilson-flow quantity w_0
HPQCD 20	[510]	2+1+1	0.06, 0.09, 0.12, 0.15	Modified z-expansion fit combining the continuum and chiral extrapolations and the momentum-transfer dependence, and, for the heavy-HISQ spectator b quark, the dependence on $1/m_Q$. The analysis combines data with NRQCD b quarks and data with HISQ heavy quarks	Scale setting from f_π via the flow quantity w_0 [14,37,1071]

Table 136 Chiral extrapolation/minimum pion mass in determinations of form factors for semileptonic decays of charmed hadrons. For actions with multiple species of pions, masses quoted are the RMS pion masses for $N_f = 2+1$ and the Goldstone mode mass for $N_f = 2+1+1$. The different $M_{\pi,\text{min}}$ entries correspond to the different lattice spacings

Collab.	Refs.	N_f	$M_{\pi,\text{min}}$ [MeV]	Description
HPQCD 21A	[61]	2+1+1	315, 329, 129, 132, 131	Modified z-expansion fit combining the continuum and chiral extrapolations and the momentum-transfer dependence. Polynomial dependence on quark masses, supplemented by a pion chiral logarithm. Fit result compared with alternative approach based on cubic splines in q^2
Zhang 21	[517]	2+1	300, 290	Dependence on pion mass neglected. No estimate of resulting systematic uncertainty
HPQCD 20	[510]	2+1+1	329, 316, 132/305, 131/305	Modified z-expansion fit combining the continuum and chiral extrapolations and the momentum-transfer dependence, and, for the heavy-HISQ spectator b quark, the dependence on $1/m_Q$. The analysis combines data with NRQCD b quarks and data with HISQ heavy quarks

Table 137 Finite-volume effects in determinations of form factors for semileptonic decays of charmed hadrons. Each L-entry corresponds to a different lattice spacing, with multiple spatial volumes at some lattice spacings. For actions with multiple species of pions, the lightest pion masses are quoted

Collab.	Refs.	N_f	L [fm]	$M_{\pi,\text{min}} L$	Description
HPQCD 21A	[61]	2+1+1	2.73, 2.72, 2.81/5.62, 2.93/5.87, 2.45/4.89	$\gtrsim 3.7$	Finite volume correction included in chiral fit, claimed to be a negligible effect. Effect of frozen topology in finest ensemble not discussed
Zhang 21	[517]	2+1+1	2.6, 2.6	$\gtrsim 3.8$	No discussion of finite-volume effects
HPQCD 20	[510]	2+1+1	2.72, 2.81, 2.93/5.87, 2.45/4.89	$\gtrsim 3.8$	Physical point ensemble at $a \simeq 0.15$ fm has $m_\pi L = 3.3$; the statement $m_\pi L \gtrsim 3.8$ applies to the other five ensembles

Table 138 Operator renormalization in determinations of form factors for semileptonic decays of charmed hadrons

Collab.	Refs.	N_f	Ren.	Description
HPQCD 21A	[61]	2+1+1	NP	Vector current normalized by imposing Ward identity at zero recoil
Zhang 21	[517]	2+1	NP	Local vector current renormalized using ratio to conserved vector current. Axial current renormalized using ratio of off-shell quark matrix elements
HPQCD 20	[510]	2+1+1	NP	Vector current normalized by imposing Ward identity at zero recoil

Table 139 Heavy-quark treatment in determinations of form factors for semileptonic decays of charmed hadrons

Collab.	Refs.	N_f	Action	Description
HPQCD 21A	[61]	2+1+1	HISQ	Bare charm-quark mass $0.194 \lesssim am_c \lesssim 0.8605$
Zhang 21	[517]	2+1+1	SW	Bare charm-quark mass $0.235 \lesssim am_c \lesssim 0.485$. No $\mathcal{O}(a)$ improvement of currents
HPQCD 20	[510]	2+1+1	Charm: HISQ Bottom (spectator): HISQ and NRQCD	Bare charm-quark HIQS mass $0.274 \lesssim am_c \lesssim 0.827$ Bare bottom-quark HIQS mass $0.274 \lesssim am_b \lesssim 0.8$

C.6 Notes to Sect. 8 on B-meson decay constants, mixing parameters and form factors

C.6.1 $B_{(s)}$-meson decay constants

See Tables 140, 141, 142, 143, 144, 145, 146, 147, 148.

Table 140 Chiral extrapolation/minimum pion mass in determinations of the B- and B_s-meson decay constants for $N_f = 2 + 1$ simulations. For actions with multiple species of pions, masses quoted are the RMS pion masses. The different $M_{\pi,\min}$ entries correspond to the different lattice spacings

Collab.	Ref.	N_f	$M_{\pi,\min}$ [MeV]	Description
RBC/UKQCD 18A	[70]	2+1	139, 139, 232	Three or four light-quark masses per lattice spacing except for the finest lattice spacing. Generic fits to $m_\pi^2 - (m_\pi^{\text{phys}})^2$ and a^2 in the combined chiral-continuum extrapolation, with systematic errors estimated to be from 0.3% to 0.5% in f_{B_s}/f_B

Table 141 Chiral extrapolation/minimum pion mass in determinations of the B- and B_s-meson decay constants for $N_f = 2$ simulations. For actions with multiple species of pions, masses quoted are the RMS pion masses (where available). The different $M_{\pi,\min}$ entries correspond to the different lattice spacings

Collab.	Ref.	N_f	$M_{\pi,\min}$ [MeV]	Description
Balasubramamian 19	[58]	2	282, 194, 269	Two pion masses for the coarsest and finest lattice spacings, and four pion masses for the intermediate lattice spacing. Generic fits to m_π^2 and a^2 in the combined continuum-chiral extrapolation, with systematic effects obtained by including a generic NLO chiral term $m_\pi^2 \log m_\pi^2$. Detailed error budget not provided, but total systematic uncertainty estimated as 1.1–1.2%

Table 142 Finite-volume effects in determinations of the B- and B_s-meson decay constants for $N_f = 2+1$ simulations. Each L-entry corresponds to a different lattice spacing, with multiple spatial volumes at some lattice spacings

Collab.	Ref.	N_f	L [fm]	$M_{\pi,\min}L$	Description
RBC/UKQCD 18A	[70]	2+1	2.65/5.47, 2.65/5.35,3.49	3.86, 3.78, 4.11	Finite-volume effects are estimated to be 0.18% in f_{B_s}/f_B

Table 143 Finite-volume effects in determinations of the B- and B_s-meson decay constants for $N_f = 2$ simulations. Each L-entry corresponds to a different lattice spacing, with multiple spatial volumes at some lattice spacings

Collab.	Ref.	N_f	L [fm]	$M_{\pi,\min}L$	Description
Balasubramamian 19	[58]	2	2.4/3.6, 2.1/3.1/4.2, 2.3/3.1	4.1, 4.1, 4.0	No explicit estimate of FV errors, but expected to be much smaller than other uncertainties

Table 144 Continuum extrapolations/estimation of lattice artifacts in determinations of the B and B_s meson decay constants for $N_f = 2 + 1$ simulations

Collab.	Ref.	N_f	a [fm]	Continuum extrapolation	Scale setting
RBC/UKQCD 18A	[70]	2+1	0.11, 0.084, 0.073	Combined continuum and chiral extrapolation with linear in a^2 term. Systematic errors estimated to be from 0.3% to 0.5% in f_{B_s}/f_B	Scale set by the Ω baryon mass. No estimate for scale uncertainty, but expected to be negligible in f_{B_s}/f_B

Table 145 Description of the renormalization/matching procedure adopted in the determinations of the B- and B_s-meson decay constants for $N_f = 2 + 1$ simulations

Collab.	Ref.	N_f	Ren.	Description
	[70]	2+1	–	Mass-independent operator renormalization cancels in f_{B_s}/f_B

Table 146 Description of the renormalization/matching procedure adopted in the determinations of the B- and B_s-meson decay constants for $N_f = 2$ simulations

Collab.	Ref.	N_f	Ren.	Description
Balasubramamian 19	[58]	2	PT2ℓ	Perturbative coefficient relating HQET and QCD currents included at NNLO in continuum perturbation theory. Systematic uncertainties estimated using fits including only NLO coefficients

Table 147 Heavy-quark treatment in $N_f = 2 + 1$ determinations of the B-and B_s-meson decay constants

Collab.	Ref.	N_f	Action	Description
RBC/UKQCD 18A	[70]	2+1	DWF	Linear extrapolation in inverse heavy quark mass $1/M_H$, with systematic errors estimated, by excluding heaviest and lightest valence quark masses, to be 0.47% in f_{B_s}/f_B. HQ discretization effects are estimated to be 0.01% in f_{B_s}/f_B

Table 148 Heavy-quark treatment in $N_f = 2$ determinations of the B-and B_s-meson decay constants

Collab.	Ref.	N_f	Action	Description
Balasubramamian 19	[58]	2	Wilson	Expansion in inverse of pseudoscalar heavy-strange meson mass, $1/M_{H_s}$. HQ discretization effects included in generic fit linear in $a^2(aM_{H_s})^2$. Detailed error budget not provided, but systematic uncertainty estimated as 1.1–2.3% in f_{B_s}

C.6.2 $B_{(s)}$-meson mixing matrix elements

See Tables 149, 150, 151, 152, 153, 154, 155, 156, 157, 158, 159.

Table 149 Continuum extrapolations/estimation of lattice artifacts in determinations of the neutral B-meson mixing matrix elements for $N_f = 2 + 1 + 1$ simulations

Collab.	Ref.	N_f	a [fm]	Continuum extrapolation	Scale setting
HPQCD 19A	[71]	2+1+1	0.15, 0.12, 0.09	Discretization errors start from $\alpha_s a^2$ and are included in the systematic error. It is estimated as 1.8% for individual bag parameters. Residual $\alpha_s a^2$ and a^4 errors from wrong-spin contributions are subtracted by including them in the chiral fit	Scale setting done using Υ and Υ' mass splitting [552]

Table 150 Continuum extrapolations/estimation of lattice artifacts in determinations of the neutral B-meson mixing matrix elements for $N_f = 2+1$ simulations

Collab.	Ref.	N_f	a [fm]	Continuum extrapolation	Scale setting
RBC/UKQCD 18A	[70]	2+1	0.11, 0.08, 0.07	Combined continuum (a^2) and heavy quark ($1/m_H$) extrapolation with the LO pion mass dependence (m_π^2) in the global fit	Lattice scale and target quark masses are set using Ω, K and π masses [8,55,117]

Table 151 Chiral extrapolation/minimum pion mass in determinations of the neutral B-meson mixing matrix elements. For actions with multiple species of pions, masses quoted are the RMS pion masses (where available). The different $M_{\pi,\mathrm{min}}$ entries correspond to the different lattice spacings

Collab.	Refs.	N_f	$M_{\pi,\mathrm{min}}$ [MeV]	Description
HPQCD 19A	[71]	2+1+1	311, 241, –	Pion mass in the Goldston channel is as small as 130 MeV for two coarser lattices. NLO HMrSχPT is used with NNLO analytic terms and other discretization errors. Staggered wrong-spin contributions are included
RBC/UKQCD 18A	[70]	2+1	139, 139, 234	Combined continuum (a^2) and heavy quark ($1/m_H$) extrapolation with the LO pion mass dependence (m_π^2) in the global fit

Table 152 Finite-volume effects in determinations of the neutral B-meson mixing matrix elements. Each L-entry corresponds to a different lattice spacing, with multiple spatial volumes at some lattice spacings. For actions with multiple species of pions, masses quoted are the RMS pion masses (where available)

Collab.	Refs.	N_f	L [fm]	$M_{\pi,\mathrm{min}}L$	Description
HPQCD 19A	[71]	2+1+1	2.4/3.5/4.6, 2.9/3.8/5.7, 2.8	7.3, 7.0, –	FV error is estimated to be negligible from FV HMχPT
RBC/UKQCD 18A	[70]	2+1	2.7/5.5, 2.6/5.3, 3.5	3.9, 3.8, 4.0	FV error is estimated to be less than 0.18% for $SU(3)$-breaking ratios from FV HMχPT

Table 153 Operator renormalization in determinations of the neutral B-meson mixing matrix elements

Collab.	Refs.	N_f	Ren.	Description
HPQCD 19A	[71]	2+1+1	PT1ℓ	HISQ-NRQCD 4-quark operators are matched through $O(1/M)$ and renormalized to 1-loop: included are those of $O(\alpha_s)$, $O(\Lambda_{\mathrm{QCD}}/M)$, $O(\alpha_s/aM)$, $O(\alpha_s\,\Lambda_{\mathrm{QCD}}/M)$. Remnant error is dominated by $O(\alpha_s\Lambda_{\mathrm{QCD}}/M)$ 2.9% and $O(\alpha_s^2)$ 2.1% for individual bag parameters. Associated error for their SU(3) breaking ratio are negligible
RBC/UKQCD 18A	[70]	2+1	–	Operators are renormalized multiplicatively due to chiral symmetry of DWF. No need to calculate the renormalization factor since only the $SU(3)$ breaking ratios are examined

Table 154 Heavy-quark treatment in determinations of the neutral B-meson mixing matrix elements

Collab.	Refs.	N_f	Action	Description
HPQCD 19A	[71]	2+1+1	NRQCD	See the entry in Table 153
RBC/UKQCD 18A	[70]	2+1	DWF	Domain-wall fermion with 3 stout-smearing extends the reach to heavy mass, allowing to simulate up to half of the b-quark mass. Heavy mass errors on ξ are estimated as 0.8% from fitting range and 0.4% from higher order $(1/M^2)$ by power counting

C.6.3 Form factors entering determinations of $|V_{ub}|$ ($B \to \pi\ell\nu$, $B_s \to K\ell\nu$, $\Lambda_b \to p\ell\bar{\nu}$)

Table 155 Continuum extrapolations/estimation of lattice artifacts in determinations of $B \to \pi\ell\nu$, $B_s \to K\ell\nu$, and $\Lambda_b \to p\ell\bar{\nu}$ form factors

Collab.	Ref.	N_f	a [fm]	Continuum extrapolation	Scale setting
FNAL/MILC 19	[573]	2+1	0.06, 0.09, 0.12	HMrSχPT expansion used at next-to-leading order in $SU(2)$ and leading order in $1/M_B$, including next-to-next-to-leading-order (NNLO) analytic and generic discretization terms. Hard kaons assumed to decouple. Systematic uncertainties estimated by varying fit ansatz and data range. The (stat + chiral extrap + HQ discretization + g_π) uncertainty dominates the error budget, ranging from 2–3% at $q^2 \gtrsim 21$ GeV^2 to up to 8–10% in the lower end of the accessed q^2 interval	Relative scale r_1/a set from the static-quark potential. Absolute scale r_1, including related uncertainty estimates, taken from [54]

Table 156 Chiral extrapolation/minimum pion mass in determinations of $B \to \pi\ell\nu$, $B_s \to K\ell\nu$, and $\Lambda_b \to p\ell\bar{\nu}$ form factors. For actions with multiple species of pions, masses quoted are the RMS pion masses. The different $M_{\pi,\text{min}}$ entries correspond to the different lattice spacings

Collab.	Ref.	N_f	$M_{\pi,\text{min}}$ [MeV]	Description
FNAL/MILC 19	[573]	2+1	255, 277, 456	HMrSχPT expansion used at next-to-leading order in $SU(2)$ and leading order in $1/M_B$, including next-to-next-to-leading-order (NNLO) analytic and generic discretization terms. Hard kaons assumed to decouple. Systematic uncertainties estimated by varying fit ansatz and data range

Table 157 Finite-volume effects in determinations of $B \to \pi\ell\nu$, $B_s \to K\ell\nu$, and $\Lambda_b \to p\ell\bar{\nu}$ form factors. Each L-entry corresponds to a different lattice spacing, with multiple spatial volumes at some lattice spacings. For actions with multiple species of pions, the lightest masses are quoted

Collab.	Ref.	N_f	L [fm]	$M_{\pi,\text{min}}L$	Description
FNAL/MILC 19	[573]	2+1	3.8, 2.5/2.9/3.6/5.8, 2.9	$\gtrsim 3.8$	FV effects estimated by comparing infinite volume integrals with finite sums in HMrSχPT, found to be negligible

Table 158 Operator renormalization in determinations of $B \to \pi\ell\nu$, $B_s \to K\ell\nu$, and $\Lambda_b \to p\ell\bar{\nu}$ form factors

Collab.	Ref.	N_f	Ren.	Description
FNAL/MILC 19	[573]	2+1	mNPR	Perturbative truncation error estimated at 1% with size of 1-loop correction on next-to-finest ensemble

Table 159 Heavy-quark treatment in determinations of $B \to \pi \ell \nu$, $B_s \to K \ell \nu$, and $\Lambda_b \to p \ell \bar{\nu}$ form factors

Collab.	Ref.	N_f	Action	Description
FNAL/MILC 19	[573]	2+1	Fermilab	(See comments for continuum limit extrapolation.)

C.6.4 Form factors for rare decays of beauty hadrons

See Tables 160, 161, 162, 163, 164.

Table 160 Continuum extrapolations/estimation of lattice artifacts in determinations of form factors for rare decays of beauty hadrons

Collab.	Ref.	N_f	a [fm]	Continuum extrapolation	Scale setting
Meinel 20	[648]	2+1	0.0828(3), 0.1106(3)	Combined chiral-continuum extrapolation as part of the expansion of form factor shape in powers of $w - 1$. Systematic uncertainty estimated by repeating fit with added higher-order terms	Scale setting using Ω mass in Ref. [8]

Table 161 Chiral extrapolation/minimum pion mass in determinations of form factors for rare decays of beauty hadrons. For actions with multiple species of pions, masses quoted are the RMS pion masses. The different $M_{\pi,\text{min}}$ entries correspond to the different lattice spacings

Collab.	Ref.	N_f	$M_{\pi,\text{min}}$ [MeV]	Description
Meinel 20	[648]	2+1	303, 340	Combined chiral-continuum extrapolation as part of the expansion of form factor shape in powers of $w - 1$. Systematic uncertainty estimated by repeating fit with added higher-order terms

Table 162 Finite-volume effects in determinations of form factors for rare decays of beauty hadrons. Each L-entry corresponds to a different lattice spacing, with multiple spatial volumes at some lattice spacings. For actions with multiple species of pions, the lightest masses are quoted

Collab.	Ref.	N_f	L [fm]	$M_{\pi,\text{min}} L$	Description
Meinel 20	[648]	2+1	2.7, 2.7	4.1, 4.6	FV effects not quantified. Effects from unstable $\Lambda^*(1520)$ not quantified

Table 163 Operator renormalization in determinations of form factors for rare decays of beauty hadrons

Collab.	Ref.	N_f	Ren.	Description
Meinel 20	[648]	2+1	mNPR	Residual matching factors ρ computed at one-loop for vector and axial-vector currents, but at tree-level only for tensor currents. A systematic uncertainty is assigned to $\rho_{T^{\mu\nu}}$ as the double of $\max(\lvert\rho_{A^\mu} - 1\rvert, \lvert\rho_{V^\mu} - 1\rvert)$

Table 164 Heavy-quark treatment in determinations of form factors for rare decays of beauty hadrons

Collab.	Ref.	N_f	Action	Description
Meinel 20	[648]	2+1	Columbia RHQ	Discretization errors discussed as part of combined chiral-continuum-w fit. Higher-order fit also includes $\mathcal{O}(\alpha_s a \lvert\mathbf{p}\rvert)$ terms to account for missing radiative corrections to $\mathcal{O}(a)$ improvement of the currents

C.6.5 Form factors entering determinations of $|V_{cb}|$ ($B_{(s)} \to D_{(s)}^{(*)}\ell\nu$, $\Lambda_b \to \Lambda_c^{(*)}\ell\bar{\nu}$) and $R(D_{(s)})$

See Tables 165, 166, 167, 168, 169.

Table 165 Continuum extrapolations/estimation of lattice artifacts in $N_f = 2+1$ determinations of $B_{(s)} \to D_{(s)}^{(*)}\ell\nu$ and $\Lambda_b \to \Lambda_c^{(*)}\ell\bar{\nu}$ form factors, and of $R(D_{(s)})$

Collab.	Refs.	N_f	a [fm]	Continuum extrapolation	Scale setting
Meinel 21	[638]	2+1	0.0828(3), 0.1106(3)	Combined chiral-continuum extrapolation as part of the expansion of form factor shape in powers of $w-1$. Systematics estimated by varying fit form	Scale setting using Ω mass in Ref. [8]
HPQCD 19	[613]	2+1+1	0.044, 0.059, ≈ 0.09	Combined chiral-continuum extrapolation. Fractional error from continuum limit and extrapolation to physical b mass at zero recoil quoted as 1.20%	Scale setting from f_π via the flow quantity w_0 [14,37,1071]
HPQCD 19B	[612]	2+1+1	0.044, 0.059, $\approx$0.09	Combined chiral-continuum extrapolation. Fractional error from continuum limit and extrapolation to physical b mass at zero recoil quoted as 0.73% and 0.69%, respectively	Scale setting from f_π via the flow quantity w_0 [14,37,1071]

Table 166 Chiral extrapolation/minimum pion mass in $N_f = 2+1$ determinations of $B_{(s)} \to D_{(s)}^{(*)}\ell\nu$ and $\Lambda_b \to \Lambda_c^{(*)}\ell\bar{\nu}$ form factors, and of $R(D_{(s)})$. For actions with multiple species of pions, masses quoted are the RMS pion masses for $N_f = 2+1$ and the Goldstone mode mass for $N_f = 2+1+1$. The different $M_{\pi,\mathrm{min}}$ entries correspond to the different lattice spacings

Collab.	Refs.	N_f	$M_{\pi,\mathrm{min}}$ [MeV]	Description
Meinel 21	[638]	2+1	303, 340	Combined chiral-continuum extrapolation as part of the expansion of form factor shape in powers of $w-1$. Systematic uncertainty estimated by repeating fit with added higher-order terms
HPQCD 19	[613]	2+1+1	315, 329, 129 [16]	Combined chiral-continuum extrapolation using rSχPT. No specific uncertainty coming from chiral extrapolation quoted
HPQCD 19B	[612]	2+1+1	315, 329, 129 [16]	Combined chiral-continuum extrapolation using rSχPT. No specific uncertainty coming from chiral extrapolation quoted

Table 167 Finite-volume effects in determinations of $B_{(s)} \to D_{(s)}^{(*)}\ell\nu$ and $\Lambda_b \to \Lambda_c^{(*)}\ell\bar{\nu}$ form factors, and of $R(D_{(s)})$. Each L-entry corresponds to a differentlattice spacing, with multiple spatial volumes at some lattice spacings. For actions with multiple species of pions, the lightest pion masses are quoted

Collab.	Refs.	N_f	L [fm]	$M_{\pi,\mathrm{min}}L$	Description
Meinel 21	[638]	2+1	2.7, 2.7	4.1, 4.6	FV effects not quantified. Effects from unstable Λ_c^* not quantified
HPQCD 19	[613]	2+1+1	2.73, 2.72,2.81/5.62	4.3, 4.5, 3.7/4.5, 3.9/4.5, 3.3/3.8	FV effects neglected. This includes the effect of frozen topology in the finest ensemble
HPQCD 19B	[612]	2+1+1	2.73, 2.72,2.81/5.62	4.3, 4.5, 3.7/4.5, 3.9/4.5, 3.3/3.8	FV effects neglected. This includes the effect of frozen topology in the finest ensemble

Table 168 Operator renormalization in determinations of $B_{(s)} \to D_{(s)}^{(*)} \ell \nu$ and $\Lambda_b \to \Lambda_c^{(*)} \ell \bar{\nu}$ form factors, and of $R(D_{(s)})$

Collab.	Refs.	N_f	Ren.	Description
Meinel 21	[638]	2+1	mNPR	Residual matching factors ρ computed at one-loop for vector and axial-vector currents, but at tree-level only for tensor currents. A systematic uncertainty is assigned to $\rho_{T^{\mu\nu}}$ as the double of $\max(\lvert\rho_{A^\mu} - 1\rvert, \lvert\rho_{V^\mu} - 1\rvert)$
HPQCD 19	[613]	2+1+1	NP	Currents normalized non-perturbatively by imposing that $f_+(0) = f_0(0) = 1$ for transitions involving initial and final mesons with identical masses
HPQCD 19B	[612]	2+1+1	NP	Currents renormalized nonperturbatively using PCAC relation

Table 169 Heavy-quark treatment in determinations of $B_{(s)} \to D_{(s)}^{(*)} \ell \nu$ and $\Lambda_b \to \Lambda_c^{(*)} \ell \bar{\nu}$ form factors, and of $R(D_{(s)})$

Collab.	Refs.	N_f	Action	Description
Meinel 21	[638]	2+1	Columbia RHQ for both the b and c quarks	Discretization errors discussed as part of combined chiral-continuum-w fit. Higher-order fit also includes $\mathcal{O}(\alpha_s a\lvert\mathbf{p}\rvert)$ terms to account for missing radiative corrections to $\mathcal{O}(a)$ improvement of the currents
HPQCD 19	[613]	2+1+1	HISQ for both the b and c quarks	Values of bare heavy quark masses up to $am_h = 0.8$. Fractional error from continuum limit and extrapolation to physical b mass at zero recoil quoted as 1.20%
HPQCD 19B	[612]	2+1+1	HISQ for both the b and c quarks	Values of bare heavy-quark masses up to $am_h = 0.8$. Fractional error from extrapolation to physical b mass quoted as 0.69%

C.7 Notes to Sect. 9 on the strong coupling α_s

In this section we provide more detailed information on the simulations used to calculate the strong coupling α_s. We present this information only for results that have appeared since FLAG 19. For information on previous calculations not listed here we refer the previous reports FLAG 19 [4] and FLAG 16 [3].

C.7.1 Renormalization scale and perturbative behaviour

See Tables 170, 171.

Table 170 Renormalization scale and perturbative behaviour of α_s determinations for $N_f = 0$

Collab.	Refs.	N_f	α_{eff}	n_l	Description
Nada 20	[694]	0	SF: 0.08–0.15 GF: 0.08–0.24	2	Step-scaling with GF, non-pert matching to SF, Same gauge configurations as in [693]
Husung 20	[695]	0	0.17−0.36	3	Estimated from α_{qq}
Dalla Brida 19	[693]	0	SF: 0.08–0.15 GF: 0.08–0.95	2	Step-scaling with GF, non-pert matching to SF

Table 171 Renormalization scale and perturbative behaviour of α_s determinations for $N_f = 3$

Collab.	Refs.	N_f	α_{eff}	n_l	Description
Petreczky 20	[696]	2+1	0.22−0.38	2	$m_h = m_c - 4m_c$
Ayala 20	[74]	2+1	0.2−0.4	3	$1/r > 2$ GeV
Cali 20	[76]	2+1	0.235−0.308	3	$\|x\| = 0.13$−0.19 fm
Boito 20	[698]	2+1	0.38	2	Only $m_h = m_c$ is used
TUMQCD 19	[75]	2+1	0.2−0.4	3	$r < 0.073$ fm
Zafeiropoulos 19	[699]	2+1	0.35–0.42	3	α_T for $p \sim 3.0$−3.7 GeV
Petreczky 19	[26]	2+1	0.31, 0.38	2	Only results for $m_h = m_c, 1.5m_c$ are reviewed

C.7.2 Continuum limit

See Tables 172, 173.

Table 172 Continuum limit for α_s determinations with $N_f = 0$

Collab.	Refs.	N_f	$a\,\mu$	Description
Nada 20	[694]	0	GF: $0.125 < a\mu < 0.042$ SF: $0.17 < a\mu < 0.063$	Step scaling GF scheme, Non-pert matching to SF scheme
Husung 20	[695]	0	$a\mu < 0.57$	Only $r/a > 3/5$ are used in the analysis
Dalla Brida 19	[693]	0	GF: $0.125 < a\mu < 0.042$ SF: $0.17 < a\mu < 0.063$	Step scaling GF scheme, Non-pert matching to SF scheme

Table 173 Continuum limit for α_s determinations with $N_f = 3$

Collab.	Refs.	N_f	$a\,\mu$	Description
Petreczky 20	[696]	2+1	$a\mu = 0.32$−5.40	$a = 0.025$−0.104 fm, $m_h = m_c - 4m_c$
Ayala 20	[74]	2+1	$a\mu < 0.71$	Only $r/a > \sqrt{8}$ are considered
Cali 20	[76]	2+1	$a\mu = 0.21$−0.58	$a = 0.039$−0.076 fm
Boito 20	[698]	2+1	NA	Previously published continuum results were used
TUMQCD 19	[75]	2+1	$a\mu < 2$	r/a values down to 1 are used but it is checked that the result does not change if only $r/a > \sqrt{8}$ are considered
Zafeiropoulos 19	[699]	2+1	$a\mu \sim 1.3$−1.6	Two lattice spacings $a = 0.11, 0.08$ fm $\alpha_{\text{eff}} = 0.3$ not reached
Petreczky 19	[26]	2+1	$a\mu < 0.49$	Only results for $m_h = m_c, 1.5m_c$ are reviewed

C.8 Notes to Sect. 10 on nucleon matrix elements

See Tables 174, 175, 176, 177, 178, 179, 180, 181, 182, 183, 184, 185, 186, 187, 188, 189, 190, 191, 192, 193, 194, 195, 196, 197, 198, 199, 200.

Table 174 Continuum extrapolations/estimation of lattice artifacts in determinations of the isovector axial, scalar and tensor charges with $N_f = 2+1+1$ quark flavours

Collab.	Refs.	N_f	a [fm]	Description
CalLat 19	[100]	2+1+1	0.15, 0.12, 0.09	Extrapolation to the physical point via simultaneous fit in the lattice spacing, M_π and $M_\pi L$, including terms of order a^2 and a^4
ETM 19	[971]	2+1+1	0.08	Single lattice spacing

Table 175 Continuum extrapolations/estimation of lattice artifacts in determinations of the isovector axial, scalar and tensor charges with $N_f = 2+1$ quark flavours

Collab.	Refs.	N_f	a [fm]	Description
χQCD 21	[978]	2+1	0.06, 0.08, 0.11, 0.14	Extrapolation performed using a quadratic term in a as part of a simultaneous fit in a, M_π and $M_\pi L$
NME 21	[972]	2+1	0.07, 0.09, 0.13	Extrapolation performed using a linear term in a as part of a simultaneous fit in a, M_π and $M_\pi L$
RBC/UKQCD 19	[977]	2+1	0.14	Single lattice spacing
LHPC 19	[851]	2+1	0.09, 0.12	No extrapolation performed; final result taken from finer lattice with an enlarged error bar to account for result at coarser a
Mainz 19	[102]	2+1	0.05, 0.06, 0.08, 0.09	Extrapolation performed as part of a simultaneous fit in a, M_π and $M_\pi L$
PACS 18A	[849]	2+1	0.085	Single lattice spacing

Table 176 Chiral extrapolation/minimum pion mass in determinations of the isovector axial, scalar and tensor charges with $N_f = 2+1+1$ quark flavours

Collab.	Ref.	N_f	$M_{\pi,\text{min}}$ [MeV]	Description
CalLat 19	[100]	2+1+1	135, 130, 220	Fit performed including analytic and non-analytic terms in M_π up to order M_π^4
ETM 19	[971]	2+1+1	139	Single pion mass within 3% of the physical value

Table 177 Chiral extrapolation/minimum pion mass in determinations of the isovector axial, scalar and tensor charges with $N_f = 2+1$ quark flavours

Collab.	Ref.	N_f	$M_{\pi,\text{min}}$ [MeV]	Description
χQCD 21	[978]	2+1	139, 171, 302, 337, 371	Extrapolation performed using quadratic terms in M_π from partially quenched chiral perturbation theory as part of a simultaneous fit in a, M_π and $M_\pi L$
NME 21	[972]	2+1	170, 170, 270, 285	Extrapolation performed using a quadratic term in M_π as part of a simultaneous fit in a, M_π and $M_\pi L$
RBC/UKQCD 19	[977]	2+1	170, 250	Does not quote extrapolated value, but shows low mass dependence
LHPC 19	[851]	2+1	133, 137	Does not perform extrapolation; comparison of results at two near-physical pion masses
Mainz 19	[102]	2+1	220, 290, 200, 260	Extrapolation performed using logarithmic and quadratic terms in M_π as part of a simultaneous fit in a, M_π and $M_\pi L$
PACS 18A	[849]	2+1	135	Single, physical pion mass

Table 178 Finite-volume effects in determinations of the isovector axial, scalar and tensor charges with $N_f = 2+1+1$ quark flavours

Collab.	Ref.	N_f	L [fm]	$M_{\pi,\min}L$	Description
CalLat 19	[100]	2+1+1	2.4–7.2, 2.9–5.8, 2.9–4.2	4.9, 3.8, 4.7	Fit performed including a term of the form $M_\pi^2 e^{-M_\pi L}/\sqrt{M_\pi L}$ as part of a simultaneous fit in a^2, M_π and $M_\pi L$
ETM 19	[971]	2+1+1	5.12, 4.5–6.0	3.62, 2.98	Final result quoted from the $M_\pi L = 3.62$ ensemble only

Table 179 Finite-volume effects in determinations of the isovector axial, scalar and tensor charges with $N_f = 2+1$ quark flavours

Collab.	Refs.	N_f	L [fm]	$M_{\pi,\min}L$	Description
χQCD 21	[978]	2+1	4.5, 5.3, 2.6, 2.6, 1.92	3.7, 3.9, 3.6, 3.8, 3.6	Extrapolation performed including a term of the form $e^{-M_\pi L}$ as part of a simultaneous fit in a, M_π and $M_\pi L$
NME 21	[972]	2+1	4.2, 2.9–4.3, 4.3–5.8, 3.4–5.0	5.87, 4.09, 3.75, 4.28	Extrapolation performed including a term of the form $M_\pi^2 e^{-M_\pi L}/\sqrt{M_\pi L}$ as part of a simultaneous fit in a^2, M_π and $M_\pi L$
RBC/UKQCD 19	[977]	2+1	4.5	4.0	Does not quote extrapolated value
LHPC 19	[851]	2+1	5.9, 5.6	4.0, 3.9	Does not quote extrapolated value
Mainz 19	[102]	2+1	2.8–4.1, 2.4–3.6, 2.1–4.1, 2.4–3.2	4.7, 5.3, 4.2, 4.3	Extrapolation performed including a term of the form $M_\pi^2 e^{-M_\pi L}/\sqrt{M_\pi L}$ as part of a simultaneous fit in a^2, M_π and $M_\pi L$
PACS 18A	[849]	2+1	10.8	7.4	Single spatial volume of 10.8 fm at physical pion mass $M_\pi L = 7.4$

Table 180 Renormalization in determinations of the isovector axial, scalar and tensor charges with $N_f = 2+1+1$ quark flavours

Collab.	Ref.	N_f	Ren.
CalLat 19	[100]	2+1+1	RI-MOM
ETM 19	[971]	2+1+1	RI-MOM

Table 181 Renormalization in determinations of the isovector axial, scalar and tensor charges with $2+1$ quark flavours

Collab.	Ref.	N_f	Ren.
χQCD 21	[978]	2+1	RI-MOM
NME 21	[972]	2+1	RI-SMOM
RBC/UKQCD 19	[977]	2+1	RI-SMOM
LHPC 19	[851]	2+1	RI-MOM, RI-SMOM
Mainz 19	[102]	2+1	RI-MOM, SF
PACS 18A	[849]	2+1	SF

Table 182 Control of excited state contamination in determinations of the isovector axial, scalar and tensor charges with $N_f = 2+1+1$ quark flavours. The comma-separated list of numbers in square brackets denote the range of source-sink separations τ (in fermi) at each value of the bare coupling

Collab.	Ref.	N_f	τ [fm]	Description
CalLat 19	[100]	2+1+1	All	Two-state fits to the τ-dependence of summed operator insertion for $\tau \geq 0.3$ fm
ETM 19	[971]	2+1+1	[0.64−1.6]	Fits to the τ- and t-dependence of three-point correlators using multiple methods (plateau, two- and three-state fits, summation), with the two-state fits quoted for the final result

Table 183 Control of excited state contamination in determinations of the isovector axial, scalar and tensor charges with $N_f = 2+1$ quark flavours. The comma-separated list of numbers in square brackets denote the range of source-sink separations τ (in fermi) at each value of the bare coupling

Collab.	Refs.	N_f	τ [fm]	Description
χQCD 21	[978]	2+1	[0.9–1.1] [1–1.2] [0.9–1.3,0.9–1.3] [1–1.5]	Fits to the τ- and t-dependence of three-point correlators using up to three lowest-lying states
NME 21	[972]	2+1	[1.0–1.8] [0.75–1.3,0.75–1.7] [0.72–1.46,0.72–1.46] [0.8–1.4,0.9–1.5]	Fits to the τ- and t-dependence of three-point correlators using three lowest-lying states.
RBC/UKQCD 19	[977]	2+1	[1.0,1.3]	Result quoted from t=1.3 fm point only; consistency in results from $t = 1.0$ fm is demonstrated
LHPC 19	[851]	2+1	[0.4–1.4] [0.9–1.5]	Multiple analysis methods used (plateau, summation, and two-state fits to each), and combined to produce final result
Mainz 19	[102]	2+1	[1.0–1.4,1.0–1.4,1.0–1.4] [1.0–1.5,1.0–1.5] [1.0–1.4,1.0–1.4,1.0–1.4,1.0–1.4] [1.0–1.4,1.0–1.3]	Fits to the τ- and t-dependence of correlator ratios using the two lowest-lying states
PACS 18A	[849]	2+1	[0.9−1.4]	Average of plateau values at the three largest source-sink separations

Table 184 Continuum extrapolations/estimation of lattice artifacts in determinations of g_A^q and g_T^q

Collab.	Ref.	N_f	a [fm]	Description
ETM 19	[971]	2+1+1	0.08	Not estimated

Table 185 Chiral extrapolation/minimum pion mass in determinations of g_A^q and g_T^q

Collab.	Ref.	N_f	$M_{\pi,\min}$ [MeV]	Description
ETM 19	[971]	2+1+1	139	Simulate close to M_π^{phys}

Table 186 Finite-volume effects in determinations of g_A^q and g_T^q

Collab.	Ref.	N_f	L [fm]	$M_{\pi,\min}L$	Description
ETM 19	[971]	2+1+1	5.1	3.6	FVE are anticipated to be small based on an investigation using two near physical point $N_f = 2$ ensembles with $M_\pi L = 3.0$ and 4.0

Table 187 Renormalization in determinations of g_A^q and g_T^q

Collab.	Ref.	N_f	Ren.
ETM 19	[971]	2+1+1	RI-SMOM

Table 188 Control of excited state contamination in determinations of g_A^q and g_T^q. The comma-separated list of numbers in square brackets denote the range of source-sink separations τ (in fermi) at each value of the bare coupling

Collab.	Ref.	N_f	τ [fm]	Description
ETM 19	[971]	2+1+1	[0.6−1.6]/all	Two-state fit to all τ. A comparison is made with three-state fits, plateau fits and the summation method

Table 189 Continuum extrapolation/estimation of lattice artifacts in direct determinations of $\sigma_{\pi N}$ and σ_s

Collab.	Ref.	N_f	a [fm]	Description
ETM 19	[971]	2+1+1	0.08	Not estimated

Table 190 Chiral extrapolation/minimum pion mass in direct determinations of $\sigma_{\pi N}$ and σ_s

Collab.	Ref.	N_f	$M_{\pi,\min}$ [MeV]	Description
ETM 19	[971]	2+1+1	139	Simulate close to M_π^{phys}

Table 191 Finite-volume effects in direct determinations of $\sigma_{\pi N}$ and σ_s

Collab.	Ref.	N_f	L [fm]	$M_{\pi,\min}L$	Description
ETM 19	[971]	2+1+1	5.1	3.6	FVE are found to be small from an investigation using two near physical point $N_f = 2$ ensembles with $M_\pi L = 3.0$ and 4.0

Table 192 Renormalization for direct determinations of $\sigma_{\pi N}$ and σ_s. The type of renormalization (Ren.) is given for $\sigma_{\pi N}$ first and σ_s second. The label 'na' indicates that no renormalization is required

Collab.	Ref.	N_f	Ren.	Description
ETM 19	[971]	2+1+1	na/na	6.3 cm

Table 193 Control of excited state contamination in direct determinations of $\sigma_{\pi N}$ and σ_s. The comma-separated list of numbers in square brackets denote the range of source-sink separations τ (in fermi) at each value of the bare coupling. The range of τ for the connected (disconnected) contributions to the three-point correlation functions is given first (second). If a wide range of τ values is available this is indicated by "all" in the table

Collab.	Ref.	N_f	τ [fm]	Description
ETM 19	[971]	2+1+1	[0.6−1.6]/all	Two-state fit to all τ. A comparison is made with three-state fits, plateau fits and the summation method

Table 194 Continuum extrapolations/estimation of lattice artifacts in determinations of $\sigma_{\pi N}$ and σ_s from the Feynman–Hellmann method

Collab.	Ref.	N_f	a [fm]	Description
BMW 20A	[1010]	1+1+1+1	0.10, 0.09, 0.08, 0.06	Combined continuum, chiral and volume fit within an extended frequentist method. $\mathcal{O}(\alpha a)$ or $\mathcal{O}(a^2)$ terms are included. M_N used to fix the lattice spacing

Table 195 Chiral extrapolation/minimum pion mass in determinations of $\sigma_{\pi N}$ and σ_s from the Feynman–Hellmann method

Collab.	Ref.	N_f	$M_{\pi,\min}$ [MeV]	Description
BMW 20A	[1010]	1+1+1+1	238, 200, 219, 199	Combined continuum, chiral and volume fit within an extended frequentist method. Terms with $M_\pi^{2,3,4}$ and M_K^2 are included and cuts of $M_\pi < 420$ MeV and $M_\pi < 360$ MeV are made
Walker-Loud 08	[1014]	2+1	294	Fit using NNLO $SU(2)$ HBχPT [1072] with a zero and non-zero value for $g_{\Delta N}$. Errors on the LECs that are not free parameters determine the systematic uncertainty

Table 196 Finite-volume effects in determinations of $\sigma_{\pi N}$ and σ_s from the Feynman–Hellmann method

Collab.	Ref.	N_f	L [fm]	$M_{\pi,\min}L$	Description
BMW 20A	[1010]	1+1+1+1	3.2, 2.9–4.3, 2.6–3.8, 1.9–3.8	4.0, 4.3, 4.1, 4.1	Combined continuum, chiral and volume fit within an extended frequentist method. FV term $M_\pi^{1/2}L^{-3/2}e^{-M_\pi L}$ added
Walker-Loud 08	[1014]	2+1	2.5	3.7	FV effects expected to be 1% or less for the lightest pion mass based on [1073]

C.9 Notes to Sect. 11 on scale setting

Table 197 Continuum extrapolations/estimation of lattice artifacts in scale determinations with $N_f = 2 + 1 + 1$ quark flavours

Collab.	Refs.	N_f	a [fm]	Description
ETM 21	[305]	2+1+1	0.069, 0.079, 0.097	
CalLat 20A	[111]	2+1+1	[0.056, 0.082, 0.11, 0.13], [0.057, 0.087, 0.12, 0.15]	Möbius Domain-wall valence quarks on HISQ/MILC sea; lattice spacings depending on scheme
BMW 20	[115]	1+1+1+1	0.0640, 0.0787, 0.0952, 0.1116, 0.1191, 0.1315	Staggered fermion computation with isospin breaking and QED
ETM 20	[1052]	2+1+1	0.069, 0.079, 0.097	Wilson TM fermions at maximal twist including clover term. Note that lattice spacings are not explicitly given in [1052]
ETM 18A	[1074]	2+1+1	0.08	Wilson TM fermions at maximal twist including clover term
FNAL/MILC 17	[16]	2+1+1	0.03, 0.042, 0.06, 0.09, 0.12, 0.15	Determination of f_{p4s}
MILC 15	[112]	2+1+1	0.06, 0.09, 0.12, 0.15	Highly improved staggered quarks
ETM 14	[7]	2+1+1	0.089, 0.082, 0.062	Wilson TM fermions at maximal twist
FNAL/MILC 14A	[17]	2+1+1	0.06, 0.09, 0.12, 0.15	
HPQCD 13A	[37]	2+1+1	0.15, 0.12, 0.09	
HPQCD 11B	[552]	2+1+1	0.09, 0.12, 0.15	NRQCD for b quark and HISQ for valence light quarks and MILC sea

Table 198 Continuum extrapolations/estimation of lattice artifacts in scale determinations with $N_f = 2 + 1$ quark flavours

Collab.	Refs.	N_f	a [fm]	Description
CLS 16	[113]	2+1	0.085, 0.065, 0.05	NP $\mathcal{O}(a)$-improved Wilson fermions with LW gauge action
QCDSF/UKQCD 15B	[713]	2+1	0.059, 0.068, 0.074, 0.082	$(a_{\max}/a_{\min})^2 = 1.94$
χQCD 14	[24]	2+1	0.084, 0.112	Valence overlap fermions on domain wall fermion gauge configurations
HotQCD 14	[116]	2+1	[0.04, 0.25]	HISQ and tree-level improved Symanzik gauge action. Several ensembles with a in the quoted range and with a single $M_\pi \approx 160$ MeV
RBC/UKQCD 14	[8]	2+1	0.06, 0.08, 0.11, 0.14	Two versions of Domain Wall Fermions combined each with the Iwasaki gauge action
BMW 12A	[114]	2+1	0.053, 0.065, 0.077, 0.093	Wilson fermion computation
HotQCD 11	[708]	2+1	[0.066, 0.25]	HISQ and tree-level improved Symanzik gauge action. Several ensembles with a in the quoted range
RBC/UKQCD 10A	[117]	2+1	0.087, 0.114	
MILC 10	[41]	2+1	0.045, 0.06, 0.09	Asqtad staggered quarks
HPQCD 09B	[120]	2+1	0.044, 0.059, 0.085, 0.12, 0.15	NRQCD for b quark and HISQ for valence light quarks on MILC asqtad sea
MILC 09	[15,157,1054]	2+1	[0.045, 0.18]	Asqtad staggered quarks, 6 different lattice spacings in the quoted range
PACS-CS 08	[193]	2+1	0.09	Several ensembles of Wilson clover quarks and Iwasaki gauge action at a single lattice spacing
HPQCD 05B	[118]	2+1	0.09, 0.12, 0.17	NRQCD with tree level tadpole improved couplings on MILC asqtad sea
Aubin 04	[119]	2+1	0.09, 0.12	Asqtad staggered quarks

Table 199 Chiral extrapolation and finite-volume effects in scale determinations with $N_f = 2 + 1 + 1$ quark flavours. We list the minimum pion mass $M_{\pi,\min}$ and $M_\pi L \equiv M_{\pi,\min}[L(M_{\pi,\min})]_{\max}$ is evaluated at the maximum value of L available at $M_\pi = M_{\pi,\min}$

Collab.	Refs.	N_f	$M_{\pi,\min}$ [MeV]	$M_\pi L$	Description
ETM 21	[305]	2+1+1			
CalLat 20A	[111]	2+1+1	130	3.9	
BMW 20	[115]	1+1+1+1	Several pion masses within $\pm 3\%$ of physical value	3.0	
ETM 20	[1052]	2+1+1	135	3.5	Only indirectly inferred
ETM 18A	[1074]	2+1+1	139.8	3.6	One ensemble only
FNAL/MILC 17	[17]	2+1+1	129	3.7	Determination of f_{4ps}, M_{4ps}
MILC 15	[112]	2+1+1	125	3.7	Four ensembles at physical point
ETM 14	[7]	2+1+1	211	3.19	
FNAL/MILC 14A	[17]	2+1+1	130	3.7	Determination of f_{4ps}, M_{4ps}
HPQCD 13A	[37]	2+1+1	128	3.7	
HPQCD 11B	[552]	2+1+1	211	4.0	NRQCD Υ 2s-1s splitting and η_s as input

Table 200 Chiral extrapolation and finite-volume effects in scale determinations with $N_f = 2+1$ quark flavours. We list the minimum pion mass $M_{\pi,\min}$ and $M_\pi L \equiv M_{\pi,\min}[L(M_{\pi,\min})]_{\max}$ is evaluated at the maximum value of L available at $M_\pi = M_{\pi,\min}$

Collab.	Refs.	N_f	$M_{\pi,\min}$ [MeV]	$M_\pi L$	Description
CLS 16	[113]	2+1	200	4.2	Extrapolation along line $m_u + m_d + m_s = \text{const.}$
QCDSF/UKQCD 15B	[713]	2+1	228	4.1	
χQCD 14	[24]	2+1	290	4.0	
HotQCD 14	[116]	2+1	160	4.8	HISQ staggered quarks, the pion mass quoted is M_π. Results on 20 ensembles with volumes in the range [2.6, 6.1] fm, we quote $M_\pi^{min} L^{max}$
RBC/UKQCD 14	[8]	2+1	139	3.9	
BMW 12A	[114]	2+1	131 and 120	3.92 and 3.0	
HotQCD 11	[708]	2+1	160	4.8	HISQ staggered quarks, the pion mass quoted is M_π. Results on 20 ensembles with volumes in the range [3.2, 6.1] fm, we quote $M_\pi^{min} L^{max}$
RBC/UKQCD 10A	[117]	2+1	290	4.0	
MILC 10	[41]	2+1	255	4.8	Determination from global fit, scale from f_π
HPQCD 09B	[120]	2+1	211	4.0	Extension of HPQCD 05B [118]
MILC 09	[15,157,1054]	2+1	258	4.3	Asqtad staggered quarks, the pion mass quoted is M_π^{RMS}
PACS-CS 08	[193]	2+1	156	2.3	Clover quarks, several pion masses in the range [156, 702] MeV, single lattice spacing
HPQCD 05B	[118]	2+1	270	3.7	NRQCD Υ 2s-1s splitting as input
Aubin 04	[119]	2+1	253	3.8	Asqtad staggered quarks, the pion mass quoted is the Goldstone mass

References

1. [FLAG 10] G. Colangelo, S. Dürr, A. Jüttner, L. Lellouch, H. Leutwyler et al., Review of lattice results concerning low energy particle physics. Eur. Phys. J. C **71**, 1695 (2011). https://doi.org/10.1140/epjc/s10052-011-1695-1. arXiv:1011.4408
2. [FLAG 13] S. Aoki, Y. Aoki, C. Bernard, T. Blum, G. Colangelo et al., Review of lattice results concerning low-energy particle physics. Eur. Phys. J. C **74**, 2890 (2014). https://doi.org/10.1140/epjc/s10052-014-2890-7. arXiv:1310.8555
3. [FLAG 16] S. Aoki et al., Review of lattice results concerning low-energy particle physics. Eur. Phys. J. C **77**, 112 (2017). https://doi.org/10.1140/epjc/s10052-016-4509-7. arXiv:1607.00299
4. [FLAG 19] S. Aoki et al., FLAG Review 2019: Flavour Lattice Averaging Group (FLAG). Eur. Phys. J. C **80**, 113 (2020). https://doi.org/10.1140/epjc/s10052-019-7354-7. arXiv:1902.08191
5. Flavour Lattice Averaging Group (FLAG), *FLAG Review*. http://flag.unibe.ch/
6. [FNAL/MILC/TUMQCD 18] A. Bazavov et al., Up-, down-, strange-, charm-, and bottom-quark masses from four-flavor lattice QCD. Phys. Rev. D **98**, 054517 (2018). https://doi.org/10.1103/PhysRevD.98.054517. arXiv:1802.04248
7. [ETM 14] N. Carrasco et al., Up, down, strange and charm quark masses with N_f = 2+1+1 twisted mass lattice QCD. Nucl. Phys. B **887**, 19 (2014). https://doi.org/10.1016/j.nuclphysb.2014.07.025. arXiv:1403.4504
8. [RBC/UKQCD 14B] T. Blum et al., Domain wall QCD with physical quark masses. Phys. Rev. D **93**, 074505 (2016). https://doi.org/10.1103/PhysRevD.93.074505. arXiv:1411.7017
9. [BMW 10A] S. Dürr, Z. Fodor, C. Hoelbling, S. Katz, S. Krieg et al., Lattice QCD at the physical point: light quark masses. Phys. Lett. B **701**, 265 (2011). https://doi.org/10.1016/j.physletb.2011.05.053. arXiv:1011.2403
10. [BMW 10B] S. Dürr, Z. Fodor, C. Hoelbling, S. Katz, S. Krieg et al., Lattice QCD at the physical point: simulation and analysis details. JHEP **1108**, 148 (2011). https://doi.org/10.1007/JHEP08(2011)148. arXiv:1011.2711

11. [HPQCD 10] C. McNeile, C.T.H. Davies, E. Follana, K. Hornbostel, G.P. Lepage, High-precision c and b masses and QCD coupling from current–current correlators in lattice and continuum QCD. Phys. Rev. D **82**, 034512 (2010). https://doi.org/10.1103/PhysRevD.82.034512. arXiv:1004.4285
12. [MILC 10A] A. Bazavov et al., Staggered chiral perturbation theory in the two-flavor case and SU(2) analysis of the MILC data. PoS LAT **2010**, 083 (2010). arXiv:1011.1792
13. [HPQCD 18] A.T. Lytle, C.T.H. Davies, D. Hatton, G.P. Lepage, C. Sturm, Determination of quark masses from $n_f = 4$ lattice QCD and the RI-SMOM intermediate scheme. Phys. Rev. D **98**, 014513 (2018). https://doi.org/10.1103/PhysRevD.98.014513. arXiv:1805.06225
14. [HPQCD 14A] B. Chakraborty, C.T.H. Davies, G.C. Donald, R.J. Dowdall, B. Galloway, P. Knecht et al., High-precision quark masses and QCD coupling from $n_f = 4$ lattice QCD. Phys. Rev. D **91**, 054508 (2015). https://doi.org/10.1103/PhysRevD.91.054508. arXiv:1408.4169
15. [MILC 09A] A. Bazavov et al., MILC results for light pseudoscalars. PoS **CD09**, 007 (2009). arXiv:0910.2966
16. [FNAL/MILC 17] A. Bazavov et al., B- and D-meson leptonic decay constants from four-flavor lattice QCD. Phys. Rev. D **98**, 074512 (2018). https://doi.org/10.1103/PhysRevD.98.074512. arXiv:1712.09262
17. [FNAL/MILC 14A] A. Bazavov et al., Charmed and light pseudoscalar meson decay constants from four-flavor lattice QCD with physical light quarks. Phys. Rev. D **90**, 074509 (2014). https://doi.org/10.1103/PhysRevD.90.074509. arXiv:1407.3772
18. [ALPHA 19] M. Bruno, I. Campos, P. Fritzsch, J. Koponen, C. Pena, D. Preti et al., Light quark masses in $N_\mathrm{f} = 2 + 1$ lattice QCD with Wilson fermions. Eur. Phys. J. C. **80**, 169 (2020). https://doi.org/10.1140/epjc/s10052-020-7698-z. arXiv:1911.08025
19. [RM123 17] D. Giusti, V. Lubicz, C. Tarantino, G. Martinelli, S. Sanfilippo, S. Simula et al., Leading isospin-breaking corrections to pion, kaon and charmed-meson masses with Twisted-Mass fermions. Phys. Rev. D **95**, 114504 (2017). https://doi.org/10.1103/PhysRevD.95.114504. arXiv:1704.06561
20. [BMW 16] Z. Fodor, C. Hoelbling, S. Krieg, L. Lellouch, T. Lippert, A. Portelli et al., Up and down quark masses and corrections to Dashen's theorem from lattice QCD and quenched QED. Phys. Rev. Lett. **117**, 082001 (2016). https://doi.org/10.1103/PhysRevLett.117.082001. arXiv:1604.07112
21. [MILC 18] S. Basak et al., Lattice computation of the electromagnetic contributions to kaon and pion masses. Phys. Rev. D **99**, 034503 (2019). https://doi.org/10.1103/PhysRevD.99.034503. arXiv:1807.05556
22. [ETM 14A] C. Alexandrou, V. Drach, K. Jansen, C. Kallidonis, G. Koutsou, Baryon spectrum with $N_f = 2 + 1 + 1$ twisted mass fermions. Phys. Rev. D **90**, 074501 (2014). https://doi.org/10.1103/PhysRevD.90.074501. arXiv:1406.4310
23. [HPQCD 20A] D. Hatton, C.T.H. Davies, B. Galloway, J. Koponen, G.P. Lepage, A.T. Lytle, Charmonium properties from lattice QCD+QED: hyperfine splitting, J/ψ leptonic width, charm quark mass, and a_μ^c. Phys. Rev. D **102**, 054511 (2020). https://doi.org/10.1103/PhysRevD.102.054511. arXiv:2005.01845
24. [χQCD 14] Y. Yi-Bo et al., Charm and strange quark masses and f_D_s from overlap fermions. Phys. Rev. D **92**, 034517 (2015). https://doi.org/10.1103/PhysRevD.92.034517. arXiv:1410.3343
25. [JLQCD 16] K. Nakayama, B. Fahy, S. Hashimoto, Short-distance charmonium correlator on the lattice with Möbius domain-wall fermion and a determination of charm quark mass. Phys. Rev. D **94**, 054507 (2016). https://doi.org/10.1103/PhysRevD.94.054507. arXiv:1606.01002
26. P. Petreczky, J. Weber, Strong coupling constant and heavy quark masses in (2+1)-flavor QCD. Phys. Rev. D **100**, 034519 (2019). https://doi.org/10.1103/PhysRevD.100.034519. arXiv:1901.06424
27. [HPQCD 09A] C.T.H. Davies et al., Precise charm to strange mass ratio and light quark masses from full lattice QCD. Phys. Rev. Lett. **104**, 132003 (2010). https://doi.org/10.1103/PhysRevLett.104.132003. arXiv:0910.3102
28. [HPQCD 21] D. Hatton, C.T.H. Davies, J. Koponen, G.P. Lepage, A.T. Lytle, Determination of $\overline{m}_b/\overline{m}_c$ and $\overline{m}_b$ from $n_f = 4$ lattice QCD+QED. Phys. Rev. D **103**, 114508 (2021). https://doi.org/10.1103/PhysRevD.103.114508. arXiv:2102.09609
29. [HPQCD 14B] B. Colquhoun, R.J. Dowdall, C.T.H. Davies, K. Hornbostel, G.P. Lepage, Υ and Υ' leptonic widths, a_μ^b and m_b from full lattice QCD. Phys. Rev. D **91**, 074514 (2015). https://doi.org/10.1103/PhysRevD.91.074514. arXiv:1408.5768
30. [ETM 16B] A. Bussone et al., Mass of the b quark and B-meson decay constants from N$_f$=2+1+1 twisted-mass lattice QCD. Phys. Rev. D **93**, 114505 (2016). https://doi.org/10.1103/PhysRevD.93.114505. arXiv:1603.04306
31. P. Gambino, A. Melis, S. Simula, Extraction of heavy-quark-expansion parameters from unquenched lattice data on pseudoscalar and vector heavy-light meson masses. Phys. Rev. D **96**, 014511 (2017). https://doi.org/10.1103/PhysRevD.96.014511. arXiv:1704.06105
32. [ETM 16] N. Carrasco, P. Lami, V. Lubicz, L. Riggio, S. Simula, C. Tarantino, $K \to \pi$ semileptonic form factors with $N_f = 2 + 1 + 1$ twisted mass fermions. Phys. Rev. D **93**, 114512 (2016). https://doi.org/10.1103/PhysRevD.93.114512. arXiv:1602.04113
33. [FNAL/MILC 18] A. Bazavov et al., $|V_{us}|$ from $K_{\ell 3}$ decay and four-flavor lattice QCD. Phys. Rev. D **99**, 114509 (2019). https://doi.org/10.1103/PhysRevD.99.114509. arXiv:1809.02827
34. [FNAL/MILC 12I] A. Bazavov, C. Bernard, C. Bouchard, C. DeTar, D. Du et al., Kaon semileptonic vector form factor and determination of $|V_{us}|$ using staggered fermions. Phys. Rev. D **87**, 073012 (2013). https://doi.org/10.1103/PhysRevD.87.073012. arXiv:1212.4993
35. [RBC/UKQCD 15A] P.A. Boyle et al., The kaon semileptonic form factor in N$_f$ = 2 + 1 domain wall lattice QCD with physical light quark masses. JHEP **1506**, 164 (2015). https://doi.org/10.1007/JHEP06(2015)164. arXiv:1504.01692
36. [ETM 09A] V. Lubicz, F. Mescia, S. Simula, C. Tarantino, $K \to \pi\, \ell\, \nu$ semileptonic form factors from two-flavor lattice QCD. Phys. Rev. D **80**, 111502 (2009). https://doi.org/10.1103/PhysRevD.80.111502. arXiv:0906.4728
37. [HPQCD 13A] R. Dowdall, C. Davies, G. Lepage, C. McNeile, V_{us} from π and K decay constants in full lattice QCD with physical u, d, s and c quarks. Phys. Rev. D **88**, 074504 (2013). https://doi.org/10.1103/PhysRevD.88.074504. arXiv:1303.1670]
38. [ETM 14E] N. Carrasco, P. Dimopoulos, R. Frezzotti, P. Lami, V. Lubicz et al., Leptonic decay constants f_K, f_D and f_{D_s} with $N_f = 2+1+1$ twisted-mass lattice QCD. Phys. Rev. D **91**, 054507 (2015). https://doi.org/10.1103/PhysRevD.91.054507. arXiv:1411.7908
39. [CalLat 20] N. Miller et al., f_k/f_π from Möbius domain-wall fermions solved on gradient-flowed hisq ensembles. Phys. Rev. D **102**, 034507 (2020). https://doi.org/10.1103/PhysRevD.102.034507. arXiv:2005.04795
40. [HPQCD/UKQCD 07] E. Follana, C.T.H. Davies, G.P. Lepage, J. Shigemitsu, High precision determination of the π, K, D and D_s decay constants from lattice QCD. Phys. Rev. Lett. **100**, 062002 (2008). https://doi.org/10.1103/PhysRevLett.100.062002. arXiv:0706.1726
41. [MILC 10] A. Bazavov et al., Results for light pseudoscalar mesons. PoS LAT **2010**, 074 (2010). arXiv:1012.0868
42. [BMW 10] S. Dürr, Z. Fodor, C. Hoelbling, S. Katz, S. Krieg et al., The ratio F_K/F_π in QCD. Phys. Rev. D **81**, 054507 (2010). https://doi.org/10.1103/PhysRevD.81.054507. arXiv:1001.4692

43. S. Dürr et al., Leptonic decay-constant ratio f_K/f_π from lattice QCD using 2+1 clover-improved fermion flavors with 2-HEX smearing. Phys. Rev. D **95**, 054513 (2017). https://doi.org/10.1103/PhysRevD.95.054513. arXiv:1601.05998
44. [QCDSF/UKQCD 16] V.G. Bornyakov, R. Horsley, Y. Nakamura, H. Perlt, D. Pleiter, P.E.L. Rakow et al., Flavour breaking effects in the pseudoscalar meson decay constants. Phys. Lett. B **767**, 366 (2017). https://doi.org/10.1016/j.physletb.2017.02.018. arXiv:1612.04798
45. [ETM 09] B. Blossier et al., Pseudoscalar decay constants of kaon and D-mesons from $N_f = 2$ twisted mass lattice QCD. JHEP **0907**, 043 (2009). https://doi.org/10.1088/1126-6708/2009/07/043. arXiv:0904.0954
46. [RBC/UKQCD 15F] T. Blum et al., $K \to \pi\pi$ $\Delta I = 3/2$ decay amplitude in the continuum limit. Phys. Rev. D **91**, 074502 (2015). https://doi.org/10.1103/PhysRevD.91.074502. arXiv:1502.00263
47. [ETM 15] N. Carrasco, P. Dimopoulos, R. Frezzotti, V. Lubicz, G.C. Rossi, S. Simula et al., $\Delta S = 2$ and $\Delta C = 2$ bag parameters in the standard model and beyond from $N_f = 2 + 1 + 1$ twisted-mass lattice QCD. Phys. Rev. D **92**, 034516 (2015). https://doi.org/10.1103/PhysRevD.92.034516. arXiv:1505.06639
48. [BMW 11] S. Dürr, Z. Fodor, C. Hoelbling, S. Katz, S. Krieg et al., Precision computation of the kaon bag parameter. Phys. Lett. B **705**, 477 (2011). https://doi.org/10.1016/j.physletb.2011.10.043. arXiv:1106.3230
49. J. Laiho, R.S. Van de Water, Pseudoscalar decay constants, light-quark masses and B_K from mixed-action lattice QCD. PoS LATTICE **2011**, 293 (2011). arXiv:1112.4861
50. [SWME 15A] Y.-C. Jang et al., Kaon BSM B-parameters using improved staggered fermions from $N_f = 2+1$ unquenched QCD. Phys. Rev. D **93**, 014511 (2016). https://doi.org/10.1103/PhysRevD.93.014511. arXiv:1509.00592
51. [ETM 12D] V. Bertone et al., Kaon mixing beyond the SM from N_f=2 tmQCD and model independent constraints from the UTA. JHEP **03** (2013) 089. https://doi.org/10.1007/JHEP07(2013)143. https://doi.org/10.1007/JHEP03(2013)089. arXiv:1207.1287] [Erratum: JHEP 07, 143 (2013)]
52. [RBC/UKQCD 16] N. Garron, R.J. Hudspith, A.T. Lytle, Neutral kaon mixing beyond the standard model with $n_f = 2 + 1$ chiral fermions part 1: bare matrix elements and physical results. JHEP **11**, 001 (2016). https://doi.org/10.1007/JHEP11(2016)001. arXiv:1609.03334
53. [HPQCD 12A] H. Na, C.T. Davies, E. Follana, G.P. Lepage, J. Shigemitsu, $|V_{cd}|$ from D meson leptonic decays. Phys. Rev. D **86**, 054510 (2012). https://doi.org/10.1103/PhysRevD.86.054510. arXiv:1206.4936
54. [FNAL/MILC 11] A. Bazavov et al., B- and D-meson decay constants from three-flavor lattice QCD. Phys. Rev. D **85**, 114506 (2012). https://doi.org/10.1103/PhysRevD.85.114506. arXiv:1112.3051
55. [RBC/UKQCD 17] P.A. Boyle, L. Del Debbio, A. Jüttner, A. Khamseh, F. Sanfilippo, J.T. Tsang, The decay constants $\mathbf{f_D}$ and $\mathbf{f_{D_s}}$ in the continuum limit of $\mathbf{N_f = 2+1}$ domain wall lattice QCD. JHEP **12**, 008 (2017). https://doi.org/10.1007/JHEP12(2017)008. arXiv:1701.02644
56. [ETM 13B] N. Carrasco et al., B-physics from N_f = 2 tmQCD: the Standard Model and beyond. JHEP **1403**, 016 (2014). https://doi.org/10.1007/JHEP03(2014)016. arXiv:1308.1851
57. [HPQCD 10A] C.T.H. Davies, C. McNeile, E. Follana, G. Lepage, H. Na et al., Update: precision D_s decay constant from full lattice QCD using very fine lattices. Phys. Rev. D **82**, 114504 (2010). https://doi.org/10.1103/PhysRevD.82.114504. arXiv:1008.4018
58. R. Balasubramamian, B. Blossier, Decay constant of B_s and B_s^* mesons from $N_f = 2$ lattice QCD. Eur. Phys. J. C **80**, 412 (2020). https://doi.org/10.1140/epjc/s10052-020-7965-z. arXiv:1912.09937
59. [ETM 17D] V. Lubicz, L. Riggio, G. Salerno, S. Simula, C. Tarantino, Scalar and vector form factors of $D \to \pi(K)\ell\nu$ decays with $N_f = 2 + 1 + 1$ twisted fermions. Phys. Rev. D **96**, 054514 (2017). https://doi.org/10.1103/PhysRevD.96.054514. arXiv:1706.03017
60. [HPQCD 11] H. Na et al., $D \to \pi\ell\nu$ semileptonic decays, $|V_{cd}|$ and 2^{nd} row unitarity from lattice QCD. Phys. Rev. D **84**, 114505 (2011). https://doi.org/10.1103/PhysRevD.84.114505. arXiv:1109.1501
61. [HPQCD 21A] B. Chakraborty, W.G. Parrott, C. Bouchard, C.T.H. Davies, J. Koponen, G.P. Lepage, Improved V_{cs} determination using precise lattice QCD form factors for $D \to K\ell\nu$. Phys. Rev. D **104**, 034505 (2021). https://doi.org/10.1103/PhysRevD.104.034505. arXiv:2104.09883
62. [HPQCD 10B] H. Na, C.T.H. Davies, E. Follana, G.P. Lepage, J. Shigemitsu, The $D \to K\ell\nu$ semileptonic decay scalar form factor and $|V_{cs}|$ from lattice QCD. Phys. Rev. D **82**, 114506 (2010). https://doi.org/10.1103/PhysRevD.82.114506. arXiv:1008.4562
63. [HPQCD 13] R.J. Dowdall, C. Davies, R. Horgan, C. Monahan, J. Shigemitsu, B-meson decay constants from improved lattice NRQCD and physical u, d, s and c sea quarks. Phys. Rev. Lett. **110**, 222003 (2013). https://doi.org/10.1103/PhysRevLett.110.222003. arXiv:1302.2644
64. [HPQCD 17A] C. Hughes, C.T.H. Davies, C.J. Monahan, New methods for B meson decay constants and form factors from lattice NRQCD. Phys. Rev. D **97**, 054509 (2018). https://doi.org/10.1103/PhysRevD.97.054509. arXiv:1711.09981
65. [HPQCD 11A] C. McNeile, C.T.H. Davies, E. Follana, K. Hornbostel, G.P. Lepage, High-precision f_{B_s} and HQET from relativistic lattice QCD. Phys. Rev. D **85**, 031503 (2012). https://doi.org/10.1103/PhysRevD.85.031503. arXiv:1110.4510
66. [HPQCD 12] H. Na, C.J. Monahan, C.T. Davies, R. Horgan, G.P. Lepage et al., The B and B_s meson decay constants from lattice QCD. Phys. Rev. D **86**, 034506 (2012). https://doi.org/10.1103/PhysRevD.86.034506. arXiv:1202.4914
67. [RBC/UKQCD 14A] Y. Aoki, T. Ishikawa, T. Izubuchi, C. Lehner, A. Soni, Neutral B meson mixings and B meson decay constants with static heavy and domain-wall light quarks. Phys. Rev. D **91**, 114505 (2015). https://doi.org/10.1103/PhysRevD.91.114505. arXiv:1406.6192
68. [RBC/UKQCD 14] N.H. Christ, J.M. Flynn, T. Izubuchi, T. Kawanai, C. Lehner et al., B-meson decay constants from 2+1-flavor lattice QCD with domain-wall light quarks and relativistic heavy quarks. Phys. Rev. D **91**, 054502 (2015). https://doi.org/10.1103/PhysRevD.91.054502. arXiv:1404.4670
69. [ALPHA 14] F. Bernardoni et al., Decay constants of B-mesons from non-perturbative HQET with two light dynamical quarks. Phys. Lett. B **735**, 349 (2014). https://doi.org/10.1016/j.physletb.2014.06.051. arXiv:1404.3590
70. [RBC/UKQCD 18A] P.A. Boyle, L. Del Debbio, N. Garron, A. Juttner, A. Soni, J.T. Tsang et al., SU(3)-breaking ratios for $D_{(s)}$ and $B_{(s)}$ mesons. arXiv:1812.08791
71. [HPQCD 19A] R.J. Dowdall, C.T.H. Davies, R.R. Horgan, G.P. Lepage, C.J. Monahan, J. Shigemitsu et al., Neutral B-meson mixing from full lattice QCD at the physical point. Phys. Rev. D **100**, 094508 (2019). https://doi.org/10.1103/PhysRevD.100.094508. arXiv:1907.01025
72. [HPQCD 09] E. Gamiz, C.T. Davies, G.P. Lepage, J. Shigemitsu, M. Wingate, Neutral B meson mixing in unquenched lattice QCD. Phys. Rev. D **80**, 014503 (2009). https://doi.org/10.1103/PhysRevD.80.014503. arXiv:0902.1815
73. [FNAL/MILC 16] A. Bazavov et al., $B^0_{(s)}$-mixing matrix elements from lattice QCD for the Standard Model and beyond. Phys. Rev. D **93**, 113016 (2016). https://doi.org/10.1103/PhysRevD.93.113016. arXiv:1602.03560

74. C. Ayala, X. Lobregat, A. Pineda, Determination of $\alpha(M_z)$ from an hyperasymptotic approximation to the energy of a static quark–antiquark pair. JHEP **09**, 016 (2020). https://doi.org/10.1007/JHEP09(2020)016. arXiv:2005.12301
75. [TUMQCD 19] A. Bazavov, N. Brambilla, X. Garcia i Tormo, P. Petreczky, J. Soto, A. Vairo, et al., Determination of the QCD coupling from the static energy and the free energy. Phys. Rev. D **100**, 114511 (2019). https://doi.org/10.1103/PhysRevD.100.114511. arXiv:1907.11747
76. S. Cali, K. Cichy, P. Korcyl, J. Simeth, Running coupling constant from position-space current-current correlation functions in three-flavor lattice QCD. Phys. Rev. Lett. **125**, 242002 (2020). https://doi.org/10.1103/PhysRevLett.125.242002. arXiv:2003.05781
77. [ALPHA 17] M. Bruno, M. Dalla Brida, P. Fritzsch, T. Korzec, A. Ramos, S. Schaefer et al., QCD coupling from a nonperturbative determination of the three-flavor Λ parameter. Phys. Rev. Lett. **119**(2017), 102001 (2017). https://doi.org/10.1103/PhysRevLett.119.102001. arXiv:1706.03821
78. [PACS-CS 09A] S. Aoki et al., Precise determination of the strong coupling constant in $N_f = 2 + 1$ lattice QCD with the Schrödinger functional scheme. JHEP **0910**, 053 (2009). https://doi.org/10.1088/1126-6708/2009/10/053. arXiv:0906.3906
79. K. Maltman, D. Leinweber, P. Moran, A. Sternbeck, The realistic lattice determination of $\alpha_s(M_Z)$ revisited. Phys. Rev. D **78**, 114504 (2008). arXiv:0807.2020
80. [ETM 13] K. Cichy, E. Garcia-Ramos, K. Jansen, Chiral condensate from the twisted mass Dirac operator spectrum. JHEP **1310**, 175 (2013). https://doi.org/10.1007/JHEP10(2013)175. arXiv:1303.1954
81. [ETMC 17E] C. Alexandrou, A. Athenodorou, K. Cichy, M. Constantinou, D.P. Horkel, K. Jansen et al., Topological susceptibility from twisted mass fermions using spectral projectors and the gradient flow. Phys. Rev. D **97**, 074503 (2018). https://doi.org/10.1103/PhysRevD.97.074503. arXiv:1709.06596
82. S. Borsanyi, S. Dürr, Z. Fodor, S. Krieg, A. Schäfer et al., SU(2) chiral perturbation theory low-energy constants from 2+1 flavor staggered lattice simulations. Phys. Rev. D **88**, 014513 (2013). https://doi.org/10.1103/PhysRevD.88.014513. arXiv:1205.0788
83. [BMW 13] S. Dürr, Z. Fodor, C. Hoelbling, S. Krieg, T. Kurth et al., Lattice QCD at the physical point meets SU(2) chiral perturbation theory. Phys. Rev. D **90**, 114504 (2014). https://doi.org/10.1103/PhysRevD.90.114504. arXiv:1310.3626
84. [RBC/UKQCD 15E] P.A. Boyle et al., Low energy constants of SU(2) partially quenched chiral perturbation theory from N_f=2+1 domain wall QCD. Phys. Rev. D **93**, 054502 (2016). https://doi.org/10.1103/PhysRevD.93.054502. arXiv:1511.01950
85. [JLQCD 16B] G. Cossu, H. Fukaya, S. Hashimoto, T. Kaneko, J.-I. Noaki, Stochastic calculation of the Dirac spectrum on the lattice and a determination of chiral condensate in 2+1-flavor QCD. PTEP **2016**, 093B06 (2016). https://doi.org/10.1093/ptep/ptw129. arXiv: 1607.01099
86. [JLQCD 17A] S. Aoki, G. Cossu, H. Fukaya, S. Hashimoto, T. Kaneko, Topological susceptibility of QCD with dynamical Möbius domain wall fermions. PTEP **2018**, 043B07 (2018). https://doi.org/10.1093/ptep/pty041. arXiv:1705.10906
87. [ETM 09C] R. Baron et al., Light meson physics from maximally twisted mass lattice QCD. JHEP **08**, 097 (2010). https://doi.org/10.1007/JHEP08(2010)097. arXiv:0911.5061
88. B.B. Brandt, A. Jüttner, H. Wittig, The pion vector form factor from lattice QCD and NNLO chiral perturbation theory. JHEP **1311**, 034 (2013). https://doi.org/10.1007/JHEP11(2013)034. arXiv:1306.2916
89. G.P. Engel, L. Giusti, S. Lottini, R. Sommer, Spectral density of the Dirac operator in two-flavor QCD. Phys. Rev. D **91**, 054505 (2015). https://doi.org/10.1103/PhysRevD.91.054505. arXiv:1411.6386
90. [ETM 11] R. Baron et al., Light hadrons from $N_f = 2+1+1$ dynamical twisted mass fermions. PoS LAT **2010**, 123 (2010). arXiv:1101.0518
91. [NPLQCD 11] S.R. Beane, W. Detmold, P. Junnarkar, T. Luu, K. Orginos et al., SU(2) low-energy constants from mixed-action lattice QCD. Phys. Rev. D **86**, 094509 (2012). https://doi.org/10.1103/PhysRevD.86.094509. arXiv:1108.1380
92. [ETM 08] R. Frezzotti, V. Lubicz, S. Simula, Electromagnetic form factor of the pion from twisted-mass lattice QCD at $N_f = 2$. Phys. Rev. D **79**, 074506 (2009). https://doi.org/10.1103/PhysRevD.79.074506. arXiv:0812.4042
93. V. Gülpers, G. von Hippel, H. Wittig, The scalar radius of the pion from lattice QCD in the continuum limit. Eur. Phys. J. A **51**, 158 (2015). https://doi.org/10.1140/epja/i2015-15158-0. arXiv:1507.01749
94. [ETM 15E] C. Helmes, C. Jost, B. Knippschild, C. Liu, J. Liu, L. Liu et al., Hadron–hadron interactions from $N_f = 2 + 1 + 1$ lattice QCD: isospin-2 π-π scattering length. JHEP **09**, 109 (2015). https://doi.org/10.1007/JHEP09(2015)109. arXiv:1506.00408
95. [ETM 09G] X. Feng, K. Jansen, D.B. Renner, The pi+ pi+ scattering length from maximally twisted mass lattice QCD. Phys. Lett. B **684**, 268 (2010). https://doi.org/10.1016/j.physletb.2010.01.018. arXiv:0909.3255
96. [ETM 18B] C. Helmes, C. Jost, B. Knippschild, B. Kostrzewa, L. Liu, F. Pittler et al., Hadron–hadron interactions from $N_f = 2+1+1$ lattice QCD: $I = 3/2$ πK scattering length. Phys. Rev. D **98**, 114511 (2018). https://doi.org/10.1103/PhysRevD.98.114511. arXiv:1809.08886
97. [ETM 17G] C. Helmes, C. Jost, B. Knippschild, B. Kostrzewa, L. Liu, C. Urbach et al., Hadron–hadron interactions from $N_f = 2+1+1$ lattice QCD: isospin-1 KK scattering length. Phys. Rev. D **96**, 034510 (2017). https://doi.org/10.1103/PhysRevD.96.034510. arXiv:1703.04737
98. [PNDME 18] R. Gupta, Y.-C. Jang, B. Yoon, H.-W. Lin, V. Cirigliano, T. Bhattacharya, Isovector charges of the nucleon from 2+1+1-flavor lattice QCD. Phys. Rev. D **98**, 034503 (2018). https://doi.org/10.1103/PhysRevD.98.034503. arXiv:1806.09006
99. [CalLat 18] C.C. Chang et al., A per-cent-level determination of the nucleon axial coupling from quantum chromodynamics. Nature (2018). https://doi.org/10.1038/s41586-018-0161-8. arXiv:1805.12130
100. [CalLat 19] A. Walker-Loud et al., Lattice QCD determination of g_A. PoS CD **2018**, 020 (2020). https://doi.org/10.22323/1.317.0020. arXiv:1912.08321
101. [χQCD 18] J. Liang, Y.-B. Yang, T. Draper, M. Gong, K.-F. Liu, Quark spins and Anomalous Ward Identity. Phys. Rev. D **98**, 074505 (2018). https://doi.org/10.1103/PhysRevD.98.074505. arXiv:1806.08366
102. [Mainz 19] T. Harris, G. von Hippel, P. Junnarkar, H.B. Meyer, K. Ottnad, J. Wilhelm et al., Nucleon isovector charges and twist-2 matrix elements with $N_f = 2 + 1$ dynamical Wilson quarks. Phys. Rev. D **100**, 034513 (2019). https://doi.org/10.1103/PhysRevD.100.034513. arXiv:1905.01291
103. [PNDME 18A] H.-W. Lin, R. Gupta, B. Yoon, Y.-C. Jang, T. Bhattacharya, Quark contribution to the proton spin from 2+1+1-flavor lattice QCD. Phys. Rev. D **98**, 094512 (2018). https://doi.org/10.1103/PhysRevD.98.094512. arXiv:1806.10604
104. [BMW 11A] S. Dürr et al., Sigma term and strangeness content of octet baryons. Phys. Rev. D **85**, 014509 (2012). https://doi.org/10.1103/PhysRevD.85.014509. https://doi.org/10.1103/PhysRevD.93.039905. arXiv:1109.4265 [Erratum: Phys. Rev. D 93(3), 039905 (2016)]
105. [BMW 15] S. Dürr et al., Lattice computation of the nucleon scalar quark contents at the physical point. Phys. Rev. Lett. **116**, 172001 (2016). https://doi.org/10.1103/PhysRevLett.116.172001. arXiv:1510.08013

106. [χQCD 15A] Y.-B. Yang, A. Alexandru, T. Draper, J. Liang, K.-F. Liu, πN and strangeness sigma terms at the physical point with chiral fermions. Phys. Rev. D **94**, 054503 (2016). https://doi.org/10.1103/PhysRevD.94.054503. arXiv:1511.09089
107. [QCDSF 12] G. Bali, P. Bruns, S. Collins, M. Deka, B. Glasle et al., Nucleon mass and sigma term from lattice QCD with two light fermion flavors. Nucl. Phys. B **866**, 1 (2013). https://doi.org/10.1016/j.nuclphysb.2012.08.009. arXiv:1206.7034
108. [MILC 12C] W. Freeman, D. Toussaint, Intrinsic strangeness and charm of the nucleon using improved staggered fermions. Phys. Rev. D **88**, 054503 (2013). https://doi.org/10.1103/PhysRevD.88.054503. arXiv:1204.3866
109. P. Junnarkar, A. Walker-Loud, Scalar strange content of the nucleon from lattice QCD. Phys. Rev. D **87**, 114510 (2013). https://doi.org/10.1103/PhysRevD.87.114510. arXiv:1301.1114
110. [PNDME 18B] [PNDME 18B] R. Gupta, B. Yoon, T. Bhattacharya, V. Cirigliano, Y.-C. Jang, H.-W. Lin, Flavor diagonal tensor charges of the nucleon from (2+1+1)-flavor lattice QCD. Phys. Rev. D **98**, 091501 (2018). https://doi.org/10.1103/PhysRevD.98.091501. arXiv:1808.07597
111. [CalLat 20A] N. Miller et al., Scale setting the Möbius domain wall fermion on gradient-flowed HISQ action using the omega baryon mass and the gradient-flow scales t_0 and w_0. Phys. Rev. D **103**, 054511 (2021). https://doi.org/10.1103/PhysRevD.103.054511. arXiv:2011.12166
112. [MILC 15] A. Bazavov et al., Gradient flow and scale setting on MILC HISQ ensembles. Phys. Rev. D **93**, 094510 (2016). https://doi.org/10.1103/PhysRevD.93.094510. arXiv:1503.02769
113. [CLS 16] M. Bruno, T. Korzec, S. Schaefer, Setting the scale for the CLS 2+1 flavor ensembles. Phys. Rev. D **95**, 074504 (2017). https://doi.org/10.1103/PhysRevD.95.074504. arXiv:1608.08900
114. [BMW 12A] S. Borsanyi, S. Dürr, Z. Fodor, C. Hoelbling, S.D. Katz et al., High-precision scale setting in lattice QCD. JHEP **1209**, 010 (2012). https://doi.org/10.1007/JHEP09(2012)010. arXiv:1203.4469
115. [BMW 20] Sz. Borsanyi et al., Leading hadronic contribution to the muon magnetic moment from lattice QCD. Nature **593**, 51 (2021). https://doi.org/10.1038/s41586-021-03418-1. arXiv:2002.12347
116. [HotQCD 14] A. Bazavov et al., Equation of state in (2+1)-flavor QCD. Phys. Rev. D **90**, 094503 (2014). https://doi.org/10.1103/PhysRevD.90.094503. arXiv:1407.6387
117. [RBC/UKQCD 10A] Y. Aoki et al., Continuum limit physics from 2+1 flavor domain wall QCD. Phys. Rev. D **83**, 074508 (2011). https://doi.org/10.1103/PhysRevD.83.074508. arXiv:1011.0892
118. [HPQCD 05B] A. Gray et al., The upsilon spectrum and m_b from full lattice QCD. Phys. Rev. D **72**, 094507 (2005). https://doi.org/10.1103/PhysRevD.72.094507. arXiv:hep-lat/0507013
119. C. Aubin et al., Light hadrons with improved staggered quarks: approaching the continuum limit. Phys. Rev. D **70**, 094505 (2004). https://doi.org/10.1103/PhysRevD.70.094505. arXiv:hep-lat/0402030
120. [HPQCD 09B] C.T.H. Davies, E. Follana, I. Kendall, G.P. Lepage, C. McNeile, Precise determination of the lattice spacing in full lattice QCD. Phys. Rev. D **81**, 034506 (2010). https://doi.org/10.1103/PhysRevD.81.034506Phys.Rev. arXiv:0910.1229
121. K. Symanzik, Continuum limit and improved action in lattice theories. 1. Principles and ϕ^4 theory. Nucl. Phys. B **226**, 187 (1983). https://doi.org/10.1016/0550-3213(83)90468-6
122. K. Symanzik, Continuum limit and improved action in lattice theories. 2. O(N) nonlinear sigma model in perturbation theory. Nucl. Phys. B **226**, 205 (1983). https://doi.org/10.1016/0550-3213(83)90469-8
123. [RBC 07A] D.J. Antonio et al., Localization and chiral symmetry in 3 flavor domain wall QCD. Phys. Rev. D **77**, 014509 (2008). https://doi.org/10.1103/PhysRevD.77.014509. arXiv:0705.2340
124. [MILC 10] A. Bazavov et al., Topological susceptibility with the asqtad action. Phys. Rev. D **81**, 114501 (2010). https://doi.org/10.1103/PhysRevD.81.114501. arXiv:1003.5695
125. [ALPHA 10C] S. Schaefer, R. Sommer, F. Virotta, Critical slowing down and error analysis in lattice QCD simulations. Nucl. Phys. Phys. B **845**, 93 (2011). https://doi.org/10.1016/j.nuclphysb.2010.11.020Nucl. arXiv:1009.5228
126. M. Lüscher, Topology, the Wilson flow and the HMC algorithm. PoS LATTICE **2010**, 015 (2010). arXiv:1009.5877
127. S. Schaefer, Algorithms for lattice QCD: progress and challenges. AIP. Conf. Proc. **1343**, 93 (2011). https://doi.org/10.1063/1.3574948. arXiv:1011.5641
128. A. Chowdhury, A. Harindranath, J. Maiti, P. Majumdar, Topological susceptibility in lattice Yang–Mills theory with open boundary condition. JHEP **02**, 045 (2014). https://doi.org/10.1007/JHEP02(2014)045. arXiv:1311.6599
129. [LSD 14] R.C. Brower et al., Maximum-likelihood approach to topological charge fluctuations in lattice Gauge theory. Phys. Rev. D **90**, 014503 (2014). https://doi.org/10.1103/PhysRevD.90.014503. arXiv:1403.2761
130. [JLQCD 15] H. Fukaya, S. Aoki, G. Cossu, S. Hashimoto, T. Kaneko, J. Noaki, η' meson mass from topological charge density correlator in QCD. Phys. Rev. D **92**, 111501 (2015). https://doi.org/10.1103/PhysRevD.92.111501. arXiv:1509.00944
131. L. Del Debbio, H. Panagopoulos, E. Vicari, Theta dependence of SU(N) gauge theories. JHEP **08**, 044 (2002). https://doi.org/10.1088/1126-6708/2002/08/044. arXiv:hep-th/0204125
132. C. Bernard et al., Topological susceptibility with the improved Asqtad action. Phys. Rev. D **68**, 114501 (2003). https://doi.org/10.1103/PhysRevD.68.114501. arXiv:hep-lat/0308019
133. M. Lüscher, S. Schaefer, Lattice QCD without topology barriers. JHEP **1107**, 036 (2011). https://doi.org/10.1007/JHEP07(2011)036. arXiv:1105.4749
134. M.G. Endres, R.C. Brower, W. Detmold, K. Orginos, A.V. Pochinsky, Multiscale Monte Carlo equilibration: pure Yang–Mills theory. Phys. Rev. D **92**, 114516 (2015). https://doi.org/10.1103/PhysRevD.92.114516. arXiv:1510.04675
135. W. Detmold, M.G. Endres, Scaling properties of multiscale equilibration. Phys. Rev. D **97**, 074507 (2018). https://doi.org/10.1103/PhysRevD.97.074507. arXiv:1801.06132
136. S. Mages, B.C. Toth, S. Borsanyi, Z. Fodor, S. Katz, K.K. Szabo, Lattice QCD on non-orientable manifolds. Phys. Rev. D **95**, 094512 (2017). https://doi.org/10.1103/PhysRevD.95.094512. arXiv:1512.06804
137. M. Bruno et al., Simulation of QCD with $N_f = 2 + 1$ flavors of non-perturbatively improved Wilson fermions. JHEP **02**, 043 (2015). https://doi.org/10.1007/JHEP02(2015)043. arXiv:1411.3982
138. R. Brower, S. Chandrasekharan, J.W. Negele, U. Wiese, QCD at fixed topology. Phys. Lett. B **560**, 64 (2003). https://doi.org/10.1016/S0370-2693(03)00369-1. arXiv:hep-lat/0302005

139. S. Aoki, H. Fukaya, S. Hashimoto, T. Onogi, Finite volume QCD at fixed topological charge. Phys. Rev. D **76**, 054508 (2007). https://doi.org/10.1103/PhysRevD.76.054508. arXiv:0707.0396
140. I. Bautista, W. Bietenholz, A. Dromard, U. Gerber, L. Gonglach, C.P. Hofmann et al., Measuring the topological susceptibility in a fixed sector. Phys. Rev. D **92**, 114510 (2015). https://doi.org/10.1103/PhysRevD.92.114510. arXiv:1503.06853
141. W. Bietenholz, C. Czaban, A. Dromard, U. Gerber, C.P. Hofmann, H. Mejía-Díaz et al., Interpreting numerical measurements in fixed topological sectors. Phys. Rev. D **93**, 114516 (2016). https://doi.org/10.1103/PhysRevD.93.114516. arXiv:1603.05630
142. C. Bernard, D. Toussaint, Effects of nonequilibrated topological charge distributions on pseudoscalar meson masses and decay constants. Phys. Rev. D **97**, 074502 (2018). https://doi.org/10.1103/PhysRevD.97.074502. arXiv:1707.05430
143. S. Duane, A.D. Kennedy, B.J. Pendleton, D. Roweth, Hybrid Monte Carlo. Phys. Lett. B **195**, 216 (1987). https://doi.org/10.1016/0370-2693(87)91197-X
144. M.A. Clark, A.D. Kennedy, Accelerating staggered fermion dynamics with the rational hybrid Monte Carlo (RHMC) algorithm. Phys. Rev. D **75**, 011502 (2007). https://doi.org/10.1103/PhysRevD.75.011502. arXiv:hep-lat/0610047
145. [MILC 12B] A. Bazavov et al., Lattice QCD ensembles with four flavors of highly improved staggered quarks. Phys. Rev. D **87**, 054505 (2013). https://doi.org/10.1103/PhysRevD.87.054505. arXiv:1212.4768
146. G. Colangelo, S. Dürr, C. Haefeli, Finite volume effects for meson masses and decay constants. Nucl. Phys. B **721**, 136 (2005). https://doi.org/10.1016/j.nuclphysb.2005.05.015. arXiv:hep-lat/0503014
147. [BMW 14] Sz. Borsanyi et al., Ab initio calculation of the neutron–proton mass difference. Science **347**, 1452 (2015). https://doi.org/10.1126/science.1257050. arXiv:1406.4088
148. Z. Davoudi, M.J. Savage, Finite-volume electromagnetic corrections to the masses of mesons, baryons and nuclei. Phys. Rev. D **90**, 054503 (2014). https://doi.org/10.1103/PhysRevD.90.054503. arXiv:1402.6741
149. V. Lubicz, G. Martinelli, C.T. Sachrajda, F. Sanfilippo, S. Simula, N. Tantalo, Finite-volume QED corrections to decay amplitudes in lattice QCD. Phys. Rev. D **95**, 034504 (2017). https://doi.org/10.1103/PhysRevD.95.034504. arXiv:1611.08497
150. Z. Davoudi, J. Harrison, A. Jüttner, A. Portelli, M.J. Savage, Theoretical aspects of quantum electrodynamics in a finite volume with periodic boundary conditions. Phys. Rev. D **99**, 034510 (2019). https://doi.org/10.1103/PhysRevD.99.034510. arXiv:1810.05923
151. [ETM 07A] Ph. Boucaud et al., Dynamical twisted mass fermions with light quarks. Phys. Lett. B **650**, 304 (2007). https://doi.org/10.1016/j.physletb.2007.04.054. arXiv:hep-lat/0701012
152. O. Bär, Chiral logs in twisted mass lattice QCD with large isospin breaking. Phys. Rev. D **82**, 094505 (2010). https://doi.org/10.1103/PhysRevD.82.094505. arXiv:1008.0784
153. S. Dürr, Theoretical issues with staggered fermion simulations. PoS LAT **2005**, 021 (2006). arXiv:hep-lat/0509026
154. S.R. Sharpe, Rooted staggered fermions: good, bad or ugly? PoS LAT **2006**, 022 (2006). arXiv:hep-lat/0610094
155. A.S. Kronfeld, Lattice gauge theory with staggered fermions: how, where, and why (not). PoS LAT **2007**, 016 (2007). arXiv:0711.0699
156. M. Golterman, QCD with rooted staggered fermions. PoS CONFINEMENT **8**, 014 (2008). arXiv:0812.3110
157. A. Bazavov et al., Full nonperturbative QCD simulations with 2+1 flavors of improved staggered quarks. Rev. Mod. Phys. **82**, 1349 (2010). arXiv:0903.3598
158. [ALPHA 14A] M. Bruno, J. Finkenrath, F. Knechtli, B. Leder, R. Sommer, Effects of heavy sea quarks at low energies. Phys. Rev. Lett. **114**, 102001 (2015). https://doi.org/10.1103/PhysRevLett.114.102001. arXiv:1410.8374
159. [ALPHA 17A] F. Knechtli, T. Korzec, B. Leder, G. Moir, Power corrections from decoupling of the charm quark. Phys. Lett. B **774**, 649 (2017). https://doi.org/10.1016/j.physletb.2017.10.025. arXiv:1706.04982
160. A. Athenodorou, J. Finkenrath, F. Knechtli, T. Korzec, B. Leder, M.K. Marinkovic et al., How perturbative are heavy sea quarks? Nucl. Phys. B **943**, 114612 (2019). https://doi.org/10.1016/j.nuclphysb.2019.114612. arXiv:1809.03383
161. S. Cali, F. Knechtli, T. Korzec, How much do charm sea quarks affect the charmonium spectrum? Eur. Phys. J. C **79**, 607 (2019). https://doi.org/10.1140/epjc/s10052-019-7108-6. arXiv:1905.12971
162. [ALPHA 21A] S. Cali, K. Eckert, J. Heitger, F. Knechtli, T. Korzec, Charm sea effects on charmonium decay constants and heavy meson masses. Eur. Phys. J. C **81**, 733 (2021). https://doi.org/10.1140/epjc/s10052-021-09520-y. arXiv:2105.12278
163. M. Schmelling, Averaging correlated data **51**, 676 (1995). https://doi.org/10.1088/0031-8949/51/6/002Phys.Scripta
164. J.L. Rosner, S. Stone, R.S. Van de Water, Leptonic decays of charged pseudoscalar mesons. Rev. Part. Phys. [201] 2015 update. arXiv:1509.02220
165. Particle Data Group collaboration, Review of Particle Physics. PTEP **2020**, 083C01 (2020). https://doi.org/10.1093/ptep/ptaa104
166. J. Gasser, H. Leutwyler, Quark masses. Phys. Rep. **87**, 77 (1982). https://doi.org/10.1016/0370-1573(82)90035-7
167. [ALPHA 20] R. Höllwieser, F. Knechtli, T. Korzec, Scale setting for $N_f = 3 + 1$ QCD. Eur. Phys. J. C **80**, 349 (2020). https://doi.org/10.1140/epjc/s10052-020-7889-7. arXiv:2002.02866
168. M. Gell-Mann, R.J. Oakes, B. Renner, Behavior of current divergences under SU(3)×SU(3). Phys. Rev. **175**, 2195 (1968). https://doi.org/10.1103/PhysRev.175.2195
169. [RBC 07] T. Blum, T. Doi, M. Hayakawa, T. Izubuchi, N. Yamada, Determination of light quark masses from the electromagnetic splitting of pseudoscalar meson masses computed with two flavors of domain wall fermions. Phys. Rev. D **76**, 114508 (2007). https://doi.org/10.1103/PhysRevD.76.114508. arXiv:0708.0484
170. T. Blum et al., Electromagnetic mass splittings of the low lying hadrons and quark masses from 2+1 flavor lattice QCD+QED. Phys. Rev. D **82**, 094508 (2010). https://doi.org/10.1103/PhysRevD.82.094508. arXiv:1006.1311
171. [RM123 11] G.M. de Divitiis, P. Dimopoulos, R. Frezzotti, V. Lubicz, G. Martinelli et al., Isospin breaking effects due to the up-down mass difference in lattice QCD. JHEP **1204**, 124 (2012). https://doi.org/10.1007/JHEP04(2012)124. arXiv:1110.6294
172. [RM123 13] G.M. de Divitiis, R. Frezzotti, V. Lubicz, G. Martinelli, R. Petronzio et al., Leading isospin breaking effects on the lattice. Phys. Rev. D **87**, 114505 (2013). https://doi.org/10.1103/PhysRevD.87.114505. arXiv:1303.4896
173. [BMW 13A] Sz. Borsanyi et al., Isospin splittings in the light baryon octet from lattice QCD and QED. Phys. Rev. Lett. **111**, 252001 (2013). https://doi.org/10.1103/PhysRevLett.111.252001. arXiv:1306.2287
174. J. Bijnens, N. Danielsson, Electromagnetic corrections in partially quenched chiral perturbation theory. Phys. Rev. D **75**, 014505 (2007). https://doi.org/10.1103/PhysRevD.75.014505. arXiv:hep-lat/0610127

175. [QCDSF/UKQCD 15A] R. Horsley et al., QED effects in the pseudoscalar meson sector. JHEP **04**, 093 (2016). https://doi.org/10.1007/JHEP04(2016)093. arXiv:1509.00799
176. M. Hansen, B. Lucini, A. Patella, N. Tantalo, Gauge invariant determination of charged hadron masses. JHEP **05**, 146 (2018). https://doi.org/10.1007/JHEP05(2018)146. arXiv:1802.05474
177. B. Lucini, A. Patella, A. Ramos, N. Tantalo, Charged hadrons in local finite-volume QED+QCD with C* boundary conditions. JHEP **02**, 076 (2016). https://doi.org/10.1007/JHEP02(2016)076. arXiv:1509.01636
178. A. Duncan, E. Eichten, H. Thacker, Electromagnetic splittings and light quark masses in lattice QCD. Phys. Rev. Lett. **76**, 3894 (1996). https://doi.org/10.1103/PhysRevLett.76.3894. arXiv:hep-lat/9602005
179. M. Hayakawa, S. Uno, QED in finite volume and finite size scaling effect on electromagnetic properties of hadrons. Prog. Theor. Phys. **120**, 413 (2008). https://doi.org/10.1143/PTP.120.413. arXiv:0804.2044
180. Z. Fodor, C. Hoelbling, S.D. Katz, L. Lellouch, A. Portelli, K.K. Szabo et al., Quantum electrodynamics in finite volume and nonrelativistic effective field theories. Phys. Lett. B **755**, 245 (2016). https://doi.org/10.1016/j.physletb.2016.01.047. arXiv:1502.06921
181. N. Tantalo, V. Lubicz, G. Martinelli, C.T. Sachrajda, F. Sanfilippo, S. Simula, Electromagnetic corrections to leptonic decay rates of charged pseudoscalar mesons: finite-volume effects. arXiv:1612.00199
182. J. Bijnens, J. Harrison, N. Hermansson-Truedsson, T. Janowski, A. Jüttner, A. Portelli, Electromagnetic finite-size effects to the hadronic vacuum polarization. Phys. Rev. D **100**, 014508 (2019). https://doi.org/10.1103/PhysRevD.100.014508. arXiv:1903.10591
183. M. Göckeler, R. Horsley, E. Laermann, P.E.L. Rakow, G. Schierholz, R. Sommer et al., QED: a lattice investigation of the chiral phase transition and the nature of the continuum limit. Nucl. Phys. B **334**, 527 (1990). https://doi.org/10.1016/0550-3213(90)90490-5
184. M.G. Endres, A. Shindler, B.C. Tiburzi, A. Walker-Loud, Massive photons: an infrared regularization scheme for lattice QCD+QED. Phys. Rev. Lett. **117**, 072002 (2016). https://doi.org/10.1103/PhysRevLett.117.072002. arXiv:1507.08916
185. U.J. Wiese, C periodic and G periodic QCD at finite temperature. Nucl. Phys. B **375**, 45 (1992). https://doi.org/10.1016/0550-3213(92)90333-7
186. L. Polley, Boundaries for SU(3)(C) x U(1)-el lattice gauge theory with a chemical potential. Z. Phys. C **59**, 105 (1993). https://doi.org/10.1007/BF01555844
187. P. Boyle, V. Gülpers, J. Harrison, A. Jüttner, C. Lehner, A. Portelli et al., Isospin breaking corrections to meson masses and the hadronic vacuum polarization: a comparative study **09**, 153 (2017). https://doi.org/10.1007/JHEP09(2017)153JHEP. arXiv:1706.05293
188. [RBC/UKQCD 12] R. Arthur et al., Domain wall QCD with near-physical pions. Phys. Rev. D **87**, 094514 (2013). https://doi.org/10.1103/PhysRevD.87.094514. arXiv:1208.4412
189. Y. Maezawa, P. Petreczky, Quark masses and strong coupling constant in 2+1 flavor QCD. Phys. Rev. D **94**, 034507 (2016). https://doi.org/10.1103/PhysRevD.94.034507. arXiv:1606.08798
190. [PACS-CS 12] S. Aoki, K.-I. Ishikawa, N. Ishizuka, K. Kanaya, Y. Kuramashi et al., 1+1+1 flavor QCD + QED simulation at the physical point. Phys. Rev. D **86**, 034507 (2012). https://doi.org/10.1103/PhysRevD.86.034507. arXiv:1205.2961
191. [PACS-CS 10] S. Aoki et al., Non-perturbative renormalization of quark mass in $N_f = 2 + 1$ QCD with the Schrödinger functional scheme. JHEP **1008**, 101 (2010). https://doi.org/10.1007/JHEP08(2010)101. arXiv:1006.1164
192. [PACS-CS 09] S. Aoki et al., Physical point simulation in 2+1 flavor lattice QCD, Phys. Rev. D **81**, 074503 (2010). https://doi.org/10.1103/PhysRevD.81.074503. arXiv:0911.2561
193. [PACS-CS 08] S. Aoki et al., 2+1 flavor lattice QCD toward the physical point. Phys. Rev. D **79**, 034503 (2009). https://doi.org/10.1103/PhysRevD.79.034503. arXiv:0807.1661
194. [RBC/UKQCD 08] C. Allton et al., Physical results from 2+1 flavor domain wall QCD and SU(2) chiral perturbation theory. Phys. Rev. D **78**, 114509 (2008). https://doi.org/10.1103/PhysRevD.78.114509. arXiv:0804.0473
195. [CP-PACS/JLQCD 07] T. Ishikawa et al., Light quark masses from unquenched lattice QCD. Phys. Rev. D **78**, 011502 (2008). https://doi.org/10.1103/PhysRevD.78.011502. arXiv:0704.1937
196. [HPQCD 05] Q. Mason, H.D. Trottier, R. Horgan, C.T.H. Davies, G.P. Lepage, High-precision determination of the light-quark masses from realistic lattice QCD. Phys. Rev. D **73**, 114501 (2006). https://doi.org/10.1103/PhysRevD.73.114501. arXiv:hep-ph/0511160
197. [MILC 04] C. Aubin et al., Light pseudoscalar decay constants, quark masses and low energy constants from three-flavor lattice QCD. Phys. Rev. D **70**, 114501 (2004). https://doi.org/10.1103/PhysRevD.70.114501. arXiv:hep-lat/0407028
198. [HPQCD/MILC/UKQCD 04] C. Aubin et al., First determination of the strange and light quark masses from full lattice QCD. Phys. Rev. D **70**, 031504 (2004). https://doi.org/10.1103/PhysRevD.70.031504. arxiv:hep-lat/0405022
199. T. van Ritbergen, J.A.M. Vermaseren, S.A. Larin, The four-loop β-function in quantum chromodynamics. Phys. Lett. B **400**, 379 (1997). https://doi.org/10.1016/S0370-2693(97)00370-5. arXiv:hep-ph/9701390
200. K.G. Chetyrkin, A. Retey, Renormalization and running of quark mass and field in the regularization invariant and $\overline{\text{MS}}$ schemes at three and four loops. Nucl. Phys. B **583**, 3 (2000). https://doi.org/10.1016/S0550-3213(00)00331-X. arXiv:hep-ph/9910332
201. Particle Data Group collaboration, Review of Particle Physics. Chin. Phys. C **38**, 090001 (2014), 2015 update. https://doi.org/10.1088/1674-1137/38/9/090001
202. [HPQCD 08B] I. Allison et al., High-precision charm-quark mass from current-current correlators in lattice and continuum QCD. Phys. Rev. D **78**, 054513 (2008). https://doi.org/10.1103/PhysRevD.78.054513. arXiv:0805.2999
203. [ALPHA 18C] I. Campos, P. Fritzsch, C. Pena, D. Preti, A. Ramos, A. Vladikas, Non-perturbative quark mass renormalisation and running in $N_f = 3$ QCD. Eur. Phys. J. C **78**, 387 (2018). https://doi.org/10.1140/epjc/s10052-018-5870-5. arXiv:1802.05243
204. [ETM 21A] C. Alexandrou et al., Quark masses using twisted mass fermion gauge ensembles. Phys. Rev. D **104**, 074515 (2021). https://doi.org/10.1103/PhysRevD.104.074515. arXiv:2104.13408
205. C.A. Dominguez, N.F. Nasrallah, R. Röntsch, K. Schilcher, Light quark masses from QCD sum rules with minimal hadronic bias. Nucl. Phys. Proc. Suppl. **186**, 133 (2009). https://doi.org/10.1016/j.nuclphysbps.2008.12.031. arXiv:0808.3909
206. K.G. Chetyrkin, A. Khodjamirian, Strange quark mass from pseudoscalar sum rule with $O(\alpha_s^4)$ accuracy. Eur. Phys. J. C **46**, 721 (2006). https://doi.org/10.1140/epjc/s2006-02508-8. arXiv:hep-ph/0512295
207. M. Jamin, J.A. Oller, A. Pich, Scalar $K\pi$ form factor and light quark masses. Phys. Rev. D **74**, 074009 (2006). https://doi.org/10.1103/PhysRevD.74.074009. arXiv:hep-ph/0605095

208. S. Narison, Strange quark mass from e^+e^- revisited and present status of light quark masses. Phys. Rev. D **74**, 034013 (2006). https://doi.org/10.1103/PhysRevD.74.034013. arXiv:hep-ph/0510108
209. A.I. Vainshtein et al., Sum rules for light quarks in Quantum Chromodynamics. Sov. J. Nucl. Phys. **27**, 274 (1978)
210. K. Maltman, J. Kambor, $m_u + m_d$ from isovector pseudoscalar sum rules. Phys. Lett. B **517**, 332 (2001). https://doi.org/10.1016/S0370-2693(01)00987-X. arXiv:hep-ph/0107060
211. J.A. Oller, L. Roca, Non-perturbative study of the light pseudoscalar masses in chiral dynamics. Eur. Phys. J. A **34**, 371 (2007). https://doi.org/10.1140/epja/i2006-10516-7. arXiv:hep-ph/0608290
212. R. Kaiser, The η and the η' at large N_c, diploma work. University of Bern (1997)
213. H. Leutwyler, On the 1/N-expansion in chiral perturbation theory. Nucl. Phys. Proc. Suppl. **64**, 223 (1998). https://doi.org/10.1016/S0920-5632(97)01065-7. arXiv:hep-ph/9709408
214. H. Leutwyler, The ratios of the light quark masses. Phys. Lett. B **378**, 313 (1996). https://doi.org/10.1016/0370-2693(96)00386-3. arXiv:hep-ph/9602366
215. S. Weinberg, The problem of mass. Trans. N. Y. Acad. Sci. **38**, 185 (1977)
216. R.F. Dashen, Chiral SU(3)×SU(3) as a symmetry of the strong interactions. Phys. Rev. **183**, 1245 (1969). https://doi.org/10.1103/PhysRev.183.1245
217. A. Portelli, Inclusion of isospin breaking effects in lattice simulations. PoS LATTICE **2014**, 013 (2015)
218. [ETM 10] R. Baron et al., Light hadrons from lattice QCD with light (u,d), strange and charm dynamical quarks. JHEP **1006**, 111 (2010). https://doi.org/10.1007/JHEP06(2010)111. arXiv:1004.5284
219. [MILC 16] S. Basak et al., Electromagnetic effects on the light pseudoscalar mesons and determination of m_u/m_d. PoS LATTICE **2015**, 259 (2016). arXiv: 1606.01228
220. H. Leutwyler, Light quark masses. PoS **CD09**, 005 (2009). arXiv:0911.1416
221. [QCDSF/UKQCD 15] R. Horsley et al., Isospin splittings of meson and baryon masses from three-flavor lattice QCD + QED, J. Phys. G **43**, 10LT02 (2016). https://doi.org/10.1088/0954-3899/43/10/10LT02. arXiv:1508.06401
222. [ALPHA 05] M. Della Morte et al., Non-perturbative quark mass renormalization in two-flavor QCD. Nucl. Phys. B **729**, 117 (2005). https://doi.org/10.1016/j.nuclphysb.2005.09.028. arXiv:hep-lat/0507035
223. [BMW 12] A. Portelli, S. Dürr, Z. Fodor, J. Frison, C. Hoelbling et al., Systematic errors in partially-quenched QCD plus QED lattice simulations. PoS LAT **2011**, 136 (2011). arXiv:1201.2787
224. J. Gasser, H. Leutwyler, $\eta \to 3\pi$ to one loop. Nucl. Phys. B **250**, 539 (1985). https://doi.org/10.1016/0550-3213(85)90494-8
225. G. Colangelo, S. Lanz, H. Leutwyler, E. Passemar, Dispersive analysis of $\eta \to 3\pi$. Eur. Phys. J. C **78**, 947 (2018). https://doi.org/10.1140/epjc/s10052-018-6377-9. arXiv:1807.11937
226. G. Amoros, J. Bijnens, P. Talavera, QCD isospin breaking in meson masses, decay constants and quark mass ratios. Nucl. Phys. B **602**, 87 (2001). https://doi.org/10.1016/S0550-3213(01)00121-3. arXiv:hep-ph/0101127
227. [ALPHA 21] J. Heitger, F. Joswig, S. Kuberski, Determination of the charm quark mass in lattice QCD with $2 + 1$ flavours on fine lattices. JHEP **05**, 288 (2021). https://doi.org/10.1007/JHEP05(2021)288. arXiv:2101.02694
228. [ETM 14B] A. Bussone et al., Heavy flavour precision physics from $N_f = 2 + 1 + 1$ lattice simulations. in *International Conference on High Energy Physics 2014 (ICHEP 2014)*, Valencia, Spain, July 2–9, 2014, vol. 273–275, pp. 273–275 (2016). https://doi.org/10.1016/j.nuclphysbps.2015.09.265DOI. arXiv:1411.0484
229. [HPQCD 13B] A.J. Lee et al., Mass of the b quark from lattice NRQCD and lattice perturbation theory. Phys. Rev. D **87**, 074018 (2013). https://doi.org/10.1103/PhysRevD.87.074018. arXiv:1302.3739
230. [ALPHA 13C] F. Bernardoni et al., The b-quark mass from non-perturbative $N_f = 2$ Heavy Quark Effective Theory at $O(1/m_h)$. Phys. Lett. B **730**, 171 (2014). https://doi.org/10.1016/j.physletb.2014.01.046. arXiv:1311.5498
231. [ETM 11A] P. Dimopoulos et al., Lattice QCD determination of m_b, f_B and f_{B_s} with twisted mass Wilson fermions. JHEP **1201**, 046 (2012). https://doi.org/10.1007/JHEP01(2012)046. arXiv:1107.1441
232. M. Moulson, Experimental determination of V_{us} from kaon decays. PoS CKM **2016**, 033 (2017). arXiv:1704.04104
233. J. Gasser, G.R.S. Zarnauskas, On the pion decay constant. Phys. Lett. B **693**, 122 (2010). https://doi.org/10.1016/j.physletb.2010.08.021. arXiv:1008.3479
234. Particle Data Group collaboration, Review of Particle Physics. Phys. C **40**, 100001 (2016). https://doi.org/10.1088/1674-1137/40/10/100001Chin
235. J. Gasser, A. Rusetsky, I. Scimemi, Electromagnetic corrections in hadronic processes. Eur. Phys. J. **C32**, 97 (2003). https://doi.org/10.1140/epjc/s2003-01383-1. arXiv:hep-ph/0305260
236. A. Rusetsky, Isospin symmetry breaking. PoS CD **09**, 071 (2009). arXiv:0910.5151
237. J. Gasser, Theoretical progress on cusp effect and $K_{\ell 4}$ decays. PoS KAON **07**, 033 (2008). arXiv:0710.3048
238. N. Carrasco, V. Lubicz, G. Martinelli, C.T. Sachrajda, N. Tantalo, C. Tarantino et al., QED corrections to hadronic processes in lattice QCD. Phys. Rev. D **91**, 074506 (2015). https://doi.org/10.1103/PhysRevD.91.074506. arXiv:1502.00257
239. D. Giusti, V. Lubicz, G. Martinelli, C.T. Sachrajda, F. Sanfilippo, S. Simula et al., First lattice calculation of the QED corrections to leptonic decay rates. Phys. Rev. Lett. **120**, 072001 (2018). https://doi.org/10.1103/PhysRevLett.120.072001. arXiv:1711.06537
240. M. Di Carlo, D. Giusti, V. Lubicz, G. Martinelli, C. Sachrajda, F. Sanfilippo et al., Light-meson leptonic decay rates in lattice QCD+QED. Phys. Rev. D **100**, 034514 (2019). https://doi.org/10.1103/PhysRevD.100.034514. arXiv:1904.08731
241. V. Cirigliano, H. Neufeld, A note on isospin violation in $P_{\ell 2}(\gamma)$ decays. Phys. Lett. B **700**, 7 (2011). https://doi.org/10.1016/j.physletb.2011.04.038. arXiv:1102.0563
242. P. Boyle, V. Guelpers, A. Juettner, C. Lehner, F. Hogain, A. Portelli et al., QED corrections to leptonic decay rates. PoS LATTICE **2018**, 267 (2019). https://doi.org/10.22323/1.334.0267. arXiv:1902.00295
243. C.Y. Seng, M. Gorchtein, M.J. Ramsey-Musolf, Dispersive evaluation of the inner radiative correction in neutron and nuclear β decay. Phys. Rev. D **100**, 013001 (2019). https://doi.org/10.1103/PhysRevD.100.013001. arXiv:1812.03352
244. C.-Y. Seng, M. Gorchtein, H.H. Patel, M.J. Ramsey-Musolf, Reduced hadronic uncertainty in the determination of V_{ud}. Phys. Rev. Lett. **121**, 241804 (2018). https://doi.org/10.1103/PhysRevLett.121.241804. arXiv:1807.10197

245. W.J. Marciano, A. Sirlin, Improved calculation of electroweak radiative corrections and the value of V(ud). Phys. Rev. Lett. **96**, 032002 (2006). https://doi.org/10.1103/PhysRevLett.96.032002. arXiv:hep-ph/0510099
246. A. Czarnecki, W.J. Marciano, A. Sirlin, Radiative corrections to neutron and nuclear beta decays revisited. Phys. Rev. D **100**, 073008 (2019). https://doi.org/10.1103/PhysRevD.100.073008. arXiv:1907.06737
247. J. Hardy, I.S. Towner, $|V_{ud}|$ from nuclear β decays. PoS CKM **2016**, 028 (2016)
248. I.S. Towner, J.C. Hardy, An improved calculation of the isospin-symmetry-breaking corrections to superallowed Fermi β decay. Phys. Rev. C **77**, 025501 (2008). https://doi.org/10.1103/PhysRevC.77.025501. arXiv:0710.3181
249. G.A. Miller, A. Schwenk, Isospin-symmetry-breaking corrections to superallowed Fermi β decay: formalism and schematic models. Phys. Rev. C **78**, 035501 (2008). https://doi.org/10.1103/PhysRevC.78.035501. arXiv:0805.0603
250. N. Auerbach, Coulomb corrections to superallowed β decay in nuclei. Phys. Rev. C **79**, 035502 (2009). https://doi.org/10.1103/PhysRevC.79.035502. arXiv:0811.4742
251. H. Liang, N. Van Giai, J. Meng, Isospin corrections for superallowed Fermi β decay in self-consistent relativistic random-phase approximation approaches. Phys. Rev. C **79**, 064316 (2009). https://doi.org/10.1103/PhysRevC.79.064316. arXiv:0904.3673
252. G.A. Miller, A. Schwenk, Isospin-symmetry-breaking corrections to superallowed Fermi β decay: radial excitations. Phys. Rev. C **80**, 064319 (2009). https://doi.org/10.1103/PhysRevC.80.064319. arXiv:0910.2790
253. I. Towner, J. Hardy, Comparative tests of isospin-symmetry-breaking corrections to superallowed $0^+ \to 0^+$ nuclear β decay. Phys. Rev. C **82**, 065501 (2010). https://doi.org/10.1103/PhysRevC.82.065501. arXiv:1007.5343
254. J.C. Hardy, I.S. Towner, Superallowed $0^+ \to 0^+$ nuclear β decays: 2014 critical survey, with precise results for V_{ud} and CKM unitarity. Phys. Rev. C **91**, 025501 (2015). https://doi.org/10.1103/PhysRevC.91.025501. arXiv:1411.5987
255. M. Gorchtein, γW Box inside out: nuclear polarizabilities distort the beta decay spectrum. Phys. Rev. Lett. **123**, 042503 (2019). https://doi.org/10.1103/PhysRevLett.123.042503. arXiv:1812.04229
256. J.C. Hardy, I.S. Towner, Superallowed $0^+ \to 0^+$ nuclear β decays: 2020 critical survey, with implications for V_{ud} and CKM unitarity. Phys. Rev. C **102**, 045501 (2020). https://doi.org/10.1103/PhysRevC.102.045501
257. E. Gamiz, M. Jamin, A. Pich, J. Prades, F. Schwab, Determination of m_s and $|V_{us}|$ from hadronic τ decays. JHEP **01**, 060 (2003). arXiv:hep-ph/0212230
258. E. Gamiz, M. Jamin, A. Pich, J. Prades, F. Schwab, V_{us} and m_s from hadronic τ decays. Phys. Rev. Lett. **94**, 011803 (2005). https://doi.org/10.1103/PhysRevLett.94.011803. arXiv:hep-ph/0408044
259. K. Maltman, A mixed τ-electroproduction sum rule for V_{us}. Phys. Lett. B **672**, 257 (2009). https://doi.org/10.1016/j.physletb.2009.01.036. arXiv:0811.1590
260. A. Pich, R. Kass, Talks given at CKM 2008. http://ckm2008.roma1.infn.it
261. Y. Amhis et al., Averages of b-hadron, c-hadron, and τ-lepton properties as of 2018. Eur. Phys. J. C **81**, 226 (2021). https://doi.org/10.1140/epjc/s10052-020-8156-7. arXiv:1909.12524
262. K. Maltman, C.E. Wolfe, S. Banerjee, J.M. Roney, I. Nugent, Status of the hadronic τ determination of V_{us}. Int. J. Mod. Phys. A **23**, 3191 (2008). https://doi.org/10.1142/S0217751X08041803. arXiv:0807.3195
263. K. Maltman, C.E. Wolfe, S. Banerjee, I.M. Nugent, J.M. Roney, Status of the hadronic τ decay determination of $|V_{us}|$. Nucl. Phys. Proc. Suppl. **189**, 175 (2009). https://doi.org/10.1016/j.nuclphysbps.2009.03.031. arXiv:0906.1386
264. E. Gamiz, M. Jamin, A. Pich, J. Prades, F. Schwab, Theoretical progress on the V_{us} determination from τ decays. PoS KAON **07**, 008 (2008). arXiv:0709.0282
265. E. Gamiz, $|V_{us}|$ from hadronic τ decays, CKM (2012). arXiv:1301.2206
266. R.J. Hudspith, R. Lewis, K. Maltman, J. Zanotti, A resolution of the inclusive flavor-breaking τ $|V_{us}|$ puzzle. Phys. Lett. B **781**, 206 (2018). https://doi.org/10.1016/j.physletb.2018.03.074. arXiv:1702.01767
267. K. Maltman, P. Boyle, R. Hudspith, T. Izubuchi, A. Juttner, C. Lehner et al., Current status of inclusive hadronic tau determinations of $|V_{us}|$. Sci. Post Phys. Proc. 6 (2019). https://doi.org/10.21468/SciPostPhysProc.1.006
268. [RBC/UKQCD 18] P. Boyle, R.J. Hudspith, T. Izubuchi, A. Jüttner, C. Lehner, R. Lewis et al., Novel |Vus| determination using inclusive strange τ decay and lattice hadronic vacuum polarization functions. Phys. Rev. Lett. **121**, 202003 (2018). https://doi.org/10.1103/PhysRevLett.121.202003. arXiv:1803.07228
269. M. Antonelli et al., An evaluation of $|V_{us}|$ and precise tests of the Standard Model from world data on leptonic and semileptonic kaon decays. Eur. Phys. J. C **69**, 399 (2010). https://doi.org/10.1140/epjc/s10052-010-1406-3. arXiv:1005.2323
270. T. Ishikawa, T. Blum, M. Hayakawa, T. Izubuchi, C. Jung et al., Full QED+QCD low-energy constants through reweighting. Phys. Rev. Lett. **109**, 072002 (2012). https://doi.org/10.1103/PhysRevLett.109.072002. arXiv:1202.6018
271. T. Izubuchi, Lattice QCD + QED − from isospin breaking to g-2 light-by-light, talk given at Lattice 2012, Cairns, Australia. http://www.physics.adelaide.edu.au/cssm/lattice2012
272. N. Tantalo, Isospin breaking effects on the lattice. PoS LATTICE **2013**, 007 (2014). arXiv:1311.2797
273. C. Sachrajda, M. Di Carlo, G. Martinelli, D. Giusti, V. Lubicz, F. Sanfilippo et al., Radiative corrections to semileptonic decay rates. PoS LATTICE **2019**, 162 (2019). https://doi.org/10.22323/1.363.0162. arXiv:1910.07342
274. C.-Y. Seng, X. Feng, M. Gorchtein, L.-C. Jin, U.-G. Meißner, New method for calculating electromagnetic effects in semileptonic beta-decays of mesons. JHEP **10**, 179 (2020). https://doi.org/10.1007/JHEP10(2020)179. arXiv:2009.00459
275. P.-X. Ma, X. Feng, M. Gorchtein, L.-C. Jin, C.-Y. Seng, Lattice QCD calculation of the electroweak box diagrams for the kaon semileptonic decays. Phys. Rev. D **103**, 114503 (2021). https://doi.org/10.1103/PhysRevD.103.114503. arXiv:2102.12048
276. C.-Y. Seng, D. Galviz, M. Gorchtein, U.-G. Meißner, Improved K_{e3} radiative corrections sharpen the $K_{\mu 2}$-K_{l3} discrepancy. JHEP **11**, 172 (2021). https://doi.org/10.1007/JHEP11(2021)172. arXiv:2103.04843
277. M. Ademollo, R. Gatto, Nonrenormalization theorem for the strangeness violating vector currents. Phys. Rev. Lett. **13**, 264 (1964). https://doi.org/10.1103/PhysRevLett.13.264
278. J. Gasser, H. Leutwyler, Low-energy expansion of meson form factors. Nucl. Phys. B **250**, 517 (1985). https://doi.org/10.1016/0550-3213(85)90493-6
279. G. Furlan, F. Lannoy, C. Rossetti, G. Segré, Symmetry-breaking corrections to weak vector currents. Nuovo Cim. **38**, 1747 (1965)

280. J. Gasser, H. Leutwyler, Chiral perturbation theory: expansions in the mass of the strange quark. Nucl. Phys. B **250**, 465 (1985). https://doi.org/10.1016/0550-3213(85)90492-4
281. C. Bernard, J. Bijnens, E. Gamiz, Semileptonic kaon decay in staggered chiral perturbation theory. Phys. Rev. D **89**, 054510 (2014). https://doi.org/10.1103/PhysRevD.89.054510. arXiv:1311.7511
282. [RBC 08A] J.M. Flynn, C.T. Sachrajda, SU(2) chiral perturbation theory for $K_{\ell 3}$ decay amplitudes. Nucl. Phys. B **812**, 64 (2009). https://doi.org/10.1016/j.nuclphysb.2008.12.001. arXiv:0809.1229
283. H. Leutwyler, M. Roos, Determination of the elements V_{us} and V_{ud} of the Kobayashi–Maskawa matrix. Phys. C **25**, 91 (1984). https://doi.org/10.1007/BF01571961Z
284. P. Post, K. Schilcher, K_{l3} form factors at order p^6 in chiral perturbation theory. Eur. Phys. J. **C25**, 427 (2002). https://doi.org/10.1007/s10052-002-0967-1. arXiv:hep-ph/0112352
285. J. Bijnens, P. Talavera, K_{l3} decays in chiral perturbation theory. Nucl. Phys. B **669**, 341 (2003). https://doi.org/10.1016/S0550-3213(03)00581-9. arXiv:hep-ph/0303103
286. M. Jamin, J.A. Oller, A. Pich, Order p^6 chiral couplings from the scalar $K\pi$ form factor. JHEP **02**, 047 (2004). arXiv:hep-ph/0401080
287. V. Cirigliano et al., The Green function and SU(3) breaking in K_{l3} decays. JHEP **04**, 006 (2005). arXiv:hep-ph/0503108
288. A. Kastner, H. Neufeld, The K_{l3} scalar form factors in the Standard Model. Eur. Phys. J. C **57**, 541 (2008). https://doi.org/10.1140/epjc/s10052-008-0703-6. arXiv:0805.2222
289. [JLQCD 17] S. Aoki, G. Cossu, X. Feng, H. Fukaya, S. Hashimoto, T. Kaneko et al., Chiral behavior of $K \to \pi l \nu$ decay form factors in lattice QCD with exact chiral symmetry. Phys. Rev. D **96**, 034501 (2017). https://doi.org/10.1103/PhysRevD.96.034501. arXiv:1705.00884
290. V. Bernard, E. Passemar, Matching chiral perturbation theory and the dispersive representation of the scalar K pi form-factor. Phys. Lett. B **661**, 95 (2008). https://doi.org/10.1016/j.physletb.2008.02.004. arXiv:0711.3450
291. [MILC 08] S. Basak et al., Electromagnetic splittings of hadrons from improved staggered quarks in full QCD. PoS LAT **2008**, 127 (2008). arXiv:0812.4486
292. [BMW 10C] A. Portelli et al., Electromagnetic corrections to light hadron masses. PoS LAT **2010**, 121 (2010). arXiv:1011.4189
293. [FNAL/MILC 13E] A. Bazavov et al., Determination of $|V_{us}|$ from a lattice-QCD calculation of the $K \to \pi \ell \nu$ semileptonic form factor with physical quark masses. Phys. Rev. Lett. **112**, 112001 (2014). https://doi.org/10.1103/PhysRevLett.112.112001. arXiv:1312.1228
294. [PACS 19] J. Kakazu, K.-i. Ishikawa, N. Ishizuka, Y. Kuramashi, Y. Nakamura, Y. Namekawa et al., K_{l3} form factors at the physical point on $(10.9\ \mathrm{fm})^3$ volume. Phys. Rev. D **101**, 094504 (2020). https://doi.org/10.1103/PhysRevD.101.094504. arXiv:1912.13127
295. [RBC/UKQCD 13] P.A. Boyle, J.M. Flynn, N. Garron, A. Jüttner, C.T. Sachrajda et al., The kaon semileptonic form factor with near physical domain wall quarks. JHEP **1308**, 132 (2013). https://doi.org/10.1007/JHEP08(2013)132. arXiv:1305.7217
296. [JLQCD 12] T. Kaneko et al., Chiral behavior of kaon semileptonic form factors in lattice QCD with exact chiral symmetry. PoS LAT **2012**, 111 (2012). arXiv:1211.6180
297. [JLQCD 11] T. Kaneko et al., Kaon semileptonic form factors in QCD with exact chiral symmetry. PoS LAT **2011**, 284 (2011). arXiv:1112.5259
298. [RBC/UKQCD 10] P.A. Boyle et al., $K \to \pi$ form factors with reduced model dependence. Eur. Phys. J. C **69**, 159 (2010). https://doi.org/10.1140/epjc/s10052-010-1405-4. arXiv:1004.0886
299. [RBC/UKQCD 07] P.A. Boyle, A. Jüttner, R. Kenway, C. Sachrajda, S. Sasaki et al., K_{l3} semileptonic form-factor from 2+1 flavour lattice QCD. Phys. Rev. Lett. **100**, 141601 (2008). https://doi.org/10.1103/PhysRevLett.100.141601. arxiv:0710.5136
300. [ETM 10D] V. Lubicz, F. Mescia, L. Orifici, S. Simula, C. Tarantino, Improved analysis of the scalar and vector form factors of kaon semileptonic decays with $N_f = 2$ twisted-mass fermions. PoS LAT **2010**, 316 (2010). arXiv:1012.3573
301. D. Guadagnoli, F. Mescia, S. Simula, Lattice study of semileptonic form-factors with twisted boundary conditions. Phys. Rev. D **73**, 1144504 (2006). https://doi.org/10.1103/PhysRevD.73.114504. arXiv:hep-lat/0512020
302. [UKQCD 07] P.A. Boyle, J. Flynn, A. Jüttner, C. Sachrajda, J. Zanotti, Hadronic form factors in lattice QCD at small and vanishing momentum transfer. JHEP **0705**, 016 (2007). https://doi.org/10.1088/1126-6708/2007/05/016. arXiv:hep-lat/0703005
303. [SPQcdR 04] D. Bećirević et al., The $K \to \pi$ vector form factor at zero momentum transfer on the lattice. Nucl. Phys. B **705**, 339 (2005). https://doi.org/10.1016/j.nuclphysb.2004.11.017. arXiv:hep-ph/0403217
304. C. Bernard, J. Bijnens, E. Gámiz, J. Relefors, Twisted finite-volume corrections to K_{l3} decays with partially-quenched and rooted-staggered quarks. JHEP **03**, 120 (2017). https://doi.org/10.1007/JHEP03(2017)120. arXiv:1702.03416
305. C. Alexandrou et al., Ratio of kaon and pion leptonic decay constants with $N_f = 2 + 1 + 1$ Wilson-clover twisted-mass fermions. Phys. Rev. D **104**, 074520 (2021). arXiv:2104.06747 [hep-lat]
306. P. Dimopoulos, R. Frezzotti, P. Lami, V. Lubicz, E. Picca et al., Pseudoscalar decay constants f_K/f_π, f_D and f_{D_s} with $N_f = 2 + 1 + 1$ ETMC configurations. PoS LATTICE **2013**, 314 (2014). arXiv:1311.3080
307. A. Bazavov, C. Bernard, C. DeTar, J. Foley, W. Freeman et al., Leptonic decay-constant ratio f_{K^+}/f_{π^+} from lattice QCD with physical light quarks. Phys. Rev. Lett. **110**, 172003 (2013). https://doi.org/10.1103/PhysRevLett.110.172003. arXiv:1301.5855
308. A. Bazavov et al., Properties of light pseudoscalars from lattice QCD with HISQ ensembles. PoS LAT **2011**, 107 (2011). arXiv:1111.4314
309. F. Farchioni, G. Herdoiza, K. Jansen, M. Petschlies, C. Urbach et al., Pseudoscalar decay constants from $N_f = 2 + 1 + 1$ twisted mass lattice QCD. PoS LAT **2010**, 128 (2010). arXiv:1012.0200
310. E.E. Scholz, S. Dürr, Leptonic decay-constant ratio f_K/f_π from clover-improved $N_f = 2 + 1$ QCD. PoS LATTICE **2016**, 283 (2016). arXiv:1610.00932
311. J. Noaki et al., Chiral properties of light mesons in $N_f = 2 + 1$ overlap QCD. PoS LAT **2010**, 117 (2010)
312. C. Aubin, J. Laiho, R.S. Van de Water, Light pseudoscalar meson masses and decay constants from mixed action lattice QCD. PoS LAT **2008**, 105 (2008). arXiv:0810.4328
313. A. Abdel-Rehim, C. Alexandrou, P. Dimopoulos, R. Frezzotti, K. Jansen et al., Progress in simulations with twisted mass fermions at the physical point. PoS LATTICE **2014**, 119 (2014). arXiv:1411.6842
314. S. Lottini, Chiral behaviour of the pion decay constant in $N_f = 2$ QCD. PoS LATTICE **2013**, 315 (2013). arXiv:1311.3081
315. G. Schierholz et al., Probing the chiral limit with clover fermions I: the meson sector, talk given at Lattice 2007, Regensburg, Germany. PoS LAT **2007**, 133 (2007)

316. B. Ananthanarayan, J. Bijnens, S. Friot, S. Ghosh, Analytic representation of f_k/f_π in two loop chiral perturbation theory. Phys. Rev. D **97** (2018). https://doi.org/10.1103/physrevd.97.091502
317. M. Lüscher, Properties and uses of the Wilson flow in lattice QCD. JHEP **08**, 071 (2010). https://doi.org/10.1007/JHEP08(2010)071. https://doi.org/10.1007/JHEP03(2014)092. arXiv:1006.4518 [Erratum: JHEP **03**, 092 (2014)]
318. D. Giusti, V. Lubicz, G. Martinelli, F. Sanfilippo, S. Simula, N. Tantalo et al., Leading isospin-breaking corrections to meson masses on the lattice. EPJ Web Conf. **175**, 06002 (2018). https://doi.org/10.1051/epjconf/201817506002. arXiv:1710.06633
319. B. Fahy, G. Cossu, S. Hashimoto, T. Kaneko, J. Noaki, M. Tomii, Decay constants and spectroscopy of mesons in lattice QCD using domain-wall fermions. PoS LATTICE **2015**, 074 (2016). arXiv:1512.08599
320. J. Gasser, H. Leutwyler, Chiral perturbation theory to one loop. Ann. Phys. **158**, 142 (1984). https://doi.org/10.1016/0003-4916(84)90242-2
321. S. Weinberg, Pion scattering lengths. Phys. Rev. Lett. **17**, 616 (1966). https://doi.org/10.1103/PhysRevLett.17.616
322. J. Gasser, H. Leutwyler, Low-energy theorems as precision tests of QCD. Phys. Lett. B **125**, 325 (1983). https://doi.org/10.1016/0370-2693(83)91294-7
323. J. Bijnens, G. Colangelo, G. Ecker, J. Gasser, M.E. Sainio, Elastic pi pi scattering to two loops. Phys. Lett. B **374**, 210 (1996). https://doi.org/10.1016/0370-2693(96)00165-7. arXiv:hep-ph/9511397
324. G. Colangelo, J. Gasser, H. Leutwyler, $\pi\pi$ scattering. Nucl. Phys. B **603**, 125 (2001). https://doi.org/10.1016/S0550-3213(01)00147-X. arXiv:hep-ph/0103088
325. J. Nebreda, J.R. Pelaez, Strange and non-strange quark mass dependence of elastic light resonances from SU(3) Unitarized Chiral Perturbation Theory to one loop. Phys. Rev. D **81**, 054035 (2010). https://doi.org/10.1103/PhysRevD.81.054035. arXiv:1001.5237
326. L. Maiani, M. Testa, Final state interactions from Euclidean correlation functions. Phys. Lett. B **245**, 585 (1990). https://doi.org/10.1016/0370-2693(90)90695-3
327. M. Lüscher, Volume dependence of the energy spectrum in massive quantum field theories. 1. Stable particle states. Commun. Math. Phys. **104**, 177 (1986). https://doi.org/10.1007/BF01211589
328. M. Lüscher, Volume dependence of the energy spectrum in massive quantum field theories. 2. Scattering states. Commun. Math. Phys. **105**, 153 (1986). https://doi.org/10.1007/BF01211097
329. M. Lüscher, Two particle states on a torus and their relation to the scattering matrix. Nucl. Phys. B **354**, 531 (1991). https://doi.org/10.1016/0550-3213(91)90366-6
330. M. Lüscher, Signatures of unstable particles in finite volume. Nucl. Phys. B **364**, 237 (1991). https://doi.org/10.1016/0550-3213(91)90584-K
331. S.M. Roy, Exact integral equation for pion pion scattering involving only physical region partial waves. Phys. Lett. B **36**, 353 (1971). https://doi.org/10.1016/0370-2693(71)90724-6
332. B. Ananthanarayan, G. Colangelo, J. Gasser, H. Leutwyler, Roy equation analysis of pi pi scattering. Phys. Rep. **353**, 207 (2001). https://doi.org/10.1016/S0370-1573(01)00009-6. arXiv:hep-ph/0005297
333. I. Caprini, G. Colangelo, H. Leutwyler, Regge analysis of the pi pi scattering amplitude. Eur. Phys. J. C **72**, 1860 (2012). https://doi.org/10.1140/epjc/s10052-012-1860-1. arXiv:1111.7160
334. [NPLQCD 07] S.R. Beane et al., Precise determination of the I=2 $\pi\pi$ scattering length from mixed-action lattice QCD. Phys. Rev. D **77**, 014505 (2008). https://doi.org/10.1103/PhysRevD.77.014505. arXiv:0706.3026
335. Z. Fu, Lattice QCD study of the s-wave $\pi\pi$ scattering lengths in the I = 0 and 2 channels. Phys. Rev. D **87**, 074501 (2013). https://doi.org/10.1103/PhysRevD.87.074501. arXiv:1303.0517
336. [ETM 16C] L. Liu et al., Isospin-0 $\pi\pi$ s-wave scattering length from twisted mass lattice QCD. Phys. Rev. D **96**, 054516 (2017). https://doi.org/10.1103/PhysRevD.96.054516. arXiv:1612.02061
337. J.-W. Chen, D. O'Connell, R.S. Van de Water, A. Walker-Loud, Ginsparg–Wilson pions scattering on a staggered sea. Phys. Rev. D **73**, 074510 (2006). https://doi.org/10.1103/PhysRevD.73.074510. arXiv:hep-lat/0510024
338. M.I. Buchoff, Isotropic and anisotropic lattice spacing corrections for I = 2 pi-pi scattering from effective field theory. Phys. Rev. D **77**, 114502 (2008). https://doi.org/10.1103/PhysRevD.77.114502. arXiv:0802.2931
339. S. Aoki, O. Bar, B. Biedermann, Pion scattering in Wilson chiral perturbation theory. Phys. Rev. D **78**, 114501 (2008). https://doi.org/10.1103/PhysRevD.78.114501. arXiv:0806.4863
340. N.R. Acharya, F.-K. Guo, U.-G. Meissner, C.-Y. Seng, Connected and disconnected contractions in pion–pion scattering. Nucl. Phys. B **922**, 480 (2017). https://doi.org/10.1016/j.nuclphysb.2017.07.012. arXiv:1704.06754
341. G. Burdman, J.F. Donoghue, Union of chiral and heavy quark symmetries. Phys. Lett. B **280**, 287 (1992). https://doi.org/10.1016/0370-2693(92)90068-F
342. M.B. Wise, Chiral perturbation theory for hadrons containing a heavy quark. Phys. Rev. D **45**, R2188 (1992). https://doi.org/10.1103/PhysRevD.45.R2188
343. T.-M. Yan, H.-Y. Cheng, C.-Y. Cheung, G.-L. Lin, Y.C. Lin, H.-L. Yu, Heavy quark symmetry and chiral dynamics. Phys. Rev. D **46**, 1148 (1992). https://doi.org/10.1103/PhysRevD.46.1148 [Erratum: Phys. Rev. D 55, 5851 (1997)]
344. [PACS-CS 13] K. Sasaki, N. Ishizuka, M. Oka, T. Yamazaki, Scattering lengths for two pseudoscalar meson systems. Phys. Rev. D **89**, 054502 (2014). https://doi.org/10.1103/PhysRevD.89.054502. arXiv:1311.7226
345. V. Bernard, N. Kaiser, U.G. Meissner, pi K scattering in chiral perturbation theory to one loop. Nucl. Phys. B **357**, 129 (1991). https://doi.org/10.1016/0550-3213(91)90461-6
346. V. Bernard, N. Kaiser, U.G. Meissner, Threshold parameters of pi K scattering in QCD. Phys. Rev. D **43**, 2757 (1991). https://doi.org/10.1103/PhysRevD.43.R2757
347. B. Kubis, U.-G. Meissner, Isospin violation in low-energy charged pion kaon scattering. Phys. Lett. B **529**, 69 (2002). https://doi.org/10.1016/S0370-2693(02)01192-9. arXiv:hep-ph/0112154
348. J.-W. Chen, D. O'Connell, A. Walker-Loud, Two meson systems with Ginsparg–Wilson valence quarks. Phys. Rev. D **75**, 054501 (2007). https://doi.org/10.1103/PhysRevD.75.054501. arXiv:hep-lat/0611003
349. [NPLQCD 06B] S.R. Beane, P.F. Bedaque, T.C. Luu, K. Orginos, E. Pallante, A. Parreno et al., pi K scattering in full QCD with domain-wall valence quarks. Phys. Rev. D **74**, 114503 (2006). https://doi.org/10.1103/PhysRevD.74.114503. arXiv:hep-lat/0607036

350. [ETM 20A] M. Fischer, B. Kostrzewa, M. Mai, M. Petschlies, F. Pittler, M. Ueding et al., The ρ-resonance with physical pion mass from $N_f = 2$ lattice QCD. Phys. Lett. B **819**, 136449 (2021). https://doi.org/10.1016/j.physletb.2021.136449. arXiv:2006.13805
351. [χQCD 21] J. Liang, A. Alexandru, Y.-J. Bi, T. Draper, K.-F. Liu, Y.-B. Yang, Detecting flavors of vacuum from the Dirac operator spectrum. arXiv:2102.05380
352. S. Dürr, Validity of ChPT—is $M_\pi = 135$ MeV small enough? PoS LATTICE **2014**, 006 (2015). arXiv:1412.6434
353. C. Wang, Y. Bi, H. Cai, Y. Chen, M. Gong, Z. Liu, Quark chiral condensate from the overlap quark propagator. Chin. Phys. C **41**, 053102 (2017). https://doi.org/10.1088/1674-1137/41/5/053102. arXiv:1612.04579
354. [JLQCD/TWQCD 10A] H. Fukaya et al., Determination of the chiral condensate from QCD Dirac spectrum on the lattice. Phys. Rev. D **83**, 074501 (2011). https://doi.org/10.1103/PhysRevD.83.074501. arXiv:1012.4052
355. [JLQCD 09] H. Fukaya et al., Determination of the chiral condensate from 2+1-flavor lattice QCD. Phys. Rev. Lett. **104**, 122002 (2010). https://doi.org/10.1103/PhysRevLett.104.122002. arXiv:0911.5555
356. [TWQCD 08] T.-W. Chiu, T.-H. Hsieh, P.-K. Tseng, Topological susceptibility in 2+1 flavors lattice QCD with domain-wall fermions. Phys. Lett. B **671**, 135 (2009). https://doi.org/10.1016/j.physletb.2008.11.058. arXiv:0810.3406
357. [ETM 12] F. Burger, V. Lubicz, M. Muller-Preussker, S. Simula, C. Urbach, Quark mass and chiral condensate from the Wilson twisted mass lattice quark propagator. Phys. Rev. D **87**, 034514 (2013). https://doi.org/10.1103/PhysRevD.87.034514. https://doi.org/10.1103/PhysRevD.87.079904. arXiv:1210.0838
358. F. Bernardoni, N. Garron, P. Hernandez, S. Necco, C. Pena, Light quark correlators in a mixed-action setup. PoS LAT **2011**, 109 (2011). arXiv:1110.0922
359. [TWQCD 11] T.-W. Chiu, T.-H. Hsieh, Y.-Y. Mao, Pseudoscalar meson in two flavors QCD with the optimal domain-wall fermion. Phys. Lett. B **717**, 420 (2012). https://doi.org/10.1016/j.physletb.2012.09.067. arXiv:1109.3675
360. [TWQCD 11A] T.-W. Chiu, T.H. Hsieh, Y.Y. Mao, Topological susceptibility in two flavors lattice QCD with the optimal domain-wall fermion. Phys. Lett. B **702**, 131 (2011). arXiv:1105.4414
361. F. Bernardoni, P. Hernandez, N. Garron, S. Necco, C. Pena, Probing the chiral regime of N_f= 2 QCD with mixed actions. Phys. Rev. D **83**, 054503 (2011). https://doi.org/10.1103/PhysRevD.83.054503. arXiv:1008.1870
362. [CERN 08] L. Giusti, M. Lüscher, Chiral symmetry breaking and the Banks–Casher relation in lattice QCD with Wilson quarks. JHEP **03**, 013 (2009). https://doi.org/10.1088/1126-6708/2009/03/013. arXiv:0812.3638
363. A. Hasenfratz, R. Hoffmann, S. Schaefer, Low energy chiral constants from ϵ-regime simulations with improved Wilson fermions. Phys. Rev. D **78**, 054511 (2008). https://doi.org/10.1103/PhysRevD.78.054511. arXiv:0806.4586
364. [JLQCD/TWQCD 08A] J. Noaki et al., Convergence of the chiral expansion in two-flavor lattice QCD. Phys. Rev. Lett. **101**, 202004 (2008). https://doi.org/10.1103/PhysRevLett.101.202004. arXiv:0806.0894
365. [JLQCD/TWQCD 07] H. Fukaya et al., Lattice study of meson correlators in the ϵ-regime of two-flavor QCD. Phys. Rev. D **77**, 074503 (2008). https://doi.org/10.1103/PhysRevD.77.074503. arXiv:0711.4965
366. [JLQCD/TWQCD 07A] S. Aoki et al., Topological susceptibility in two-flavor lattice QCD with exact chiral symmetry. Phys. Lett. B **665**, 294 (2008). https://doi.org/10.1016/j.physletb.2008.06.039. arXiv:0710.1130
367. Y. Aoki, S. Borsanyi, S. Dürr, Z. Fodor, S.D. Katz, S. Krieg et al., The QCD transition temperature: results with physical masses in the continuum limit II. JHEP **06**, 088 (2009). https://doi.org/10.1088/1126-6708/2009/06/088. arXiv:0903.4155
368. [ETM 15A] A. Abdel-Rehim et al., Simulating QCD at the physical point with $N_f = 2$ Wilson twisted mass fermions at maximal twist. Phys. Rev. D **95**, 094515 (2015). https://doi.org/10.1103/PhysRevD.95.094515. arXiv:1507.05068
369. [QCDSF 13] R. Horsley, Y. Nakamura, A. Nobile, P. Rakow, G. Schierholz et al., Nucleon axial charge and pion decay constant from two-flavor lattice QCD. Phys. Lett. B **732**, 41 (2014). https://doi.org/10.1016/j.physletb.2014.03.002. arXiv:1302.2233
370. G. Colangelo, S. Dürr, The pion mass in finite volume. Eur. Phys. J. C **33**, 543 (2004). https://doi.org/10.1140/epjc/s2004-01593-y. arXiv:hep-lat/0311023
371. V. Gülpers, G. von Hippel, H. Wittig, The scalar pion form factor in two-flavor lattice QCD. Phys. Rev. D **89**, 094503 (2014). https://doi.org/10.1103/PhysRevD.89.094503. arXiv:1309.2104
372. [JLQCD/TWQCD 09] S. Aoki et al., Pion form factors from two-flavor lattice QCD with exact chiral symmetry. Phys. Rev. D **80**, 034508 (2009). https://doi.org/10.1103/PhysRevD.80.034508. arXiv:0905.2465
373. [CERN-TOV 06] L. Del Debbio, L. Giusti, M. Lüscher, R. Petronzio, N. Tantalo, QCD with light Wilson quarks on fine lattices (I): first experiences and physics results. JHEP **02**, 056 (2007). arXiv:hep-lat/0610059
374. [HPQCD 15B] J. Koponen, F. Bursa, C.T.H. Davies, R.J. Dowdall and G.P. Lepage, The size of the pion from full lattice QCD with physical u, d, s and c quarks. Phys. Rev. D **93**, 054503 (2016). https://doi.org/10.1103/PhysRevD.93.054503. arXiv:1511.07382
375. X. Gao, N. Karthik, S. Mukherjee, P. Petreczky, S. Syritsyn, Y. Zhao, Pion form factor and charge radius from Lattice QCD at physical point. Phys. Rev. D **104**, 114515 (2021). https://doi.org/10.1103/PhysRevD.104.114515. arXiv:2102.06047
376. [χQCD 20] G. Wang, J. Liang, T. Draper, K.-F. Liu, Y.-B. Yang, Lattice calculation of pion form factor with overlap fermions. Phys. Rev. D **104**, 074502 (2021). https://doi.org/10.1103/PhysRevD.104.074502. arXiv:2006.05431
377. X. Feng, Y. Fu, L.-C. Jin, Lattice QCD calculation of the pion charge radius using a model-independent method. Phys. Rev. D **101**, 051502 (2020). https://doi.org/10.1103/PhysRevD.101.051502. arXiv:1911.04064
378. [JLQCD 15A] S. Aoki, G. Cossu, X. Feng, S. Hashimoto, T. Kaneko, J. Noaki et al., Light meson electromagnetic form factors from three-flavor lattice QCD with exact chiral symmetry. Phys. Rev. D **93**, 034504 (2016). https://doi.org/10.1103/PhysRevD.93.034504. arXiv:1510.06470
379. [JLQCD 14] H. Fukaya, S. Aoki, S. Hashimoto, T. Kaneko, H. Matsufuru, J. Noaki, Computation of the electromagnetic pion form factor from lattice QCD in the ϵ regime. Phys. Rev. D **90**, 034506 (2014). https://doi.org/10.1103/PhysRevD.90.034506. arXiv:1405.4077
380. [PACS-CS 11A] O.H. Nguyen, K.-I. Ishikawa, A. Ukawa, N. Ukita, Electromagnetic form factor of pion from $N_f = 2 + 1$ dynamical flavor QCD. JHEP **04**, 122 (2011). https://doi.org/10.1007/JHEP04(2011)122. arXiv:1102.3652
381. [RBC/UKQCD 08A] P.A. Boyle et al., The pion's electromagnetic form factor at small momentum transfer in full lattice QCD. JHEP **07**, 112 (2008). https://doi.org/10.1088/1126-6708/2008/07/112. arXiv:0804.3971
382. [LHP 04] F.D.R. Bonnet, R.G. Edwards, G.T. Fleming, R. Lewis, D.G. Richards, Lattice computations of the pion form factor. Phys. Rev. D **72**, 054506 (2005). https://doi.org/10.1103/PhysRevD.72.054506. arXiv:hep-lat/0411028

383. [ETM 17F] C. Alexandrou et al., Pion vector form factor from lattice QCD at the physical point. Phys. Rev. D **97**, 014508 (2018). https://doi.org/10.1103/PhysRevD.97.014508. arXiv:1710.10401
384. [QCDSF/UKQCD 06A] D. Brömmel et al., The pion form factor from lattice QCD with two dynamical flavours. Eur. Phys. J. C **51**, 335 (2007). https://doi.org/10.1140/epjc/s10052-007-0295-6. arXiv:hep-lat/0608021
385. J. Bijnens, G. Colangelo, P. Talavera, The vector and scalar form factors of the pion to two loops. JHEP **05**, 014 (1998). arXiv:hep-ph/9805389
386. S.R. Amendolia et al., A measurement of the space-like pion electromagnetic form factor. Nucl. Phys. B **277**, 168 (1986). https://doi.org/10.1016/0550-3213(86)90437-2
387. B. Hörz, A. Hanlon, Two- and three-pion finite-volume spectra at maximal isospin from lattice QCD. Phys. Rev. Lett. **123**, 142002 (2019). https://doi.org/10.1103/PhysRevLett.123.142002. arXiv:1905.04277
388. J. Bulava, B. Fahy, B. Horz, K.J. Juge, C. Morningstar, C.H. Wong, $I = 1$ and $I = 2$ $\pi - \pi$ scattering phase shifts from $N_{\rm f} = 2 + 1$ lattice QCD. Nucl. Phys. B **910**, 842 (2016). https://doi.org/10.1016/j.nuclphysb.2016.07.024. arXiv:1604.05593
389. T.D. Blanton, F. Romero-López, S.R. Sharpe, $I = 3$ Three-pion scattering amplitude from lattice QCD. Phys. Rev. Lett. **124**, 032001 (2020). https://doi.org/10.1103/PhysRevLett.124.032001. arXiv:1909.02973
390. C. Culver, M. Mai, A. Alexandru, M. Döring, F.X. Lee, Pion scattering in the isospin $I = 2$ channel from elongated lattices. Phys. Rev. D **100**, 034509 (2019). https://doi.org/10.1103/PhysRevD.100.034509. arXiv:1905.10202
391. M. Mai, C. Culver, A. Alexandru, M. Döring, F.X. Lee, Cross-channel study of pion scattering from lattice QCD. Phys. Rev. D **100**, 114514 (2019). https://doi.org/10.1103/PhysRevD.100.114514. arXiv:1908.01847
392. [ETM 20B] M. Fischer, B. Kostrzewa, L. Liu, F. Romero-López, M. Ueding, C. Urbach, Scattering of two and three physical pions at maximal isospin from lattice QCD. Eur. Phys. J. C **81**, 436 (2021). https://doi.org/10.1140/epjc/s10052-021-09206-5. arXiv:2008.03035
393. Z. Fu, X. Chen, $I = 0$ $\pi\pi$ s-wave scattering length from lattice QCD. Phys. Rev. D **98**, 014514 (2018). https://doi.org/10.1103/PhysRevD.98.014514. arXiv:1712.02219
394. Z. Fu, Lattice QCD calculation of $\pi\pi$ scattering length. Commun. Theor. Phys. **57**, 78 (2012). https://doi.org/10.1088/0253-6102/57/1/13. arXiv:1110.3918
395. [NPLQCD 11A] S.R. Beane, E. Chang, W. Detmold, H.W. Lin, T.C. Luu, K. Orginos et al., The I=2 pipi S-wave scattering phase shift from lattice QCD. Phys. Rev. D **85**, 034505 (2012). https://doi.org/10.1103/PhysRevD.85.034505. arXiv:1107.5023
396. [NPLQCD 05] S.R. Beane, P.F. Bedaque, K. Orginos, M.J. Savage, I = 2 pi-pi scattering from fully-dynamical mixed-action lattice QCD. Phys. Rev. D **73**, 054503 (2006). https://doi.org/10.1103/PhysRevD.73.054503. arXiv:hep-lat/0506013
397. T. Yagi, S. Hashimoto, O. Morimatsu, M. Ohtani, I=2 π-π scattering length with dynamical overlap fermion. arXiv:1108.2970
398. [CP-PACS 04] T. Yamazaki et al., I = 2 pi pi scattering phase shift with two flavors of O(a) improved dynamical quarks. Phys. Rev. D **70**, 074513 (2004). https://doi.org/10.1103/PhysRevD.70.074513. arXiv:hep-lat/0402025
399. Z. Fu, Lattice study on πK scattering with moving wall source. Phys. Rev. D **85**, 074501 (2012). https://doi.org/10.1103/PhysRevD.85.074501. arXiv:1110.1422
400. Z. Fu, Preliminary lattice study of the I = 1 $K\bar{K}$ scattering length. Eur. Phys. J. **72**, 2159 (2012). https://doi.org/10.1140/epjc/s10052-012-2159-y. arXiv:1201.3708
401. [NPLQCD 07B] S.R. Beane et al., The K+K+ scattering length from lattice QCD. Phys. Rev. D **77**, 094507 (2008). https://doi.org/10.1103/PhysRevD.77.094507. arXiv:0709.1169
402. C.B. Lang, L. Leskovec, D. Mohler, S. Prelovsek, K pi scattering for isospin 1/2 and 3/2 in lattice QCD. Phys. Rev. D **86**, 054508 (2012). https://doi.org/10.1103/PhysRevD.86.054508. arXiv:1207.3204
403. D.J. Wilson, J.J. Dudek, R.G. Edwards, C.E. Thomas, Resonances in coupled πK, ηK scattering from lattice QCD. Phys. Rev. D **91**, 054008 (2015). https://doi.org/10.1103/PhysRevD.91.054008. arXiv:1411.2004
404. R. Brett, J. Bulava, J. Fallica, A. Hanlon, B. Hörz, C. Morningstar, Determination of s- and p-wave $I = 1/2$ $K\pi$ scattering amplitudes in $N_{\rm f} = 2 + 1$ lattice QCD. Nucl. Phys. B **932**, 29 (2018). https://doi.org/10.1016/j.nuclphysb.2018.05.008. arXiv:1802.03100
405. B. Moussallam, N(f) dependence of the quark condensate from a chiral sum rule. Eur. Phys. J. C **14**, 111 (2000). https://doi.org/10.1007/s100520050738. arXiv:hep-ph/9909292
406. S. Descotes-Genon, L. Girlanda, J. Stern, Paramagnetic effect of light quark loops on chiral symmetry breaking. JHEP **01**, 041 (2000). arXiv:hep-ph/9910537
407. G.C. Branco, L. Lavoura, J.P. Silva, CP violation. Int. Ser. Monogr. Phys. **103**, 1 (1999)
408. M. Sozzi, Discrete Symmetries and CP Violation: From Experiment to Theory. Oxford University Press (2008). https://doi.org/10.1093/acprof:oso/9780199296668.001.0001
409. A. Buras, Gauge Theories of Weak Decays. Cambridge University Press (2020). https://doi.org/10.1017/9781139524100
410. G. Buchalla, A.J. Buras, M.E. Lautenbacher, Weak decays beyond leading logarithms. Rev. Mod. Phys. **68**, 1125 (1996). https://doi.org/10.1103/RevModPhys.68.1125. arXiv:hep-ph/9512380
411. A.J. Buras, C.P. Weak Hamiltonian, violation and rare decays, Published in Les Houches, Probing the standard model of particle interactions. Pt. 1, 281–539 (1997). arxiv:hep-ph9806471
412. L. Lellouch, Flavor physics and lattice quantum chromodynamics, in Modern perspectives in lattice QCD: Quantum field theory and high performance computing. Proceedings, International School, 93rd Session, Les Houches, France, August 3–28, 2009, pp. 629–698 (2011). arXiv:1104.5484
413. K. Anikeev et al., B physics at the Tevatron: Run II and beyond. arXiv:hep-ph/0201071
414. U. Nierste, Three lectures on meson mixing and CKM phenomenology, published in Dubna 2008, Heavy Quark Physics (HQP08), pp. 1–39. arXiv:0904.1869
415. A.J. Buras, D. Guadagnoli, Correlations among new CP violating effects in $\Delta F = 2$ observables. Phys. Rev. D **78**, 033005 (2008). https://doi.org/10.1103/PhysRevD.78.033005. arXiv:0805.3887
416. A.J. Buras, D. Guadagnoli, G. Isidori, On ϵ_K beyond lowest order in the operator product expansion. Phys. Lett. B **688**, 309 (2010). https://doi.org/10.1016/j.physletb.2010.04.017. arXiv:1002.3612
417. T. Inami, C.S. Lim, Effects of superheavy quarks and leptons in low-energy weak processes $K_L \to \mu\bar{\mu}$, $K^+ \to \pi^+\nu\bar{\nu}$ and $K^0 \leftrightarrow \bar{K}^0$. Prog. Theor. Phys. **65**, 297 (1981). https://doi.org/10.1143/PTP.65.297

418. J. Brod, M. Gorbahn, Next-to-next-to-leading-order charm-quark contribution to the CP violation parameter ϵ_K and ΔM_K. Phys. Rev. Lett. **108**, 121801 (2012). https://doi.org/10.1103/PhysRevLett.108.121801. arXiv:1108.2036
419. J. Brod, M. Gorbahn, ϵ_K at next-to-next-to-leading order: the charm-top-quark contribution. Phys. Rev. D **82**, 094026 (2010). https://doi.org/10.1103/PhysRevD.82.094026. arXiv:1007.0684
420. G. Martinelli, C. Pittori, C.T. Sachrajda, M. Testa, A. Vladikas, A general method for nonperturbative renormalization of lattice operators. Nucl. Phys. B **445**, 81 (1995). https://doi.org/10.1016/0550-3213(95)00126-D. arXiv:hep-lat/9411010
421. M. Lüscher, R. Narayanan, P. Weisz, U. Wolff, The Schrödinger functional: a renormalizable probe for non-abelian gauge theories. Nucl. Phys. B **384**, 168 (1992). https://doi.org/10.1016/0550-3213(92)90466-O. arXiv:hep-lat/9207009
422. T. Bae et al., Improved determination of B_K with staggered quarks. Phys. Rev. D **89**, 074504 (2014). https://doi.org/10.1103/PhysRevD.89.074504. arXiv:1402.0048
423. [ALPHA 07A] P. Dimopoulos et al., Non-perturbative renormalisation of $\Delta F = 2$ four-fermion operators in two-flavour QCD. JHEP **0805**, 065 (2008). https://doi.org/10.1088/1126-6708/2008/05/065. arXiv:0712.2429
424. [ALPHA 18B] P. Dimopoulos et al., Non-perturbative renormalisation and running of BSM four-quark operators in $N_f = 2$ QCD. Eur. Phys. J. C **78**, 579 (2018). https://doi.org/10.1140/epjc/s10052-018-6002-y. arXiv:1801.09455
425. [RBC/UKQCD 12F] N.H. Christ, T. Izubuchi, C.T. Sachrajda, A. Soni, J. Yu, Long distance contribution to the KL-KS mass difference. Phys. Rev. D **88**, 014508 (2013). https://doi.org/10.1103/PhysRevD.88.014508. arXiv:1212.5931
426. J. Brod, M. Gorbahn, E. Stamou, Standard-model prediction of ϵ_K with manifest CKM unitarity. Phys. Rev. Lett. **125**, 171803 (2020). https://doi.org/10.1103/PhysRevLett.125.171803. arXiv:1911.06822
427. V. Cirigliano, A. Pich, G. Ecker, H. Neufeld, Isospin violation in epsilon-prime. Phys. Rev. Lett. **91**, 162001 (2003). https://doi.org/10.1103/PhysRevLett.91.162001. arXiv:hep-ph/0307030
428. V. Cirigliano, H. Gisbert, A. Pich, A. Rodríguez-Sánchez, Isospin-violating contributions to ϵ'/ϵ. JHEP **02**, 032 (2020). https://doi.org/10.1007/JHEP02(2020)032. arXiv:1911.01359
429. [RBC/UKQCD 20] R. Abbott et al., Direct CP violation and the $\Delta I = 1/2$ rule in $K \to \pi\pi$ decay from the Standard Model. Phys. Rev. D **102**, 054509 (2020). https://doi.org/10.1103/PhysRevD.102.054509. arXiv:2004.09440
430. [RBC/UKQCD 15G] Z. Bai et al., Standard model prediction for direct CP violation in $K \to \pi\pi$ decay. Phys. Rev. Lett. **115**, 212001 (2015). https://doi.org/10.1103/PhysRevLett.115.212001. arXiv:1505.07863
431. Particle Data Group collaboration, Review of Particle Physics. Phys. Rev. D **98**, 030001 (2018). https://doi.org/10.1103/PhysRevD.98.030001
432. Z. Bai, Long distance part of ϵ_K from lattice QCD. PoS LATTICE **2016**, 309 (2017). https://doi.org/10.22323/1.256.0309. arXiv:1611.06601
433. Z. Bai, N.H. Christ, T. Izubuchi, C.T. Sachrajda, A. Soni, J. Yu, $K_L - K_S$ mass difference from lattice QCD. Phys. Rev. Lett. **113**, 112003 (2014). https://doi.org/10.1103/PhysRevLett.113.112003. arXiv:1406.0916
434. N.H. Christ, X. Feng, G. Martinelli, C.T. Sachrajda, Effects of finite volume on the KL-KS mass difference. Phys. Rev. D **91**, 114510 (2015). https://doi.org/10.1103/PhysRevD.91.114510. arXiv:1504.01170
435. B. Wang, Calculation of the $K_L - K_S$ mass difference for physical quark masses. PoS LATTICE **2019**, 093 (2019). https://doi.org/10.22323/1.363.0093. arXiv:2001.06374
436. Z. Bai et al., Erratum: Standard-model prediction for direct CP violation in $K \to \pi\pi$ decay. arXiv:1603.03065
437. M. Gaillard, B.W. Lee, Δ I = 1/2 rule for nonleptonic decays in asymptotically free field theories. Phys. Rev. Lett. **33**, 108 (1974). https://doi.org/10.1103/PhysRevLett.33.108
438. G. Altarelli, L. Maiani, Octet enhancement of nonleptonic weak interactions in asymptotically free gauge theories. Phys. Lett. B **52**, 351 (1974). https://doi.org/10.1016/0370-2693(74)90060-4
439. [RBC/UKQCD 21] T. Blum et al., Lattice determination of $I = 0$ and 2 $\pi\pi$ scattering phase shifts with a physical pion mass. Phys. Rev. D **104**, 114506 (2021). https://doi.org/10.1103/PhysRevD.104.114506. arXiv:2103.15131
440. N. Ishizuka, K.I. Ishikawa, A. Ukawa, T. Yoshié, Calculation of $K \to \pi\pi$ decay amplitudes with improved Wilson fermion action in lattice QCD. Phys. Rev. D **92**, 074503 (2015). https://doi.org/10.1103/PhysRevD.92.074503. arXiv:1505.05289
441. N. Ishizuka, K.I. Ishikawa, A. Ukawa, T. Yoshié, Calculation of $K \to \pi\pi$ decay amplitudes with improved Wilson fermion action in non-zero momentum frame in lattice QCD. Phys. Rev. **D98**, 114512 (2018). https://doi.org/10.1103/PhysRevD.98.114512. arXiv:1809.03893
442. A. Donini, P. Hernández, C. Pena, F. Romero-López, Nonleptonic kaon decays at large N_c. Phys. Rev. D **94**, 114511 (2016). https://doi.org/10.1103/PhysRevD.94.114511. arXiv:1607.03262
443. A. Donini, P. Hernández, C. Pena, F. Romero-López, Dissecting the $\Delta I = 1/2$ rule at large N_c. Eur. Phys. J. C **80**, 638 (2020). https://doi.org/10.1140/epjc/s10052-020-8192-3. arXiv:2003.10293
444. N. Christ, X. Feng, Including electromagnetism in $K \to \pi\pi$ decay calculations. EPJ Web Conf. **175**, 13016 (2018). https://doi.org/10.1051/epjconf/201817513016. arXiv:1711.09339
445. Y. Cai, Z. Davoudi, QED-corrected Lellouch–Luescher formula for $K \to \pi\pi$ decay. PoS LATTICE **2018**, 280 (2018). https://doi.org/10.22323/1.334.0280. arXiv:1812.11015
446. [SWME 15B] J.A. Bailey, Y.-C. Jang, W. Lee, S. Park, Standard Model evaluation of ε_K using lattice QCD inputs for $\hat{B}_K$ and V_{cb}. Phys. Rev. D **92**, 034510 (2015). https://doi.org/10.1103/PhysRevD.92.034510. arXiv:1503.05388
447. J.A. Bailey, S. Lee, W. Lee, J. Leem, S. Park, Updated evaluation of ϵ_K in the standard model with lattice QCD inputs. Phys. Rev. D **98**, 094505 (2018). https://doi.org/10.1103/PhysRevD.98.094505. arXiv:1808.09657
448. [LANL-SWME 19] J. Kim, S. Lee, W. Lee, Y.-C. Jang, J. Leem, S. Park, 2019 update of ε_K with lattice QCD inputs. PoS LATTICE **2019**, 029 (2019). https://doi.org/10.22323/1.363.0029. arXiv:1912.03024
449. D. Bećirević et al., $K^0\bar{K}^0$ mixing with Wilson fermions without subtractions. Phys. Lett. B **487**, 74 (2000). https://doi.org/10.1016/S0370-2693(00)00797-8. arXiv:hep-lat/0005013
450. R. Frezzotti, P.A. Grassi, S. Sint, P. Weisz, Lattice QCD with a chirally twisted mass term. JHEP **08**, 058 (2001). arXiv:hep-lat/0101001
451. [ALPHA 06] P. Dimopoulos et al., A precise determination of B_K in quenched QCD. Nucl. Phys. B **749**, 69 (2006). https://doi.org/10.1016/j.nuclphysb.2006.04.033. arXiv:hep-ph/0601002
452. [ALPHA 07] P. Dimopoulos et al., Flavour symmetry restoration and kaon weak matrix elements in quenched twisted mass QCD. Nucl. Phys. B **776**, 258 (2007). https://doi.org/10.1016/j.nuclphysb.2007.03.051. arXiv:hep-lat/0702017

453. R.S. Van de Water, S.R. Sharpe, B_K in staggered chiral perturbation theory. Phys. Rev. D **73**, 014003 (2006). https://doi.org/10.1103/PhysRevD.73.014003. arXiv:hep-lat/0507012
454. J.A. Bailey, H.-J. Kim, W. Lee, S.R. Sharpe, Kaon mixing matrix elements from beyond-the-Standard-Model operators in staggered chiral perturbation theory. Phys. Rev. D **85**, 074507 (2012). https://doi.org/10.1103/PhysRevD.85.074507. arXiv:1202.1570
455. P.H. Ginsparg, K.G. Wilson, A remnant of chiral symmetry on the lattice. Phys. Rev. D **25**, 2649 (1982). https://doi.org/10.1103/PhysRevD.25.2649
456. Y. Aoki et al., The Kaon B-parameter from quenched domain-wall QCD. Phys. Rev. D **73**, 094507 (2006). https://doi.org/10.1103/PhysRevD.73.094507. arXiv:hep-lat/0508011
457. [RBC/UKQCD] N. Christ, Estimating domain wall fermion chiral symmetry breaking. PoS LAT **2005**, 345 (2006). https://doi.org/10.22323/1.020.0345
458. V. Cirigliano, J.F. Donoghue, E. Golowich, Dimension eight operators in the weak OPE. JHEP **10**, 048 (2000). https://doi.org/10.1088/1126-6708/2000/10/048. arXiv:hep-ph/0007196
459. A.J. Buras, M. Jamin, P.H. Weisz, Leading and next-to-leading QCD corrections to ϵ parameter and $B_0 - \bar{B}_0$ mixing in the presence of a heavy top quark. Nucl. Phys. B **347**, 491 (1990). https://doi.org/10.1016/0550-3213(90)90373-L
460. A. Suzuki, Y. Taniguchi, H. Suzuki, K. Kanaya, Four quark operators for kaon bag parameter with gradient flow. Phys. Rev. D **102**, 034508 (2020). https://doi.org/10.1103/PhysRevD.102.034508. arXiv:2006.06999
461. [SWME 13A] T. Bae et al., Neutral kaon mixing from new physics: matrix elements in $N_f = 2 + 1$ lattice QCD. Phys. Rev. D **88**, 071503 (2013). https://doi.org/10.1103/PhysRevD.88.071503. arXiv:1309.2040
462. [SWME 13] T. Bae et al., Update on B_K and ε_K with staggered quarks. PoS LATTICE **2013**, 476 (2013). arXiv:1310.7319
463. [SWME 11A] T. Bae et al., Kaon B-parameter from improved staggered fermions in $N_f = 2 + 1$ QCD. Phys. Rev. Lett. **109**, 041601 (2012). https://doi.org/10.1103/PhysRevLett.109.041601. arXiv:1111.5698
464. [RBC/UKQCD 10B] Y. Aoki et al., Continuum limit of B_K from 2+1 flavor domain wall QCD. Phys. Rev. D **84**, 014503 (2011). https://doi.org/10.1103/PhysRevD.84.014503. arXiv:1012.4178
465. [SWME 10] T. Bae et al., B_K using HYP-smeared staggered fermions in $N_f = 2 + 1$ unquenched QCD. Phys. Rev. D **82**, 114509 (2010). https://doi.org/10.1103/PhysRevD.82.114509. arXiv:1008.5179
466. C. Aubin, J. Laiho, R.S. Van de Water, The neutral kaon mixing parameter B_K from unquenched mixed-action lattice QCD. Phys. Rev. D **81**, 014507 (2010). https://doi.org/10.1103/PhysRevD.81.014507. arXiv:0905.3947
467. [ETM 10A] M. Constantinou et al., BK-parameter from $N_f = 2$ twisted mass lattice QCD. Phys. Rev. D **83**, 014505 (2011). https://doi.org/10.1103/PhysRevD.83.014505. arXiv:1009.5606
468. [ETM 10C] M. Constantinou et al., Non-perturbative renormalization of quark bilinear operators with $N_f = 2$ (tmQCD) Wilson fermions and the tree-level improved gauge action. JHEP **08**, 068 (2010). https://doi.org/10.1007/JHEP08(2010)068. arXiv:1004.1115
469. F. Gabbiani, E. Gabrielli, A. Masiero, L. Silvestrini, A complete analysis of FCNC and CP constraints in general SUSY extensions of the standard model. Nucl. Phys. B **477**, 321 (1996). https://doi.org/10.1016/0550-3213(96)00390-2. arXiv:hep-ph/9604387
470. [RBC/UKQCD 12E] P.A. Boyle, N. Garron, R.J. Hudspith, Neutral kaon mixing beyond the standard model with $n_f = 2+1$ chiral fermions. Phys. Rev. D **86**, 054028 (2012). https://doi.org/10.1103/PhysRevD.86.054028. arXiv:1206.5737
471. A.J. Buras, M. Misiak, J. Urban, Two loop QCD anomalous dimensions of flavor changing four quark operators within and beyond the standard model. Nucl. Phys. B **586**, 397 (2000). https://doi.org/10.1016/S0550-3213(00)00437-5. arXiv:hep-ph/0005183
472. C.R. Allton, L. Conti, A. Donini, V. Gimenez, L. Giusti, G. Martinelli et al., B parameters for Delta S = 2 supersymmetric operators. Phys. Lett. B **453**, 30 (1999). https://doi.org/10.1016/S0370-2693(99)00283-X. arXiv:hep-lat/9806016
473. A. Donini, V. Gimenez, L. Giusti, G. Martinelli, Renormalization group invariant matrix elements of Delta S = 2 and Delta I = 3/2 four fermion operators without quark masses. Phys. Lett. B **470**, 233 (1999). https://doi.org/10.1016/S0370-2693(99)01300-3. arXiv:hep-lat/9910017
474. R. Babich, N. Garron, C. Hoelbling, J. Howard, L. Lellouch, C. Rebbi, K0–anti-K0 mixing beyond the standard model and CP-violating electroweak penguins in quenched QCD with exact chiral symmetry. Phys. Rev. D **74**, 073009 (2006). https://doi.org/10.1103/PhysRevD.74.073009. arXiv:hep-lat/0605016
475. A.J. Buras, J.-M. Gérard, Dual QCD insight into BSM hadronic matrix elements for $K^0 - \bar{K}^0$ mixing from lattice QCD. Acta Phys. Polon. B **50**, 121 (2019). https://doi.org/10.5506/APhysPolB.50.121. arXiv:1804.02401
476. [SWME 14C] J. Leem et al., Calculation of BSM Kaon B-parameters using Staggered Quarks. PoS LATTICE **2014**, 370 (2014). arXiv:1411.1501
477. [RBC/UKQCD 17A] P. Boyle et al., Neutral kaon mixing beyond the Standard Model with $n_f = 2 + 1$ chiral fermions. Part 2: non perturbative renormalisation of the $\Delta F = 2$ four-quark operators. JHEP **10**, 054 (2017). https://doi.org/10.1007/JHEP10(2017)054. arXiv:1708.03552
478. P. Boyle, N. Garron, R.J. Hudspith, A. Juttner, J. Kettle, A. Khamseh et al., Beyond the Standard Model kaon mixing with physical masses, in Proceedings, 36th International Symposium on Lattice Field Theory (Lattice 2018): East Lansing, MI, United States, July 22–28, 2018, vol. LATTICE2018, p. 285 (2019). https://doi.org/10.22323/1.334.0285. arXiv:1812.04981
479. B. Blossier, J. Heitger, M. Post, Leptonic D_s decays in two-flavour lattice QCD. Phys. Rev. D **98**, 054506 (2018). https://doi.org/10.1103/PhysRevD.98.054506. arXiv:1803.03065
480. [FNAL/MILC 13] A. Bazavov et al., Charmed and strange pseudoscalar meson decay constants from HISQ simulations. PoS LATTICE **2013**, 405 (2014). arXiv:1312.0149
481. [FNAL/MILC 12B] A. Bazavov et al., Pseudoscalar meson physics with four dynamical quarks. PoS LAT **2012**, 159 (2012). arXiv:1210.8431
482. [χQCD 20A] Y. Chen, W.-F. Chiu, M. Gong, Z. Liu, Y. Ma, Charmed and ϕ meson decay constants from 2+1-flavor lattice QCD. Chin. Phys. C **45**, 023109 (2021). https://doi.org/10.1088/1674-1137/abcd8f. arXiv:2008.05208
483. [PACS-CS 11] Y. Namekawa et al., Charm quark system at the physical point of 2+1 flavor lattice QCD. Phys. Rev. D **84**, 074505 (2011). https://doi.org/10.1103/PhysRevD.84.074505. arXiv:1104.4600
484. [FNAL/MILC 05] C. Aubin, C. Bernard, C.E. DeTar, M. Di Pierro, E.D. Freeland et al., Charmed meson decay constants in three-flavor lattice QCD. Phys. Rev. Lett. **95**, 122002 (2005). https://doi.org/10.1103/PhysRevLett.95.122002. arXiv:hep-lat/0506030
485. [TWQCD 14] W. Chen et al., Decay constants of pseudoscalar D-mesons in lattice QCD with domain-wall fermion. Phys. Lett. B **736**, 231 (2014). https://doi.org/10.1016/j.physletb.2014.07.025. arXiv:1404.3648

486. [ALPHA 13B] J. Heitger, G.M. von Hippel, S. Schaefer, F. Virotta, Charm quark mass and D-meson decay constants from two-flavour lattice QCD. PoS LATTICE **2013**, 475 (2014). arXiv:1312.7693
487. C. Kane, C. Lehner, S. Meinel, A. Soni, Radiative leptonic decays on the lattice. PoS LATTICE **2019**, 134 (2019). https://doi.org/10.22323/1.363.0134. arXiv:1907.00279
488. A. Desiderio et al., First lattice calculation of radiative leptonic decay rates of pseudoscalar mesons. Phys. Rev. D **103**, 014502 (2021). https://doi.org/10.1103/PhysRevD.103.014502. arXiv:2006.05358
489. CLEO collaboration, Improved measurements of D meson semileptonic decays to π and K mesons. Phys. Rev. D **80**, 032005 (2009). https://doi.org/10.1103/PhysRevD.80.032005. arXiv:0906.2983
490. BESIII collaboration, Measurement of $e^+e^- \to \pi^+\pi^-\psi(3686)$ from 4.008 to 4.600 GeV and observation of a charged structure in the $\pi^\pm\psi(3686)$ mass spectrum. Phys. Rev. D **96**, 032004 (2017). https://doi.org/10.1103/PhysRevD.96.032004. arXiv:1703.08787
491. BESIII collaboration, Measurement of the branching fraction for the semi-leptonic decay $D^{0(+)} \to \pi^{-(0)}\mu^+\nu_\mu$ and test of lepton universality. Phys. Rev. Lett. **121**, 171803 (2018). https://doi.org/10.1103/PhysRevLett.121.171803. arXiv:1802.05492
492. P.F. Bedaque, Aharonov–Bohm effect and nucleon nucleon phase shifts on the lattice. Phys. Lett. B **593**, 82 (2004). https://doi.org/10.1016/j.physletb.2004.04.045. arXiv:nucl-th/0402051
493. C. Sachrajda, G. Villadoro, Twisted boundary conditions in lattice simulations. Phys. Lett. B **609**, 73 (2005). https://doi.org/10.1016/j.physletb.2005.01.033. arXiv:hep-lat/0411033
494. [ETM 11B] S. Di Vita, B. Haas, V. Lubicz, F. Mescia, S. Simula, C. Tarantino, Form factors of the $D \to \pi$ and $D \to K$ semileptonic decays with $N_f = 2$ twisted mass lattice QCD. PoS LATTICE **2010**, 301 (2010). arXiv:1104.0869
495. [HPQCD 11C] J. Koponen et al., The D to K and D to π semileptonic decay form factors from lattice QCD. PoS LAT **2011**, 286 (2011). arXiv:1111.0225
496. [HPQCD 12B] J. Koponen, C. Davies, G. Donald, D to K and D to π semileptonic form factors from lattice QCD, Charm (2012). arXiv:1208.6242
497. [HPQCD 13C] J. Koponen, C.T.H. Davies, G.C. Donald, E. Follana, G.P. Lepage et al., The shape of the $D \to K$ semileptonic form factor from full lattice QCD and V_{cs}. arXiv:1305.1462
498. [ETM 18] V. Lubicz, L. Riggio, G. Salerno, S. Simula, C. Tarantino, Tensor form factor of $D \to \pi(K)\ell\nu$ and $D \to \pi(K)\ell\ell$ decays with $N_f = 2+1+1$ twisted-mass fermions. Phys. Rev. D **98**, 014516 (2018). https://doi.org/10.1103/PhysRevD.98.014516. arXiv:1803.04807
499. D. Bećirević, B. Haas, F. Mescia, Semileptonic D-decays and lattice QCD. PoS LAT **2007**, 355 (2007). arXiv:0710.1741
500. D. Bećirević, A.B. Kaidalov, Comment on the heavy $\to$ light form-factors. Phys. Lett. B **478**, 417 (2000). https://doi.org/10.1016/S0370-2693(00)00290-2. arXiv:hep-ph/9904490
501. [FNAL/MILC 04] C. Aubin et al., Semileptonic decays of D mesons in three-flavor lattice QCD. Phys. Rev. Lett. **94**, 011601 (2005). https://doi.org/10.1103/PhysRevLett.94.011601. arXiv:hep-ph/0408306
502. FOCUS collaboration, Measurements of the q^2 dependence of the $D^0 \to K^-\mu^+\nu$ and $D^0 \to \pi^-\mu^+\nu$ form factors. Phys. Lett. B **607**, 233 (2005). https://doi.org/10.1016/j.physletb.2004.12.036. arXiv:hep-ex/0410037
503. Belle collaboration, Measurement of $D^0 \to \pi l\nu(Kl\nu)$ and their form-factors. arXiv:hep-ex/0510003
504. [FNAL/MILC 12G] J.A. Bailey et al., Charm semileptonic decays and $|V_{cs(d)}|$ from heavy clover quarks and 2+1 flavor asqtad staggered ensembles. PoS LAT **2012**, 272 (2012). arXiv:1211.4964
505. [JLQCD 17B] T. Kaneko, B. Colquhoun, H. Fukaya, S. Hashimoto, D meson semileptonic form factors in N_f = 3 QCD with Möbius domain-wall quarks. EPJ. Web Conf. **175**, 13007 (2018). https://doi.org/10.1051/epjconf/201817513007. arXiv:1711.11235
506. G. Colangelo, M. Procura, L. Rothen, R. Stucki, J. Tarrus Castella, On the factorization of chiral logarithms in the pion form factors. JHEP **09**, 081 (2012). https://doi.org/10.1007/JHEP09(2012)081. arXiv:1208.0498
507. J. Bijnens, I. Jemos, Hard pion chiral perturbation theory for $B \to \pi$ and $D \to \pi$ formfactors. Nucl. Phys. B **840**, 54 (2010). https://doi.org/10.1016/j.nuclphysb.2010.06.021. https://doi.org/10.1016/j.nuclphysb.2010.10.024. arXiv:1006.1197 [Erratum: Nucl. Phys. B 844, 182 (2011)]
508. [FNAL/MILC 15B] T. Primer, C. Bernard, C. DeTar, A. El-Khadra, E. Gámiz, J. Komijani et al., D-meson semileptonic form factors at zero momentum transfer in (2+1+1)-flavor lattice QCD. PoS LATTICE **2015**, 338 (2016). arXiv:1511.04000
509. [FNAL/MILC 17B] T. Primer et al., D meson semileptonic form factors with HISQ valence and sea quarks. PoS LATTICE **2016**, 305 (2017). https://doi.org/10.22323/1.256.0305
510. [HPQCD 20] L.J. Cooper, C.T.H. Davies, J. Harrison, J. Komijani, M. Wingate, $B_c \to B_{s(d)}$ form factors from lattice QCD. Phys. Rev. D **102**, 014513 (2020). https://doi.org/10.1103/PhysRevD.102.014513. arXiv:2003.00914] [Erratum: Phys. Rev. D 103, 099901 (2021)]
511. T. Feldmann, M.W.Y. Yip, Form factors for $Lambda_b \to \Lambda$ transitions in SCET. Phys. Rev. D **85**, 014035 (2012). https://doi.org/10.1103/PhysRevD.85.014035. https://doi.org/10.1103/PhysRevD.86.079901. arXiv:1111.1844 [Erratum: Phys. Rev. D 86, 079901 (2012)]
512. S. Meinel, $\Lambda_c \to \Lambda l^+\nu_l$ form factors and decay rates from lattice QCD with physical quark masses. Phys. Rev. Lett. **118**, 082001 (2017). https://doi.org/10.1103/PhysRevLett.118.082001. arXiv:1611.09696
513. BESIII collaboration, Measurement of the absolute branching fraction for $\Lambda_c^+ \to \Lambda e^+\nu_e$. Phys. Rev. Lett. **115**, 221805 (2015). https://doi.org/10.1103/PhysRevLett.115.221805. arXiv:1510.02610
514. BESIII collaboration, Measurement of the absolute branching fraction for $\Lambda_c^+ \to \Lambda\mu^+\nu_\mu$. Phys. Lett. B **767**, 42 (2017). https://doi.org/10.1016/j.physletb.2017.01.047. arXiv:1611.04382
515. S. Meinel, $\Lambda_c \to N$ form factors from lattice QCD and phenomenology of $\Lambda_c \to n\ell^+\nu_\ell$ and $\Lambda_c \to p\mu^+\mu^-$ decays. Phys. Rev. D **97**, 034511 (2018). https://doi.org/10.1103/PhysRevD.97.034511. arXiv:1712.05783
516. W. Detmold, C. Lehner, S. Meinel, $\Lambda_b \to p\ell^-\bar{\nu}_\ell$ and $\Lambda_b \to \Lambda_c\ell^-\bar{\nu}_\ell$ form factors from lattice QCD with relativistic heavy quarks. Phys. Rev. D **92**, 034503 (2015). https://doi.org/10.1103/PhysRevD.92.034503. arXiv:1503.01421
517. Q.-A. Zhang, J. Hua, F. Huang, R. Li, Y. Li, C.-D. Lu et al., $\Xi_c \to \Xi$ form factors and $\Xi_c \to \Xi\ell^+\nu_\ell$ decay rates from lattice QCD. Phys. C **46**, 011002 (2022). https://doi.org/10.1088/1674-1137/ac2b12. arXiv:2103.07064
518. Belle collaboration, Measurements of the branching fractions of semileptonic decays $\Xi_c^0 \to \Xi^-\ell^+\nu_\ell$ and asymmetry parameter of $\Xi_c^0 \to \Xi^-\pi^+$ decay. arXiv:2103.06496

519. B.A. Dobrescu, A.S. Kronfeld, Accumulating evidence for nonstandard leptonic decays of D_s mesons. Phys. Rev. Lett. **100**, 241802 (2008). https://doi.org/10.1103/PhysRevLett.100.241802. arXiv:0803.0512
520. V. Cirigliano, I. Rosell, $\pi/K \to e\bar{\nu}_e$ branching ratios to $O(e^2p^4)$ in Chiral Perturbation Theory. JHEP **10**, 005 (2007). https://doi.org/10.1088/1126-6708/2007/10/005. arXiv:0707.4464
521. L. Riggio, G. Salerno, S. Simula, Extraction of $|V_{cd}|$ and $|V_{cs}|$ from experimental decay rates using lattice QCD $D \to \pi(K)\ell\nu$ form factors. Eur. Phys. J. **C78**, 501 (2018). https://doi.org/10.1140/epjc/s10052-018-5943-5. arXiv:1706.03657
522. BESIII collaboration, Study of the $D^0 \to K^-\mu^+\nu_\mu$ dynamics and test of lepton flavor universality with $D^0 \to K^-\ell^+\nu_\ell$ decays. Phys. Rev. Lett. **122**, 011804 (2019). https://doi.org/10.1103/PhysRevLett.122.011804. arXiv:1810.03127
523. BaBar collaboration, Measurement of the hadronic form-factor in $D^0 \to K^-e^+\nu_e$ 1. Phys. Rev. D **76**, 052005 (2007). https://doi.org/10.1103/PhysRevD.76.052005. arXiv:0704.0020
524. BESIII collaboration, Study of dynamics of $D^0 \to K^-e^+\nu_e$ and $D^0 \to \pi^-e^+\nu_e$ decays. Phys. Rev. D **92**, 072012 (2015). https://doi.org/10.1103/PhysRevD.92.072012. arXiv:1508.07560
525. BESIII collaboration, Analysis of $D^+ \to \bar{K}^0e^+\nu_e$ and $D^+ \to \pi^0e^+\nu_e$ semileptonic decays. Phys. Rev. D **96**, 012002 (2017). https://doi.org/10.1103/PhysRevD.96.012002. arXiv:1703.09084
526. Belle collaboration, Measurement of D0 → pi l nu (Kl nu) form factors and absolute branching fractions. Phys. Rev. Lett. **97**, 061804 (2006). https://doi.org/10.1103/PhysRevLett.97.061804. arXiv:hep-ex/0604049
527. Babar collaboration, Evidence of $B \to \tau\nu$ decays with hadronic B tags. Phys. Rev. D **88**, 031102 (2013). https://doi.org/10.1103/PhysRevD.88.031102. arXiv:1207.0698
528. Belle collaboration, Measurement of the branching fraction of $B^+ \to \tau^+\nu_\tau$ decays with the semileptonic tagging method. Phys. Rev. D **92**, 051102 (2015). https://doi.org/10.1103/PhysRevD.92.051102. arXiv:1503.05613
529. G. Buchalla, A.J. Buras, QCD corrections to rare K and B decays for arbitrary top quark mass. Nucl. Phys. B **400**, 225 (1993). https://doi.org/10.1016/0550-3213(93)90405-E
530. LHCb, CMS collaboration, Observation of the rare $B_s^0 \to \mu^+\mu^-$ decay from the combined analysis of CMS and LHCb data. Nature **522**, 68 (2015). https://doi.org/10.1038/nature14474. arXiv:1411.4413
531. ATLAS collaboration, Combination of the ATLAS, CMS and LHCb results on the $B_{(s)}^0 \to \mu^+\mu^-$ decays
532. M. Beneke, C. Bobeth, R. Szafron, Power-enhanced leading-logarithmic QED corrections to $B_q \to \mu^+\mu^-$. JHEP **10**, 232 (2019). https://doi.org/10.1007/JHEP10(2019)232. arXiv:1908.07011
533. [ETM 13E] N. Carrasco, P. Dimopoulos, R. Frezzotti, V. Giménez, P. Lami et al., A $N_f = 2+1+1$ 'twisted' determination of the b-quark mass, f_B and f_{B_s}. PoS LATTICE **2013**, 313 (2014). arXiv:1311.2837
534. [RBC/UKQCD 13A] O. Witzel, B-meson decay constants with domain-wall light quarks and nonperturbatively tuned relativistic b-quarks. PoS LATTICE **2013**, 377 (2014). arXiv:1311.0276
535. [ALPHA 13] F. Bernardoni, B. Blossier, J. Bulava, M. Della Morte, P. Fritzsch et al., B-physics with $N_f = 2$ Wilson fermions. PoS LATTICE **2013**, 381 (2014). arXiv:1309.1074
536. [ETM 13C] N. Carrasco et al., B-physics computations from Nf=2 tmQCD. PoS LATTICE **2013**, 382 (2014). arXiv:1310.1851
537. [ALPHA 12A] F. Bernardoni, B. Blossier, J. Bulava, M. Della Morte, P. Fritzsch et al., B-physics from HQET in two-flavour lattice QCD. PoS LAT **2012**, 273 (2012). arXiv:1210.7932
538. [ETM 12B] N. Carrasco, P. Dimopoulos, R. Frezzotti, V. Gimenez, G. Herdoiza et al., B-physics from the ratio method with Wilson twisted mass fermions. PoS LAT **2012**, 104 (2012). arXiv:1211.0568
539. [ALPHA 11] B. Blossier, J. Bulava, M. Della Morte, M. Donnellan, P. Fritzsch et al., M_b and f_B from non-perturbatively renormalized HQET with $N_f = 2$ light quarks. PoS LAT **2011**, 280 (2011). arXiv:1112.6175
540. [ETM 09D] B. Blossier et al., A proposal for B-physics on current lattices. JHEP **1004**, 049 (2010). https://doi.org/10.1007/JHEP04(2010)049. arXiv:0909.3187
541. [RBC/UKQCD 10C] C. Albertus et al., Neutral B-meson mixing from unquenched lattice QCD with domain-wall light quarks and static b-quarks. Phys. Rev. D **82**, 014505 (2010). https://doi.org/10.1103/PhysRevD.82.014505. arXiv:1001.2023
542. D.J. Broadhurst, A.G. Grozin, Matching QCD and HQET heavy-light currents at two loops and beyond. Phys. Rev. D **52**, 4082 (1995). https://doi.org/10.1103/PhysRevD.52.4082. arXiv:hep-ph/9410240
543. K. Chetyrkin, A. Grozin, Three loop anomalous dimension of the heavy light quark current in HQET. Nucl. Phys. B **666**, 289 (2003). https://doi.org/10.1016/S0550-3213(03)00490-5. arXiv:hep-ph/0303113
544. S. Bekavac, A.G. Grozin, P. Marquard, J.H. Piclum, D. Seidel, M. Steinhauser, Matching QCD and HQET heavy-light currents at three loops. Nucl. Phys. B **833**, 46 (2010). https://doi.org/10.1016/j.nuclphysb.2010.02.025. arXiv:0911.3356
545. P. Boyle, A. Jüttner, M.K. Marinkovic, F. Sanfilippo, M. Spraggs, J.T. Tsang, An exploratory study of heavy domain wall fermions on the lattice. JHEP **04**, 037 (2016). https://doi.org/10.1007/JHEP04(2016)037. arXiv:1602.04118
546. A. Lenz, U. Nierste, Theoretical update of $B_s - \bar{B}_s$ mixing. JHEP **0706**, 072 (2007). https://doi.org/10.1088/1126-6708/2007/06/072. arXiv:hep-ph/0612167
547. M. Beneke, G. Buchalla, I. Dunietz, Width difference in the $B_s - \bar{B}_s$ system. Phys. Rev. D **54**, 4419 (1996). https://doi.org/10.1103/PhysRevD.54.4419. https://doi.org/10.1103/PhysRevD.83.119902. arXiv:hep-ph/9605259
548. [FNAL/MILC 11A] C.M. Bouchard, E. Freeland, C. Bernard, A. El-Khadra, E. Gamiz et al., Neutral B mixing from $2+1$ flavor lattice-QCD: the Standard Model and beyond. PoS LAT **2011**, 274 (2011). arXiv:1112.5642
549. [HPQCD 06A] E. Dalgic, A. Gray, E. Gamiz, C.T. Davies, G.P. Lepage et al., $B_s^0 - \bar{B}_s^0$ mixing parameters from unquenched lattice QCD. Phys. Rev. D **76**, 011501 (2007). https://doi.org/10.1103/PhysRevD.76.011501. arXiv:hep-lat/0610104
550. [ETM 12A] N. Carrasco et al., Neutral meson oscillations in the Standard Model and beyond from $N_f = 2$ twisted mass lattice QCD. PoS LAT **2012**, 105 (2012). arXiv:1211.0565
551. [FNAL/MILC 12] A. Bazavov, C. Bernard, C. Bouchard, C. DeTar, M. Di Pierro et al., Neutral B-meson mixing from three-flavor lattice QCD: determination of the SU(3)-breaking ratio ξ. Phys. Rev. D **86**, 034503 (2012). https://doi.org/10.1103/PhysRevD.86.034503. arXiv:1205.7013

552. [HPQCD 11B] R.J. Dowdall et al., The upsilon spectrum and the determination of the lattice spacing from lattice QCD including charm quarks in the sea. Phys. Rev. D **85**, 054509 (2012). https://doi.org/10.1103/PhysRevD.85.054509. arXiv:1110.6887
553. M. Della Morte, B. Jäger, T. Rae, H. Wittig, Improved interpolating fields for hadrons at non-zero momentum. Eur. Phys. J. A **48**, 139 (2012). https://doi.org/10.1140/epja/i2012-12139-9. arXiv:1208.0189
554. [HPQCD 06] E. Dalgic et al., B meson semileptonic form-factors from unquenched lattice QCD, Phys. Rev. D **73**, 074502 (2006). https://doi.org/10.1103/PhysRevD.73.074502. https://doi.org/10.1103/PhysRevD.75.119906. arXiv:hep-lat/0601021
555. [FNAL/MILC 08A] J.A. Bailey et al., The $B \to \pi \ell \nu$ semileptonic form factor from three-flavor lattice QCD: a model-independent determination of $|V_{ub}|$. Phys. Rev. D **79**, 054507 (2009). https://doi.org/10.1103/PhysRevD.79.054507. arXiv:0811.3640
556. [FNAL/MILC 15] J. A. Bailey et al., $|V_{ub}|$ from $B \to \pi \ell \nu$ decays and (2+1)-flavor lattice QCD. Phys. Rev. D **92**, 014024 (2015). https://doi.org/10.1103/PhysRevD.92.014024. arXiv:1503.07839
557. [RBC/UKQCD 15] J. M. Flynn, T. Izubuchi, T. Kawanai, C. Lehner, A. Soni, R.S. Van de Water et al., $B \to \pi \ell \nu$ and $B_s \to K \ell \nu$ form factors and $|V_{ub}|$ from 2+1-flavor lattice QCD with domain-wall light quarks and relativistic heavy quarks. Phys. Rev. D **91**, 074510 (2015). https://doi.org/10.1103/PhysRevD.91.074510. arXiv:1501.05373
558. [HPQCD 15A] B. Colquhoun, R.J. Dowdall, J. Koponen, C.T.H. Davies, G.P. Lepage, $B \to \pi \ell \nu$ at zero recoil from lattice QCD with physical u/d quarks. Phys. Rev. D **93**, 034502 (2016). https://doi.org/10.1103/PhysRevD.93.034502. arXiv:1510.07446
559. [HPQCD 12C] C.M. Bouchard, G.P. Lepage, C.J. Monahan, H. Na, J. Shigemitsu, Form factors for B and B_s semileptonic decays with NRQCD/HISQ quarks. PoS LAT **2012**, 118 (2012). arXiv:1210.6992
560. [HPQCD 13F] C.M. Bouchard, G.P. Lepage, J.C. Monahan, H. Na, J. Shigemitsu, B and B_s semileptonic decay form factors with NRQCD/HISQ quarks. PoS LATTICE **2013**, 387 (2014). arXiv:1310.3207
561. B. Colquhoun, S. Hashimoto, T. Kaneko, $B \to \pi \ell \nu$ with Möbius domain wall fermions. EPJ Web Conf. **175**, 13004 (2018). https://doi.org/10.1051/epjconf/201817513004. arXiv:1710.07094
562. B. Colquhoun, S. Hashimoto, T. Kaneko, Heavy quark scaling of $B \to \pi \ell \nu$ form factors with Möbius domain wall fermions. PoS LATTICE **2018**, 274 (2018). https://doi.org/10.22323/1.334.0274. arXiv:1811.00227
563. [JLQCD 19] B. Colquhoun, S. Hashimoto, T. Kaneko, J. Koponen, $B \to \pi \ell \nu$ form factors and $|V_{ub}|$ with Möbius domain wall fermions. PoS LATTICE **2019**, 143 (2019). https://doi.org/10.22323/1.363.0143. arXiv:1912.02409
564. Z. Gelzer et al., Semileptonic B-meson decays to light pseudoscalar mesons on the HISQ ensembles. EPJ Web Conf. **175**, 13024 (2018). https://doi.org/10.1051/epjconf/201817513024. arXiv:1710.09442
565. [FNAL/MILC 19A] Z. Gelzer et al., B-meson semileptonic form factors on (2+1+1)-flavor HISQ ensembles. PoS LATTICE **2019**, 236 (2019). https://doi.org/10.22323/1.363.0236. arXiv:1912.13358
566. J. Flynn, R. Hill, A. Jüttner, A. Soni, J.T. Tsang, O. Witzel, Semileptonic $B \to \pi \ell \nu$, $B \to D \ell \nu$, $B_s \to K \ell \nu$, and $B_s \to D_s \ell \nu$ decays. PoS LATTICE **2019**, 184 (2019). https://doi.org/10.22323/1.363.0184. arXiv:1912.09946
567. P. Ball, R. Zwicky, $|V_{ub}|$ and constraints on the leading-twist pion distribution amplitude from $B \to \pi l \nu$. Phys. Lett. B **625**, 225 (2005). https://doi.org/10.1016/j.physletb.2005.08.070. arXiv:hep-ph/0507076
568. R.J. Hill, Heavy-to-light meson form-factors at large recoil. Phys. Rev. D **73**, 014012 (2006). https://doi.org/10.1103/PhysRevD.73.014012. arXiv:hep-ph/0505129
569. C.G. Boyd, B. Grinstein, R.F. Lebed, Constraints on form-factors for exclusive semileptonic heavy to light meson decays. Phys. Rev. Lett. **74**, 4603 (1995). https://doi.org/10.1103/PhysRevLett.74.4603. arXiv:hep-ph/9412324
570. [HPQCD 14] C.M. Bouchard, G.P. Lepage, C. Monahan, H. Na, J. Shigemitsu, $B_s \to K \ell \nu$ form factors from lattice QCD. Phys. Rev. D **90**, 054506 (2014). https://doi.org/10.1103/PhysRevD.90.054506. arXiv:1406.2279
571. C.J. Monahan, C.M. Bouchard, G.P. Lepage, H. Na, J. Shigemitsu, Form factor ratios for $B_s \to K \ell \nu$ and $B_s \to D_s \ell \nu$ semileptonic decays and $|V_{ub}/V_{cb}|$. arXiv:1808.09285
572. [FNAL/MILC 17A] Y. Liu et al., $B_s \to K \ell \nu$ form factors with 2+1 flavors. EPJ Web Conf. **175**, 13008 (2018). https://doi.org/10.1051/epjconf/201817513008. arXiv:1711.08085
573. [FNAL/MILC 19] A. Bazavov et al., $B_s \to K \ell \nu$ decay from lattice QCD. Phys. Rev. D **100**, 034501 (2019). https://doi.org/10.1103/PhysRevD.100.034501. arXiv:1901.02561
574. F. Bahr, D. Banerjee, F. Bernardoni, M. Koren, H. Simma, R. Sommer, Extraction of bare form factors for $B_s \to K \ell \nu$ decays in nonperturbative HQET. Int. J. Mod. Phys. A **34**, 1950166 (2019). https://doi.org/10.1142/S0217751X19501665. arXiv:1903.05870
575. [ALPHA 14B] F. Bahr, F. Bernardoni, J. Bulava, A. Joseph, A. Ramos, H. Simma et al., Form factors for $B_s \to K \ell \nu$ decays in lattice QCD, in 8th International Workshop on the CKM Unitarity Triangle (CKM2014) Vienna, Austria, September 8–12, 2014 (2014). arXiv:1411.3916
576. M. Antonelli et al., Flavor physics in the quark sector. Phys. Rep. **494**, 197 (2010). https://doi.org/10.1016/j.physrep.2010.05.003. arXiv:0907.5386
577. Z. Liu et al., Form factors for rare B decays: strategy, methodology, and numerical study. PoS LAT **2009**, 242 (2009). arXiv:0911.2370
578. [FNAL/MILC 15D] J.A. Bailey et al., $B \to K l^+ l^-$ decay form factors from three-flavor lattice QCD. Phys. Rev. D **93**, 025026 (2016). https://doi.org/10.1103/PhysRevD.93.025026. arXiv:1509.06235
579. [HPQCD 13E] C. Bouchard, G.P. Lepage, C. Monahan, H. Na, J. Shigemitsu, Rare decay $B \to K \ell^+ \ell^-$ form factors from lattice QCD. Phys. Rev. D **88**, 054509 (2013). https://doi.org/10.1103/PhysRevD.88.079901. https://doi.org/10.1103/PhysRevD.88.054509. arXiv:1306.2384 [Erratum: Phys. Rev. D **88**(7), 079901 (2013)]
580. [FNAL/MILC 15E] J.A. Bailey et al., $B \to \pi \ell \ell$ form factors for new-physics searches from lattice QCD. Phys. Rev. Lett. **115**, 152002 (2015). https://doi.org/10.1103/PhysRevLett.115.152002. arXiv:1507.01618
581. [HPQCD 13D] C. Bouchard, G.P. Lepage, C. Monahan, H. Na, J. Shigemitsu, Standard Model predictions for $B \to K ll$ with form factors from lattice QCD. Phys. Rev. Lett. **111**, 162002 (2013). https://doi.org/10.1103/PhysRevLett.112.149902. https://doi.org/10.1103/PhysRevLett.111.162002. arXiv:1306.0434 [Erratum: Phys. Rev. Lett. **112**, 149902 (2014)]
582. [FNAL/MILC 15F] D. Du, A.X. El-Khadra, S. Gottlieb, A.S. Kronfeld, J. Laiho, E. Lunghi et al., Phenomenology of semileptonic B-meson decays with form factors from lattice QCD. Phys. Rev. D **93**, 034005 (2016). https://doi.org/10.1103/PhysRevD.93.034005. arXiv:1510.02349
583. LHCb collaboration, First measurement of the differential branching fraction and CP asymmetry of the $B^\pm \to \pi^\pm \mu^+ \mu^-$ decay. JHEP **10**, 034 (2015). https://doi.org/10.1007/JHEP10(2015)034. arXiv:1509.00414

584. C.B. Lang, D. Mohler, S. Prelovsek, R.M. Woloshyn, Predicting positive parity B_s mesons from lattice QCD. Phys. Lett. B **750**, 17 (2015). https://doi.org/10.1016/j.physletb.2015.08.038. arXiv:1501.01646
585. M. Lage, U.-G. Meissner, A. Rusetsky, A method to measure the antikaon-nucleon scattering length in lattice QCD. Phys. Lett. B **681**, 439 (2009). https://doi.org/10.1016/j.physletb.2009.10.055. arXiv:0905.0069
586. V. Bernard, M. Lage, U.G. Meissner, A. Rusetsky, Scalar mesons in a finite volume. JHEP **01**, 019 (2011). https://doi.org/10.1007/JHEP01(2011)019. arXiv:1010.6018
587. M. Doring, U.-G. Meissner, E. Oset, A. Rusetsky, Unitarized chiral perturbation theory in a finite volume: scalar meson sector. Eur. Phys. J. A **47**, 139 (2011). https://doi.org/10.1140/epja/i2011-11139-7. arXiv:1107.3988
588. M.T. Hansen, S.R. Sharpe, Multiple-channel generalization of Lellouch–Luscher formula. Phys. Rev. D **86**, 016007 (2012). https://doi.org/10.1103/PhysRevD.86.016007. arXiv:1204.0826
589. R.A. Briceno, Z. Davoudi, Moving multichannel systems in a finite volume with application to proton-proton fusion. Phys. Rev. D **88**, 094507 (2013). https://doi.org/10.1103/PhysRevD.88.094507. arXiv:1204.1110
590. [HS 14] J.J. Dudek, R.G. Edwards, C.E. Thomas, D.J. Wilson, Resonances in coupled $\pi K - \eta K$ scattering from quantum chromodynamics. Phys. Rev. Lett. **113**, 182001 (2014). https://doi.org/10.1103/PhysRevLett.113.182001. arXiv:1406.4158
591. R.A. Briceño, M.T. Hansen, A. Walker-Loud, Multichannel $1 \to 2$ transition amplitudes in a finite volume. Phys. Rev. D **91**, 034501 (2015). https://doi.org/10.1103/PhysRevD.91.034501. arXiv:1406.5965
592. R.A. Briceño, M.T. Hansen, Multichannel $0 \to 2$ and $1 \to 2$ transition amplitudes for arbitrary spin particles in a finite volume. Phys. Rev. D **92**, 074509 (2015). https://doi.org/10.1103/PhysRevD.92.074509. arXiv:1502.04314
593. R.R. Horgan, Z. Liu, S. Meinel, M. Wingate, Lattice QCD calculation of form factors describing the rare decays $B \to K^* \ell^+ \ell^-$ and $B_s \to \phi \ell^+ \ell^-$. Phys. Rev. D **89**, 094501 (2014). https://doi.org/10.1103/PhysRevD.89.094501. arXiv:1310.3722
594. R.R. Horgan, Z. Liu, S. Meinel, M. Wingate, Calculation of $B^0 \to K^{*0} \mu^+ \mu^-$ and $B_s^0 \to \phi \mu^+ \mu^-$ observables using form factors from lattice QCD. Phys. Rev. Lett. **112**, 212003 (2014). https://doi.org/10.1103/PhysRevLett.112.212003. arXiv:1310.3887
595. R.R. Horgan, Z. Liu, S. Meinel, M. Wingate, Rare B decays using lattice QCD form factors. PoS LATTICE **2014**, 372 (2015). https://doi.org/10.22323/1.214.0372. arXiv:1501.00367
596. [RBC/UKQCD 15B] J. Flynn, A. Jüttner, T. Kawanai, E. Lizarazo, O. Witzel, Hadronic form factors for rare semileptonic B decays, in Proceedings, 33rd International Symposium on Lattice Field Theory (Lattice 2015), vol. LATTICE2015, p. 345 (2016). arXiv:1511.06622
597. J. Flynn, T. Izubuchi, A. Jüttner, T. Kawanai, C. Lehner, E. Lizarazo et al., Form factors for semi-leptonic B decays. PoS LATTICE **2016**, 296 (2016). https://doi.org/10.22323/1.256.0296. arXiv:1612.05112
598. E. Lizarazo, O. Witzel, Non-perturbative determinations of B-meson decay constants and semi-leptonic form factors. PoS ICHEP **2016**, 558 (2016). https://doi.org/10.22323/1.282.0558. arXiv:1612.06113
599. A. Sirlin, Large m_W, m_Z behavior of the $O(\alpha)$ corrections to semileptonic processes mediated by W. Nucl. Phys. B **196**, 83 (1982). https://doi.org/10.1016/0550-3213(82)90303-0
600. M.E. Luke, Effects of subleading operators in the heavy quark effective theory. Phys. Lett. B **252**, 447 (1990). https://doi.org/10.1016/0370-2693(90)90568-Q
601. [FNAL/MILC 04A] M. Okamoto et al., Semileptonic $D \to \pi/K$ and $B \to \pi/D$ decays in 2+1 flavor lattice QCD. Nucl. Phys. Proc. Suppl. **140**, 461 (2005). https://doi.org/10.1016/j.nuclphysbps.2004.11.151. arXiv:hep-lat/0409116
602. [FNAL/MILC 13B] S.-W. Qiu , C. DeTar, A.X. El-Khadra, A.S. Kronfeld, J. Laiho et al., Semileptonic decays $B \to D^{(*)} l \nu$ at nonzero recoil. PoS LATTICE **2013**, 385 (2014). arXiv:1312.0155
603. M. Atoui, V. Morenas, D. Becirevic, F. Sanfilippo, $b_s \to d_s \ell \nu_\ell$ near zero recoil in and beyond the standard model. Eur. Phys. J. C **74**, 2861 (2014). https://doi.org/10.1140/epjc/s10052-014-2861-z. arXiv:1310.5238
604. [FNAL/MILC 08] C. Bernard et al., The $\bar{B} \to D^* \ell \bar{\nu}$ form factor at zero recoil from three-flavor lattice QCD: a model independent determination of $|V_{cb}|$. Phys. Rev. D **79**, 014506 (2009). https://doi.org/10.1103/PhysRevD.79.014506. arXiv:0808.2519
605. [FNAL/MILC 14] J.A. Bailey et al., Update of $|V_{cb}|$ from the $\bar{B} \to D^* \ell \bar{\nu}$ form factor at zero recoil with three-flavor lattice QCD. Phys. Rev. D **89**, 114504 (2014). https://doi.org/10.1103/PhysRevD.89.114504. arXiv:1403.0635
606. [FNAL/MILC 15C] J.A. Bailey et al., $B \to D \ell \nu$ form factors at nonzero recoil and $|V_{cb}|$ from 2+1-flavor lattice QCD. Phys. Rev. D **92**, 034506 (2015). https://doi.org/10.1103/PhysRevD.92.034506. arXiv:1503.07237
607. [HPQCD 15] H. Na, C.M. Bouchard, G.P. Lepage, C. Monahan, J. Shigemitsu, $B \to D \ell \nu$ form factors at nonzero recoil and extraction of $|V_{cb}|$. Phys. Rev. D **92**, 054510 (2015). https://doi.org/10.1103/PhysRevD.92.054510. arXiv:1505.03925
608. C.J. Monahan, H. Na, C.M. Bouchard, G.P. Lepage, J. Shigemitsu, $B_{(s)} \to D_{(s)}$ semileptonic decays with NRQCD-HISQ valence quarks. PoS LATTICE **2016**, 298 (2016). arXiv:1611.09667
609. [HPQCD 17] C.J. Monahan, H. Na, C.M. Bouchard, G.P. Lepage, J. Shigemitsu, $B_s \to D_s \ell \nu$ form factors and the fragmentation fraction ratio f_s/f_d. Phys. Rev. D **95**, 114506 (2017). https://doi.org/10.1103/PhysRevD.95.114506. arXiv:1703.09728
610. J. Harrison, C. Davies, M. Wingate, $|V_{cb}|$ from the $\bar{B}^0 \to D^{*+} \ell^- \bar{\nu}$ zero-recoil form factor using $2+1+1$ flavour HISQ and NRQCD. PoS LATTICE **2016**, 287 (2017). https://doi.org/10.22323/1.256.0287. arXiv:1612.06716
611. [HPQCD 17B] J. Harrison, C. Davies, M. Wingate, Lattice QCD calculation of the $B_{(s)} \to D^*_{(s)} \ell \nu$ form factors at zero recoil and implications for $|V_{cb}|$. Phys. Rev. D **97**, 054502 (2018). https://doi.org/10.1103/PhysRevD.97.054502. arXiv:1711.11013
612. [HPQCD 19B] E. McLean, C.T.H. Davies, A.T. Lytle, J. Koponen, Lattice QCD form factor for $B_s \to D_s^* l \nu$ at zero recoil with non-perturbative current renormalisation. Phys. Rev. D **99**, 114512 (2019). https://doi.org/10.1103/PhysRevD.99.114512. arXiv:1904.02046
613. [HPQCD 19] E. McLean, C.T.H. Davies, J. Koponen, A.T. Lytle, $B_s \to D_s \ell \nu$ Form Factors for the full q^2 range from Lattice QCD with non-perturbatively normalized currents. Phys. Rev. D **101**, 074513 (2020). https://doi.org/10.1103/PhysRevD.101.074513. arXiv:1906.00701
614. LHCb collaboration, Measurement of $|V_{cb}|$ with $B_s^0 \to D_s^{(*)-} \mu^+ \nu_\mu$ decays. Phys. Rev. D **101**, 072004 (2020). https://doi.org/10.1103/PhysRevD.101.072004. arXiv:2001.03225
615. LHCb collaboration, Precise measurement of the f_s/f_d ratio of fragmentation fractions and of B_s^0 decay branching fractions. Phys. Rev. D **104**, 032005 (2021). https://doi.org/10.1103/PhysRevD.104.032005. arXiv:2103.06810

616. A. Vaquero, C. DeTar, A.X. El-Khadra, A.S. Kronfeld, J. Laiho, R.S. Van de Water, $B \to D^* \ell \nu$ at non-zero recoil, in 17th Conference on Flavor Physics and CP Violation, 6 (2019). arXiv:1906.01019
617. [JLQCD 19A] T. Kaneko, Y. Aoki, G. Bailas, B. Colquhoun, H. Fukaya, S. Hashimoto et al., $B \to D^{(*)} \ell \nu$ form factors from lattice QCD with relativistic heavy quarks. PoS LATTICE **2019**, 139 (2019). https://doi.org/10.22323/1.363.013. arXiv:1912.11770
618. [ETM 10B] B. Blossier et al., Average up/down, strange and charm quark masses with $N_f = 2$ twisted mass lattice QCD. Phys. Rev. D **82**, 114513 (2010). https://doi.org/10.1103/PhysRevD.82.114513. arXiv:1010.3659
619. [HFLAV 16] Y. Amhis et al., Averages of b-hadron, c-hadron, and τ-lepton properties as of summer 2016. Eur. Phys. J. C **77**, 895 (2017). https://doi.org/10.1140/epjc/s10052-017-5058-4. arXiv:1612.07233
620. D. Bigi, P. Gambino, Revisiting $B \to D \ell \nu$. Phys. Rev. D **94**, 094008 (2016). https://doi.org/10.1103/PhysRevD.94.094008. arXiv:1606.08030
621. BaBar collaboration, Determination of the form-factors for the decay $B^0 \to D^{*-} \ell^+ \nu_l$ and of the CKM matrix element $|V_{cb}|$. Phys. Rev. D **77**, 032002 (2008). https://doi.org/10.1103/PhysRevD.77.032002. arXiv:0705.4008
622. Belle collaboration, Measurement of the decay $B \to D \ell \nu_\ell$ in fully reconstructed events and determination of the Cabibbo–Kobayashi–Maskawa matrix element $|V_{cb}|$. Phys. Rev. D **93**, 032006 (2016). https://doi.org/10.1103/PhysRevD.93.032006. arXiv:1510.03657
623. A. Vaquero, Colloquium given in the MIT Virtual Lattice Field Theory Colloquium Series. http://ctp.lns.mit.edu/latticecolloq/
624. R. Fleischer, N. Serra, N. Tuning, A new strategy for B_s branching ratio measurements and the search for new physics in $B_s^0 \to \mu^+ \mu^-$. Phys. Rev. D **82**, 034038 (2010). https://doi.org/10.1103/PhysRevD.82.034038. arXiv:1004.3982
625. LHCb collaboration, Determination of f_s/f_d for 7 TeV pp collisions and a measurement of the branching fraction of the decay $B_d \to D^- K^+$. Phys. Rev. Lett. **107**, 211801 (2011). https://doi.org/10.1103/PhysRevLett.107.211801. arXiv:1106.4435
626. [FNAL/MILC 12C] J.A. Bailey et al., $B_s \to D_s/B \to D$ semileptonic form-factor ratios and their application to BR($B_s^0 \to \mu^+ \mu^-$). Phys. Rev. D **85**, 114502 (2012). https://doi.org/10.1103/PhysRevD.85.114502. https://doi.org/10.1103/PhysRevD.86.039904. arXiv:1202.6346
627. L. Randall, M.B. Wise, Chiral perturbation theory for $B \to D^*$ and $B \to D$ semileptonic transition matrix elements at zero recoil. Phys. Lett. B **303**, 135 (1993). https://doi.org/10.1016/0370-2693(93)90057-O. arXiv:hep-ph/9212315
628. M.J. Savage, Heavy meson observables at one loop in partially quenched chiral perturbation theory. Phys. Rev. D **65**, 034014 (2002). https://doi.org/10.1103/PhysRevD.65.034014. arXiv:hep-ph/0109190
629. S. Hashimoto, A.S. Kronfeld, P.B. Mackenzie, S.M. Ryan, J.N. Simone, Lattice calculation of the zero recoil form-factor of $\bar{B} \to D^* \ell \bar{\nu}$: toward a model independent determination of $|V_{cb}|$. Phys. Rev. D **66**, 014503 (2002). https://doi.org/10.1103/PhysRevD.66.014503. arXiv:hep-ph/0110253
630. [FNAL/MILC 21] A. Bazavov et al., Semileptonic form factors for $B \to D^* \ell \nu$ at nonzero recoil from 2 + 1-flavor lattice QCD. arXiv:2105.14019
631. [HPQCD 21B] J. Harrison, C.T.H. Davies, $B_s \to D_s^*$ form factors for the full q^2 range from Lattice QCD. arXiv:2105.11433
632. [HPQCD 20B] J. Harrison, C.T.H. Davies, A. Lytle, $B_c \to J/\psi$ form factors for the full q^2 range from lattice QCD. Phys. Rev. D **102**, 094518 (2020). https://doi.org/10.1103/PhysRevD.102.094518. arXiv:2007.06957
633. A. Lytle, B. Colquhoun, C. Davies, J. Koponen, C. McNeile, Semileptonic B_c decays from full lattice QCD. PoS BEAUTY **2016**, 069 (2016). https://doi.org/10.22323/1.273.0069. arXiv:1605.05645
634. [HPQCD 16] B. Colquhoun, C. Davies, J. Koponen, A. Lytle, C. McNeile, B_c decays from highly improved staggered quarks and NRQCD. PoS LATTICE **2016**, 281 (2016). https://doi.org/10.22323/1.256.0281. arXiv:1611.01987
635. LHCb RICH Group collaboration, Performance of the LHCb RICH detector at the LHC. Eur. Phys. J. C **73**, 2431 (2013). https://doi.org/10.1140/epjc/s10052-013-2431-9. arXiv:1211.6759
636. LHCb collaboration, Determination of the quark coupling strength $|V_{ub}|$ using baryonic decays. Nat. Phys. **11**, 743 (2015). https://doi.org/10.1038/nphys3415. arXiv:1504.01568
637. A. Datta, S. Kamali, S. Meinel, A. Rashed, Phenomenology of $\Lambda_b \to \Lambda_c \tau \overline{\nu}_\tau$ using lattice QCD calculations. JHEP **08**, 131 (2017). https://doi.org/10.1007/JHEP08(2017)131. arXiv:1702.02243
638. S. Meinel, G. Rendon, $\Lambda_b \to \Lambda_c^*(2595, 2625) \ell^- \bar{\nu}$ form factors from lattice QCD. Phys. Rev. D **103**, 094516 (2021). https://doi.org/10.1103/PhysRevD.103.094516. arXiv:2103.08775
639. T.D. Cohen, H. Lamm, R.F. Lebed, Precision model-independent bounds from global analysis of $b \to c \ell \nu$ form factors. Phys. Rev. D **100**, 094503 (2019). https://doi.org/10.1103/PhysRevD.100.094503. arXiv:1909.10691
640. T. Blake, M. Kreps, Angular distribution of polarised Λ_b baryons decaying to $\Lambda \ell^+ \ell^-$. JHEP **11**, 138 (2017). https://doi.org/10.1007/JHEP11(2017)138. arXiv:1710.00746
641. LHCb collaboration, Angular moments of the decay $\Lambda_b^0 \to \Lambda \mu^+ \mu^-$ at low hadronic recoil. JHEP **09**, 146 (2018). https://doi.org/10.1007/JHEP09(2018)146. arXiv:1808.00264
642. W. Detmold, C.J.D. Lin, S. Meinel, M. Wingate, $\Lambda_b \to \Lambda \ell^+ \ell^-$ form factors and differential branching fraction from lattice QCD. Phys. Rev. D **87**, 074502 (2013). https://doi.org/10.1103/PhysRevD.87.074502. arXiv:1212.4827
643. W. Detmold, S. Meinel, $\Lambda_b \to \Lambda \ell^+ \ell^-$ form factors, differential branching fraction, and angular observables from lattice QCD with relativistic b quarks. Phys. Rev. D **93**, 074501 (2016). https://doi.org/10.1103/PhysRevD.93.074501. arXiv:1602.01399
644. T. Blake, S. Meinel, D. van Dyk, Bayesian analysis of $b \to s \mu^+ \mu^-$ Wilson coefficients using the full angular distribution of $\Lambda_b \to \Lambda(\to p \pi^-) \mu^+ \mu^-$ decays. Phys. Rev. D **101**, 035023 (2020). https://doi.org/10.1103/PhysRevD.101.035023. arXiv:1912.05811
645. LHCb collaboration, Differential branching fraction and angular analysis of $\Lambda_b^0 \to \Lambda \mu^+ \mu^-$ decays. JHEP **06**, 115 (2015). https://doi.org/10.1007/JHEP06(2015)115. arXiv:1503.07138] [Erratum: JHEP 09, 145 (2018)]
646. M. Algueró, B. Capdevila, A. Crivellin, S. Descotes-Genon, P. Masjuan, J. Matias et al., Emerging patterns of new physics with and without lepton flavour universal contributions. Eur. Phys. J. C **79**, 714 (2019). https://doi.org/10.1140/epjc/s10052-019-7216-3. arXiv:1903.09578] [Addendum: Eur. Phys. J. C 80, 511 (2020)]
647. W. Altmannshofer, P. Stangl, New physics in rare B decays after Moriond 2021. Eur. Phys. J. C **81**, 952 (2021). https://doi.org/10.1140/epjc/s10052-021-09725-1. arXiv:2103.13370
648. S. Meinel, G. Rendon, $\Lambda_b \to \Lambda^*(1520) \ell^+ \ell^-$ form factors from lattice QCD. Phys. Rev. D **103**, 074505 (2021). https://doi.org/10.1103/PhysRevD.103.074505. arXiv:2009.09313

649. W. Detmold, C.J.D. Lin, S. Meinel, M. Wingate, $\Lambda_b \to p l^- \bar{\nu}_\ell$ form factors from lattice QCD with static b quarks. Phys. Rev. D **88**, 014512 (2013). https://doi.org/10.1103/PhysRevD.88.014512. arXiv:1306.0446
650. Belle collaboration, Measurement of $B^- \to \tau^- \bar{\nu}_\tau$ with a hadronic tagging method using the full data sample of Belle. Phys. Rev. Lett. **110**, 131801 (2013). https://doi.org/10.1103/PhysRevLett.110.131801. arXiv:1208.4678
651. Babar collaboration, A search for $B^+ \to \ell^+ \nu_\ell$ recoiling against $B^- \to D^0 \ell^- \bar{\nu} X$. Phys. Rev. D **81**, 051101 (2010). https://doi.org/10.1103/PhysRevD.81.051101. arXiv:0912.2453
652. Babar collaboration, Study of $B \to \pi \ell \nu$ and $B \to \rho \ell \nu$ Decays and Determination of $|V_{ub}|$. Phys. Rev. D **83**, 032007 (2011). https://doi.org/10.1103/PhysRevD.83.032007. arXiv:1005.3288] **(47 pages, 26 postscript figures, accepted)**
653. Babar collaboration, Branching fraction and form-factor shape measurements of exclusive charmless semileptonic B decays, and determination of $|V_{ub}|$. Phys. Rev. D **86**, 092004 (2012). https://doi.org/10.1103/PhysRevD.86.092004. arXiv:1208.1253
654. Belle collaboration, Measurement of the decay $B^0 \to \pi^- \ell^+ \nu$ and determination of $|V_{ub}|$. Phys. Rev. D **83**, 071101 (2011). https://doi.org/10.1103/PhysRevD.83.071101. arXiv:1012.0090
655. Belle collaboration, Study of exclusive $B \to X_u \ell \nu$ decays and extraction of $\|V_{ub}\|$ using full reconstruction tagging at the Belle experiment. Phys. Rev. D **88**, 032005 (2013). https://doi.org/10.1103/PhysRevD.88.032005. arXiv:1306.2781
656. P. Gambino, P. Giordano, G. Ossola, N. Uraltsev, Inclusive semileptonic B decays and the determination of $|V_{ub}|$. JHEP **0710**, 058 (2007). https://doi.org/10.1088/1126-6708/2007/10/058. arXiv:0707.2493
657. P. Urquijo, Physics prospects at the Belle II experiment. Nucl. Part. Phys. Proc. **263–264**, 15 (2015). https://doi.org/10.1016/j.nuclphysbps.2015.04.004l
658. E. Kou et al., The Belle II Physics Book. PTEP **2019**, 123C01 (2019). https://doi.org/10.1093/ptep/ptz106. arXiv:1808.10567 [Erratum: PTEP 2020, 029201 (2020)]
659. I. Caprini, L. Lellouch, M. Neubert, Dispersive bounds on the shape of $\bar{B} \to D^{(*)}$ lepton anti-neutrino form-factors. Nucl. Phys. B **530**, 153 (1998). https://doi.org/10.1016/S0550-3213(98)00350-2. arXiv:hep-ph/9712417
660. Belle collaboration, Measurement of the CKM matrix element $|V_{cb}|$ from $B^0 \to D^{*-} \ell^+ \nu_\ell$ at Belle. Phys. Rev. D **100**, 052007 (2019). https://doi.org/10.1103/PhysRevD.100.052007. arXiv:1809.03290 [Erratum: Phys. Rev. D 103, 079901 (2021)]
661. D. Bigi, P. Gambino, S. Schacht, A fresh look at the determination of $|V_{cb}|$ from $B \to D^* \ell \nu$. Phys. Lett. B **769**, 441 (2017). https://doi.org/10.1016/j.physletb.2017.04.022. arXiv:1703.06124
662. F.U. Bernlochner, Z. Ligeti, M. Papucci, D.J. Robinson, Tensions and correlations in $|V_{cb}|$ determinations. Phys. Rev. D **96**, 091503 (2017). https://doi.org/10.1103/PhysRevD.96.091503. arXiv:1708.07134
663. B. Grinstein, A. Kobach, Model-independent extraction of $|V_{cb}|$ from $\bar{B} \to D^* \ell \overline{\nu}$. Phys. Lett. B **771**, 359 (2017). https://doi.org/10.1016/j.physletb.2017.05.078. arXiv:1703.08170
664. C.G. Boyd, B. Grinstein, R.F. Lebed, Precision corrections to dispersive bounds on form-factors. Phys. Rev. D **56**, 6895 (1997). https://doi.org/10.1103/PhysRevD.56.6895. arXiv:hep-ph/9705252
665. P. Gambino, M. Jung, S. Schacht, The V_{cb} puzzle: an update. Phys. Lett. B **795**, 386 (2019). https://doi.org/10.1016/j.physletb.2019.06.039. arXiv:1905.08209
666. Belle collaboration, Measurement of the decay $B \to D \ell \nu_\ell$ in fully reconstructed events and determination of the Cabibbo–Kobayashi–Maskawa matrix element $|V_{cb}|$. Phys. Rev. D **93**, 032006 (2016). https://doi.org/10.1103/PhysRevD.93.032006. arXiv:1510.03657
667. BaBar collaboration, Measurement of $|V(cb)|$ and the form-factor slope in $\overline{B} \to D \ell^- \overline{\nu}_\ell$ decays in events tagged by a fully reconstructed B meson. Phys. Rev. Lett. **104**, 011802 (2010). https://doi.org/10.1103/PhysRevLett.104.011802. arXiv:0904.4063
668. P. Gambino, K.J. Healey, S. Turczyk, Taming the higher power corrections in semileptonic B decays. Phys. Lett. B **763**, 60 (2016). https://doi.org/10.1016/j.physletb.2016.10.023. arXiv:1606.06174
669. LHCb collaboration, First observation of the decay $B_s^0 \to K^- \mu^+ \nu_\mu$ and measurement of $|V_{ub}|/|V_{cb}|$. Phys. Rev. Lett. **126**, 081804 (2021). https://doi.org/10.1103/PhysRevLett.126.081804. arXiv:2012.05143
670. Belle collaboration, Measurements of partial branching fractions of inclusive $B \to X_u \ell \nu_\ell$ decays with hadronic tagging. Phys. Rev. D **104**, 012008 (2021). https://doi.org/10.1103/PhysRevD.104.012008. arXiv:2102.00020
671. S. Dittmaier et al., Handbook of LHC Higgs cross sections: 2. Differential distributions. arXiv:1201.3084
672. LHC Higgs Cross Section Working Group collaboration, Handbook of LHC Higgs cross sections: 3. Higgs properties. arXiv:1307.1347
673. LBNE collaboration, Scientific opportunities with the long-baseline neutrino experiment. arXiv:1307.7335
674. S. Dawson, A. Gritsan, H. Logan, J. Qian, C. Tully et al., Higgs Working Group Report of the Snowmass 2013 Community Planning Study. arXiv:1310.8361
675. A. Accardi et al., A critical appraisal and evaluation of modern PDFs. Eur. Phys. J. C **76**, 471 (2016). https://doi.org/10.1140/epjc/s10052-016-4285-4. arXiv:1603.08906
676. G.P. Lepage, P.B. Mackenzie, M.E. Peskin, Expected precision of Higgs boson partial widths within the Standard Model. arXiv:1404.0319
677. D. Buttazzo, G. Degrassi, P.P. Giardino, G.F. Giudice, F. Sala, A. Salvio et al., Investigating the near-criticality of the Higgs boson. JHEP **12**, 089 (2013). https://doi.org/10.1007/JHEP12(2013)089. arXiv:1307.3536
678. J.R. Espinosa, Vacuum stability and the Higgs boson. PoS LATTICE **2013**, 010 (2014). arXiv:1311.1970
679. G.P. Salam, The strong coupling: a theoretical perspective, in From My Vast Repertoire ...: Guido Altarelli's Legacy, A. Levy, S. Forte, G. Ridolfi, editors. pp. 101–121 (2019). https://doi.org/10.1142/9789813238053_0007DOI. arXiv:1712.05165
680. M. Czakon, The four-loop QCD beta-function and anomalous dimensions. Nucl. Phys. B **710**, 485 (2005). https://doi.org/10.1016/j.nuclphysb.2005.01.012. arXiv:hep-ph/0411261
681. T. Luthe, A. Maier, P. Marquard, Y. Schröder, Towards the five-loop beta function for a general gauge group. JHEP **07**, 127 (2016). https://doi.org/10.1007/JHEP07(2016)127. arXiv:1606.08662
682. F. Herzog, B. Ruijl, T. Ueda, J.A.M. Vermaseren, A. Vogt, The five-loop beta function of Yang–Mills theory with fermions. JHEP **02**, 090 (2017). https://doi.org/10.1007/JHEP02(2017)090. arXiv:1701.01404
683. P.A. Baikov, K.G. Chetyrkin, J.H. Kuhn, Five-loop running of the QCD coupling constant. Phys. Rev. Lett. **118**, 082002 (2017). https://doi.org/10.1103/PhysRevLett.118.082002. arXiv:1606.08659

684. W. Bernreuther, W. Wetzel, Decoupling of heavy quarks in the minimal subtraction scheme. Nucl. Phys. B **197**, 228 (1982). https://doi.org/10.1016/0550-3213(82)90288-7
685. K. Chetyrkin, J.H. Kuhn, C. Sturm, QCD decoupling at four loops. Nucl. Phys. B **744**, 121 (2006). https://doi.org/10.1016/j.nuclphysb.2006.03.020. arXiv:hep-ph/0512060
686. Y. Schröder, M. Steinhauser, Four-loop decoupling relations for the strong coupling. JHEP **01**, 051 (2006). https://doi.org/10.1088/1126-6708/2006/01/051. arXiv:hep-ph/0512058
687. B.A. Kniehl, A.V. Kotikov, A.I. Onishchenko, O.L. Veretin, Strong-coupling constant with flavor thresholds at five loops in the anti-MS scheme. Phys. Rev. Lett. **97**, 042001 (2006). https://doi.org/10.1103/PhysRevLett.97.042001. arXiv:hep-ph/0607202
688. A.G. Grozin, M. Hoeschele, J. Hoff, M. Steinhauser, Simultaneous decoupling of bottom and charm quarks. JHEP **09**, 066 (2011). https://doi.org/10.1007/JHEP09(2011)066. arXiv:1107.5970
689. K.G. Chetyrkin, J.H. Kuhn, M. Steinhauser, RunDec: a Mathematica package for running and decoupling of the strong coupling and quark masses. Comput. Phys. Commun. **133**, 43 (2000). https://doi.org/10.1016/S0010-4655(00)00155-7. arXiv:hep-ph/0004189
690. F. Herren, M. Steinhauser, Version 3 of RunDec and CRunDec. Comput. Phys. Commun. **224**, 333 (2018). https://doi.org/10.1016/j.cpc.2017.11.014. arXiv:1703.03751
691. L. Del Debbio, A. Ramos, Lattice determinations of the strong coupling. Phys. Rep. **920**, 1 (2021). https://doi.org/10.1016/j.physrep.2021.03.005. arXiv:2101.04762
692. [ALPHA 19A] M. Dalla Brida, R. Höllwieser, F. Knechtli, T. Korzec, A. Ramos, R. Sommer, Non-perturbative renormalization by decoupling. Phys. Lett. B **807**, 135571 (2020). https://doi.org/10.1016/j.physletb.2020.135571. arXiv:1912.06001
693. M. Dalla Brida, A. Ramos, The gradient flow coupling at high-energy and the scale of SU(3) Yang–Mills theory. Eur. Phys. J. C **79**, 720 (2019). https://doi.org/10.1140/epjc/s10052-019-7228-z. arXiv:1905.05147
694. A. Nada, A. Ramos, An analysis of systematic effects in finite size scaling studies using the gradient flow. Eur. Phys. J. C **81**, 1 (2021). https://doi.org/10.1140/epjc/s10052-020-08759-1. arXiv:2007.12862
695. N. Husung, A. Nada, R. Sommer, Yang Mills short distance potential and perturbation theory. PoS LATTICE **2019**, 263 (2020). https://doi.org/10.22323/1.363.0263
696. P. Petreczky, J.H. Weber, Strong coupling constant from moments of quarkonium correlators revisited. Eur. Phys. J. C **82**, 64 (2022). https://doi.org/10.1140/epjc/s10052-022-09998-0. arXiv:2012.06193
697. D. Boito, V. Mateu, Precise α_s determination from charmonium sum rules. Phys. Lett. B **806**, 135482 (2020). https://doi.org/10.1016/j.physletb.2020.135482. arXiv:1912.06237
698. D. Boito, V. Mateu, Precise determination of α_s from relativistic quarkonium sum rules. JHEP **03**, 094 (2020). https://doi.org/10.1007/JHEP03(2020)094. arXiv:2001.11041
699. S. Zafeiropoulos, P. Boucaud, F. De Soto, J. Rodríguez-Quintero, J. Segovia, Strong running coupling from the gauge sector of domain wall lattice QCD with physical quark masses. Phys. Rev. Lett. **122**, 162002 (2019). https://doi.org/10.1103/PhysRevLett.122.162002. arXiv:1902.08148
700. R. Sommer, A new way to set the energy scale in lattice gauge theories and its applications to the static force and α_s in SU(2) Yang–Mills theory. Nucl. Phys. B **411**, 839 (1994). https://doi.org/10.1016/0550-3213(94)90473-1. arXiv:hep-lat/9310022
701. C.W. Bernard et al., The static quark potential in three flavor QCD. Phys. Rev. D **62**, 034503 (2000). https://doi.org/10.1103/PhysRevD.62.034503. arXiv:hep-lat/0002028
702. G. Martinelli, C.T. Sachrajda, On the difficulty of computing higher twist corrections. Nucl. Phys. B **478**, 660 (1996). https://doi.org/10.1016/0550-3213(96)00415-4. arXiv:hep-ph/9605336
703. A.H. Hoang, C. Regner, On the difference between FOPT and CIPT for hadronic tau decays, vol. 230 (2021). https://doi.org/10.1140/epjs/s11734-021-00257-z. arXiv:2105.11222
704. S. Bethke, A.H. Hoang, S. Kluth, J. Schieck, I.W. Stewart et al., Workshop on precision measurements of α_s. arXiv:1110.0016
705. D. Boito, M. Golterman, K. Maltman, J. Osborne, S. Peris, Strong coupling from the revised ALEPH data for hadronic τ decays. Phys. Rev. D **91**, 034003 (2015). https://doi.org/10.1103/PhysRevD.91.034003. arXiv:1410.3528
706. D. Boito, M. Golterman, K. Maltman, S. Peris, Strong coupling from hadronic τ decays: a critical appraisal. Phys. Rev. D **95**, 034024 (2017). https://doi.org/10.1103/PhysRevD.95.034024. arXiv:1611.03457
707. [ALPHA 12] P. Fritzsch, F. Knechtli, B. Leder, M. Marinkovic, S. Schaefer et al., The strange quark mass and the Λ parameter of two flavor QCD. Nucl. Phys. B **865**, 397 (2012). https://doi.org/10.1016/j.nuclphysb.2012.07.026. arXiv:1205.5380
708. [HotQCD 11] A. Bazavov, T. Bhattacharya, M. Cheng, C. DeTar, H. Ding et al., The chiral and deconfinement aspects of the QCD transition. Phys. Rev. D **85**, 054503 (2012). https://doi.org/10.1103/PhysRevD.85.054503. arXiv:1111.1710
709. S. Necco, R. Sommer, The $N_f = 0$ heavy quark potential from short to intermediate distances. Nucl. Phys. B **622**, 328 (2002). https://doi.org/10.1016/S0550-3213(01)00582-X. arXiv:hep-lat/0108008
710. M. Lüscher, P. Weisz, Quark confinement and the bosonic string. JHEP **0207**, 049 (2002). https://doi.org/10.1088/1126-6708/2002/07/049. arXiv:hep-lat/0207003
711. S. Sint, A. Ramos, On O(a^2) effects in gradient flow observables. PoS LATTICE **2014**, 329 (2015). arXiv:1411.6706
712. Z. Fodor, K. Holland, J. Kuti, S. Mondal, D. Nogradi et al., The lattice gradient flow at tree-level and its improvement. JHEP **1409**, 018 (2014). https://doi.org/10.1007/JHEP09(2014)018. arXiv:1406.0827
713. [QCDSF/UKQCD 15B] V.G. Bornyakov et al., Wilson flow and scale setting from lattice QCD. arXiv:1508.05916
714. R. Sommer, Scale setting in lattice QCD. PoS LATTICE **2013**, 015 (2014). https://doi.org/10.22323/1.187.0015. arXiv:1401.3270
715. [ALPHA 16] M. Dalla Brida, P. Fritzsch, T. Korzec, A. Ramos, S. Sint, R. Sommer, Determination of the QCD Λ-parameter and the accuracy of perturbation theory at high energies. Phys. Rev. Lett. **117**, 182001 (2016). https://doi.org/10.1103/PhysRevLett.117.182001. arXiv:1604.06193
716. [ALPHA 18] M. Dalla Brida, P. Fritzsch, T. Korzec, A. Ramos, S. Sint, R. Sommer, A non-perturbative exploration of the high energy regime in $N_f = 3$ QCD. Eur. Phys. J. C **78**, 372 (2018). https://doi.org/10.1140/epjc/s10052-018-5838-5. arXiv:1803.10230
717. M. Lüscher, P. Weisz, U. Wolff, A numerical method to compute the running coupling in asymptotically free theories. Nucl. Phys. B **359**, 221 (1991). https://doi.org/10.1016/0550-3213(91)90298-C

718. S. Sint, On the Schrödinger functional in QCD. Nucl. Phys. B **421**, 135 (1994). https://doi.org/10.1016/0550-3213(94)90228-3. arXiv:hep-lat/9312079
719. A. Coste, A. Gonzalez-Arroyo, J. Jurkiewicz, C. Korthals Altes, Zero momentum contribution to Wilson loops in periodic boxes. Nucl. Phys. B **262**, 67 (1985). https://doi.org/10.1016/0550-3213(85)90064-1
720. M. Lüscher, R. Sommer, P. Weisz, U. Wolff, A precise determination of the running coupling in the $SU(3)$ Yang–Mills theory. Nucl. Phys. B **413**, 481 (1994). https://doi.org/10.1016/0550-3213(94)90629-7. arXiv:hep-lat/9309005
721. S. Sint, R. Sommer, The running coupling from the QCD Schrödinger functional: a one loop analysis. Nucl. Phys. B **465**, 71 (1996). https://doi.org/10.1016/0550-3213(96)00020-X. arXiv:hep-lat/9508012
722. [ALPHA 99] A. Bode, P. Weisz, U. Wolff, Two loop computation of the Schrödinger functional in lattice QCD. Nucl. Phys. B **576**, 517 (2000). https://doi.org/10.1016/S0550-3213(00)00187-5. https://doi.org/10.1016/S0550-3213(00)00187-5. arXiv:hep-lat/9911018
723. [CP-PACS 04] S. Takeda, S. Aoki, M. Fukugita, K.-I. Ishikawa, N. Ishizuka et al., A scaling study of the step scaling function in $SU(3)$ gauge theory with improved gauge actions. Phys. Rev. D **70**, 074510 (2004). https://doi.org/10.1103/PhysRevD.70.074510. arXiv:hep-lat/0408010
724. M. Lüscher, A semiclassical formula for the topological susceptibility in a finite space-time volume. Nucl. Phys. B **205**, 483 (1982). https://doi.org/10.1016/0550-3213(82)90371-6
725. P. Fritzsch, A. Ramos, F. Stollenwerk, Critical slowing down and the gradient flow coupling in the Schrödinger functional. PoS Lattice **2013**, 461 (2014). arXiv:1311.7304
726. M. Dalla Brida, P. Fritzsch, T. Korzec, A. Ramos, S. Sint, R. Sommer, Slow running of the gradient flow coupling from 200 MeV to 4 GeV in $N_{\rm f} = 3$ QCD. Phys. Rev. D **95**, 014507 (2017). https://doi.org/10.1103/PhysRevD.95.014507. arXiv:1607.06423
727. M. Lüscher, Step scaling and the Yang–Mills gradient flow. JHEP **06**, 105 (2014). https://doi.org/10.1007/JHEP06(2014)105. arXiv:1404.5930
728. R. Narayanan, H. Neuberger, Infinite N phase transitions in continuum Wilson loop operators. JHEP **03**, 064 (2006). https://doi.org/10.1088/1126-6708/2006/03/064. arXiv:hep-th/0601210
729. Z. Fodor, K. Holland, J. Kuti, D. Nogradi, C.H. Wong, The Yang–Mills gradient flow in finite volume. JHEP **1211**, 007 (2012). https://doi.org/10.1007/JHEP11(2012)007. arXiv:1208.1051
730. P. Fritzsch, A. Ramos, The gradient flow coupling in the Schrödinger functional. JHEP **1310**, 008 (2013). https://doi.org/10.1007/JHEP10(2013)008. arXiv:1301.4388
731. A. Ramos, The gradient flow running coupling with twisted boundary conditions. JHEP **11**, 101 (2014). https://doi.org/10.1007/JHEP11(2014)101. arXiv:1409.1445
732. K.-I. Ishikawa, I. Kanamori, Y. Murakami, A. Nakamura, M. Okawa, R. Ueno, Non-perturbative determination of the Λ-parameter in the pure SU(3) gauge theory from the twisted gradient flow coupling. JHEP **12**, 067 (2017). https://doi.org/10.1007/JHEP12(2017)067. arXiv:1702.06289
733. M. Dalla Brida, M. Lüscher, SMD-based numerical stochastic perturbation theory. Eur. Phys. J. C **77**, 308 (2017). https://doi.org/10.1140/epjc/s10052-017-4839-0. arXiv:1703.04396
734. E.I. Bribian, M. Garcia Perez, The twisted gradient flow coupling at one loop. JHEP **03**, 200 (2019). https://doi.org/10.1007/JHEP03(2019)200. arXiv:1903.08029
735. [ALPHA 10A] F. Tekin, R. Sommer and U. Wolff, The running coupling of QCD with four flavors. Nucl. Phys. B **840**, 114 (2010). https://doi.org/10.1016/j.nuclphysb.2010.07.002. arXiv:1006.0672
736. P. Perez-Rubio, S. Sint, Non-perturbative running of the coupling from four flavour lattice QCD with staggered quarks. PoS LAT **2010**, 236 (2010). arXiv:1011.6580
737. [ALPHA 04] M. Della Morte et al., Computation of the strong coupling in QCD with two dynamical flavours. Nucl. Phys. B **713**, 378 (2005). https://doi.org/10.1016/j.nuclphysb.2005.02.013. arXiv:hep-lat/0411025
738. [ALPHA 01A] A. Bode et al., First results on the running coupling in QCD with two massless flavors. Phys. Lett. B **515**, 49 (2001). https://doi.org/10.1016/S0370-2693(01)00857-7. arXiv:hep-lat/0105003
739. [ALPHA 98] S. Capitani, M. Lüscher, R. Sommer, H. Wittig, Nonperturbative quark mass renormalization in quenched lattice QCD. Nucl. Phys. B **544**, 669 (1999). https://doi.org/10.1016/S0550-3213(98)00857-8. arXiv:hep-lat/9810063
740. J. Bulava, S. Schaefer, Improvement of $N_f = 3$ lattice QCD with Wilson fermions and tree-level improved gauge action. Nucl. Phys. B **874**, 188 (2013). https://doi.org/10.1016/j.nuclphysb.2013.05.019. arXiv:1304.7093
741. M. Lüscher, P. Weisz, On-shell improved lattice gauge theories. Commun. Math. Phys. **97**, 59 (1985). https://doi.org/10.1007/BF01206178
742. [JLQCD/CP-PACS 04] N. Yamada et al., Non-perturbative O(a)-improvement of Wilson quark action in three-flavor QCD with plaquette gauge action. Phys. Rev. D **71**, 054505 (2005). https://doi.org/10.1103/PhysRevD.71.054505. arXiv:hep-lat/0406028
743. A. Gonzalez-Arroyo, M. Okawa, The string tension from smeared Wilson loops at large N. Phys. Lett. B **718**, 1524 (2013). https://doi.org/10.1016/j.physletb.2012.12.027. arXiv:1206.0049
744. M. Dalla Brida, Past, present, and future of precision determinations of the QCD parameters from lattice QCD. Eur. Phys. J. A **57**, 66 (2021). https://doi.org/10.1140/epja/s10050-021-00381-3. arXiv:2012.01232
745. ALPHA collaboration, Results for α_s from the decoupling strategy, in 38th International Symposium on Lattice Field Theory, 12 (2021). arXiv:2112.09623
746. M. Gerlach, F. Herren, M. Steinhauser, Wilson coefficients for Higgs boson production and decoupling relations to $\mathcal{O}\left(\alpha_s^4\right)$. JHEP **11**, 141 (2018). https://doi.org/10.1007/JHEP11(2018)141. arXiv:1809.06787
747. C. Michael, The running coupling from lattice gauge theory. Phys. Lett. B **283**, 103 (1992). https://doi.org/10.1016/0370-2693(92)91435-C. arXiv:hep-lat/9205010
748. [UKQCD 92] S.P. Booth et al., The running coupling from SU(3) lattice gauge theory. Phys. Lett. B **294**, 385 (1992). https://doi.org/10.1016/0370-2693(92)91538-K. arXiv:hep-lat/9209008
749. W. Fischler, Quark–antiquark potential in QCD. Nucl. Phys. B **129**, 157 (1977). https://doi.org/10.1016/0550-3213(77)90026-8
750. A. Billoire, How heavy must be quarks in order to build coulombic $q\bar{q}$ bound states. Phys. Lett. B **92**, 343 (1980). https://doi.org/10.1016/0370-2693(80)90279-8
751. M. Peter, The static potential in QCD: a full two loop calculation. Nucl. Phys. B **501**, 471 (1997). https://doi.org/10.1016/S0550-3213(97)00373-8. arXiv:hep-ph/9702245

752. Y. Schröder, The static potential in QCD to two loops. Phys. Lett. B **447**, 321 (1999). https://doi.org/10.1016/S0370-2693(99)00010-6. arXiv:hep-ph/9812205
753. N. Brambilla, A. Pineda, J. Soto, A. Vairo, The infrared behavior of the static potential in perturbative QCD. Phys. Rev. D **60**, 091502 (1999). https://doi.org/10.1103/PhysRevD.60.091502. arXiv:hep-ph/9903355
754. A.V. Smirnov, V.A. Smirnov, M. Steinhauser, Three-loop static potential. Phys. Rev. Lett. **104**, 112002 (2010). https://doi.org/10.1103/PhysRevLett.104.112002. arXiv:0911.4742
755. C. Anzai, Y. Kiyo, Y. Sumino, Static QCD potential at three-loop order. Phys. Rev. Lett **104**, 112003 (2010). https://doi.org/10.1103/PhysRevLett.104.112003. arXiv:0911.4335
756. N. Brambilla, A. Vairo, X. Garcia i Tormo, J. Soto, The QCD static energy at NNNLL. Phys. Rev. D **80**, 034016 (2009). https://doi.org/10.1103/PhysRevD.80.034016. arXiv:0906.1390
757. S. Necco, R. Sommer, Testing perturbation theory on the $N_f = 0$ static quark potential. Phys. Lett. B **523**, 135 (2001). https://doi.org/10.1016/S0370-2693(01)01298-9. arXiv:hep-ph/0109093
758. H. Takaura, T. Kaneko, Y. Kiyo, Y. Sumino, Determination of α_s from static QCD potential with renormalon subtraction. Phys. Lett. B **789**, 598 (2019). https://doi.org/10.1016/j.physletb.2018.12.060. arXiv:1808.01632
759. H. Takaura, T. Kaneko, Y. Kiyo, Y. Sumino, Determination of α_s from static QCD potential: OPE with renormalon subtraction and Lattice QCD. JHEP **04**, 155 (2019). https://doi.org/10.1007/JHEP04(2019)155. arXiv:1808.01643
760. A. Bazavov, N. Brambilla, X. Garcia i Tormo, P. Petreczky, J. Soto, A. Vairo, Determination of α_s from the QCD static energy: an update. Phys. Rev. D **90**, 074038 (2014). https://doi.org/10.1103/PhysRevD.90.074038. arXiv:1407.8437
761. A. Bazavov, N. Brambilla, X. Garcia i Tormo, P. Petreczky, J. Soto, et al., Determination of α_s from the QCD static energy. Phys. Rev. D **86**, 114031 (2012). https://doi.org/10.1103/PhysRevD.86.114031. arXiv:1205.6155
762. F. Karbstein, M. Wagner, M. Weber, Determination of $\Lambda_{\overline{\rm MS}}^{(n_f=2)}$ and analytic parameterization of the static quark-antiquark potentialDetermination of $\Lambda_{\overline{\rm MS}}^{(n_f=2)}$ and analytic parametrization of the static quark-antiquark potential. Phys. Rev. D **98**, 114506 (2018). https://doi.org/10.1103/PhysRevD.98.114506. arXiv:1804.10909
763. F. Karbstein, A. Peters, M. Wagner, $\Lambda_{\overline{\rm MS}}^{(n_f=2)}$ from a momentum space analysis of the quark-antiquark static potential. JHEP **1409**, 114 (2014). https://doi.org/10.1007/JHEP09(2014)114. arXiv:1407.7503
764. [ETM 11C] K. Jansen, F. Karbstein, A. Nagy, M. Wagner, $\Lambda_{\overline{\rm MS}}$ from the static potential for QCD with $N_f = 2$ dynamical quark flavors. JHEP **1201**, 025 (2012). https://doi.org/10.1007/JHEP01(2012)025. arXiv:1110.6859
765. N. Husung, M. Koren, P. Krah, R. Sommer, SU(3) Yang Mills theory at small distances and fine lattices. EPJ Web Conf. **175**, 14024 (2018). https://doi.org/10.1051/epjconf/201817514024. arXiv:1711.01860
766. N. Brambilla, X. Garcia i Tormo, J. Soto, A. Vairo, Precision determination of $r_0\,\Lambda_{\overline{MS}}$ from the QCD static energy. Phys. Rev. Lett. **105**, 212001 (2010). https://doi.org/10.1103/PhysRevLett.105.212001. arXiv:1006.2066
767. G.S. Bali, K. Schilling, Running coupling and the Λ-parameter from $SU(3)$ lattice simulations. Phys. Rev. D **47**, 661 (1993). https://doi.org/10.1103/PhysRevD.47.661. arXiv:hep-lat/9208028
768. N. Husung, P. Marquard, R. Sommer, Asymptotic behavior of cutoff effects in Yang–Mills theory and in Wilson's lattice QCD. Eur. Phys. J. C **80**, 200 (2020). https://doi.org/10.1140/epjc/s10052-020-7685-4. arXiv:1912.08498
769. A. Bazavov, P. Petreczky, J. Weber, Equation of state in 2+1 flavor QCD at high temperatures. Phys. Rev. D **97**, 014510 (2018). https://doi.org/10.1103/PhysRevD.97.014510. arXiv:1710.05024
770. J.H. Weber, A. Bazavov, P. Petreczky, Equation of state in (2+1) flavor QCD at high temperatures. PoS Confinement **2018**, 166 (2019). https://doi.org/10.22323/1.336.0166. arXiv:1811.12902
771. M. Berwein, N. Brambilla, P. Petreczky, A. Vairo, Polyakov loop correlator in perturbation theory. Phys. Rev. D **96**, 014025 (2017). https://doi.org/10.1103/PhysRevD.96.014025. arXiv:1704.07266 [Addendum: Phys. Rev. D 101, 099903 (2020)]
772. K.G. Chetyrkin, A.L. Kataev, F.V. Tkachov, Higher order corrections to sigma-t (e+ e− → hadrons) in quantum chromodynamics. Phys. Lett. B **85**, 277 (1979). https://doi.org/10.1016/0370-2693(79)90596-3
773. L.R. Surguladze, M.A. Samuel, Total hadronic cross-section in e+ e− annihilation at the four loop level of perturbative QCD. Phys. Rev. Lett. **66**, 560 (1991). https://doi.org/10.1103/PhysRevLett.66.560 [Erratum: Phys. Rev. Lett. 66, 2416 (1991)]
774. S.G. Gorishnii, A.L. Kataev, S.A. Larin, The O(α_s^3) corrections to tot($e^+e^- \to$ hadrons) and $\Gamma(\tau^- \to \nu_\tau +$ hadrons) in QCD. Phys. Lett. B **259**, 144 (1991). https://doi.org/10.1016/0370-2693(91)90149-K
775. P.A. Baikov, K.G. Chetyrkin, J.H. Kuhn, Order α_s^4 QCD corrections to Z and tau decays. Phys. Rev. Lett. **101**, 012002 (2008). https://doi.org/10.1103/PhysRevLett.101.012002. arXiv:0801.1821
776. I. Balitsky, M. Beneke, V.M. Braun, Instanton contributions to the τ decay widths. Phys. Lett. B **318**, 371 (1993). https://doi.org/10.1016/0370-2693(93)90142-5. arXiv:hep-ph/9309217
777. K. Chetyrkin, A. Maier, Massless correlators of vector, scalar and tensor currents in position space at orders α_s^3 and α_s^4: explicit analytical results. Nucl. Phys. B **844**, 266 (2011). https://doi.org/10.1016/j.nuclphysb.2010.11.007. arXiv:1010.1145
778. [JLQCD/TWQCD 08C] E. Shintani et al., Lattice study of the vacuum polarization function and determination of the strong coupling constant. Phys. Rev. D **79**, 074510 (2009). https://doi.org/10.1103/PhysRevD.79.074510. arXiv:0807.0556
779. [JLQCD 10] E. Shintani, S. Aoki, H. Fukaya, S. Hashimoto, T. Kaneko et al., Strong coupling constant from vacuum polarization functions in three-flavor lattice QCD with dynamical overlap fermions. Phys. Rev. D **82**, 074505 (2010). https://doi.org/10.1103/PhysRevD.82.074505. arXiv:1002.0371
780. R.J. Hudspith, R. Lewis, K. Maltman, E. Shintani, α_s from the lattice hadronic vacuum polarisation. arXiv:1804.10286
781. R.J. Hudspith, R. Lewis, K. Maltman, E. Shintani, Determining the QCD coupling from lattice vacuum polarization, in Proceedings, 33rd International Symposium on Lattice Field Theory (Lattice 2015), vol. LATTICE2015, p. 268 (2016). arXiv:1510.04890
782. R. Hudspith, R. Lewis, K. Maltman, E. Shintani, α_s from the hadronic vacuum polarisation. EPJ. Web Conf. **175**, 10006 (2018). https://doi.org/10.1051/epjconf/201817510006

783. [HPQCD 05A] Q. Mason et al., Accurate determinations of α_s from realistic lattice QCD. Phys. Rev. Lett. **95**, 052002 (2005). https://doi.org/10.1103/PhysRevLett.95.052002. arXiv:hep-lat/0503005
784. [HPQCD 08A] C.T.H. Davies et al., Update: accurate determinations of α_s from realistic lattice QCD. Phys. Rev. D **78**, 114507 (2008). arXiv:0807.1687
785. G.P. Lepage, P.B. Mackenzie, On the viability of lattice perturbation theory. Phys. Rev. D **48**, 2250 (1993). https://doi.org/10.1103/PhysRevD.48.2250. arXiv:hep-lat/9209022
786. K. Hornbostel, G. Lepage, C. Morningstar, Scale setting for α_s beyond leading order. Phys. Rev. D **67**, 034023 (2003). https://doi.org/10.1103/PhysRevD.67.034023. arXiv:hep-ph/0208224
787. [QCDSF/UKQCD 05] M. Göckeler, R. Horsley, A. Irving, D. Pleiter, P. Rakow, G. Schierholz et al., A determination of the Lambda parameter from full lattice QCD. Phys. Rev. D **73**, 014513 (2006). https://doi.org/10.1103/PhysRevD.73.014513. arXiv:hep-ph/0502212
788. [SESAM 99] A. Spitz et al., α_s from upsilon spectroscopy with dynamical Wilson fermions. Phys. Rev. D **60**, 074502 (1999). https://doi.org/10.1103/PhysRevD.60.074502. arXiv:hep-lat/9906009
789. M. Wingate, T.A. DeGrand, S. Collins, U.M. Heller, From spectroscopy to the strong coupling constant with heavy Wilson quarks. Phys. Rev. D **52**, 307 (1995). https://doi.org/10.1103/PhysRevD.52.307. arXiv:hep-lat/9501034
790. C.T.H. Davies, K. Hornbostel, G. Lepage, A. Lidsey, J. Shigemitsu et al., A precise determination of α_s from lattice QCD. Phys. Lett. B **345**, 42 (1995). https://doi.org/10.1016/0370-2693(94)01598-7. arXiv:hep-ph/9408328
791. S. Aoki, M. Fukugita, S. Hashimoto, N. Ishizuka, H. Mino et al., Manifestation of sea quark effects in the strong coupling constant in lattice QCD. Phys. Rev. Lett. **74**, 22 (1995). https://doi.org/10.1103/PhysRevLett.74.22. arXiv:hep-lat/9407015
792. M. Kitazawa, T. Iritani, M. Asakawa, T. Hatsuda, H. Suzuki, Equation of state for SU(3) gauge theory via the energy–momentum tensor under gradient flow. Phys. Rev. D **94**, 114512 (2016). https://doi.org/10.1103/PhysRevD.94.114512. arXiv:1610.07810
793. [FlowQCD 15] M. Asakawa, T. Iritani, M. Kitazawa, H. Suzuki, Determination of reference scales for Wilson gauge action from Yang–Mills gradient flow. arXiv:1503.06516
794. A.X. El-Khadra, G. Hockney, A.S. Kronfeld, P.B. Mackenzie, A determination of the strong coupling constant from the charmonium spectrum. Phys. Rev. Lett **69**, 729 (1992). https://doi.org/10.1103/PhysRevLett.69.729
795. [QCDSF/UKQCD 04A] M. Göckeler, R. Horsley, A. Irving, D. Pleiter, P. Rakow, G. Schierholz et al., Determination of Λ in quenched and full QCD: an update. Nucl. Phys. Proc. Suppl.**140**, 228 (2005). https://doi.org/10.1016/j.nuclphysbps.2004.11.295. arXiv:hep-lat/0409166
796. S. Booth, M. Göckeler, R. Horsley, A. Irving, B. Joo, S. Pickles et al., The strong coupling constant from lattice QCD with $N_f = 2$ dynamical quarks. Nucl. Phys. Proc. Suppl. **106**, 308 (2002). https://doi.org/10.1016/S0920-5632(01)01697-8. arXiv:hep-lat/0111006
797. [QCDSF/UKQCD 01] S. Booth, M. Göckeler, R. Horsley, A. Irving, B. Joo, S. Pickles et al., Determination of $\Lambda_{\overline{\rm MS}}$ from quenched and $N_f = 2$ dynamical QCD. Phys. Lett. B **519**, 229 (2001). https://doi.org/10.1016/S0370-2693(01)01103-0. arXiv:hep-lat/0103023
798. [HPQCD 03A] C.T.H. Davies et al., High-precision lattice QCD confronts experiment. Phys. Rev. Lett. **92**, 022001 (2004). https://doi.org/10.1103/PhysRevLett.92.022001. arXiv:hep-lat/0304004
799. Q.J. Mason, High-precision lattice QCD: perturbations in a non-perturbative world, Ph.D. thesis, Cornell U., LNS (2004)
800. K. Maltman, Two recent high-precision determinations of alpha(s). AIP. Conf. Proc. **1261**, 159 (2010). https://doi.org/10.1063/1.3479337
801. A. Bochkarev, P. de Forcrand, Determination of the renormalized heavy quark mass in lattice QCD. Nucl. Phys. B **477**, 489 (1996). https://doi.org/10.1016/0550-3213(96)00396-3. arXiv:hep-lat/9505025
802. B. Dehnadi, A.H. Hoang, V. Mateu, Bottom and charm mass determinations with a convergence test. JHEP **08**, 155 (2015). https://doi.org/10.1007/JHEP08(2015)155. arXiv:1504.07638
803. K. Chetyrkin, J.H. Kuhn, C. Sturm, Four-loop moments of the heavy quark vacuum polarization function in perturbative QCD. Eur. Phys. J. C **48**, 107 (2006). https://doi.org/10.1140/epjc/s2006-02610-y. arXiv:hep-ph/0604234
804. R. Boughezal, M. Czakon, T. Schutzmeier, Charm and bottom quark masses from perturbative QCD. Phys. Rev. D **74**, 074006 (2006). https://doi.org/10.1103/PhysRevD.74.074006. arXiv:hep-ph/0605023
805. A. Maier, P. Maierhofer, P. Marqaurd, The second physical moment of the heavy quark vector correlator at $O(\alpha_s^3)$. Phys. Lett. B **669**, 88 (2008). https://doi.org/10.1016/j.physletb.2008.09.041. arXiv:0806.3405
806. A. Maier, P. Maierhofer, P. Marquard, A. Smirnov, Low energy moments of heavy quark current correlators at four loops. Nucl. Phys. B **824**, 1 (2010). https://doi.org/10.1016/j.nuclphysb.2009.08.011. arXiv:0907.2117
807. Y. Kiyo, A. Maier, P. Maierhofer, P. Marquard, Reconstruction of heavy quark current correlators at $O(\alpha_s^3)$. Nucl. Phys. B **823**, 269 (2009). https://doi.org/10.1016/j.nuclphysb.2009.08.010. arXiv:0907.2120
808. J.H. Kühn, M. Steinhauser, C. Sturm, Heavy quark masses from sum rules in four-loop approximation. Nucl. Phys. B **778**, 192 (2007). https://doi.org/10.1016/j.nuclphysb.2007.04.036. arXiv:hep-ph/0702103
809. K. Chetyrkin, J. Kuhn, A. Maier, P. Maierhofer, P. Marquard et al., Charm and bottom quark masses: an update. Phys. Rev. D **80**, 074010 (2009). https://doi.org/10.1103/PhysRevD.80.074010. arXiv:0907.2110
810. A. Cucchieri, Gribov copies in the minimal Landau gauge: the influence on gluon and ghost propagators. Nucl. Phys. B **508**, 353 (1997). https://doi.org/10.1016/S0550-3213(97)00629-9. arXiv:hep-lat/9705005
811. L. Giusti, M. Paciello, C. Parrinello, S. Petrarca, B. Taglienti, Problems on lattice gauge fixing. Int. J. Mod. Phys. A **16**, 3487 (2001). https://doi.org/10.1142/S0217751X01004281. arXiv:hep-lat/0104012
812. A. Maas, J.M. Pawlowski, D. Spielmann, A. Sternbeck, L. von Smekal, Strong-coupling study of the Gribov ambiguity in lattice Landau gauge. Eur. Phys. J. C **68**, 183 (2010). https://doi.org/10.1140/epjc/s10052-010-1306-6. arXiv:0912.4203
813. B. Alles, D. Henty, H. Panagopoulos, C. Parrinello, C. Pittori et al., α_s from the nonperturbatively renormalised lattice three gluon vertex. Nucl. Phys. B **502**, 325 (1997). https://doi.org/10.1016/S0550-3213(97)00483-5. arXiv:hep-lat/9605033
814. P. Boucaud, J. Leroy, H. Moutarde, J. Micheli, O. Pene et al., Preliminary calculation of α_s from Green functions with dynamical quarks. JHEP **0201**, 046 (2002). arXiv:hep-ph/0107278
815. P. Boucaud, J. Leroy, A. Le Yaouanc, A. Lokhov, J. Micheli et al., Asymptotic behavior of the ghost propagator in SU(3) lattice gauge theory. Phys. Rev. D **72**, 114503 (2005). https://doi.org/10.1103/PhysRevD.72.114503. arXiv:hep-lat/0506031
816. P. Boucaud, J. Leroy, A. Le Yaouanc, A. Lokhov, J. Micheli et al., Non-perturbative power corrections to ghost and gluon propagators. JHEP **0601**, 037 (2006). https://doi.org/10.1088/1126-6708/2006/01/037. arXiv:hep-lat/0507005

817. A. Sternbeck, K. Maltman, L. von Smekal, A. Williams, E. Ilgenfritz et al., Running α_s from Landau-gauge gluon and ghost correlations. PoS LAT **2007**, 256 (2007). arXiv:0710.2965
818. Ph. Boucaud, F. De Soto, J. Leroy, A. Le Yaouanc, J. Micheli et al., Ghost-gluon running coupling, power corrections and the determination of $\Lambda_{\overline{\rm MS}}$. Phys. Rev. D **79**, 014508 (2009). https://doi.org/10.1103/PhysRevD.79.014508. arXiv:0811.2059
819. [ETM 13D] B. Blossier et al., High statistics determination of the strong coupling constant in Taylor scheme and its OPE Wilson coefficient from lattice QCD with a dynamical charm. Phys. Rev. D **89**, 014507 (2014). https://doi.org/10.1103/PhysRevD.89.014507. arXiv:1310.3763
820. [ETM 12C] B. Blossier, P. Boucaud, M. Brinet, F. De Soto, X. Du et al., The strong running coupling at τ and Z_0 mass scales from lattice QCD. Phys. Rev. Lett. **108**, 262002 (2012). https://doi.org/10.1103/PhysRevLett.108.262002. arXiv:1201.5770
821. [ETM 11D] B. Blossier, P. Boucaud, M. Brinet, F. De Soto, X. Du et al., Ghost-gluon coupling, power corrections and $\Lambda_{\overline{\rm MS}}$ from lattice QCD with a dynamical charm. Phys. Rev. D **85**, 034503 (2012). https://doi.org/10.1103/PhysRevD.85.034503. arXiv:1110.5829
822. A. Sternbeck, K. Maltman, M. Müller-Preussker, L. von Smekal, Determination of $\Lambda_{\overline{\rm MS}}$ from the gluon and ghost propagators in Landau gauge. PoS LAT **2012**, 243 (2012). arXiv:1212.2039
823. A. Sternbeck, E.-M. Ilgenfritz, K. Maltman, M. Müller-Preussker, L. von Smekal et al., QCD Lambda parameter from Landau-gauge gluon and ghost correlations. PoS LAT **2009**, 210 (2009). arXiv:1003.1585
824. [ETM 10F] B. Blossier et al., Ghost-gluon coupling, power corrections and $\Lambda_{\overline{\rm MS}}$ from twisted-mass lattice QCD at $N_f = 2$. Phys. Rev. D **82**, 034510 (2010). https://doi.org/10.1103/PhysRevD.82.034510. arXiv:1005.5290
825. E.-M. Ilgenfritz, C. Menz, M. Müller-Preussker, A. Schiller, A. Sternbeck, $SU(3)$ Landau gauge gluon and ghost propagators using the logarithmic lattice gluon field definition. Phys. Rev. D **83**, 054506 (2011). https://doi.org/10.1103/PhysRevD.83.054506. arXiv:1010.5120
826. F. De Soto, J. Rodriguez-Quintero, Notes on the determination of the Landau gauge OPE for the asymmetric three gluon vertex. Phys. Rev. D **64**, 114003 (2001). https://doi.org/10.1103/PhysRevD.64.114003. arXiv:hep-ph/0105063
827. P. Boucaud, A. Le Yaouanc, J. Leroy, J. Micheli, O. Pene et al., Testing Landau gauge OPE on the lattice with a $\langle A^2 \rangle$ condensate. Phys. Rev. D **63**, 114003 (2001). https://doi.org/10.1103/PhysRevD.63.114003. arXiv:hep-ph/0101302
828. P. Boucaud, A. Le Yaouanc, J. Leroy, J. Micheli, O. Pene et al., Consistent OPE description of gluon two point and three point Green function? Phys. Lett. B **493**, 315 (2000). https://doi.org/10.1016/S0370-2693(00)01149-7. arXiv:hep-ph/0008043
829. P. Boucaud, G. Burgio, F. Di Renzo, J. Leroy, J. Micheli et al., Lattice calculation of $1/p^2$ corrections to α_s and of $\Lambda_{\rm QCD}$ in the MOM scheme. JHEP **0004**, 006 (2000). arXiv:hep-ph/0003020
830. D. Bećirević, P. Boucaud, J. Leroy, J. Micheli, O. Pene et al., Asymptotic scaling of the gluon propagator on the lattice. Phys. Rev. D **61**, 114508 (2000). https://doi.org/10.1103/PhysRevD.61.114508. arXiv:hep-ph/9910204
831. D. Bećirević, P. Boucaud, J. Leroy, J. Micheli, O. Pene et al., Asymptotic behavior of the gluon propagator from lattice QCD. Phys. Rev. D **60**, 094509 (1999). https://doi.org/10.1103/PhysRevD.60.094509. arXiv:hep-ph/9903364
832. P. Boucaud, J. Leroy, J. Micheli, O. Pene, C. Roiesnel, Three loop beta function and nonperturbative α_s in asymmetric momentum scheme. JHEP **9812**, 004 (1998). https://doi.org/10.1088/1126-6708/1998/12/004. arXiv:hep-ph/9810437
833. P. Boucaud, J. Leroy, J. Micheli, O. Pene, C. Roiesnel, Lattice calculation of α_s in momentum scheme. JHEP **9810**, 017 (1998). arXiv:hep-ph/9810322
834. P. Boucaud, F. De Soto, K. Raya, J. Rodríguez-Quintero, S. Zafeiropoulos, Discretization effects on renormalized gauge-field Green's functions, scale setting, and the gluon mass. Phys. Rev. D **98**, 114515 (2018). https://doi.org/10.1103/PhysRevD.98.114515. arXiv:1809.05776
835. K.G. Chetyrkin, J.H. Kuhn, Quartic mass corrections to R(had). Nucl. Phys. B **432**, 337 (1994). https://doi.org/10.1016/0550-3213(94)90605-X. arXiv:hep-ph/9406299
836. J.-L. Kneur, A. Neveu, Chiral condensate from renormalization group optimized perturbation. Phys. Rev. D **92**, 074027 (2015). https://doi.org/10.1103/PhysRevD.92.074027. arXiv:1506.07506
837. K. Nakayama, H. Fukaya, S. Hashimoto, Lattice computation of the Dirac eigenvalue density in the perturbative regime of QCD. Phys. Rev. D **98**, 014501 (2018). https://doi.org/10.1103/PhysRevD.98.014501. arXiv:1804.06695
838. Particle Data Group collaboration, Review of Particle Physics. Phys. Rev. D **86**, 010001 (2012) and 2013 partial update for the 2014 edition. https://doi.org/10.1103/PhysRevD.86.010001
839. S. Syritsyn, Review of hadron structure calculations on a lattice. PoS LATTICE **2013**, 009 (2014). https://doi.org/10.22323/1.187.0009. arXiv:1403.4686
840. S. Capitani, M. Della Morte, D. Djukanovic, G. von Hippel, J. Hua, B. Jäger et al., Nucleon electromagnetic form factors in two-flavor QCD. Phys. Rev. D **92**, 054511 (2015). https://doi.org/10.1103/PhysRevD.92.054511. arXiv:1504.04628
841. R.S. Sufian, Y.-B. Yang, A. Alexandru, T. Draper, J. Liang, K.-F. Liu, Strange quark magnetic moment of the nucleon at the physical point. Phys. Rev. Lett. **118**, 042001 (2017). https://doi.org/10.1103/PhysRevLett.118.042001. arXiv:1606.07075
842. R. Gupta, Y.-C. Jang, H.-W. Lin, B. Yoon, T. Bhattacharya, Axial vector form factors of the nucleon from lattice QCD. Phys. Rev. D **96**, 114503 (2017). https://doi.org/10.1103/PhysRevD.96.114503. arXiv:1705.06834
843. J. Green, N. Hasan, S. Meinel, M. Engelhardt, S. Krieg, J. Laeuchli et al., Up, down, and strange nucleon axial form factors from lattice QCD. Phys. Rev. D **95**, 114502 (2017). https://doi.org/10.1103/PhysRevD.95.114502. arXiv:1703.06703
844. [CSSM/QCDSF/UKQCD 17] A.J. Chambers et al., Electromagnetic form factors at large momenta from lattice QCD. Phys. Rev. D **96**, 114509 (2017). https://doi.org/10.1103/PhysRevD.96.114509. arXiv:1702.01513
845. C. Alexandrou, M. Constantinou, K. Hadjiyiannakou, K. Jansen, C. Kallidonis, G. Koutsou et al., Nucleon electromagnetic form factors using lattice simulations at the physical point. Phys. Rev. D **96**, 034503 (2017). https://doi.org/10.1103/PhysRevD.96.034503. arXiv:1706.00469
846. C. Alexandrou, M. Constantinou, K. Hadjiyiannakou, K. Jansen, C. Kallidonis, G. Koutsou et al., Strange nucleon electromagnetic form factors from lattice QCD. Phys. Rev. D **97**, 094504 (2018). https://doi.org/10.1103/PhysRevD.97.094504. arXiv:1801.09581
847. [PACS 18] K.-I. Ishikawa, Y. Kuramashi, S. Sasaki, N. Tsukamoto, A. Ukawa, T. Yamazaki, Nucleon form factors on a large volume lattice near the physical point in 2+1 flavor QCD. Phys. Rev. D **98**, 074510 (2018). https://doi.org/10.1103/PhysRevD.98.074510. arXiv:1807.03974
848. C. Alexandrou, S. Bacchio, M. Constantinou, J. Finkenrath, K. Hadjiyiannakou, K. Jansen et al., Proton and neutron electromagnetic form factors from lattice QCD. Phys. Rev. D **100**, 014509 (2019). https://doi.org/10.1103/PhysRevD.100.014509. arXiv:1812.10311

849. [PACS 18A] E. Shintani, K.-I. Ishikawa, Y. Kuramashi, S. Sasaki and T. Yamazaki, Nucleon form factors and root-mean-square radii on a $(10.8\ \text{fm})^4$ lattice at the physical point. Phys. Rev. D **99**, 014510 (2019). https://doi.org/10.1103/PhysRevD.99.014510. arXiv:1811.07292] [Erratum: Phys. Rev. D 102, 019902 (2020)]
850. [RQCD 19] G.S. Bali, L. Barca, S. Collins, M. Gruber, M. Löffler, A. Schäfer et al., Nucleon axial structure from lattice QCD. JHEP **05**, 126 (2020). https://doi.org/10.1007/JHEP05(2020)126. arXiv:1911.13150
851. [LHPC 19] N. Hasan, J. Green, S. Meinel, M. Engelhardt, S. Krieg, J. Negele et al., Nucleon axial, scalar, and tensor charges using lattice QCD at the physical pion mass. Phys. Rev. D **99**, 114505 (2019). https://doi.org/10.1103/PhysRevD.99.114505. arXiv:1903.06487
852. C. Alexandrou et al., Nucleon axial and pseudoscalar form factors from lattice QCD at the physical point. Phys. Rev. D **103**, 034509 (2021). https://doi.org/10.1103/PhysRevD.103.034509. arXiv:2011.13342
853. D. Djukanovic, T. Harris, G. von Hippel, P.M. Junnarkar, H.B. Meyer, D. Mohler et al., Isovector electromagnetic form factors of the nucleon from lattice QCD and the proton radius puzzle. Phys. Rev. D **103**, 094522 (2021). https://doi.org/10.1103/PhysRevD.103.094522. arXiv:2102.07460
854. H.-W. Lin et al., Parton distributions and lattice QCD calculations: a community white paper. Prog. Part. Nucl. Phys. **100**, 107 (2018). https://doi.org/10.1016/j.ppnp.2018.01.007. arXiv:1711.07916
855. M. Constantinou, The x-dependence of hadronic parton distributions: a review on the progress of lattice QCD. Eur. Phys. J. A **57**, 77 (2021). https://doi.org/10.1140/epja/s10050-021-00353-7. arXiv:2010.02445
856. M. Constantinou et al., Parton distributions and lattice QCD calculations: toward 3D structure. Prog. Part. Nucl. Phys. **121**, 103908 (2021). https://doi.org/10.1016/j.ppnp.2021.103908. arXiv:2006.08636
857. K. Cichy, M. Constantinou, A guide to light-cone PDFs from Lattice QCD: an overview of approaches, techniques and results. Adv. High Energy Phys. **2019**, 3036904 (2019). https://doi.org/10.1155/2019/3036904. arXiv:1811.07248
858. C. Monahan, Recent developments in x-dependent structure calculations. PoS LATTICE **2018**, 018 (2018). https://doi.org/10.22323/1.334.0018. arXiv:1811.00678
859. M.J. Savage, Nuclear physics from lattice QCD. Prog. Part. Nucl. Phys. **67**, 140 (2012). https://doi.org/10.1016/j.ppnp.2011.12.008. arXiv:1110.5943
860. [NPLQCD 17] E. Chang, Z. Davoudi, W. Detmold, A.S. Gambhir, K. Orginos, M.J. Savage et al., Scalar, axial, and tensor interactions of light nuclei from lattice QCD. Phys. Rev. Lett. **120**, 152002 (2018). https://doi.org/10.1103/PhysRevLett.120.152002. arXiv:1712.03221
861. J. Carlson, S. Gandolfi, F. Pederiva, S.C. Pieper, R. Schiavilla, K.E. Schmidt et al., Quantum Monte Carlo methods for nuclear physics. Rev. Mod. Phys. **87**, 1067 (2015). https://doi.org/10.1103/RevModPhys.87.1067. arXiv:1412.3081
862. M.L. Wagman, F. Winter, E. Chang, Z. Davoudi, W. Detmold, K. Orginos et al., Baryon-baryon interactions and spin-flavor symmetry from lattice quantum chromodynamics. Phys. Rev. D **96**, 114510 (2017). https://doi.org/10.1103/PhysRevD.96.114510. arXiv:1706.06550
863. T. Iritani, Two-baryon systems from HAL QCD method and the mirage in the temporal correlation of the direct method. EPJ Web Conf. **175**, 05008 (2018). https://doi.org/10.1051/epjconf/201817505008. arXiv:1710.06147
864. Y.-C. Jang, R. Gupta, B. Yoon, T. Bhattacharya, Axial vector form factors from lattice QCD that satisfy the PCAC relation. Phys. Rev. Lett. **124**, 072002 (2020). https://doi.org/10.1103/PhysRevLett.124.072002. arXiv:1905.06470
865. H.W. Hamber, E. Marinari, G. Parisi, C. Rebbi, Considerations on numerical analysis of QCD. Nucl. Phys. B **225**, 475 (1983). https://doi.org/10.1016/0550-3213(83)90528-X
866. G.P. Lepage, The analysis of algorithms for lattice field theory, in Boulder ASI 1989:97-120, pp. 97–120 (1989). http://alice.cern.ch/format/showfull?sysnb=0117836
867. [QCDSF 06] A.A. Khan, M. Göckeler, P. Hägler, T. Hemmert, R. Horsley et al., Axial coupling constant of the nucleon for two flavours of dynamical quarks in finite and infinite volume. Phys. Rev. D **74**, 094508 (2006). https://doi.org/10.1103/PhysRevD.74.094508. arXiv:hep-lat/0603028
868. [Mainz 12] S. Capitani, M. Della Morte, G. von Hippel, B. Jager, A. Jüttner et al., The nucleon axial charge from lattice QCD with controlled errors. Phys. Rev. D **86**, 074502 (2012). https://doi.org/10.1103/PhysRevD.86.074502. arXiv:1205.0180
869. [RQCD 14] G.S. Bali, S. Collins, B. Glässle, M. Göckeler, J. Najjar, R.H. Rödl et al., Nucleon isovector couplings from $N_f = 2$ lattice QCD. Phys. Rev. D **91**, 054501 (2015). https://doi.org/10.1103/PhysRevD.91.054501. arXiv:1412.7336
870. [RQCD 16] G.S. Bali, S. Collins, D. Richtmann, A. Schäfer, W. Söldner, A. Sternbeck, Direct determinations of the nucleon and pion σ terms at nearly physical quark masses. Phys. Rev. D **93**, 094504 (2016). https://doi.org/10.1103/PhysRevD.93.094504. arXiv:1603.00827
871. [Mainz 17] S. Capitani, M. Della Morte, D. Djukanovic, G.M. von Hippel, J. Hua, B. Jäger et al., Iso-vector axial form factors of the nucleon in two-flavor lattice QCD. Int. J. Mod. Phys. A **34**, 1950009 (2019). https://doi.org/10.1142/S0217751X1950009X. arXiv:1705.06186
872. [PACS-CS 09] K.-I. Ishikawa et al., SU(2) and SU(3) chiral perturbation theory analyses on baryon masses in 2+1 flavor lattice QCD. Phys. Rev. D **80**, 054502 (2009). https://doi.org/10.1103/PhysRevD.80.054502. arXiv:0905.0962
873. [ETM 15D] A. Abdel-Rehim et al., Nucleon and pion structure with lattice QCD simulations at physical value of the pion mass. Phys. Rev. D **92**, 114513 (2015). https://doi.org/10.1103/PhysRevD.92.114513. https://doi.org/10.1103/PhysRevD.93.039904. arXiv:1507.04936] [Erratum: Phys. Rev. D 93(3), 039904 (2016)]
874. [ETM 16A] A. Abdel-Rehim, C. Alexandrou, M. Constantinou, K. Hadjiyiannakou, K. Jansen, C. Kallidonis et al., Direct evaluation of the quark content of nucleons from lattice QCD at the physical point. Phys. Rev. Lett. **116**, 252001 (2016). https://doi.org/10.1103/PhysRevLett.116.252001. arXiv:1601.01624
875. [ETM 17B] C. Alexandrou, M. Constantinou, K. Hadjiyiannakou, K. Jansen, C. Kallidonis, G. Koutsou et al., Nucleon axial form factors using $N_f = 2$ twisted mass fermions with a physical value of the pion mass. Phys. Rev. D **96**, 054507 (2017). https://doi.org/10.1103/PhysRevD.96.054507. arXiv:1705.03399
876. [ETM 17C] C. Alexandrou, M. Constantinou, K. Hadjiyiannakou, K. Jansen, C. Kallidonis, G. Koutsou et al., Nucleon spin and momentum decomposition using lattice QCD simulations. Phys. Rev. Lett. **119**, 142002 (2017). https://doi.org/10.1103/PhysRevLett.119.142002. arXiv:1706.02973
877. [ETM 17] C. Alexandrou et al., Nucleon scalar and tensor charges using lattice QCD simulations at the physical value of the pion mass. Phys. Rev. D **95**, 114514 (2017). https://doi.org/10.1103/PhysRevD.96.099906. https://doi.org/10.1103/PhysRevD.95.114514. arXiv:1703.08788] [Erratum: Phys. Rev. D 96(9), 099906 (2017)]

878. [PNDME 13] T. Bhattacharya, S.D. Cohen, R. Gupta, A. Joseph, H.-W. Lin, B. Yoon, Nucleon charges and electromagnetic form factors from 2+1+1-flavor lattice QCD. Phys. Rev. D **89**, 094502 (2014). https://doi.org/10.1103/PhysRevD.89.094502. arXiv:1306.5435
879. [PNDME 15A] T. Bhattacharya, V. Cirigliano, S. Cohen, R. Gupta, A. Joseph, H.-W. Lin et al., Iso-vector and iso-scalar tensor charges of the nucleon from lattice QCD. Phys. Rev. D **92**, 094511 (2015). https://doi.org/10.1103/PhysRevD.92.094511. arXiv:1506.06411
880. [PNDME 15] T. Bhattacharya, V. Cirigliano, R. Gupta, H.-W. Lin, B. Yoon, Neutron electric dipole moment and tensor charges from lattice QCD. Phys. Rev. Lett. **115**, 212002 (2015). https://doi.org/10.1103/PhysRevLett.115.212002. arXiv:1506.04196
881. [PNDME 16] T. Bhattacharya, V. Cirigliano, S. Cohen, R. Gupta, H.-W. Lin, B. Yoon, Axial, scalar and tensor charges of the nucleon from 2+1+1-flavor lattice QCD. Phys. Rev. D **94**, 054508 (2016). https://doi.org/10.1103/PhysRevD.94.054508. arXiv:1606.07049
882. [CalLat 17] E. Berkowitz et al., An accurate calculation of the nucleon axial charge with lattice QCD. arXiv:1704.01114
883. [RBC/UKQCD 08B] T. Yamazaki et al., Nucleon axial charge in 2+1 flavor dynamical lattice QCD with domain wall fermions. Phys. Rev. Lett. **100**, 171602 (2008). https://doi.org/10.1103/PhysRevLett.100.171602. arXiv:0801.4016
884. [RBC/UKQCD 09B] T. Yamazaki, Y. Aoki, T. Blum, H.-W. Lin, S. Ohta, S. Sasaki et al., Nucleon form factors with 2+1 flavor dynamical domain-wall fermions. Phys. Rev. D **79**, 114505 (2009). https://doi.org/10.1103/PhysRevD.79.114505. arXiv:0904.2039
885. [RBC/UKQCD 10D] Y. Aoki, T. Blum, H.-W. Lin, S. Ohta, S. Sasaki, R. Tweedie et al., Nucleon isovector structure functions in (2+1)-flavor QCD with domain wall fermions. Phys. Rev. D **82**, 014501 (2010). https://doi.org/10.1103/PhysRevD.82.014501. arXiv:1003.3387
886. [χQCD 13A] M. Gong et al., Strangeness and charmness content of the nucleon from overlap fermions on 2+1-flavor domain-wall fermion configurations. Phys. Rev. D **88**, 014503 (2013). https://doi.org/10.1103/PhysRevD.88.014503. arXiv:1304.1194
887. [χ QCD 15] M. Gong, Y.-B. Yang, J. Liang, A. Alexandru, T. Draper, K.-F. Liu, Strange and charm quark spins from the anomalous Ward identity. Phys. Rev. D **95**, 114509 (2017). https://doi.org/10.1103/PhysRevD.95.114509. arXiv:1511.03671
888. [JLQCD 08B] H. Ohki, H. Fukaya, S. Hashimoto, T. Kaneko, H. Matsufuru, J. Noaki et al., Nucleon sigma term and strange quark content from lattice QCD with exact chiral symmetry. Phys. Rev. D **78**, 054502 (2008). https://doi.org/10.1103/PhysRevD.78.054502. arXiv:0806.4744
889. [JLQCD 12A] H. Ohki, K. Takeda, S. Aoki, S. Hashimoto, T. Kaneko, H. Matsufuru et al., Nucleon strange quark content from $N_f = 2 + 1$ lattice QCD with exact chiral symmetry. Phys. Rev. D **87**, 034509 (2013). https://doi.org/10.1103/PhysRevD.87.034509. arXiv:1208.4185
890. [JLQCD 18] N. Yamanaka, S. Hashimoto, T. Kaneko, H. Ohki, Nucleon charges with dynamical overlap fermions. Phys. Rev. D **98**, 054516 (2018). https://doi.org/10.1103/PhysRevD.98.054516. arXiv:1805.10507
891. R. Babich, J. Brannick, R.C. Brower, M.A. Clark, T.A. Manteuffel, S.F. McCormick et al., Adaptive multigrid algorithm for the lattice Wilson–Dirac operator. Phys. Rev. Lett. **105**, 201602 (2010). https://doi.org/10.1103/PhysRevLett.105.201602. arXiv:1005.3043
892. M. Lüscher, Deflation acceleration of lattice QCD simulations. JHEP **12**, 011 (2007). https://doi.org/10.1088/1126-6708/2007/12/011. arXiv:0710.5417
893. G.S. Bali, S. Collins, A. Schafer, Effective noise reduction techniques for disconnected loops in Lattice QCD. Comput. Phys. Commun. **181**, 1570 (2010). https://doi.org/10.1016/j.cpc.2010.05.008. arXiv:0910.3970
894. T. Blum, T. Izubuchi, E. Shintani, New class of variance-reduction techniques using lattice symmetries. Phys. Rev. D **88**, 094503 (2013). https://doi.org/10.1103/PhysRevD.88.094503. arXiv:1208.4349
895. A. Stathopoulos, J. Laeuchli, K. Orginos, Hierarchical probing for estimating the trace of the matrix inverse on toroidal lattices. arXiv:1302.4018
896. A.S. Gambhir, A. Stathopoulos, K. Orginos, B. Yoon, R. Gupta, S. Syritsyn, Algorithms for disconnected diagrams in lattice QCD. PoS LATTICE **2016**, 265 (2016). https://doi.org/10.22323/1.256.0265. arXiv:1611.01193
897. [LHPC 10] J.D. Bratt et al., Nucleon structure from mixed action calculations using 2+1 flavors of asqtad sea and domain wall valence fermions. Phys. Rev. D **82**, 094502 (2010). https://doi.org/10.1103/PhysRevD.82.094502. arXiv:1001.3620
898. B. Yoon et al., Controlling excited-state contamination in nucleon matrix elements. Phys. Rev. D **93**, 114506 (2016). https://doi.org/10.1103/PhysRevD.93.114506. arXiv:1602.07737
899. T.A. DeGrand, S. Schaefer, Improving meson two point functions in lattice QCD. Comput. Phys. Commun. **159**, 185 (2004). https://doi.org/10.1016/j.cpc.2004.02.006. arXiv:hep-lat/0401011
900. L. Giusti, P. Hernandez, M. Laine, P. Weisz, H. Wittig, Low-energy couplings of QCD from current correlators near the chiral limit. JHEP **0404**, 013 (2004). https://doi.org/10.1088/1126-6708/2004/04/013. arXiv:hep-lat/0402002
901. R. Gupta, A. Patel, C.F. Baillie, G. Guralnik, G.W. Kilcup, S.R. Sharpe, QCD with dynamical Wilson fermions. Phys. Rev. D **40**, 2072 (1989). https://doi.org/10.1103/PhysRevD.40.2072
902. C. Thron, S. Dong, K. Liu, H. Ying, Pade-Z(2) estimator of determinants. Phys. Rev. D **57**, 1642 (1998). https://doi.org/10.1103/PhysRevD.57.1642. arXiv:hep-lat/9707001
903. S. Bernardson, P. McCarty, C. Thron, Monte Carlo methods for estimating linear combinations of inverse matrix entries in lattice QCD. Comput. Phys. Commun. **78**, 256 (1993). https://doi.org/10.1016/0010-4655(94)90004-3
904. J. Foley et al., Practical all-to-all propagators for lattice QCD. Comput. Phys. Commun. **172**, 145 (2005). https://doi.org/10.1016/j.cpc.2005.06.008. arXiv:hep-lat/0505023
905. S. Güsken, U. Löw, K.H. Mütter, R. Sommer, A. Patel, K. Schilling, Nonsinglet axial vector couplings of the baryon octet in lattice QCD. Phys. Lett. B **227**, 266 (1989). https://doi.org/10.1016/S0370-2693(89)80034-6
906. C. Alexandrou, F. Jegerlehner, S. Gusken, K. Schilling, R. Sommer, B meson properties from lattice QCD. Phys. Lett. B **256**, 60 (1991). https://doi.org/10.1016/0370-2693(91)90219-G
907. B.C. Tiburzi, Time dependence of nucleon correlation functions in chiral perturbation theory. Phys. Rev. D **80**, 014002 (2009). https://doi.org/10.1103/PhysRevD.80.014002. arXiv:0901.0657
908. O. Bär, Multi-hadron-state contamination in nucleon observables from chiral perturbation theory. EPJ Web Conf. **175**, 01007 (2018). https://doi.org/10.1051/epjconf/201817501007. arXiv:1708.00380
909. O. Bär, Nucleon-pion-state contribution in lattice calculations of the nucleon charges g_A, g_T and g_S. Phys. Rev. D **94**, 054505 (2016). https://doi.org/10.1103/PhysRevD.94.054505. arXiv:1606.09385
910. O. Bär, Nucleon-pion-state contribution in lattice calculations of moments of parton distribution functions. Phys. Rev. D **95**, 034506 (2017). https://doi.org/10.1103/PhysRevD.95.034506. arXiv:1612.08336
911. M.T. Hansen, H.B. Meyer, On the effect of excited states in lattice calculations of the nucleon axial charge. Nucl. Phys. B **923**, 558 (2017). https://doi.org/10.1016/j.nuclphysb.2017.08.017. arXiv:1610.03843

912. B. Yoon et al., Isovector charges of the nucleon from 2+1-flavor QCD with clover fermions. Phys. Rev. D **95**, 074508 (2017). https://doi.org/10.1103/PhysRevD.95.074508. arXiv:1611.07452
913. L. Maiani, G. Martinelli, M.L. Paciello, B. Taglienti, Scalar densities and baryon mass differences in lattice QCD with Wilson fermions. Nucl. Phys. B **293**, 420 (1987). https://doi.org/10.1016/0550-3213(87)90078-2
914. S.J. Dong, K.F. Liu, A.G. Williams, Lattice calculation of the strangeness magnetic moment of the nucleon. Phys. Rev. D **58**, 074504 (1998). https://doi.org/10.1103/PhysRevD.58.074504. arXiv:hep-ph/9712483
915. S. Capitani, B. Knippschild, M. Della Morte, H. Wittig, Systematic errors in extracting nucleon properties from lattice QCD. PoS LATTICE **2010**, 147 (2010). https://doi.org/10.22323/1.105.0147. arXiv:1011.1358
916. J. Bulava, M. Donnellan, R. Sommer, On the computation of hadron-to-hadron transition matrix elements in lattice QCD. JHEP **01**, 140 (2012). https://doi.org/10.1007/JHEP01(2012)140. arXiv:1108.3774
917. S. Güsken, K. Schilling, R. Sommer, K.H. Mütter, A. Patel, Mass splittings in the baryon octet and the nucleon σ term in lattice QCD. Phys. Lett. B **212**, 216 (1988). https://doi.org/10.1016/0370-2693(88)90528-X
918. R. Sommer, Current matrix elements with quenched Wilson fermions. Nucl. Phys. Proc. Suppl. **17**, 513 (1990). https://doi.org/10.1016/0920-5632(90)90304-D
919. C. Bouchard, C.C. Chang, T. Kurth, K. Orginos, A. Walker-Loud, On the Feynman–Hellmann theorem in quantum field theory and the calculation of matrix elements. Phys. Rev. D **96**, 014504 (2017). https://doi.org/10.1103/PhysRevD.96.014504. arXiv:1612.06963
920. [CSSM/QCDSF/UKQCD 14] A.J. Chambers et al., Feynman–Hellmann approach to the spin structure of hadrons. Phys. Rev. D **90**, 014510 (2014). https://doi.org/10.1103/PhysRevD.90.014510. arXiv:1405.3019
921. A.J. Chambers et al., Disconnected contributions to the spin of the nucleon. Phys. Rev. D **92**, 114517 (2015). https://doi.org/10.1103/PhysRevD.92.114517. arXiv:1508.06856
922. B.J. Owen, J. Dragos, W. Kamleh, D.B. Leinweber, M.S. Mahbub, B.J. Menadue et al., Variational approach to the calculation of gA. Phys. Lett. B **723**, 217 (2013). https://doi.org/10.1016/j.physletb.2013.04.063. arXiv:1212.4668
923. C. Egerer, D. Richards, F. Winter, Controlling excited-state contributions with distillation in lattice QCD calculations of nucleon isovector charges g_S^{u-d}, g_A^{u-d}, g_T^{u-d}. Phys. Rev. D **99**, 034506 (2019). https://doi.org/10.1103/PhysRevD.99.034506. arXiv:1810.09991
924. G. Fox, R. Gupta, O. Martin, S. Otto, Monte Carlo estimates of the mass gap of the O(2) and O(3) spin models in (1+1)-dimensions. Nucl. Phys. B **205**, 188 (1982). https://doi.org/10.1016/0550-3213(82)90384-4
925. C. Michael, Adjoint sources in lattice gauge theory. Nucl. Phys. B **259**, 58 (1985). https://doi.org/10.1016/0550-3213(85)90297-4
926. M. Lüscher, U. Wolff, How to calculate the elastic scattering matrix in two-dimensional quantum field theories by numerical simulation. Nucl. Phys. B **339**, 222 (1990). https://doi.org/10.1016/0550-3213(90)90540-T
927. B. Blossier, M. Della Morte, G. von Hippel, T. Mendes, R. Sommer, On the generalized eigenvalue method for energies and matrix elements in lattice field theory. JHEP **04**, 094 (2009). https://doi.org/10.1088/1126-6708/2009/04/094. arXiv:0902.1265
928. J. Dragos, R. Horsley, W. Kamleh, D.B. Leinweber, Y. Nakamura, P.E.L. Rakow et al., Nucleon matrix elements using the variational method in lattice QCD. Phys. Rev. D **94**, 074505 (2016). https://doi.org/10.1103/PhysRevD.94.074505. arXiv:1606.03195
929. K. Jansen, C. Liu, M. Luscher, H. Simma, S. Sint, R. Sommer et al., Nonperturbative renormalization of lattice QCD at all scales. Phys. Lett. B **372**, 275 (1996). https://doi.org/10.1016/0370-2693(96)00075-5. arXiv:hep-lat/9512009
930. M. Lüscher, S. Sint, R. Sommer, P. Weisz, Chiral symmetry and O(a) improvement in lattice QCD. Nucl. Phys. B **478**, 365 (1996). https://doi.org/10.1016/0550-3213(96)00378-1. arXiv:hep-lat/9605038
931. [RQCD 16A] G.S. Bali, E.E. Scholz, J. Simeth, W. Söldner, Lattice simulations with $N_f = 2+1$ improved Wilson fermions at a fixed strange quark mass. Phys. Rev. D **94**, 074501 (2016). https://doi.org/10.1103/PhysRevD.94.074501. arXiv:1606.09039
932. A. Gerardin, T. Harris, H.B. Meyer, Non-perturbative renormalization and O(a)-improvement of the non-singlet vector current with $N_{\rm f} = 2+1$ Wilson fermions and tree-level Symanzik improved gauge action. Phys. Rev. D **99**, 014519 (2019). https://doi.org/10.1103/PhysRevD.99.014519. arXiv:1811.08209
933. R. Frezzotti, G.C. Rossi, Chirally improving Wilson fermions. I: O(a) improvement. JHEP **08**, 007 (2004). arXiv:hep-lat/0306014
934. R. Frezzotti, G.C. Rossi, Twisted mass lattice QCD with mass nondegenerate quarks. Nucl. Phys. Proc. Suppl. **128**, 193 (2004). https://doi.org/10.1016/S0920-5632(03)02477-0. arxiv:hep-lat/0311008
935. S. Capitani, M. Göckeler, R. Horsley, H. Perlt, P.E.L. Rakow, G. Schierholz et al., Renormalization and off-shell improvement in lattice perturbation theory. Nucl. Phys. B **593**, 183 (2001). https://doi.org/10.1016/S0550-3213(00)00590-3. arXiv:hep-lat/0007004
936. T. Bhattacharya, R. Gupta, W. Lee, S.R. Sharpe, J.M.S. Wu, Improved bilinears in lattice QCD with non-degenerate quarks. Phys. Rev. D **73**, 034504 (2006). https://doi.org/10.1103/PhysRevD.73.034504. arXiv:hep-lat/0511014
937. M. Bochicchio, L. Maiani, G. Martinelli, G.C. Rossi, M. Testa, Chiral symmetry on the lattice with Wilson fermions. Nucl. Phys. B **262**, 331 (1985). https://doi.org/10.1016/0550-3213(85)90290-1
938. S. Sint, P. Weisz, Further results on O(a) improved lattice QCD to one loop order of perturbation theory. Nucl. Phys. B **502**, 251 (1997). https://doi.org/10.1016/S0550-3213(97)00372-6. arXiv:hep-lat/9704001
939. Y. Taniguchi, A. Ukawa, Perturbative calculation of improvement coefficients to O(g**2a) for bilinear quark operators in lattice QCD. Phys. Rev. D **58**, 114503 (1998). https://doi.org/10.1103/PhysRevD.58.114503. arXiv:hep-lat/9806015
940. P. Korcyl, G.S. Bali, Non-perturbative determination of improvement coefficients using coordinate space correlators in $N_f = 2+1$ lattice QCD. Phys. Rev. D **95**, 014505 (2017). https://doi.org/10.1103/PhysRevD.95.014505. arXiv:1607.07090
941. M. Constantinou, M. Hadjiantonis, H. Panagopoulos, G. Spanoudes, Singlet versus nonsinglet perturbative renormalization of fermion bilinears. Phys. Rev. D **94**, 114513 (2016). https://doi.org/10.1103/PhysRevD.94.114513. arXiv:1610.06744
942. G.S. Bali, S. Collins, M. Göckeler, S. Piemonte, A. Sternbeck, Non-perturbative renormalization of flavor singlet quark bilinear operators in lattice QCD. PoS LATTICE **2016**, 187 (2016). https://doi.org/10.22323/1.256.0187. arXiv:1703.03745
943. S. Dinter, V. Drach, R. Frezzotti, G. Herdoiza, K. Jansen, G. Rossi, Sigma terms and strangeness content of the nucleon with $N_f = 2+1+1$ twisted mass fermions. JHEP **08**, 037 (2012). https://doi.org/10.1007/JHEP08(2012)037. arXiv:1202.1480
944. E.E. Jenkins, A.V. Manohar, Baryon chiral perturbation theory using a heavy fermion Lagrangian. Phys. Lett. B **255**, 558 (1991). https://doi.org/10.1016/0370-2693(91)90266-S

945. V. Bernard, N. Kaiser, U.-G. Meissner, Chiral dynamics in nucleons and nuclei. Int. J. Mod. Phys. E **4**, 193 (1995). https://doi.org/10.1142/S0218301395000092. arXiv:hep-ph/9501384
946. T.N. Truong, Chiral perturbation theory and final state theorem. Phys. Rev. Lett. **61**, 2526 (1988). https://doi.org/10.1103/PhysRevLett.61.2526
947. T. Becher, H. Leutwyler, Baryon chiral perturbation theory in manifestly Lorentz invariant form. Eur. Phys. J. C **9**, 643 (1999). https://doi.org/10.1007/PL00021673. arXiv:hep-ph/9901384
948. T. Fuchs, J. Gegelia, G. Japaridze, S. Scherer, Renormalization of relativistic baryon chiral perturbation theory and power counting. Phys. Rev. D **68**, 056005 (2003). https://doi.org/10.1103/PhysRevD.68.056005. arXiv:hep-ph/0302117
949. A. Walker-Loud et al., Light hadron spectroscopy using domain wall valence quarks on an Asqtad sea. Phys. Rev. D **79**, 054502 (2009). https://doi.org/10.1103/PhysRevD.79.054502. arXiv:0806.4549
950. A. Torok, S.R. Beane, W. Detmold, T.C. Luu, K. Orginos, A. Parreno et al., Meson-baryon scattering lengths from mixed-action lattice QCD. Phys. Rev. D **81**, 074506 (2010). https://doi.org/10.1103/PhysRevD.81.074506. arXiv:0907.1913
951. E.E. Jenkins, A.V. Manohar, J.W. Negele, A. Walker-Loud, A lattice test of 1/N(c) baryon mass relations. Phys. Rev. D **81**, 014502 (2010). https://doi.org/10.1103/PhysRevD.81.014502. arXiv:0907.0529
952. A. Walker-Loud, Evidence for non-analytic light quark mass dependence in the baryon spectrum. Phys. Rev. D **86**, 074509 (2012). https://doi.org/10.1103/PhysRevD.86.074509. arXiv:1112.2658
953. V. Bernard, N. Kaiser, J. Kambor, U.G. Meissner, Chiral structure of the nucleon. Nucl. Phys. **B388**, 315 (1992). https://doi.org/10.1016/0550-3213(92)90615-I
954. S.R. Beane, M.J. Savage, Baryon axial charge in a finite volume. Phys. Rev. D **70**, 074029 (2004). https://doi.org/10.1103/PhysRevD.70.074029. arXiv:hep-ph/0404131
955. R.E. Kass, A.E. Raftery, Bayes factors. J. Am. Stat. Assoc. **90**, 773 (1995). https://doi.org/10.1080/01621459.1995.10476572
956. H. Akaike, A new look at the statistical model identification. IEEE. Trans. Autom. Control **19**, 716 (1974). https://doi.org/10.1109/TAC.1974.1100705
957. T. Bhattacharya, V. Cirigliano, S.D. Cohen, A. Filipuzzi, M. Gonzalez-Alonso et al., Probing novel scalar and tensor interactions from (ultra)cold neutrons to the LHC. Phys. Rev. D **85**, 054512 (2012). https://doi.org/10.1103/PhysRevD.85.054512. arXiv:1110.6448
958. UCNA collaboration, Precision measurement of the neutron β-decay asymmetry. Phys. Rev. C **87**, 032501 (2013). https://doi.org/10.1103/PhysRevC.87.032501. arXiv:1210.7048
959. UCNA collaboration, New result for the neutron β-asymmetry parameter A_0 from UCNA. Phys. Rev. C **97**, 035505 (2018). https://doi.org/10.1103/PhysRevC.97.035505. arXiv:1712.00884
960. D. Mund, B. Maerkisch, M. Deissenroth, J. Krempel, M. Schumann, H. Abele et al., Determination of the weak axial vector coupling from a measurement of the beta-asymmetry parameter a in neutron beta decay. Phys. Rev. Lett. **110**, 172502 (2013). https://doi.org/10.1103/PhysRevLett.110.172502. arXiv:1204.0013
961. M. Ademollo, R. Gatto, Nonrenormalization theorem for the strangeness violating vector. Phys. Rev. Lett. Curr. **13**, 264 (1964). https://doi.org/10.1103/PhysRevLett.13.264
962. J.F. Donoghue, D. Wyler, Isospin breaking and the precise determination of V_{ud}. Phys. Lett. B **241**, 243 (1990). https://doi.org/10.1016/0370-2693(90)91287-L
963. R. Alarcon et al., Precise Measurement of Neutron Decay Parameters (2007)
964. W. Wilburn et al., Measurement of the neutrino-spin correlation parameter b in neutron decay using ultracold neutrons. Rev. Mex. Fis. Suppl. **55**, 119 (2009)
965. Nab collaboration, Nab: measurement principles, apparatus and uncertainties. Nucl. Instrum. Methods A **611**, 211 (2009). https://doi.org/10.1016/j.nima.2009.07.065. arXiv:0810.0251
966. M. Gonzalez-Alonso, J. Martin Camalich, Isospin breaking in the nucleon mass and the sensitivity of β decays to new physics. Phys. Rev. Lett. **112**, 042501 (2014). https://doi.org/10.1103/PhysRevLett.112.042501. arXiv:1309.4434
967. J. Dudek et al., Physics opportunities with the 12 GeV upgrade at Jefferson Lab. Eur. Phys. J. A **48**, 187 (2012). https://doi.org/10.1140/epja/i2012-12187-1. arXiv:1208.1244
968. Z. Ye, N. Sato, K. Allada, T. Liu, J.-P. Chen, H. Gao et al., Unveiling the nucleon tensor charge at Jefferson Lab: a study of the SoLID case. Phys. Lett. B **767**, 91 (2017). https://doi.org/10.1016/j.physletb.2017.01.046. arXiv:1609.02449
969. H.-W. Lin, W. Melnitchouk, A. Prokudin, N. Sato, H. Shows, First Monte Carlo global analysis of nucleon transversity with lattice QCD constraints. Phys. Rev. Lett. **120**, 152502 (2018). https://doi.org/10.1103/PhysRevLett.120.152502. arXiv:1710.09858
970. M. Radici, A. Bacchetta, First extraction of transversity from a global analysis of electron–proton and proton–proton data. Phys. Rev. Lett. **120**, 192001 (2018). https://doi.org/10.1103/PhysRevLett.120.192001. arXiv:1802.05212
971. [ETM 19] C. Alexandrou, S. Bacchio, M. Constantinou, J. Finkenrath, K. Hadjiyiannakou, K. Jansen et al., Nucleon axial, tensor, and scalar charges and σ-terms in lattice QCD. Phys. Rev. D **102**, 054517 (2020). https://doi.org/10.1103/PhysRevD.102.054517. arXiv:1909.00485
972. [NME 21] S. Park, R. Gupta, B. Yoon, S. Mondal, T. Bhattacharya, Y.-C. Jang et al., Precision nucleon charges and form factors using 2+1-flavor lattice QCD. arXiv:2103.05599
973. [LHPC 12A] J.R. Green, M. Engelhardt, S. Krieg, J.W. Negele, A.V. Pochinsky, S.N. Syritsyn, Nucleon structure from lattice QCD using a nearly physical pion mass. Phys. Lett. B **734**, 290 (2014). https://doi.org/10.1016/j.physletb.2014.05.075. arXiv:1209.1687
974. [LHPC 05] R.G. Edwards et al., The nucleon axial charge in full lattice QCD. Phys. Rev. Lett. **96**, 052001 (2006). https://doi.org/10.1103/PhysRevLett.96.052001. arXiv:hep-lat/0510062
975. [RBC 08] H.-W. Lin, T. Blum, S. Ohta, S. Sasaki, T. Yamazaki, Nucleon structure with two flavors of dynamical domain-wall fermions. Phys. Rev. D **78**, 014505 (2008). https://doi.org/10.1103/PhysRevD.78.014505. arXiv:0802.0863
976. [Mainz 18] K. Ottnad, T. Harris, H. Meyer, G. von Hippel, J. Wilhelm, H. Wittig, Nucleon charges and quark momentum fraction with $N_f = 2 + 1$ Wilson fermions, in Proceedings, 36th International Symposium on Lattice Field Theory (Lattice 2018): East Lansing, MI, United States, July 22–28, 2018, vol. LATTICE2018, p. 129 (2018). https://doi.org/10.22323/1.334.0129. arXiv:1809.10638

977. [RBC/UKQCD 19] M. Abramczyk, T. Blum, T. Izubuchi, C. Jung, M. Lin, A. Lytle et al., Nucleon mass and isovector couplings in 2+1-flavor dynamical domain-wall lattice QCD near physical mass. Phys. Rev. D **101**, 034510 (2020). https://doi.org/10.1103/PhysRevD.101.034510. arXiv:1911.03524
978. [χQCD 21A] L. Liu, T. Chen, T. Draper, J. Liang, K.-F. Liu, G. Wang et al., Nucleon isovector scalar charge from overlap fermions. Phys. Rev. D **104**, 094503 (2021). https://doi.org/10.1103/PhysRevD.104.094503. arXiv:2103.12933
979. [LHPC 12] J.R. Green, J.W. Negele, A.V. Pochinsky, S.N. Syritsyn, M. Engelhardt, S. Krieg, Nucleon scalar and tensor charges from lattice QCD with light Wilson quarks. Phys. Rev. D **86**, 114509 (2012). https://doi.org/10.1103/PhysRevD.86.114509. arXiv:1206.4527
980. A. Walker-Loud, C.E. Carlson, G.A. Miller, The electromagnetic self-energy contribution to $M_p - M_n$ and the isovector nucleon magnetic polarizability. Phys. Rev. Lett. **108**, 232301 (2012). https://doi.org/10.1103/PhysRevLett.108.232301. arXiv:1203.0254
981. P.E. Shanahan, A.W. Thomas, R.D. Young, Strong contribution to octet baryon mass splittings. Phys. Lett. B **718**, 1148 (2013). https://doi.org/10.1016/j.physletb.2012.11.072. arXiv:1209.1892
982. S.R. Beane, K. Orginos, M.J. Savage, Strong-isospin violation in the neutron proton mass difference from fully-dynamical lattice QCD and PQQCD. Nucl. Phys. B **768**, 38 (2007). https://doi.org/10.1016/j.nuclphysb.2006.12.023. arXiv:hep-lat/0605014
983. [QCDSF/UKQCD 12A] R. Horsley, J. Najjar, Y. Nakamura, D. Pleiter, P.E.L. Rakow, G. Schierholz et al., Isospin breaking in octet baryon mass splittings. Phys. Rev. D **86**, 114511 (2012). https://doi.org/10.1103/PhysRevD.86.114511. arXiv:1206.3156
984. [BMW 13A] Sz. Borsanyi et al., Isospin splittings in the light baryon octet from lattice QCD and QED. Phys. Rev. Lett. **111**, 252001 (2013). https://doi.org/10.1103/PhysRevLett.111.252001. arXiv:1306.2287
985. D.A. Brantley, B. Joo, E.V. Mastropas, E. Mereghetti, H. Monge-Camacho, B.C. Tiburzi et al., Strong isospin violation and chiral logarithms in the baryon spectrum. arXiv:1612.07733
986. M. Radici, A. Courtoy, A. Bacchetta, M. Guagnelli, Improved extraction of valence transversity distributions from inclusive dihadron production. JHEP **05**, 123 (2015). https://doi.org/10.1007/JHEP05(2015)123. arXiv:1503.03495
987. Z.-B. Kang, A. Prokudin, P. Sun, F. Yuan, Extraction of quark transversity distribution and Collins fragmentation functions with QCD evolution. Phys. Rev. D **93**, 014009 (2016). https://doi.org/10.1103/PhysRevD.93.014009. arXiv:1505.05589
988. Z.-B. Kang, Private communication (2015)
989. G.R. Goldstein, J.O. Gonzalez Hernandez, S. Liuti, Flavor dependence of chiral odd generalized parton distributions and the tensor charge from the analysis of combined π^0 and η exclusive electroproduction data. arXiv:1401.0438
990. M. Pitschmann, C.-Y. Seng, C.D. Roberts, S.M. Schmidt, Nucleon tensor charges and electric dipole moments. Phys. Rev. D **91**, 074004 (2015). https://doi.org/10.1103/PhysRevD.91.074004. arXiv:1411.2052
991. M.A. Shifman, A.I. Vainshtein, V.I. Zakharov, Remarks on Higgs boson interactions with nucleons. Phys. Lett. B **78**, 443 (1978). https://doi.org/10.1016/0370-2693(78)90481-1
992. K.G. Chetyrkin, B.A. Kniehl, M. Steinhauser, Decoupling relations to O (alpha-s**3) and their connection to low-energy theorems. Nucl. Phys. B **510**, 61 (1998). https://doi.org/10.1016/S0550-3213(98)81004-3. https://doi.org/10.1016/S0550-3213(97)00649-4. arXiv:hep-ph/9708255
993. R.J. Hill, M.P. Solon, Standard Model anatomy of WIMP dark matter direct detection II: QCD analysis and hadronic matrix elements. Phys. Rev. D **91**, 043505 (2015). https://doi.org/10.1103/PhysRevD.91.043505. arXiv:1409.8290
994. European Muon collaboration, A measurement of the spin asymmetry and determination of the structure function g(1) in deep inelastic muon–proton scattering. Phys. Lett. B **206**, 364 (1988). https://doi.org/10.1016/0370-2693(88)91523-7
995. X.-D. Ji, Gauge-invariant decomposition of nucleon spin. Phys. Rev. Lett. **78**, 610 (1997). https://doi.org/10.1103/PhysRevLett.78.610. arXiv:hep-ph/9603249
996. R.L. Jaffe, A. Manohar, The G(1) problem: fact and fantasy on the spin of the proton. Nucl. Phys. B **337**, 509 (1990). https://doi.org/10.1016/0550-3213(90)90506-9
997. M. Pospelov, A. Ritz, Electric dipole moments as probes of new physics. Ann. Phys. **318**, 119 (2005). https://doi.org/10.1016/j.aop.2005.04.002. arXiv:hep-ph/0504231
998. C. Baker, D. Doyle, P. Geltenbort, K. Green, M. van der Grinten et al., An improved experimental limit on the electric dipole moment of the neutron. Phys. Rev. Lett. **97**, 131801 (2006). https://doi.org/10.1103/PhysRevLett.97.131801. arXiv:hep-ex/0602020
999. C.-Y. Seng, Reexamination of the standard model nucleon electric dipole moment. Phys. Rev. C **91**, 025502 (2015). https://doi.org/10.1103/PhysRevC.91.025502. arXiv:1411.1476
1000. [PNDME 20] S. Park, T. Bhattacharya, R. Gupta, Y.-C. Jang, B. Joo, H.-W. Lin et al., Nucleon charges and form factors using clover and HISQ ensembles. PoS LATTICE **2019**, 136 (2020). https://doi.org/10.22323/1.363.0136. arXiv:2002.02147
1001. [Mainz 19A] D. Djukanovic, H. Meyer, K. Ottnad, G. von Hippel, J. Wilhelm, H. Wittig, Strange nucleon form factors and isoscalar charges with $N_f = 2 + 1$ $mathcal O(a)$-improved Wilson fermions. PoS LATTICE **2019**, 158 (2019). https://doi.org/10.22323/1.363.0158. arXiv:1911.01177
1002. M. Engelhardt, Strange quark contributions to nucleon mass and spin from lattice QCD. Phys. Rev. D **86**, 114510 (2012). https://doi.org/10.1103/PhysRevD.86.114510. arXiv:1210.0025
1003. J.M. Alarcon, J. Martin Camalich, J.A. Oller, The chiral representation of the πN scattering amplitude and the pion-nucleon sigma term. Phys. Rev. D **85**, 051503 (2012). https://doi.org/10.1103/PhysRevD.85.051503. arXiv:1110.3797
1004. Y.-H. Chen, D.-L. Yao, H.Q. Zheng, Analyses of pion-nucleon elastic scattering amplitudes up to $O(p^4)$ in extended-on-mass-shell subtraction scheme. Phys. Rev. D **87**, 054019 (2013). https://doi.org/10.1103/PhysRevD.87.054019. arXiv:1212.1893
1005. M. Hoferichter, J. Ruiz de Elvira, B. Kubis, U.-G. Meissner, High-precision determination of the pion-nucleon σ term from Roy–Steiner equations. Phys. Rev. Lett. **115**, 092301 (2015). https://doi.org/10.1103/PhysRevLett.115.092301. arXiv:1506.04142
1006. [PNDME 21] R. Gupta, S. Park, M. Hoferichter, E. Mereghetti, B. Yoon, T. Bhattacharya, Pion–nucleon sigma term from lattice QCD. Phys. Rev. Lett. **127**, 242002 (2021). https://doi.org/10.1103/PhysRevLett.127.242002. arXiv:2105.12095
1007. [MILC 09D] D. Toussaint, W. Freeman, The strange quark condensate in the nucleon in 2+1 flavor QCD. Phys. Rev. Lett. **103**, 122002 (2009). https://doi.org/10.1103/PhysRevLett.103.122002. arXiv:0905.2432
1008. [JLQCD 10A] K. Takeda, S. Aoki, S. Hashimoto, T. Kaneko, J. Noaki, T. Onogi, Nucleon strange quark content from two-flavor lattice QCD with exact chiral symmetry. Phys. Rev. D **83**, 114506 (2011). https://doi.org/10.1103/PhysRevD.83.114506. arXiv:1011.1964

1009. C. McNeile, A. Bazavov, C.T.H. Davies, R.J. Dowdall, K. Hornbostel, G.P. Lepage et al., Direct determination of the strange and light quark condensates from full lattice QCD. Phys. Rev. D **87**, 034503 (2013). https://doi.org/10.1103/PhysRevD.87.034503. arXiv:1211.6577
1010. [BMW 20A] Sz. Borsanyi, Z. Fodor, C. Hoelbling, L. Lellouch, K. Szabo, C. Torrero et al., Ab-initio calculation of the proton and the neutron's scalar couplings for new physics searches. arXiv:2007.03319
1011. P.E. Shanahan, A.W. Thomas, R.D. Young, Sigma terms from an SU(3) chiral extrapolation. Phys. Rev. D **87**, 074503 (2013). https://doi.org/10.1103/PhysRevD.87.074503. arXiv:1205.5365
1012. [QCDSF/UKQCD 11] R. Horsley, Y. Nakamura, H. Perlt, D. Pleiter, P.E.L. Rakow, G. Schierholz et al., Hyperon sigma terms for 2+1 quark flavours. Phys. Rev. D **85**, 034506 (2012). https://doi.org/10.1103/PhysRevD.85.034506. arXiv:1110.4971
1013. J. Martin Camalich, L.S. Geng, M.J. Vicente Vacas, The lowest-lying baryon masses in covariant SU(3)-flavor chiral perturbation theory. Phys. Rev. D **82**, 074504 (2010). https://doi.org/10.1103/PhysRevD.82.074504. arXiv:1003.1929
1014. A. Walker-Loud et al., Light hadron spectroscopy using domain wall valence quarks on an Asqtad sea. Phys. Rev. D **79**, 054502 (2009). https://doi.org/10.1103/PhysRevD.79.054502. arXiv:0806.4549
1015. [ETM 17A] C. Alexandrou, C. Kallidonis, Low-lying baryon masses using $N_f = 2$ twisted mass clover-improved fermions directly at the physical pion mass. Phys. Rev. D **96**, 034511 (2017). https://doi.org/10.1103/PhysRevD.96.034511. arXiv:1704.02647
1016. C. Kallidonis, Private communication (2018)
1017. [ETM 09H] C. Alexandrou, R. Baron, J. Carbonell, V. Drach, P. Guichon, K. Jansen et al., Low-lying baryon spectrum with two dynamical twisted mass fermions. Phys. Rev. D **80**, 114503 (2009). https://doi.org/10.1103/PhysRevD.80.114503. arXiv:0910.2419
1018. [BMW 08] S. Dürr et al., Ab-initio determination of light hadron masses. Science **322**, 1224 (2008). https://doi.org/10.1126/science.1163233. arXiv:0906.3599
1019. A. Crivellin, M. Hoferichter, M. Procura, Accurate evaluation of hadronic uncertainties in spin-independent WIMP-nucleon scattering: disentangling two- and three-flavor effects. Phys. Rev. D **89**, 054021 (2014). https://doi.org/10.1103/PhysRevD.89.054021. arXiv:1312.4951
1020. Y.-B. Yang, J. Liang, Y.-J. Bi, Y. Chen, T. Draper, K.-F. Liu et al., Proton mass decomposition from the QCD energy momentum tensor. Phys. Rev. Lett. **121**, 212001 (2018). https://doi.org/10.1103/PhysRevLett.121.212001. arXiv:1808.08677
1021. M. Procura, B.U. Musch, T. Wollenweber, T.R. Hemmert, W. Weise, Nucleon mass: from lattice QCD to the chiral limit. Phys. Rev. D **73**, 114510 (2006). https://doi.org/10.1103/PhysRevD.73.114510. arXiv:hep-lat/0603001
1022. R.D. Young, A.W. Thomas, Octet baryon masses and sigma terms from an SU(3) chiral extrapolation. Phys. Rev. D **81**, 014503 (2010). https://doi.org/10.1103/PhysRevD.81.014503. arXiv:0901.3310
1023. X.L. Ren, L.S. Geng, J. Martin Camalich, J. Meng, H. Toki, Octet baryon masses in next-to-next-to-next-to-leading order covariant baryon chiral perturbation theory. JHEP **12**, 073 (2012). https://doi.org/10.1007/JHEP12(2012)073. arXiv:1209.3641
1024. L. Alvarez-Ruso, T. Ledwig, J. Martin Camalich, M.J. Vicente-Vacas, Nucleon mass and pion-nucleon sigma term from a chiral analysis of lattice QCD data. Phys. Rev. D **88**, 054507 (2013). https://doi.org/10.1103/PhysRevD.88.054507. arXiv:1304.0483
1025. M.F.M. Lutz, R. Bavontaweepanya, C. Kobdaj, K. Schwarz, Finite volume effects in the chiral extrapolation of baryon masses. Phys. Rev. D **90**, 054505 (2014). https://doi.org/10.1103/PhysRevD.90.054505. arXiv:1401.7805
1026. X.-L. Ren, L.-S. Geng, J. Meng, Scalar strangeness content of the nucleon and baryon sigma terms. Phys. Rev. D **91**, 051502 (2015). https://doi.org/10.1103/PhysRevD.91.051502. arXiv:1404.4799
1027. X.-L. Ren, L. Alvarez-Ruso, L.-S. Geng, T. Ledwig, J. Meng, M.J. Vicente Vacas, Consistency between SU(3) and SU(2) covariant baryon chiral perturbation theory for the nucleon mass. Phys. Lett. B **766**, 325 (2017). https://doi.org/10.1016/j.physletb.2017.01.024. arXiv:1606.03820
1028. X.-Z. Ling, X.-L. Ren, L.-S. Geng, Pion-nucleon sigma term revisited in covariant baryon chiral perturbation theory. Phys. Lett. B **783**, 7 (2018). https://doi.org/10.1016/j.physletb.2018.05.063. arXiv:1710.07164
1029. M.F.M. Lutz, Y. Heo, X.-Y. Guo, On the convergence of the chiral expansion for the baryon ground-state masses. Nucl. Phys. A **977**, 146 (2018). https://doi.org/10.1016/j.nuclphysa.2018.05.007. arXiv:1801.06417
1030. J. Ruiz de Elvira, M. Hoferichter, B. Kubis, U.-G. Meissner, Extracting the σ-term from low-energy pion-nucleon scattering. J. Phys. G **45**, 024001 (2018). https://doi.org/10.1088/1361-6471/aa9422. arXiv:1706.01465
1031. T. Aoyama et al., The anomalous magnetic moment of the muon in the Standard Model. Phys. Rep. **887**, 1 (2020). https://doi.org/10.1016/j.physrep.2020.07.006. arXiv:2006.04822
1032. M. Della Morte, A. Francis, V. Gülpers, G. Herdoíza, G. von Hippel, H. Horch et al., The hadronic vacuum polarization contribution to the muon $g-2$ from lattice QCD. JHEP **10**, 020 (2017). https://doi.org/10.1007/JHEP10(2017)020. arXiv:1705.01775
1033. M. Luscher, Computational strategies in lattice QCD, in Les Houches Summer School: session 93: modern perspectives in lattice QCD: quantum field theory and high performance computing, 2 (2010). arXiv:1002.4232
1034. B. Jäger, T.D. Rae, S. Capitani, M. Della Morte, D. Djukanovic, G. von Hippel et al., A high-statistics study of the nucleon EM form factors, axial charge and quark momentum fraction. PoS LATTICE **2013**, 272 (2014). https://doi.org/10.22323/1.187.0272. arXiv:1311.5804
1035. S. Capitani, M. Della Morte, G. von Hippel, B. Knippschild, H. Wittig, Scale setting via the Ω baryon mass. PoS LATTICE **2011**, 145 (2011). https://doi.org/10.22323/1.139.0145. arXiv:1110.6365
1036. M. Creutz, Monte Carlo study of quantized SU(2) Gauge theory. Phys. Rev. **D21**, 2308 (1980). https://doi.org/10.1103/PhysRevD.21.2308
1037. A. Patella, QED corrections to hadronic observables. PoS LATTICE **2016**, 020 (2017). https://doi.org/10.22323/1.256.0020. arXiv:1702.03857
1038. F. Bloch, A. Nordsieck, Note on the radiation field of the electron. Phys. Rev. **52**, 54 (1937). https://doi.org/10.1103/PhysRev.52.54
1039. B. Ananthanarayan, B. Moussallam, Four-point correlator constraints on electromagnetic chiral parameters and resonance effective Lagrangians. JHEP **06**, 047 (2004). https://doi.org/10.1088/1126-6708/2004/06/047. arXiv:hep-ph/0405206
1040. O. Bar, Chiral perturbation theory and nucleon-pion-state contaminations in lattice QCD. Int. J. Mod. Phys. A **32**, 1730011 (2017). https://doi.org/10.1142/S0217751X17300113. arXiv:1705.02806
1041. F. Niedermayer, P. Rufenacht, U. Wenger, Fixed point gauge actions with fat links: scaling and glueballs. Nucl. Phys. B **597**, 413 (2001). https://doi.org/10.1016/S0550-3213(00)00731-8. arXiv:hep-lat/0007007
1042. M. Della Morte, A. Shindler, R. Sommer, On lattice actions for static quarks. JHEP **08**, 051 (2005). https://doi.org/10.1088/1126-6708/2005/08/051. arXiv:hep-lat/0506008

1043. M. Donnellan, F. Knechtli, B. Leder, R. Sommer, Determination of the static potential with dynamical fermions. Nucl. Phys. B **849**, 45 (2011). https://doi.org/10.1016/j.nuclphysb.2011.03.013. arXiv:1012.3037
1044. A. Hasenfratz, F. Knechtli, Flavor symmetry and the static potential with hypercubic blocking. Phys. Rev. D **64**, 034504 (2001). https://doi.org/10.1103/PhysRevD.64.034504. arXiv:hep-lat/0103029
1045. M. Lüscher, P. Weisz, Perturbative analysis of the gradient flow in non-abelian gauge theories. JHEP **02**, 051 (2011). https://doi.org/10.1007/JHEP02(2011)051. arXiv:1101.0963
1046. A. Deuzeman, U. Wenger, Gradient flow and scale setting for twisted mass fermions. PoS LATTICE **2012**, 162 (2012). https://doi.org/10.22323/1.164.0162
1047. O. Bär, M. Golterman, Chiral perturbation theory for gradient flow observables. Phys. Rev. D **89**, 034505 (2014). https://doi.org/10.1103/PhysRevD.89.099905. https://doi.org/10.1103/PhysRevD.89.034505. arxiv:1312.4999 [Erratum: Phys. Rev. D **89**, 099905 (2014)]
1048. S. Schaefer, Status and challenges of simulations with dynamical fermions. PoS LATTICE **2012**, 001 (2012). https://doi.org/10.22323/1.164.0001. arXiv:1211.5069
1049. A. Ramos, S. Sint, Symanzik improvement of the gradient flow in lattice gauge theories. Eur. Phys. J. C **76**, 15 (2016). https://doi.org/10.1140/epjc/s10052-015-3831-9. arXiv:1508.05552
1050. [MILC 13B] A. Bazavov et al., Symanzik flow on HISQ ensembles. PoS LATTICE **2013**, 269 (2014). https://doi.org/10.22323/1.187.0269. arXiv:1311.1474
1051. A. Cheng, A. Hasenfratz, Y. Liu, G. Petropoulos, D. Schaich, Improving the continuum limit of gradient flow step scaling. JHEP **05**, 137 (2014). https://doi.org/10.1007/JHEP05(2014)137. arXiv:1404.0984
1052. [ETM 20] G. Bergner, P. Dimopoulos, J. Finkenrath, E. Fiorenza, R. Frezzotti, M. Garofalo et al., Quark masses and decay constants in $N_f = 2+1+1$ isoQCD with Wilson clover twisted mass fermions, in 37th International Symposium on Lattice Field Theory (Lattice 2019) Wuhan, Hubei, China, June 16–22, 2019, vol. LATTICE2019, p. 181 (2020). https://doi.org/10.22323/1.363.0181. arXiv:2001.09116
1053. V. Bornyakov et al., Determining the scale in Lattice QCD, 12 (2015). arXiv:1512.05745
1054. [MILC 09B] A. Bazavov et al., Results from the MILC collaboration's SU(3) chiral perturbation theory analysis. PoS LAT **2009**, 079 (2009). arXiv:0910.3618
1055. [HPQCD 03] M. Wingate, C.T. Davies, A. Gray, G.P. Lepage, J. Shigemitsu, The B_s and D_s decay constants in three flavor lattice QCD. Phys. Rev. Lett. **92**, 162001 (2004). https://doi.org/10.1103/PhysRevLett.92.162001. arxiv:hep-ph/0311130
1056. A. Duncan, E. Eichten, H. Thacker, Electromagnetic structure of light baryons in lattice QCD. Phys. Lett. B **409**, 387 (1997). https://doi.org/10.1016/S0370-2693(97)00850-2. arXiv:hep-lat/9607032
1057. P. Ball, R. Zwicky, New results on $B \to \pi, K, \eta$ decay form factors from light-cone sum rules. Phys. Rev. D **71**, 014015 (2005). https://doi.org/10.1103/PhysRevD.71.014015. arXiv:hep-ph/0406232
1058. D. Becirevic, A.L. Yaouanc, A. Oyanguren, P. Roudeau, F. Sanfilippo, Insight into $D/B \to \pi \ell \nu_\ell$ decay using the pole models. arXiv:1407.1019
1059. G.P. Lepage, S.J. Brodsky, Exclusive processes in perturbative Quantum Chromodynamics. Phys. Rev. D **22**, 2157 (1980). https://doi.org/10.1103/PhysRevD.22.2157
1060. R. Akhoury, G.F. Sterman, Y. Yao, Exclusive semileptonic decays of B mesons into light mesons. Phys. Rev. D **50**, 358 (1994). https://doi.org/10.1103/PhysRevD.50.358
1061. L. Lellouch, Lattice constrained unitarity bounds for $\bar{B}^0 \to \pi^+ \ell \bar{\nu}_l$ decays. Nucl. Phys. B **479**, 353 (1996). https://doi.org/10.1016/0550-3213(96)00443-9. arXiv:hep-ph/9509358
1062. C. Bourrely, I. Caprini, L. Lellouch, Model-independent description of $B \to \pi \ell \nu$ decays and a determination of $|V_{ub}|$. Phys. Rev. D **79**, 013008 (2009). https://doi.org/10.1103/PhysRevD.82.099902. https://doi.org/10.1103/PhysRevD.79.013008. arXiv:0807.2722
1063. C. Bourrely, B. Machet, E. de Rafael, Semileptonic decays of pseudoscalar particles (M $\to M' \ell \nu_\ell$) and short distance behavior of Quantum Chromodynamics. Nucl. Phys. B **189**, 157 (1981). https://doi.org/10.1016/0550-3213(81)90086-9
1064. C.G. Boyd, M.J. Savage, Analyticity, shapes of semileptonic form-factors, and $\bar{B} \to \pi \ell \bar{\nu}$. Phys. Rev. D **56**, 303 (1997). https://doi.org/10.1103/PhysRevD.56.303. arXiv:hep-ph/9702300
1065. M.C. Arnesen, B. Grinstein, I.Z. Rothstein, I.W. Stewart, A precision model independent determination of $|V_{ub}|$ from $B \to \pi e \nu$. Phys. Rev. Lett. **95**, 071802 (2005). https://doi.org/10.1103/PhysRevLett.95.071802. arXiv:hep-ph/0504209
1066. T. Becher, R.J. Hill, Comment on form-factor shape and extraction of $|V_{ub}|$ from $B \to \pi l \nu$. Phys. Lett. B **633**, 61 (2006). https://doi.org/10.1016/j.physletb.2005.11.063. arXiv:hep-ph/0509090
1067. R.J. Hill, The Modern description of semileptonic meson form factors. eConf **C060409**, 027 (2006). arXiv:hep-ph/0606023
1068. R.J. Hill, G. Paz, Model independent extraction of the proton charge radius from electron scattering. Phys. Rev. D **82**, 113005 (2010). https://doi.org/10.1103/PhysRevD.82.113005. arXiv:1008.4619
1069. R.J. Hill, G. Paz, Model independent analysis of proton structure for hydrogenic bound states. Phys. Rev. Lett. **107**, 160402 (2011). https://doi.org/10.1103/PhysRevLett.107.160402. arXiv:1103.4617
1070. Z. Epstein, G. Paz, J. Roy, Model independent extraction of the proton magnetic radius from electron scattering. Phys. Rev. D **90**, 074027 (2014). https://doi.org/10.1103/PhysRevD.90.074027. arXiv:1407.5683
1071. B. Chakraborty, C.T.H. Davies, P.G. de Oliviera, J. Koponen, G.P. Lepage, R.S. Van de Water, The hadronic vacuum polarization contribution to a_μ from full lattice QCD. Phys. Rev. D **96**, 034516 (2017). https://doi.org/10.1103/PhysRevD.96.034516. arXiv:1601.03071
1072. B.C. Tiburzi, A. Walker-Loud, Strong isospin breaking in the nucleon and Delta masses. Nucl. Phys. A **764**, 274 (2006). https://doi.org/10.1016/j.nuclphysa.2005.08.013. arXiv:hep-lat/0501018
1073. S.R. Beane, Nucleon masses and magnetic moments in a finite volume. Phys. Rev. D **70**, 034507 (2004). https://doi.org/10.1103/PhysRevD.70.034507. arXiv:hep-lat/0403015
1074. [ETM 18A] C. Alexandrou et al., Simulating twisted mass fermions at physical light, strange and charm quark masses. Phys. Rev. D **98**, 054518 (2018). https://doi.org/10.1103/PhysRevD.98.054518. arXiv:1807.00495